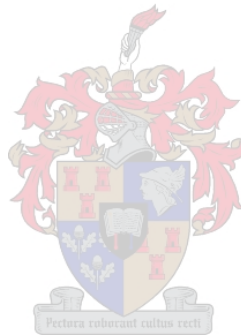


**Chemostratigraphic trends and provenance of the  
Permian Tanqua and Laingsburg depocentres,  
southwestern Karoo Basin,  
South Africa**

by

**Belinda van Lente**



Dissertation presented in partial fulfilment for the Degree of Doctor of  
Philosophy at the University of Stellenbosch

Promotors: Dr. H. deV. Wickens  
Prof. S. S. Flint

December 2004

Declaration

I, the undersigned, hereby declare that the work contained in this dissertation is my own original work and that I have not previously in its entirety or in part submitted it at any university for a degree.

Signature:  .....

Date: 8 November 2004

## Abstract

### Chemostratigraphic trends and provenance of the Permian Tanqua and Laingsburg depocentres, southwestern Karoo Basin, South Africa

Belinda van Lente

Foreland basins commonly fill with sediment derived from the adjacent fold/thrust belt, providing a relatively simple source-to-basin configuration. However, that is not true for the early southwestern Karoo Basin, since the composition of the Ecca Group sedimentary rocks do not match the composition of the adjacent fold/thrust belt.

The southwestern Karoo Basin is bordered to the west and south by the Cape Fold Belt (CFB) and provides the opportunity to study the linkage between its early structural evolution and deposition in the two spatially and temporally distinct Tanqua and Laingsburg depocentres. The CFB was formed when the early Palaeozoic passive continental margin, which formed a large section of the southern edge of Gondwana, evolved into an active convergent margin during the late Palaeozoic. Orogenesis resulted in a northwest-trending Cedarberg branch and an eastwest-trending Swartberg branch. The oroclinal bend between the two branches includes large-scale northeast-trending syntaxis structures, such as the Hex River and Baviaanshoek anticlinoria, which influenced the sedimentation path into the basin.

Spectral gamma ray (SGR), mineralogical and geochemical studies of exposed rocks from the Tanqua and Laingsburg depocentres indicate a near uniform provenance for both, dominated by granitic and metamorphic material derived from a provenance seemingly far beyond the CFB.

SGR data, combined with lithology, show that regional stratigraphic correlation is possible in the Skoorsteenberg, Kookfontein and Waterford Formations in the Tanqua depocentre. The same is true for the Laingsburg and Fort Brown Formations in the Laingsburg depocentre. There are no major changes in the SGR data set between the successive sandstone or shale units that could imply different origin, and no distinct signals in the SGR pattern of the shale intervals that could potentially correspond to maximum flooding surfaces.

The Tanqua and Laingsburg depocentre sandstones are very fine- to lower medium-grained, tightly packed, poorly to well sorted, and have undergone mechanical compaction and pressure solution. The mineralogical composition and texture of these sandstones suggest that they have undergone high-grade diagenesis to low-grade regional burial metamorphism to the lower greenschist facies ( $250 \pm 50^\circ\text{C}$ ;  $\sim 2$  kbars). They are mineralogically and geochemically classified as lithic arenites and greywackes, and the Tanqua depocentre sandstones are slightly more mature than the Laingsburg depocentre

sandstones. REE patterns for the Tanqua and Laingsburg depocentre sandstones are similar, suggesting that both form part of the same evolutionary pattern and that the sediments have one common origin, i.e. a provenance predominantly composed of granitic material.

Homogenous  $\epsilon_{Nd}$ -values for all sandstone samples of around  $-5$  at the time of deposition indicate that there is little or no variation in provenance between the Tanqua and Laingsburg depocentre sediments.  $T_{CHUR}$  model ages of 0.70 to 0.95 Ga, and  $T_{DM}$  model ages of 1.19 to 1.49 Ga, resulted from a mixture of Archaean and Proterozoic material in unknown proportions. The most likely source terrane is thought to be the North Patagonian Massif. The latter show Nd isotopic compositions corresponding to an average  $\epsilon_{Nd}$ -value of  $-5$  at 265 Ma.

---

## Uittreksel

Voorlandkomme word oor die algemeen gevul met sediment afkomstig van die aanliggende plooi gordel, wat lei tot 'n redelik eenvoudige brongebied-tot-afsettingskom konfigurasie. Dit is egter nie van toepassing vir die vroeë suidwestelike Karookom nie, aangesien die samestelling van die Ecca Groep sedimentêre gesteentes nie ooreenstem met die samestelling van die aanliggende plooi gordel nie.

Die suidwestelike Karookom word aan die weste en suide begrens deur die Kaapse Plooi gordel en bied die geleentheid om die verwantskap tussen die vroeë strukturele evolusie en afsetting in die twee ruimtelik en temporeel afsonderlike Tankwa en Laingsburg subkomme te bestudeer. Die Kaapse Plooi gordel het gevorm toe die vroeë Palaeosoïkum kontinentale grens, wat 'n groot deel van die suidelike grens van Gondwana was, ontwikkel het tot 'n aktiewe konvergerende grens gedurende die laat Palaeosoïkum. Orogenese het gelei tot die vorming van 'n noordwes-strekkende Sederberg tak en 'n ooswes-strekkende Swartberg tak. Die oroklinale buig tussen die twee takke sluit grootskaalse noordoos-strekkende sintaksis strukture in, soos die Hex Rivier en Baviaanshoek antiklinoria, wat die sedimentasie rigtings na die kom beïnvloed het.

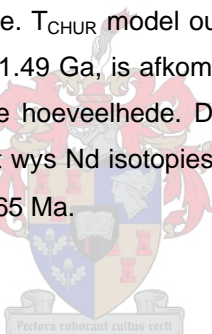
Spektrale gammastraal (SGR), mineralogiese en geochemiese studies op die dagsome van die Tankwa en Laingsburg subkomme dui 'n byna identiese brongebied aan vir beide, oorheers deur granitiese en metamorfe materiaal vanaf 'n brongebied oënskynlik vër vanaf die Kaapse Plooi gordel.

SGR data, gekombineer met litologie, dui aan dat dit moontlik is om regionale stratigrafiese korrelasies in the Skoorsteenberge, Kookfontein en Waterford Formasies in die Tankwa subkom te maak. Dieselfde geld vir die Laingsburg en Fort Brown Formasies in die Laingsburg subkom. Daar is geen groot veranderinge, wat 'n verskil in oorsprong kan aandui, in the SGR datastel tussen die opeenvolgende sandsteen of skalie eenhede nie, en ook geen

uitstaande tekens in the SGR patroon van die skalie-intervalle wat moontlik kan ooreenstem met 'n maksimum vloedingsvlak nie.

Die Tankwa en Laingsburg subkom sandsteenlae is baie fyn- tot laervlak medium-korrelrig, dig gekompakteer, swak tot goed gesorteer, en het meganiese kompaksie en drukoplossing ondergaan. Die mineralogiese samestelling en tekstuur van hierdie sandsteenlae dui daarop dat hulle hoë-gradse diagenese tot lae-gradse regionale begrawingsmetamorfose tot laervlak groenskis fasies ( $250 \pm 50^{\circ}\text{C}$ ;  $\sim 2$  kbars) ondergaan het. Hulle word mineralogies en geochemies geklassifiseer as litiese areniete en grouwakke. Die Tankwa subkom sandsteenlae is effens meer volwasse as die Laingsburg subkom sandsteenlae. Die lantanietgroep patroon vir die Tankwa en Laingsburg sandsteenlae is eenders, wat aandui dat beide deel gevorm het van dieselfde evolusionêre ontwikkeling en dat die sedimente een gesamentlike oorsprong gehad het, naamlik 'n brongebied bestaande hoofsaaklik uit granitiese materiaal.

Homogene  $\epsilon_{\text{Nd}}$ -waardes van ongeveer  $-5$  by tye van afsetting vir al die sandsteen monsters dui daarop dat daar min of geen verandering in brongebied vir die Tankwa en Laingsburg subkom sedimente was nie.  $T_{\text{CHUR}}$  model ouderdomme van 0.70 tot 0.95 Ga, en  $T_{\text{DM}}$  model ouderdomme van 1.19 tot 1.49 Ga, is afkomstig van 'n mengsel van Argeïese en Proterosoïese materiaal in onbekende hoeveelhede. Die mees waarskynlike brongebied is die Noord Patagoniese Gebergtes. Dit wys Nd isotopiese samestellings wat ooreenstem met 'n gemiddelde  $\epsilon_{\text{Nd}}$ -waarde van  $-5$  by 265 Ma.



## Acknowledgements

Firstly, I would like to give thanks to my Creator.

My sincerest thanks to De Ville Wickens (University of Stellenbosch), for the opportunity that he has given me in conducting this study, as well as his continued support throughout the past three years. I would also like to thank Stephen Flint (University of Liverpool), who was always available to help and discuss new ideas. Helpful discussions offered by Dave Hodgson and Richard Wild (University of Liverpool) is much appreciated. Thank you also to Richard Worden and Nick Kushner (University of Liverpool) for their interest and discussion on the geochemistry and burial history of the sediments from this study. Daniel Andersson (University of Stockholm) is thanked for his help and advice in the field on the uses of the portable multi-channel scintillation spectrometer (Exploranium GR320) and detector (GPX-21), its software and manipulation of the data.

Financial support for this project was received through the Universities of Stellenbosch and Liverpool and a consortium of international oil companies (ExxonMobil, ChevronTexaco, ConocoPhillips and Statoil). The Association of Commonwealth Universities made it possible for me to spend a year in Liverpool, which proved to be invaluable in the forward progress of this thesis.

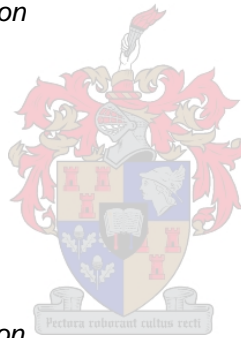
My field assistants, Danie Botha and André Gous, are thanked for their patience with the scintillation spectrometer and detector in 40°C in the middle of desert, an experience I'm sure they're not eager to repeat. Additionally I would also like to thank all colleagues, both at the Universities of Stellenbosch and Liverpool, for their kindness and academic, as well as non-academic, discussions.

I am grateful to my parents, Robbert and Helen, and family, who were always there when I needed support. Thank you very much mom, dad, Bernard, Charmaine and Renier. I would also like to thank my friends, who've helped me through some tough times, and partied through the better times. They always manage to somehow make life more interesting.

# Contents

	<b>Page:</b>
Abstract	i
Acknowledgements	iv
<b>Chapter 1: Introduction</b>	<b>1</b>
1.1 Aims of the project	1
1.2 Present models on basin setting	3
1.2.1 <i>Sedimentary basins</i>	3
1.2.2 <i>Foreland basins</i>	3
1.2.3 <i>Submarine slope systems</i>	7
1.2.4 <i>Provenance studies</i>	11
1.2.5 <i>Provenance studies comparable to the Karoo Basin</i>	14
1.3 Previous work	16
1.4 Methodology of data collection and processing	21
<b>Chapter 2: Geological Framework</b>	<b>24</b>
2.1 Tectonic evolution of southern Africa	24
2.1.1 <i>Introduction</i>	24
2.1.2 <i>Pre-Karoo setting</i>	24
2.1.3 <i>Cape Fold Belt (CFB)</i>	27
2.1.4 <i>Karoo Basin development</i>	29
2.2 Karoo Basin stratigraphy	31
2.2.1 <i>Introduction</i>	31
2.2.2 <i>Dwyka Group</i>	33
2.2.3 <i>Ecca Group</i>	34
2.2.3.1 <i>Tanqua depocentre</i>	34
2.2.3.1.1 <i>Skoorsteenbergs Formation</i>	35
2.2.3.1.2 <i>Kookfontein Formation</i>	35
2.2.3.1.3 <i>Waterford Formation</i>	36
2.2.3.2 <i>Laingsburg depocentre</i>	36
2.2.3.2.1 <i>Collingham Formation</i>	36
2.2.3.2.2 <i>Vischkuil Formation</i>	37
2.2.3.2.3 <i>Laingsburg Formation</i>	37
2.2.3.2.4 <i>Fort Brown Formation</i>	38
2.2.4 <i>Beaufort Group and overlying formations</i>	39
<b>Chapter 3: Spectral Gamma Ray Analyses</b>	<b>41</b>
3.1 Analytical techniques	41
3.2 Objectives	43

3.3	Sequence stratigraphy and shelf edge deltas	43
3.3.1	<i>The highstand systems tract (HST)</i>	44
3.3.2	<i>The falling stage systems tract (FSST)</i>	44
3.3.3	<i>The lowstand systems tract (LST)</i>	44
3.3.4	<i>The transgressive systems tract (TST)</i>	44
3.3.5	<i>Application to the study area</i>	46
3.3.5.1	<i>Introduction</i>	46
3.3.5.2	<i>Shelf edge deltas and shelf construction</i>	46
3.4	Tanqua depocentre	51
3.4.1	<i>Skoorsteenberg Formation</i>	53
3.4.2	<i>Kookfontein Formation</i>	61
3.4.3	<i>Waterford Formation</i>	77
3.4.4	<i>Discussion on gamma ray characteristics of the Tanqua depocentre</i>	83
3.5	Laingsburg depocentre	88
3.5.1	<i>Collingham Formation</i>	88
3.5.2	<i>Vischkuil Formation</i>	94
3.5.3	<i>Laingsburg Formation</i>	94
3.5.3.1	<i>Fan A</i>	96
3.5.3.2	<i>Fan B</i>	96
3.5.3.3	<i>Fan C</i>	103
3.5.3.4	<i>Fan D</i>	103
3.5.3.5	<i>Fan E</i>	106
3.5.3.6	<i>Fan F</i>	106
3.5.4	<i>Fort Brown Formation</i>	109
3.5.5	<i>Discussion on gamma ray characteristics of the Laingsburg depocentre</i>	112
3.6	Discussion on general gamma ray characteristics and their significance in both the Tanqua and Laingsburg depocentres	115
3.7	Conclusions (answer to initial objectives)	118
<b>Chapter 4: Petrography</b>		<b>121</b>
4.1	Analytical techniques	121
4.2	Objectives	122
4.3	Tanqua depocentre	122
4.3.1	<i>Skoorsteenberg Formation (Unit 5)</i>	122
4.3.1.1	<i>Interchannel/overbank deposits</i>	128
4.3.1.2	<i>Slope channel-fill complex deposits</i>	128
4.3.2	<i>Kookfontein Formation</i>	136
4.3.2.1	<i>Lower slope, low-density turbidite deposits</i>	136
4.3.2.2	<i>Sandstone with soft-sediment deformational features</i>	136



4.3.2.3	<i>Mid-slope to shelf edge delta deposits</i>	136
4.3.2.4	<i>Channel-fill deposits</i>	142
4.3.2.5	<i>Upper slope to pro-delta deposits</i>	142
4.3.2.6	<i>Pro-delta to delta front deposits</i>	142
4.3.3	<i>Waterford Formation</i>	143
4.3.3.1	<i>Pro-delta and delta front deposits</i>	143
4.3.3.2	<i>Channel-fill deposits</i>	143
4.4	<i>Laingsburg depocentre</i>	146
4.4.1	<i>Collingham Formation</i>	146
4.4.1.1	<i>Basin-floor, very fine-grained turbidites</i>	146
4.4.1.2	<i>Matjiesfontein Chert Bed</i>	153
4.4.2	<i>Vischkuil Formation</i>	153
4.4.2.1	<i>Basin-floor, muddy turbidites</i>	153
4.4.2.2	<i>Sandstone with soft-sediment deformational features</i>	153
4.4.3	<i>Laingsburg Formation</i>	159
4.4.3.1	<i>Fan A</i>	159
4.4.3.1.1	<i>Basin-floor turbidite deposits</i>	159
4.4.3.2	<i>Fan B</i>	166
4.4.3.2.1	<i>Base of slope turbidite deposits</i>	166
4.4.3.3	<i>Fan C</i>	167
4.4.3.3.1	<i>Slope facies deposits</i>	167
4.4.3.4	<i>Fan D</i>	167
4.4.3.4.1	<i>Slope facies deposits</i>	167
4.4.3.5	<i>Fan E</i>	168
4.4.3.5.1	<i>Slope facies deposits</i>	168
4.4.3.6	<i>Fan F</i>	168
4.4.3.6.1	<i>Slope facies deposits</i>	168
4.4.4	<i>Fort Brown Formation</i>	169
4.4.4.1	<i>Pro-delta deposits</i>	169
4.4.4.2	<i>Sandstone with soft-sediment deformational features</i>	172
4.4.4.3	<i>Distal delta front deposits</i>	172
4.5	<i>Discussion</i>	173
4.5.1	<i>Detrital and authigenic mineralogy</i>	173
4.5.2	<i>Burial history</i>	176
4.5.2.1	<i>Pressure/temperature processes</i>	176
4.5.2.2	<i>Sensitivity models</i>	182
4.5.3	<i>Petrographic differences between depositional facies</i>	187
4.5.4	<i>Petrographic differences between the Tanqua and Laingsburg depocentre sandstones</i>	187
4.5.5	<i>Synthesis of the textural and detrital mineralogy data</i>	188
4.6	<i>Gondwana palaeogeography and possible source area(s)</i>	189

4.7	Conclusions (answers to initial objectives)	199
<b>Chapter 5: Geochemistry</b>		<b>200</b>
5.1	Analytical techniques	200
5.1.1	<i>X-ray Fluorescence (XRF) Spectrometry</i>	200
5.1.2	<i>Inductively Coupled Plasma Emission Mass Spectrometry (ICP-MS)</i>	201
5.2	Objectives	202
5.3	Major element chemistry	202
5.3.1	<i>Tanqua depocentre</i>	202
5.3.1.1	<i>Skoorsteenbergr Formation</i>	202
5.3.1.2	<i>Kookfontein Formation</i>	205
5.3.1.3	<i>Discussion on trends in the Tanqua depocentre rocks</i>	211
5.3.2	<i>Laingsburg depocentre</i>	213
5.3.2.1	<i>Laingsburg Formation</i>	213
5.3.2.2	<i>Fort Brown Formation</i>	217
5.3.2.3	<i>Discussion on trends in the Laingsburg depocentre rocks</i>	217
5.3.2.4	<i>Discussion on the major element chemistry of the Tanqua and Laingsburg depocentres</i>	218
5.4	Trace and rare earth element chemistry	221
5.4.1	<i>Tanqua depocentre</i>	221
5.4.1.1	<i>Skoorsteenbergr Formation</i>	221
5.4.1.2	<i>Kookfontein Formation</i>	223
5.4.1.3	<i>Discussion on trends in the Tanqua depocentre rocks</i>	226
5.4.2	<i>Laingsburg depocentre</i>	226
5.4.2.1	<i>Laingsburg Formation</i>	226
5.4.2.2	<i>Fort Brown Formation</i>	228
5.4.2.3	<i>Discussion on trends in the Laingsburg depocentre rocks</i>	229
5.4.2.4	<i>Discussion on trace and rare earth element chemistry of the Tanqua and Laingsburg depocentres</i>	229
5.5	Tectonic discrimination	230
5.5.1	<i>Tanqua depocentre</i>	231
5.5.2	<i>Laingsburg depocentre</i>	231
5.5.3	<i>Discussion on the tectonic setting of Tanqua and Laingsburg depocentre source rocks</i>	237
5.6	Source terrane identification	240
5.7	Geological overview of central South America	249
5.7.1	<i>Introduction</i>	249
5.7.2	<i>Sierras Pampeanas (SP)</i>	250
5.7.3	<i>North Patagonian Massif (NPM)</i>	252
5.8	Conclusions (answers to initial objectives)	253

<b>Chapter 6: Sm-Nd Isotope Chemistry</b>	<b>255</b>
6.1 Analytical techniques	255
6.1.1 <i>Isotope dilution analyses</i>	256
6.2 Objectives	257
6.3 Examples of Sm-Nd isotope studies of sedimentary rock from the literature	257
6.4 Tanqua and Laingsburg depocentres	260
6.5 Provenance	268
6.6 Discussion	269
6.7 Conclusions (answers to initial objectives)	272
<b>Chapter 7: Conclusions</b>	<b>276</b>
7.1 Spectral gamma ray (SGR)	276
7.2 Mineralogy	277
7.3 General geochemical characteristics of the southwestern Karoo Basin	278
7.4 Sm-Nd isotope chemistry constraints	279
7.5 Provenance and tectonic setting	279
7.6 Suggestions for future work	280
<b>References</b>	<b>281</b>
<b>Appendix A: Table for modal compositions of Tanqua and Laingsburg depocentre rocks</b>	<b>306</b>
<b>Appendix B: Sample microphotographs</b>	<b>310</b>
<b>Appendix C: Table for major, trace and rare earth elements for the Tanqua and Laingsburg depocentre rocks</b>	<b>322</b>
<b>Appendix D: Table for average major, trace and rare earth element compositions of sandstones and siltstones from the Tanqua and Laingsburg depocentres</b>	<b>333</b>

**Enclosures:**

Enlargements of Figures 3.27 and 3.44 are contained on the inside back cover of the thesis.

# Chapter One

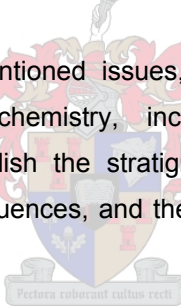
## 1 Introduction

### 1.1 Aims of the project

Foreland basins commonly fill with sediments derived from the adjacent fold/thrust belt, with the mineralogical and textural compositions of the sediments 'fingerprinting' this adjacent fold/thrust belt, and providing a relatively simple source-to-basin configuration. The early Permian Karoo foreland basin of South Africa is bounded to the west and south by the Cape Fold Belt (CFB) and provides an opportunity to study the linkages between early foldbelt development and deep-water turbidite sandstone deposition (Figure 1.1).

This study is devoted to the chemostratigraphic, petrographic and geochemical characterisation of the Permian Ecca Group strata in the Tanqua and Laingsburg depocentres, their stratigraphic evolution and regional stratal relationships, and the construction of a model for the evolution of the provenance and depositional environments.

In order to resolve the aforementioned issues, detailed field and laboratory studies (petrography, mineral and rock chemistry, including trace element and isotopic measurements) were used to establish the stratigraphy of the Tanqua and Laingsburg depocentres, in terms of orogenic influences, and the resultant diagenetic and metamorphic grade signatures.



The following relevant questions arising from previous studies on outcrop material will be addressed in this study:

- Can spectral gamma ray (SGR) data be used as a correlation tool in establishing a high-resolution stratigraphic framework throughout the Tanqua and Laingsburg depocentres?
- Do changes in major, trace and rare earth element chemistry relate to the chemical index of alteration (CIA), palaeocurrent direction, and stratigraphic position, within and between these depocentres?
- Are there any differences in geochemical and petrographic classification for the Tanqua and Laingsburg strata and what do they indicate?
- Are the provenance signatures and tectonic settings within the individual depocentres reflecting similar stratigraphic and geographic positions?
- What was the most probable provenance for the deep-water and deltaic deposits of the southwestern Karoo Basin during the late Palaeozoic?
- Does the Karoo Basin reflect a true foreland basin setting?



## **1.2 Present models on basin setting**

### **1.2.1 Sedimentary basins**

Horizontal movements of lithospheric plates induce vertical movements due to changes in crustal thickness, thermal character and isostatic adjustment (Dickinson, 1974). These vertical movements cause uplift of sediment source areas, reorganisation of dispersal paths and the formation of sedimentary basins. The type of substratum (continental, oceanic, transitional and anomalous crust), the proximity to plate boundary(s) and the type of nearest plate boundary(s) (divergent, convergent and transform) control basin evolution (Ingersoll and Busby, 1995). A list of basin types in convergent settings is given in Table 1.1. The preservation potential of tectonostratigraphic assemblages is an important factor in basin analysis and palaeotectonic reconstruction (Ingersoll and Busby, 1995).

### **1.2.2 Foreland basins**

A foreland basin is defined as an elongate trough that forms between a linear contractional orogenic belt and the stable craton, mainly in response to flexural subsidence that is driven by thrust-sheet loading in the orogen, with sediment derived principally from the adjacent thrust belt and minor sediment contributions from the cratonward side of the basin, providing a relatively simple source-to-basin configuration (Figure 1.2) (Dickinson and Suczek, 1979). Foreland basin sediment fill is wedge-shaped in transverse cross-section, with the thickest part located directly adjacent to the associated thrust belt (Jordan, 1995), and a forebulge may separate the main part of the foreland basin from the craton (Crampton and Allen, 1995). DeCelles and Giles (1996) define foreland basin systems as: (i) elongate regions of potential sediment accommodation that form on continental crust between contractional orogenic belts and cratons in response to geodynamic processes related to the orogenic belt and its associated subduction system, (ii) consist of four discrete depozones, referred to as wedge-top, foredeep, forebulge and backbulge depozones, and (iii) have longitudinal dimensions roughly equal to the lengths of the adjacent fold/thrust belts (Figure 1.2). Foreland basins can be subdivided into peripheral (collisional) foreland basins, and retro-arc foreland basins (form along the continental-interior flanks of continental-margin orogenic belts) (Figure 1.3) (Dickinson, 1974; Jordan, 1995).

Retro-arc foreland basins are large-scale (100s of kilometres wide and 1000s of kilometres long, with many kilometres of lateral strata), long-lived (10 to 100 million years in duration) features, with the majority of foreland basin development being related to thin-skinned thrust belts, where sedimentary cover rocks are shortened by folding and thrusting above undeformed basement (Jordan, 1995).

Table 1.1 Basin classification (after Ingersoll and Busby, 1995 and references therein).

Convergent settings

Trenches:	deep throughs formed by subduction of oceanic lithosphere
Trench-slope basins:	local structural depressions developed on subduction complexes
Fore-arc basins:	basins within arc-trench gaps
Intra-arc basins:	basins along arc platform, which includes superposed and overlapping volcanoes
Retro-arc basins:	oceanic basins behind intraoceanic magmatic arcs (including inter-arc basins between active and remnant arcs), and continental basins behind continental margin magmatic arcs without foreland fold/thrust belts
<b>Retro-arc foreland basins:</b>	<b>foreland basins on continental sides of continental-margin arc-trench systems (formed by subduction-generated compression and/or collision)</b>
Remnant ocean basins:	shrinking ocean basins caught between colliding continental margins and/or arc-trench systems, and ultimately subducted or deformed within suture belts
Peripheral foreland basins:	foreland basins above rifted continental margins that have been pulled into subduction zones during crustal collision (primary type of collision-related forelands)
Piggyback basins:	basins formed and carried atop moving thrust sheets
Foreland intermontane basins (broken forelands):	basins formed among basement-cored uplifts in foreland settings

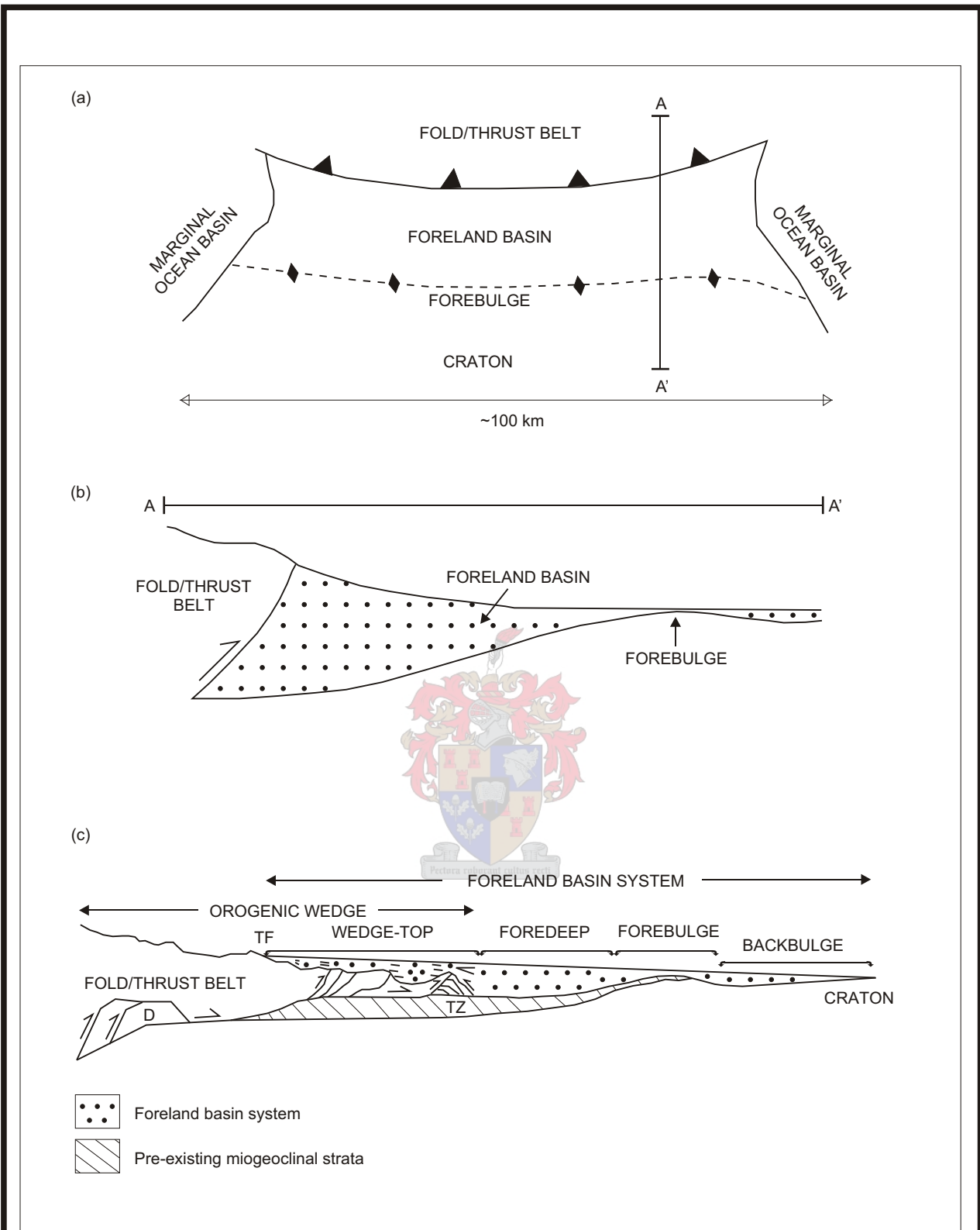


Figure 1.2 (a) Schematic view of a 'typical' foreland basin, bounded longitudinally by a pair of marginal ocean basins. (b) The generally accepted notion of foreland basin geometry in transverse cross-section. Note the unrealistic geometry of the boundary between the basin and the thrust belt. Vertical exaggeration is of the order of 10 times. (c) Schematic cross-section depicting a revised concept of a foreland basin system, with the wedge-top, foredeep, forebulge and backbulge depozones shown at approximately true scale. Topographic front of the thrust belt is labeled TF. A schematic duplex (D) is depicted in the hinterland part of the orogenic wedge, and a frontal triangle zone (TZ) and progressive deformation in the wedge-top depozone are also shown (DeCelles and Giles, 1996).

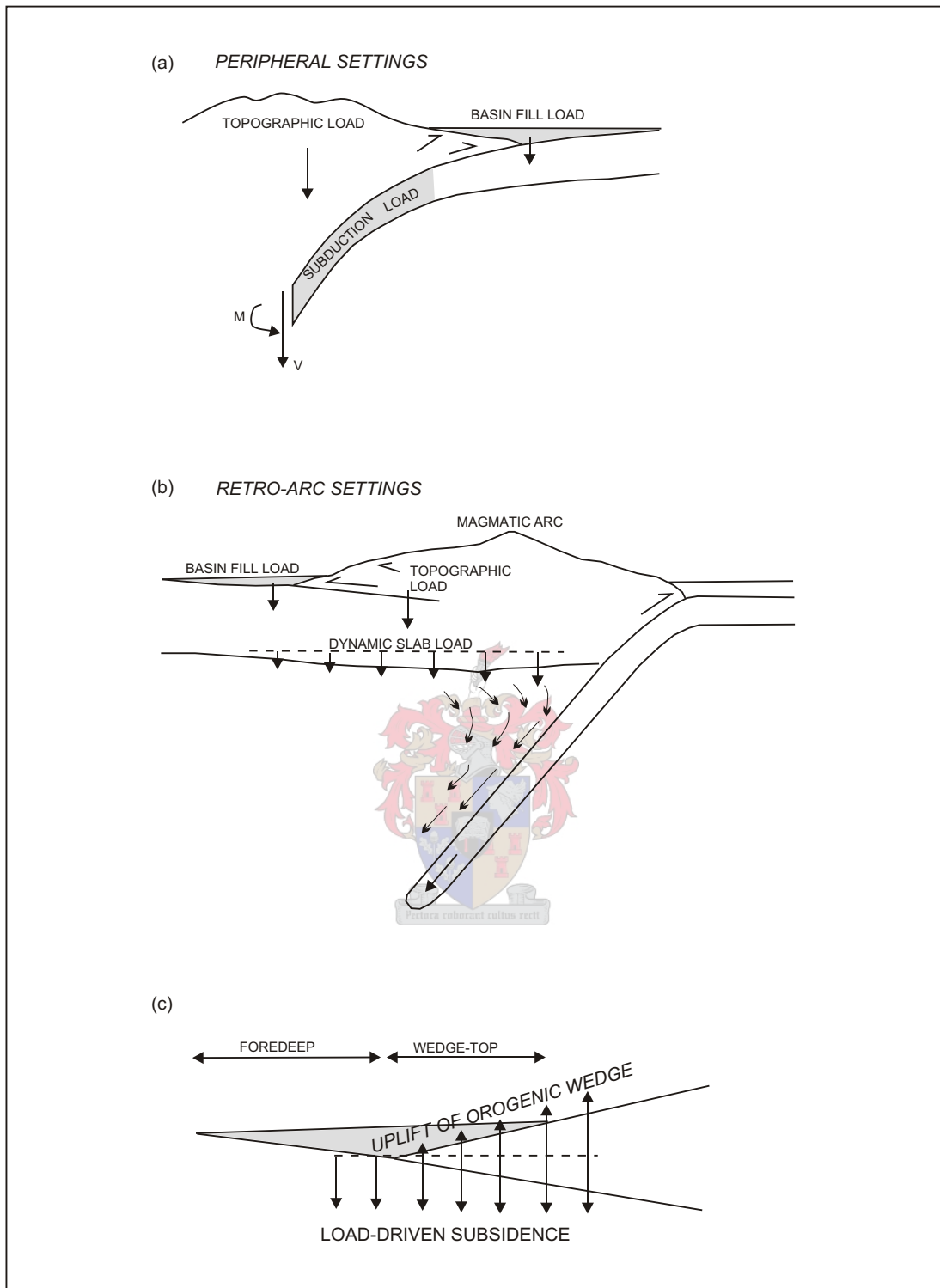


Figure 1.3 (a) Schematic diagram showing the principle loads in peripheral foreland basin systems. In addition to the topographical and sediment loads, a subduction load, due to a vertical shear force ( $V$ ) and bending moment ( $M$ ) on the end of the subducted slab, may exist at depths of 50 - 200 km. (b) Retro-arc foreland basin systems involve topographic and sediment loads as well as dynamic slab load caused by viscous coupling between the subducting slab, overlying mantle-wedge material and the base of the overlying continental plate. (c) Accumulation in the wedge-top depozone takes place under competing influences of regional, load-driven subsidence (downward pointing arrows), and local uplift of the orogenic wedge in response to shortening and thickening (upward pointing arrows) (DeCelles and Giles, 1996).

The Karoo Basin is widely accepted as a retro-arc foreland system that formed in front of the CFB in response to crustal shortening brought about by the subduction of the palaeo-Pacific plate beneath the Gondwana plate (Lock, 1980; De Wit *et al.*, 1988; Johnson, 1991; De Wit and Ransome, 1992). However, the Karoo Basin does not fit a simple foreland basin model. Reciprocal stratigraphic modelling of non-marine type foreland basins are predicted to be dominated by coarsening-upward sequences (Turner, 1999), and not the fining-upward sequences that dominate the stratigraphy of the non-marine upper Karoo succession (Triassic-Jurassic).

The prediction of tectonic subsidence curves due to dynamic topography over subducting slabs is possible through the modelling of mantle dynamics (Figure 1.4). However, subsidence due to other processes such as lithospheric extension and flexural loading by orogenic wedges that is likely to be superimposed on the dynamic topographic signature, complicates this process (Burgess and Moresi, 1999). Subsidence due to dynamic topography in retro-arc basins should be distinguishable from this superimposition by the fact that extensional tectonics is based simply on the temporal subsidence evolution expressed in the subsidence curve shapes. In a foreland basin setting dynamic topography causes subsidence over significantly greater wavelengths than in forward models of flexural loading, even though temporal subsidence patterns are similar (Burgess and Moresi, 1999).

Flexural and surface profiles for the evolution of the Karoo Basin foreland system during stages of orogenic loading and unloading suggest that both flexural tectonics and dynamic loading have contributed to the total amount of subsidence (Catuneanu *et al.*, 1998). The composition of the turbidite sediments in the Tanqua and Laingsburg depocentres also does not match the composition of the adjacent CFB.

### **1.2.3 Submarine slope systems**

The submarine slope connects basin-floor fans to shelf feeder systems/bypass zones (Figure 1.5). It consists of a range of erosional, bypass and depositional sites that evolve temporally and spatially. Until the mid 1990's, many geoscientists working on ancient basin margin systems regarded the slope as a simple zone of sand bypass to the basin floor (Figure 1.6). Over the last 10 years, the understanding of slope systems has been revolutionised by the acquisition and interpretation of high-resolution 3D seismic datasets from areas such as the Gulf of Mexico, offshore Angola and Nigeria. These allowed the mapping of slope channel systems, slope mini-basins and their fills. The studies of slope profile and its changing character in space and time, and the development of facies and stratigraphic models for slope channel systems, have led to predictive stratigraphic models for slope systems (Figure 1.7) that bear little resemblance to the simple bypass model. Many of these advances are discussed by Mayall and Stewart (2000) and Prather (2000, 2003).

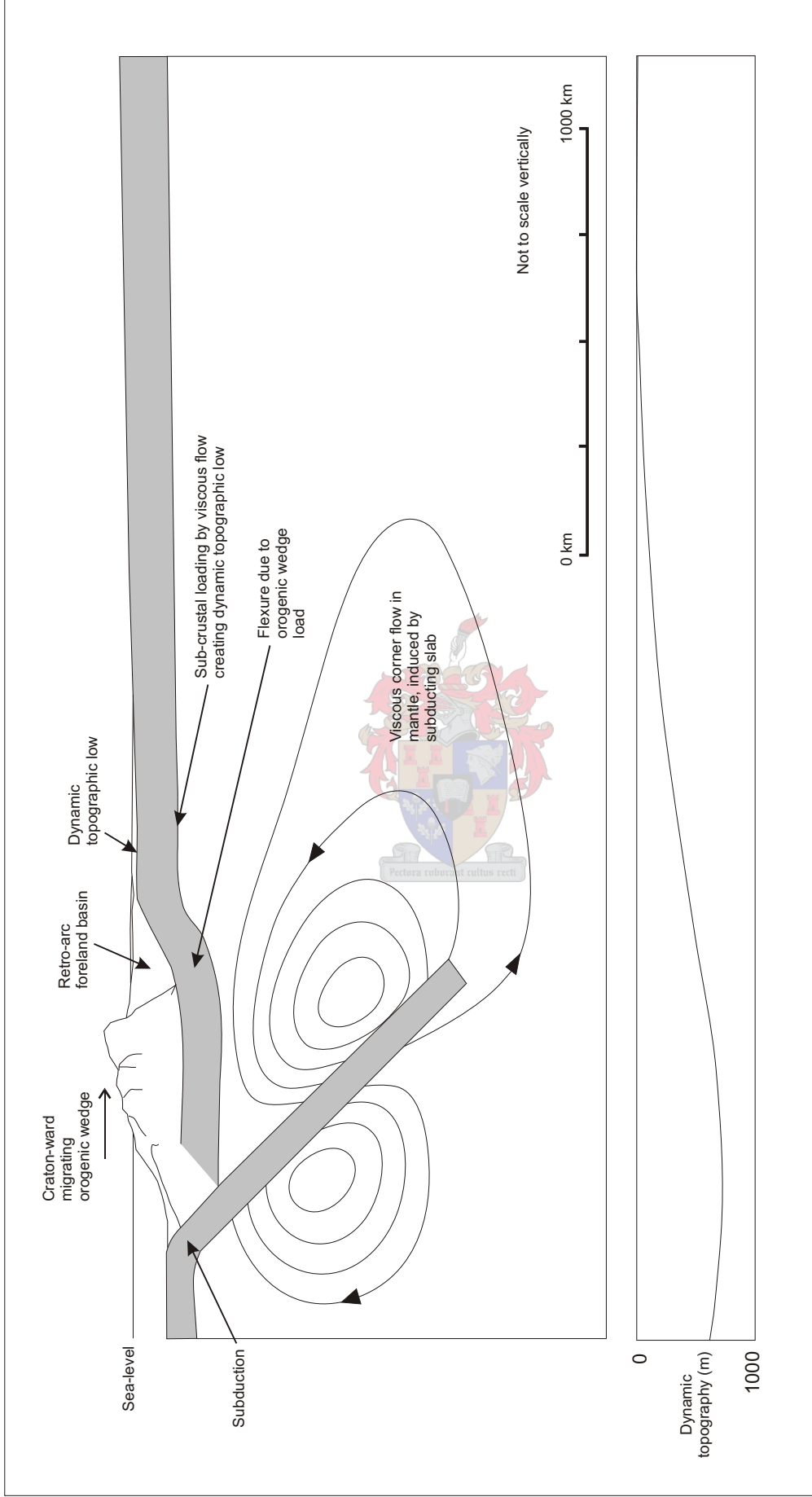


Figure 1.4 Dynamic topography forms above subducting slabs due to stresses generated on the base of the lithosphere by the slab's negative mass anomaly in the mantle. These stresses are transferred to the base of the lithosphere by viscous mantle flow. Retro-arc foreland basins are also commonly present on convergent margins so that dynamic topography and flexural loading may be superimposed (from Burgess and Moresi, 1999).

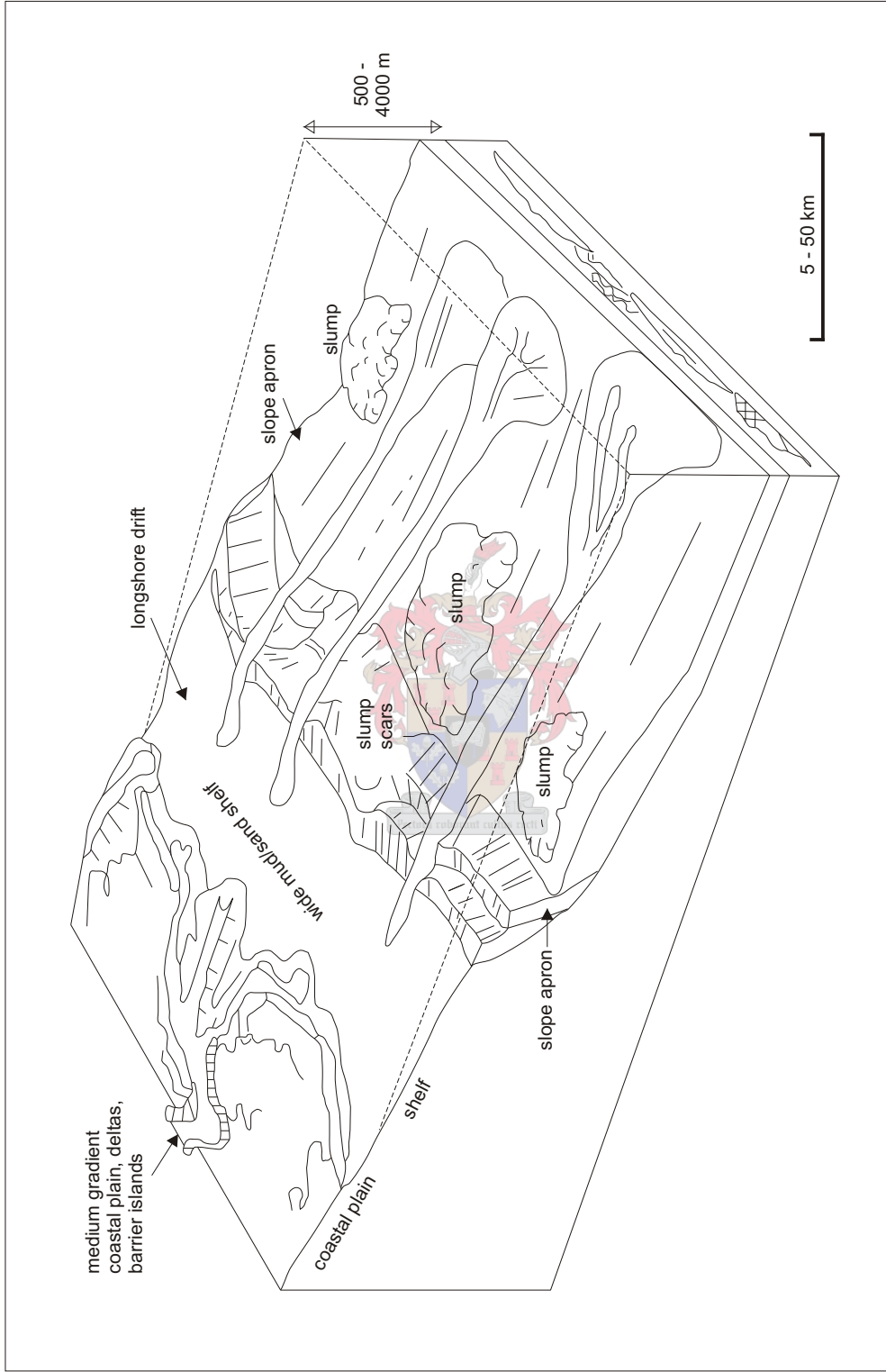


Figure 1.5 Depositional model for mud/sand-rich slope apron (from Reading and Richards, 1994).

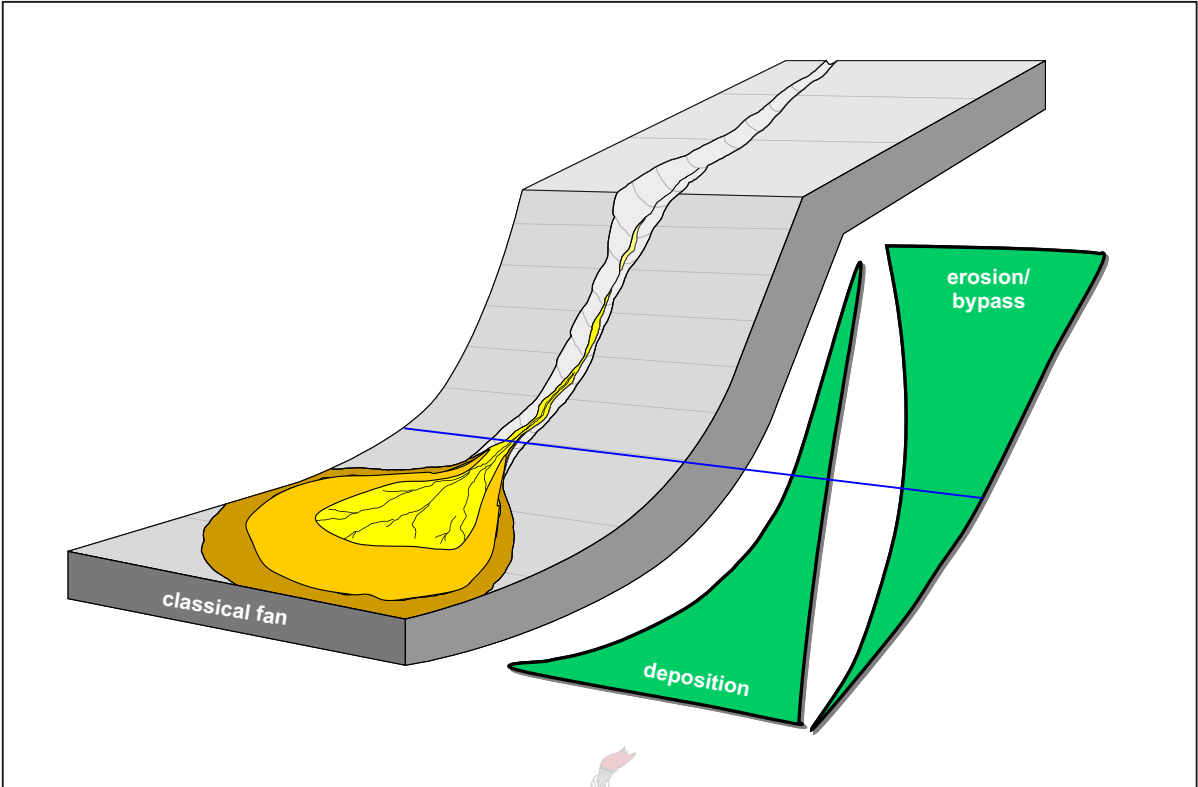


Figure 1.6 Classical model for a slope to basin profile. The slope is dominated by bypass, with almost all sand being supplied to the basin floor (after Sprague *et al.*, 2003).

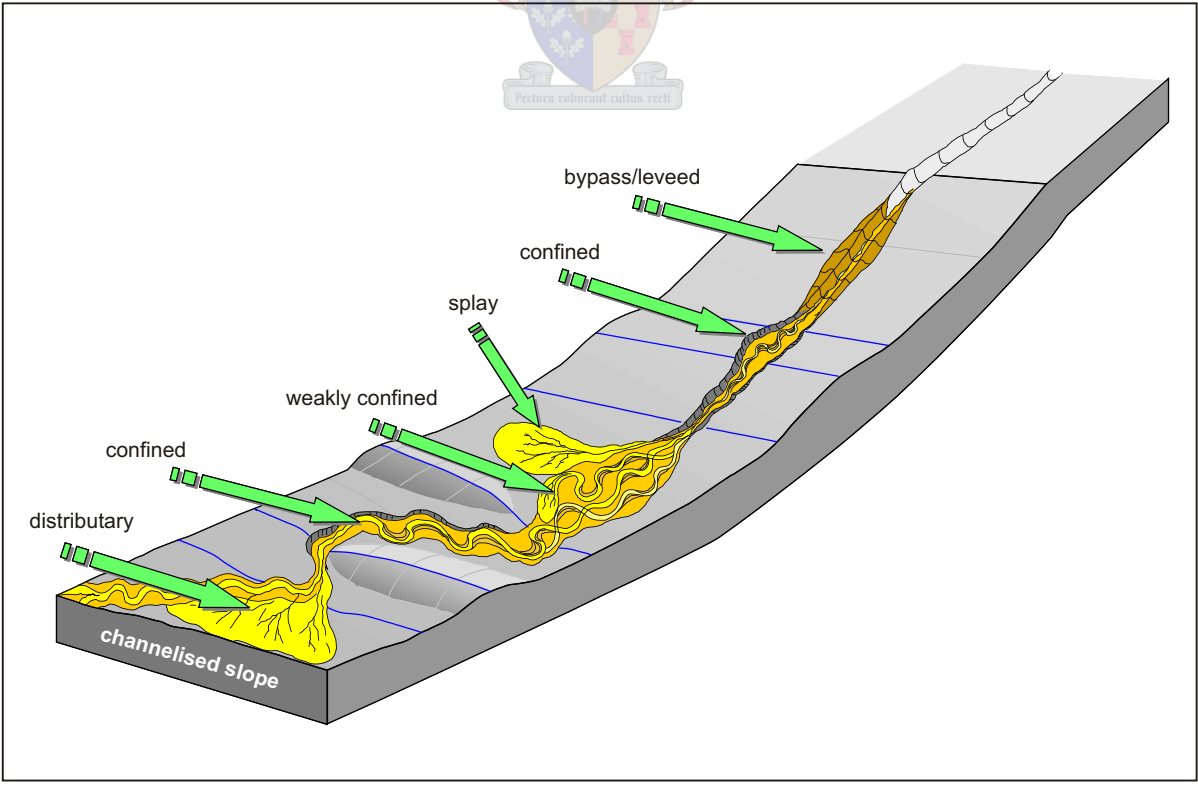


Figure 1.7 Stratigraphic and facies model for a channelised slope, taking into account recent advances in the understanding of slope systems (after Sprague *et al.*, 2003).

Slope topography is an essential element influencing the distribution, quality, and architecture of submarine fan reservoirs (Prather, 2003). Accommodation, the space available for deposition, on a submarine slope is controlled by the topography of the depositional surface and its graded or steady state profile. Prather (2003) identified several types of accommodation that exist across most continental slopes: (i) ponded; (ii) healed-slope in upper slope, mid-slope, lower slope, base of slope, and basin floor positions; (iii) slope; and (iv) incised submarine valley (Figures 1.8 and 1.9).

#### **1.2.4 Provenance studies**

The composition of terrigenous sedimentary rocks is a function of the interplay of variables such as provenance, weathering, transportation and diagenesis (Bhatia, 1983). Framework modes of terrigenous sandstones reflect derivation from various types of provenance terranes and are related to the tectonic setting of sedimentary basins (Dickinson *et al.*, 1983). However, the plate tectonic setting of the provenance exerts primary control on sandstone composition (Dickinson, 1985). The main classes of provenance originally identified are stable cratons, basement uplifts, magmatic arcs, and recycled orogens (Dickinson and Suczek, 1979).

Relative proportions of different types of terrigenous sand grains are guides to the nature of the source rocks in the provenance terrane from which sandy detritus was derived. Compositional variations between these terrigenous sandstones can be displayed as ternary plots on triangular diagrams (Dickinson, 1985), where the three poles represent recalculated proportions of key categories of the grain types determined by modal point counts. These key categories are quartz (Q or Qm), feldspar (F) and lithic fragments (L or Lt) (Figure 1.10). The three main categories of provenance terranes as defined by Dickinson *et al.* (1983) are: (i) continental blocks – sources are either stable shields and platforms or in uplifts marking plate boundaries and trends of intraplate deformation that transects the continental blocks; (ii) active magmatic arcs – sediment sources are mainly in the volcanic sheet capping the igneous belt and in granitic plutons of the arc roots; and (iii) recycled orogens – sediment sources are dominantly sedimentary strata and subordinate volcanic rocks, in part metamorphosed, exposed to erosion by the orogenic uplift of fold belts and thrust sheets. However, the relationship between tectonic setting and sandstone composition, mainly based on framework modes, may not always reflect the true crustal setting, since the nature of grains could be obliterated or destroyed by post-depositional changes, such as diagenesis and metamorphism (Bhatia, 1983).

Geochemical characteristics in the compositions of sandstone suites can be used to identify signatures of source rocks and tectonic settings, as well as infer the redistribution of elements during and after deposition. Four types of plate tectonic classifications of continental

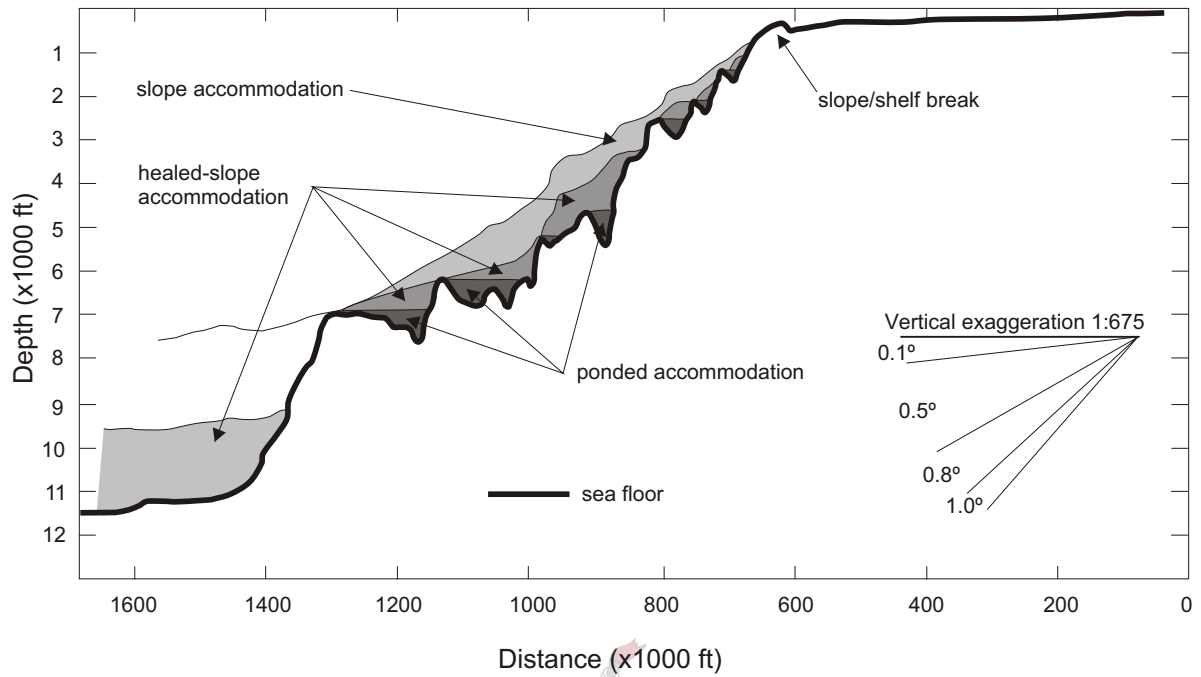


Figure 1.8 A sea floor profile shows the distribution of accommodation on an end-member above-grade slope profile with ponded basins (from Prather, 2003).

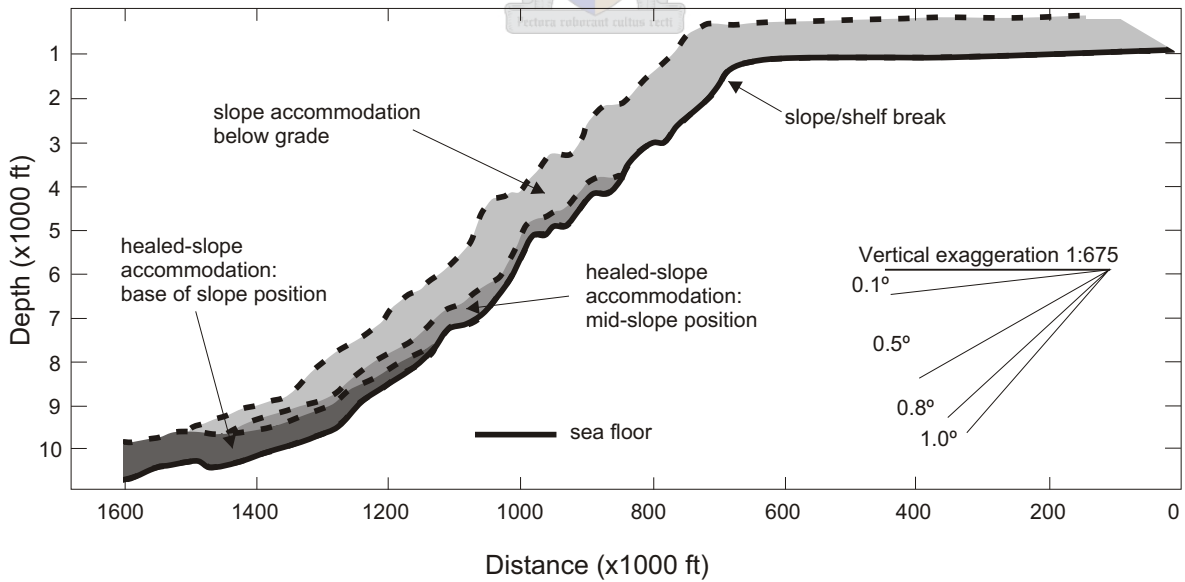


Figure 1.9 A sea floor profile shows the distribution of accommodation on a graded slope profile (from Prather, 2003).

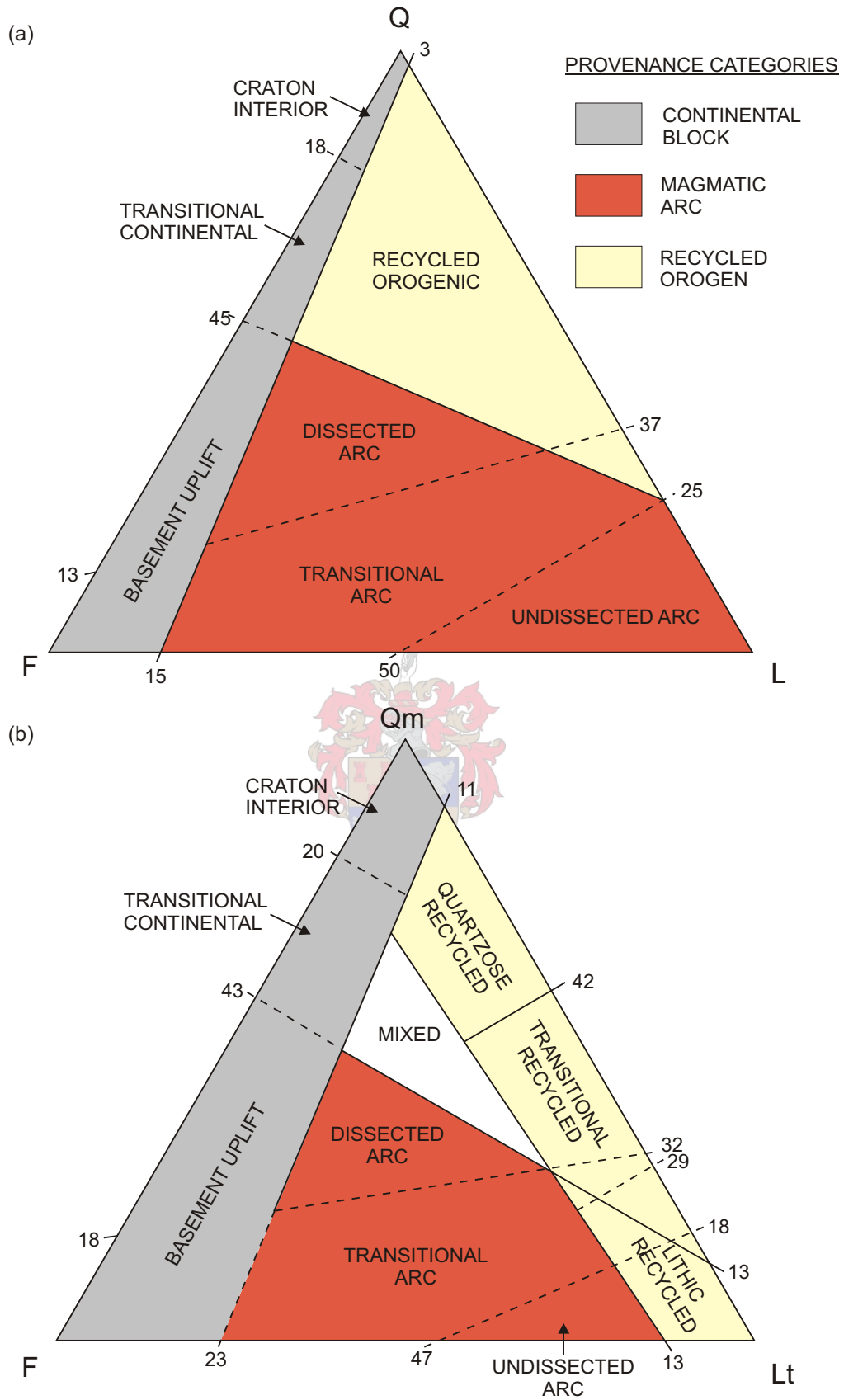


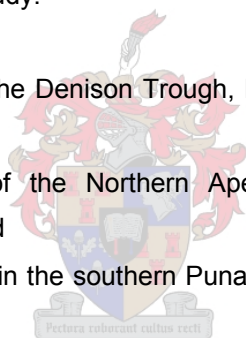
Figure 1.10 (a) QFL and (b) QmFLt plots for framework modes of terrigenous sandstones showing provisional subdivisions according to inferred provenance type. Numbered ticks on legs of triangles denote positions of empirical provenance division lines in percentage units measured from nearest apical pole (from Dickinson *et al.*, 1983).

margins and oceanic basins based on the nature of the crust have been recognised by Bhatia (1983) and Bhatia and Crook (1986). These are: (i) oceanic island-arc – sedimentary basins adjacent to oceanic island-arcs or island-arcs partly formed on thin continental crust (sediment derived from calc-alkaline or tholeiitic arcs); (ii) continental island-arc – sedimentary basins adjacent to island-arcs formed on a well-developed continental crust or on thin continental margins (sediments derived from felsic volcanic rocks); (iii) passive margins – comprise rifted continental margins of the Atlantic-type developed along the edges of the continents, remnant ocean basins adjacent to collision orogens, and inactive or extinct convergent margins (sediment derived by the recycling of older sedimentary and metamorphic rocks of platforms or recycled orogens); and (iv) active continental margins - sedimentary basins of the Andean-type thick continental margins and strike-slip types (sediments derived from granite-gneisses and siliceous volcanics of the uplifted basement).

### **1.2.5 Provenance studies comparable to the Karoo Basin**

Three examples from the literature have been chosen to illustrate the effectiveness of the above approaches in the present study:

- Permian sandstones from the Denison Trough, Bowen Basin (time equivalent to the Karoo Basin);
- Oligo-Miocene turbidites of the Northern Apennines foreland basin (sediments compositionally similar); and
- Ordovician clastic deposits in the southern Puna Basin, NW Argentina (sourced from South America).



*(i) Permian sandstones from the Denison Trough, Bowen Basin (Ahmad et al., 1994).*

The retro-arc foreland Bowen Basin of east central Queensland developed during Permo-Triassic time coeval with the final stages of the Tasman Orogenic Phase. The Denison Through is an elongate N-S trending downwarp, one of the two principal depocentres in the southern Bowen Basin and accumulated more than 3500 m of Permian sediments, largely sandstones. The Peawaddy Formation, attaining a thickness of 210 m, consists of medium-grained, moderately to well sorted sandstones, alternately bedded with either siltstone or mudstone, with several tuff beds near the base of the succession.

Quartz (mostly monocrystalline), feldspar, chert, and volcanic rock fragments constitute the significant detrital grains. The feldspar grains are considerably altered due to dissolution and partial replacement by calcite and/or ankerite/siderite and the matrix is largely replaced by carbonates, such as calcite, high-Mg calcite, ankerite and siderite.

The Peawaddy Formation sediments were deposited during the renewal of compressional tectonics and arc volcanic activity in the region, resulting in a great supply of recycled sediment and volcanic detritus to the Denison Trough from the east. This was accompanied by folding and uplift of sedimentary strata that created a largely fluvial depositional environment in the trough.

*(ii) Oligo-Miocene turbidites of the Northern Apennines foreland basin (Valloni et al., 1991).*

The 700 to 1400 m turbiditic sandstone succession of the Cervarola Formation was deposited during Lower to Middle Miocene times in one of the foreland basins of the Northern Apennines. The deposits have experienced mainly physical compaction processes, the effects of which are controlled by the abundance of grains susceptible to deformation. Palaeocurrents and petrography indicate that the Cervarola Basin was fed from the northwest and that the clastic supply probably travelled along the front of the collided plates and entered the basin from the northern apex.

The Cervarola sandstones are lithofeldspathic with an essentially metamorphic lithic assemblage, quartzite grains averaging 50% and fine-grained lithic grains ranging from 5 to 25%. The essential framework grains account for 70 – 80% of the bulk composition, while micas and altered or deformed framework grains vary from 5 to 15%.

The unstable components of the turbidite sandstones show a sequence of mineralogical-textural transformations, making it possible to determine the diagenetic stage using parameters (such as the secondary matrix) that can be measured on thin-sections. Provenance information in several sandstone components (dissolution of heavy minerals; plagioclase and unstable grain replacement by albite, muscovite and chlorite; diagenetic calcite; and the formation of pseudomatrix) can thus be lost due to the selective alteration of framework grains.

*(iii) Ordovician clastic deposits in the southern Puna Basin, NW Argentina (Zimmermann and Bahlburg, 2003).*

The Lower Ordovician clastic sedimentary formations in the southern Puna include synsedimentary lava flows and are tectonically associated with mafic to ultramafic rocks. Very coarse-grained debris-flow deposits and fine- to coarse-grained greywackes and siltstones representing turbidites, with rhyolitic and andesitic lavas forming occasional intercalations, dominate the Diablo Formation, in the central part of the Sierra de Calalaste. Analyses of illite and chlorite indicated that the sedimentary succession of the Diablo Formation underwent very low-grade metamorphism. Flute marks indicate a uniform axial sediment transport from

the S and SSW to the N and NNE, and the sedimentary succession is isoclinally folded with folds commonly verging westwards.

The sedimentological features, the petrological, geochemical and isotope geochemical similarities of coeval sedimentary and volcanic rocks in the Diablo Formation indicate that this formation formed as a marine volcanic apron close to an eruption centre. Also transported into the depositional area are minor amounts of older crustal material. The preservation of the compositionally immature detrital material in the same strata is indicative of minor weathering and sorting influence on the detritus on its way from source-to-basin. This implies relatively short transport paths and potentially marked relief and minor intermediate storage of sediment. As there is no evidence of exotic sources, the deposits reflect the composition of adjacent continental regions represented by the Sierras Pampeanas (SP) basement, i.e. the Pampeanas Terrane including the Puncoviscana Fold Belt.

The reconstructions of the palaeogeographies outlined above were facilitated by the recognition of temporal, spatial and compositional grain signatures, in combination with geochemical analyses. Successful results in provenance studies based on framework modes alone do, however, depend to a large extent on the degree to which diagenetic processes have obscured the original features of palaeo- and neovolcanic grains (Zuffa, 1991).

### 1.3 Previous work

The Karoo Basin, generally interpreted as a foreland basin, developed during the late Palaeozoic on the Archean Kaapvaal Craton in the north and the Mesozoic Namaqua-Natal Belt in the east, west and south (Cole, 1992). It formed inbound of the CFB, which wraps around the southwestern margin of South Africa (Figure 1.1). The evolving structures of the CFB are believed to have caused the development of, and also influenced, the sediment pathways in this part of the Karoo Basin to the Tanqua and Laingsburg depocentres. The Permian Ecca Group in the southwestern Karoo Basin comprises an approximately 1300 m thick, seemingly conformable succession of siliciclastic sediments, occupying a stratigraphic position between the glacial deposits of the Dwyka Group and the fluvial deposits of the Beaufort Group (Wickens, 1994). The Tanqua and Laingsburg depocentres each contain a separate sequence of Ecca Group stratigraphic units above the Collingham Formation (Figure 1.11).

The Tanqua depocentre is located in the low-lying regions of the Tanqua and Ceres Karoo, between the Cedarberg Mountains in the west, the Roggeveld escarpment to the east and the Klein Roggeveld Mountains to the southeast (Figure 1.12). The Laingsburg depocentre, elongated from Matjiesfontein in the west to east of Klaarstroom, borders the

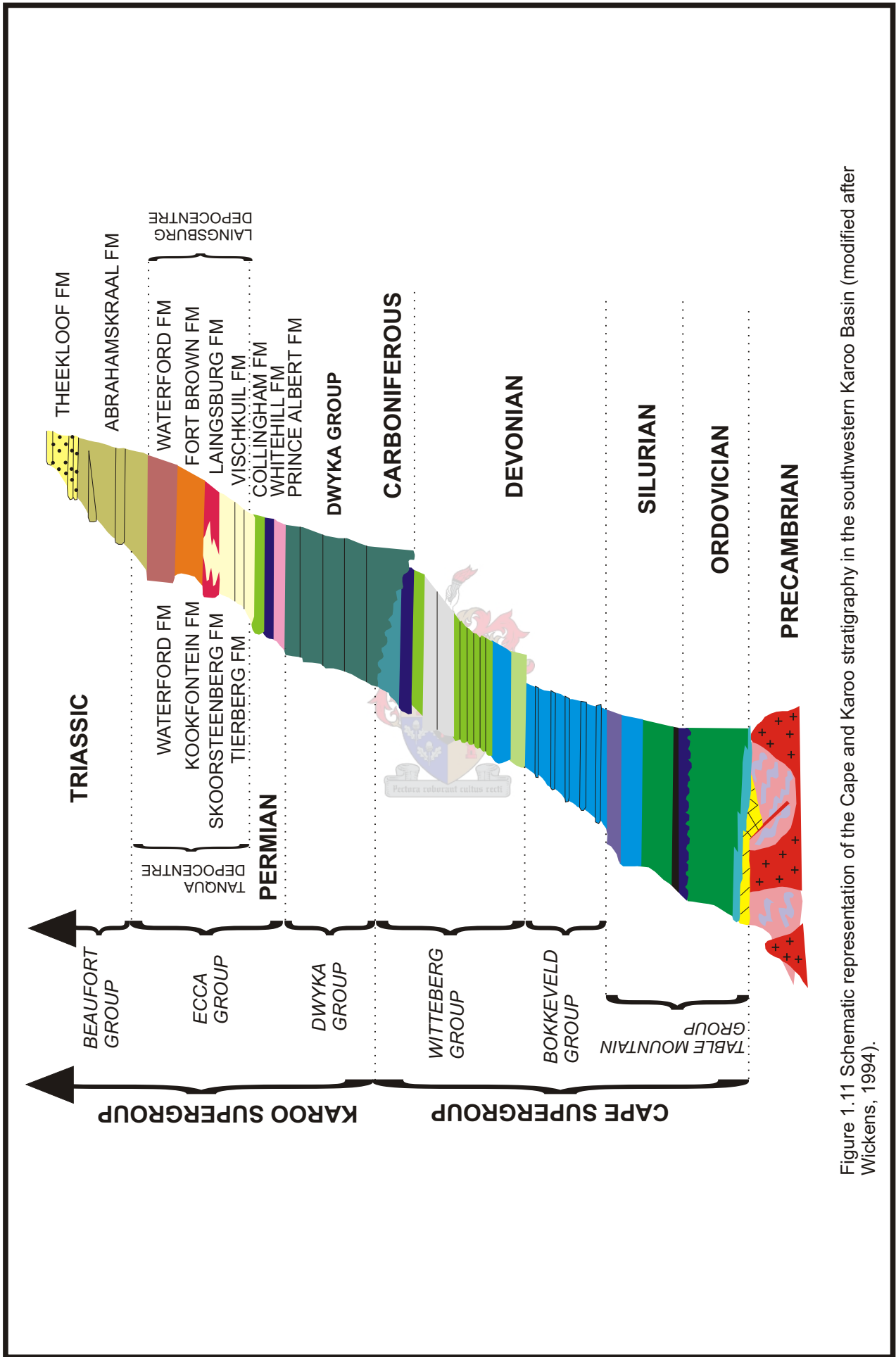
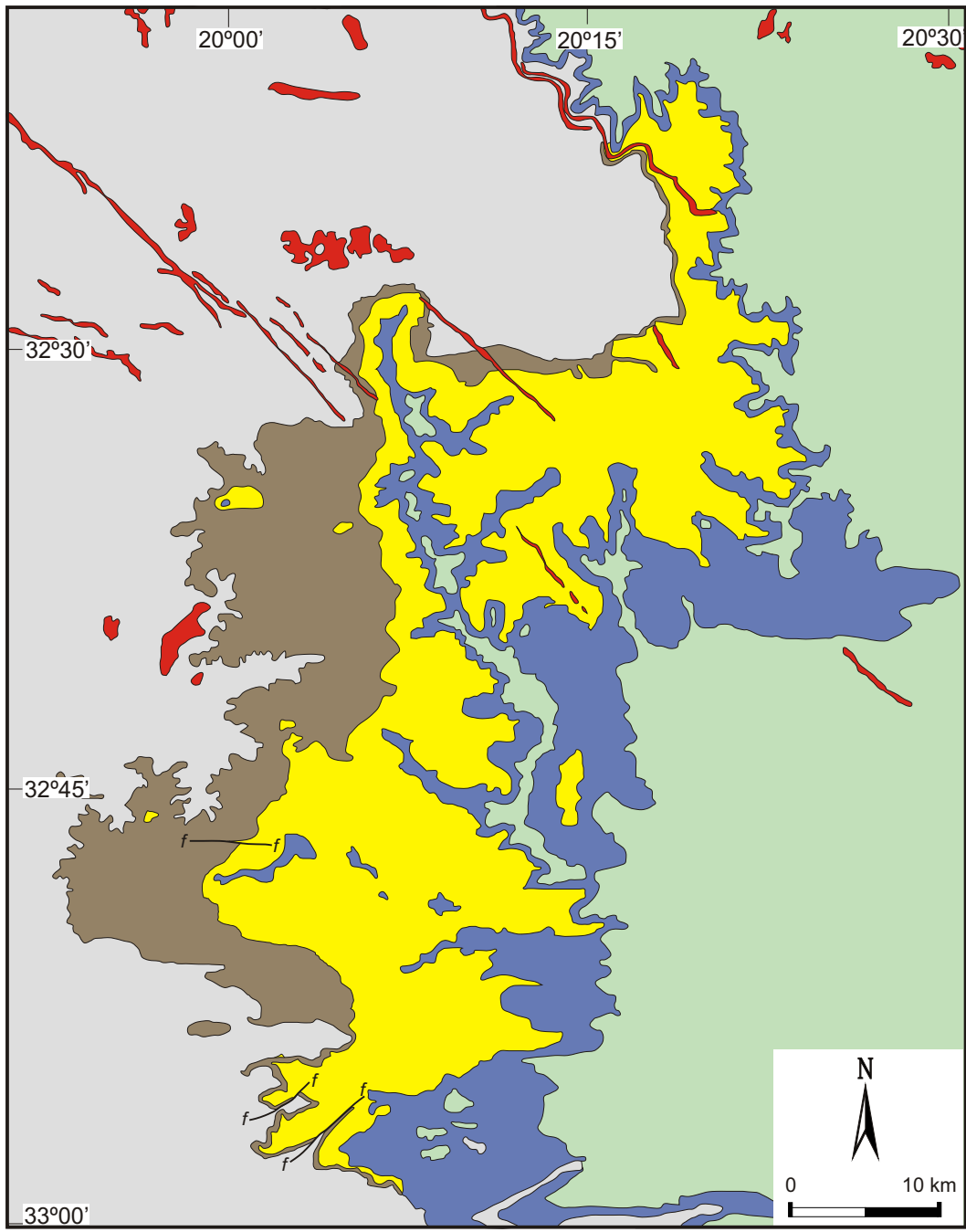


Figure 1.11 Schematic representation of the Cape and Karoo stratigraphy in the southwestern Karoo Basin (modified after Wicks, 1994).



Geological legend

Mesozoic	Jurassic
Palaeozoic	Permian

Lithostratigraphy

Karoo Supergroup	▲ Beaufort Group	Abrahamskraal Fm
		Waterford Fm
		Kookfontein Fm
	Ecca Group	Skoorsteenberg Fm
		Tierberg Fm

Lithology

<span style="display: inline-block; width: 15px; height: 15px; background-color: red; border: 1px solid black;"></span>	Dolerite
<span style="display: inline-block; width: 15px; height: 15px; background-color: #c8e6c9; border: 1px solid black;"></span>	Mudstone, siltstone, sandstone, thin cherty beds
<span style="display: inline-block; width: 15px; height: 15px; background-color: #bbdefb; border: 1px solid black;"></span>	Sandstone, siltstone, mudstone, shale
<span style="display: inline-block; width: 15px; height: 15px; background-color: #fff176; border: 1px solid black;"></span>	Shale, siltstone, thin sandstone beds
<span style="display: inline-block; width: 15px; height: 15px; background-color: #d7ccc8; border: 1px solid black;"></span>	Sandstone, siltstone, shale
<span style="display: inline-block; width: 15px; height: 15px; background-color: #e0e0e0; border: 1px solid black;"></span>	Shale

Figure 1.12 Geological map of the Tanqua depocentre, Karoo Basin, South Africa. Geological information compiled from the Clanwilliam 3218 and Sutherland 3220 maps. 1:250 000 Geological series, Geological Survey of South Africa.

Swartberg Mountains (Figure 1.13). Both these depocentres are situated in the Western Cape Province of South Africa.

The earliest observations on changing character of landscape in the area of the southwestern Karoo Basin, was made by Burchell (1811) while collecting and describing plant species. Investigations on the geology of the Laingsburg/Beaufort West region were carried out by Dunn (1879, 1886) and Schwarz (1897) and were later incorporated by Rogers and Schwarz (1902), Rogers and Du Toit (1903) and Rogers (1910) in reports to the Cape Geological Commission. These reports contain the first comprehensive descriptions on the geomorphology, structural geology and regional characteristics of the major lithological units. The first geological map of the area, Cape Sheet No. 5 (Laingsburg), supplemented by an explanation of the geology of the area, was produced by Rogers in 1925.

The Karoo sequence was originally subdivided on the basis of the presence of reptilian and plant remains (Bain, 1856). Rogers and Du Toit (1903) stratigraphically subdivided the Ecca Series into three units, namely the lower shale unit, the middle Laingsburg beds, and the upper sandstone and shale unit. Blignaut *et al.* (1948) and Rossouw *et al.* (1964) recognised a Lower Ecca sandstone and shale, a Middle Ecca shale, and an Upper Ecca sandstone and shale for the area east of Laingsburg.

Recognition of basin-wide lithofacies variations in the Ecca Group resulted from the work of Du Toit (1954) and Ryan (1967). Four area-characteristic facies, namely a Northern, Western, Southern and Central Facies, were identified, based upon palaeotransport flow direction.

Keunen (1963) was the first to describe the Lower Ecca sandstones (Laingsburg Formation) as a flysch-like succession and suggested a turbiditic origin. These ideas were followed up by Theron (1967) who did a detailed study close to the town of Laingsburg, interpreting the Vischkuil Formation as a succession of “distal turbidites” that changes upwards into “proximal turbidites” of the Laingsburg Formation. It was only in 1977 when research on the Ecca turbidites was resumed, this time in the Eastern Cape by Kingsley. He subdivided and characterised the Ripon Formation (stratigraphic equivalent of the Vischkuil and Laingsburg Formations) based on stratigraphy and sedimentology (NW of Grahamstown to NE of Port Alfred).

Rowsell and De Swardt (1976) presented a comprehensive summary of petrographical, geophysical and geochemical results based on data from deep boreholes drilled by SOEKOR in the southwestern Karoo, and showed that there was a general southward increase in diagenesis. The depositional environments of the Ecca in the southwestern Karoo Basin was reviewed, and various aspects of the nature of the deltaic deposition, water depth and

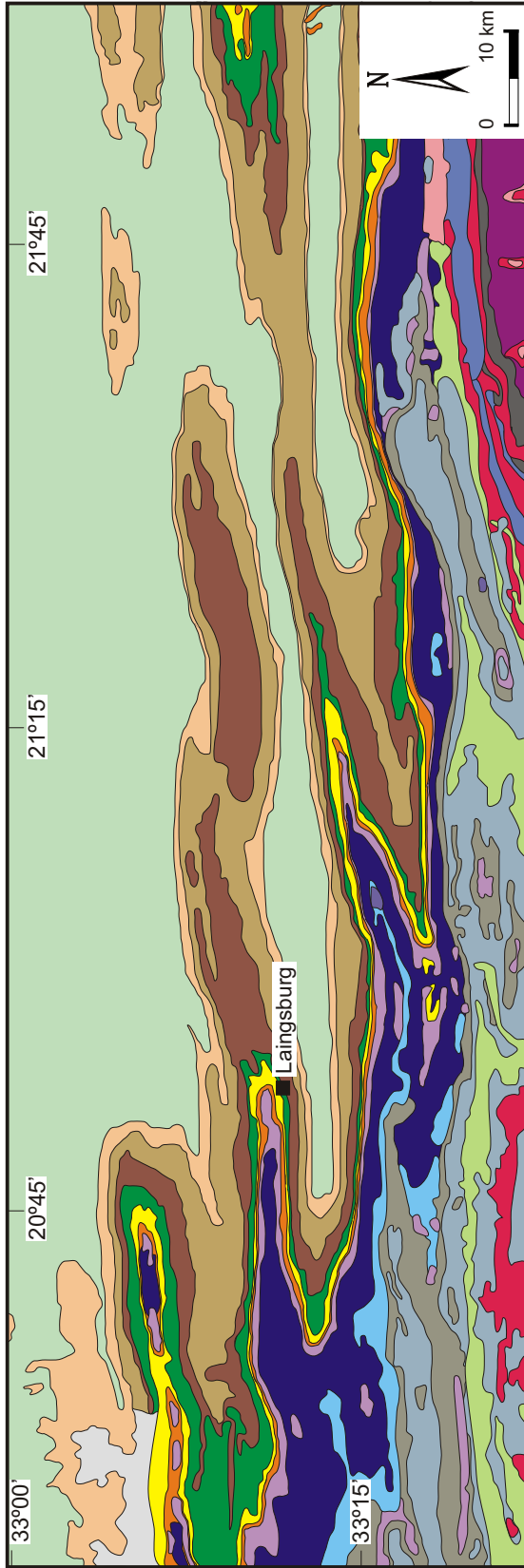


Figure 1.13 Geological map of the Laingsburg deopcentre, Karoo Basin, South Africa. Geological information from the Ladismith 3320 map. 1:250 000 Geological series, Geological Survey of South Africa.

palaeotransport directions, was addressed by Visser and Looek (1978) and Visser *et al.* (1980).

A research program aimed at the development of depositional models for the hydrocarbon-bearing submarine fan deposits in the offshore Cretaceous Bredasdorp Basin was started on the Tanqua fan complex by SOEKOR in 1989 (Wickens *et al.*, 1990; Bouma and Wickens, 1991; Wickens *et al.*, 1992).

Wickens (1994) was the first to interpret and compare the depositional environments of the Vischkuil, Laingsburg and Fort Brown Formations in the Laingsburg depocentre to the stratigraphic equivalent units in the Tanqua depocentre, based on stratigraphic and regional sedimentological correlations. Scott (1997) and Adelman and Fiedler (1998) further attempted comparisons with the use of petrographical and geochemical analyses. It was found that both depocentres most likely had a single point source and that active submarine fan deposition only occurred in one depocentre at a time (Scott, 1997). Basu and Bouma (2000) worked on the channel-fills of Unit 5 of the Skoorsteenberg Formation in the Tanqua depocentre, whereas Scott *et al.* (2000) described the influence of tectonics on submarine fan deposition in the Tanqua and Laingsburg depocentres.

Recent studies focussed on high-resolution stratigraphy of the deep water successions of the Tanqua and Laingsburg basin-floor to slope turbidites, establishing and advancing analogous features to many modern fine-grained submarine fans in passive margin settings (Grecula, 2000; Sixsmith, 2000; Johnson *et al.*, 2001; Grecula *et al.*, 2003). Grecula (2000) found that local tectonic segmentation of the Laingsburg depocentre produced highly variable vertical facies development of coeval depositional cycles in different parts of the deep water systems. Sixsmith (2000) established a high-frequency cyclic subdivision of the lowermost fan system within the Laingsburg Formation (Laingsburg depocentre) and recognised changes in palaeotransport patterns, attributed to local syndepositional tectonic activity.

Recent mineralogical, geochemical and SGR studies of sedimentary rocks from the Tanqua submarine fan complex focussed on the sedimentary processes that acted during the deposition of these rocks and the characteristics and evolution of the source area (Andersson *et al.*, 2003; Andersson and Worden, 2004). The principal findings of these studies revealed that little or no variation in provenance occurred between the different fans of the Skoorsteenberg Formation (Tanqua depocentre).

#### **1.4 Methodology of data collection and processing**

Sedimentary outcrop logging, measurement of gamma radiation profiles and sample collection for petrography and geochemical analyses were carried out over the last two years

in the Tanqua and Laingsburg Karoo, South Africa. Samples were characterised through petrographic analyses, and the effects of alteration and possible contamination were determined.

This study forms part of the SLOPE project, which is an interdisciplinary geochemical, sedimentological and structural study of the deep water Karoo deposits. A summary diagram of the methodology is given in Figure 1.14.

Sedimentological and gamma ray profiles were measured from the basin-floor deposits to the base of the deltaic successions in both the Tanqua and Laingsburg depocentres. The locations for these profiles were chosen on best outcrop positions for regional correlation between the depocentres. Profile names differ from names on topo-cadastral maps. Samples were taken from fresh outcrop surfaces where possible, concentrating mudstone sampling between fans/units, and sandstone samples at the start and end of major depositional facies. All samples within a specific profile were taken at vertical intervals, for the purpose of constraining regional correlations based on geochemistry.

Further studies involving X-ray fluorescence (XRF), inductively coupled plasma mass emission spectrometry (ICP-MS) and isotope dilution mass spectrometry (ID-TIMS) were used to measure the major element oxides, the trace and rare earth elements and the Sm-Nd concentrations. XRF and ICP-MS studies and results are further discussed in Chapter Four, whereas Chapter Six includes a detailed discussion on Sm-Nd isotope analyses.

High-resolution stratigraphy aids in predicting facies distribution. Integration of new chemostratigraphic data with existing litho- and sequence stratigraphy leads to a better understanding of the sequence stratigraphy and basin-fill evolution of the Karoo Basin. This project thus provides an increased understanding on the early Karoo Basin and Gondwana geodynamics that benefit South Africa in terms of (a) regional tectonostratigraphic models, and (b) generic understanding of chemostratigraphic correlation in deep-water systems, for application to offshore petroleum exploration.

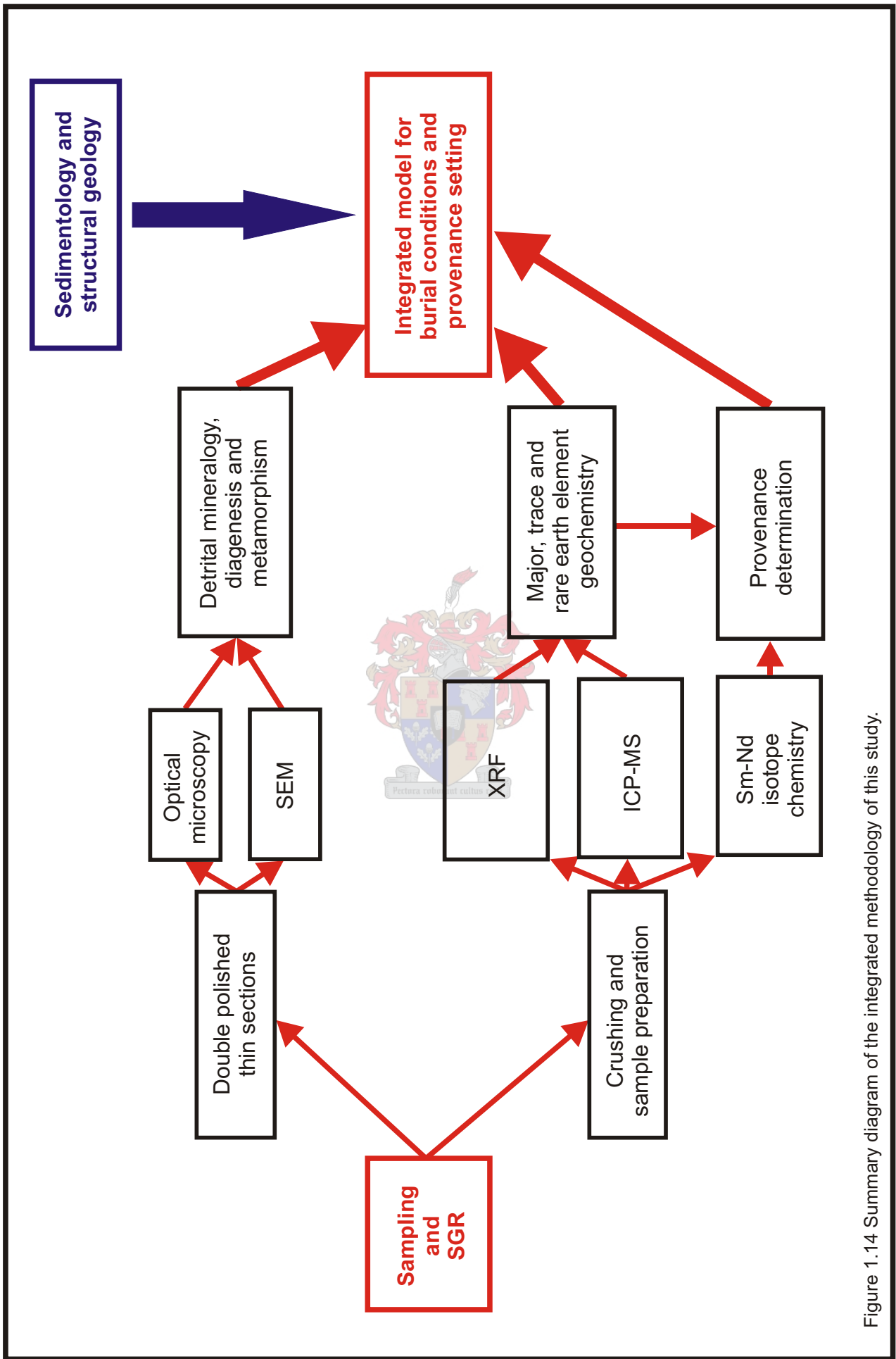


Figure 1.14 Summary diagram of the integrated methodology of this study.

## Chapter Two

### 2 Geological Framework

#### 2.1 Tectonic evolution of southern Africa

##### 2.1.1 Introduction

Episodic terrane accretion during the mid-Archean led to the growth of ancient continental fragments, culminating in the juxtaposition of the Kaapvaal and Zimbabwe granitoids-greenstone terranes during the Limpopo orogeny at ~2.7 Ga (Figure 2.1). Intracratonic sedimentary basins developed on this stable cratonic block from the late Archean to mid-Proterozoic, whereas crustal growth occurred during the successive Eburnian (~2.0 – 1.8 Ga), Kibaran (~1.2 - 1.0 Ga) and Pan-African (~550 Ma) global accretionary events (Thomas *et al.*, 1993).

The supercontinent of Gondwana existed from about the Cambrian-Ordovician boundary until latest Devonian to early Carboniferous when it collided with Laurasia and became part of the amalgamated landmass known as Pangea (Visser and Praekelt, 1998). During the late Permian, the relative movement between Gondwana and Laurasia changed from mid-Carboniferous–early Permian suturing (which resulted in the formation of Pangea), to late Jurassic–early Cretaceous extension, which ultimately led to the break-up of Pangea and Gondwana (Smith, 1999).



The Karoo Basin is a retro-arc foreland basin that developed inbound of the Cape Fold Belt (CFB), in relationship to late Palaeozoic–early Mesozoic subduction episode of the palaeo-Pacific plate underneath the Gondwana plate (De Wit *et al.*, 1988; Johnson, 1991; De Wit and Ransome, 1992). The foreland basins, which formed part of the extensive Pan-Gondwanian Mobile Belt, were fragmented as a result of Gondwana break-up, and are preserved today in southern Africa (Karoo Basin), South America (Paraná Basin), Australia (Bowen Basin) and Antarctica (Beacon Basin) (Figure 2.2).

##### 2.1.2 Pre-Karoo setting

Pre-Cambrian basement structures that were active during the Pan-African orogeny controlled the geographical positioning of the Cape and Karoo Basins. The Karoo Basin overlies the Archean Kaapvaal Province in the north and northeast, the Precambrian rocks of the Namaqua-Natal Belt to the north, and the Ordovician to upper Devonian rocks of the Cape Supergroup in the south (Figure 2.3). The Cape Supergroup succession overlies Pre-Cape rocks belonging to the late Proterozoic Gariiep, Saldania and Mozambique Provinces.

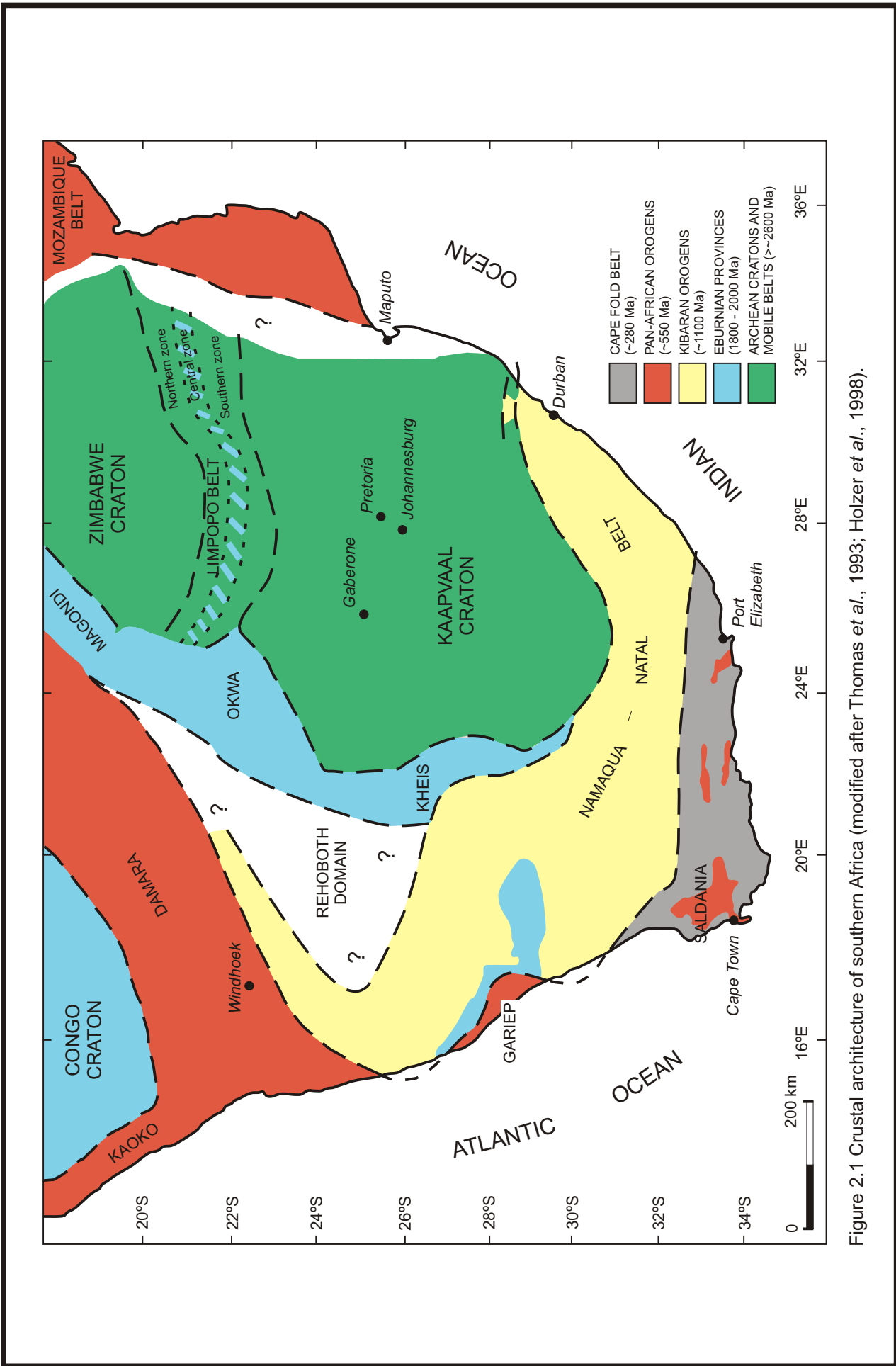


Figure 2.1 Crustal architecture of southern Africa (modified after Thomas et al., 1993; Holzer et al., 1998).

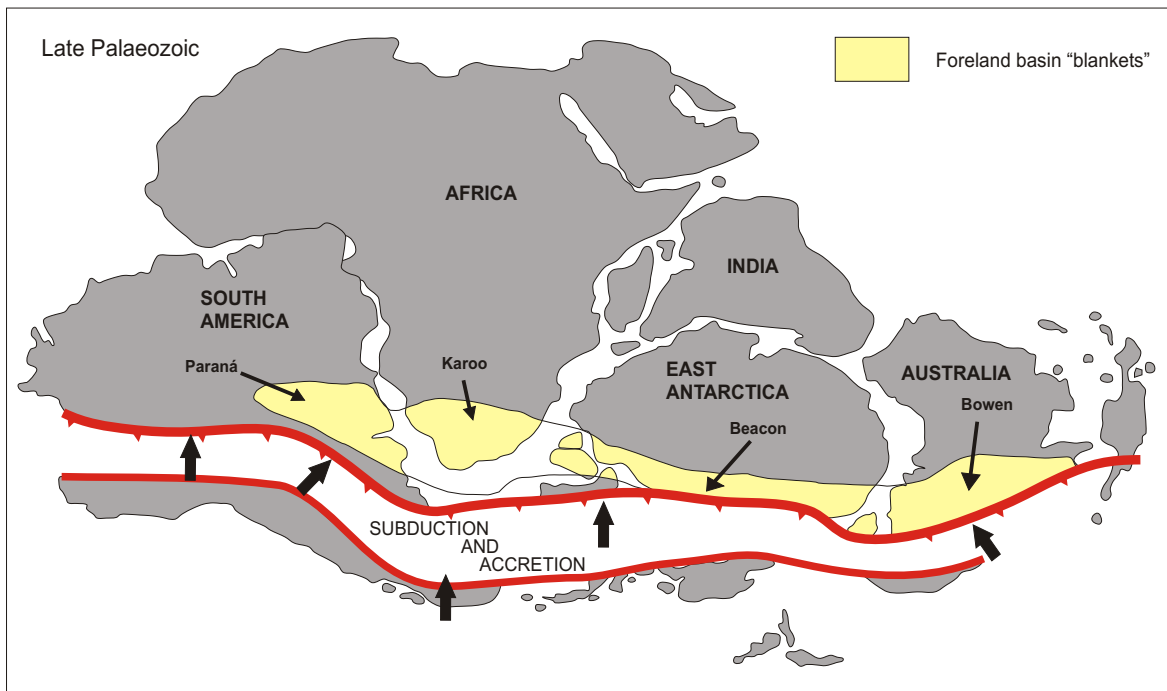


Figure 2.2 Karoo, Paraná and Beacon Basins in response to accretion tectonics during the late Palaeozoic along the southern margin of Gondwana (after De Wit and Ransome, 1992).

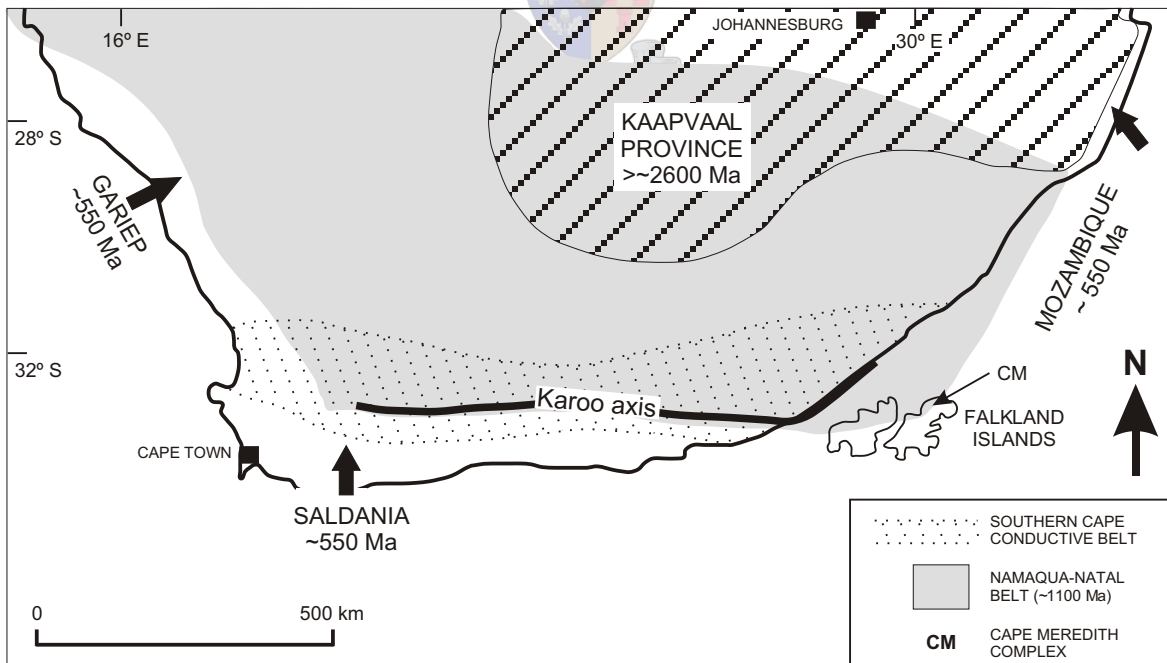


Figure 2.3 Map of southern Africa showing the locations of the Precambrian Provinces (from Cole, 1992). The depositional axis of the Karoo Sequence and the zone of the Southern Cape Conductive Belt positions are indicated (after De Beer *et al.*, 1982).

The latter are composed of gneisses, schists, quartzites and metamorphosed carbonates. A deep-seated magnetic feature with low electrical resistivity, called the Southern Cape Conductive Belt (SCCB), occurs as an east-west elongated anomaly between the Namaqua-Natal Belt and the Saldania Province (Figure 2.3) (De Beer *et al.*, 1982). This zone, thought to consist of serpentinitised basalt (De Beer *et al.*, 1982), has been interpreted to be 30 km wide and 7 km below the surface, dipping south (Pitts *et al.*, 1992), and obducted against the Namaqua-Natal Belt at 0.8 Ga. The Gariep, Saldania and Mozambique Provinces, comprising metasediments, were periodically deformed by the Pan-African orogeny as a result of plate convergence. The final phase of development of these provinces lasted until 0.6 and 0.5 Ga, with the intrusion of syn- and post-tectonic granitoids of the Cape Granite Suite (CGS) into the oldest rocks of the Saldania Belt (Tankard *et al.*, 1982; Scheepers and Rozendaal, 1995).

Strata of the Cape Supergroup (the Table Mountain, Bokkeveld and Witteberg Groups) comprise an 8000 m thick sequence of clastic sediments, deposited in a passive margin setting during the early to mid-Palaeozoic (Tankard *et al.*, 1982; Thomas *et al.*, 1993). The Cape Supergroup succession, deposited as beach, deltaic and shallow marine clastic sediments and derived from a granitic source to the north (Johnson, 1991; Thomas *et al.*, 1993), were deformed and metamorphosed to lower greenschist facies during the late Palaeozoic/early Mesozoic (Broquet, 1992). The depositional environment changes progressively from shallow-marine and terrestrial for the Table Mountain Group to deltaic and shallow-marine shelf in the Bokkeveld and Witteberg Groups (Tankard *et al.*, 1982). The Table Mountain Group is mainly composed of orthoquartzite, with siltstone occurring in lesser proportions, the Bokkeveld Group is predominantly argillaceous, with fewer quartzites, and the Witteberg Group has approximately equal amounts of quartzite and shales, with a diamictite horizon occurring in the upper part of the succession (Booth and Shone, 2002).

Deposition of the Karoo Supergroup commenced after a hiatus of approximately 30 Ma, caused by eustatic sea-level fall and subsequent erosion of the newly exposed continental shelves (Visser, 1992). The latter was due to a series of glacial episodes that enveloped southern Gondwana at the start of the Carboniferous (Veevers and Powell, 1987). However, mass balance suggests that the volume of shelf incision is only minor during sea-level lowstands. An increase in plate motion rates, linked to the onset of the palaeo-Pacific plate beneath southern Gondwana, accompanied the glacial episode (Visser, 1992). The evolution of this active collisional margin during the late Palaeozoic led to the formation of the CFB (Tankard *et al.*, 1982; De Wit and Ransome, 1992).

### **2.1.3 Cape Fold Belt (CFB)**

The CFB was formed when the early Palaeozoic passive continental margin, which formed a large section of the southern edge of Gondwana, evolved into an active convergent

margin during the late Palaeozoic (De Wit and Ransome, 1992). The cover rocks involved in the Permo-Triassic CFB orogeny are composed of the Cape Supergroup, of which about 5000 m is exposed in the syntaxis (De Beer, 1995). Deformation in the region adjacent to the CFB affected the lower part of the Karoo Supergroup.

The CFB extends east-west for more than 800 km along the southern margin of Africa and may be divided into three domains in the Western Cape, based upon structural grain, fold style and the amount of shortening: (i) the north-trending western branch (Cedarberg; displays relatively open, upright, first-order folds and monoclines), (ii) the east-trending southern branch (Swartberg; much higher deformational intensity, with north-verging, recumbent first-order folds, a high incidence of second-order folds and local out-of-the-forelimb thrusting), and (iii) the area of intersection of the two belts at the core of the regional curve defined by the western and southern branches (Hälbich, 1983; De Beer, 1995). Both branches are cut by numerous post-tectonic normal faults. Some northerly directed thrusts cut through basement and cover alike, whereas the area of merge between the western and southern branch folds is characterised by numerous NE-trending folds (Hälbich, 1983; De Beer, 1995).

The high-angle thrusts of the CFB dip steeply to the south. This sense of displacement was reversed during the early Cretaceous rifting of the South Atlantic, causing the faults to become down-thrown to the south, with a strong dextral component (Lock, 1980). Less than 10% crustal shortening was involved in the Cedarberg branch, while the Swartberg branch underwent more intense S-N local horizontal shortening of approximately 40%, decreasing to 25% towards the east (Hälbich and Swart, 1983; De Beer, 1989).

First-order folds involving the quartz arenites of the Table Mountain Group and part of the basement form the structural backbone of the CFB (Gresse *et al.*, 1992). The folds usually have monoclinical geometry on their limbs, possess wavelengths of up to 11 km and have amplitudes of hundreds of metres (De Beer, 1995). The Bokkeveld Group consists of sandstone units embedded in a ductile mudstone matrix. These are folded into sinusoidal forms with wavelengths of 0.5 – 2 km and amplitudes of a few metres to a few tens of metres. The Witteberg Group is mainly composed of thin- and well-bedded arenites that have been shortened. This led to the formation of folds with kink geometries in which the bedding maintained a near-constant inclination between adjacent hinges (De Beer, 1995).

Similar deformational peaks at 278, 258, 247 and 230 Ma ( $^{40}\text{Ar}/^{39}\text{Ar}$  stepwise heating analysis on micas in cleaved rocks) were obtained from samples in the southern branch, the syntaxis and the western branch (Hälbich *et al.*, 1983). Further  $^{40}\text{Ar}/^{39}\text{Ar}$  dating of deformations in Saldania rocks revealed pulses of tectonism at 294, 276, 259, 239, and 223 Ma (Gresse *et al.*, 1992). It thus seems as if the western branch, the syntaxis and the

southern branch were formed during the same general orogeny (De Beer, 1995).

#### **2.1.4 Karoo Basin development**

The Karoo Basin is believed to have developed as part of a series of basins associated with the subduction of the palaeo-Pacific plate under the southern margin of Gondwana and has been subdivided into the Permian Tanqua and Laingsburg depocentres (270 – 255 Ma) (Figure 2.4) (Wickens, 1994). Recent studies by Wickens (1994) and Scott (1997), clearly illustrate that the evolving structures of the CFB influenced the sediment pathways to the depocentres.

The major depositional basins in the late Palaeozoic of southwestern Gondwana (consisting of South America, southern Africa, Falkland Islands, East Antarctica and the microplates in West Antarctica and inundated microplates in the southern Atlantic Ocean) developed between the uplifted landmass to the south and southwest and cratonic highlands to the north, in response to accretion tectonics along the southern margin of Gondwana (Visser, 1991; De Wit and Ransome, 1992). Previous workers have interpreted the development and origin of the Karoo Basin and the CFB in terms of (a) continent-continent collision, (b) Andean-type subduction, and (c) orogenic processes unrelated to subduction.

Hälbich (1983) opted for an orogeny without subduction, which he based on the absence of high-grade metamorphic rocks, ocean floor derivatives, any kind of suture, and major shear zone and melange points against the plate collision or subduction-related models. He suggested instead the presence of a mantle plume under southern Gondwana, compatible with the deformation episode of the CFB. There is, however, no evidence for this. In contrast, a collision of the 'proto-African' plate with a southern continental plate (probably including Patagonia, the continental Falkland Plateau, and part of Antarctica), following southward subduction of oceanic floor beneath the southern continent, has been suggested (Winter, 1984; Ramos, 1986).

The most widely accepted mechanism for the evolution of the Karoo Basin and CFB is the northward subduction of an oceanic plate under the palaeo-Pacific margin of Gondwana (De Wit *et al.*, 1988; Visser, 1991). This concept also points to the existence of a subduction-related, volcanically active source area situated somewhere between the CFB and the palaeo-Pacific subduction site (De Wit *et al.*, 1988).

Visser (1985, 1989, 1992) placed the early Karoo Basin in a retro-arc position north of a northward migrating orogenic belt at the palaeo-Pacific margin of Gondwana. He postulated that during Dwyka times, the uplifted region was initially situated more than 1200 km south of South Africa, but only a few hundred kilometres to the south during Ecca Group deposition.

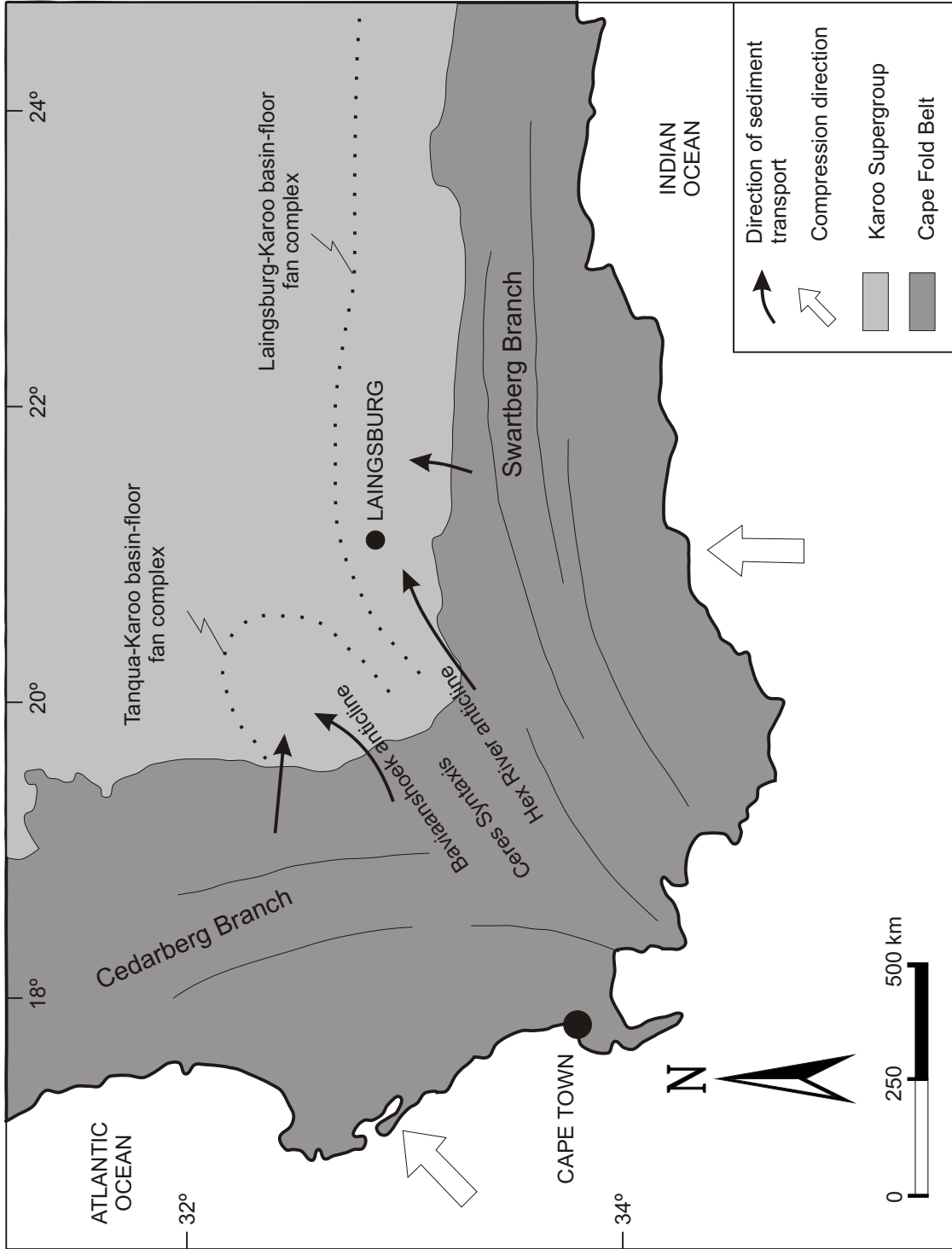


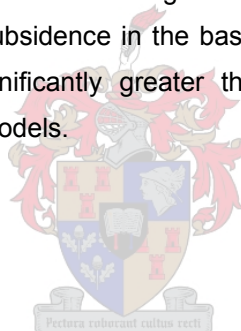
Figure 2.4 Influence of the Cape folding event upon Ecca deprecentre development (from Wickers, 1994).

The large volcanoclastic component in the lower Karoo succession, led Johnson (1991) to consider a retro-arc foreland setting during Ecca and Lower Beaufort times. It indicated that the magmatic arc source at that time was located much closer than 1500 to 2000 km south of the basin (Lock, 1980; Smellie, 1981).

The main Karoo Basin succession forms the thickest and stratigraphically most complete megasequence of Permo-Carboniferous to Jurassic age rocks in southwestern Gondwana (Veevers *et al.*, 1994; Catuneanu *et al.*, 1998). Eight coaxial compressional deformation events are thought by some authors to have produced varying sedimentary responses within the foreland setting, interpreted as having occurred within a single subsiding basin characterised by continuous base-level rise in any of its parts (Rust, 1975; Turner, 1975; Hälbich, 1983, 1992; Cole, 1992; Gresse *et al.*, 1992). However, this interpretation ignored the effects of the flexural response of the foreland lithosphere to the orogenic tectonism, and explained the stratigraphic features based only on the interplay between varying subsidence and sedimentation rates in time and across the basin (Jordan and Flemings, 1991; Sinclair *et al.*, 1991; Watts, 1992; DeCelles and Giles, 1996; Catuneanu *et al.*, 1998). Pysklywec and Mitrovica (1999) pointed out that a flexural loading mechanism couldn't explain the complete Karoo Basin evolution, since the subsidence in the basin, extending horizontally for at least 1300 km from the trench, is significantly greater than the length scales of deflection suggested by lithospheric flexural models.

## 2.2 Karoo Basin stratigraphy

### 2.2.1 Introduction



The Karoo Basin fill (Karoo Supergroup) in the southwestern Karoo Basin is divided into the Dwyka Group (Westphalian to early Permian), the Ecca Group (Permian), the Beaufort Group (Permo-Triassic) and Stormberg Group (late Triassic to early Jurassic) (Figures 1.11 and 2.5) (Tankard *et al.*, 1982; Smith *et al.*, 1993; Catuneanu *et al.*, 1998; Turner, 1999). The succession is conformable with the underlying Cape Supergroup in the south, but unconformable with the progressively older rocks (including crystalline and metasedimentary basement) to the north (Tankard *et al.*, 1982).

The Karoo succession has a maximum cumulative thickness of approximately 12000 m in the eastern and southern Karoo foredeep (Johnson, 1976) that is almost completely preserved in the central parts of the basin, in and around Lesotho, whereas the upper part of the succession has been eroded (Cole, 1992).

The glaciogenic Dwyka Group is overlain by mudrock-dominated sediments (marine and brackish to fresh water) of the Lower Ecca Group, followed by the sand-dominated fluvio-

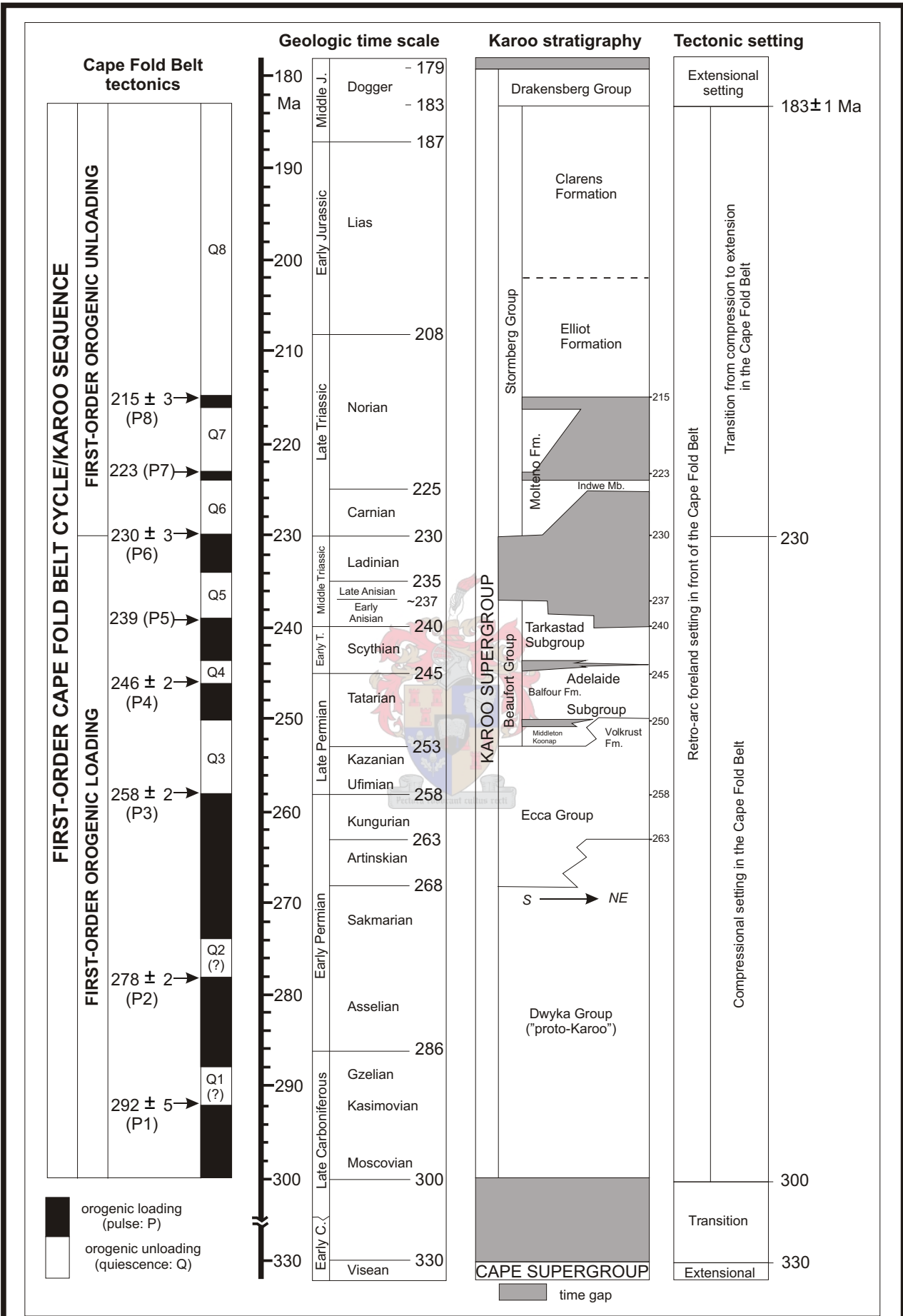


Figure 2.5 Tectonic regimes during the evolution of the Karoo foreland basin (from Catuneanu *et al.*, 1998).

deltaic systems of the Upper Ecca and Lower Beaufort Groups, prograding into the basin from the northeast and southwest (Smith *et al.*, 1993; Veevers *et al.*, 1994; Johnson *et al.*, 1996; Turner, 1999). The Stormberg Group comprises the Upper Karoo, and forms a southeast thickening clastic wedge capped by approximately 1400 m of basaltic lava of the Drakensberg Group, dated at  $183 \pm 1$  Ma (Tankard *et al.*, 1982; Duncan *et al.*, 1997; Hawkesworth *et al.*, 1999; Turner, 1999). The Middle Jurassic Drakensberg lavas terminated Karoo sedimentation and are interpreted to represent early rifting of Gondwana prior to its eventual fragmentation in Cretaceous times (Dingle *et al.*, 1983; Turner, 1999).

### **2.2.2 Dwyka Group**

Dwyka sedimentation was initiated about 300 Ma ago, following a 30 Ma stratigraphic break after the end of the Visean, when sedimentation in the Cape Basin was terminated (Visser, 1989; Cole, 1992). The glacially influenced Dwyka deposits (800 m thick succession) of the Karoo Basin show three distinct facies associations, which are: (i) the valley glacier facies association (restricted to the margins of the basin and consisting of diamictites and mudstones with ice-rafted material), (ii) the platform facies association (rainout tills and gravity flow diamictites), and (iii) scarce mudstones (the product of fall-out from sediment plumes) (Visser, 1991; López-Gamundi and Rossello, 1998). The composition of volcanic ash beds that occur within the lower 100 m of the Dwyka Group, suggests continental arc volcanism in a convergent margin setting (Johnson, 1991), signalling the initiation of subduction of the palaeo-Pacific plate beneath Gondwana (Smellie, 1981).

There is a clear distinction between the southern (proximal) and northern (distal) Dwyka successions, in that nine fining-upwards cycles with uniform character and lateral continuity in the layers have been recognised in the south (thicknesses varying between 60 and 100 m). Lateral correlation in the two fining-upwards cycles in the northern Dwyka facies is very difficult due to their irregular thicknesses and complex facies relationships (Visser, 1986; Tankard *et al.*, 1982; Visser, 1997). Ground ice dominated deposition in the northern Dwyka, whereas southern Dwyka deposition was dominated by floating ice. The overall pattern of palaeotransport shows southward ice movement (Tankard *et al.*, 1982).

The northern Dwyka succession has coal-bearing fluvio-deltaic sequences, as a result of the gradual deglaciation of the continental areas, and is overlain in places by the marine shales of the Ecca Group (Smith *et al.*, 1993; Catuneanu *et al.*, 1998). The transition from glaciomarine in the Dwyka Group to fully marine in the Ecca Group was gradual in the southern part of the Karoo Basin. The percentage of dropstones in the rock gradually decreases upwards as a result of the melting and disintegration of the floating ice.

### **2.2.3 *Ecca Group***

The Dwyka ice-sheet retreated in the west and south during the early Asselian (290 – 286 Ma), although tide-water glaciers persisted along the northern basin margin until ca. 265 Ma (Visser, 1989). The southern Ecca stratigraphy includes the Prince Albert and Whitehill Formations, with exposure of the Skoorsteenberg, Kookfontein and Waterford Formations in the Tanqua depocentre, and the Collingham, Vischkuil, Laingsburg, Fort Brown and Waterford Formations in the Laingsburg depocentre.

The open-marine shales of the Prince Albert Formation at the base of the Ecca Group sharply and conformably overlies the Dwyka diamictites, recording a rapid glacial retreat (Visser, 1991). This dark greenish-grey shale, with some graded silty layers, is of Artinskian to Middle Kungurian age (Visser, 1992) and reaches a thickness of 165 m in the Laingsburg area, but thins out northwards and eastwards (Visser, 1991). Four phases of deposition have been recorded, with the lower part of the Prince Albert Formation dominated by mudstone containing dropstones and other ice-rafted detritus, the middle and upper part dominated by mudstone and isolated mud-rich turbidite deposits, and the uppermost unit dominated by shale, containing phosphatic nodules (Visser and Looek, 1978; Visser, 1991). Marine fossils, as well as plant and palaeoniscoid fish remains and coprolites, have been recorded from near the base of the formation (Johnson *et al.*, 1997). The upper contact with the Whitehill Formation commonly overlies a thin upward-coarsening sequence grading from carbonaceous mudrock into silty shale (Johnson *et al.*, 1997).

The Whitehill Formation (early to late Permian) covers much of southern Gondwana and consists of carbonaceous shale, weathering white, with chert bands and lenses, deposited in a deep water, pelagic, non-marine and reducing environment (Visser, 1992; Catuneanu *et al.*, 1998). The lower contact of the formation is always sharp and well defined. Ferruginous carbonate concretions with a dolomitic composition are dispersed throughout the formation, whereas the biostratigraphy suggests synchronous deposition in the Karoo Basin (Johnson *et al.*, 1997). The succeeding deposits of the overlying formations were deposited in deeper, fully marine environments.

#### **2.2.3.1 *Tanqua depocentre***

The Tanqua depocentre is located in the southwestern Karoo foreland basin and is bounded by the western and southern branches of the CFB. The Skoorsteenberg Formation represents gravity flow deposits, whereas the Tierberg Formation, which is overlain by the Skoorsteenberg Formation, consists of grey shale and subordinate thin siltstone layers and represents deposition mainly from suspension (Wickens, 1994). Water depths most likely did not exceed 500 m and the dominant sedimentary process was the deposition of mud from

suspension (Visser and Loock, 1978). The Skoorsteenberg, Kookfontein and Waterford Formations represent the sequence under study in the Tanqua depocentre.

#### **2.2.3.1.1 Skoorsteenberg Formation**

The Skoorsteenberg Formation comprises five deep-water turbidite fan systems, almost completely exposed over 650 km<sup>2</sup>. The formation thins out in a northerly and easterly direction. A progradational trend can be seen in the approximately 450 m thick succession, from distal basin-floor (Fan 1) through basin-floor sub-environments (Fans 2, 3 and 4) to a slope setting for Fan 5 (Goldhammer *et al.*, 2000; Wach *et al.*, 2000; Wickens and Bouma, 2000; Johnson *et al.*, 2001). Deposition was unrestricted in the broad, open style N-S trending Tanqua depocentre and the sandstones are very fine- to fine-grained.

Each fan system has a high sandstone-to-shale ratio, whereas the interfan units comprise finely laminated shale and silty shales of hemipelagic and tubiditic origin (Wickens and Bouma, 2000). The thickness of the sand-rich turbidite systems vary from 20 – 60 m, and are separated by basin shales, with varying thickness of 20 – 75 m (Wickens and Bouma, 2000). The sandstones are virtually without any porosity or permeability, resulting from high-grade diagenetic to low-grade metamorphic changes during burial to depths of about 7 km (Rowell and De Swardt, 1976; Wickens and Bouma, 2000).

Five major lithofacies have been recognised, namely massively bedded sandstone, horizontally and ripple cross-laminated sandstone, parallel-laminated siltstone, parallel-laminated shale and a micaceous, silty plant-fragment facies (Wickens and Bouma, 2000). Tuff, limestone beds, calcareous concretions, and cherty layers are present as subordinate facies. Palaeocurrent and isopach data were used by Wickens *et al.* (1990) in the initial studies to reconstruct the fan systems. They found that each successive fan system prograded further into the basin, with an offset stacking pattern to compensate for basin floor topography. Fans 2 and 3, for example, show an eastward shift compared to the position of Fan 1.

#### **2.2.3.1.2 Kookfontein Formation**

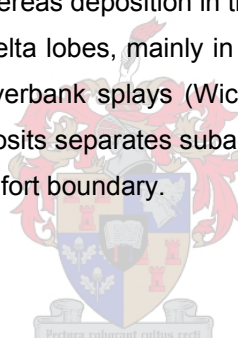
The Kookfontein Formation occurs above the turbidite fan complex and is an upwards coarsening succession, reflecting progressive shallowing conditions associated with deltaic progradation (Wickens, 1994). The upper part of the formation shows very subtle, upward thickening cycles (2 – 10 m thick) that generally commence with dark grey shale and siltstone derived from suspension, followed upwards by a rhythmic alternation of shale, siltstone and sandstone (Wickens, 1994). Traction and wave-produced ripple-lamination become more pronounced upwards in the succession. The thin lower beds mostly resulted from suspension

settling, whereas the thicker beds (up to 20 cm) towards the top resulted from sediment-laden traction currents (Wickens, 1994). Thick-bedded mouth bar sandstones, in places modified by wave and tide produced structures, occur in many places and are often associated with soft-sediment deformational features (Flint *et al.*, 2004).

### **2.2.3.1.3 Waterford Formation**

The Waterford Formation consists of delta front, lower delta plain and upper delta plain deposits, dominated by fine- to medium-grained sandstone and a thickness of ca. 200 m (Wickens, 1994).

The proximal delta front succession is arenaceous and contrasts sharply with the distal delta front and pro-delta deposits. Characteristic to the delta front succession is the vertically stacked, upward coarsening cycles (10 – 20 m in thickness) and a variety of syn- and post-depositional deformational structures (Wickens, 1994). The lower delta plain deposits accumulated as distributory channel-fills, crevasse channel-fills, crevasse splays and interdistributory bay-fill deposits, whereas deposition in the upper delta plain environment took place landward of the prograding delta lobes, mainly in the form of aggrading overbank mud deposits and thin-bedded sandy overbank splays (Wickens, 1994). The boundary between the upper and lower delta plain deposits separates subaqueous from subaerial deposition, i.e. the position taken as the Ecca-Beaufort boundary.



### **2.2.3.2 Laingsburg depocentre**

The Laingsburg depocentre, elongated from Matjiesfontein in the west to east of Klaarstroom, borders the Swartberg Mountains along the southern margin of the Karoo Basin. The Collingham, Vischkuil, Laingsburg and Fort Brown Formations represent the sequence under study in this depocentre. Sediments in the Laingsburg depocentre were deposited in a tectonically active elongated setting where confinement and basin floor topography have played a major role in the distribution of the fan systems (Wickens and Bouma, 2000).

#### **2.2.3.2.1 Collingham Formation**

The Collingham Formation (thickness of 30 – 70 m) overlies the Whitehill Formation with a sharp conformable contact and consists of alternating beds of dark grey mudstone and cherty mudstone, yellowish tuff beds, siltstone and very fine- to fine-grained sandstone (Viljoen, 1992a). It is interpreted as a distal submarine fan facies of late Permian age, associated with pelagic sedimentation and wind-blown interbedded volcanic ash (Martini, 1974; Cole, 1992; Viljoen, 1995). The volcanic ash, indicating a dramatic change in the tectonomagmatic activity along the Panthalassan continental margin of Gondwana, were most

probably derived from volcanoes located in what is now northern Patagonia, where Permian silicic-andesitic volcanic and plutonic rocks crop out (Wickens and Bouma, 2000). The tuff layers, deposited from suspension, range in thickness from 1 – 20 cm (commonly < 5 cm thick) and are sharp-based and infrequently reworked in their upper portions (Viljoen, 1992a). The Matjiesfontein Chert Bed, a regionally extensive marker bed, occurs in the lower part of the formation. Tractional structures and occasional sole structures exhibited by the fine siltstone and sandstone beds, and their association with typical deep-water shale, confirm a turbiditic origin (Viljoen, 1992a; Wickens, 1994).

#### **2.2.3.2.2 Vischkuil Formation**

The contact of the Vischkuil Formation with the Collingham Formation is conformable and clearly defined. The Vischkuil Formation attains a thickness of 200 to 400 m and consists predominantly of mudstone, siltstone and fine-grained sandstone (Viljoen and Wickens, 1992; Wickens, 1994). The lower part of the Vischkuil Formation is dominated by mudstone, with occasional thin siltstone beds and several slump horizons, whereas the upper 40 m consists of metre-scale fining-upward beds separated by mudstone (Viljoen and Wickens, 1992; Wickens, 1994). The thickest beds of this facies (max. 15 m) occur in the lower half of the formation where they contain calcareous and phosphatic lenses and ferruginous layers (Johnson *et al.*, 1997). Tuff layers (1 to 20 cm in thickness) occur sporadically throughout the formation and are laterally persistent, lack any traction structures and sometimes show normal grading with slight mottling near the base (Johnson *et al.*, 1997). Theron (1967) interpreted the Vischkuil Formation as the distal end of a turbidite system, which becomes gradually more proximal in the upper parts. The slump zones in the upper Vischkuil Formation were interpreted by Wickens (1994) as an indication of slope conditions, and the entire formation itself as “background” hemipelagic deposits, interrupted by mud-rich and very fine-grained, low-density turbidites in the distal deep part of the basin. Current work is re-evaluating this model.

#### **2.2.3.2.3 Laingsburg Formation**

The boundary between the Vischkuil and Laingsburg Formation is gradational and defined as a horizon above which sandstone predominates over mudrock (Viljoen, 1992b). The Laingsburg Formation, consisting predominantly of very fine- to medium-grained sandstone and attaining a thickness of 750 m, is made up of six turbidite fan systems, informally called Fans A to F, each separated by a significant thickness (10 – 90 m) of hemipelagic and turbiditic mudstone (Sixsmith, 2000). The term ‘Fan’ is used to distinguish informally a sandstone-dominated unit of deep-water origin, without implications for its geometry (Grecula *et al.*, 2003). Fan A is interpreted as being deposited in a basin floor setting, constituting ~40% of the Laingsburg Formation with a thickness of 350 m southeast of

Laingsburg. Fan B, deposited in a base of slope setting, attains a thickness of 80 – 150 m, and Fans C to F (slope depositional setting) have thicknesses ranging between 10 – 100 m (Grecula, 2000; Sixsmith, 2000).

Sixsmith (2000) developed a high-resolution stratigraphic framework for Fan A in the Laingsburg area. He subdivided Fan A into seven time-stratigraphic depositional units (Units 1 to 7), bounded by regionally correlatable key surfaces, interpreted as flooding surfaces and sequence boundaries. Fan A is predominantly composed of alternating sheet-like, medium- to thick-bedded sandstone, rhythmic thin-bedded sandstone/siltstone units and shale units of varying thickness (Wickens, 1994). Fans B to F exhibit a more amalgamated internal character and stacked channel intervals (Grecula *et al.*, 2003).

Fan B is separated from Fan A by a shale unit, which is persistent over the entire outcrop region. In places along the base of the Fan B succession, are stacked, thick-bedded, mostly amalgamated, sandstone beds that are overlain by progressively thinner beds towards the top; elsewhere thin overbank deposits occur at the base (Grecula, 2000).

Fan C is separated from Fan B by a shale unit that attains a thickness of approximately 150 m. The fan itself is predominantly comprised of thick-bedded, massive and mostly amalgamated sandstone beds at the base, succeeded by thinner-bedded turbidites towards the top (Wickens, 1994; Grecula, 2000).

Fan D is comprised of two closely spaced sandstone-rich units and is separated from Fan C by 180 m of basin shale (Wickens, 1994; Grecula, 2000). A thick unit of mudstone separates Fan E from Fan D and is dominated by muddy sandstone and thin beds of massive sandstone (Grecula, 2000). Fan F is separated from Fan E by a thick unit of mudstone as well, and consists predominantly of muddy sandstone and thin beds of massive and parallel-laminated sandstone (Grecula, 2000).

#### **2.2.3.2.4 Fort Brown Formation**

The Fort Brown Formation overlies the Laingsburg Formation with a gradational contact at the top of Fan F, attains a thickness of 205 m in the Laingsburg area, and is predominantly comprised of slope and pro-delta mudstones with thick intervals of siltstone and sandstone (Smith *et al.*, 1993; Sixsmith, 2000). The lower part of the Fort Brown Formation is dominantly mud-rich, whereas the upper part becomes silt-dominated and exhibits traction structures, with high-frequency thickening upward cycles of 2 – 10 m thick (Wickens, 1994; Sixsmith, 2000). Soft-sediment deformation, including large-scale slumping, indicates the presence of unstable slope conditions from time to time.

Slow mud deposition characterised the initial stage of sedimentation of the Fort Brown

Formation (Kingsley, 1981). Subsequent fast regression occurred during which time a typical coarsening-upward sequence was formed. This is characteristic of progradation of a delta front into a relatively shallow water body with a depth above wave base. Cole (1992) interpreted the Fort Brown Formation to have been deposited in an overall regressive shallow marine environment during the late Permian.

#### **2.2.4 Beaufort Group and overlying formations**

The Beaufort Group is subdivided into the lower Beaufort Group (Adelaide Subgroup) and the upper Beaufort Group (Tarkastad Subgroup). It is exposed over an area of some 200 000 km<sup>2</sup> and attains a maximum thickness of approximately 7 km in the foredeep (Tankard *et al.*, 1982; Johnson, 1991). It thins gradually northward across the basin. Fluvial deposition of the Adelaide Subgroup commenced approximately 255 Ma ago, with palaeocurrents of the Abrahamskraal Formation trending NE. The Baviaanshoek and Hex River anticlinoria are believed to have controlled transport directions of the lower Beaufort Group, whereas east-trending megafolds in the southern CFB controlled the thickness distribution of individual sandstone bodies (De Beer, 1992).

The Adelaide Subgroup (late Permian) consists of the Koonap, Middleton and Balfour Formations in the southern (proximal) sector of the Karoo Basin (Tankard *et al.*, 1982; Smith *et al.*, 1993; Johnson *et al.*, 1996; Catuneanu *et al.*, 1998). The Koonap and Middleton Formations together form a single fining-upward unit, with an arbitrary contact between them based on a general change in lithofacies. The Koonap Formation is dominated by fining-upward cycles of silty mudstones and sandstones (deposited in braided and meandering river systems), whereas the Middleton Formation consists of an overall fining-upward succession of mudstones interbedded with sandstones (deposited in meandering and lacustrine systems) (Smith *et al.*, 1993; Catuneanu *et al.*, 1998). The contact relationship with the overlying Balfour Formation is unconformable. The latter formation consists of thick sandstone units deposited in a high-energy braided river environment.

The Tarkastad Subgroup (Triassic) consists of the Katberg and Burgersdorp Formations in the southern (proximal) sector of the Karoo Basin (Tankard *et al.*, 1982; Smith *et al.*, 1993; Johnson *et al.*, 1996; Catuneanu *et al.*, 1998). The Katberg Formation unconformably overlies the Balfour Formation and consists of thick, laterally extensive sandstones (deposited in a shallow, braided environment with pulsatory discharge), whereas the overlying Burgersdorp Formation (conformable contact) consists of thick fining-upward units of laterally extensive sandstones, overlain by siltstones and mudstones (deposited in mixed-load meandering river and floodplain environments) (Hiller and Stavakis, 1984; Smith *et al.*, 1993; Catuneanu *et al.*, 1998). The contact between the Tarkastad Subgroup and the overlying Molteno Formation of

the Stormberg Group is unconformable across the entire area of occurrence (Smith *et al.*, 1993; Catuneanu *et al.*, 1998).

Uplift of southern Africa, related to the final coalescence of Pangea (Veevers *et al.*, 1994), occurred after the deposition of the upper Beaufort Group and resulted in the consequent erosion of the Beaufort Group strata during this Middle Triassic hiatus. Renewed subsidence in the Carnian (235 – 223 Ma) was associated with the deposition of the fining-upward fluvial sediments of the Molteno and Elliot Formations of the Stormberg Group (Turner, 1983; Smith *et al.*, 1983; Johnson *et al.*, 1996).

The Stormberg Group consists of the Molteno, Elliot and Clarens Formations. Braided low-sinuosity rivers deposited the sandstone-rich Molteno Formation, whereas high-sinuosity meandering rivers deposited the Elliot Formation. The overlying Clarens Formation, which typifies the culmination of the upper Karoo Supergroup at the end of the late Triassic, was deposited during arid, aeolian conditions, with massive, loess-type deposits as well as cross-bedded dunes being present (Visser, 1984; Johnson *et al.*, 1996). Wetter climatic episodes during the Clarens Formation deposition have been identified by the presence of fluvial and playa lake deposits (Smith *et al.*, 1993).

The Clarens Formation is overlain by the basaltic lavas of the Drakensberg Group (1400 m thick), and its equivalents (Tankard *et al.*, 1982; Smith *et al.*, 1993; Johnson *et al.*, 1996; Turner, 1999). This volcanic episode lasted until the early Jurassic and terminated Karoo Basin development. This was followed by mid- to late Mesozoic extension, leading to the break-up of Gondwana (De Wit and Ransome, 1992).

## Chapter Three

### 3 Spectral Gamma Ray Analyses

#### 3.1 Analytical techniques

Natural radioactivity in sedimentary rocks originates from the decay of unstable isotopes, which emit alpha, beta and gamma rays. The spectral gamma ray (SGR) tool measures the total gamma ray (GR) and the individual contribution from the three major radioactive sources, namely  $^{40}\text{K}$ ,  $^{238}\text{U}$  and  $^{232}\text{Th}$ , in a given time. The total radioactive component of a sedimentary rock could thus be estimated, which is a function of its chemical and mineralogical composition. It can therefore be regarded as a real time multi-element profile.

The GR log is extremely useful, since it is a first indicator of lithology. Higher GR values indicate a higher percentage of shale. Sandstones usually show low GR values. The reason for this is based in the mineralogy of the rocks. K occurs in the clay silicate structure (including micas) and in rock-forming minerals, such as feldspars; U behaves as an independent constituent, is loosely associated with secondary components and peaks on logs are commonly associated with condensed sequences and unconformities; Th is extremely stable and is associated with heavy minerals such as zircon, thorite, monazite, epidote and titanite (Rider, 1986). Shales thus show high GR values due to their mineralogy of primarily clay minerals (including micas), as well as possible fine fractions of feldspar. Quartz, the principal component of coarse-grained detrital rocks, shows no radioactivity, the reason for sandstones showing low GR values (Rider, 1986).

It should be noted that problems could arise from using only the GR log for facies interpretation. In sedimentary rocks consisting of a mixture of quartz sand and clay, high GR readings are usually taken to indicate high clay content. However, this is not always the case, since all that is radioactive is not necessarily clay and clay is not always radioactive (Rider, 1990). Sandstones that contain, for example, a high modal percentage of K-feldspar (increase in K), a relatively large amount of heavy minerals such as zircon, monazite or titanite (increase in U), or even a large amount of phosphates (increase in Th), will strongly influence the natural radioactivity of the rocks and thus give high GR values, comparable to those normally given by clay sediments. A silty clay, composed mainly of kaolinite, will give a very low natural radioactivity. Clay mineral diagenesis in sandstones also commonly causes changes in the distribution of natural radioactivity in minerals (Rider, 1990). For example, dissolution of detrital K-feldspar and neof ormation of illite will change the location of K in minerals and thereby increase the radioactivity present in the clay-size fraction (Rider, 1990). GR log shapes are also often used to determine sandstone grain size trends and hence depositional facies. However, natural variability in the relationships between GR log values

and clay content and between clay content and grain size make this tenable only under very limited (and definable) conditions (Rider, 1990). This means that a universal application of GR log shape to grain size trend and depositional facies should be approached with care.

U, Th and K abundances were measured from the sections with a portable multi-channel scintillation spectrometer (Exploranium GR320) and detector (GPX-21). The sedimentary successions were logged by measuring the gamma radiation at an average vertical spacing of 50 - 75 cm over a selected time interval, namely 180 seconds for the argillaceous units and 240 seconds for sandstone. Instrument precision is better than  $\pm 10\%$  for all elements when using these durations (Løvborg and Mose, 1987; Andersson and Worden, 2004). Th/K and Th/U ratios are not measured automatically by this device and must be derived by extraction of the U, Th and K counts from the combined K + U + Th measurements. Graphic sedimentological logs were constructed at the same time and the GR sample points were correlated to these logs.

The detector-formation contact is critical, since the crystal mounted in the detector records the radiation to an approximate depth of 14 cm penetration and a surface diameter of 80 cm (Løvborg *et al.*, 1971; Andersson and Worden, 2004). This is for a flat, unweathered rock surface. A convex surface will give underestimated readings, whereas a concave surface will give overestimated readings (Svendsen and Hartley, 2001). For this study, great care was taken to ensure representative sampling. However, in practice, measurements have to be recorded from surfaces with irregularities. Due to weathering and rubble coverage of minor parts of some sections, trenching was sometimes necessary to expose unweathered surface exposures. Readings from a reference point were taken at the start and end of every field day to identify potential analytical drift of the instrument, which showed a precision of  $\pm 5\%$ .

SGR data successfully illustrate lateral and vertical variations in the geochemistry of sandstones and siltstones (Andersson and Worden, 2004). Sedimentological changes in measured vertical sections show close similarity to high-resolution SGR logs. Genetic sandstone units, which often form fluid flow units as well, are recognisable in GR logs and application of this technique is promising for integrated sequence stratigraphic analyses and reservoir characterisation (Aigner *et al.*, 1995). SGR logs help define bed boundaries and are useful in solving correlation problems.

The surface GR logs (scintillation spectrometer profiles) constructed for the Tanqua region adds to 1922 readings in total, 14 vertical profiles with a total length of 1212.24 m and 13 horizontal profiles of 430 m in total. For the Laingsburg area there are 2566 readings in total, consisting of 4 vertical profiles with a total length of 2175.35 m. The SGR logs from the measured total counts (cps), K (%), U (ppm), Th (ppm), along with ratios of Th/U, Th/K and U/K data, were plotted against height above the base of measured sedimentological sections.

This enables the study of Th/U, Th/K, U/K and total radioactivity as a function of stratigraphy and the gross radioactive character of the lithostratigraphic units.

Vertical profiles are denoted as V1 – V20 and horizontal profiles as H1 – H13. In both the Tanqua and Laingsburg depocentre sections, work done are presented and discussed against the background of basin stratigraphy: in the Tanqua depocentre from the uppermost unit of the Skoorsteenberg Formation (Unit 5) to the upper slope and deltaic deposits of the Kookfontein and Waterford Formations; and in the Laingsburg depocentre from the basin-floor deposits of the Collingham Formation, the basin-floor and slope deposits of the Vischkuil and Laingsburg Formations and the shelf edge deposits of the Fort Brown Formation.

### 3.2 Objectives

- i. To what extent do the SGR data for the sandstones and siltstones differ within each of the depocentres?
- ii. Can SGR data be used as a correlation tool for high-resolution stratigraphy throughout both depocentres?
- iii. Are there differences in the average SGR data for the sandstones and siltstones in a downcurrent direction in the Tanqua depocentre?
- iv. Are there differences in the SGR data between the Collingham, Vischkuil, Laingsburg and Fort Brown Formations in the Laingsburg depocentre?
- v. Are there differences or any significant trends in the SGR data between Fans A to F of the Laingsburg Formation?
- vi. How do the SGR data relate to K, Th and U geochemical data obtained from XRF analyses?

### 3.3 Sequence stratigraphy and shelf edge deltas

Sequence stratigraphy has evolved over the past few decades and changed the way in which geologists interpret the development of sedimentary environments in time and space.

The term “sequence” in stratigraphic analysis is defined as “a stratigraphic unit composed of genetically related strata bound at the top and bottom by unconformities or their correlative conformities” (Vail *et al.*, 1977; Posamentier *et al.*, 1988; Van Wagoner *et al.*, 1990). This definition provides us with a genetic stratigraphic unit that has unconformities, across which significant changes in the depositional regime occur, rather than within. Stratal architecture and lithologies can thus potentially be predicted and modelled with this method (Jervey, 1988; Van Wagoner *et al.*, 1990). The detailed sequence stratigraphic model from Exxon scientists has been well established (Jervey, 1988; Posamentier *et al.*, 1988; Van Wagoner *et al.*, 1990; Haq, 1991; Vail *et al.*, 1991). However, for successful application of this model, local control

mechanisms, such as subsidence rate, type of basin, sediment supply rate and the nature of the depositional system must be taken into account (Posamentier and Vail, 1988).

### **3.3.1 The highstand systems tract (HST)**

Within a cycle of relative sea-level change, the package of sediment deposited between the point of maximum relative sea-level rise (maximum flooding surface) and the highest point of relative sea-level is termed the highstand systems tract or HST (Figure 3.1) (Vail *et al.*, 1977; Posamentier *et al.*, 1988; Coe *et al.*, 2003). On the shelf it is composed of aggradational to progradational parasequence sets and the time-equivalent slope and deep basin environment are marked by suspension deposition, resulting in condensed shale intervals.

### **3.3.2 The falling stage systems tract (FSST)**

The combined effect of slow, but increasing rate of relative sea-level fall, and hence increased erosion and reducing accommodation, will be to increase supply of siliciclastic sediment into a reducing space on the shelf. This leads to an increasing rate of shoreline progradation (Plint and Nummedal, 2000; Coe *et al.*, 2003). Sediment will mainly be sourced from rivers that are incising valleys and transporting sediment into the sea in response to the fall in relative sea-level. When shorelines reach the shelf edge, progradation into excessive slope accommodation results in delta front collapse and initiation of basin-floor fan deposition. These sediments are termed the falling stage systems tract (FSST) or forced regressive deposits (Figure 3.2).



### **3.3.3 The lowstand systems tract (LST)**

The lowstand systems tract (LST) is developed from the point of maximum rate of sea-level fall (sequence boundary) through the lowstand of sea-level, to the point where sea-level begins to rise (Figure 3.3). This period is when the deep basin receives the maximum supply of sand, due to new or negative accommodation on the shelf.

### **3.3.4 The transgressive systems tract (TST)**

A transgressive surface will be formed when the rise in sea-level reaches a point where the long-term rate of creation of accommodation space is greater than the rate of sediment supply (Coe *et al.*, 2003). The sediments immediately overlying the transgressive surface form the transgressive systems tract (TST) (Figure 3.4).

**Highstand systems tract (HST)**

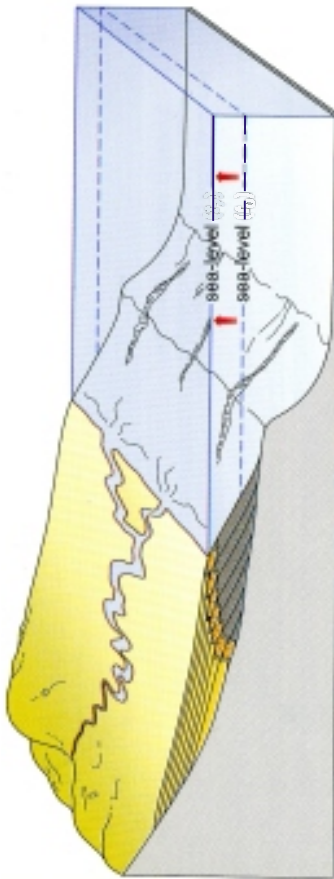


Figure 3.1 Typical geometry and features of the HST along a margin with a shelf break (after Coe *et al.*, 2003). Note that in the example illustrated, the HST did not prograde as far as the shelf break. Not to scale.

**Lowstand systems tract (LST)**

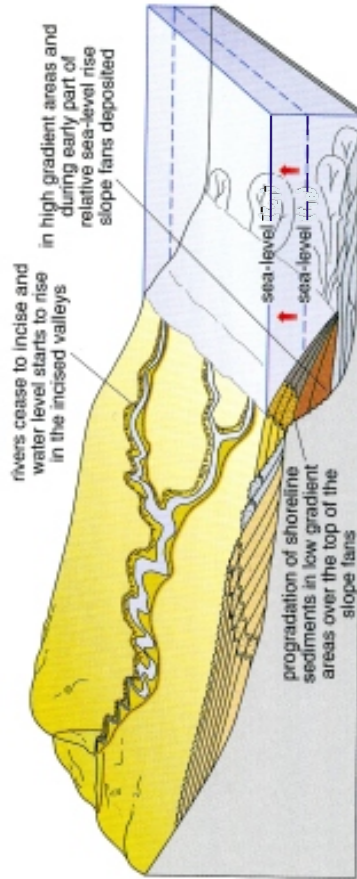


Figure 3.3 Geometry and features of the LST along a margin with a shelf break (after Coe *et al.*, 2003). Initially, submarine slope fans may be deposited until the gradient is low enough and sea-level high enough that the shoreline can prograde out into the basin and coastline sediments can be deposited. Not to scale.

**Falling stage systems tract (FSST)**

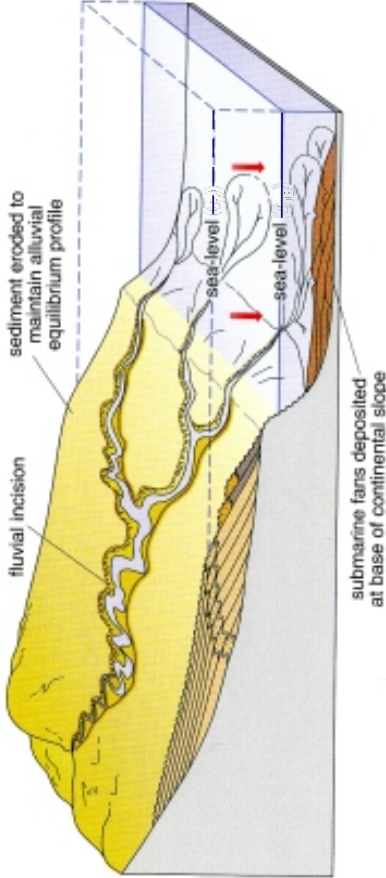


Figure 3.2 Geometry and features of the FSST along a margin with a shelf break (after Coe *et al.*, 2003). After relative sea-level fall below the shelf break, all further sediment was transported down the steep continental slope into the deep water where it was deposited as submarine fans on the basin floor. Not to scale.

**Transgressive systems tract (TST)**

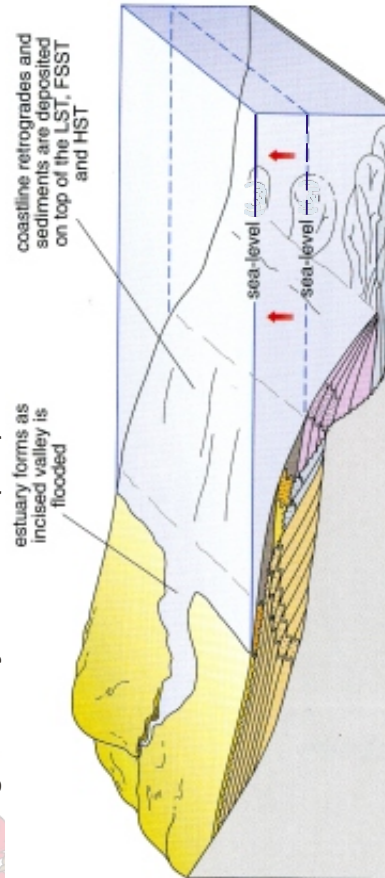


Figure 3.4 Geometry and features of the TST along a margin with a shelf break (after Coe *et al.*, 2003). Not to scale.

### **3.3.5 Application to the study area**

#### **3.3.5.1 Introduction**

The Kookfontein Formation represents a transition from lower slope (Unit 5, Skoorsteenberg Formation) to shelfal (Waterford Formation) deposits, thus marking construction of the slope and shelf edge in the Karoo Basin. Liverpool Ph.D. student, R.J. Wild, is currently concluding a detailed sedimentological study, and the results are serving to add further detail to the earlier studies by Wickens (1994). Fieldwork for this project was undertaken in collaboration with Wild, within the Slope project and therefore some of the sedimentological interpretations are taken from his work (with due acknowledgement). These new findings indicate that the prograding Ecca coastline was subject to mixed influences of river, waves and minor tidal processes. No evidence for subaerial exposure was found in the Kookfontein Formation. The key points in terms of facies associations defined by Flint *et al.* (2004) and Wild (*in preparation*) within the Slope project are summarised in Table 3.1.

#### **3.3.5.2 Shelf edge deltas and shelf construction**

Shelf edge deltas typically develop during and immediately after a significant fall in sea-level (Porębski and Steel, 2003). In this setting, deltaic shorelines can move far out across the shelf, often into a position at or near the shelf-slope break (Coleman *et al.*, 1983; Mellere *et al.*, 2002).

In well-documented examples from the Eocene of Spitsbergen (Plink-Björklund *et al.*, 2001; Mellere *et al.*, 2002; Plink-Björklund and Steel, 2002), the upper slope apron consists of distributary channel and mouth bar deposits in the shelf edge reaches, passing downslope to slope channels/chutes that feeds turbiditic lobes and spillover sheets. During subsequent sea-level rise, estuaries develop at the shelf edge and are marked by tidal deposits, overlain by marine flooding surfaces.

The occurrence of six regionally identified coarsening- and thickening-upward cycles have been identified within the Kookfontein Formation (Flint *et al.*, 2004; Wild, *in preparation*). Each of these is shortly described below, using the north-facing slope of Pienaarsfontein se Berg as type locality (Figure 3.5).

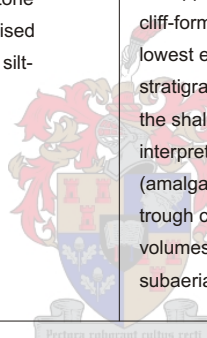
Cycle 1: Cycle 1 is ca. 75 m thick and overlies the regionally developed 12 m thick shale unit that overlies Unit 5. The lowermost 38 m of stratigraphy is represented by thin-bedded, ripple-laminated siltstones and very fine-grained sandstones, interbedded with claystones and fine siltstones. This is overlain by a coarsening- and thickening-upward succession of thin-bedded, ripple-laminated sandstones. Overlying the thin-bedded material is

Table 3.1 Interpretation of the sedimentology and depositional environments of the Kookfontein Formation/lower Waterford Formation, Tanqua depocentre.

OBSERVATIONS	INTERPRETATIONS
<b>Lithologies and sedimentary structures</b>	<b>Flint <i>et al.</i> (2004); Wild (<i>in preparation</i>)</b>
<p>Claystone, siltstone-claystone interbeds and concretionary horizons. Usually structureless or parallel-laminated.</p>	<p><b>Hemipelagic association</b>            Fall-out of clay from suspension in the water column and deposition of silt from extremely weak, distal turbidity currents during times of low sediment supply, marking times of flooding and storage of sand on the shelf. Found in basin-floor, slope and shelf positions.</p>
<p>Claystone, siltstone-claystone interbeds, siltstone-sandstone interbeds, sandstone interbeds, medium-bedded sandstone, structureless sandstone sheets, structureless sandstone channels, concretionary horizons, and lag. Channel-fills consist of well-sorted and very fine- to fine-grained sandstones, massive to planar-laminated, commonly pervasive soft-sediment deformation and dewatering. Sandstone-siltstone interbeds show parallel-, current- and climbing ripple-lamination. Interbedded heterolithic units are often intercalated with intensely dewatered homogenous coarse siltstones, sandstones commonly exhibit loaded bases and low intensity soft-sediment deformation features.</p>	<p><b>Lower slope association</b>            Early bypass in channels that fed basin-floor fans and later deposition included episodes of channel axis aggradation followed by 'spill' into overbank areas. Different channel systems were active at the same time, leading to a complex mosaic of channelised and sheet turbidite deposits, commonly modified by instability processes.</p>
<p>Claystone, siltstone-claystone interbeds, siltstone-sandstone interbeds, sandstone interbeds, medium-bedded sandstone and mass transport complexes. Thin-bedded graded and ripple-laminated siltstones and fine-grained sandstones, and very fine-grained graded sandstones interbedded with claystones and fine siltstones form aggradational packages. Ripple-laminated sandstone beds commonly have erosive bases, marked by claystone rip-up clasts.</p>	<p><b>Mid-slope association</b>            Accretion to the mid-slope of thinly bedded sheet turbidites, commonly but not always exhibiting instability features. These deposits may be interrupted by mass transport complexes that represent remobilisation of shelf material during lowering of relative sea-level and also by slope channels.</p>
<p>Siltstone-claystone interbeds, siltstone-sandstone interbeds, medium-bedded sandstones and mass transport complex. Thin-bedded, sheet-like sandstones are common, occurring in thickening-upward packages. In addition, thin-bedded successions of plane parallel-laminated and graded, current ripple-laminated very fine-grained sandstones, marked by small (0.5 - 1 m) deep incision surfaces occur locally. Also present are interbedded organic-rich, ungraded fine-grained sandstones, climbing ripple-laminated graded fine-grained sandstones and thin deformed siltstone units. Locally, zones of highly deformed sandstone, with large blocks of sandstone supported by a very fine-grained matrix are found.</p>	<p><b>Upper slope association</b>            Accretion of turbidites to the upper slope and local preservation of the products of episodes of shelf edge collapse and the influence of oversteepened shelf edge shorefaces. The presence of scour surfaces and parallel-laminations within the turbidites may indicate deposition via sustained turbidity currents originating from shelf edge deltas.</p>

Table 3.1 continued

<p>Siltstone-sandstone interbeds, sandstone interbeds, deformed-homogeneous, deformed-heterogeneous and channelised cross- and planar-laminated sandstones. Interbedded, ripple-laminated very fine-grained graded sandstones and siltstones with common dewatering fabrics.</p>	<p><b>Offshore transition/pro-delta association</b> Deposition below storm wave base by a mixture of density underflows from the toes of shorefaces and via suspension fall-out. The pervasive destabilisation is due to prograding over the shelf edge and onto the upper slope.</p>
<p>Siltstone-sandstone interbeds, sandstone interbeds, medium-bedded sandstone, channelised cross- and planar-laminated sandstone and rippled silt-sand-clay interbeds. Some of these deposits are highly regular with thick mudstone drapes to ripples.</p>	<p><b>Mid-shoreface/delta front association</b> The presence of amalgamated hummocky cross-stratification (HCS) signifies deposition above fairweather wave base, typical of lower to middle shoreface environments. The sharp bases of these units and common evidence for missing typical lower shoreface facies (such as non-amalgamated HCS beds) indicate a basinward shift in facies. Due to the regular development of thick mud drapes to ripples, these are interpreted as tidal flat deposits.</p>
<p>Siltstone-sandstone interbeds, sandstone interbeds, structureless sandstone sheets, structureless sandstone channels, lag, medium-bedded sandstones, channelised cross- and planar-laminated sandstones and rippled silt-sand-clay interbeds.</p>	<p><b>Upper shoreface association</b> Only present above a regionally mapped sharp surface in the upper Kookfontein Formation. It forms a prominent cliff-forming sandstone layer and includes the stratigraphically lowest extra-formational conglomerate layer in the Ecca Group stratigraphy. The facies organisation is interpreted to represent the shallowest water environments present. These are interpreted as a complex association of upper shoreface (amalgamated HCS to swaley cross-stratification (SCS) and trough cross-bedding), tidally influenced channels and minor volumes of tidal flat deposits. There is no evidence of subaerial exposure.</p>



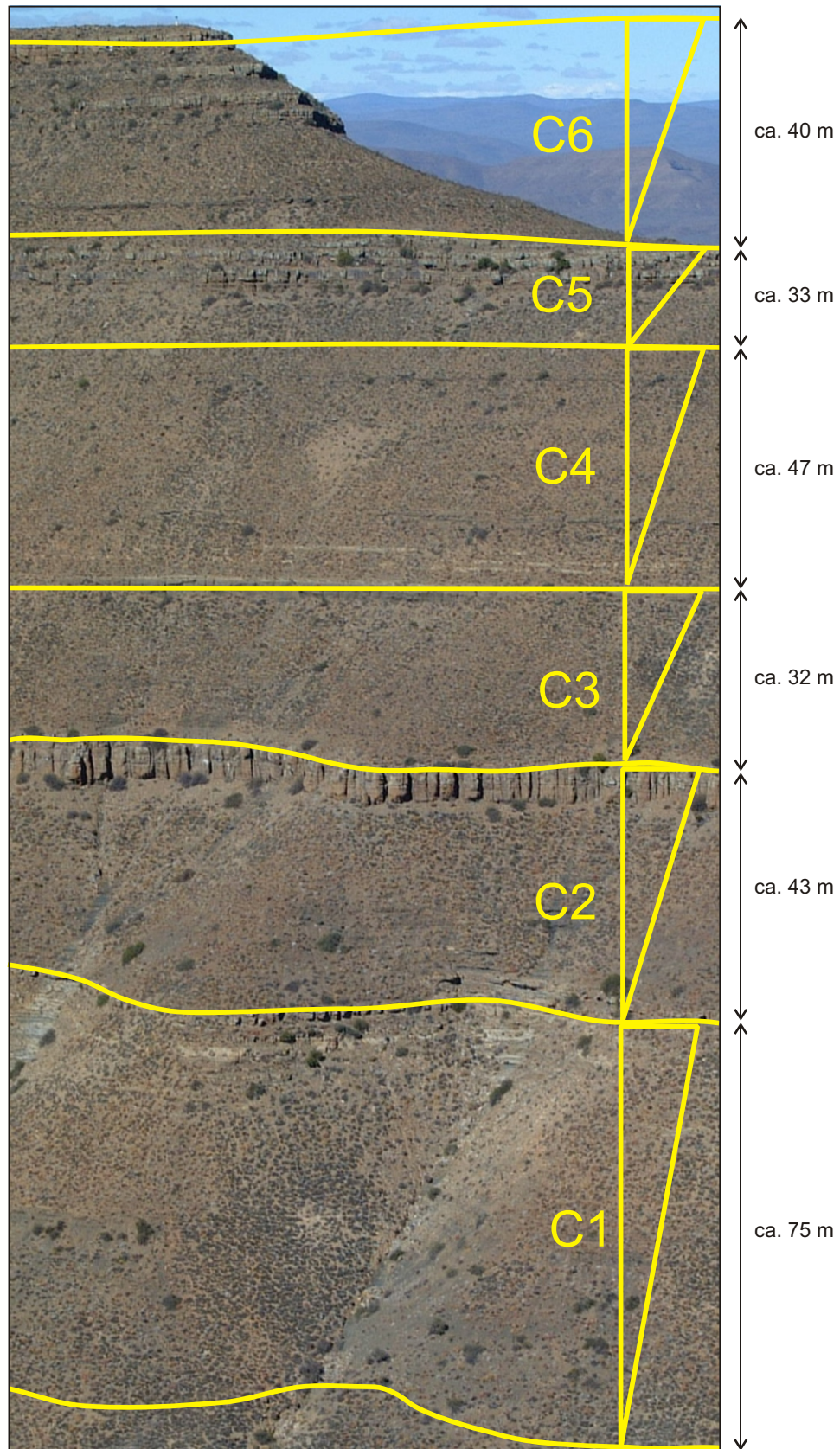


Figure 3.5 Photograph of Pienaarsfontein se Berg, showing the key stratigraphic sections (coarsening- and thickening-upward cycles 1 to 6) of the Kookfontein Formation (after Flint *et al.*, 2004; Wild, *in preparation*). View is to the south.

a 10 m thick package of highly deformed strata, which in turn is overlain by an abrupt change in facies, namely fine-grained sandstone with concave-up lamination that pass into ripple-laminated, fine-grained sandstones displaying bioturbation (bioturbation index of 2 – 3).

*Interpretation:* The lower part of the cycle is interpreted as the deposition of sheet-like turbidites that accreted on the mid- to lower slope. This cycle represents the first sedimentation following a period of starvation in the outer shelf, slope and basin-floor depositional environments due to a relative sea-level rise above Unit 5. The upper part of the cycle marks the accumulation of mid-slope sheet-like turbidites.

Cycle 2: Cycle 2 is ca. 32 m thick and a return to thin-bedded, ripple-laminated very fine-grained sandstones immediately above Cycle 1. The thin-bedded succession slowly thickens upwards, although it is abruptly overlain by a 4 - 5 m thick package of interbedded organic-rich fine-grained sandstones, ripple-laminated, fine-grained sandstones and thin deformed siltstone units. The interbedded package is abruptly overlain by ripple-laminated, fine-grained sandstones, representing a distinct change in facies. The top of Cycle 2 is marked by a 1 - 2 m thick package of interbedded organic-rich, ripple-laminated, fine-grained sandstone that has a distinctive mottled appearance, which is due to the pervasive burrows (bioturbation index 2 - 5). This facies is similar to that observed at the top of Cycle 1.

*Interpretation:* The base of this cycle represents the accumulation of sheet-like turbidity currents in an upper to mid-slope environment. Thin-bedded slope sediments are abruptly overlain by a ripple-laminated, fine-grained sandstone unit that forms a tabular architecture at outcrop, and is, therefore, interpreted as a lower shoreface that stepped out onto the upper-slope, leading to local gravitational failures and reworking by storm events. The well bioturbated organic-rich upper surface marks a depositional hiatus.

Cycle 3: Cycle 3 is ca. 36 m thick and the base is marked by a return to thin-bedded, ripple-laminated, very fine-grained sandstones, interbedded with claystones and siltstones. The top 10 m of Cycle 3 is marked by the abrupt transition to a 'striped' facies (cm-scale interbeds of white-coloured ripple-laminated sandstones and green-black siltstones). Soft-sediment deformed intervals are preferentially found towards the top of Cycle 3. The top 1 m of Cycle 3 is composed of fine-grained organic-rich, ripple-laminated sandstones displaying mud-filled burrows (bioturbation index 2 - 4) that give the sediment a mottled appearance, similar to that observed at the top of Cycles 1 and 2.

*Interpretation:* The thin-bedded facies represent accumulation of sheet-flow turbidity currents in an outer shelf to upper slope environment. Due to the stratigraphic position, regional extent and local soft-sediment deformation structures of this facies, it is interpreted as lower shoreface deposits, reflecting a period of starvation in clastic supply. The bioturbated organic-rich upper beds mark a depositional hiatus.

Cycle 4: Cycle 4 is ca. 50 m thick and composed of three approximately 15 m thick coarsening- and thickening-upward cycles that is broadly similar to the top of Cycle 3. Typically the lower 5 - 6 metres of each 15 m thick sub-cycle comprises interbedded ripple-laminated, very fine-grained sandstones and siltstones, with common dewatering fabrics. The upper 3 - 4 m of the sub-cycles is marked by highly deformed units containing contorted sandstone blocks supported by a coarse siltstone matrix. Some sections demonstrate that nearly the entire Cycle 4 succession is disrupted by soft-sediment deformation features.

*Interpretation:* The widespread soft-sediment deformation indicates the presence of local gradients, although an outer shelf environment of deposition is interpreted. The sub-cycles of Cycle 4 are therefore interpreted to reflect the progressive progradation of the lower shoreface to the shelf edge.

Cycle 5: Cycle 5 is ca. 32 m thick and composed of two sub-cycles. The coarse-grained component of the sub-cycles is more sand-prone than the underlying sub-cycles. The basal portion of the 16 m thick lower sub-cycle is composed of thin-bedded, ripple-laminated, very fine-grained sandstones interbedded with siltstones. The bulk of the 10 m thick sand-prone package at the top of Cycle 5 is composed of aggradational thin-bedded, fine-grained, ripple-laminated sandstones.

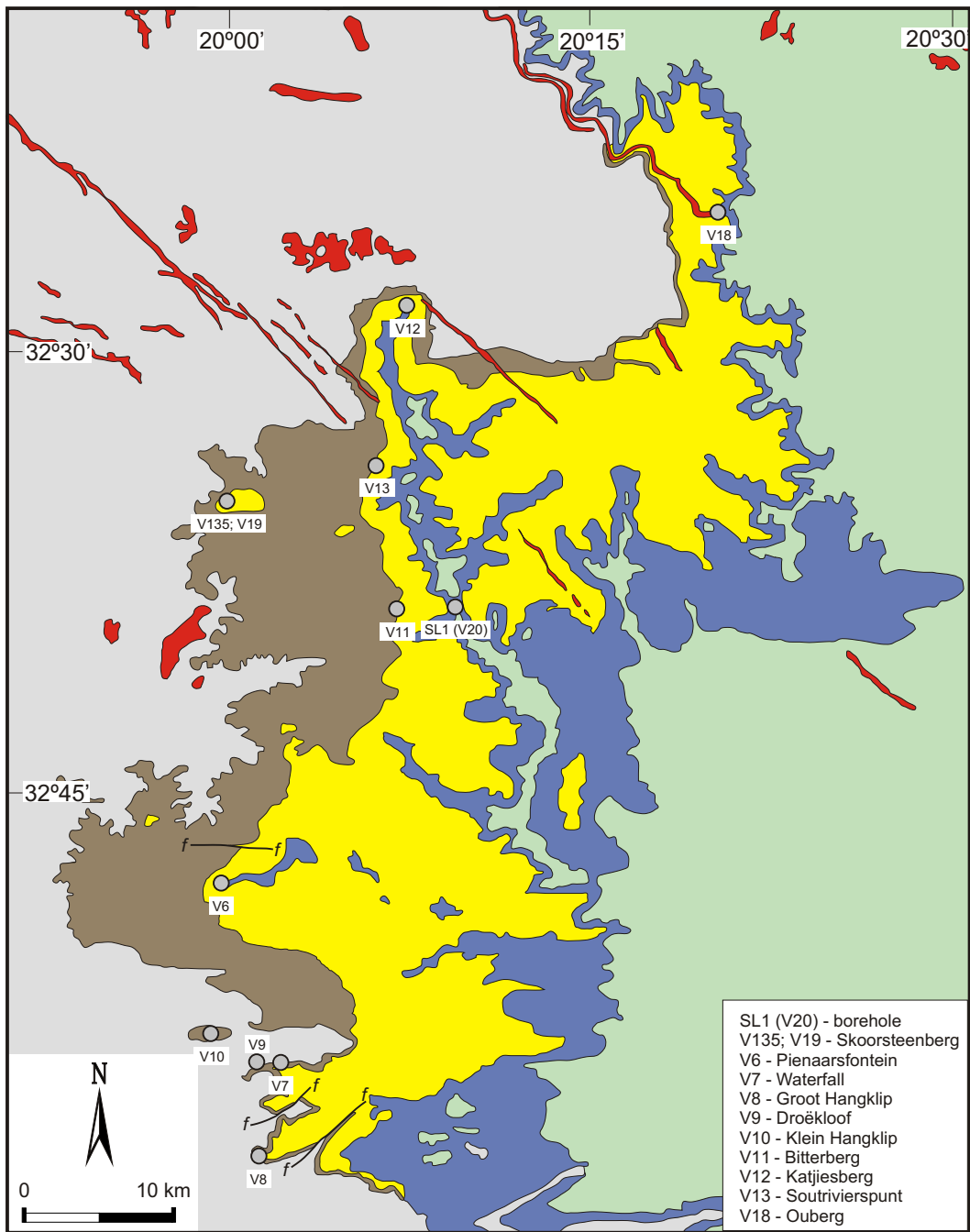
*Interpretation:* The coarser-grained nature of Cycle 5 suggests a more proximal depositional setting. This is supported by pervasive and large-scale hummocky cross-stratification and scour surfaces indicating the regular influence of storm events on the shelf. These cycles are interpreted to represent the progradation of the shoreface across the mid- to outer shelf.

Cycle 6: Cycle 6 is marked by a change in facies as a result of a period of high sediment supply. The cycle is ca. 20 m thick, with the lower 10 m comprising a unit of thickening upwards, thin-bedded, ripple-laminated sandstone. The upper sand-prone part of the cycle is dominantly composed of low-angle concave-up lamination (up to 20 cm in amplitude) that are commonly mantled by claystone rip-up clasts.

*Interpretation:* The marked increase in the supply of sediment across the basin above Cycle 5 is in part due to the construction of the shelf edge by the underlying progradational shoreface cycles, thereby reducing gradient. The increased availability of sand on the shelf either indicates that less sand were being transported to deeper water, and/or more sand-grade material was available.

### **3.4 Tanqua depocentre**

The regional development of the Skoorsteenberg, Kookfontein and Waterford Formations, with the locations of the measured sedimentological and GR profiles, are shown in Figure 3.6.



- SL1 (V20) - borehole
- V135; V19 - Skoorsteenberg
- V6 - Pienaarsfontein
- V7 - Waterfall
- V8 - Groot Hangklip
- V9 - Droëkloof
- V10 - Klein Hangklip
- V11 - Bitterberg
- V12 - Katjiesberg
- V13 - Soutrivierspunt
- V18 - Ouberg

**Geological legend**

Mesozoic	Jurassic	Palaeozoic	Karoo Supergroup	▲ Beaufort Group	Abrahamskraal Fm	Dolerite	Mudstone, siltstone, sandstone, thin cherty beds
				Waterford Fm	Sandstone, siltstone, mudstone, shale		
	Permian		Ecca Group	Kookfontein Fm	Shale, siltstone, thin sandstone beds	Sandstone, siltstone, shale	
			Skoorsteenberg Fm	Tierberg Fm		Shale	

Figure 3.6 Geological map of the Tanqua depocentre, Karoo Basin, South Africa, showing the Skoorsteenberg, Kookfontein and Waterford Formations and measured sedimentological and SGR profile locations. Geological information compiled from the Clanwilliam 3218 and Sutherland 3220 maps. 1:250 000 Geological series, Geological Survey of South Africa.

### 3.4.1 Skoorsteenberg Formation

The Skoorsteenberg Formation contains five deep-water turbidite depositional systems, almost completely exposed over 650 km<sup>2</sup>. A progradational trend can be seen in the more than 450 m thick succession, from distal basin-floor (Fan 1) through basin-floor sub-environments (Fans 2, 3 and 4) to a slope setting for Unit 5 (Johnson *et al.*, 2000; Wach *et al.*, 2000; Wickens and Bouma, 2000; Goldhammer *et al.*, 2000). Deposition was unrestricted in the broad, open style N-S trending Tanqua depocentre. The sandstones are very fine- to fine-grained, virtually without any porosity or permeability, resulting from high-grade diagenetic to low-grade metamorphic changes during burial to depths of about 7 km (Rowell and De Swardt, 1976; Wickens and Bouma, 2000). The thickness of the sand-rich turbidite systems vary from 20 – 60 m, and are separated by basin shales, with varying thickness of 20 – 75 m (Wickens and Bouma, 2000). Five major lithofacies have been recognised, namely massively bedded sandstone, horizontally and ripple cross-laminated sandstone, parallel-laminated siltstone, parallel-laminated shale and a micaceous, silty plant-fragment facies (Wickens and Bouma, 2000).

The outcrop section of Groot Hangklip (V8) can be interpreted as pro-delta deposits, followed by channel-fill complex and slump deposits. The SGR logs measured at Groot Hangklip (V8) in the southern part of the Tanqua depocentre (Figure 3.7) display a relatively non-uniform response for the U/K, Th/U and Th/K data (Figure 3.8). U/K for the sandstones are rather constant, at between 0.85 – 2.22 (avg. = 1.55, n = 97), whereas the Th/K data are between 2.93 and 8.22 (avg. 6.25, n = 97), across the section. The sandstone Th/U data are all slightly higher, with a more erratic response ranging between 3.08 and 8.50 and showing an average of 4.09 (n = 97). Higher values of both the Th/K and Th/U data are present in the soft-sediment deformation deposits. The sandstones' total counts log displays an erratic response as well.

The average total count (62 cps, n = 97) is intermittently disturbed by higher values (up to 101 cps), corresponding to zones of soft-sediment deformation. These higher values might be due to the zones containing a slightly higher clay fraction. Table 3.2 shows the averages and standard deviations of the total counts and ratios for the sandstones and siltstones.

The siltstone total counts have a higher average value than that of the sandstones, 70 cps (n = 38). There appears to be minor correlations between the Th/U log and the total counts log for the entire profile (Figure 3.8).

The proximal interchannel/overbank deposits at the Waterfall (V7) section consist of thin-bedded siltstones, interbedded with thin-bedded climbing ripple cross-laminated sandstone. The trends for the sandstone U/K, Th/K and Th/U measured at Waterfall (V7) (Figure 3.9) are

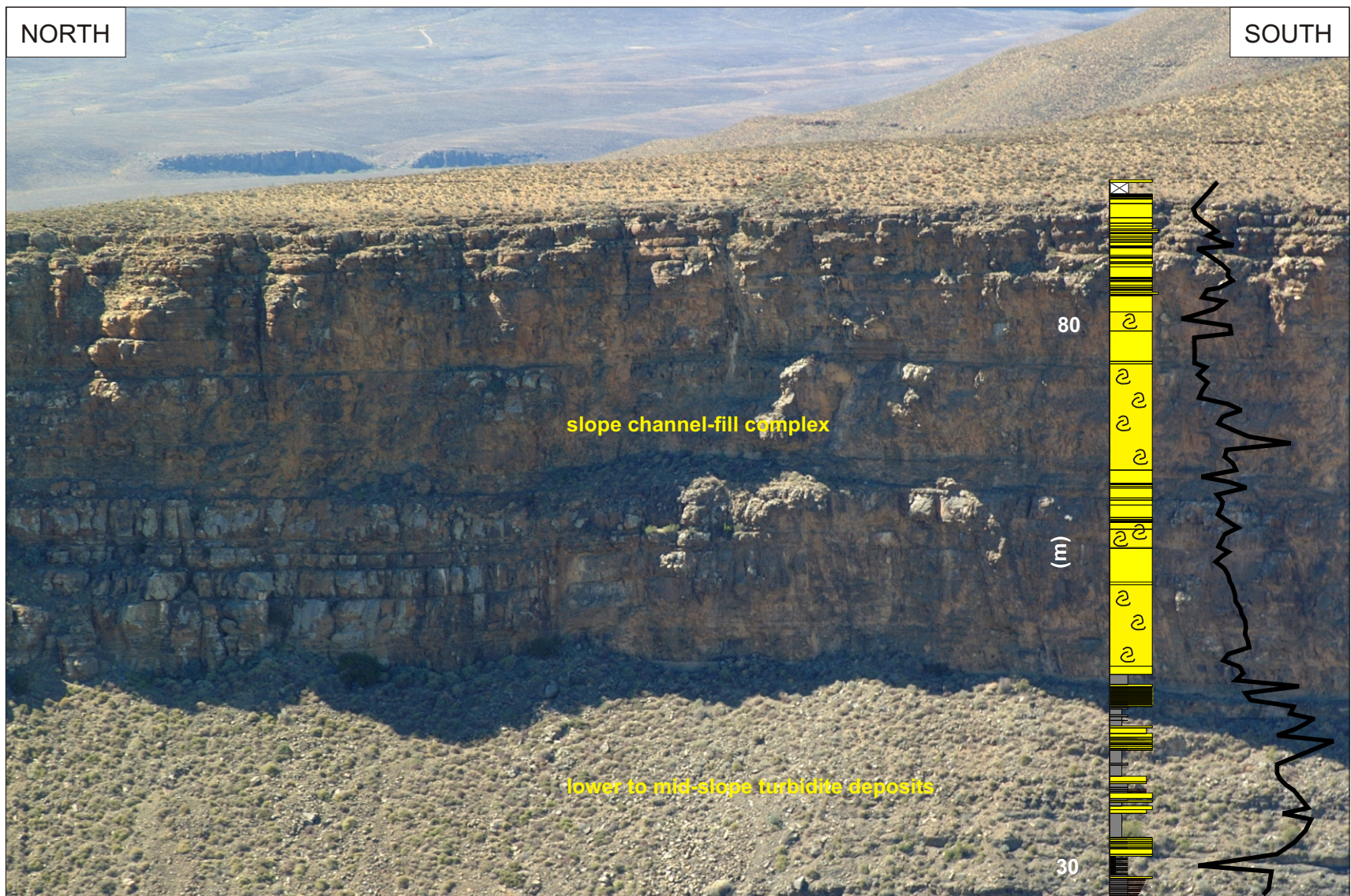
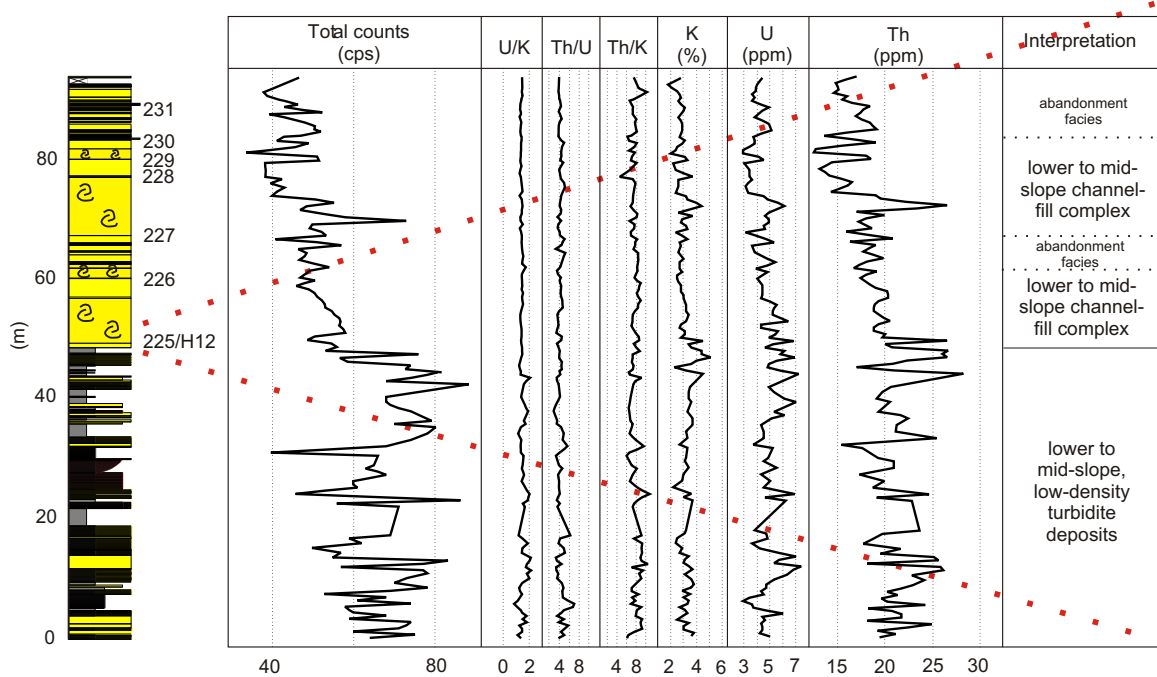
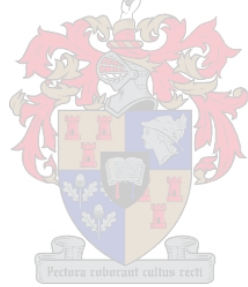


Figure 3.7 Outcrop setting of Unit 5 at Groot Hangklip (V8). Thick-bedded, predominantly structureless sandstones in a lower slope channel-fill complex. The upper part of the measured sedimentological and GR logs are shown. The logs were measured 10 m to the right within a gully. Location: GPS 32°56'23.6"S, 020°01'06.0"E

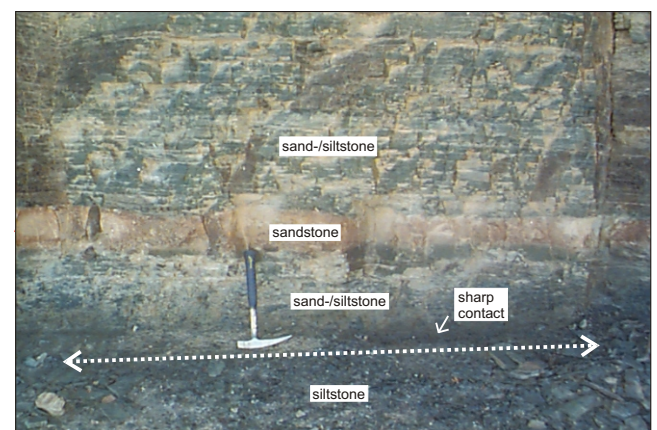


Facies key:

- Mudstone
- Siltstone
- Very fine to low medium sandstone
- Sandstone with soft-sediment deformational features



Soft-sediment deformation within an amalgamated sandstone succession. Hammer for scale (30 cm) is circled.



Alternating sandstone and siltstone facies below the overlying channelised sandstones.

Figure 3.8 Groot Hangklip (V8), representing the lower slope setting of the upper turbidite depositional sequence. Comparison between SGR logs and lithology. SGR results are from 152 measurements at an average vertical spacing of 50 cm. The location of a horizontal profile measured is indicated as H12 next to the lithology and samples taken as 225 - 231.

Table 3.2 Average total counts (cps), U/K, Th/K and Th/U from SGR measurements for profiles in Unit 5 of the Skoorsteenberg Formation. Confidence levels are at 95%.

Stratigraphy	Profile	n	Avg.		S <sub>e</sub>	Lower limit	Upper limit
Skoorsteenberg Formation (Unit 5)	<u>Groot Hangklip (V8)</u>						
	Sandstone	97					
	Total counts		62	8.42	1.71	40	90
	U/K		1.55	0.23	0.05	0.92	2.22
	Th/K		6.25	0.62	0.13	3.81	8.22
	Th/U		4.09	0.50	0.10	2.93	6.72
	Siltstone	38					
	Total counts		70	12.4	4.02	46	101
	U/K		1.56	0.29	0.09	0.85	2.18
	Th/K		6.49	0.85	0.27	5.20	8.50
	Th/U		4.27	0.77	0.25	3.42	6.97
	<u>Waterfall (V7)</u>						
	Sandstone	17					
	Total counts		64	11.3	5.46	46	82
	U/K		1.49	0.22	0.10	1.14	2.05
	Th/K		5.92	0.33	0.16	5.43	6.53
	Th/U		4.05	0.59	0.29	3.18	5.27
	<u>Droëkloof (V9)</u>						
	Sandstone	91					
	Total counts		55	6.41	1.34	38	79
	U/K		1.55	0.22	0.05	1.04	2.47
	Th/K		6.84	0.90	0.19	5.55	11.4
	Th/U		4.43	0.51	0.11	3.37	6.60
	Siltstone	5					
	Total counts		58	2.03	1.81	56	61
	U/K		1.54	0.09	0.08	1.42	1.62
	Th/K		6.56	0.13	0.12	6.39	6.71
	Th/U		4.27	0.23	0.21	3.98	4.54
<u>Klein Hangklip (V10)</u>							
Sandstone	66						
Total counts		56	6.73	1.66	39	83	
U/K		1.51	0.23	0.06	1.15	2.41	
Th/K		6.47	0.54	0.13	5.61	8.00	
Th/U		4.34	0.49	0.12	3.29	5.92	
Siltstone	3						
Total counts		62	6.62	7.64	55	68	
U/K		1.52	0.11	0.13	1.41	1.64	
Th/K		6.53	0.16	0.18	6.40	6.70	
Th/U		4.31	0.43	0.50	3.90	4.76	

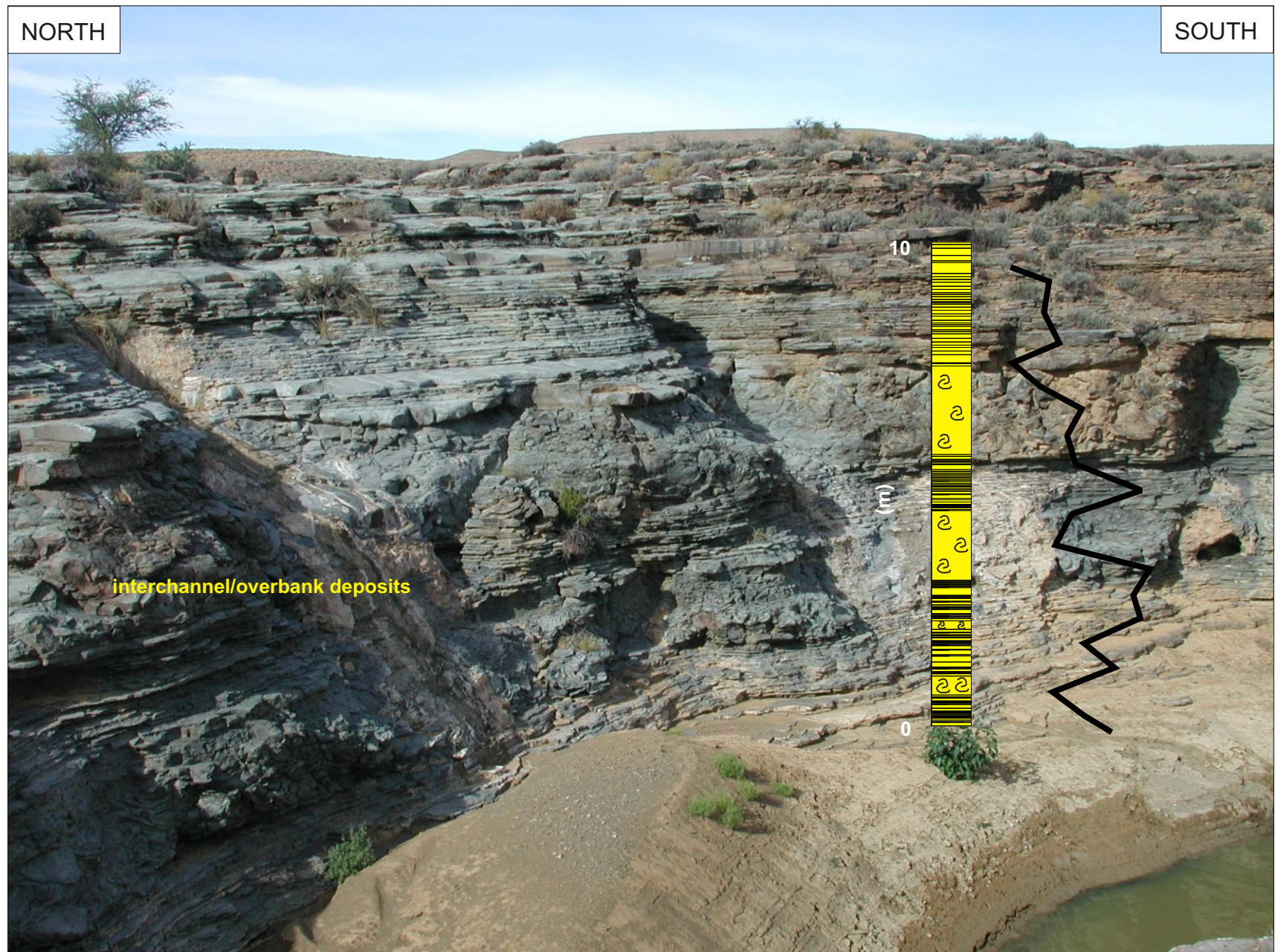
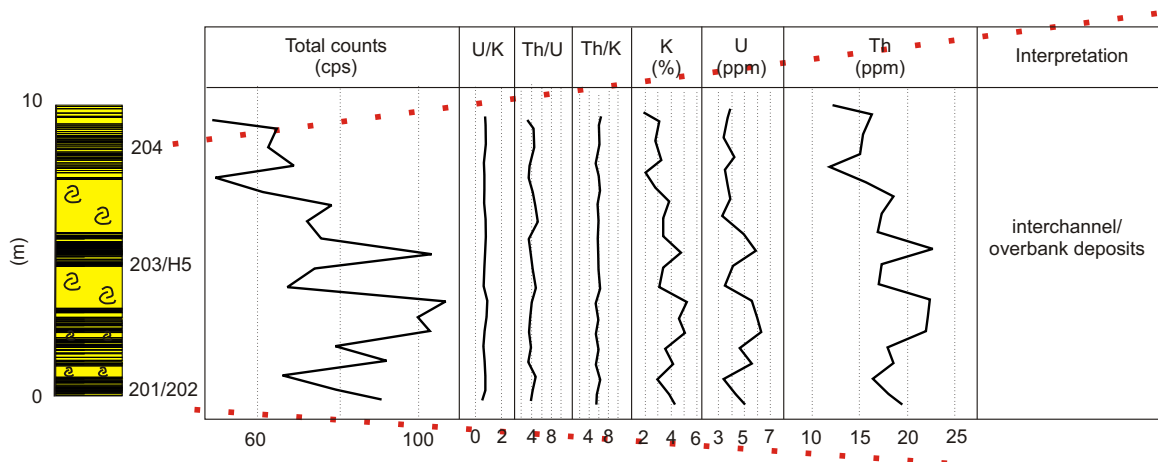
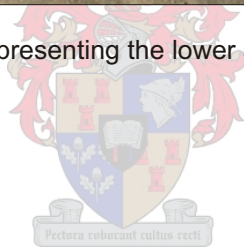
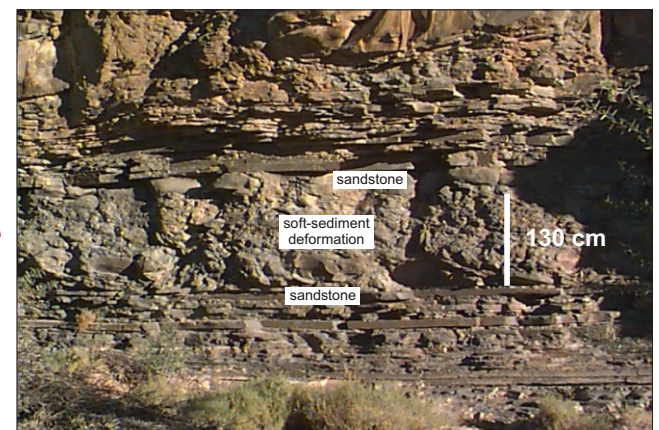


Figure 3.9 Sedimentological and GR logs at Waterfall (V7), representing the lower slope setting of the uppermost turbidite depositional sequence. Location: GPS 32°54'34.8"S, 020°02'15.5"E



Facies key:

- Mudstone
- Siltstone
- Very fine- to lower medium-grained sandstone
- Sandstone with soft-sediment deformational features



Soft-sediment deformation within an interchannel/overbank succession.



Low-amplitude sandstone wavy beds with thin silty intercalations and intermittent beds showing soft-sediment deformation.

Figure 3.10 Waterfall (V7), representing the lower slope setting of the uppermost turbidite depositional sequence. Comparison between SGR logs and lithology. SGR results are from 20 measurements at an average vertical spacing of 50 cm. The location of a horizontal profile measured is indicated as H5 next to the lithology and samples taken as 201 - 204.

relatively flat (Figure 3.10), with average values of 1.49 (n = 17), 5.92 (n = 17) and 4.05 (n = 17), respectively (Table 3.2). The total counts data are more erratic, showing an average value of 64 cps (n = 17) (Table 3.2; Figure 3.10). A horizontal profile, H5, measured in a sandstone bed below a unit displaying soft-sediment deformation, exhibits similar values for Th/K and Th/U, although the average total counts value is slightly higher (avg. = 78 cps, n = 6). The variation in data over distance measured is higher for V7 than for H5. Changes in U/K appear to be constant throughout, for both the vertical and horizontal profiles. The Waterfall unit can be traced throughout profiles V8, V9 and V10, and show similar patterns for the total counts profiles, with a sharp peak at the base of the unit (Figure 3.11).

The stacked channel-fill complex measured at Droëkloof (V9) overlies mid- to lower slope turbidite deposits. The sandstone and siltstone averages of U/K, Th/K and Th/U values measured at Droëkloof (V9) (Figure 3.12) are shown in Table 3.2. Sandstone Th/K and Th/U data show small deviations, corresponding to apparent anomalies in the total counts data, such as a high of 79 cps, compared to an average of 55 cps (n = 91) (Figure 3.13). It also corresponds to H13, which was taken in a sandstone bed with similar anomalous total counts values (highest value of 80 cps, avg. = 66 cps, n = 7). The total counts values increase with increase in the siltstone: sandstone ratio and units displaying soft-sediment deformation. Changes in U/K appear to be constant throughout, for both the vertical and horizontal profiles.

The outcrop section at Klein Hangklip (V10) can be interpreted as a channel-fill complex containing slump deposits. The total counts log measured at Klein Hangklip (V10) (Figure 3.12) is erratic, ranging between 39 – 83 cps. The sandstone average value is 56 cps (n = 66), whereas the siltstone average value is 62 cps (n = 3). The highest values correspond to alternating beds of sandstone and siltstone (Figure 3.13). The U/K, Th/K and Th/U data are relatively uniform (Table 3.2). It was not possible to measure any horizontal logs in this section.

The average Th/K and Th/U values for the measured profiles are all relatively uniform, as are the total counts values, with the slight exceptions of V7 and V8. These show slightly higher values, corresponding to increased siltstone: sandstone ratios and units displaying soft-sediment deformation within these profiles (Figures 3.8 and 3.10). Changes in the U/K data appear to be constant throughout, for both the vertical and horizontal profiles.

The outcrop sections of Skoorsteenbergrug (V19 and V135) show thick-bedded and amalgamated sandstone units, large-scale channel-fills and sheet deposits, with the first appearance of wave ripple-marked thickening upward cycles and slump units approximately 60 m above the top of Unit 5. These can be interpreted as the products of basin-floor to delta front deposition under gradually shoaling conditions.

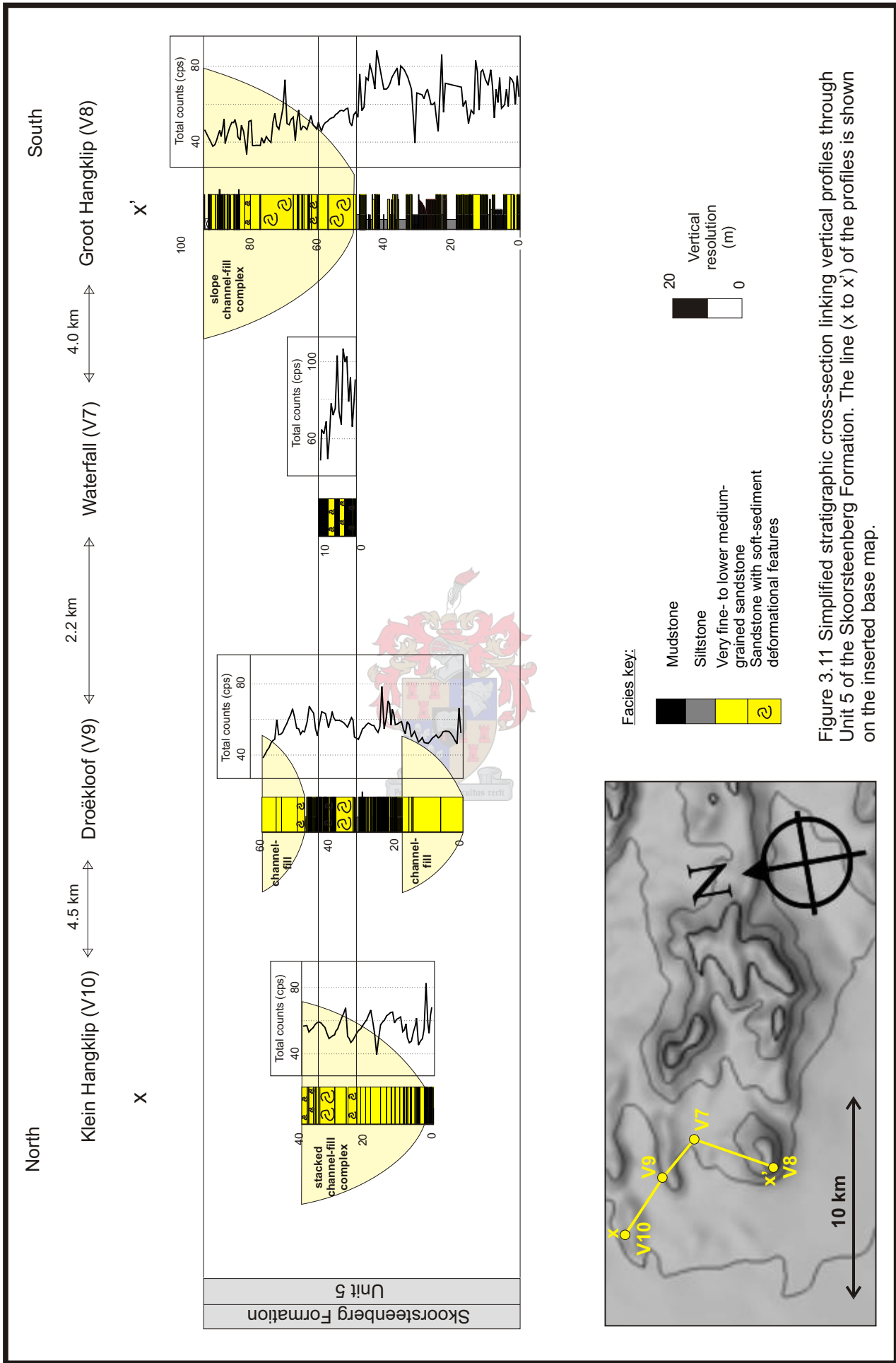


Figure 3.11 Simplified stratigraphic cross-section linking vertical profiles through Unit 5 of the Skoorsteenberg Formation. The line (x to x') of the profiles is shown on the inserted base map.

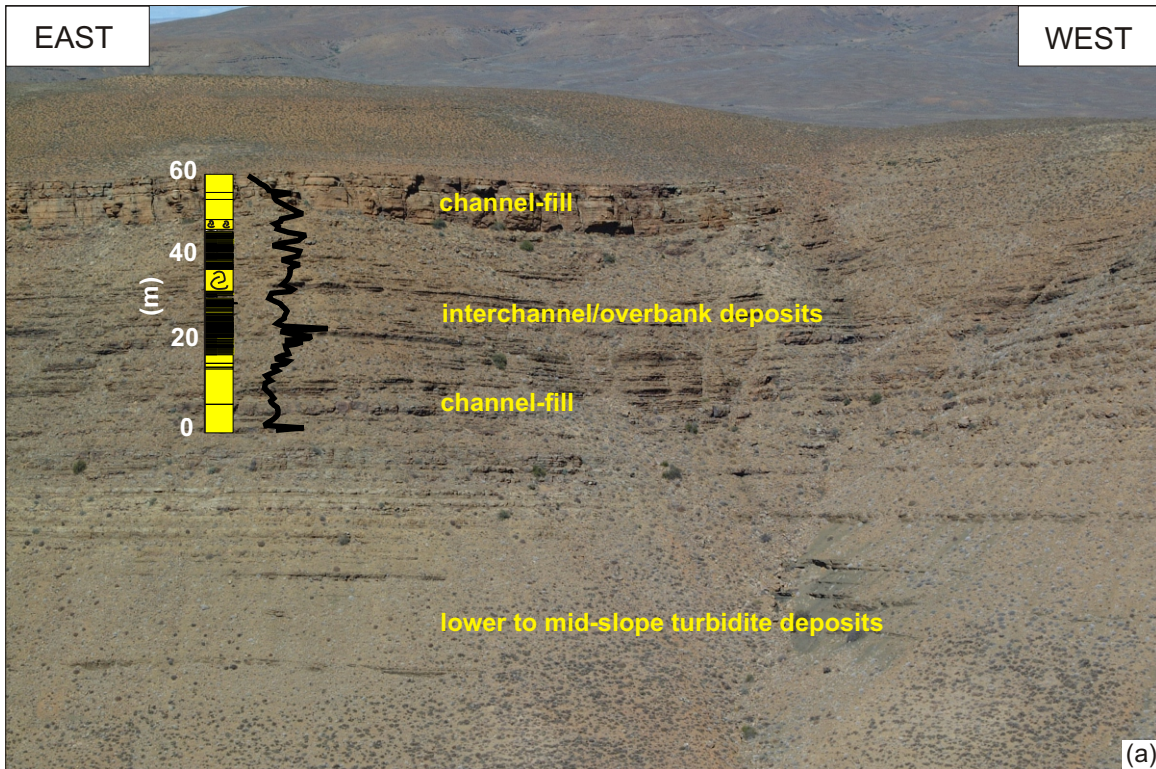


Figure 3.12 (a) Outcrop locality for the Droëkloof (V9) section. The E-W orientation of exposure resembles an oblique dip section. The sedimentological and GR logs are shown. Location: GPS 32°53'54.9"S, 020°00'57.8"E

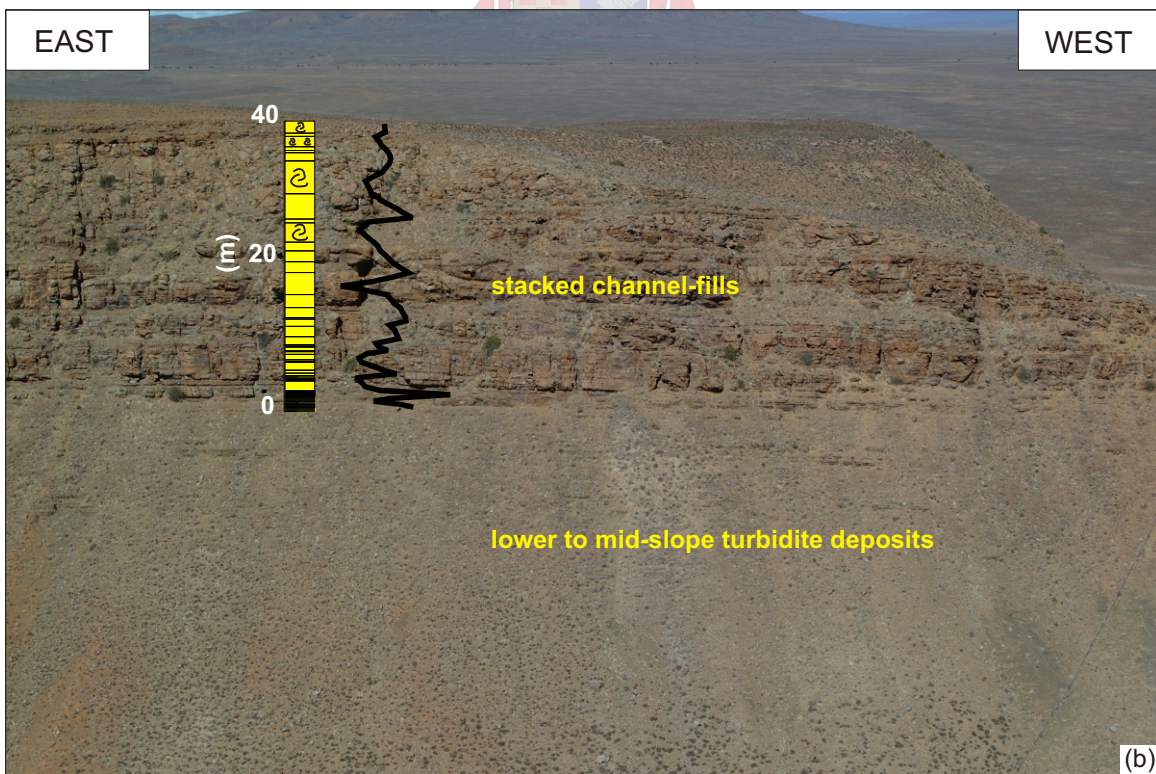
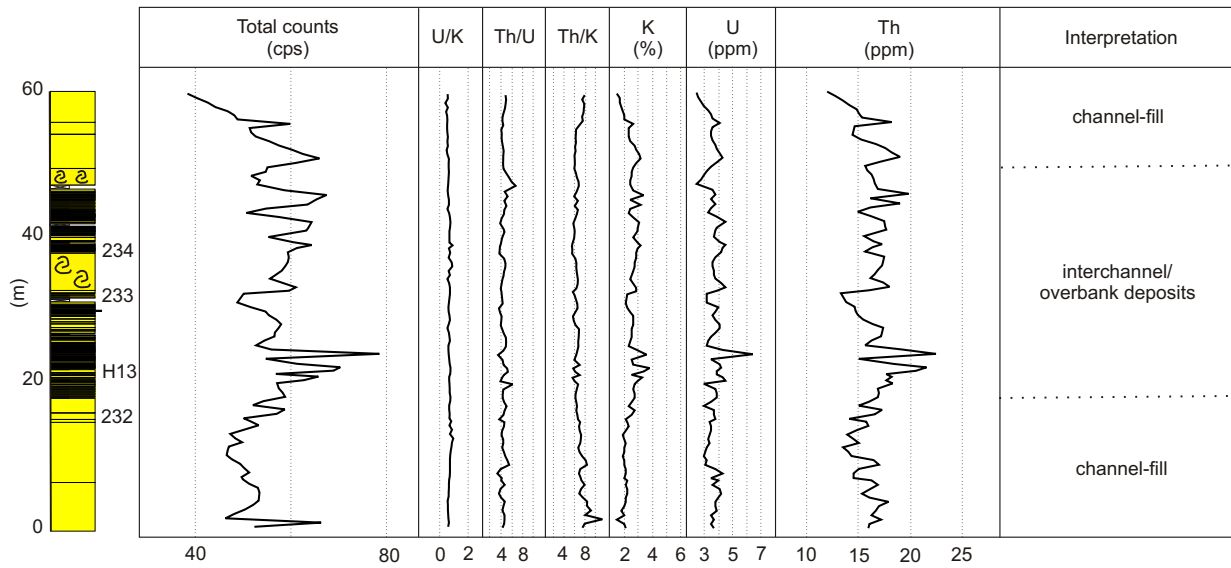


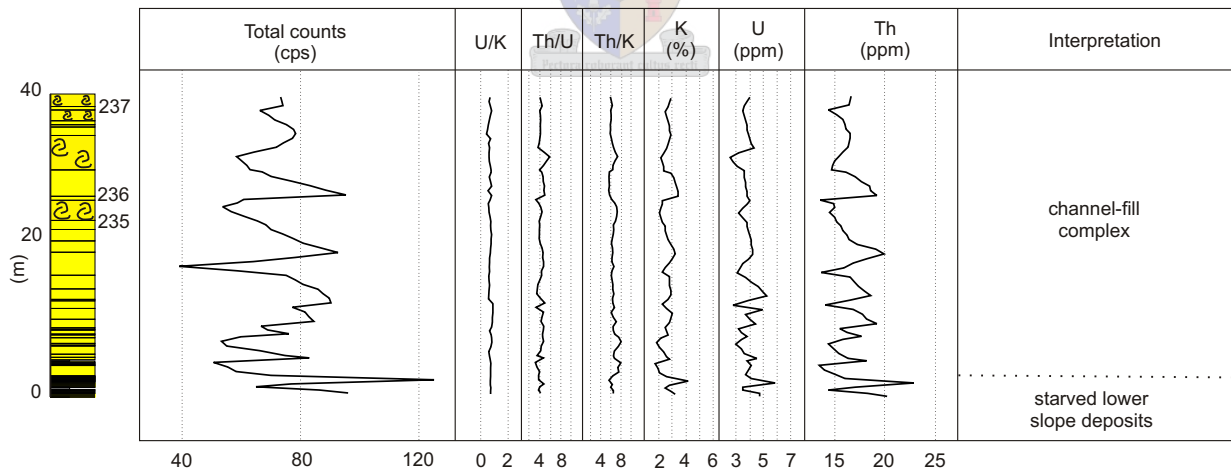
Figure 3.12 (b) The outcrop setting of Klein Hangklip (V10), interpreted as a lower slope channel-fill complex. Looking south, approximate dip section. The measured sedimentological and GR logs are shown. Location: GPS 32°52'40.5"S, 019°58'27.1"E



Facies key:

- Mudstone
- Siltstone
- Very fine- to lower medium-grained sandstone
- Sandstone with soft-sediment deformational features

Figure 3.13 (a) Droëkloof (V9), showing channel-fill and interchannel/overbank deposits on the slope setting of the upper turbidite depositional sequence. Comparison between SGR logs and lithology. SGR results are from 102 measurements at an average vertical spacing of 50 cm. The location of a horizontal profile measured is indicated as H13 next to the lithology and samples taken as 232 - 234.



Facies key:

- Mudstone
- Siltstone
- Very fine- to lower medium-grained sandstone
- Sandstone with soft-sediment deformational features

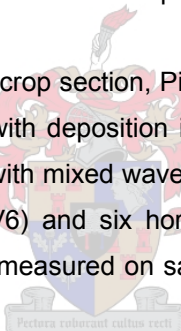
Figure 3.13 (b) Klein Hangklip (V10), showing lower slope turbidite deposits and a stacked channel-fill complex. Comparison between SGR logs and lithology. SGR results are from 69 measurements at an average vertical spacing of 50 cm. The location of samples taken are indicated next to the lithology as 235 - 237.

The total counts GR log of the Skoorsteenberg Formation is dominated by the Th content, as shown by the correlation between the Th counts and the total counts ( $r = 0.29$  for sandstones and  $r = 0.30$  for siltstones). K and U show very low correlations with total counts (Table 3.3). K-Th cross-plots show positive correlation between the K and Th content for both the siltstones and the sandstones from GR analyses (Figure 3.14).

### 3.4.2 Kookfontein Formation

The Kookfontein Formation occurs above the turbidite complex and is an upwards coarsening succession, reflecting progressive shallowing conditions associated with deltaic progradation (Wickens, 1994). The upper part of the formation shows very subtle, small upward thickening cycles (2 – 10 m thick) (Kingsley, 1977; Visser and Young, 1990; Wickens, 1994). These cycles generally commence with horizontally-laminated dark grey shale and siltstone derived from suspension settling, followed upwards by a rhythmic alteration of shale, siltstone and sandstone, whereas the thicker beds (up to 20 cm) towards the top resulted from sediment-laden traction currents (Wickens, 1994). Symmetrical wave ripple form sets and wave-produced ripple-lamination become more pronounced upwards in the succession.

Interpretation of the measured outcrop section, Pienaarsfontein (V6), suggests a slope to deltaic basin-fill succession, starting with deposition in wave influenced lower slope to shelf edge delta environments and ending with mixed wave and fluvial influenced pro-delta to delta front deposits. One vertical profile (V6) and six horizontal profiles were measured at this location. The horizontal profiles were measured on sandstone beds and designated as H6 – H11 (Figure 3.15).



The sandstone U/K, Th/K and Th/U data show similar trends with relatively uniform values throughout (Table 3.4), although some anomalies can be seen in the Th/K and Th/U logs (Figure 3.16). The sandstone total counts data are erratic, ranging from 38 – 94 cps (avg. = 59 cps,  $n = 173$ ). The siltstone average U/K, Th/K, Th/U and total counts data are shown in Table 3.4. There is a definite decrease in the total counts data upwards in the section, along with an increase in the sandstone: siltstone ratio.

The horizontal profiles (H6 – H11) exhibit SGR profiles correlative with their positions within the vertical profile (V6). The Th/K and Th/U logs are relatively uniform, with some of the total counts logs showing erratic responses. On average, however, the data are similar to that of V6 and can be characterised as follows: H6 (avg. = 48 cps,  $n = 10$ ), H7 (avg. = 64 cps,  $n = 10$ ), H8 (avg. = 55 cps,  $n = 10$ ), H9 (avg. = 53 cps,  $n = 10$ ), H10 (avg. = 59 cps,  $n = 4$ ) and H11 (avg. = 60 cps,  $n = 6$ ). H6 and H7 were measured in the lower section of V6, where siltstone is more common than higher up in the section (Figure 3.16). Changes in the U/K appear to be constant throughout, for both the vertical and horizontal profiles.

Table 3.3 Correlation matrix for radioactive elements determined by SGR for the Tanqua and Laingsburg depocentres. These are all r-values. The minimum figure for a significant pattern is ~0.7.

Tanqua depocentre					Laingsburg depocentre				
Skoorsteenberg Formation (Unit 5)					Collingham Formation				
<b>Sandstones</b>					<b>Sandstones</b>				
	$K_{SGR}$	$U_{SGR}$	$Th_{SGR}$	Total counts		$K_{SGR}$	$U_{SGR}$	$Th_{SGR}$	Total counts
$K_{SGR}$	1.00				$K_{SGR}$	1.00			
$U_{SGR}$	0.66	1.00			$U_{SGR}$	0.43	1.00		
$Th_{SGR}$	0.16	0.24	1.00		$Th_{SGR}$	0.14	0.33	1.00	
Total counts	0.05	0.07	0.29	1.00	Total counts	0.04	0.09	0.28	1.00
<b>Siltstones</b>					<b>Siltstones</b>				
	$K_{SGR}$	$U_{SGR}$	$Th_{SGR}$	Total counts		$K_{SGR}$	$U_{SGR}$	$Th_{SGR}$	Total counts
$K_{SGR}$	1.00				$K_{SGR}$	1.00			
$U_{SGR}$	0.65	1.00			$U_{SGR}$	0.58	1.00		
$Th_{SGR}$	0.16	0.24	1.00		$Th_{SGR}$	0.18	0.32	1.00	
Total counts	0.05	0.07	0.30	1.00	Total counts	0.05	0.09	0.28	1.00
Kookfontein Formation					Vischkuil Formation				
<b>Sandstones</b>					<b>Sandstones</b>				
	$K_{SGR}$	$U_{SGR}$	$Th_{SGR}$	Total counts		$K_{SGR}$	$U_{SGR}$	$Th_{SGR}$	Total counts
$K_{SGR}$	1.00				$K_{SGR}$	1.00			
$U_{SGR}$	0.74	1.00			$U_{SGR}$	0.53	1.00		
$Th_{SGR}$	0.16	0.22	1.00		$Th_{SGR}$	0.14	0.26	1.00	
Total counts	0.05	0.06	0.29	1.00	Total counts	0.04	0.08	0.28	1.00
<b>Siltstones</b>					<b>Siltstones</b>				
	$K_{SGR}$	$U_{SGR}$	$Th_{SGR}$	Total counts		$K_{SGR}$	$U_{SGR}$	$Th_{SGR}$	Total counts
$K_{SGR}$	1.00				$K_{SGR}$	1.00			
$U_{SGR}$	0.77	1.00			$U_{SGR}$	0.63	1.00		
$Th_{SGR}$	0.17	0.23	1.00		$Th_{SGR}$	0.16	0.26	1.00	
Total counts	0.05	0.07	0.30	1.00	Total counts	0.05	0.08	0.31	1.00
Waterford Formation					Laingsburg Formation				
<b>Sandstones</b>					<b>Sandstones</b>				
	$K_{SGR}$	$U_{SGR}$	$Th_{SGR}$	Total counts		$K_{SGR}$	$U_{SGR}$	$Th_{SGR}$	Total counts
$K_{SGR}$	1.00				$K_{SGR}$	1.00			
$U_{SGR}$	0.72	1.00			$U_{SGR}$	0.66	1.00		
$Th_{SGR}$	0.17	0.24	1.00		$Th_{SGR}$	0.15	0.23	1.00	
Total counts	0.05	0.07	0.29	1.00	Total counts	0.04	0.07	0.29	1.00
<b>Siltstones</b>					<b>Siltstones</b>				
	$K_{SGR}$	$U_{SGR}$	$Th_{SGR}$	Total counts		$K_{SGR}$	$U_{SGR}$	$Th_{SGR}$	Total counts
$K_{SGR}$	1.00				$K_{SGR}$	1.00			
$U_{SGR}$	0.73	1.00			$U_{SGR}$	0.70	1.00		
$Th_{SGR}$	0.18	0.24	1.00		$Th_{SGR}$	0.16	0.23	1.00	
Total counts	0.05	0.07	0.30	1.00	Total counts	0.05	0.07	0.31	1.00
Fort Brown Formation					Fort Brown Formation				
<b>Sandstones</b>					<b>Sandstones</b>				
	$K_{SGR}$	$U_{SGR}$	$Th_{SGR}$	Total counts		$K_{SGR}$	$U_{SGR}$	$Th_{SGR}$	Total counts
$K_{SGR}$	1.00				$K_{SGR}$	1.00			
$U_{SGR}$	0.67	1.00			$U_{SGR}$	0.67	1.00		
$Th_{SGR}$	0.15	0.23	1.00		$Th_{SGR}$	0.15	0.23	1.00	
Total counts	0.05	0.07	0.29	1.00	Total counts	0.05	0.07	0.29	1.00
<b>Siltstones</b>					<b>Siltstones</b>				
	$K_{SGR}$	$U_{SGR}$	$Th_{SGR}$	Total counts		$K_{SGR}$	$U_{SGR}$	$Th_{SGR}$	Total counts
$K_{SGR}$	1.00				$K_{SGR}$	1.00			
$U_{SGR}$	0.74	1.00			$U_{SGR}$	0.74	1.00		
$Th_{SGR}$	0.17	0.23	1.00		$Th_{SGR}$	0.17	0.23	1.00	
Total counts	0.05	0.07	0.30	1.00	Total counts	0.05	0.07	0.30	1.00

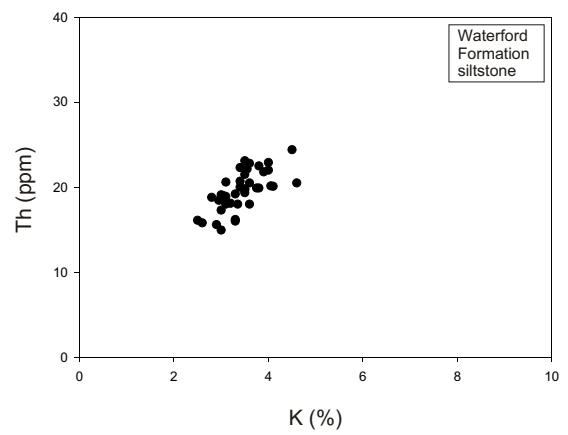
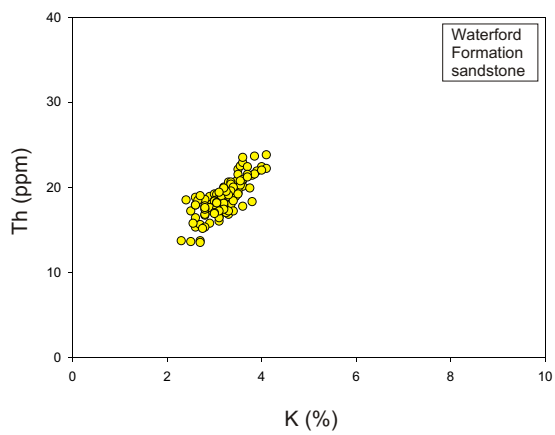
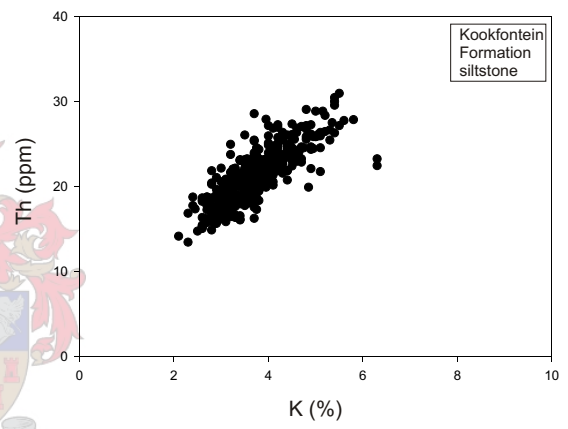
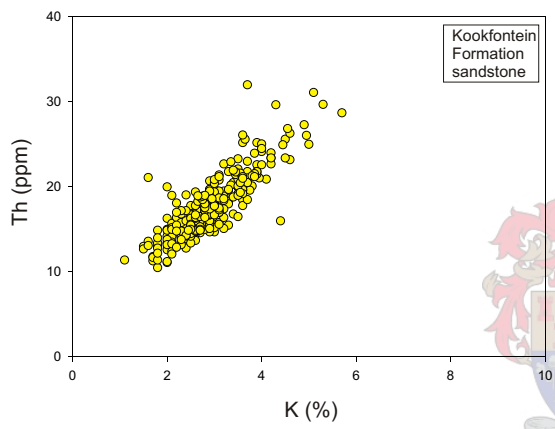
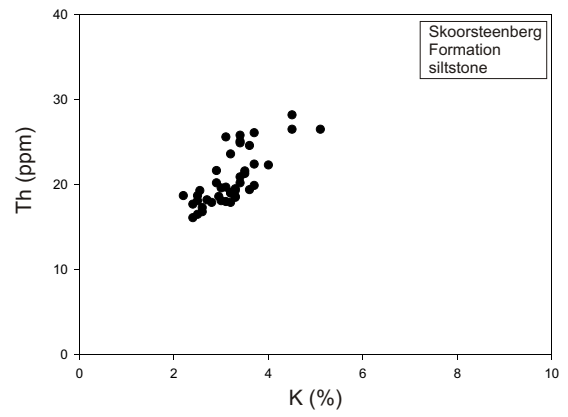
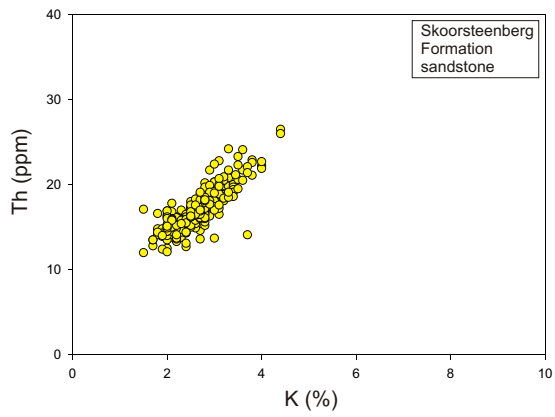


Figure 3.14 K vs. Th cross-plots for the sandstones and siltstones from the Tanqua depocentre, used to distinguish between the different facies associations and formations from GR analyses (method after Myers and Bristow, 1989).

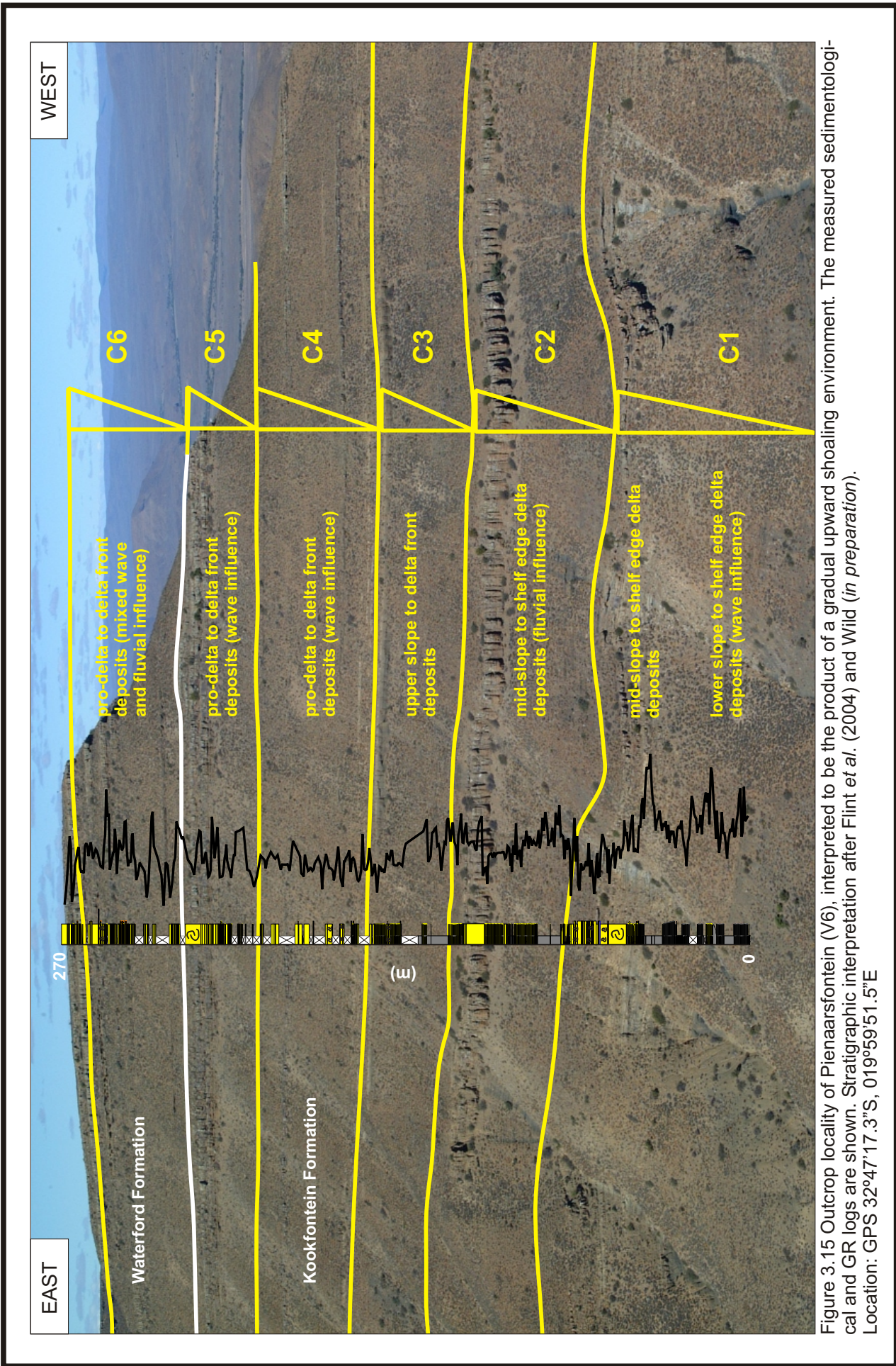
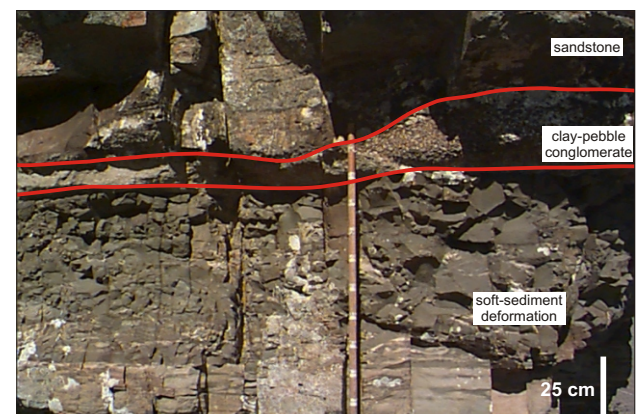
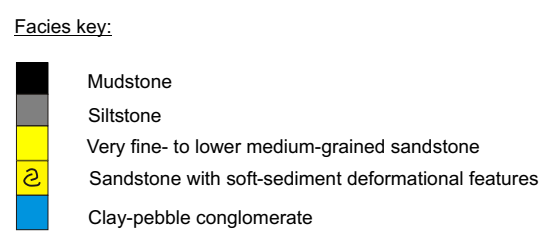
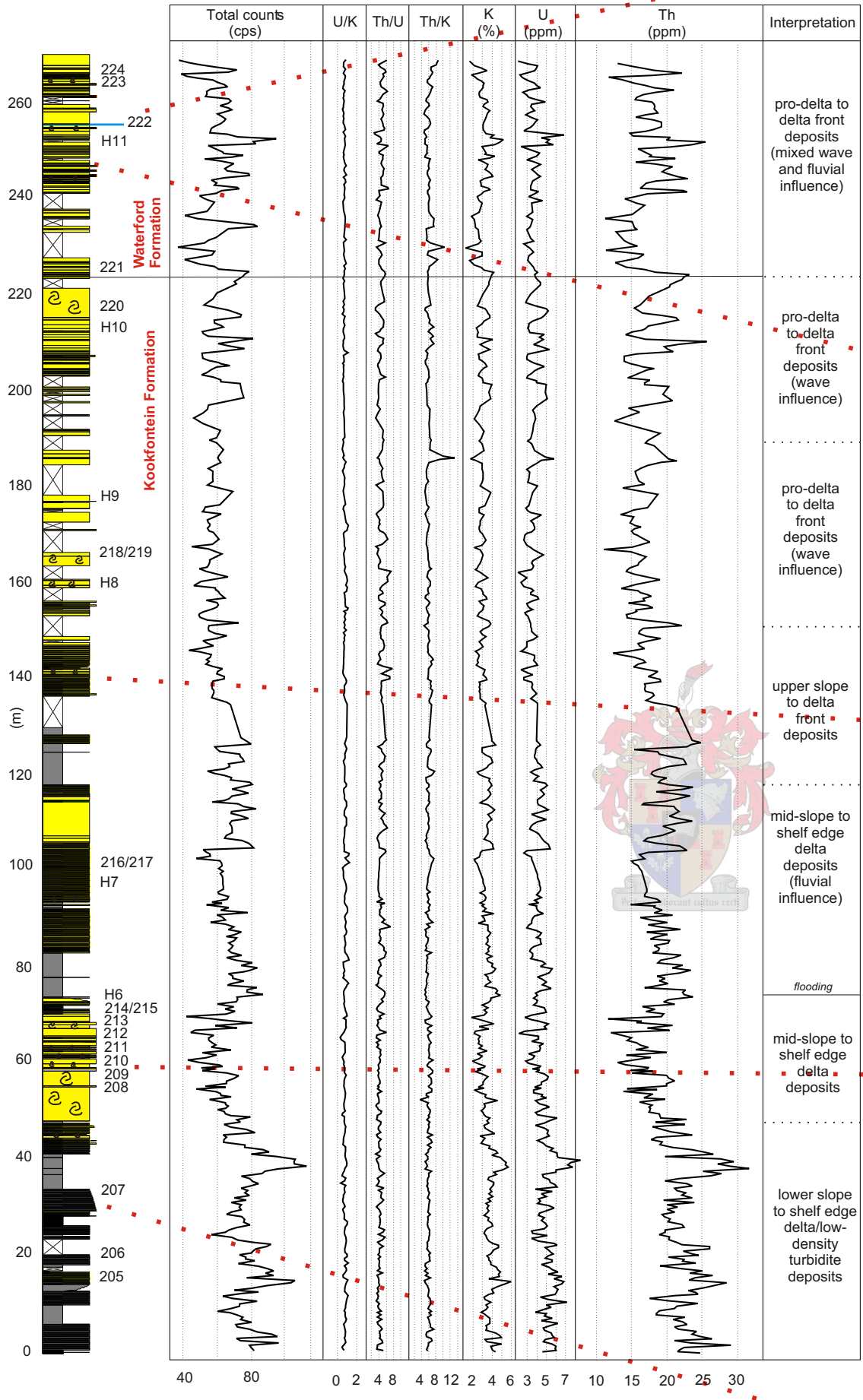


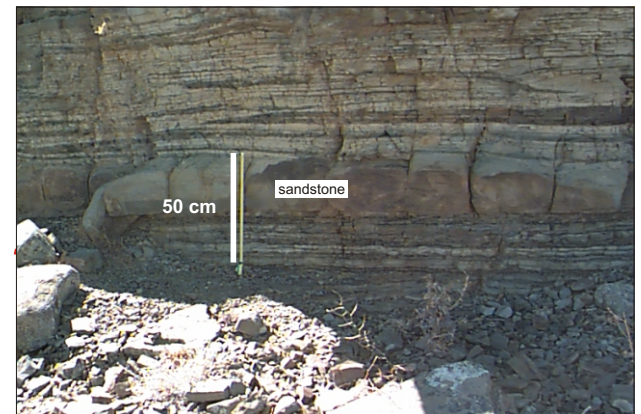
Figure 3.15 Outcrop locality of Pienaarsfontein (V6), interpreted to be the product of a gradual upward shoaling environment. The measured sedimentological and GR logs are shown. Stratigraphic interpretation after Flint *et al.* (2004) and Wild (*in preparation*). Location: GPS 32°47'17.3"S, 019°59'51.5"E

Table 3.4 Average total counts (cps), U/K, Th/K and Th/U from SGR measurements for profiles in the Kookfontein Formation. Confidence levels are at 95%.

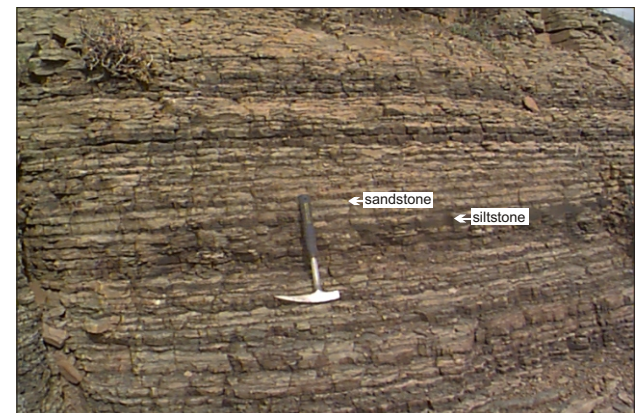
Stratigraphy	Profile	n	Avg.		S <sub>e</sub>	Lower limit	Upper limit
Kookfontein Formation	<u>Pienaarsfontein (V6)</u>						
	Sandstone	173					
	Total counts		59	7.15	1.09	38	94
	U/K		1.40	0.31	0.05	0.81	3.63
	Th/K		6.14	0.87	0.13	4.70	13.19
	Th/U		4.51	0.74	0.11	2.85	7.29
	Siltstone	167					
	Total counts		74	9.99	1.55	59	112
	U/K		1.32	0.21	0.03	0.82	2.04
	Th/K		5.78	0.47	0.07	4.81	7.04
	Th/U		4.49	0.76	0.12	3.15	7.20
	<u>Bitterberg (V11)</u>						
	Sandstone	59					
	Total counts		68	13.9	3.62	46	110
	U/K		1.24	0.26	0.07	0.92	2.44
	Th/K		6.12	0.64	0.17	5.04	8.50
	Th/U		5.06	0.87	0.23	3.49	7.64
	Siltstone	119					
	Total counts		68	8.10	1.49	47	92
	U/K		1.24	0.19	0.03	0.67	1.86
	Th/K		5.82	0.50	0.09	4.41	7.28
	Th/U		4.80	0.73	0.13	3.40	8.38
	<u>Skoorsteenberg (V135)</u>						
	Sandstone	36					
	Total counts		53	7.57	2.52	39	73
	U/K		1.45	0.29	0.10	0.94	2.20
	Th/K		6.19	0.49	0.16	5.21	7.44
	Th/U		4.43	0.98	0.33	2.80	7.53
	Siltstone	13					
	Total counts		66	13.6	7.54	51	96
	U/K		1.56	0.18	0.10	1.30	1.94
	Th/K		5.92	0.60	0.33	5.16	7.35
	Th/U		3.83	0.50	0.28	3.21	4.83
	<u>Soutrivierspunt (V13)</u>						
	Sandstone	68					
	Total counts		68	8.95	2.17	45	88
	U/K		1.46	0.30	0.07	1.06	2.06
	Th/K		6.39	0.83	0.20	5.13	8.65
	Th/U		4.46	0.61	0.15	2.78	6.03
	Siltstone	149					
	Total counts		76	12.7	2.08	41	98
	U/K		1.28	0.22	0.04	0.59	1.75
	Th/K		5.74	0.62	0.10	4.11	7.46
	Th/U		4.60	0.96	0.16	3.13	8.80
	<u>Katjiesberg (V12)</u>						
	Sandstone	19					
	Total counts		55	10.8	4.96	35	66
	U/K		1.34	0.18	0.08	1.07	1.68
Th/K		5.89	0.41	0.19	5.33	6.73	
Th/U		4.48	0.73	0.33	3.60	5.70	
Siltstone	169						
Total counts		67	10.4	1.60	42	101	
U/K		1.39	0.19	0.03	0.87	1.82	
Th/K		5.97	0.50	0.08	5.03	7.82	
Th/U		4.38	0.73	0.11	3.35	7.61	
<u>Ouberg (V18)</u>							
Sandstone	134						
Total counts		64	6.43	1.11	39	86	
U/K		1.39	0.20	0.03	0.91	1.96	
Th/K		5.95	0.52	0.09	4.82	8.19	
Th/U		4.38	0.77	0.13	2.78	7.23	
Siltstone	84						
Total counts		65	8.00	1.75	35	86	
U/K		1.39	0.17	0.04	1.07	1.76	
Th/K		5.75	0.55	0.12	4.46	6.73	
Th/U		4.18	0.55	0.12	3.20	5.70	



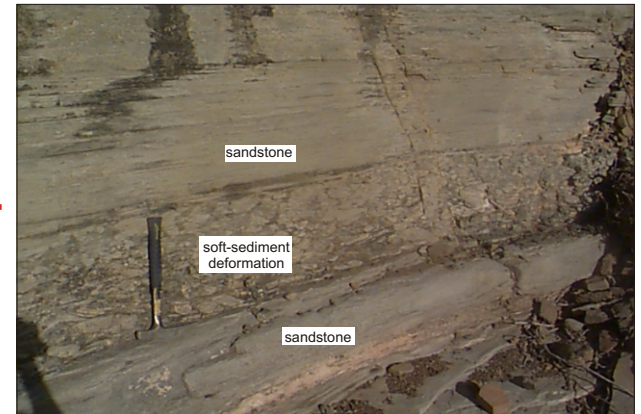
Clay-pebble conglomerate bed (between red lines) above a sandstone bed that has undergone soft-sediment deformation, and overlain by a parallel-laminated sandstone bed.



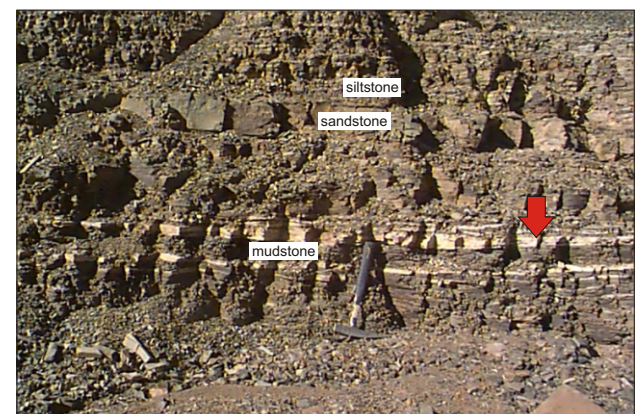
Parallel-stratified sandstone bed within a unit of thin wavy sandstone beds with thin silty intercalations.



Rhythmic ripple cross-laminated beds of alternating sandstone and siltstone.



Soft-sediment deformation between beds of parallel-laminated sandstone.



Alternating thin mudstone and siltstone beds, with intermittent sandstone beds and thin intercalated calcareous beds (red arrow).

Figure 3.16 Outcrop locality of Pienaarsfontein (V6), representing a slope setting containing turbidites, moving upwards into a deltaic depositional environment. Comparison between SGR logs and lithology. SGR results are from 489 measurements at an average vertical spacing of 50 cm. The location of horizontal profiles measured are indicated as H6 - H11 next to the lithology and samples taken as 205 - 224. Stratigraphic interpretation after Flint *et al.* (2004) and Wild (*in preparation*).

The outcrop section of Bitterberg (V11) can be interpreted as deposition in mid-slope to pro-delta to delta front environments. The Bitterberg (V11) (Figure 3.17) sedimentary log shows cycles of alternating sandstone and siltstone units separated by siltstone units. This is reflected in the GR profiles at the contacts between the sandstone and siltstone, and larger siltstone units (Figure 3.18). The average sandstone and siltstone GR data are shown in Table 3.4.

Three separate vertical profiles (V1, V3 and V5) and five horizontal profiles (H1 within V1, H2 within V3 and H3a and H3b within V5) were measured at Skoorsteenberg (V135) (Figures 3.19 and 3.20). The horizontal profiles were measured along sandstone beds and a unit of alternating sandstone and siltstone.

The sandstone trends for U/K, Th/K and Th/U in V135 are generally flat (Table 3.4), whereas the total counts data show an average value of 53 cps ( $n = 36$ ). The siltstone values are shown in Table 3.4. The total counts values for the siltstones show an increase with movement to the top of the measured succession. Horizontal sandstone bed profile H3a was taken in section V1 and shows total counts values of avg. = 83 cps ( $n = 5$ ). The variation in data from H3b, measured in a sandstone bed above H3b, show flat trends for Th/K (avg. = 5.51,  $n = 5$ ) and Th/U (avg. = 4.85,  $n = 5$ ) as well, although there is some variation in the total counts data, ranging from 38 – 59 cps (avg. = 51 cps,  $n = 5$ ). H1, measured in a sandstone bed in V5, show an average Th/K of 5.83 ( $n = 5$ ), an average Th/U of 3.98 ( $n = 5$ ) and an average total counts value of 66 cps ( $n = 5$ ). Changes in the U/K appear to be constant throughout, for both the vertical and horizontal profiles.

The pro-delta slope deposits measured at Soutrivierspunt (V13) progrades into delta front deposits. Larger areas of unexposed outcrop were present at Soutrivierspunt (V13), however, the exposed sections show non-uniform patterns in all the GR profiles (Figure 3.21). Most peaks are at the contacts between the sandstone and siltstone, and larger siltstone units (Figure 3.22). The sandstone and siltstone average data collected for these profiles are shown in Table 3.4.

Interpretation of the Katjiesberg (V12) outcrop section shows background slope and pro-delta deposits, followed by delta front progradation. The Katjiesberg (V12) (Figure 3.23) log ratio profiles are uniform, however, the total counts profile exhibits sharp deviations from uniformity at the first appearance of interlaminated sandstone and siltstone layers above the shale (Figure 3.24). This continues up to the top of the measured section. The average sandstone and siltstone values are shown in Table 3.4.

The outcrop section of Ouberg (V18) (Figure 3.25) can be interpreted as upper slope, pro-delta and delta front deposits. The trends for U/K, Th/K, Th/U and total counts data in V18

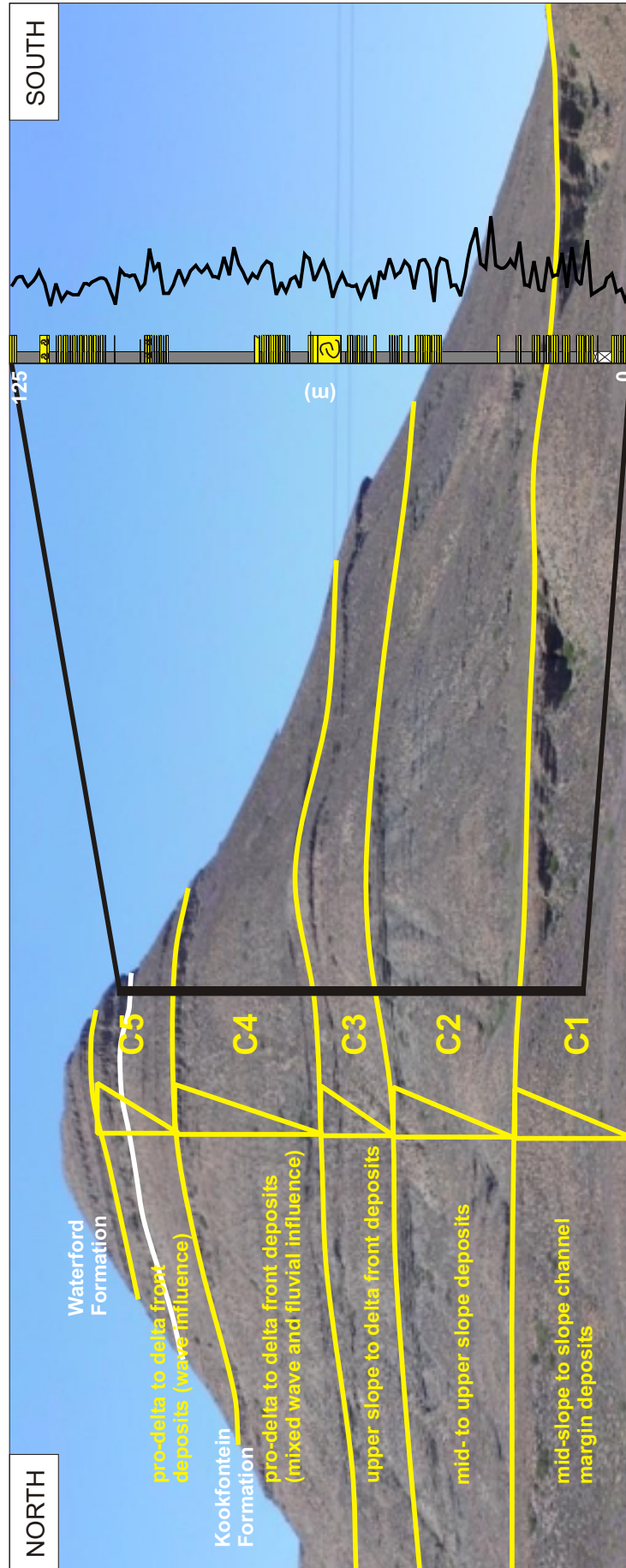
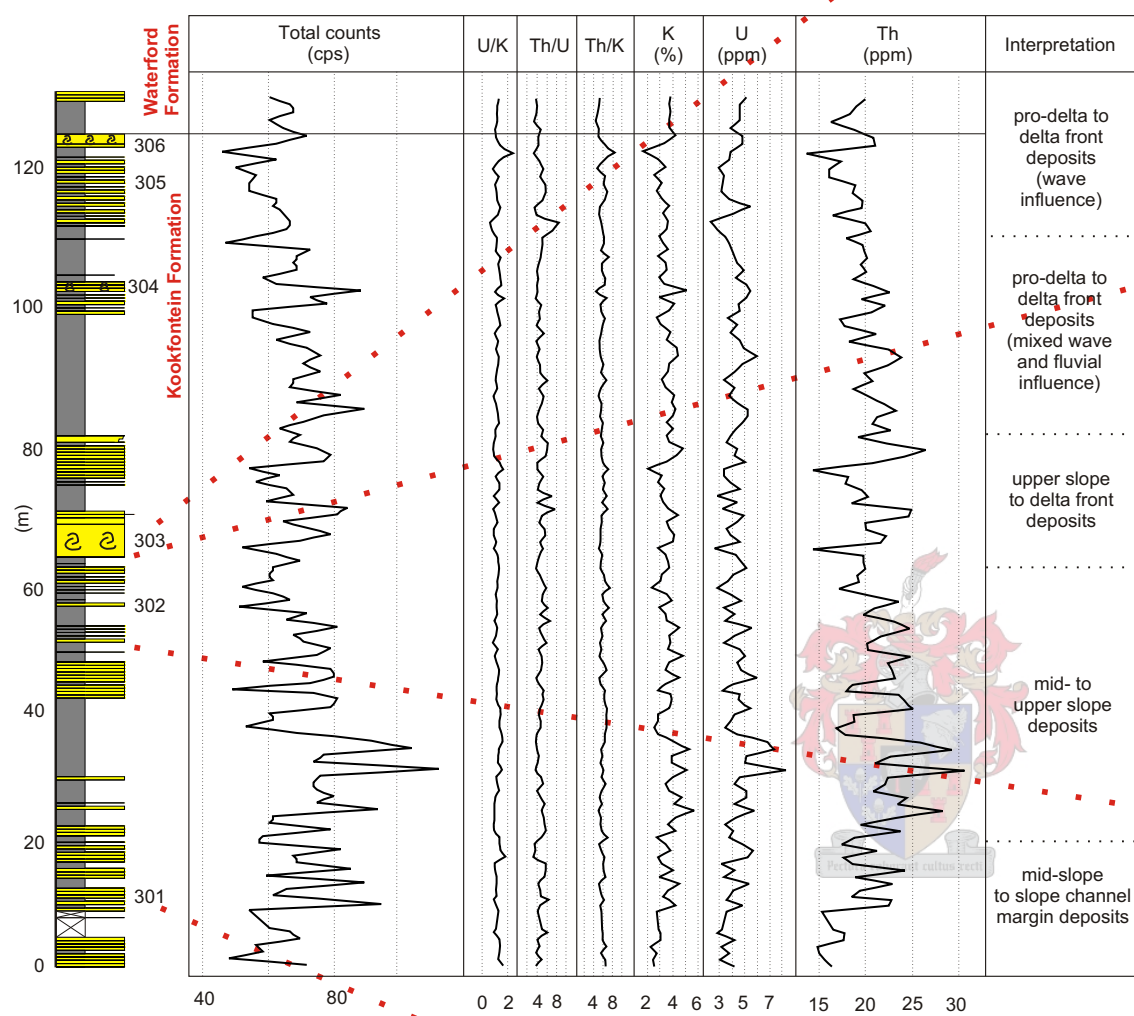
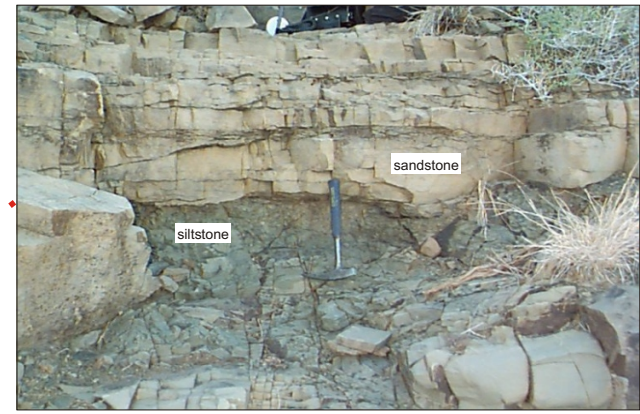


Figure 3.17 Position for the V11 section at Bitterberg, western side of the Koedoesberg Mountain Range. View to the east. The pro-delta slope facies are interpreted as low-density, thin-bedded turbidite deposits. The measured section and corresponding GR log are shown. Stratigraphic interpretation after Flint *et al.* (2004) and Wild (*in preparation*).  
 Location: GPS 32°39'19.2"S, 020°06'58.3"E

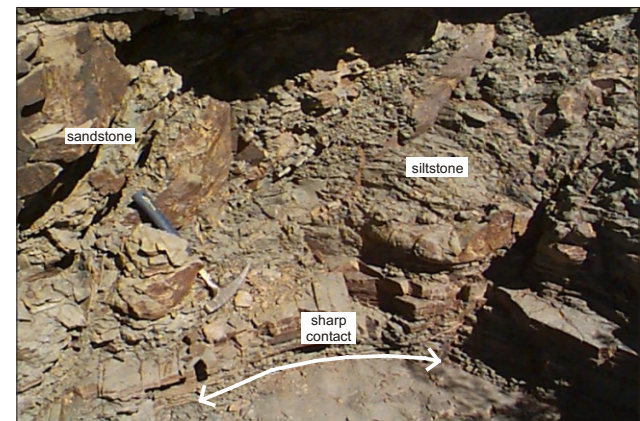


Facies key:

- Mudstone
- Siltstone
- Very fine- to lower medium-grained sandstone
- Sandstone with soft-sediment deformational features



Siltstone capped by a parallel-stratified sandstone bed.



Soft-sediment deformation within a succession of sandstone and siltstone. The contact with the underlying ripple cross-laminated siltstone bed is sharp.



Weathered-out spherical concretion showing internal circular growth boundaries.



Rhythmic ripple cross-laminated beds of alternating sandstone and siltstone.

Figure 3.18 Bitterberg (V11), interpreted as a pro-delta and delta front slope setting containing slope channel-fill and slope turbidite facies. Comparison between SGR logs and lithology. SGR results are from 244 measurements at an average vertical spacing of 50 cm. The location of samples taken are indicated next to the lithology as 301 - 306. Stratigraphic interpretation after Flint *et al.* (2004) and Wild (*in preparation*).

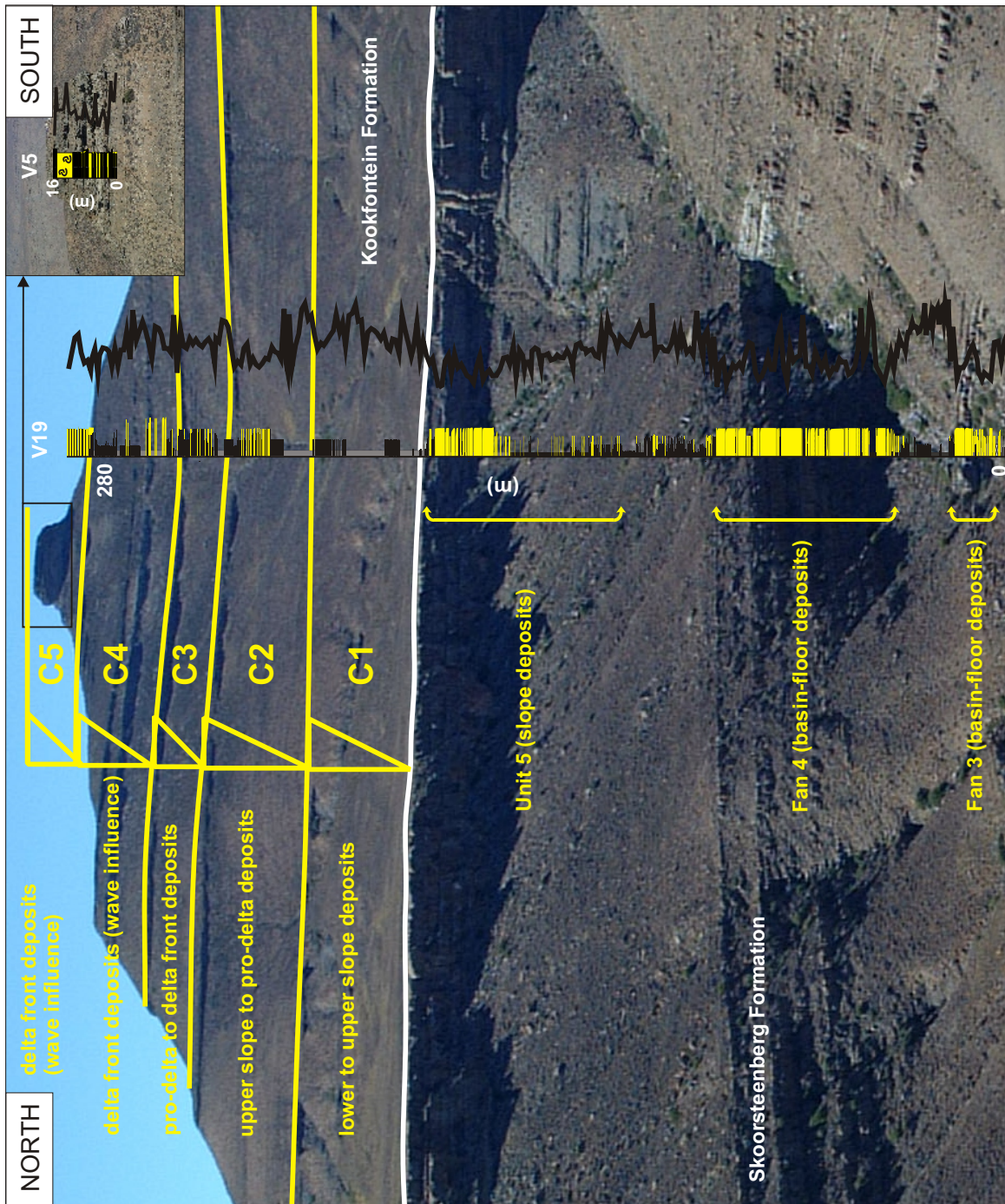
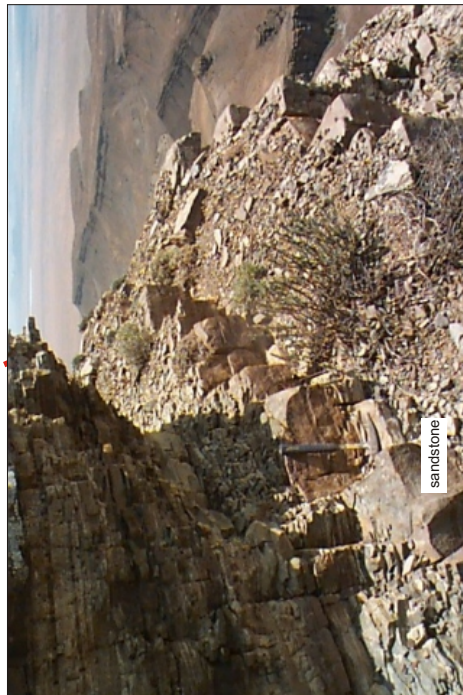
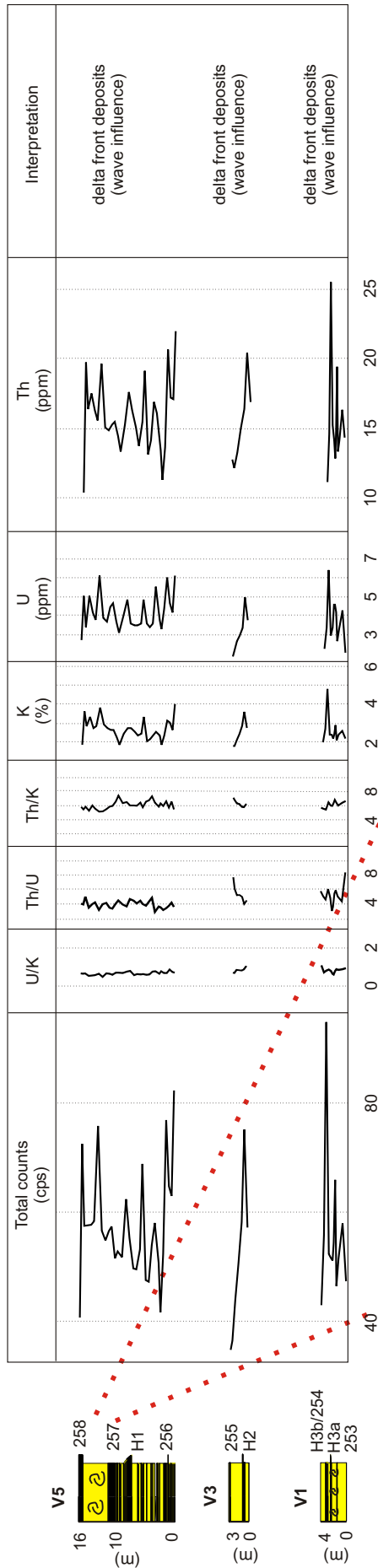


Figure 3.19 Outcrops of Fans 3, 4, Unit 5 and deltaic slope succession at Skoorsteenberg. The succession is interpreted to be a product of basin-floor to delta front deposition under gradual shoaling conditions. The measured sedimentological (V135 and V19) and GR logs are shown. V19 is after Andersson and Worden (2004). Stratigraphic interpretation after Flint *et al.* (2004) and Wild (*in preparation*).

Location: GPS 32°35'19.8"S, 019°59'42.1"E



Hummocky cross-stratified sandstone beds alternating with thin beds of siltstone and sandstone, the latter displaying wavy lamination.



Soft-sediment deformation (ball-and-pillow) layer consisting of sandstone and siltstone.

Facies key:



Figure 3.20 Skoorsteenberg (V135), interpreted as a wave-dominated delta front under gradual shoaling-upward conditions. Comparison between SGR logs and lithology. SGR results are from 50 measurements at an average vertical spacing of 50 cm. The location of horizontal profiles measured and samples taken, are indicated as H3a and H3b, and 253 - 258, next to the lithology. Stratigraphic interpretation after Flint *et al.* (2004) and Wild (*in preparation*).

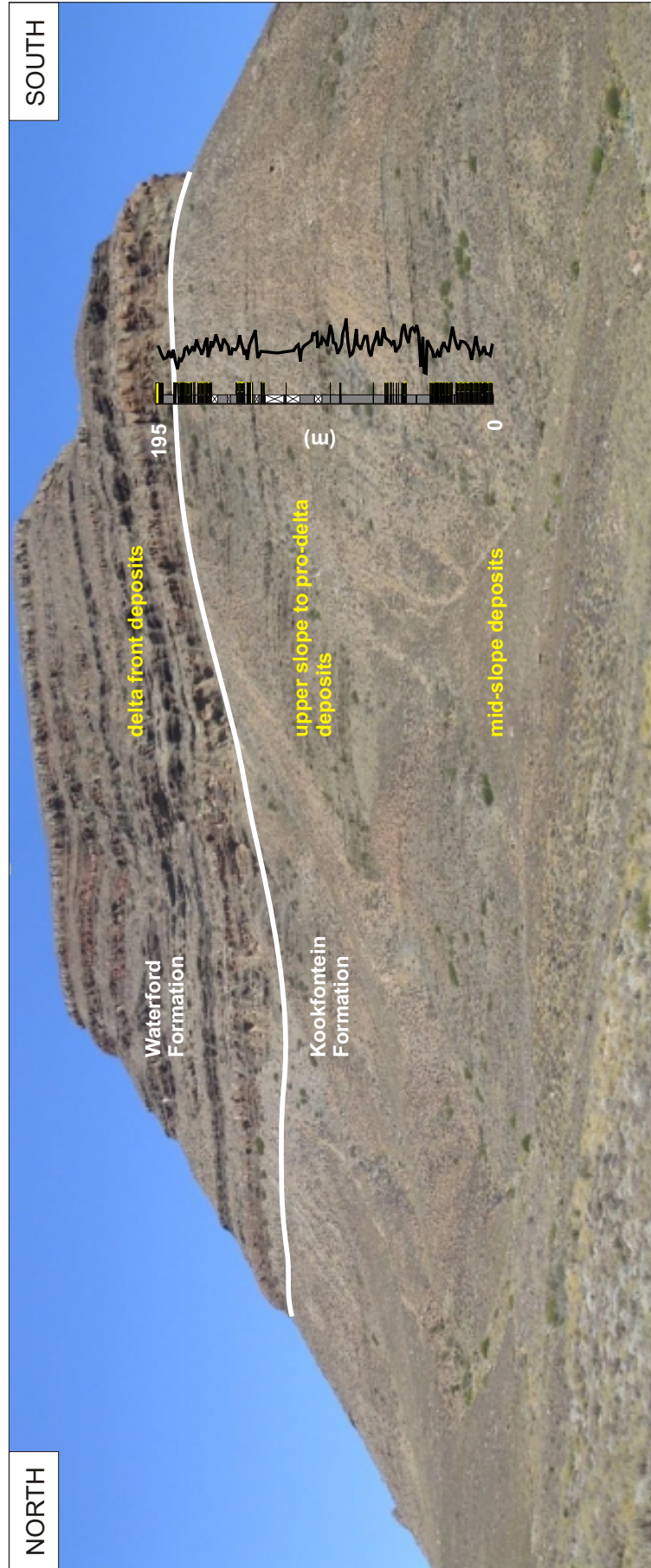
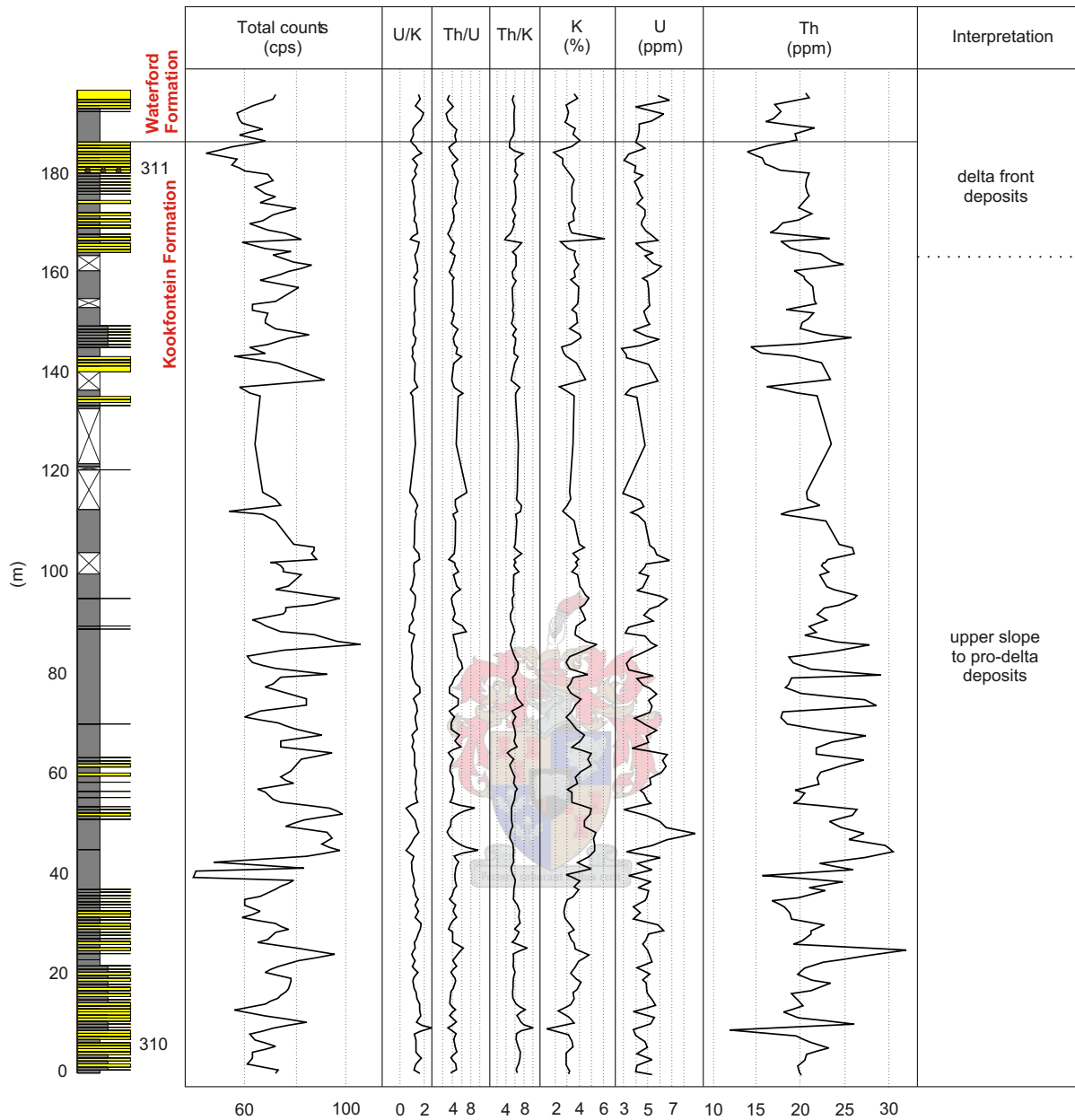


Figure 3.21 Outcrop of Kookfontein and Waterford Formations at Soutrivierspunt in the eastern part of the Tanqua depocentre, interpreted as pro-delta slope and delta front depositional settings, respectively. The sedimentological (V13) and GR logs are shown. Location: GPS 32°34'48.0"S, 020°05'26.6"E



Facies key:

- Mudstone
- Siltstone
- Very fine- to lower medium-grained sandstone
- Sandstone with soft-sediment deformational features

Figure 3.22 Soutrivierspunt (V13), interpreted as slope and lower delta front depositional settings. Comparison between SGR logs and lithology. SGR results are from 250 measurements at an average vertical spacing of 50 cm. The location of samples taken are indicated next to the lithology as 310 - 311.

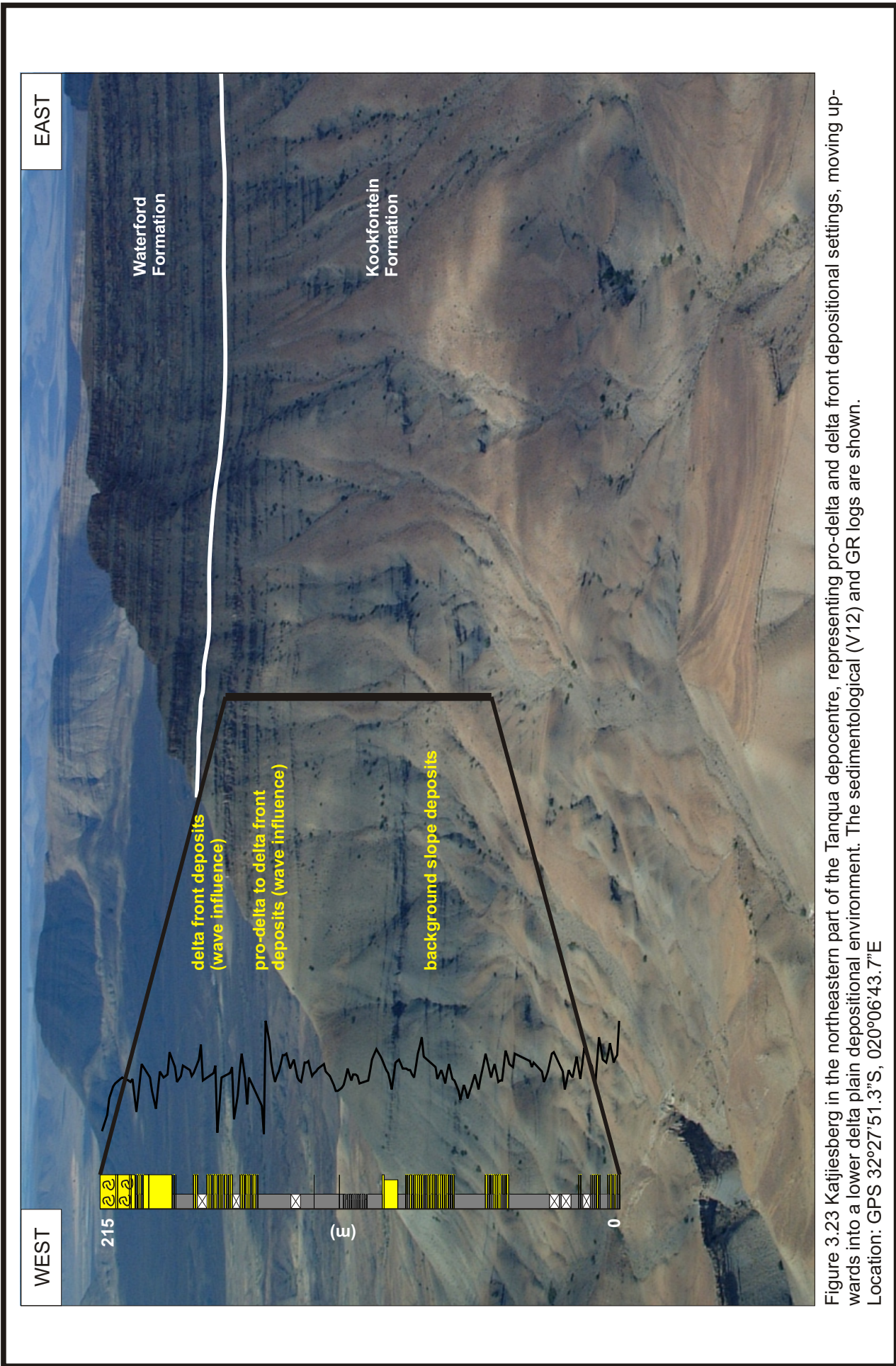
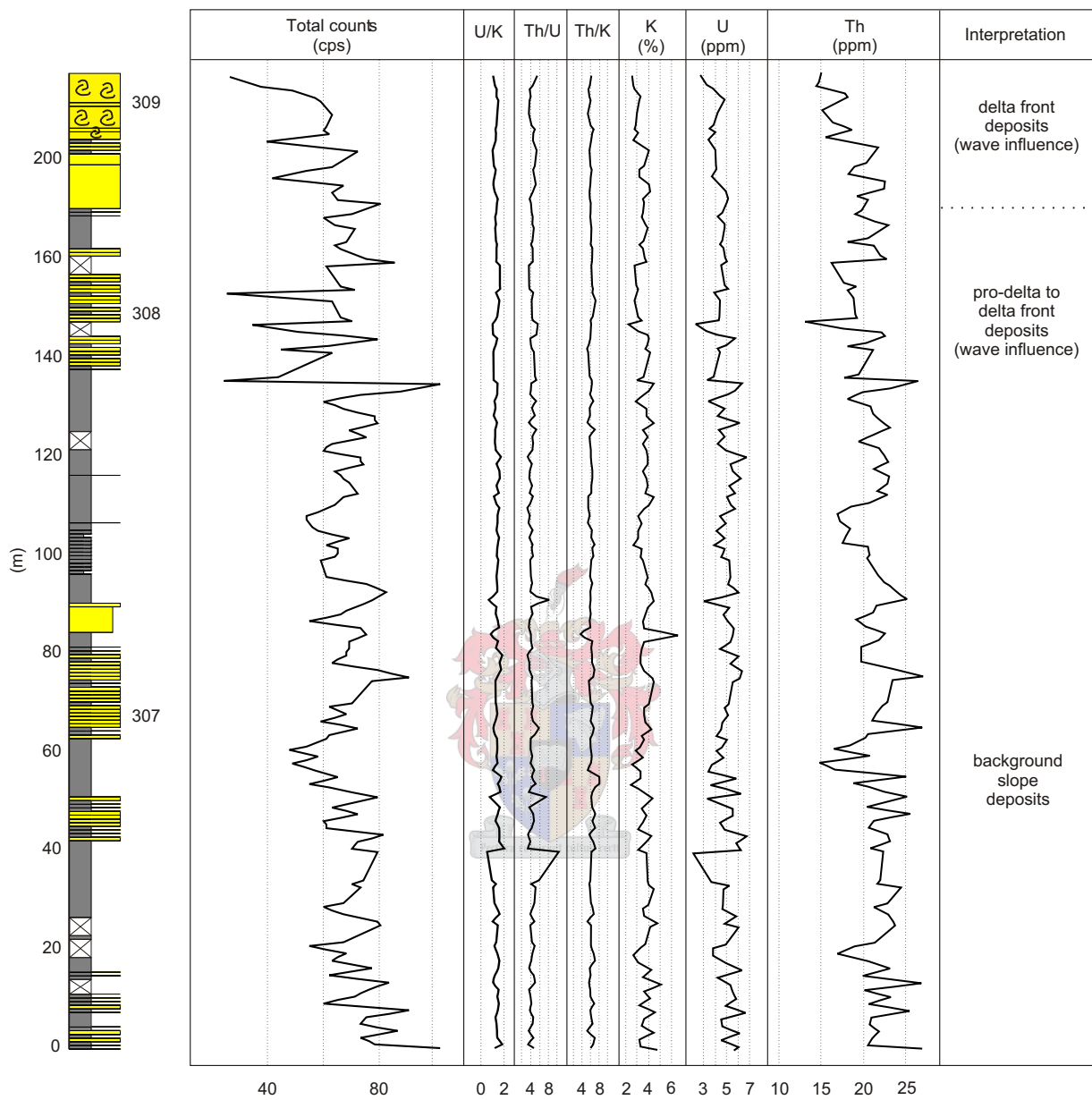


Figure 3.23 Katjiesberg in the northeastern part of the Tanqua depocentre, representing pro-delta and delta front depositional settings, moving upwards into a lower delta plain depositional environment. The sedimentological (V12) and GR logs are shown. Location: GPS 32°27'51.3"S, 020°06'43.7"E



Facies key:

- Mudstone
- Siltstone
- Very fine- to lower medium-grained sandstone
- Sandstone with soft-sediment deformational features

Figure 3.24 Katjiesberg (V12), representing pro-delta and delta front depositional settings, moving upwards into a lower delta plain depositional environment. Comparison between SGR logs and lithology. SGR results are from 208 measurements at an average vertical spacing of 50 cm. The location of samples taken are indicated next to the lithology as 307 - 309.

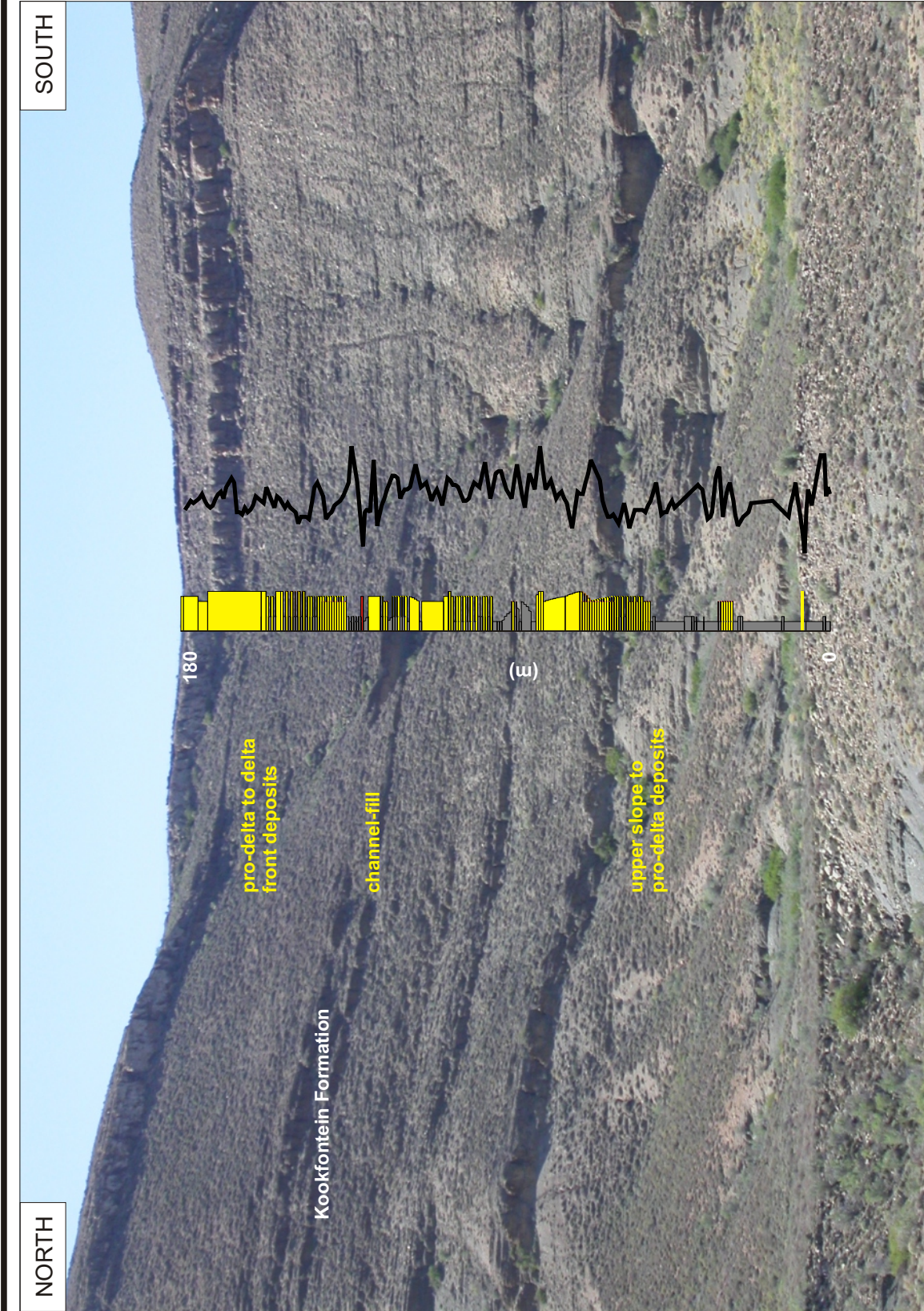


Figure 3.25 Ouberg (V18) outcrop setting, representing upper slope, pro-delta and delta front depositional settings. The sedimentological (V18) and GR logs are shown. Location: GPS 32°24'39.3"S, 020°17'14.1"E

show small spikes for the coarser siltstone relative to the finer siltstone (Figure 3.26). The U/K and Th/U profiles show spikes at the base and the top of a unit of thin sandstone beds within the siltstone. The sandstone U/K, Th/K and Th/U data show similar trends with relatively uniform values throughout. The sandstone average total counts data are 64 cps ( $n = 134$ ) (Table 3.4). The siltstone average U/K, Th/K, Th/U and total counts data are shown in Table 3.4.

The total counts GR log for the Kookfontein Formation is dominated by the Th content, as shown by the correlation between the Th counts and the total counts ( $r = 0.29$  for sandstones and  $r = 0.30$  for siltstones). K and U show very low correlations with total counts (Table 3.3). K and Th show positive correlation on K-Th cross-plots for both the siltstones and sandstones from GR analyses (Figure 3.14).

The stratigraphic interval correlation of the Kookfontein Formation, in relation to the Skoorsteenberg and Waterford Formations, are shown in Figure 3.27.

### **3.4.3 Waterford Formation**

The Waterford Formation consists of delta front and delta topset deposits, dominated by lower medium-grained sandstone and an average thickness of 200 m (Wickens, 1994).

The total counts GR log for the Waterford Formation is dominated by the Th content, as shown by the correlation between Th counts and the total counts ( $r = 0.29$  for sandstones and  $r = 0.30$  for siltstones). K and U show very low correlations with total counts (Table 3.3).

The SGR data show an increase in Th/K and U/K for sandstone and siltstone in the Skoorsteenberg Formation, and an increase in Th/K for sandstone in the Kookfontein Formation, with the down-current direction, and no obvious patterns for total counts and Th/U in either the sandstones or siltstones from the Skoorsteenberg and Kookfontein Formations in the direction of the palaeocurrent (Figure 3.28). Graphs of the geochemical data obtained on samples with XRF, show no obvious trends in Th/K, Th/U and U/K upwards in the stratigraphic succession from the Skoorsteenberg to the Kookfontein Formation and along the palaeocurrent direction (Figure 3.29). The diagrams based on geochemistry of sandstones do, however, show relatively lower U and K values in the Kookfontein Formation, compared to the Skoorsteenberg Formation. A plot of the Th/K vs. the Th/U ratios for the SGR data of the siltstones of the Skoorsteenberg and Kookfontein Formations show narrow trends (Figure 3.30). K-Th plots from GR analyses show positive correlation for sandstones and siltstones (Figure 3.14).

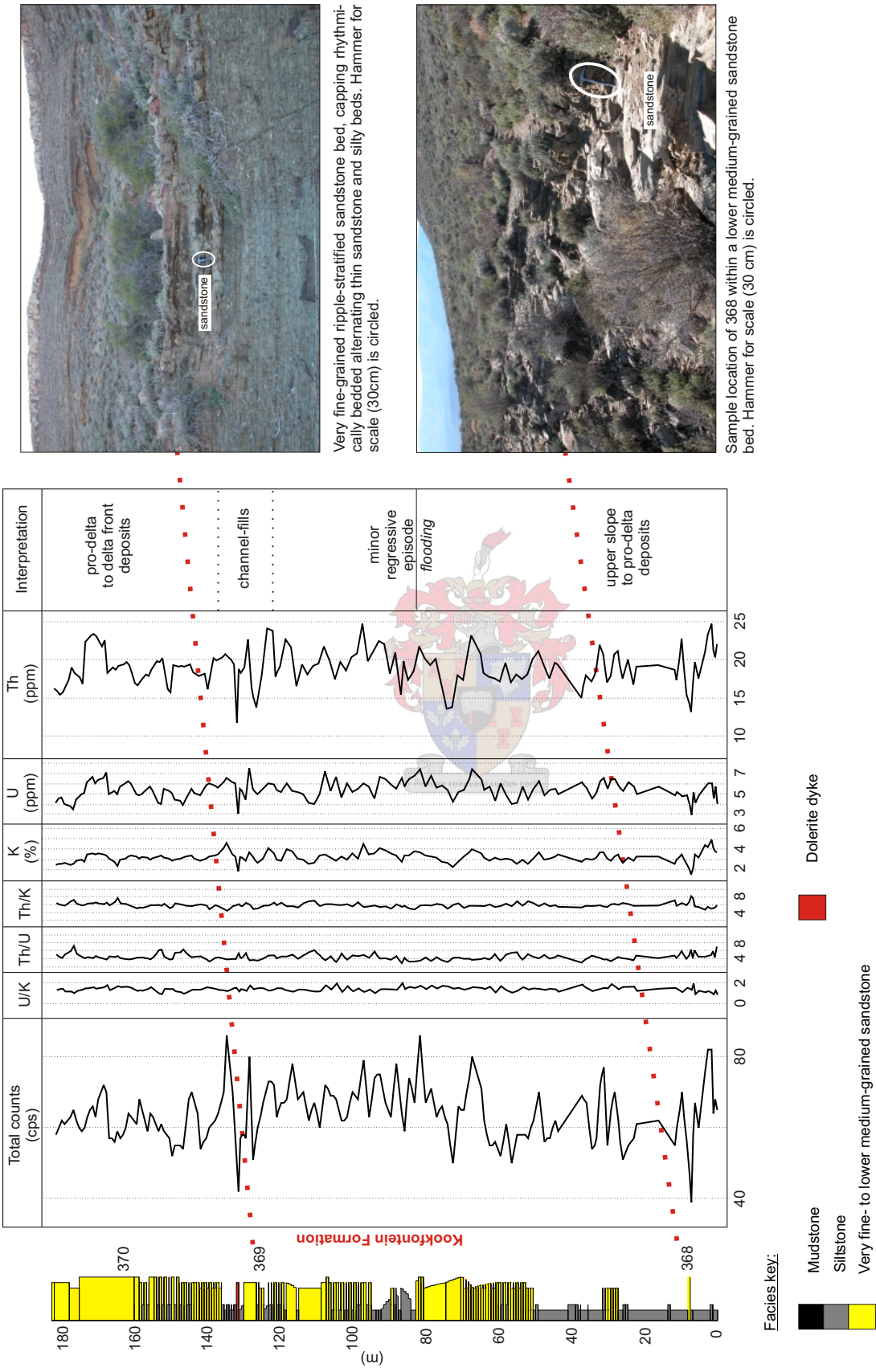
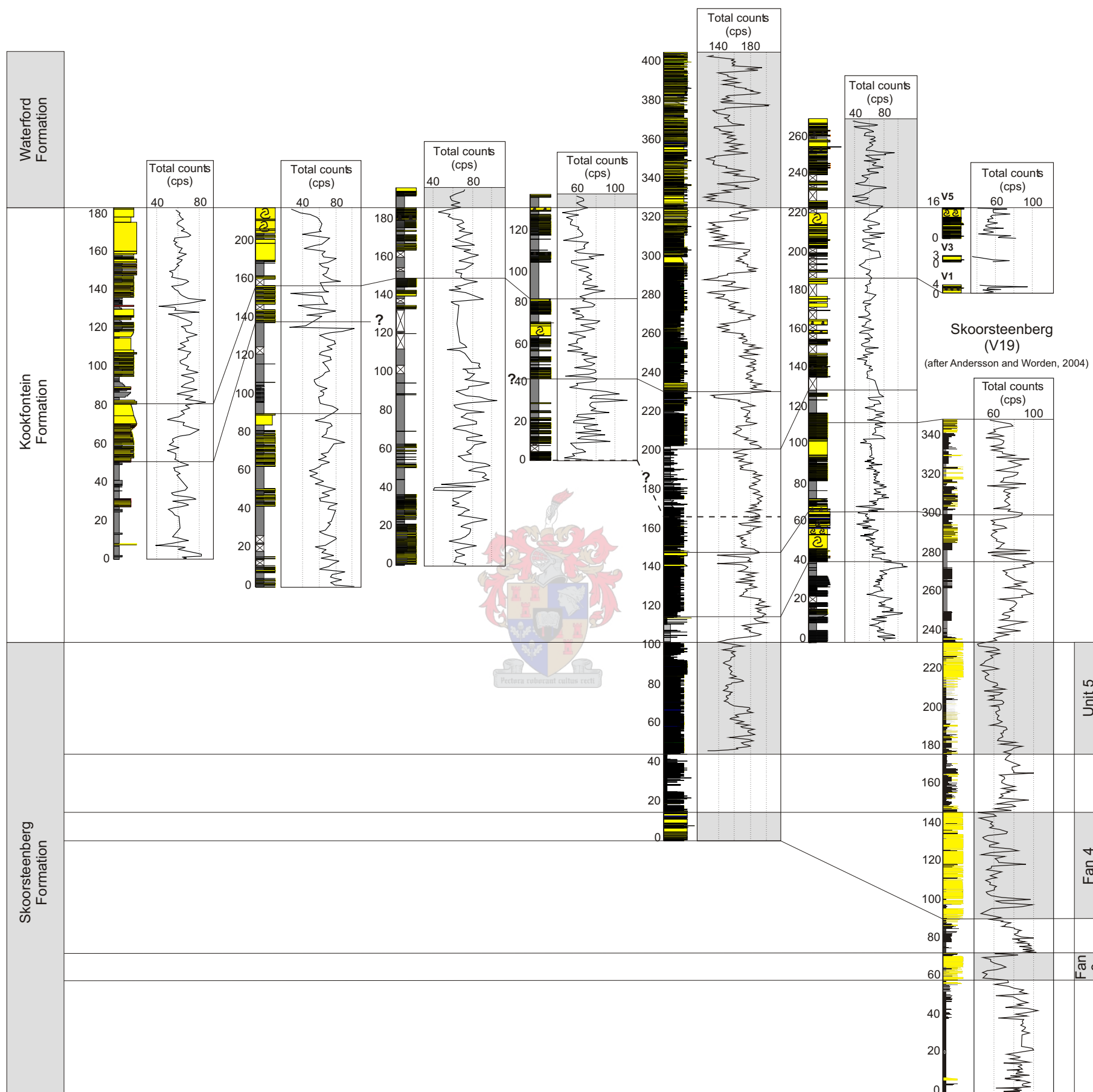


Figure 3.26 Ouberg (V18) measured section, representing upper slope, pro-delta and delta front depositional settings. Comparison between SGR logs and lithology. SGR results are from 228 measurements at an average vertical spacing of 75 cm. Sample positions are indicated next to the lithology as 368 - 270.

Ouberg (V18) ← 17.3 km → Katjiesberg (V12) ← 12.8 km → Soutrivierspunt (V13) ← 8.9 km → Bitterberg (V11) ← 3.9 km → SL1 (V20) ← 22.2 km → Pienaarsfontein (V6) ← 22.1 km → Skoorsteenberg (V135)



Facies key:

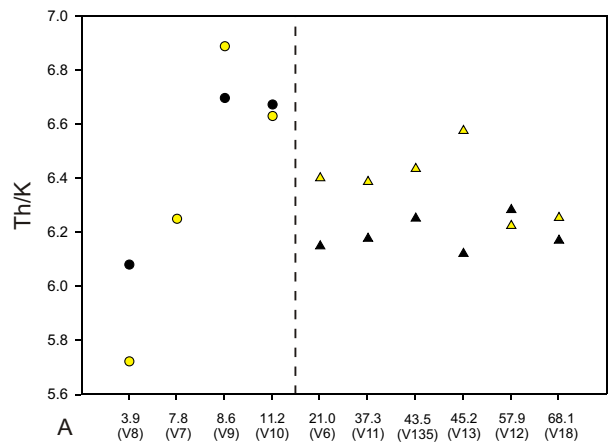
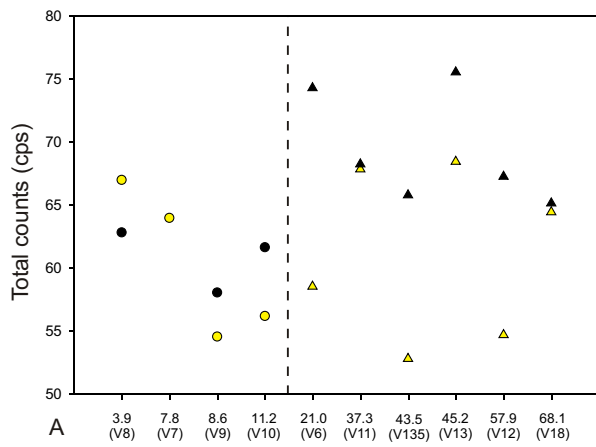
- Mudstone
- Siltstone
- Very fine- to lower medium-grained sandstone
- Sandstone with soft-sediment deformational features
- Clay-pebble conglomerate

Dolerite dyke

--- ? --- Less confident correlation

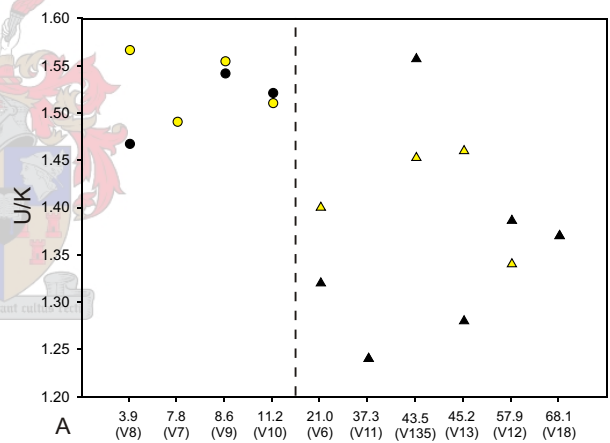
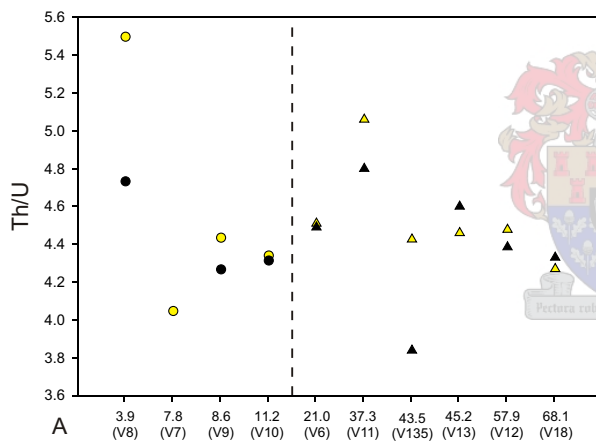
40  
Vertical resolution (m)  
0

Figure 3.27 Tanqua depocentre. Stratigraphic cross-section illustrating correlation of the turbidite and deltaic units of the Skoorsteenberg, Kookfontein and Waterford Formations, respectively, in the study area. Correlations are based upon gross thicknesses of corresponding facies.



Distance (in km) from arbitrary point A → palaeocurrent direction

Distance (in km) from arbitrary point A → palaeocurrent direction



Distance (in km) from arbitrary point A → palaeocurrent direction

Distance (in km) from arbitrary point A → palaeocurrent direction

- ▲ Kookfontein Formation sandstone
- ▲ Kookfontein Formation siltstone
- Skoorsteenberg Formation sandstone
- Skoorsteenberg Formation siltstone

Figure 3.28 SGR data of the average total counts (cps) and Th/K, Th/U and U/K ratios for sandstones and siltstones of the Skoorsteenberg and Kookfontein Formations, plotted against distance (in km) down-current from an arbitrary point A. The dashed line separates the Skoorsteenberg Formation (basin-floor and slope deposits) and Kookfontein Formation (slope and deltaic deposits). Based on the assumption that the provenance was the same for both formations, they have been linked in these diagrams to determine any variations in the SGR data along the transport direction.

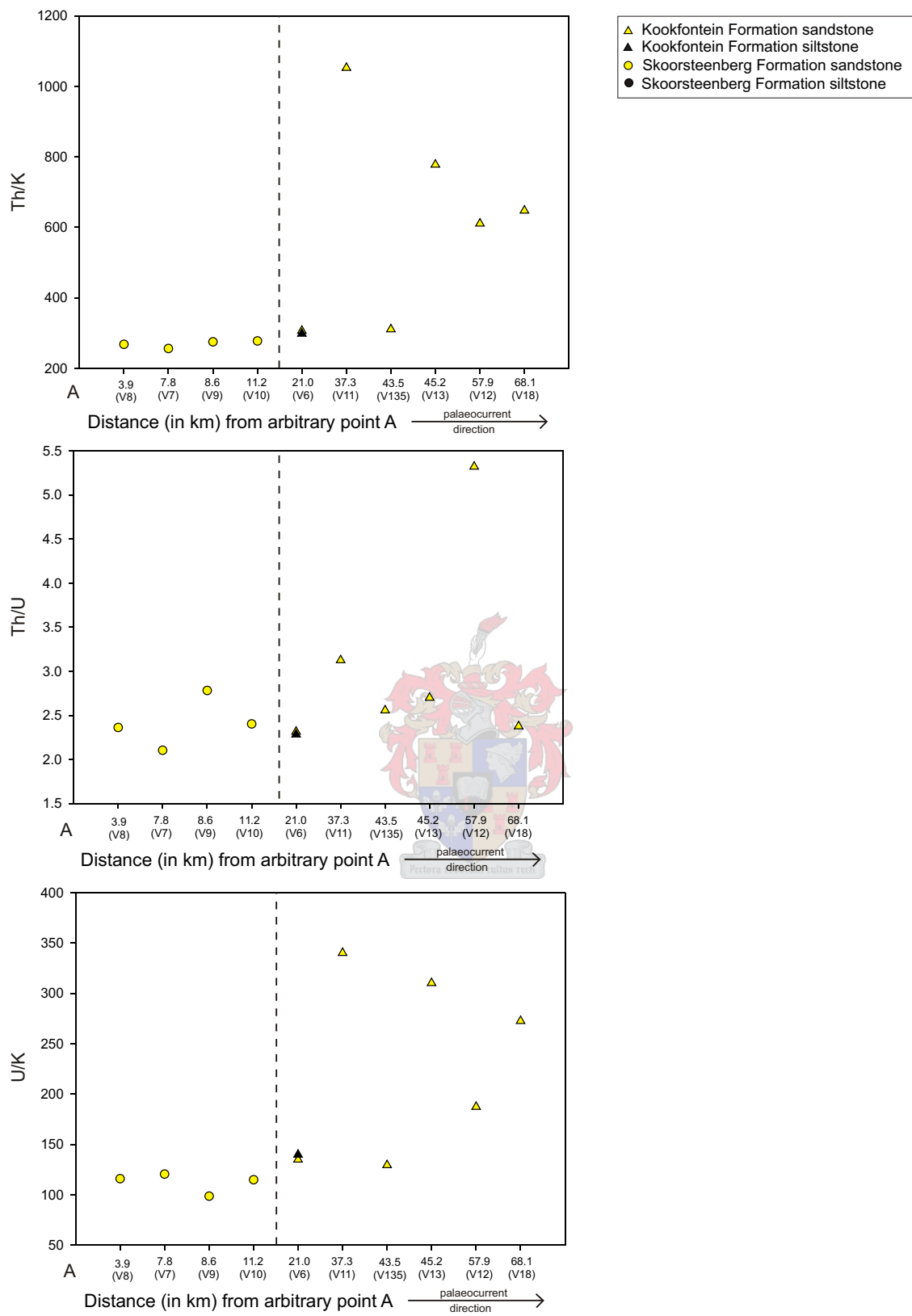


Figure 3.29 Geochemical data of the average Th/K, Th/U and U/K ratios for sandstones and siltstones of the Skoorsteenberg and Kookfontein Formations, plotted against distance (in km) down-current from an arbitrary point A. The dashed line separates the Skoorsteenberg Formation (basin-floor and slope deposits) and Kookfontein Formation (slope and deltaic deposits). Based on the assumption that the provenance was the same for both formations, they have been linked in these diagrams to determine any variations in the geochemical data along the transport direction.

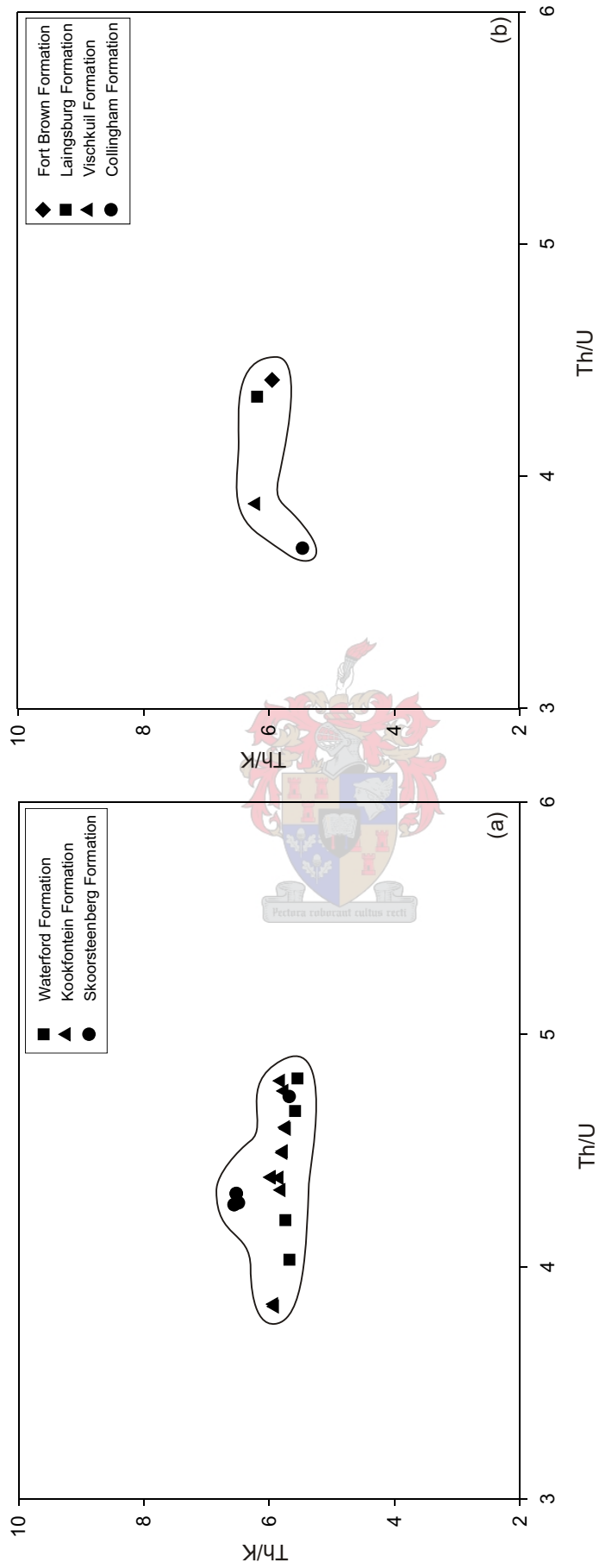


Figure 3.30 Th/K vs. Th/U for the average siltstone SGR analyses from (a) the Tanqua depocentre, and (b) the Laingsburg depocentre. The narrow trends in the Th/K ratios can be explained by relatively constant clay mineralogy. The Th/K ratios, ranging around 6 to 8, is compatible with average concentrations of kaolinite and illite/smectite (Hesselbo, 1996).

The sedimentological profiles measured at Pienaarsfontein (V6), Bitterberg (V11) and Soutrivierspunt (V13) includes Waterford Formation deposits. The sandstone and siltstone average data are shown in Table 3.5. The profiles are all relatively uniform, with occasional spikes at contact surfaces between sandstone and siltstone.

#### **3.4.4 Discussion on gamma ray characteristics of the Tanqua depocentre**

The total counts GR logs for the Tanqua depocentre are dominated by the Th content, as shown by the correlation between the Th counts and the total counts (Table 3.3). Relative concentration of Th at the expense of K during the generally palaeopedologic conditions of kaolinite formation might have caused this (Hesselbo, 1996). Th is concentrated in sand and silt-sized heavy minerals (zircon, thorite, monazite, epidote and titanite), phosphates or adsorbed and concentrated in clays. The relationships between SGR-derived K, U and Th (U/K, Th/K and Th/U), show correlations that are statistically significant, but which are less significant than the relationship between the elements and the total counts (Svensen and Hartley, 2001). A positive correlation on cross-plots between K and Th from GR analyses is shown for the sandstones and siltstones from the Tanqua depocentre. The diagrams (Figure 3.14) all show an intercept of ~4 ppm Th for 0% K. This is probably due to a calibration error. The compositional fields are all similar and distinct and reflect similarities in original mineralogy (Myers and Bristow, 1989), and thus the same source terrane(s). The original mineralogy of the Tanqua depocentre sandstones has been identified as quartz, albite, K-feldspar, opaques, biotite, lithic fragments and accessory muscovite and zircon.

The narrow trends in the Th/K ratios summarised in Figure 3.30 for the Tanqua depocentre can be explained by relatively constant clay mineralogy. The Th/K ratios, ranging around 6 to 8, is compatible with average concentrations of kaolinite and illite/smectite (Hesselbo, 1996), and in this study mostly illite, as can be seen from the petrography.

The Th/U and U/K ratios recorded from the GR measurements and from XRF measurements (Table 3.6), show a basinward and stratigraphic evolution in the Tanqua depocentre, mostly from the sandstones. The SGR K (%) data was plotted against the stratigraphic successions of the profiles measured in the Skoorsteenberg, Kookfontein and Waterford Formations (Figure 3.31). On average, the SGR K (%) values are higher in the Kookfontein Formation than in the Skoorsteenberg Formation. However, the geochemical data show the opposite. The longest section measured in the Kookfontein Formation (V6), shows an overall decrease in K (%) upwards in the succession. The possible reasons for this might be: (i) the source(s) became more depleted in K, or (ii) the formation waters were rich in Th, and K was inhibited during the formation of kaolinite. Differences in SGR and geochemical data might be due to a calibration error on the SGR tool. It should also be noted that the geochemical data is primarily based on sandstone analyses. If the trend (more K in

Table 3.5 Average total counts (cps), U/K, Th/K and Th/U from SGR measurements for profiles in the Waterford Formation. Confidence levels are at 95%.

Stratigraphy	Profile	n	Avg.		$S_e$	Lower limit	Upper limit
Waterford Formation	<u>Piensaarsfontein (V6)</u>						
	Sandstone	70					
	Total counts		60	10.7	2.50	42	89
	U/K		1.32	0.33	0.06	0.89	1.96
	Th/K		6.22	0.98	0.22	3.64	7.45
	Th/U		4.82	0.68	0.15	3.30	6.09
	Siltstone	8					
	Total counts		70	6.13	8.68	71	95
	U/K		1.24	0.19	0.17	1.21	1.69
	Th/K		5.59	0.47	0.53	5.28	7.44
	Th/U		4.67	1.20	0.64	3.68	4.96
	<u>Bitterberg (V11)</u>						
	Sandstone	2					
	Total counts		63	2.23	3.15	61	64
	U/K		1.61	0.03	0.04	1.59	1.63
	Th/K		6.53	0.04	0.06	6.50	6.56
	Th/U		4.02	0.07	0.10	3.97	4.07
	Siltstone	5					
	Total counts		65	2.82	2.52	63	88
	U/K		1.23	0.01	0.01	1.14	1.42
Th/K		4.81	0.30	0.27	4.35	6.17	
Th/U		3.91	0.25	0.22	3.51	4.82	
<u>Soutrivierspunt (V13)</u>							
Sandstone	5						
Total counts		62	6.11	5.46	60	73	
U/K		1.68	0.28	0.25	1.25	1.74	
Th/K		5.75	0.03	0.03	5.25	6.86	
Th/U		3.51	0.61	0.55	3.13	4.98	
Siltstone	4						
Total counts		63	3.85	3.85	40	79	
U/K		1.16	0.05	0.05	1.05	1.29	
Th/K		5.55	0.30	0.30	5.35	6.05	
Th/U		4.81	0.17	0.17	4.66	5.00	

Table 3.6 Average U/K, Th/K and Th/U from XRF measurements for profiles in the Tanqua depocentre. Confidence levels are at 95%.

Stratigraphy	Profile	n	Avg.		S <sub>e</sub>	Lower limit	Upper limit
Kookfontein Formation	<u>Pienaarsfontein (V6)</u>	16			17.8	91	217
	Sandstone						
	U/K		135	35.5			
		Th/K	306	48.9	24.5	242	431
		Th/U	2.31	0.35	0.18	1.60	2.69
	Siltstone	3			94.0	83.7	233
	U/K		140	81.4			
	Th/K		298	122			
		Th/U	2.28	0.50	0.58	1.88	2.84
	<u>Bitterberg (V11)</u>	6			46.9	285	425
	Sandstone						
	U/K		340	57.4			
		Th/K	1052	248	202	773	1351
		Th/U	3.13	0.73	0.60	2.29	4.20
	<u>Skoorsteenberg (V135)</u>	5			25.2	105	160
Sandstone							
U/K	129		28.2				
	Th/K	311	45.4	40.6	302	387	
	Th/U	2.56	0.16	0.14	2.41	2.73	
<u>Soutrivierspunt (V13)</u>	2			171	225	396	
Sandstone							
U/K		310	121				
	Th/K	778	19.5	27.6	764	792	
	Th/U	2.70	0.90	1.27	2.00	3.40	
<u>Katjiesberg (V12)</u>	3			143	71.1	318	
Sandstone							
U/K		187	124				
	Th/K	611	181	209	484	818	
	Th/U	5.32	5.38	6.21	1.67	11.5	
<u>Ouberg (V18)</u>	3			70.4	151	273	
Sandstone							
U/K		215	61.0				
	Th/K	469	157	181	352	648	
	Th/U	2.18	0.29	0.33	1.85	2.38	
Skoorsteenberg Formation	<u>Groot Hangklip (V8)</u>	7			10.8	103	137
	Sandstone						
	U/K		116	14.3			
		Th/K	268	43.6	33.0	205.00	319
		Th/U	2.36	0.59	0.45	1.83	3.10
	<u>Waterfall (V7)</u>	4			14.8	102	135
	Sandstone						
	U/K		121	14.8			
		Th/K	256	62.5	62.5	167	309
		Th/U	2.10	0.33	0.3	1.63	2.39
	<u>Droëkloof (V9)</u>	3			2.25	97.2	100
	Sandstone						
U/K	98.6		1.95				
	Th/K	275	6.90	7.97	267	281	
	Th/U	2.78	0.15	0.17	2.67	2.89	
<u>Klein Hangklip (V10)</u>	3			42.5	89	141	
Sandstone							
U/K		115	36.8				
	Th/K	278	42.1	48.6	231	312	
	Th/U	2.40	0.27	0.31	2.21	2.59	

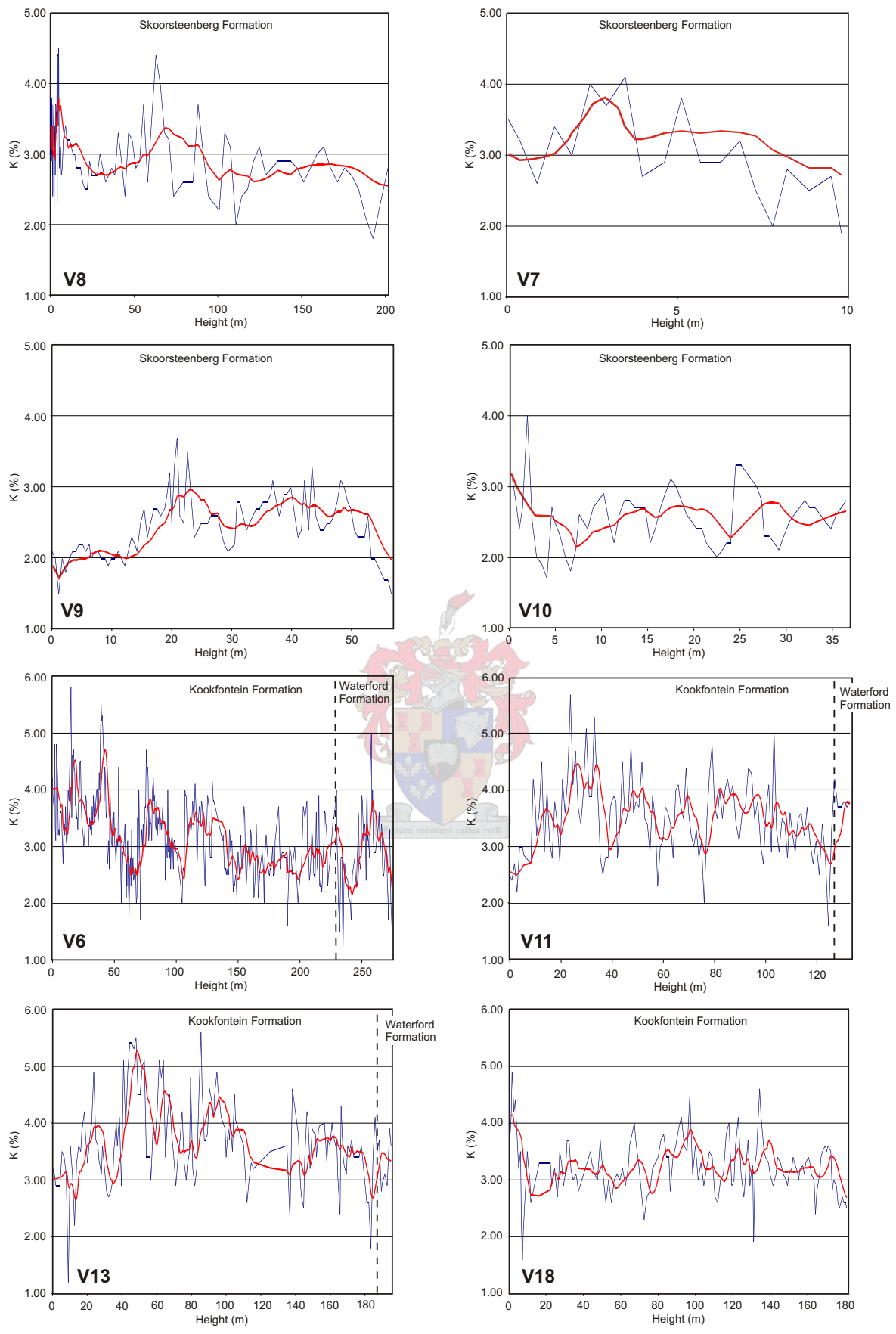


Figure 3.31 SGR data of K (%) for measured profiles in the Skoorsteenberg, Kookfontein and Waterford Formations, plotted against height (m). The dashed line separates the formations, whereas the red line represents a moving point average of 10, which decreases noise and makes it easier to identify K trends.

the Kookfontein than Skoorsteenberg Formation) is due to kaolinite formation (altered to illite), it will be concentrated in the clays (mud- and siltstones). The main source of K in the sandstones is K-feldspar. Geochemically the sandstone from the Kookfontein Formation has less K than the sandstone from the Skoorsteenberg Formation. However, petrography shows similar compositions for both formations. Illite and chlorite in sandstone thus play an important role. It is also possible that differences are due to the difference in sampling volume for the two analytical techniques. A gamma radiation reading is influenced by approximately 49 kg of rock (Løvborg *et al.*, 1971), whereas approximately 0.5 kg of rock was sampled for laboratory XRF and ICP-MS analyses.

$Al_2O_3$  is characteristic of clay minerals and feldspar, and in siltstones the  $Al_2O_3$  content is broadly indicative of the overall clay content.  $TiO_2$  can be abundant in heavy minerals such as rutile and ilmenite in sandstones (Andersson and Worden, 2004).  $TiO_2$  and  $Al_2O_3$  are only lost from a weathering profile under conditions of extreme weathering (Hill *et al.*, 2000). In this study, there were not enough data to draw any conclusions from  $TiO_2/Al_2O_3$  vs. stratigraphy. Higher ratios of  $TiO_2/Al_2O_3$  through the stratigraphy may indicate derivation from subtly different sediment source lithologies in the hinterland (Andersson and Worden, 2004). The study of these authors on the mudstones from the Skoorsteenberg Formation in the Tanqua depocentre showed increases in  $TiO_2/Al_2O_3$  upwards in the stratigraphic succession, which would suggest that the source area(s) became more enriched in ferromagnesian minerals, perhaps due to an unroofing trend.

Andersson and Worden (2004) carried out extensive SGR studies on the Skoorsteenberg Formation. They found the following:

1. The total GR motif for the sand-rich fans generally showed a blocky character with a sharp base and top, typical for basin-floor fans;
2. The SGR pattern for total counts, K, U, Th and ratios of these elements were erratic in the mudstone successions;
3. K-bearing minerals (illite and chlorite) were responsible for the majority of the total gamma radiation in the mudstones and identified clay mineral peaks;
4. No major changes between the interfan and intrafan mudstones were observed in the SGR data set that could imply a different origin;
5. There were no distinct signals in the SGR pattern of the mudstone intervals, which could potentially correspond to maximum flooding surfaces;
6. Lateral changes along both intrafan and interfan mudstones were observed in SGR data, concerning particularly the concentration of U, which increases basinwards;
7. No other geochemical or mineralogical signals that vary along the sediment flow path were found.

The SGR data from this study correspond to points 1 to 5 above. No lateral changes were found in the U SGR data in either the siltstones or sandstones. However, there is an overall decrease in K upwards in the succession in the Kookfontein Formation.

The net relative basinward increase in U in the inter- and intrafan mudstones, studied by Andersson and Worden (2004), was attributed to there being less clastic material to dilute the U. It is possible that this effect is only applicable to the mudstones within Fans 1 to 4 and Unit 5 of the Skoorsteenberg Formation, and not to the succession from Unit 5 in the Skoorsteenberg Formation to the Waterford Formation.

### **3.5 Laingsburg depocentre**

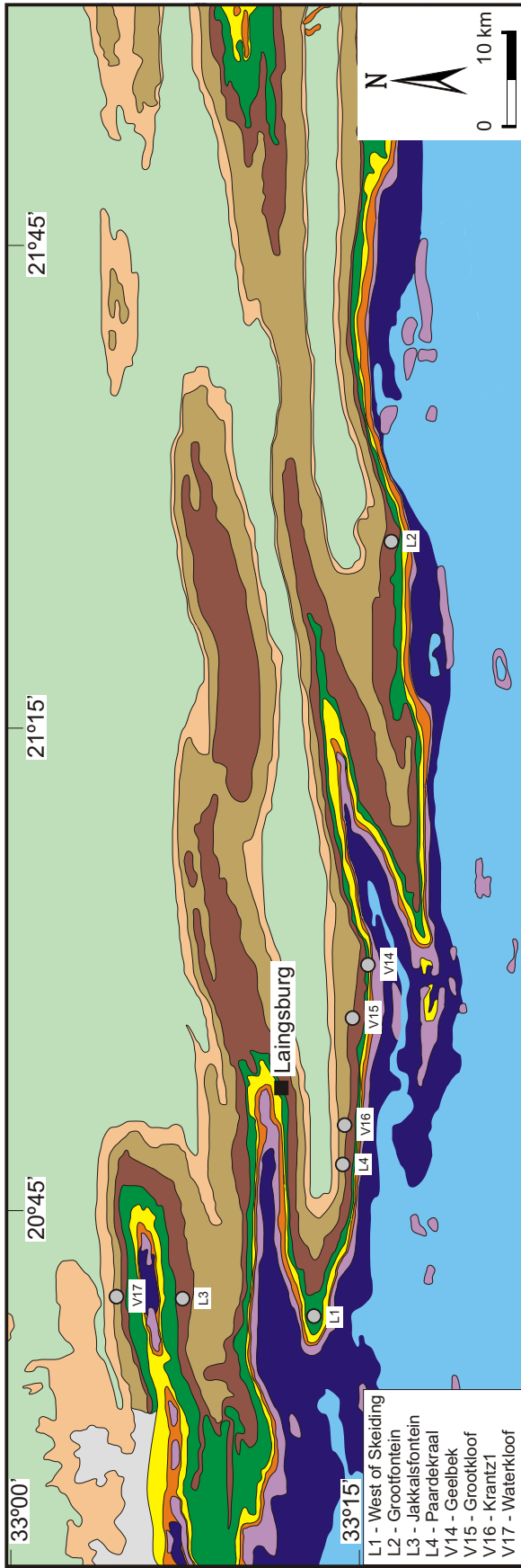
The regional distribution of the Collingham, Vischkuil, Laingsburg and Fort Brown Formations, with the localities of the measured sedimentological and GR profiles, are shown in Figure 3.32.

#### **3.5.1 Collingham Formation**

The Collingham Formation (30 – 70 m thick) overlies the Whitehill Formation with a sharp conformable contact and consists of alternating beds of dark grey mudstone and cherty mudstone, yellowish tuff beds, siltstone and very fine- to fine-grained sandstone (Viljoen, 1992a). The Matjiesfontein Chert Bed occurs in the lower part of the formation. The tuff layers, deposited from suspension, range in thickness from 1 – 20 cm (commonly < 5 cm thick) and are sharp-based and infrequently reworked in their upper portions (Viljoen, 1992a). Tractional structures and occasional sole structures exhibited by the fine siltstone and sandstone beds, and their association with typical deep-water shale, confirm a turbiditic origin (Wickens, 1994; Viljoen, 1995).

The outcrop section of Geelbek (V14) is interpreted as a shelf to basin-floor depositional environment for the Collingham Formation (Figure 3.33). The trends for U/K, Th/K, Th/U and total counts data are erratic compared to any of the other GR profiles measured (Figure 3.34). Spikes of higher values can especially be seen for measurements taken from the tuff (K-bentonite) beds. The sandstone and siltstone average U/K, Th/K, Th/U and total counts are shown in Table 3.7.

The total counts GR log is dominated by the Th content, as shown by the correlation between the Th counts and the total counts ( $r = 0.28$  for both the sandstones and siltstones). K and U show very low correlations with total counts (Table 3.3). K-Th cross-plots from GR analyses show positive correlation between the K and Th for sandstones and siltstones (Figure 3.35).



- L1 - West of Skeiding
- L2 - Grootfontein
- L3 - Jakkalsfontein
- L4 - Paardekraal
- V14 - Geelbek
- V15 - Grootkloof
- V16 - Krantz1
- V17 - Waterkloof

**Geological legend**



- Mudstone, siltstone, sandstone, thin cherty beds
- Sandstone, mudstone, shale
- a - Shale
- b - Shale with thin siltstone and sandstone beds
- c - Sandstone, greywacke and siltstone
- d - Arenaceous shale, siltstone and thin sandstone beds
- Siltstone, chert and sandstone with thin interbedded shale and yellow-weathering mudstone/tuff
- Dark grey shale, light grey weathering with cherty siltstone beds in upper part
- Dark grey shale with reddish brown weathering siltstone
- Tillite, diamictite, subsidiary shale

Figure 3.32 Geological map of the Laingsburg depocentre, Karoo Basin, South Africa, showing the Collingham, Vischkuil, Laingsburg and Fort Brown Formations and measured sedimentological and SGR profile locations. Geological information from the Ladismith 3320 map. 1:250 000 Geological series, Geological Survey of South Africa.

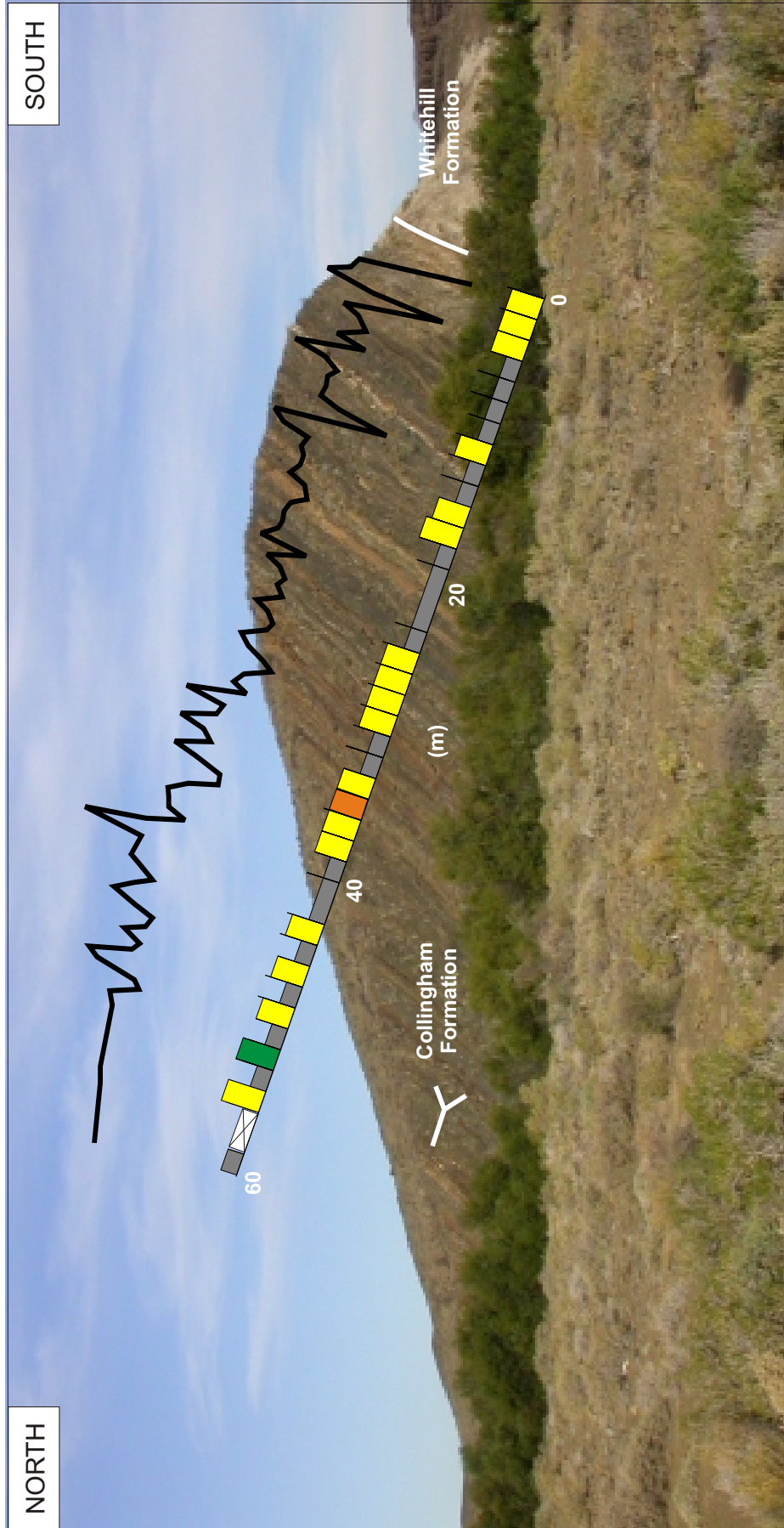
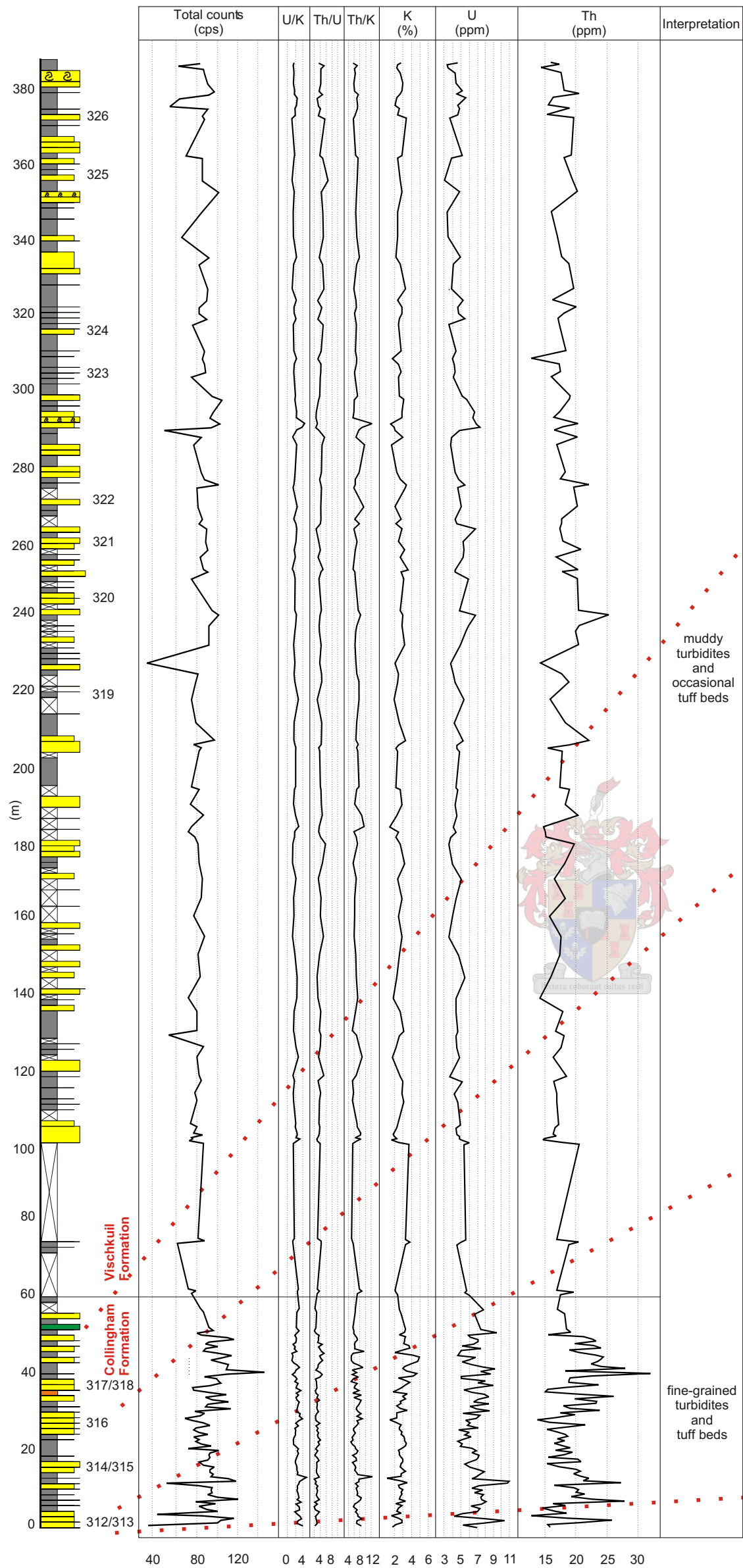
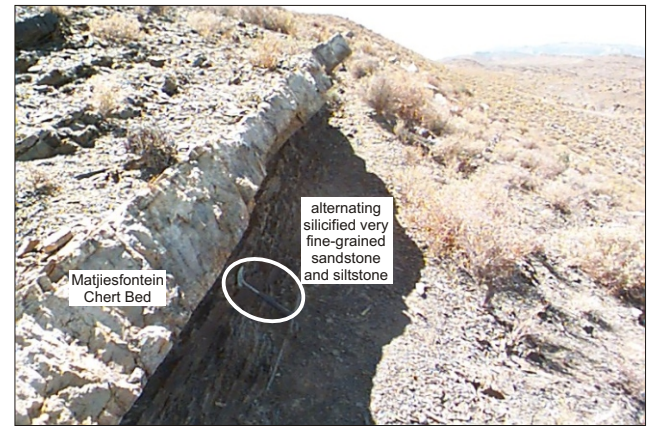


Figure 3.33 The outcrop section of the Collingham Formation at Geelbek (V14) southeast of Laingsburg. The Collingham Formation is dominated by sheet-like mud-rich turbidites, intercalated with thin, volcanic ash layers. Part of the sedimentological (V14) and GR logs are shown. Location: GPS 33°14'50.3"S, 020°59'54.1"E



Facies key:

- Mudstone
- Siltstone
- Very fine- to lower medium-grained sandstone
- Sandstone with soft-sediment deformational features
- Bentonite
- Matjiesfontein Chert Bed



The Matjiesfontein Chert Bed in alternating, silicified, very fine-grained sandstone and siltstone. Hammer for scale (30 cm) is circled.



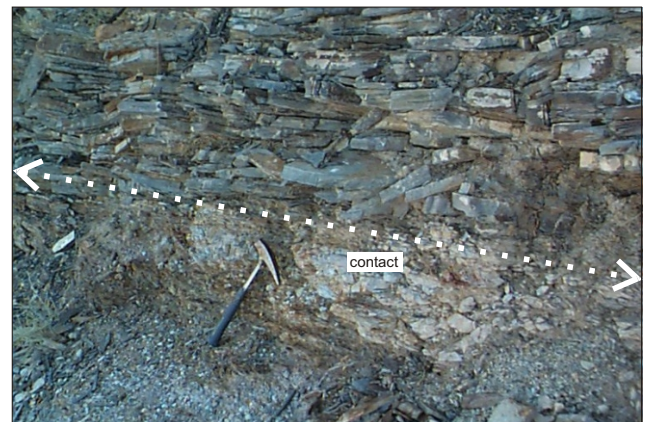
Tuff (K-bentonite) bed, within the Collingham Formation. Pocket-knife for scale (7 cm) is circled.



Alternating siltstone and tuff beds, including the Matjiesfontein Chert Bed, within the Collingham Formation.



Thin-bedded, alternating silicified beds of sandstone and siltstone, intercalated with tuff beds.



Sharp contact between the Whitehill Formation and the overlying sheet-like mud-rich turbidites and thin tuff beds of the Collingham Formation.

Figure 3.34 Geelbek (V14) outcrop section, interpreted as a shelf to basin-floor depositional environment. Comparison between SGR logs and lithology. SGR results are from 195 measurements at an average vertical spacing of 50 cm. The location of samples taken are indicated next to the lithology as 312 - 326.

Table 3.7 Average total counts (cps), U/K, Th/K and Th/U from SGR measurements for profiles in the Collingham Formation. Confidence levels are at 95%.

Stratigraphy	Profile	n	Avg.		S <sub>e</sub>	Lower limit	Upper limit					
Collingham Formation	Geelbek (V14)	77										
	Sandstone											
	Total counts							72	15.3	3.49	49	98
	U/K							2.42	0.63	0.14	1.22	3.85
		Th/K	7.17	1.67	0.38	5.38	9.81					
		Th/U	3.05	0.56	0.13	2.23	4.52					
	Siltstone	7										
	Total counts							65	6.03	4.56	57	73
U/K	1.53							0.33	0.25	1.09	2.18	
Th/K	5.45							0.45	0.34	4.85	6.22	
	Th/U	3.69	0.74	0.56	2.57	4.65						



Table 3.8 Average total counts (cps), U/K, Th/K and Th/U from SGR measurements for profiles in the Vischkuil Formation. Confidence levels are at 95%.

Stratigraphy	Profile	n	Avg.		S <sub>e</sub>	Lower limit	Upper limit					
Vischkuil Formation	Geelbek (V14)	79										
	Sandstone											
	Total counts							63	11.0	2.48	30	81
	U/K							1.94	0.50	0.11	1.24	3.55
		Th/K	7.26	1.14	0.26	5.69	9.94					
		Th/U	3.87	0.65	0.15	2.60	5.32					
	Siltstone	17										
	Total counts							60	10.40	5.04	42	76
U/K	1.64							0.39	0.19	1.19	2.67	
Th/K	6.19							0.77	0.37	5.39	8.05	
	Th/U	3.88	0.59	0.29	3.02	5.05						

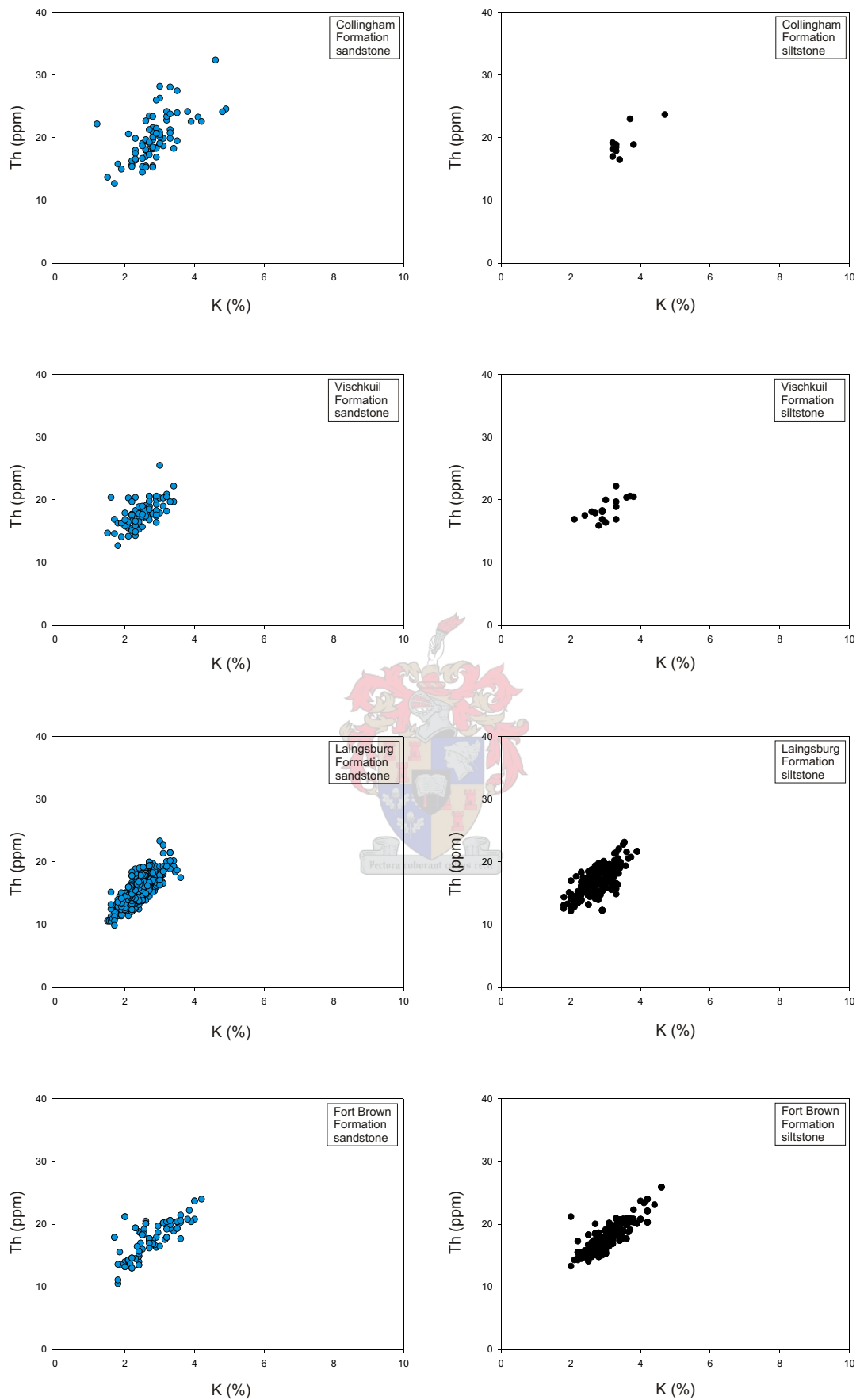


Figure 3.35 K vs. Th cross-plots for the sandstones and siltstones from the Laingsburg depocentre, used to distinguish between the different facies associations and formations from GR analyses (method after Myers and Bristow, 1989).

### 3.5.2 *Vischkuil Formation*

The contact between the Vischkuil Formation and Collingham Formation is conformable and clearly defined. The Vischkuil Formation attains a thickness of 200 to 400 m and consists predominantly of mudstone, siltstone and fine-grained sandstone (Viljoen and Wickens, 1992). The lower part of the Vischkuil Formation is dominated by mudstone, with occasional thin siltstone beds and several slump horizons, whereas the upper 40 m consists of metre-scale fining-upward beds separated by mudstone (Viljoen and Wickens, 1992). The slump zones in the upper Vischkuil Formation is interpreted by Wickens (1994) as an indication of the proximity to a slope, and the entire formation itself as the distal end of a turbidite system which becomes gradually more proximal in the upper parts.

The outcrop section of Geelbek (V14) is interpreted as a basin-floor depositional environment for the Vischkuil Formation (Figure 3.36). The U/K (sandstone avg. = 1.94, n = 79; siltstone avg. = 1.64, n = 17) is relatively uniform, only showing spikes of higher values along with spikes in the Th/K and Th/U profiles. These spikes are related to the total counts profile, in that they show increases in values, compared to spikes of lower total counts values (Figure 3.34). The spikes are generally present on contacts between very fine siltstone, coarse siltstone and sandstone lithologies, showing differences in mineralogy and grain size. The average data for Th/K, Th/U and total counts for sandstones and siltstones are shown in Table 3.8.

There is a slight overall decrease in the total counts data upwards in the section, along with an increase in the sandstone: siltstone ratio. The total counts GR log is dominated by the Th content, as shown by the correlation between the Th counts and the total counts ( $r = 0.28$  for sandstones and  $r = 0.31$  for siltstones). This is discussed later on in this chapter. K and U show very low correlations with total counts (Table 3.3). Positive correlation is shown between K and Th for sandstones and siltstones on cross-plots from GR measurements (Figure 3.35).

### 3.5.3 *Laingsburg Formation*

The boundary between the Vischkuil and Laingsburg Formation is gradational and defined as a horizon above which sandstone predominates over mudrock (Viljoen, 1992b). The Laingsburg Formation, consisting predominantly of very fine- to lower medium-grained sandstone and attaining a thickness of 750 m, is made up of six turbidite fans, informally called Fans A to F, each separated by a significant thickness of hemipelagic and turbiditic mudstone (Sixsmith, 2000). The fans represent a basin-fill succession with Fan A (basin-floor) constituting ~40% of the Laingsburg Formation with a thickness of 350 m southeast of Laingsburg, Fan B (base of slope) attaining a thickness of 80 – 150 m, and Fans C to F (slope) having thicknesses ranging between 10 – 100 m (Grecula, 2000; Sixsmith, 2000). The

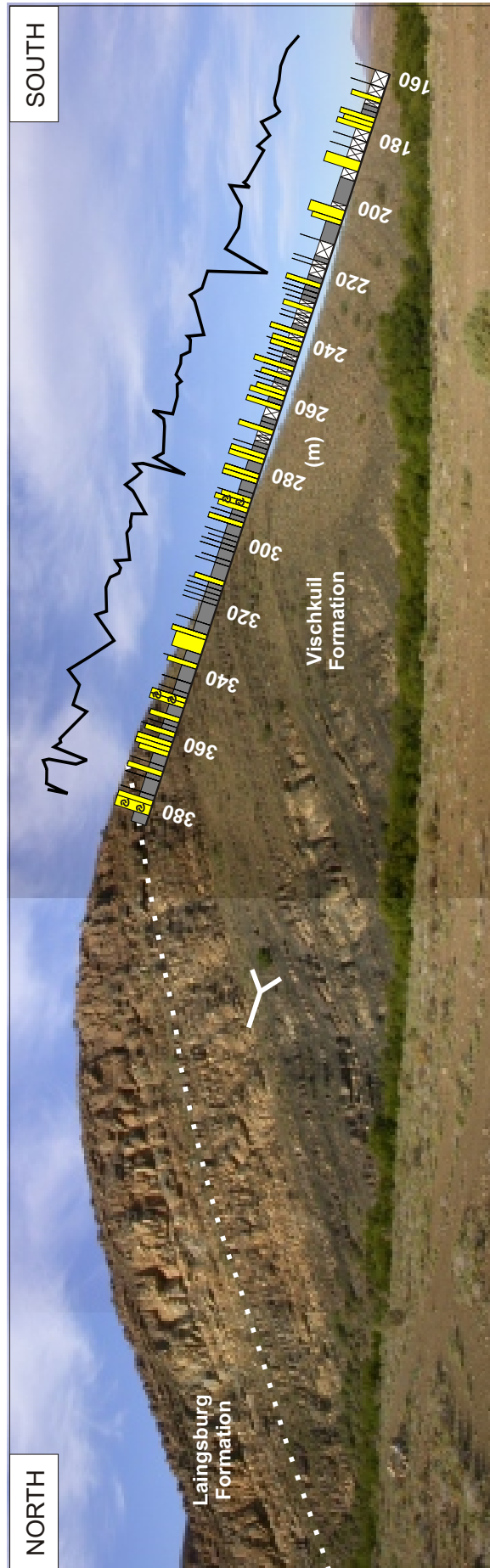


Figure 3.36 The outcrop setting of the Vischkuil Formation at Geelbek (V14), southeast of Laingsburg. Note the gradational contact between the mud-prone turbidite succession of the Vischkuil Formation and the sand-rich turbidites of the Laingsburg Formation. Part of the sedimentological (V14) and GR logs from above the Collingham Formation are shown. Location: GPS 33°14'50.3"S, 020°59'54.1"E

key sedimentological features, which control SGR signatures, of Fans A to F are shown in Table 3.9.

### 3.5.3.1 Fan A

Sixsmith (2000) has done extensive sequence stratigraphic work on Fan A in the Laingsburg area. He subdivided Fan A into seven time-stratigraphic depositional units (Units 1 to 7) bounded by regionally correlatable key surfaces, such as flooding surfaces and sequence boundaries. The present study attempted to compare these subdivisions to the SGR data and determine whether it is possible to make the same characteristic subdivisions based on GR data. Fan A is predominantly composed of alternating sheet-like, medium- to thick-bedded sandstone, rhythmic thin-bedded sandstone/siltstone units and shale units of varying thickness (Wickens, 1994).

The profile for Fan A was measured at Grootkloof (V15) (Figure 3.37). The trends for U/K, Th/K, Th/U and total counts data in V15 show small spikes for the fine- and lower medium-grained sandstone, relative to the very fine-grained sandstone and siltstone (Figure 3.38). The sedimentological profile has a large sandstone: siltstone ratio. The average SGR data for the sandstones and siltstones are shown in Table 3.10.

The stratigraphic interval correlation of the Collingham and Vischkuil Formations, in relation to Fan A of the Laingsburg Formation, is shown in Figure 3.39.

### 3.5.3.2 Fan B

Fan B is separated from Fan A by a shale unit persistent over the entire outcrop region. Along the base of the Fan B succession, are stacked, thick-bedded, mostly amalgamated, sandstone beds that are overlain by progressively thinner beds towards the top (Wickens, 1994). The channel fills in Fan B widen down-fan and are directly attached to the extensive transitional and proximal thick-bedded sheet elements (Grecula, 2000). These channel fills are grouped into complexes, which create a branching network fringed by overbank sheet-like deposits, extending over 40 km down depositional dip to the east (Grecula *et al.*, 2003). The sand-prone overbank elements coalesce between the channel branches and thus there is no significant mudstone accumulation in the interchannel areas. The vertical succession of facies in their stages of growth is generally accepted as being the product of gradual reduction in the volume of the mass flows, associated with a progressive relative rise in sea-level (Mutti, 1984; Bouma *et al.*, 1985, 1989; Posamentier and Vail, 1988; Wickens, 1994).

The outcrop sections of Krantz1 (V16) (Figure 3.40) and Waterkloof (V17), (Figure 3.41) measured from Fans B and C of the Laingsburg Formation to the overlying Fort Brown

Table 3.9 Comparison of key features of Fans A to F of the Laingsburg Formation (after Viljoen and Wickens, 1995; Grecula, 2000; Sixsmith, 2000).

Fan number	Lithology and sedimentary structures	Depositional setting	Process of deposition	Thickness
A	Alternating sheet-like, medium- to thick-bedded sandstone, rhythmic thin-bedded sandstone/siltstone units and shale; occasional large-scale channel-fills.	Basin-floor	Deposition from high-concentration turbidity currents and hemipelagic suspension. Variety of flow types dominated by depletive steady flow.	160 - 350 m
B	Stacked, thick-bedded, mostly amalgamated, sandstone beds, overlain by progressively thinner beds towards the top.	Base of slope	High-concentration turbidity currents, becoming more depletive.	80 - 150 m
C	Thick-bedded, massive and mostly amalgamated sandstone beds at their base, succeeded by thinner-bedded turbidites.	Slope	High-concentration turbidity currents, becoming more depletive.	10 - 100 m
D	Two closely spaced sandstone-rich units. Channel-fill and overbank deposits.	Slope	High-concentration turbidity currents.	10 - 100 m
E	Muddy sandstone and thin beds of massive sandstone.	Slope	Low-high concentration turbidity currents.	10 - 100 m
F	Muddy sandstone and thin beds of massive and parallel-stratified sandstone.	Slope	Low-high concentration turbidity currents.	10 - 100 m

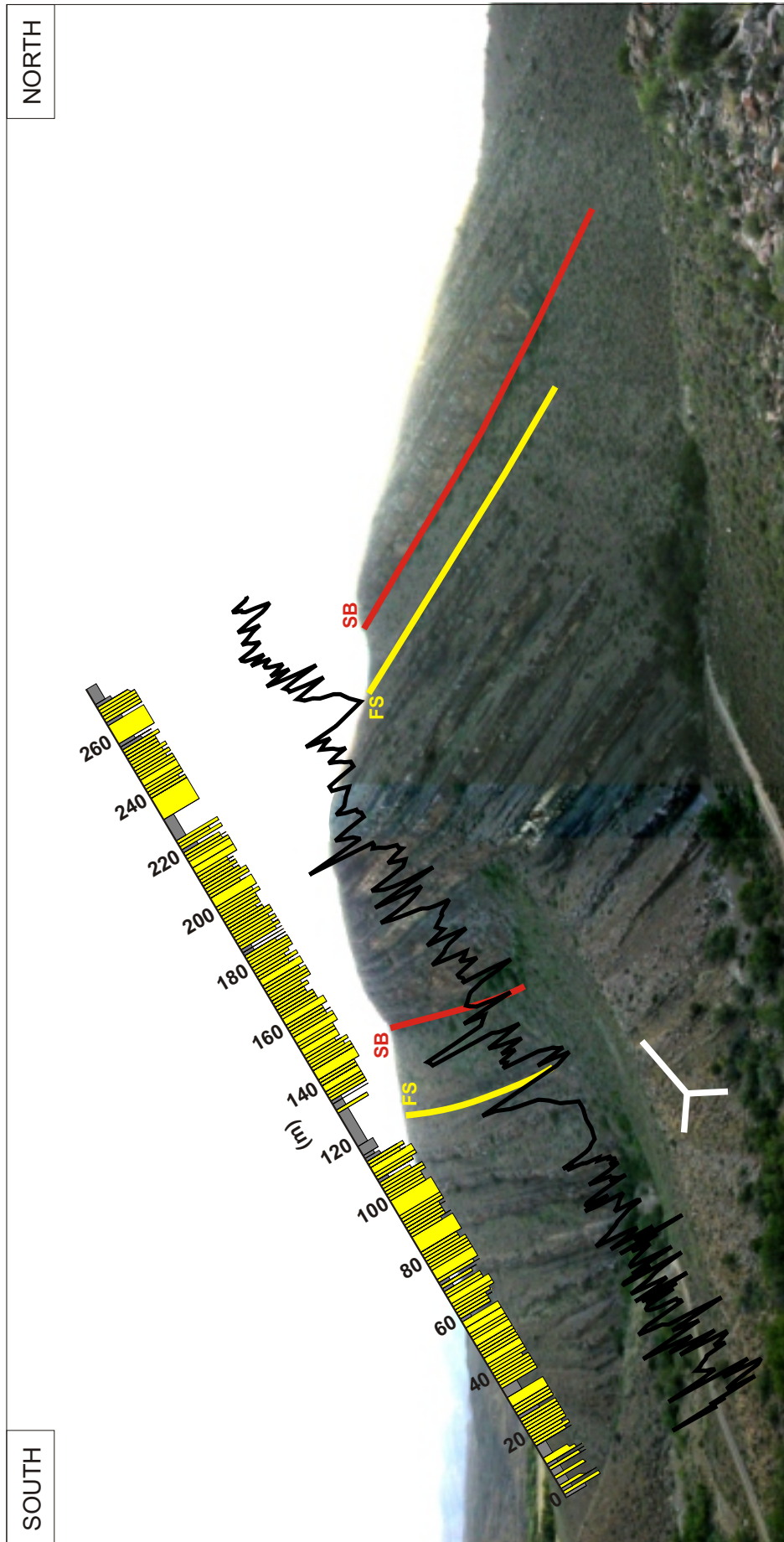
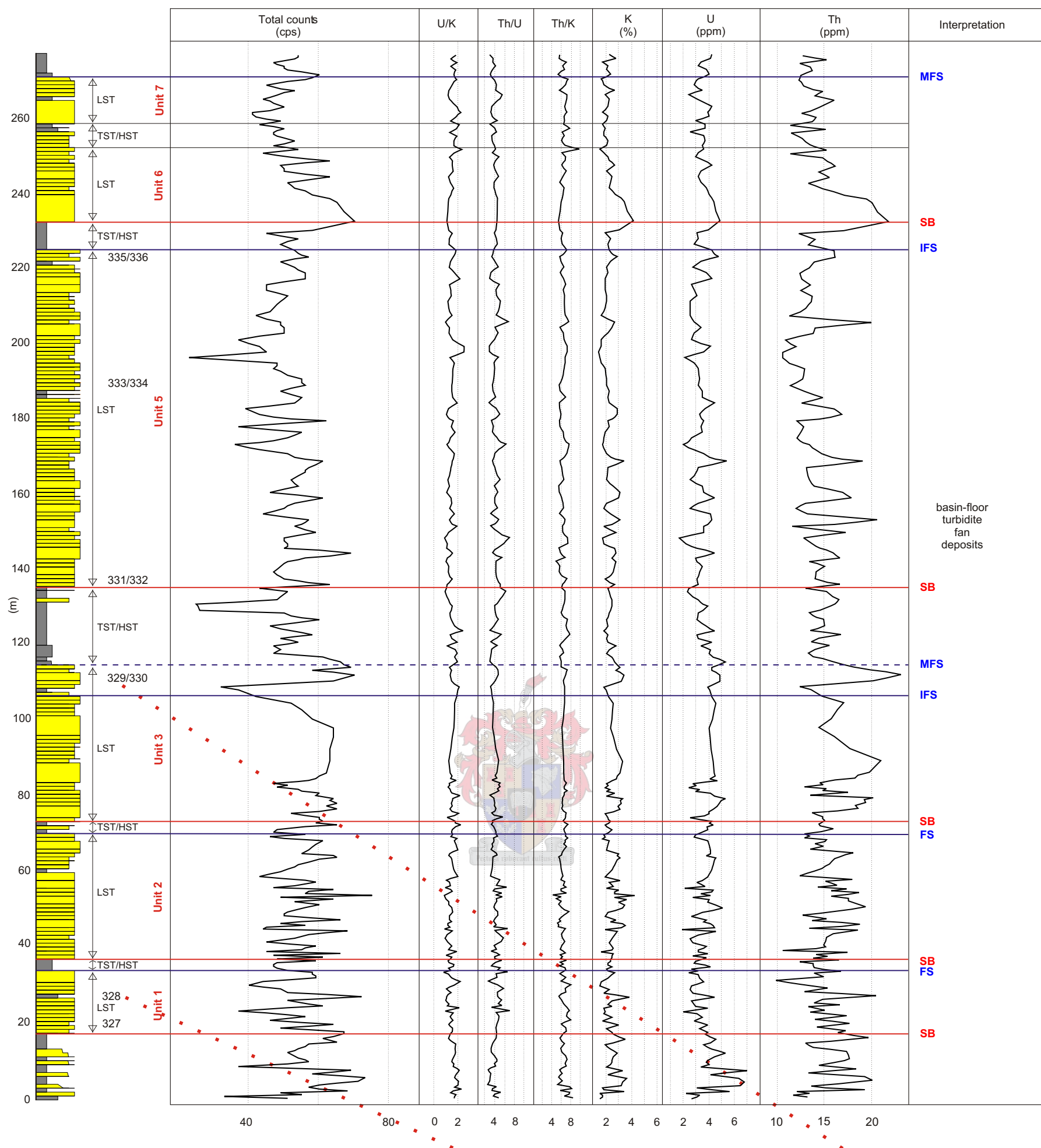


Figure 3.37 The outcrop setting of Grootkloof (V15), south of Laingsburg, representing a basin-floor succession. FS - Flooding Surface (not differentiated). SB - Sequence Boundary. Stratigraphic interpretation after Sixsmith (2000). The sedimentological (V15) and GR logs are shown. Location: GPS 33°14'32.1"S, 020°56'29.1"E



**Facies key:**

- Mudstone
- Siltstone
- Very fine- to lower medium-grained sandstone

SB - Sequence Boundary  
 FS - High order Flooding Surface (undistinguished)  
 IFS - High order Initial Flooding Surface  
 MFS - High order Maximum Flooding Surface  
 LST - Lowstand Systems Tract  
 TST - Transgressive Systems Tract  
 HST - Highstand Systems Tract



Progressively upward-thinning sandstone beds in a siltstone/sandstone/mudstone succession. Hammer for scale (30 cm) is circled. Sample location of 327 and 328.



Low-amplitude wavy beds of alternating sandstone and siltstone, capped by a thicker bed of parallel-stratified sandstone. Sample location of 329 and 330.

Figure 3.38 Grootkloof (V15), south of Laingsburg, representing the basin-floor turbidite deposits of Fan A in the Laingsburg Formation. Stratigraphic interpretation after Sixsmith (2000). Comparison between SGR logs and lithology. SGR results are from 407 measurements at an average vertical spacing of 50 cm. The location of samples taken are indicated next to the lithology as 327 - 336. Note that Unit 4 has shaled out at this position.

Table 3.10 Average total counts (cps), U/K, Th/K and Th/U from SGR measurements for profiles in Fans A - F in the Laingsburg Formation. Confidence levels are at 95%.

Stratigraphy	Profile	n	Avg.		S <sub>e</sub>	Lower limit	Upper limit		
Laingsburg Formation	<u>Krantz1 (V16) and Waterkloof (V17)</u>								
	Fan F	Sandstone	61						
		Total counts		59	8.22	2.10	45	87	
		U/K		1.68	0.25	0.06	1.23	2.19	
		Th/K		6.70	0.65	0.17	5.70	8.09	
		Th/U		4.06	0.55	0.14	3.02	5.58	
		Siltstone	249						
		Total counts		57	4.92	0.62	46	87	
		U/K		1.50	0.25	0.03	0.76	2.15	
		Th/K		6.12	0.49	0.06	5.20	8.50	
		Th/U		4.19	0.78	0.10	2.78	8.32	
		<u>Krantz1 (V16) and Waterkloof (V17)</u>							
		Fan E	Sandstone	42					
	Total counts			53	4.94	1.52	43	61	
	U/K			1.45	0.22	0.07	1.12	2.00	
	Th/K			6.75	0.74	0.23	5.43	8.50	
	Th/U			4.70	0.46	0.14	3.39	5.41	
	Siltstone		266						
	Total counts			56	4.46	0.55	38	73	
	U/K			1.42	0.26	0.03	0.83	2.12	
	Th/K			6.15	0.71	0.09	4.52	8.50	
	Th/U			4.42	0.72	0.09	2.95	7.84	
	<u>Krantz1 (V16) and Waterkloof (V17)</u>								
	Fan D		Sandstone	92					
		Total counts		52	5.69	1.19	38	65	
		U/K		1.68	0.22	0.05	1.04	2.13	
		Th/K		6.71	0.46	0.10	5.34	7.60	
		Th/U		4.05	0.66	0.14	2.98	6.72	
		Siltstone	221						
		Total counts		54	5.45	0.73	38	66	
		U/K		1.57	0.26	0.03	0.83	2.19	
		Th/K		6.33	0.60	0.08	4.24	8.09	
		Th/U		4.14	0.75	0.10	3.09	7.58	
		<u>Krantz1 (V16) and Waterkloof (V17)</u>							
		Fan C	Sandstone	67					
	Total counts			56	9.15	2.24	41	83	
U/K			1.43	0.24	0.06	1.00	2.10		
Th/K			7.11	0.52	0.13	5.76	8.14		
Th/U			5.12	0.91	0.22	3.45	7.13		
Siltstone	267								
Total counts			55	5.68	0.70	41	75		
U/K			1.30	0.22	0.03	0.87	2.10		
Th/K			6.12	0.55	0.07	5.21	7.73		
Th/U			4.83	0.80	0.10	3.30	7.00		
<u>Krantz1 (V16) and Waterkloof (V17)</u>									
Fan B	Sandstone		183						
	Total counts		61	7.53	1.11	41	77		
	U/K		1.47	0.21	0.03	1.07	2.00		
	Th/K		6.78	0.49	0.07	5.85	8.36		
	Th/U		4.71	0.67	0.10	3.30	6.36		
	Siltstone	35							
	Total counts		59	7.56	2.56	48	81		
	U/K		1.50	0.25	0.08	1.17	2.00		
	Th/K		6.40	0.47	0.16	5.50	7.00		
	Th/U		4.36	0.67	0.23	2.91	5.70		
	<u>Geelbek (V14)</u>								
	Fan A	Sandstone	340						
Total counts			52	7.48	0.81	23	75		
U/K			1.54	0.26	0.03	0.93	2.41		
Th/K			6.37	0.59	0.06	4.17	9.50		
Th/U			4.24	0.77	0.08	2.75	7.14		
Siltstone		67							
Total counts			57	7.92	1.94	39	73		
U/K			1.46	0.23	0.06	1.11	2.06		
Th/K			5.91	0.47	0.11	4.79	7.04		
Th/U			4.14	0.59	0.14	2.60	5.53		

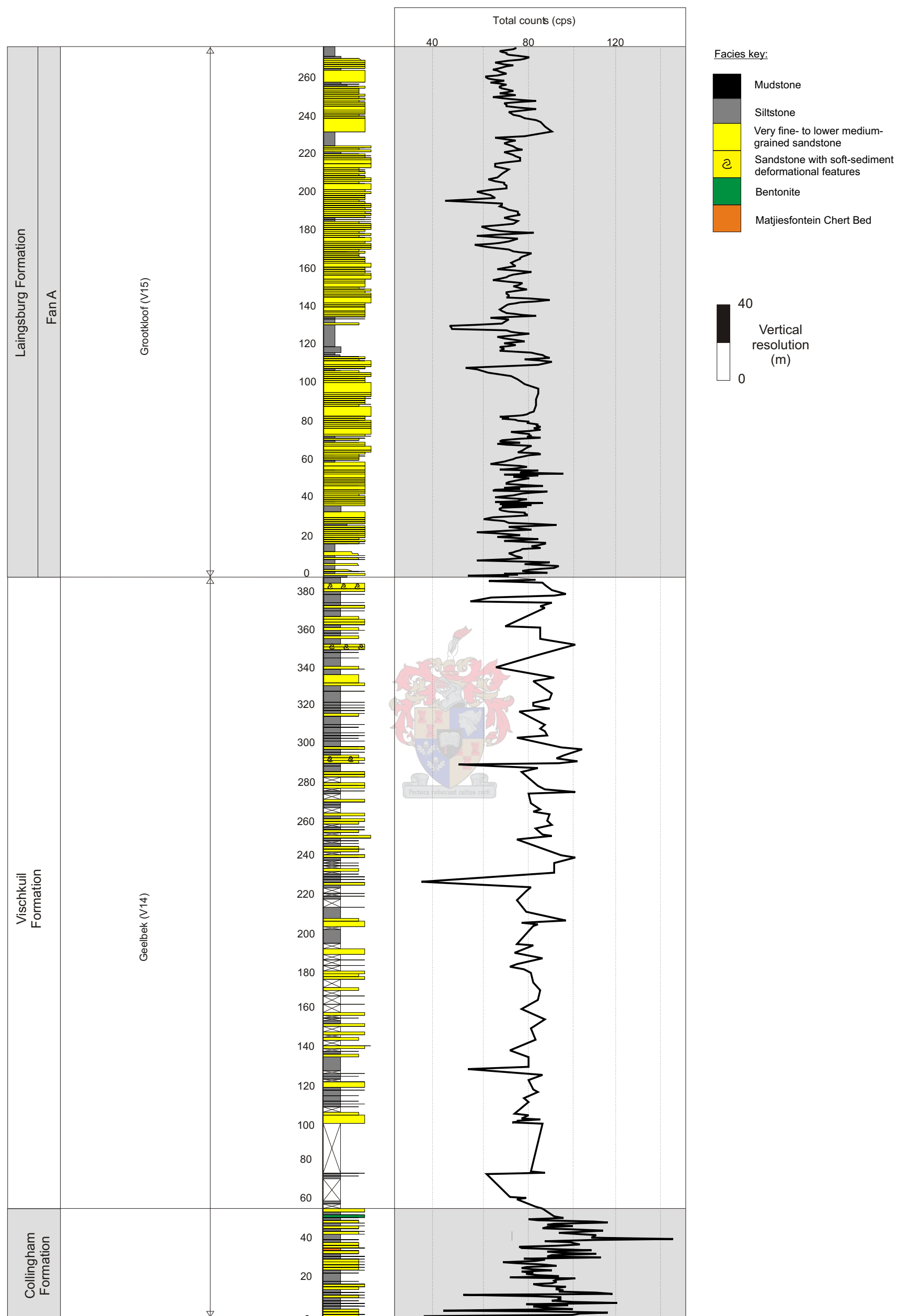


Figure 3.39 Laingsburg depocentre. Simplified stratigraphic cross-section of the Collingham and Vischkuil Formations combined with Fan A of the Laingsburg Formation to visually compare the SGR log with the sedimentological profile. The section logged at Grootkloof (V15) is situated 5.3 km west of the section logged at Geelbek (V14).

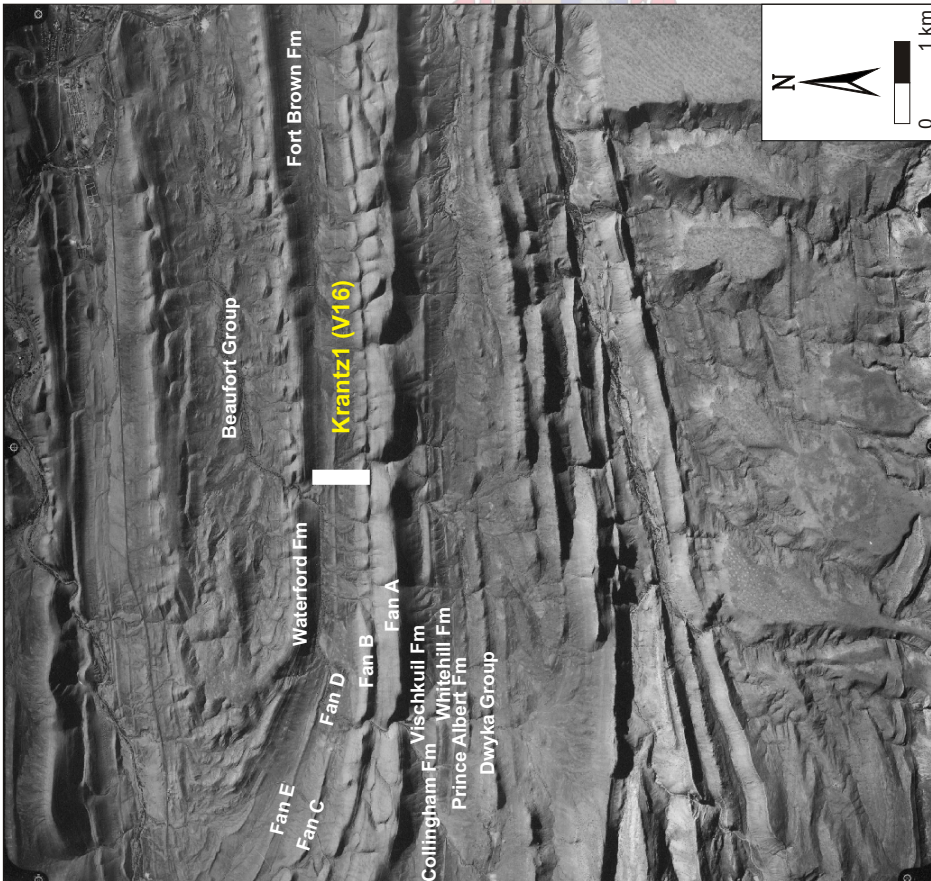


Figure 3.40 Aerial photograph (Job1025, Strip 4/2521) to indicate the position of the Krantz1 (V16) log and stratigraphic units cropping out along the southern limb of the Skeiding syncline, south of Laingsburg. (Photograph courtesy of the Chief Directorate of Surveys and Mapping, South Africa.)

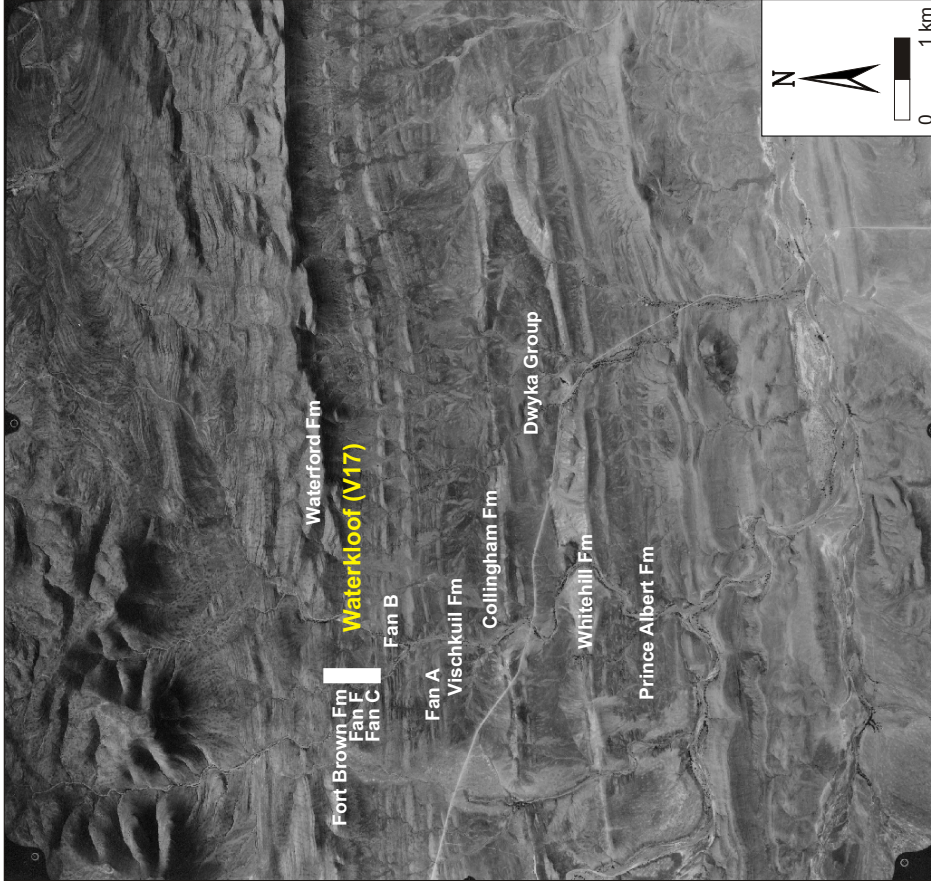


Figure 3.41 Aerial photograph (Job 1025, Strip 2/1586) to indicate the position of the Waterkloof (V17) log and stratigraphic units cropping out, northwest of Laingsburg. (Photograph courtesy of the Chief Directorate of Surveys and Mapping, South Africa.)

Formation, are interpreted to represent base of slope deposits (Fan B), slope deposits (Fans C to F) and pro-delta deposits (Fort Brown Formation). The Krantz1 (V16) and Waterkloof (V17) total counts logs show spikes at the top of Fan B (Figures 3.42 and 3.43). The profiles for the ratios are uniform. The sandstone average total counts data are 61 cps (n = 183). Further peaks are at the contacts between the sandstone and coarse siltstone, and very fine siltstone. The sandstone and siltstone average SGR data collected are shown in Table 3.10.

### **3.5.3.3 Fan C**

Fan C is separated from Fan B by a shale unit that attains a thickness of approximately 150 m, and the fan itself is predominantly comprised of thick-bedded, massive and mostly amalgamated sandstone beds at their base, succeeded by thinner-bedded turbidites (Wickens, 1994).

The trends for U/K, Th/K, Th/U and total counts measured at Krantz1 (V16) and Waterkloof (V17) become more uniform with movement from the base to the top of Fan C (Figures 3.42 and 3.43), with sandstone and siltstone average values shown in Table 3.10.

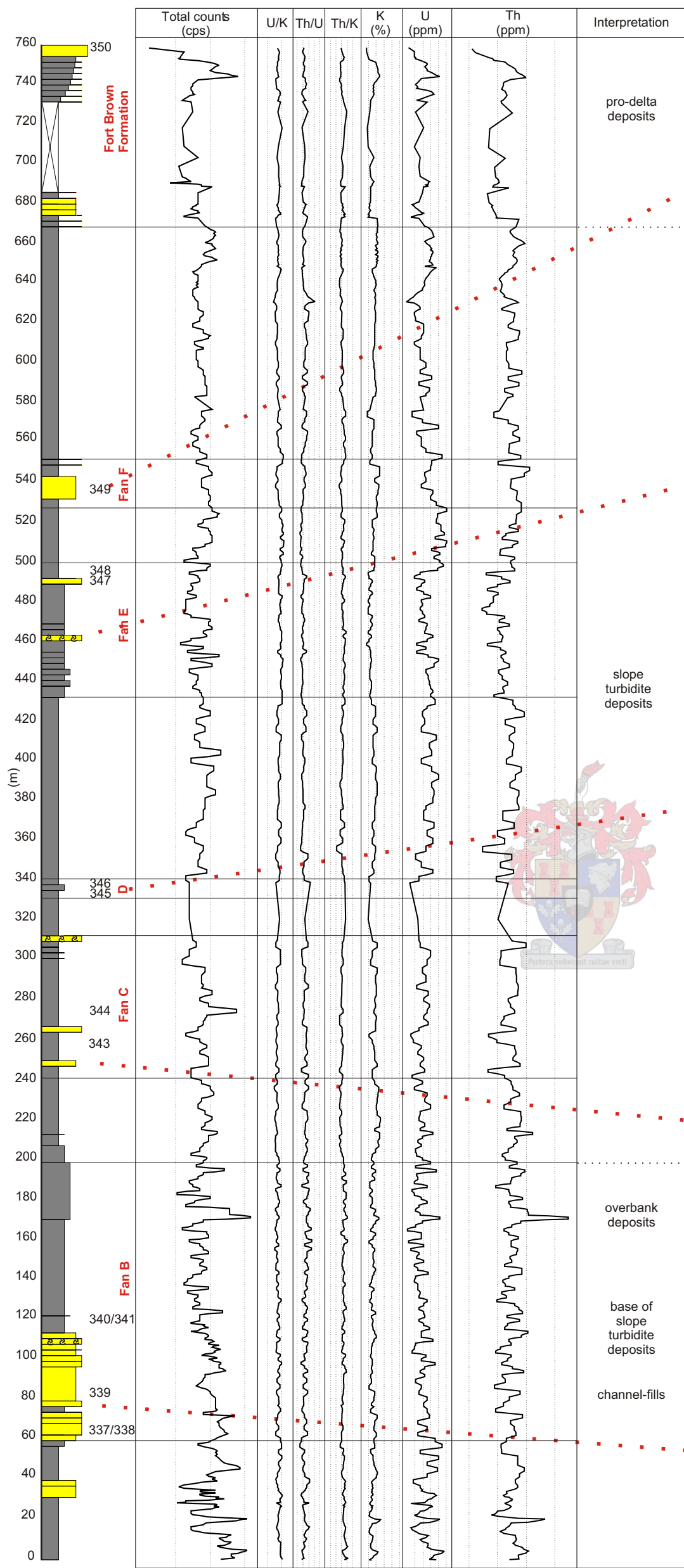
U/K, Th/K and total counts data show deviations of smaller values, corresponding to increasing sandstone. The total counts data are more erratic at the base of the sections, showing a distinction between very fine siltstone and coarse siltstone. The values also decrease with decrease in the siltstone: sandstone ratio, with the Waterkloof section being sandier than the Krantz1 section. No obvious correlations based on SGR data could be drawn between the two sections measured for Fan C at these locations.

### **3.5.3.4 Fan D**

Fan D is comprised of two closely spaced sandstone-rich units and is separated from Fan C by 180 m of basin shale (Wickens, 1994).

The trends for Th/K, Th/U and total counts data measured at Waterkloof (V17) are erratic, due to the contacts between the sandstone, coarse siltstone and very fine siltstone (Figure 3.43). The U/K profile is relatively uniform. The SGR logs measured at Krantz1 (V16) display a relatively non-uniform response for the U/K, Th/U, Th/K and total counts data (Figure 3.42). Small spikes with lower values can be seen for coarser sediments. The sandstone and siltstone average recorded GR data are shown in Table 3.10.

The U/K, Th/K, Th/U and total data profiles for Fan D at the Krantz1 locality are more uniform in comparison to Fan D in the Waterkloof log, due to the larger siltstone: sandstone ratio.



Inclined succession of alternating sandstone and siltstone beds, Fan F, Laingsburg Formation.



Thin alternating siltstone and sandstone beds, intercalated with thicker sandstone beds within Fan E, Laingsburg Formation.



Succession of thin-bedded, ripple-laminated sandstone alternating with siltstone in Fan D, Laingsburg Formation.



Rhythmically bedded, silty deposits, overlain by thicker sandstone layers of Fan C, Laingsburg Formation.

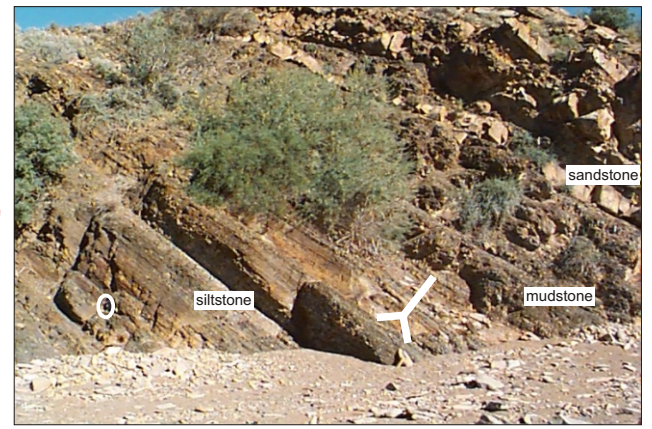
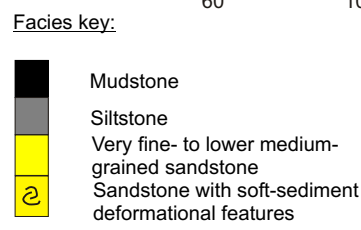
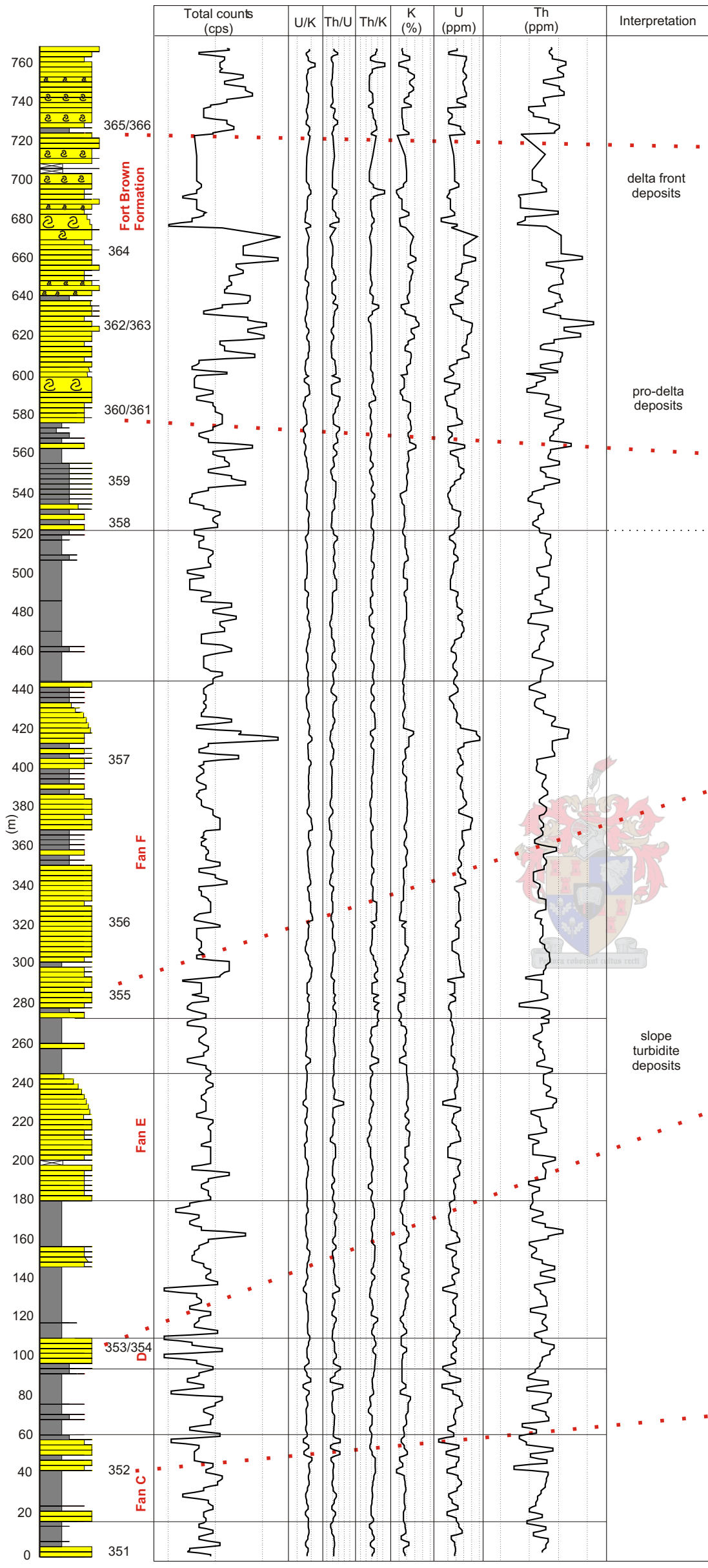


Mudstone and siltstone capped by thick beds of sandstone at the base of Fan B (dashed line), Laingsburg Formation.

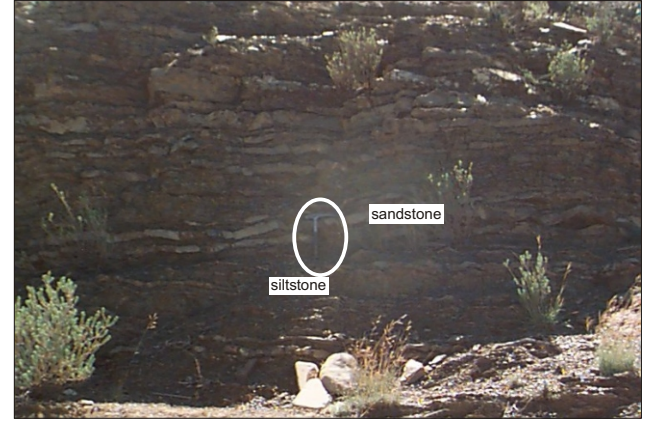
Facies key:

- Mudstone
- Siltstone
- Very fine- to lower medium-grained sandstone
- Sandstone with soft-sediment deformational features

Figure 3.42 Outcrop setting of Krantz 1 (V16), representing the Laingsburg (Fans B - F) and Fort Brown Formations, interpreted as base of slope to pro-delta deposits (after Grecula, 2000). Comparison between SGR logs and lithology. SGR results are from 1060 measurements at an average vertical spacing of 75 cm. The location of samples taken are indicated next to the lithology as 337 - 341 and 343 - 350.



Inclined succession of sandstone, siltstone and mudstone beds within the Fort Brown Formation. Hammer for scale (30 cm) is circled.



Succession of thin-bedded, ripple-laminated sandstone and siltstone. Hammer for scale (30 cm) is circled.



Inclined succession of sandstone, siltstone and mudstone beds within Fan F of the Laingsburg Formation. Hammer for scale (30 cm) is circled.



Small-scale folding in a succession of sandstone beds with thin silty intercalations. Hammer for scale (30 cm) is circled.



Sandstone bed capping mudstone within Fan C of the Laingsburg Formation.

Figure 3.43 Outcrop setting of Waterkloof (V17), representing the Laingsburg (Fans C - F) and Fort Brown Formations, interpreted as slope turbidite to pro-delta deposits (after Grecula, 2000). Comparison between SGR logs and lithology. SGR results are from 904 measurements at an average vertical spacing of 75 cm. The location of samples taken are indicated next to the lithology as 351 - 366.

### 3.5.3.5 Fan E

Fan E is separated from Fan D by a thick unit of mudstone and is dominated by muddy sandstone and thin beds of massive sandstone (Grecula, 2000).

The sedimentological profile measured at Krantz1 (V16) (Figure 3.42) consists almost entirely of shale, with a unit of very fine-grained sandstone. The GR profiles are uniform, with smaller values for the sandstone unit. The average sandstone and siltstone values measured at Krantz1 (V16) and Waterkloof (V17) (Figure 3.43) are shown in Table 3.10.

No correlations can be seen between Fan E measured at Waterkloof and Krantz1, due to the fact that the measured Fan E section at Waterkloof is much sandier than the one at Krantz1.

### 3.5.3.6 Fan F

Fan F is separated from Fan E by a thick unit of mudstone and consists predominantly of muddy sandstone and thin beds of massive and parallel-laminated sandstone (Grecula, 2000).

The Krantz1 (V16) and Waterkloof (V17) logs are relatively uniform, with some spikes in the total counts profile on the contacts between coarse siltstone, very fine-grained sandstone and fine-grained sandstone (Figures 3.42 and 3.43). The sandstone and siltstone average data collected for these profiles are shown in Table 3.10.

As with Fan E, no correlations based on SGR data can be seen between Fan F measured at Waterkloof and Krantz1, due to the fact that the measured Fan F section at Waterkloof is much sandier than the one at Krantz1.

The SGR data for Fans A to F of the Laingsburg Formation were combined in Table 3.11 for comparison to measurements taken in the Collingham, Vischkuil and Fort Brown Formations.

The total counts GR log is dominated by the Th content, as shown by the correlation between the Th counts and the total counts ( $r = 0.29$  for sandstones and  $r = 0.31$  for siltstones). K and U show very low correlations with total counts (Table 3.3).

The stratigraphic interval correlation of the Laingsburg (Fans B – F) and Fort Brown Formations is shown in Figure 3.44.

Table 3.11 Average total counts (cps), U/K, Th/K and Th/U from SGR measurements for the Laingsburg Formation. Confidence levels are at 95%.

Stratigraphy	Profile	n	Avg.		$S_e$	Lower limit	Upper limit	
Laingsburg Formation	Sandstone	785	Total counts	55	8.30	0.59	23	87
			U/K	1.54	0.25	0.02	0.93	2.41
			Th/K	6.61	0.61	0.04	4.17	9.50
			Th/U	4.41	0.79	0.06	2.75	7.14
	Siltstone	249	Total counts	56	5.52	0.70	38	87
			U/K	1.44	0.26	0.03	0.76	2.19
			Th/K	6.17	0.59	0.07	4.24	8.50
			Th/U	4.39	0.80	0.10	2.60	8.32

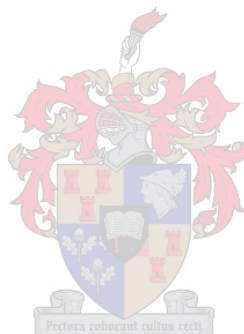


Table 3.12 Average total counts (cps), U/K, Th/K and Th/U from SGR measurements for the Fort Brown Formation. Confidence levels are at 95%.

Stratigraphy	Profile	n	Avg.		$S_e$	Lower limit	Upper limit						
Fort Brown Formation	<u>Krantz1 (V16) and Waterkloof (V17)</u>		99	60	11.0	2.21	40	88					
	Sandstone	Total counts											
		U/K							1.51	0.25	0.05	1.00	2.55
		Th/K							6.64	1.11	0.22	5.20	10.6
		Th/U	4.46	0.78	0.16	3.10	5.56						
	Siltstone	263	Total counts	60	8.96	1.10	42	87					
			U/K	1.37	0.22	0.03	0.86	2.55					
			Th/K	5.94	0.58	0.07	4.83	10.6					
Th/U			4.42	0.71	0.09	3.08	6.54						

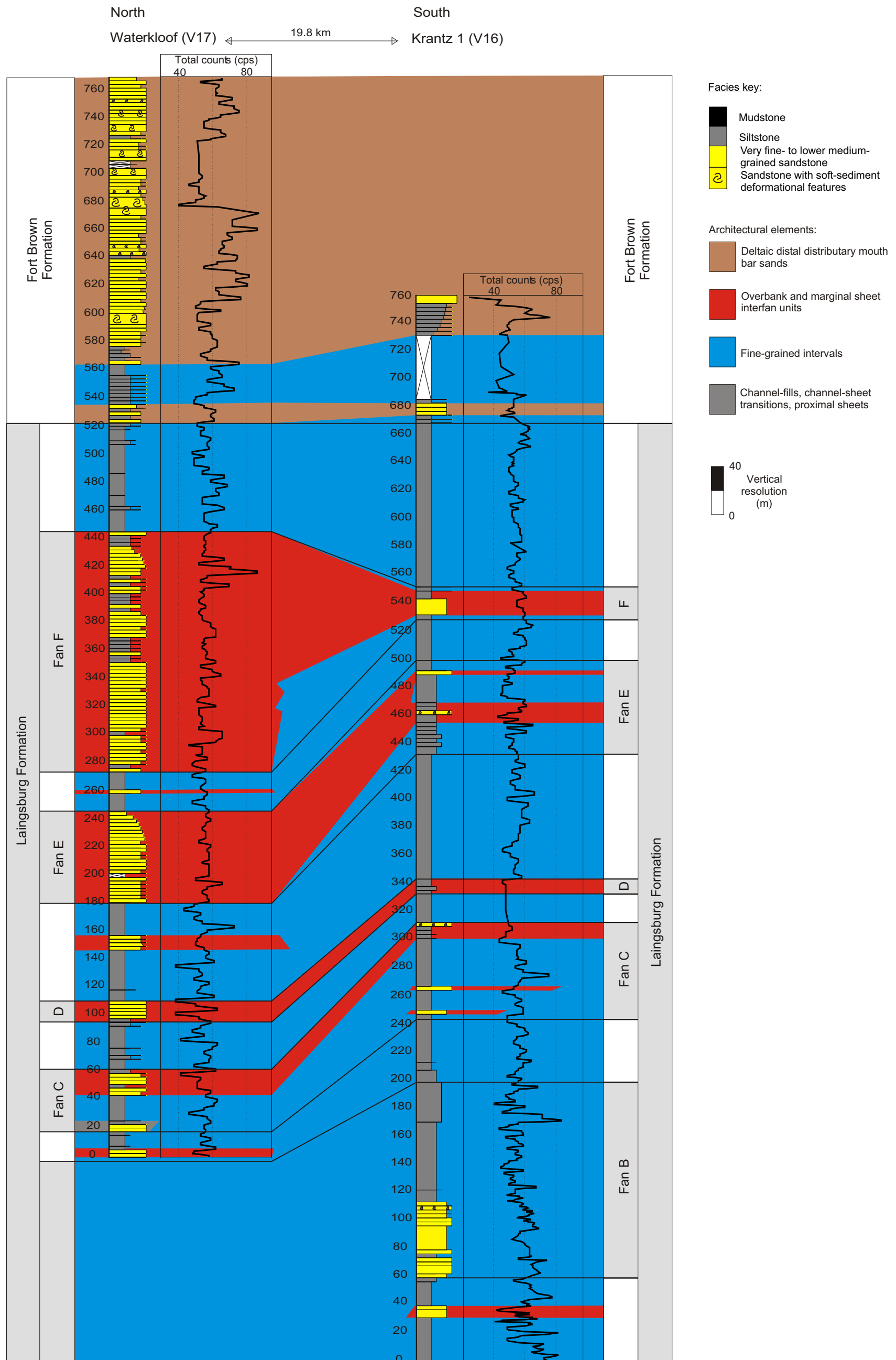


Figure 3.44. Laingsburg depocentre. Simplified stratigraphic cross-section of the Laingsburg Formation (Fans B - F) and the Fort Brown Formation in the study area (oriented north to south), displaying thickness and large-scale geometry (after Grecula, 2000; Sixsmith, 2000).

K-Th cross-plots show positive correlation between the K and Th content for both the siltstones and the sandstones from GR analyses (Figure 3.35).

### **3.5.4 Fort Brown Formation**

The Fort Brown Formation overlies the Laingsburg Formation with a gradational contact at the top of Fan F, attains a thickness of 205 m, and is predominantly comprised of slope and pro-delta mudstones with thick internal divisions of siltstone and sandstone (Sixsmith, 2000). The lower part of the Fort Brown Formation is dominantly mud-rich, whereas the upper part becomes silt-dominated and exhibits current structures, with high-frequency thickening upward cycles 2 – 10 m thick (Wickens, 1994; Sixsmith, 2000).

The top parts of the sections measured at Krantz1 (V16) and Waterkloof (V17), fall within the Fort Brown Formation (Figures 3.42 and 3.43).

The GR profiles for the section measured at Waterkloof are relatively erratic, showing spikes at the contacts between shale, siltstone, very fine-grained sandstone and fine-grained sandstone, probably due to the change in mineralogy (Figure 3.43). Larger areas of unexposed outcrop are present at Krantz1 (Figure 3.42). The measured section, however, shows an upwards-coarsening profile, which can be seen in the total counts log as well. The sandstone and siltstone average data for these profiles are shown in Table 3.12.

There is a slight decrease in the total counts data upwards in the succession, along with an increase in the sandstone: siltstone ratio. The total counts GR log is dominated by the Th content, as shown by the correlation between Th counts and total counts ( $r = 0.29$  for sandstones and  $r = 0.31$  for siltstones).

K and U show very low correlations with total counts (Table 3.3). K-Th cross-plots show positive correlation between the K and Th content from GR analyses for both the sandstones and siltstones (Figure 3.35).

Graphs of the stratigraphic positions of the Collingham, Vischkuil, Laingsburg and Fort Brown Formations against the SGR data show an upward increase in Th/U for both the sandstones and siltstones (Figure 3.45). Graphs of the same profiles, but with geochemical data obtained on samples from XRF, show an overall increase in Th/K and Th/U upwards in the stratigraphic succession (Figure 3.46). A plot of the Th/K vs. the Th/U ratios for the SGR of the siltstones of the Collingham, Vischkuil, Laingsburg and Fort Brown Formations show narrow trends (Figure 3.30).

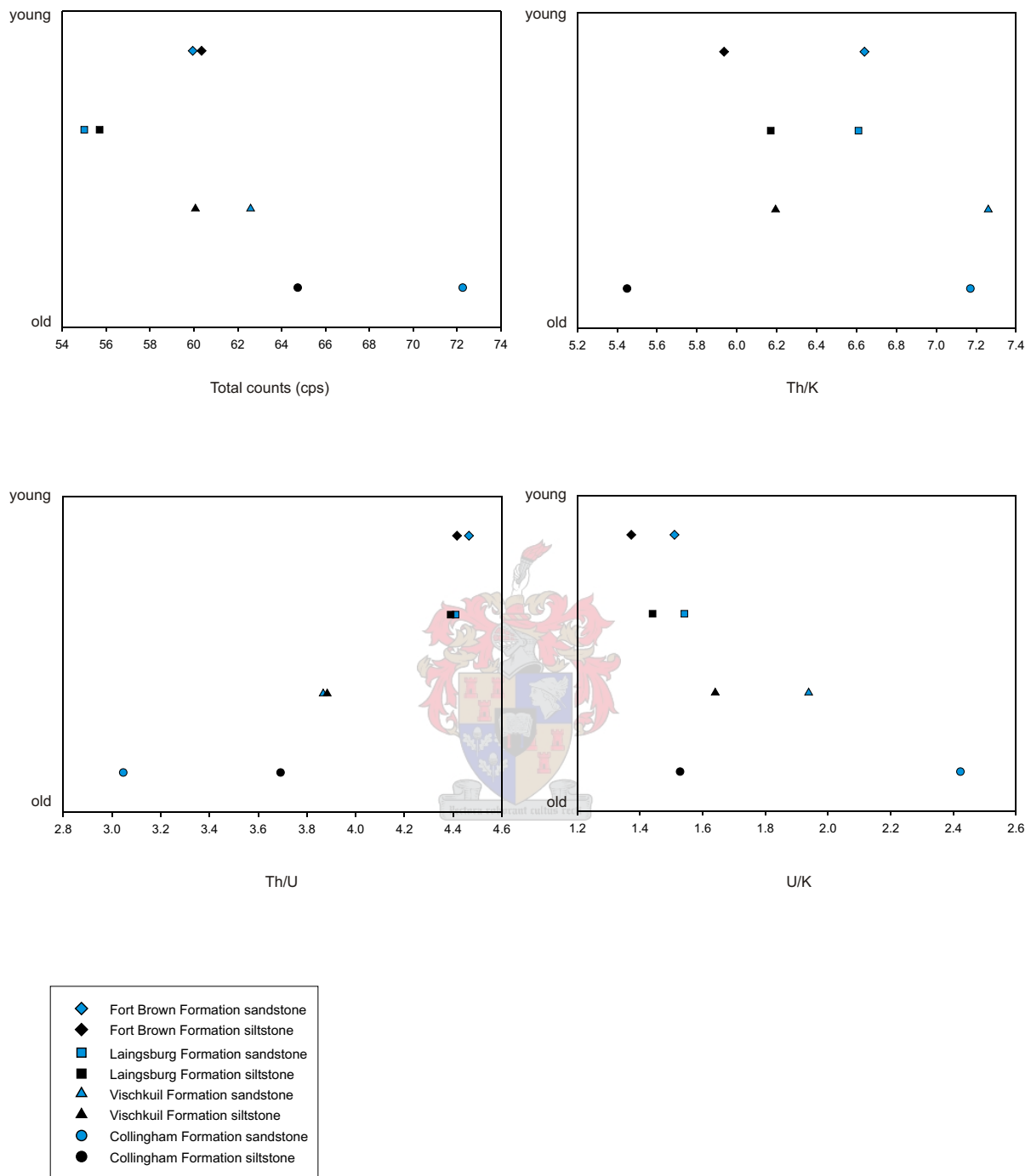


Figure 3.45 SGR data of the average total counts (cps) and Th/K, Th/U and U/K ratios for sandstones and siltstones in the Collingham, Vischkuil, Laingsburg and Fort Brown Formations, plotted against the representative stratigraphic location from an arbitrary point. Based on the assumption that the provenance was the same for the formations, they have been linked in these diagrams to determine any variation in the SGR data with stratigraphy.

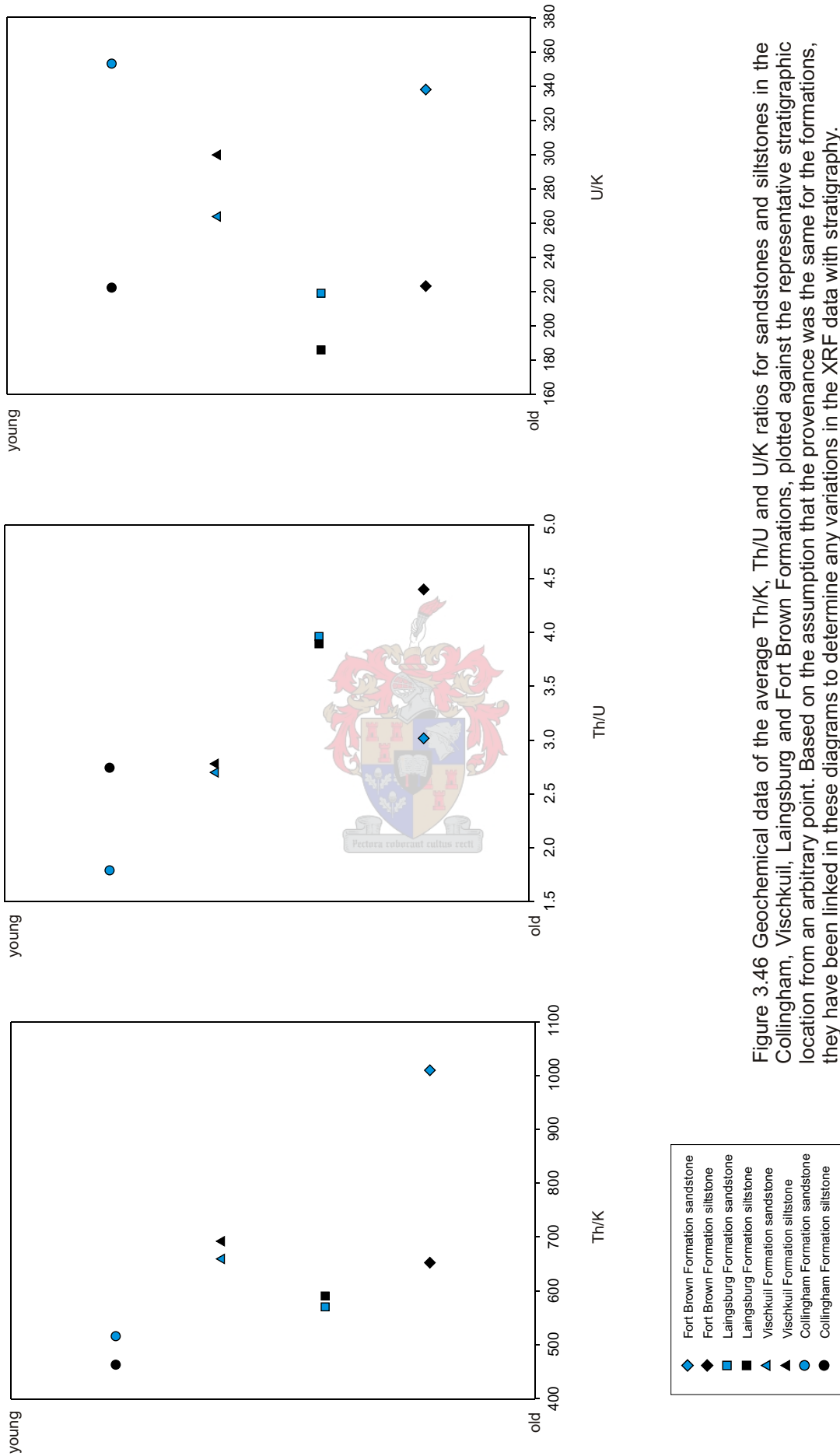


Figure 3.46 Geochemical data of the average Th/K, Th/U and U/K ratios for sandstones and siltstones in the Collingham, Vischkuil, Laingsburg and Fort Brown Formations, plotted against the representative stratigraphic location from an arbitrary point. Based on the assumption that the provenance was the same for the formations, they have been linked in these diagrams to determine any variations in the XRF data with stratigraphy.

### 3.5.5 Discussion on gamma ray characteristics of the Laingsburg depocentre

The narrow trends in the Th/K ratios summarised in Figure 3.30 for the Laingsburg depocentre can be explained by relatively uniform clay mineralogy. The Th/K ratios, ranging around 6 to 8, is compatible with average concentrations of kaolinite and illite/smectite (Hesselbo, 1996), and in this study, mostly illite, as can be seen from the petrography.

The total counts GR logs for the Laingsburg depocentre is dominated by the Th content, as shown by the correlation between the Th counts and the total counts (Table 3.3). Relative concentration of Th at the expense of K during the usually palaeopedologic conditions of kaolinite formation might have caused this (Hesselbo, 1996). Th is concentrated in sand and silt-sized heavy minerals (zircon, thorite, monazite, epidote and titanite), phosphates or adsorbed and concentrated in clays. The relationships between SGR derived K, U and Th (U/K, Th/K and Th/U), show correlations that are statistically significant, but which are less significant than the relationship between the elements and the total counts (Svendsen and Hartley, 2001). A positive correlation on cross-plots between K and Th from GR analyses is shown for the sandstones and siltstones from the Laingsburg depocentre. The compositional fields are all similar and distinct and reflect similarities in original mineralogy (Myers and Bristow, 1989). The original mineralogy of the Laingsburg depocentre sandstones has been identified as quartz, albite, K-feldspar, opaques, biotite, lithic fragments and accessory muscovite and zircon. The diagrams (Figure 3.35) all show an intercept of ~4 ppm Th for 0% K. This is probably due to a calibration error.

The Th/U and U/K ratios recorded from the GR measurements and from XRF measurements (Table 3.13), show a stratigraphic evolution in the Laingsburg depocentre, from both the siltstones and sandstones. The Th/U ratio increases, indicating an overall decrease in U. This could be due to either a decrease in the amount of U from the source area(s), or a decrease in U as a result of the early settling out of U-bearing heavy minerals, such as zircon. The SGR K (%) data was plotted against the stratigraphic successions of the profiles measured in the Collingham, Vischkuil, Laingsburg and Fort Brown Formations (Figure 3.47). The SGR K (%) values are higher in the Collingham Formation than in the overlying Vischkuil Formation, which is probably due to the high percentage of K-bentonite layers in the Collingham Formation. On average, the SGR K (%) values are higher in the Fort Brown Formation than in the Laingsburg Formation. The geochemical data show the same, i.e. higher K values for samples from the Collingham Formation compared to the Vischkuil Formation. The possible reasons for the Fort Brown Formation to be slightly more enriched in K might be: (i) the source(s) became more enriched in K, or (ii) the formation waters were poor in Th, and K was not inhibited during the formation of kaolinite. If the trend (more K in the Fort Brown than Laingsburg Formation) is a result of kaolinite formation (altered to illite), it will be concentrated in the clays (mud- and siltstones). The main source of K in the sandstones is K-feldspar. It is also possible that differences in SGR and geochemical data are due to the

Table 3.13 Average U/K, Th/K and Th/U from XRF measurements for profiles in the Laingsburg deponentre. Confidence levels are at 95%.

Stratigraphy		n	Avg.		S <sub>e</sub>	Lower limit	Upper limit	
Fort Brown Formation	Sandstone	5	U/K	338	124	111	226	495
			Th/K	1010	503	450	684	1892
			Th/U	3.02	0.86	0.77	1.92	4.29
	Siltstone	5	U/K	223	115	102.9	310	345
			Th/K	653	101	90.3	553	803
			Th/U	4.40	3.80	3.40	1.83	11.0
Laingsburg Formation	Sandstone	30	U/K	219	141	51.5	20.2	508
			Th/K	571	210	76.7	266	984
			Th/U	3.96	3.69	1.35	1.33	20.0
	Siltstone	13	U/K	186	82.8	45.9	78.7	295
			Th/K	591	84.0	46.6	432	745
			Th/U	3.89	1.94	1.08	2.00	7.67
Vischkuil Formation	Sandstone	6	U/K	263	98.1	80.1	161	391
			Th/K	658	278	227	381	1039
			Th/U	2.69	1.43	1.17	1.40	5.50
	Siltstone	3	U/K	299	199	230	119	513
			Th/K	690	266	307	494	993
			Th/U	2.77	1.22	1.41	1.94	4.17
Collingham Formation	Sandstone	2	U/K	353	257	363	171	534
			Th/K	516	142	201	416	616
			Th/U	1.79	0.90	1.27	1.15	2.43
	Siltstone	3	U/K	222	97.6	113	110	285
			Th/K	463	107	124	387	585
			Th/U	2.74	2.25	2.60	1.36	5.33

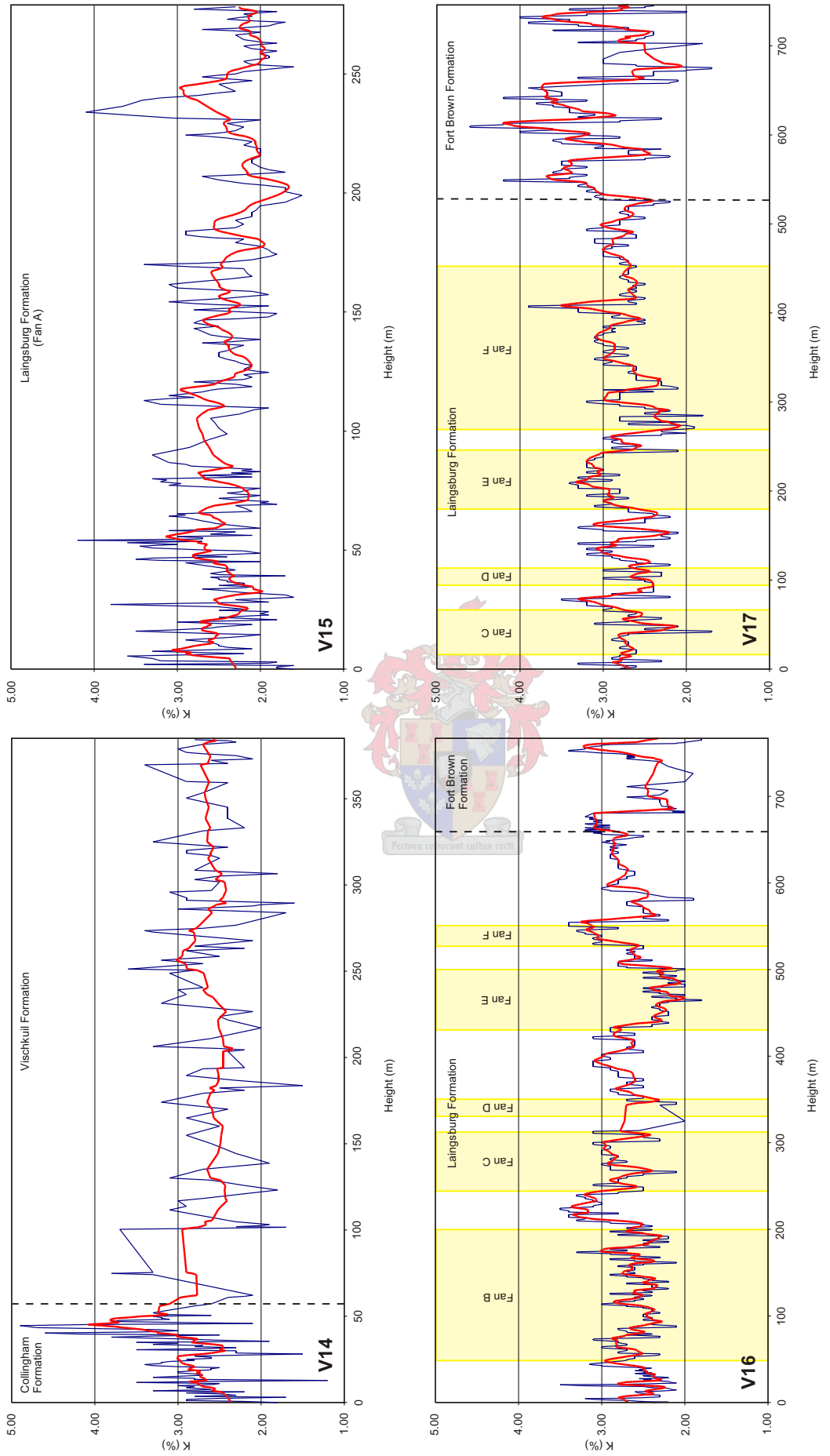


Figure 3.47 SGR data of K (%) for measured profiles in the Collingham, Vischkuil, Laingsburg and Fort Brown Formations, plotted against height (m). The dashed line separates the Collingham Formation (basin-floor deposits) from the Vischkuil Formation (basin-floor and slope deposits) and the Laingsburg Formation (basin-floor and slope deposits) from the Fort Brown Formation (deltaic deposits). The red line represents a moving point average of 10, which decreases noise and makes it easier to identify K trends.

difference in sampling volume for the analytical techniques. A gamma radiation reading is influenced by approximately 49 kg of rock (Løvborg *et al.*, 1971), whereas approximately 0.5 kg of rock was sampled for laboratory XRF and ICP-MS analyses.

The total GR motif for the sand-rich Fan A of the Laingsburg Formation shows a blocky character with a sharp base and top, typical for basin-floor fans. It was not possible to identify the subdivisions (Unit 1 to 7; Sixsmith, 2000) in Fan A by applying the SGR data. The SGR pattern for total counts, K, U, Th and ratios of these elements are erratic in the mudstone successions and K-bearing minerals (illite and chlorite) are responsible for the majority of the total gamma radiation in the mudstones and identified clay mineral peaks. There are no major changes between the interfan mudstones in the SGR data set that could imply different origin, and no distinct signals in the SGR pattern of the mudstone intervals, which potentially correspond, to maximum flooding surfaces.

### **3.6 Discussion on general gamma ray characteristics and their significance in both the Tanqua and Laingsburg depocentres**

Both total counts and element ratios are controlled primarily by lithology. The more clay minerals there are in a sample, the higher the total gamma radiation and elemental ratios containing K. Sandstones have the lowest total gamma radiation, increasing in alternating sandstone and siltstone with the highest values in siltstone and shale. Soft-sediment deformation deposits, generally being a mix of sandstone and siltstone with various degrees of deformation, show similar values as alternating sandstone and siltstone and are commonly erratic, depending on the sandstone: siltstone ratio.

Primary sedimentary structures, including bioturbation, appear to have no effect on the Th/K, Th/U, U/K and total gamma radiation. The data do, however, reflect changes in grain size, e.g. fine-grained sandstone shows higher total gamma radiation than lower medium-grained sandstone. GR peaks that are not affected by changes in grain size can be seen above basal erosional surfaces in logs V8 and V9. The average SGR data for sandstone and siltstones in the Tanqua and Laingsburg depocentres are very similar, as shown in Table 3.14.

This could indicate that the mineralogy of the sediments is very similar as well, which can be seen to be true from the petrography. Another explanation for this might be a result of the occurrence of clay mineral diagenesis in the sandstones of both the Tanqua and Laingsburg depocentres. Diagenesis may involve both clay mineral neoformation and destruction. Both change the clay to grain size relationships and, consequently, the relationship between the location of natural radioactivity in specific minerals and in grain size classes (Rider, 1990). The dissolution of the detrital K-feldspar in the sandstones and resulting formation of illite has

Table 3.14 Comparison between the average total counts (cps), U/K, Th/K and Th/U from SGR measurements for the Tanqua (Skoorsteenberg (Unit 5), Kookfontein and Waterford Formations) and Laingsburg (Collingham, Vischkuil, Laingsburg and Fort Brown Formations) depocentres. Confidence levels are at 95%.

Depocentre		n	Avg.		S <sub>e</sub>	Lower limit	Upper limit
TANQUA DEPOCENTRE	Sandstone	837					
	Total counts		61	6.11	0.42	35	110
	U/K		1.44	0.10	0.01	0.81	3.63
	Th/K		6.11	0.44	0.03	3.64	13.19
	Th/U	4.55	0.42	0.03	2.78	6.72	
	Siltstone	764					
	Total counts		67	5.66	0.41	35	112
	U/K		1.41	0.12	0.01	0.59	2.18
Th/K	5.98		0.33	0.02	4.11	8.50	
Th/U	4.42	0.29	0.02	3.13	8.80		
LAINGSBURG DEPOCENTRE	Sandstone	1040					
	Total counts		59	3.85	0.24	23	98
	U/K		1.66	0.24	0.01	0.98	3.85
	Th/K		6.84	0.37	0.02	4.17	7.14
	Th/U	4.25	0.33	0.02	2.23	10.6	
	Siltstone	536					
	Total counts		59	2.61	0.23	38	87
	U/K		1.48	0.14	0.01	0.76	2.67
Th/K	6.10		0.14	0.01	4.24	10.60	
Th/U	4.23	0.30	0.03	2.57	8.32		

changed the location of K in the minerals and thereby increased the radioactivity present in the clay-sized fraction. The result is that the GR logs are rather featureless and differentiates poorly between sandstone and siltstone.

There appears to be higher U radioactivity in fractures and faults in V135, V6 and V8 in the Tanqua depocentre. These zones of higher U radiation, present in coffinite, uraninite and zircon (Kübler, 1977), can be due to U mobility and its presence in formation waters (Rider, 1986). Tectonic deformation in the Tanqua depocentre occurred after the deposition of the Skoorsteenberg, Kookfontein and Waterford Formations (Wickens, 1994). The U was thus brought in with hydrothermal fluids at a later stage in the tectonic evolution of the depocentre. Turner (1985) studied U mineralization, identified in the Upper Permian Beaufort Group (overlying the Eccca Group) that was mainly confined to one sandstone-rich unit. He related the reason for the stratigraphic confinement of the mineralization to the geomorphic evolution of the Karoo Basin and the deposition of host sandstones at a time when gradients and sediment input were declining in response to weathering and denudation of an initially uplifted, volcanically active source area. Mineralization in some of the main U-bearing sandbodies in the Beaufort Group seems to correlate in time with major paroxysms of the Cape orogeny (Le Roux, 1993). Extra-basinal leaching of Beaufort Group granitic and volcanic source rocks, and the expulsion of U-rich pore waters from tuffs interbedded with mud-rich sediments during early diagenesis, probably account for most of the U, with minor contributions from the breakdown of feldspars, glass shards and heavy minerals within the sandstones (Le Roux, 1993). These low-temperature ore fluids migrated down the palaeoslope along permeable conduits in channel sands, migrating and accumulating in the fractures and faults that formed during the tectonic instability.

Some minerals have characteristic concentrations of Th, K and U. SGR logs can thus be used to identify them. The heavy minerals and clay content determine the Th levels in sandstones, whereas K is usually contained in micas and feldspars. The peaks in the Th/K profiles for the sandbodies could possibly be related to the concentration of heavy minerals at the bases of these sandbodies. This is confirmed by the presence of apatite in these sandstones, as identified with petrography. The K content in siltstones indicates clay minerals and mica, whereas the Th level depends on the amount of detrital material (Schlumberger, 1987). The Th/K data of the logs can be correlated with the quartz/feldspar ratio, with decreases in the Th/K data pointing to decreases in the quartz/feldspar ratio. The petrography confirms this as well, with samples containing more illite (illite replaced most of the K-feldspar) showing lower values of Th/K.

On the SGR logs of the measured vertical profiles, a change in the level of radiation can be detected, from high (about 80 cps) in the siltstone at the base of upward thickening sections, to low (about 40 cps) in the sandstone. This aids in the identification of gradual

coarsening-upward sequences. The box-shaped total GR motif of the profiles measured in the Tanqua and Laingsburg depocentres is typical for fluvial channel sands and turbidites. However, the SGR reading is not a function of grain size, but of mineralogy. The siltstone, containing the bulk of the radioactive elements, produces the long-term trend in radioactivity (Van Buchem *et al.*, 1992).

Genetically related sedimentary strata, bounded by unconformities or their correlative conformities, compose depositional sequences and are related to cycles of eustatic change (Posamentier and Vail, 1988). The building blocks of the classic Exxon sequence stratigraphy scheme are the purely asymmetrical shallowing-upward parasequences bounded by sharp flooding surfaces (Pawellek and Aigner, 2003). The cycles observed in this study, however, are mostly coarsening-upward half-cycles, consisting of silt-rich mudstones at the base to fine- and lower medium-grained sandstones at the top, bounded by gradational contacts. These stratigraphic cycles can generally be regionally correlated and most likely record phases of sea-level fluctuation resulting in deepening followed by progradation. Cyclicity in the Tanqua depocentre varies from 20 to 200 metres in thickness, and in the Laingsburg depocentre from 20 to 300 metres. Both auto- and allo-cyclicity played a role.

The distribution of the SGR data, in combination with lithology, show that it is possible to correlate successions in the Skoorsteenberg, Kookfontein and Waterford Formations in the Tanqua depocentre. GR data collected from a borehole (SL1; V20) also show good correlation with GR data measured at outcrops (Figure 3.27). The data show that it is not possible to discriminate between the Laingsburg and Fort Brown Formations in the Laingsburg depocentre using GR data alone. However, the exceptions are with the Collingham and Vischkuil Formations, particularly the Collingham Formation, which show higher values for all the GR data when compared to the rest of the measured stratigraphic sections. The higher values in some formations compared to others are a function of higher siltstone: sandstone ratios. The reason for this in the Collingham Formation is that it contains a large amount of pyroclastic deposits in the form of K-bentonites (Viljoen, 1995), which result in the higher gamma radiation.

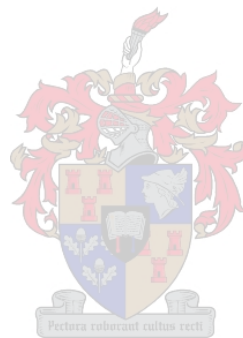
### **3.7 Conclusions (answers to initial objectives)**

- i. The SGR data for the siltstones in the Skoorsteenberg, Kookfontein and Waterford Formations in the Tanqua depocentre show higher values for total counts, K, Th and U than the sandstones. This is also true for the siltstones and sandstones in the Collingham, Vischkuil, Laingsburg and Fort Brown Formations in the Laingsburg depocentre. Average GR data for the Tanqua and Laingsburg depocentres are very similar, indicating that the mineralogy of the sediments is closely related. The original mineral constituents for the sandstones from both the Tanqua and Laingsburg

depocentres are primarily quartz, albite, K-feldspar, opaques, biotite, lithic fragments and accessory muscovite and zircon.

- ii. Apart from the Collingham Formation, which have higher average SGR values, due to the abundant K-bentonite layers, than any of the other formations in either the Tanqua or Laingsburg depocentres, it is not possible to discriminate between the Vischkuil, Laingsburg and Fort Brown Formations in the Laingsburg depocentre using GR data alone. However, correlations between successions can be identified in the Skoorsteenberg, Kookfontein and Waterford Formations based on a combination of lithology and SGR data. Decreases in K have also been identified from the Skoorsteenberg to the Kookfontein and Waterford Formations in the Tanqua depocentre, and increases from the Laingsburg to the Fort Brown Formation in the Laingsburg depocentre. It is not clear whether these are constant trends throughout the individual depocentres, since they were not shown in all the measured sections. The increase in K is most likely a result of the provenance becoming more enriched in this element, maybe as a result of unroofing. Radioactivity from Th normally contributes about half of the total counts. It is not clear why the Th measured in this study has a much larger contribution to the total counts, to an extent of apparently controlling the GR profile.
- iii. No significant geochemical or mineralogical signals that vary along the sediment flow path were found for the sandstones or siltstones within the Tanqua depocentre.
- iv. GR data from the Collingham, Vischkuil, Laingsburg and Fort Brown Formations should differ on the basis of mineralogy. However, petrographic studies showed that the mineral constituents for sandstone from the Vischkuil and Laingsburg Formations are very similar, and that the Fort Brown Formation sandstone mineralogy is closely related to them as well, apart from a slight increase in lithic fragments. The Collingham Formation sandstone mineralogy differ from these, in that, on average, it contains some volcanic lithic fragments, as well as a larger original percentage of K-feldspar, due to the abundant K-bentonite tuff layers. The mineralogy is reflected in the SGR measurements, with the Collingham Formation showing more erratic patterns, with higher values of especially K. The Vischkuil and Laingsburg Formation SGR measurement are very similar, as is the Fort Brown Formation measurements. There is, however, a slight increase in K from the Laingsburg to Fort Brown Formation. This might be a direct result of the more lithic sandstones in the Fort Brown Formation, and thus dependant on the source composition(s).
- v. No significant differences in the SGR data between Fans A to F within the Laingsburg Formation in the Laingsburg depocentre were noted.
- vi. Differences in SGR and geochemical data might be due to the difference in sampling volume for the two analytical techniques. It should be noted that the geochemical data is primarily based on sandstone analyses. If the K trends noted in the SGR data are a result of kaolinite formation (altered to illite), it will be concentrated in the clays

(mud- and siltstones). In terms of total radioactivity, illite has a much greater contribution than kaolinite or chlorite. The main source of K in the sandstones is K-feldspar. Illite and chlorite in sandstone play an important role as well, however, the K concentration of illite is normally insignificant in terms of the bulk K content of a rock unless concentrations of K-feldspar and micas are negligible. The difference between the data sets may also be a result of the fact that in the case of Th and U measurement by XRF, the elements themselves are measured. In using the SGR spectrometer,  $^{214}\text{Bi}$  is measured and not U. U is highly mobile during oxidising conditions, therefore it may not be present to the extent of  $^{214}\text{Bi}$  in the sample. Th is less mobile, but the problem of disequilibrium still holds.



## Chapter Four

### 4 Petrography

#### 4.1 Analytical techniques

The study of petrographic fabrics forms the basis for analytical research. Mineralogical and grain size data obtained from sandstone and siltstone samples are presented. The studied sandstones fall in the subfeldspathic, feldspathic and lithofeldspathic sandstone fields in QmFLt diagrams. For grain size determination and the modal analyses, photomicrographs were taken of representative thin sections; these were converted to greyscale images and analysed using the computer program ANALYSIS. The results are shown in Appendix A. Samples are grouped according to stratigraphy and photomicrographs are shown in Appendix B.

Relative proportions of different types of terrigenous sand grains are guides to the nature of the source rocks in the provenance terrane from which sandy detritus was derived (Dickinson *et al.*, 1983). Plate-tectonic settings are the basis on which provenance terranes and related basins of deposition are classified. As a result, detrital framework modes of sandstone suites provide information about tectonic setting of basins of depositions and associated provenances (Dickinson and Suczek, 1979; Dickinson *et al.*, 1983).

The most significant compositional variations among terrigenous sandstones can be displayed in ternary plots on triangular diagrams (Dickinson *et al.*, 1983). The three apices, or poles, represent recalculated proportions of key categories of grain types. Two alternate sets of poles (QmFLt and QFL) are useful (Graham *et al.*, 1976; Dickinson *et al.*, 1983):

- QmFLt diagrams: the poles are (i) quartz grains (Qm) that are exclusively monocrystalline, (ii) monocrystalline feldspar grains (F), and (iii) total polycrystalline lithic fragments (Lt), including quartzose varieties.
- QFL diagrams: the poles are (i) total quartzose grains (Q), including polycrystalline lithic fragments such as quartzite and chert, (ii) monocrystalline feldspar grains (F), and (iii) unstable polycrystalline lithic fragments (L) of either sedimentary or igneous parentage, including metamorphic varieties.

Framework constituents may be affected by diagenetic growth of interstitial matrix or cement through the processes of intrastratal solution and replacement (Dickinson *et al.*, 1983). The influence of diagenetic effects on detrital modes can never be avoided entirely. To insure that diagenetic changes lay within acceptable limits, all sandstones containing more than 25% matrix or cement, or both in combination, was arbitrarily excluded from the data compilation.

A Philips XL30 scanning electron microprobe (SEM) was used for the identification of minerals that were too fine-grained to identify with standard petrography, as well as identifying overgrowths, zoning and compaction features. The basic function and modes of operation of the SEM are discussed in Tucker (1988). A high-energy (20 kV) electron beam was scanned across the surface of a carbon-coated thin section, from which electrons scattered from the surface of the sample generated an image. The number of electrons scattered is a function of the average atomic number of each phase and the brightness of the phases varies with the atomic number. The working distance was ca. 13 mm that generated images that show intergrowths of the crystals. An energy discriminating system (EDS) was then used to detect the elements present in the mineral and thus identify it.

## 4.2 Objectives

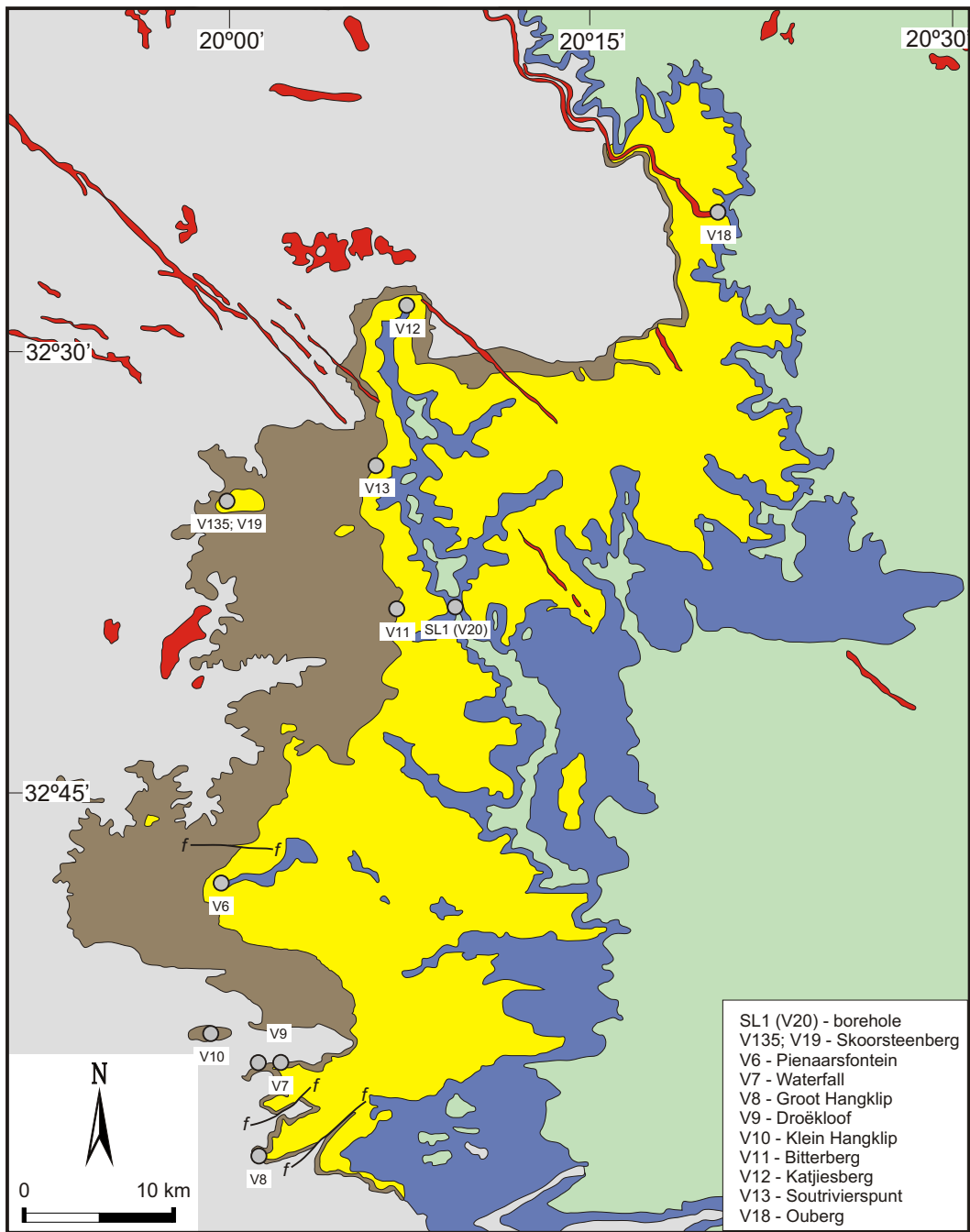
- i. What was the primary detrital mineralogy of the sandstones in both the Tanqua and Laingsburg depocentres before burial, metamorphism and alteration?
- ii. What are the main secondary mineral assemblages in these sandstones and what is their metamorphic grade?
- iii. Based upon the identified primary mineralogy, what are the sandstone classifications and what are the likely provenance(s)?
- iv. Are there any petrographic differences (mineralogy, textures, sorting, degree of alteration, etc.) between sandstones at different stratigraphic levels within the different formations of the individual depocentres, as well as between the two depocentres?
- v. What does cathodoluminescence (CL) tell us about the original mineralogy and the effect of burial diagenesis on the sandstones?

## 4.3 Tanqua depocentre

The Skoorsteenberg, Kookfontein and Waterford Formations, with the measured sedimentological profiles and sample locations, are shown in Figure 4.1.

### 4.3.1 Skoorsteenberg Formation (Unit 5)

The schematic stratigraphy of the upper unit of the Skoorsteenberg Formation (Unit 5) and sample locations relative to the overall stratigraphy are shown in Figure 4.2. Figure 4.3 shows the lithology and stratigraphy from a borehole, SL1 (V20). A summary of the texture and composition of the sandstones are given in Table 4.1. Photographs of sample locations within Unit 5 are shown in Figure 4.4.



- SL1 (V20) - borehole
- V135; V19 - Skoorsteenberg
- V6 - Pienaarsfontein
- V7 - Waterfall
- V8 - Groot Hangklip
- V9 - Droëkloof
- V10 - Klein Hangklip
- V11 - Bitterberg
- V12 - Katjiesberg
- V13 - Soutrivierspunt
- V18 - Ouberg

**Geological legend**

Mesozoic	Jurassic	Karoo Supergroup	▲ Beaufort Group	Abrahamskraal Fm	Mudstone, siltstone, sandstone, thin cherty beds
				Waterford Fm	Sandstone, siltstone, mudstone, shale
Palaeozoic	Permian		Ecce Group	Kookfontein Fm	Shale, siltstone, thin sandstone beds
				Skoorsteenberg Fm	Sandstone, siltstone, shale
				Tierberg Fm	Shale
					Dolerite

Figure 4.1 Geological map of the Tanqua depocentre, Karoo Basin, South Africa, showing the Skoorsteenberg, Kookfontein and Waterford Formations and measured sedimentological profiles and sample locations. Geological information compiled from the Clanwilliam 3218 and Sutherland 3220 maps. 1:250 000 Geological series, Geological Survey of South Africa.

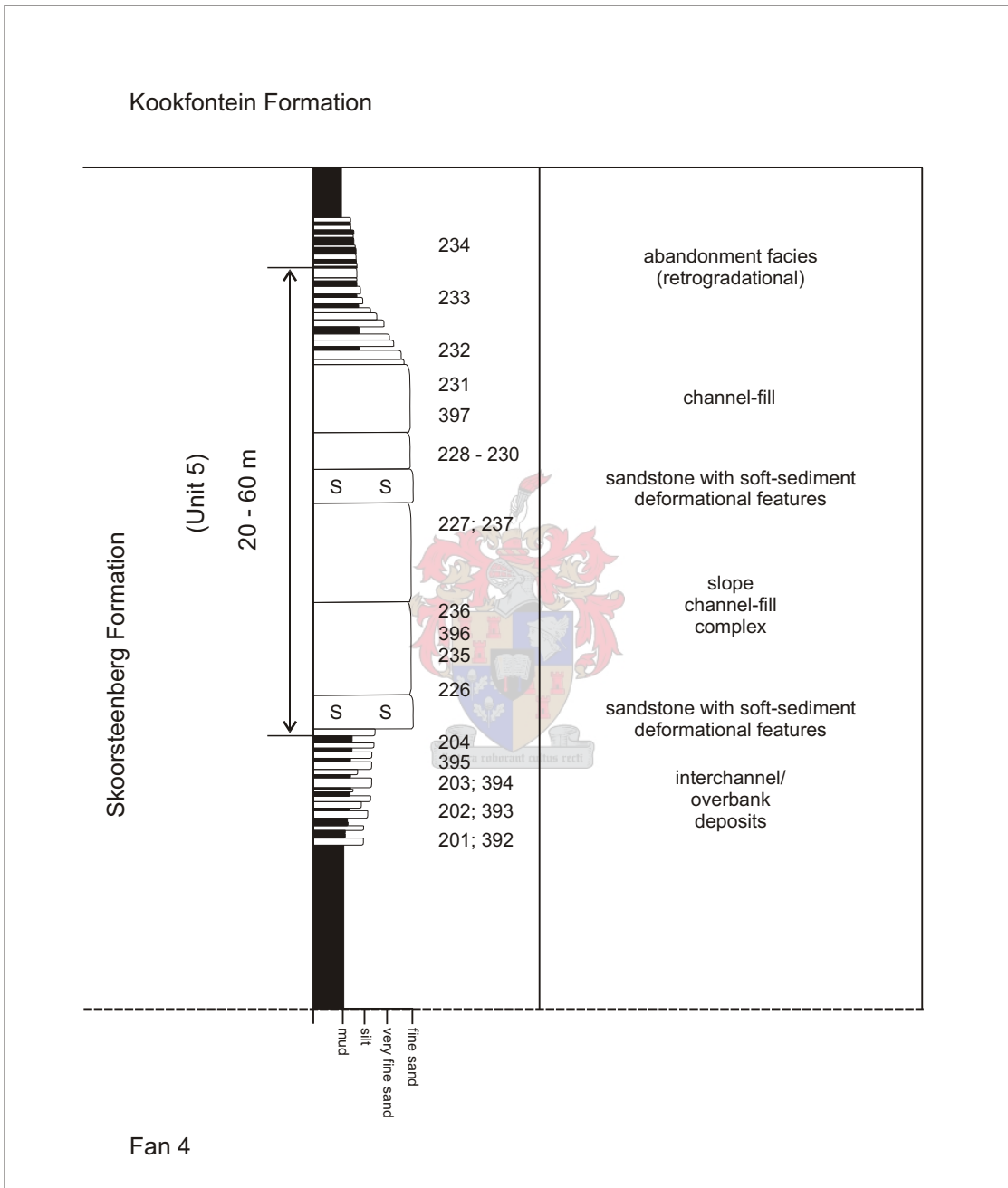


Figure 4.2 Schematic stratigraphy of the upper unit (Unit 5) of the Skoorsteenberg Formation, Tanqua depocentre. The sample locations relative to the overall stratigraphy are shown.

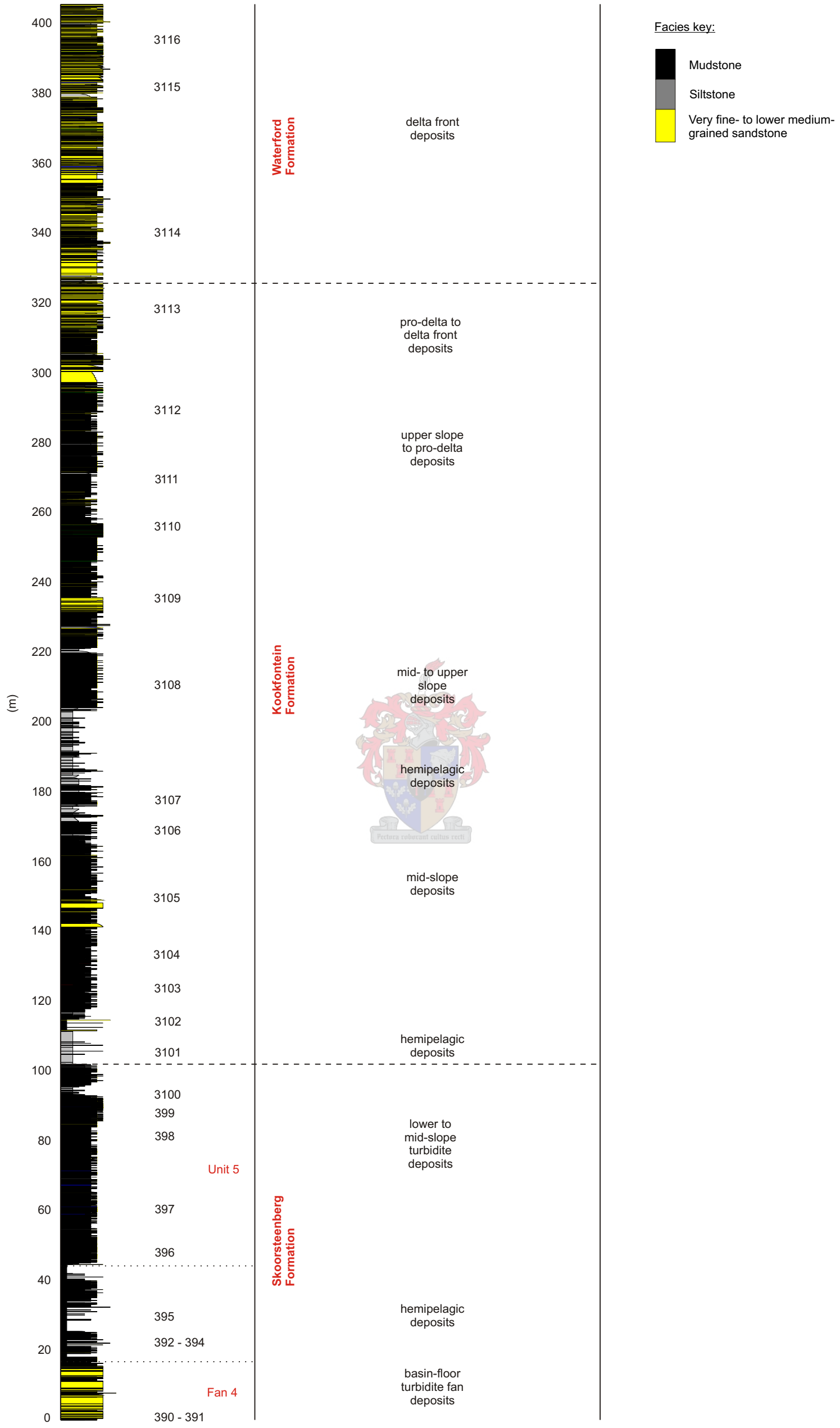


Figure 4.3 Stratigraphy from a borehole, SL1 (V20) of the upper part of the Skoorsteenberg Formation, the Kookfontein and Waterford Formations, Tanqua depocentre. The sample locations are indicated next to the lithology as 390 - 3116.

Table 4.1 Summary of texture and composition (%) of sandstones from Unit 5 of the Skoorsteenberg Formation, Tanqua depocentre.

Stratigraphic unit	Detrital components						Authigenic minerals					Texture		Rock classification	
	Quartz	Feldspar	Mica	Litho-clasts	Accessory minerals	Matrix	Opauques	Quartz cement and overgrowths	Illite	Chlorite	Calcite	Mica	Grain size		Sorting
Unit 5															
Interchannel/ overbank deposits	38.80	17.17	8.21	3.12	0.57	15.60	5.68	3.98	3.32	1.23	1.17	2.05	fine-grained	poorly to well sorted	feldspathic
Slope channel-fill complex	36.43	20.71	12.49	5.56	0.82	4.63	2.72	4.47	7.81	0.81	1.27	3.12	fine- to medium-grained	poorly to well sorted	feldspathic to lithofeldspathic

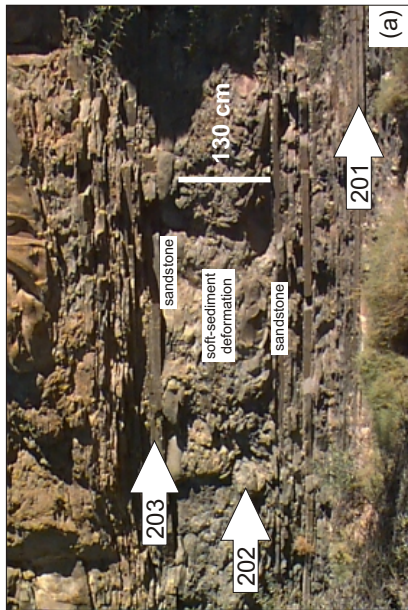
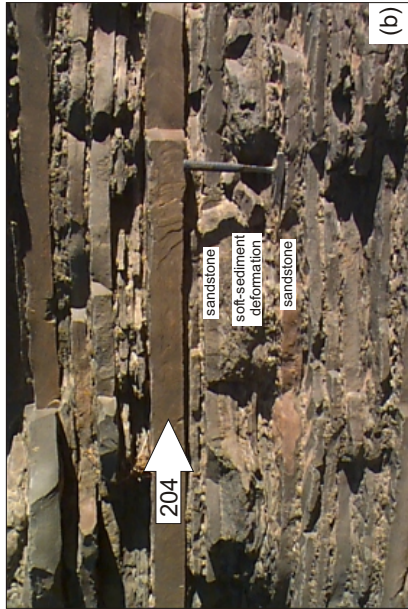
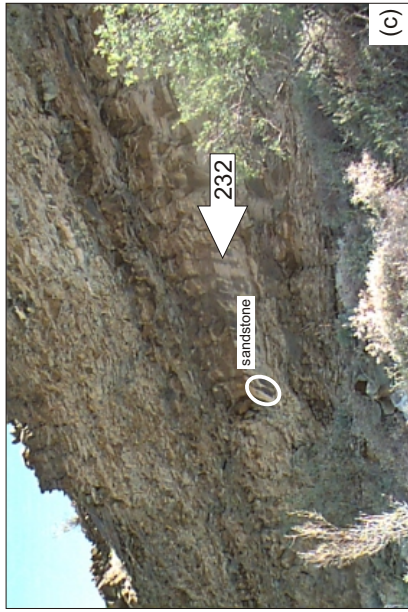


Figure 4.4 Skoorsteenberg Formation (Unit 5), Tanqua depocentre. Sample locations:  
 (a) Samples 201 - 203 (Waterfall (V7)).  
 (b) Sample 204 (Waterfall (V7)).  
 (c) Sample 232 (Droëkloof (V9)). Hammer for scale (30 cm) is circled.  
 (d) Sample 225 (Groot Hangklip (V8)).  
 (e) Samples 226 and 227 (Groot Hangklip (V8)). Hammer for scale (30 cm) is circled.

#### **4.3.1.1 Interchannel/overbank deposits**

The sandstones are feldspathic, brown to grey coloured and fine-grained (avg. grain size ~0.25 mm), with a colour index ~10. Most grains show a preferred orientation consistent with the ripple-lamination. Grain boundaries are mostly obscured by quartz overgrowths, but appear to be angular to sub-rounded. The grains are poorly to well sorted, and there is no obvious grading, with very little compaction, due to early cementation.

#### **4.3.1.2 Slope channel-fill complex deposits**

The sandstones are feldspathic to lithofeldspathic, light brown to grey coloured and fine- to lower medium-grained (max. grain size ~0.25 mm), with a colour index of ~20. The grains are poorly to well sorted, angular to sub-rounded and show no obvious grading. Preferred grain orientation parallel to the ripple-lamination is present and there is very little compaction, due to early cementation. There are quartz grain overgrowths, obscuring some of the boundaries.

The sandstones from the slope channel-fill complex are texturally and mineralogically very similar to those of the interchannel/overbank deposits. However, sandstones from the channel-fills are generally slightly coarser grained, due to the higher energy depositional environments of channels compared to those of interchannel/overbank areas.

Sample 202 falls in the subfeldspathic sandstone field, samples 203, 204, 226, 228 and 231 – 235 fall in the feldspathic sandstone field and samples 227, 229, 230, 236 and 398 fall in the lithofeldspathic field on the sandstone classification QmFLt diagram (Table 4.2; Figure 4.5). The provenance categories, based on QmFLt and QFL diagrams, show that sandstone samples 202 – 204, 226 – 228, 231 – 235 and 398 fall in the continental block field, sample 229 in the magmatic arc field and samples 230 and 236 in the mixed orogen field (Table 4.2; Figures 4.6 and 4.7).

SEM images show quartz overgrowths on quartz grains, quartz cement, replacement of albite and K-feldspar with illite, and minor calcite cement (Figure 4.8). The relative timing for these processes are suggested to be albite and K-feldspar weathering and alteration to kaolinite and smectite, pore filling and alteration of kaolinite/smectite to illite, ductile deformation of detrital biotite and chlorite, followed by the formation of quartz overgrowths while the movement of formation waters were still relatively unrestricted and porosity and permeability much higher, followed by the formation of authigenic chlorite, which further decreased porosity and permeability.

Table 4.2 Tanqua and Laingsburg depocentre sandstone compositional and provenance categories based upon framework mineralogy (monocrystalline quartz, feldspar and lithic fragments) of studied samples.

Tanqua depocentre

Skoorsteenberg Formation (Unit 5)		
No. of samples	Percentages	No. of samples
Subfeldspathic	7.14	11
Feldspathic	57.14	0
Lithofeldspathic	35.71	1
Lithic	0	2
	100.00	14

Kookfontein Formation		
No. of samples	Percentages	No. of samples
Subfeldspathic	0	13
Feldspathic	26.47	0
Lithofeldspathic	73.53	1
Lithic	0	20
	100.00	34

Waterford Formation		
No. of samples	Percentages	No. of samples
Subfeldspathic	0	2
Feldspathic	0	0
Lithofeldspathic	100.00	1
Lithic	0	1
	100.00	4

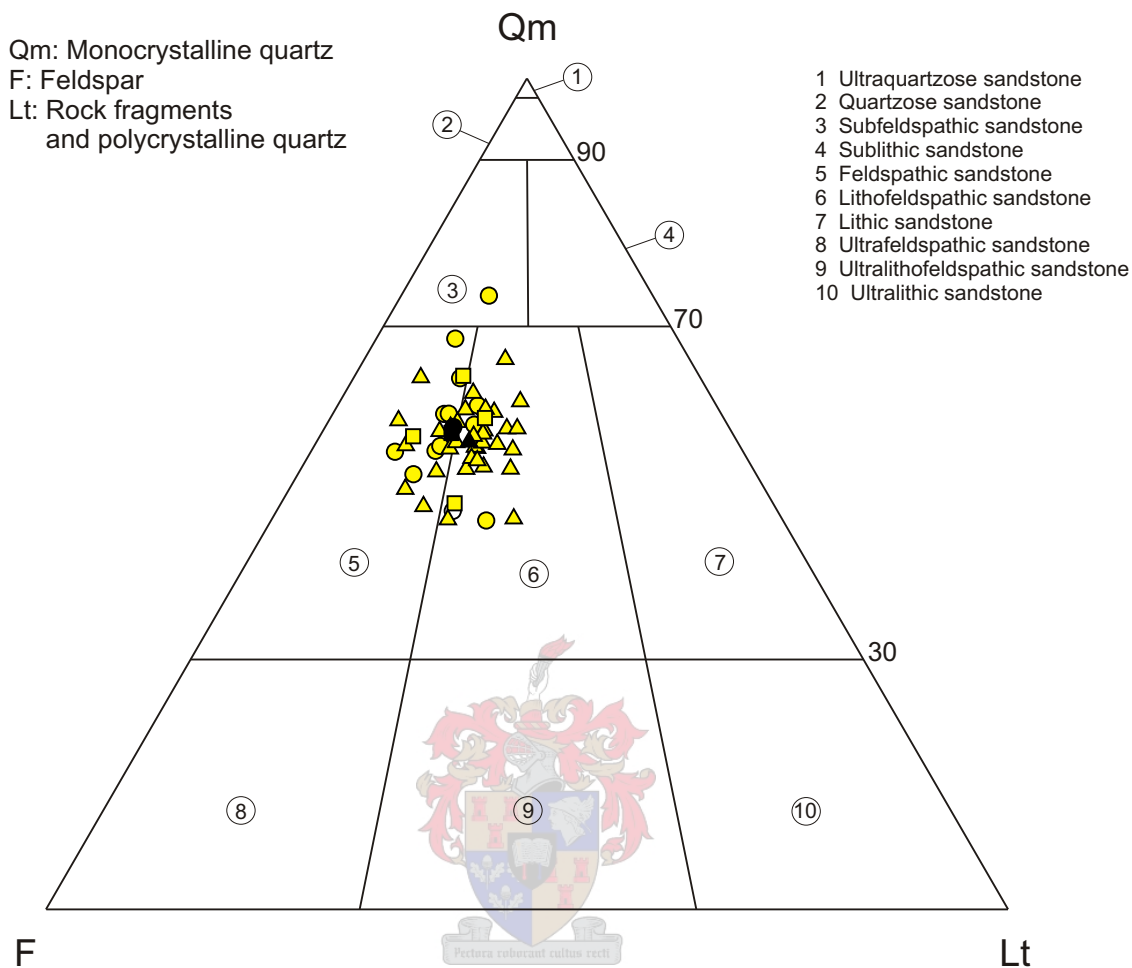
Laingsburg depocentre

Collingham Formation		
No. of samples	Percentages	No. of samples
Subfeldspathic	0	0
Feldspathic	0	1
Lithofeldspathic	100.00	0
Lithic	0	0
	100.00	1

Vischkuil Formation		
No. of samples	Percentages	No. of samples
Subfeldspathic	0	0
Feldspathic	0	0
Lithofeldspathic	100.00	1
Lithic	0	1
	100.00	2

Laingsburg Formation		
No. of samples	Percentages	No. of samples
Subfeldspathic	3	10
Feldspathic	5	0
Lithofeldspathic	14	0
Lithic	1	13
	100.00	23

Fort Brown Formation		
No. of samples	Percentages	No. of samples
Subfeldspathic	0	2
Feldspathic	2	0
Lithofeldspathic	3	0
Lithic	0	3
	100.00	5

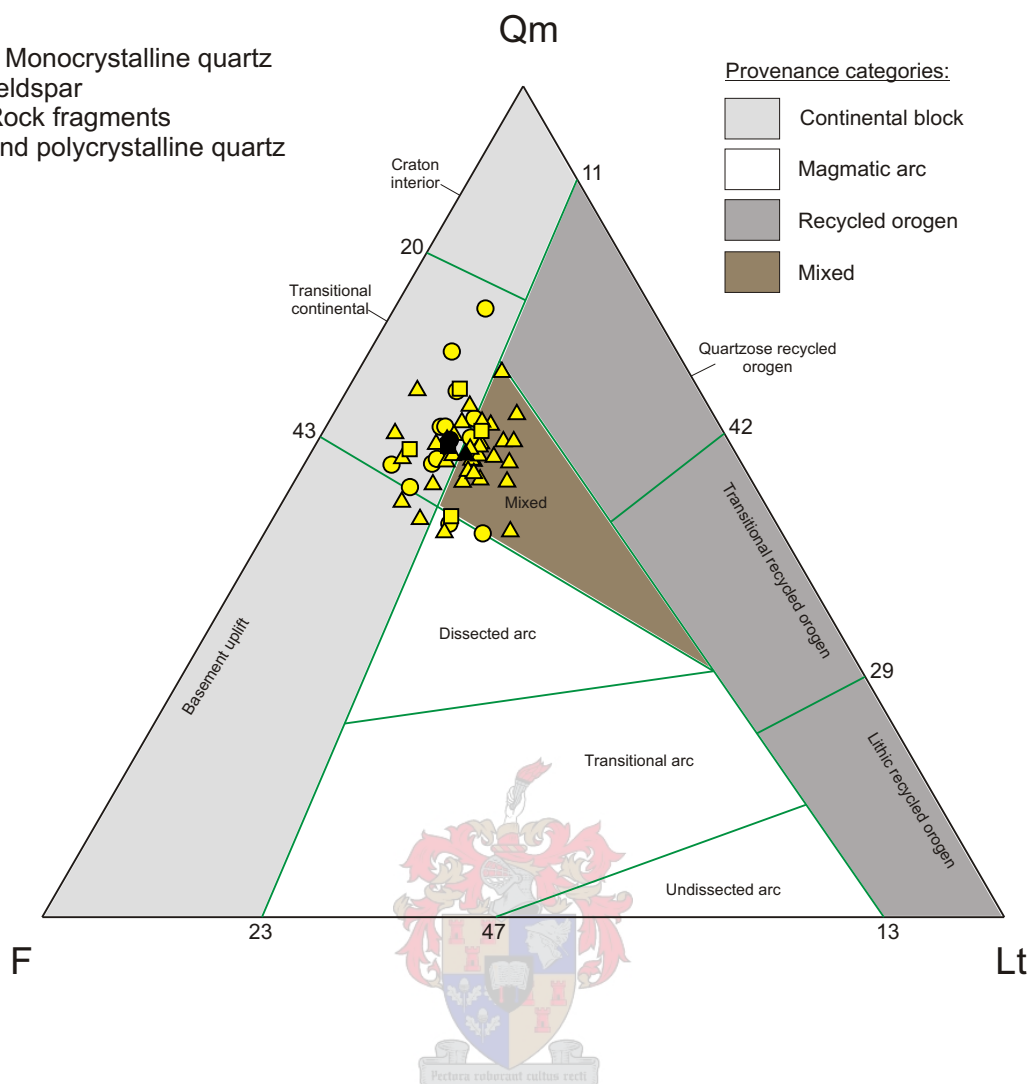


Tanqua depocentre:

- Waterford Formation
- Average Waterford Formation (n = 4)
- ▲ Kookfontein Formation
- ▲ Average Kookfontein Formation (n = 34)
- Skoorsteenberg Formation (Unit 5)
- Average Skoorsteenberg Formation (Unit 5) (n = 14)

Figure 4.5 Sandstone classification (method after Johnson, 1976) and framework mineralogy (method after Johnson, 1991).

Qm: Monocrystalline quartz  
 F: Feldspar  
 Lt: Rock fragments  
 and polycrystalline quartz



Tanqua depocentre:

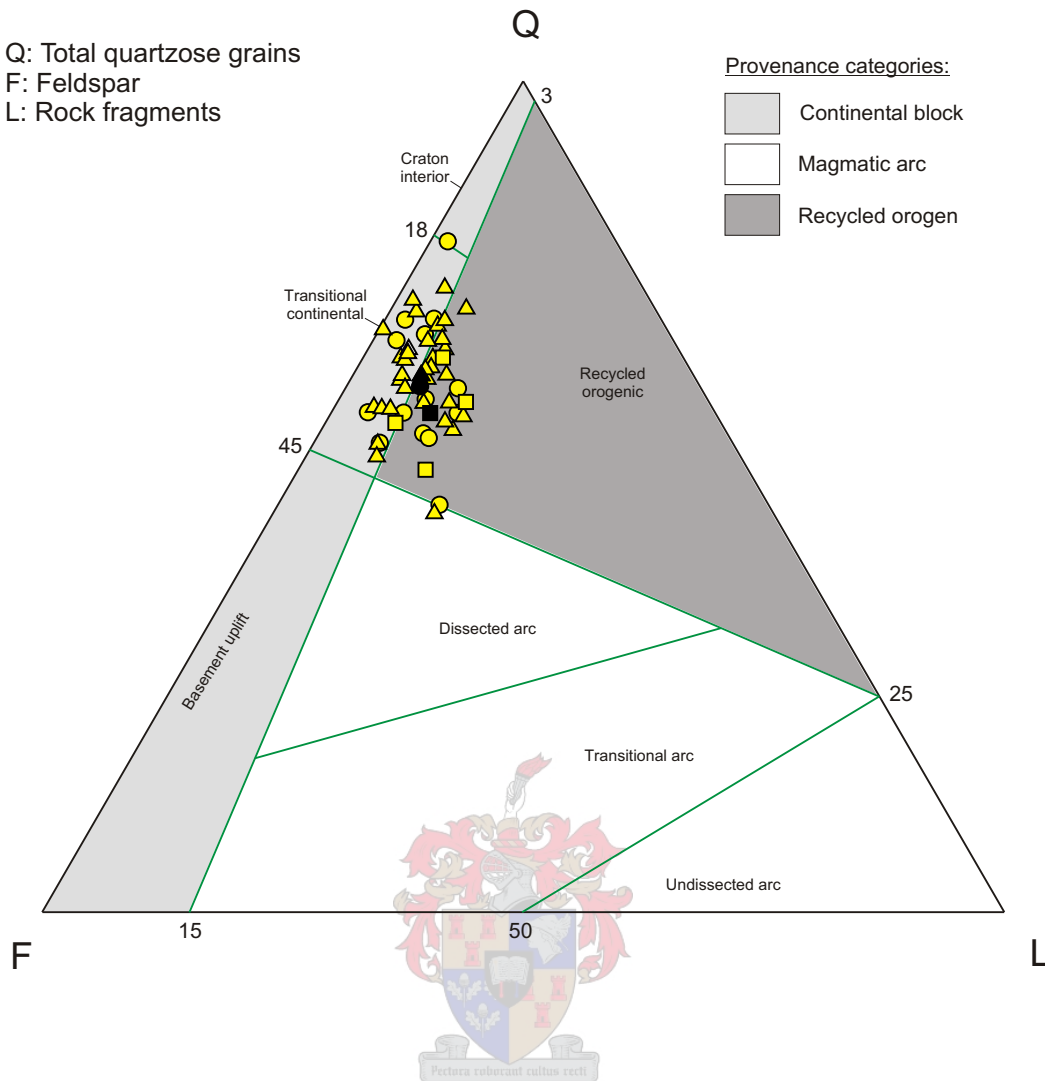
- Waterford Formation
- Average Waterford Formation (n = 4)
- ▲ Kookfontein Formation
- ▲ Average Kookfontein Formation (n = 34)
- Skoorsteenberg Formation (Unit 5)
- Average Skoorsteenberg Formation (Unit 5) (n = 14)

Figure 4.6 QmFLt plot for framework modes of sandstones showing provisional subdivisions according to inferred provenance type (method after Dickinson *et al.*, 1983). Within continental blocks, sources are either on stable shields and platforms or in uplifts marking plate boundaries and trends of intraplate deformation that transects the continental blocks (Dickinson, 1985). Commonly granitic or gneissic exposures are supplemented by recycling of associated sediments (Dickinson, 1985; McCann, 1998). Within active magmatic arcs, sediment sources are mainly in the volcanic carapace capping the igneous belt and in granitic plutons of the arc roots (Dickinson *et al.*, 1983). Within recycled orogens, sediment sources are dominantly sedimentary strata and subordinate volcanic rocks, in part metamorphosed, exposed to erosion by the orogenic uplift of fold belts and thrust sheets (Dickinson and Suszek, 1979; Dickinson, 1985; McCann, 1998). Basement uplifts occur along incipient rift belts, transform ruptures, deep-seated thrusts, and zones of wrench tectonism (Dickinson *et al.*, 1983).

Q: Total quartzose grains  
 F: Feldspar  
 L: Rock fragments

Provenance categories:

- Continental block
- Magmatic arc
- Recycled orogen



Tanqua depocentre:

- Waterford Formation
- Average Waterford Formation (n = 4)
- Kookfontein Formation
- Average Kookfontein Formation (n = 34)
- Skoorsteenberg Formation (Unit 5)
- Average Skoorsteenberg Formation (Unit 5) (n = 14)

Figure 4.7 QFL plot for framework modes of sandstones showing provisional subdivisions according to inferred provenance type (method after Dickinson *et al.*, 1983). Within continental blocks, sources are either on stable shields and platforms or in uplifts marking plate boundaries and trends of intraplate deformation that transects the continental blocks (Dickinson, 1985). Commonly granitic or gneissic exposures are supplemented by recycling of associated sediments (Dickinson, 1985; McCann, 1998). Within active magmatic arcs, sediment sources are mainly in the volcanic carapace capping the igneous belt and in granitic plutons of the arc roots (Dickinson *et al.*, 1983). Within recycled orogens, sediment sources are dominantly sedimentary strata and subordinate volcanic rocks, in part metamorphosed, exposed to erosion by the orogenic uplift of fold belts and thrust sheets (Dickinson and Suszek, 1979; Dickinson, 1985; McCann, 1998). Basement uplifts occur along incipient rift belts, transform ruptures, deep-seated thrusts, and zones of wrench tectonism (Dickinson *et al.*, 1983).

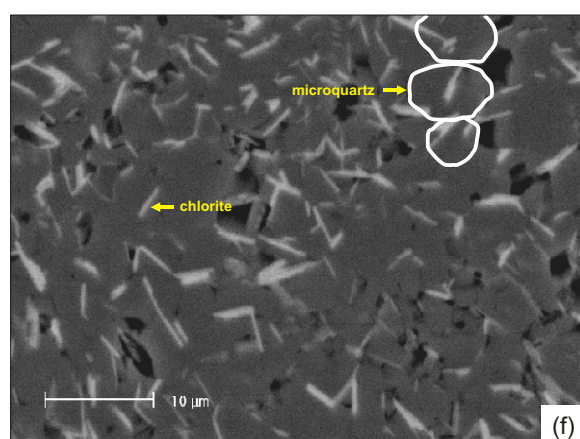
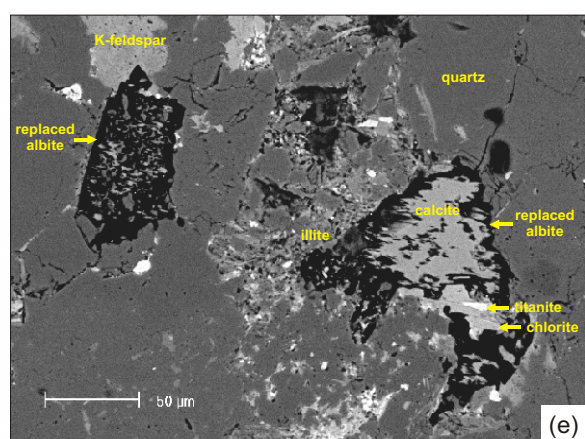
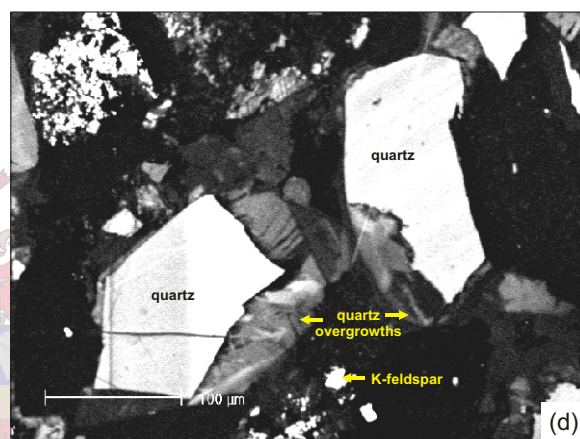
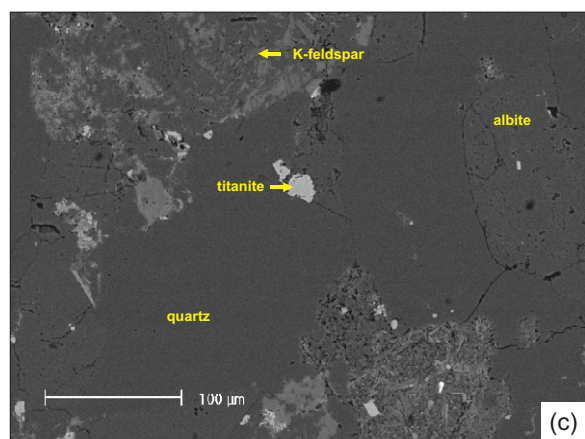
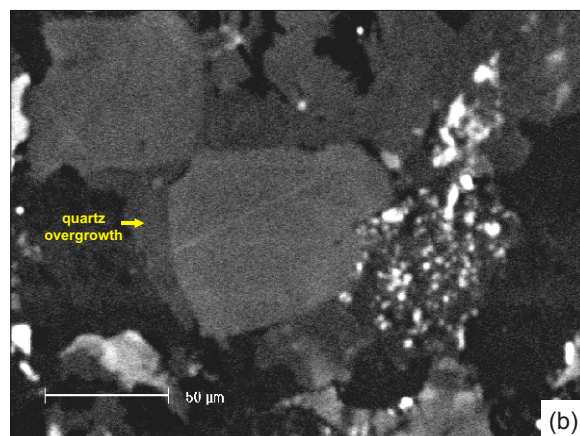
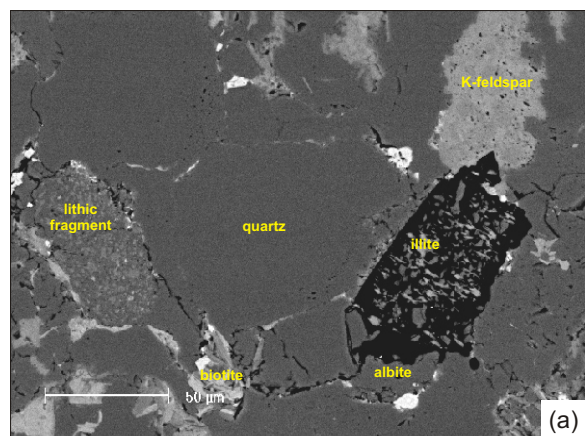


Figure 4.8 Images of sandstone (235) from a slope channel-fill complex in Unit 5 of the Skoorsteenber Formation, Tanqua depocentre. (a) Scanning electron microscopy (SEM) image of a lithic fragment, K-feldspar (darker colouring on grain shows lower K content), biotite and albite replaced by illite. (b) Same field of view under cathodoluminescence (CL) showing the extent of quartz overgrowths. (c) SEM image of quartz, albite, K-feldspar and titanite. (d) Same field of view under CL showing the extent of quartz overgrowths. (e) K-feldspar with calcite cement and illite on the rim of the grain, SEM. (f) Authigenic microquartz and chlorite, SEM. The white lines show some microquartz boundaries.

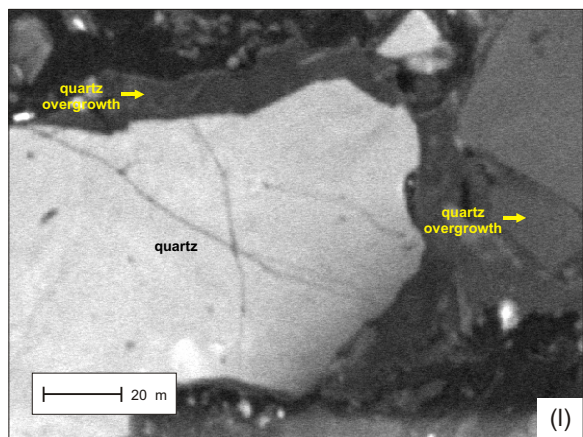
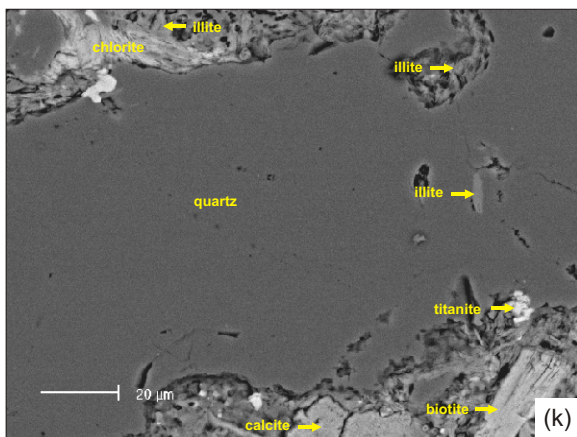
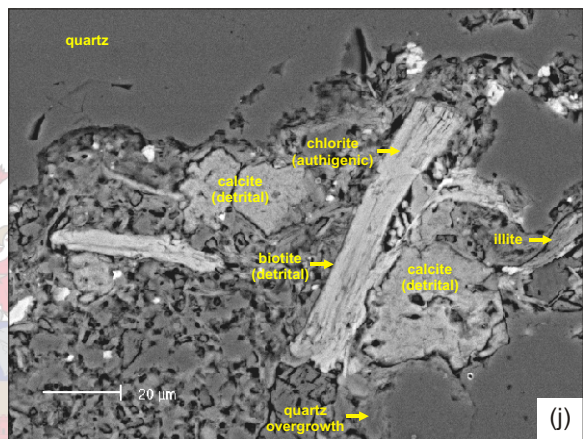
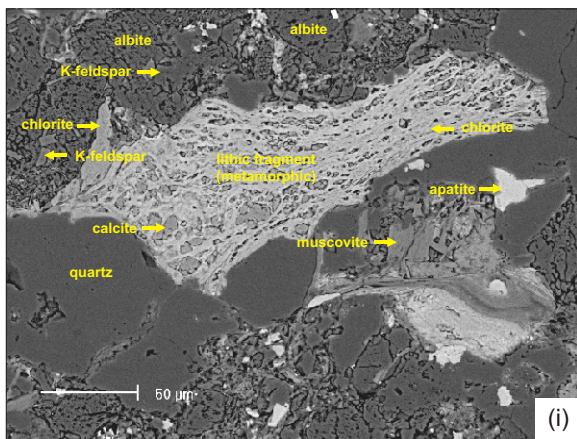
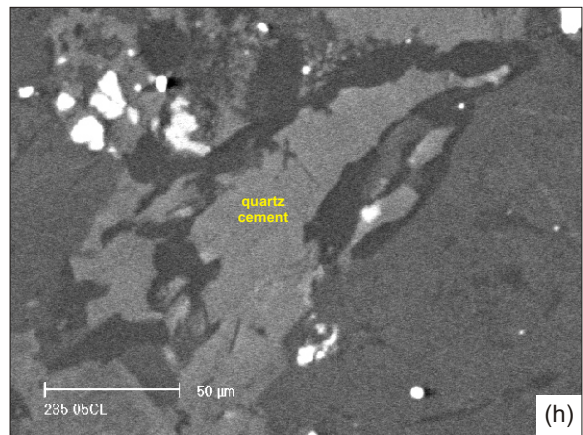
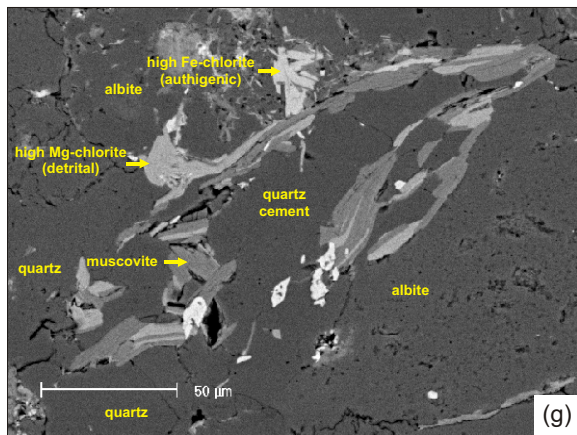


Figure 4.8 continued. Images of sandstone (235) from a slope channel-fill complex in Unit 5 of the Skoorsteenberg Formation (g and h), and sandstone (398) from pro-delta turbidites of the Kookfontein Formation (i - l), Tanqua depocentre. (g) Muscovite and chlorite grains intergrown with quartz cement, SEM. (h) Same field of view under CL showing the extent of quartz cement and overgrowths. (i) SEM image of the complete replacement of an albite grain by calcite cement and chlorite. (j) Detrital biotite and calcite, with authigenic illite and chlorite, SEM. Chlorite is replacing biotite along the cleavage planes. (k) Quartz overgrowths, chlorite and illite, SEM. (l) Same field of view under CL showing the extent of quartz overgrowths.

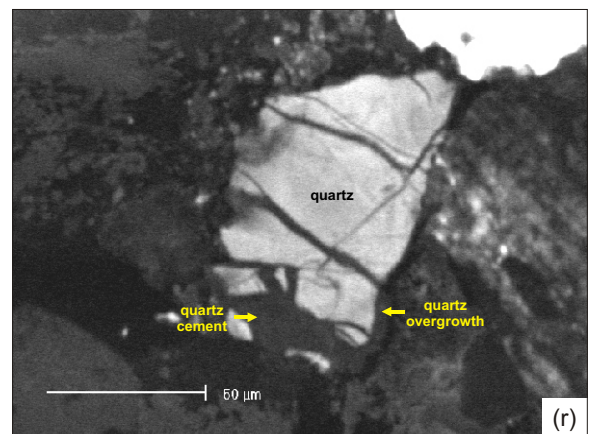
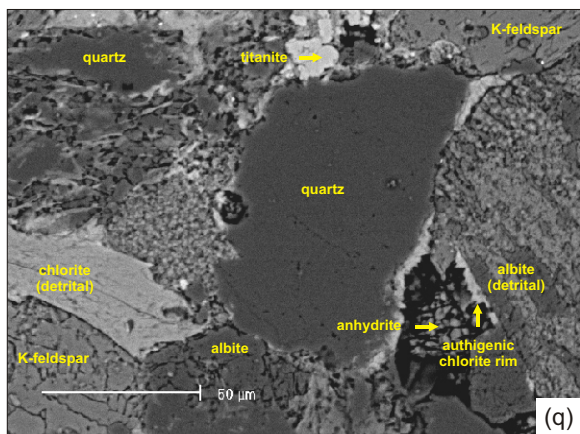
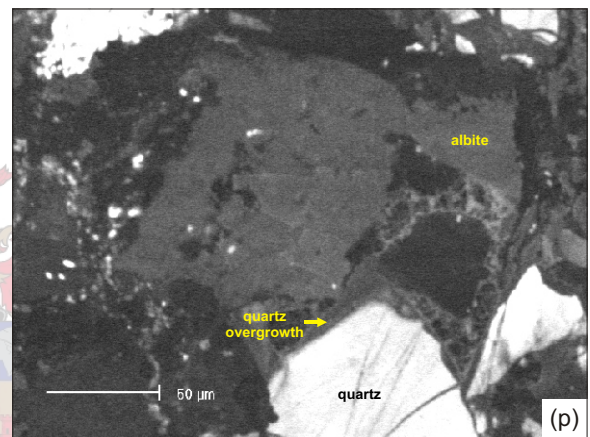
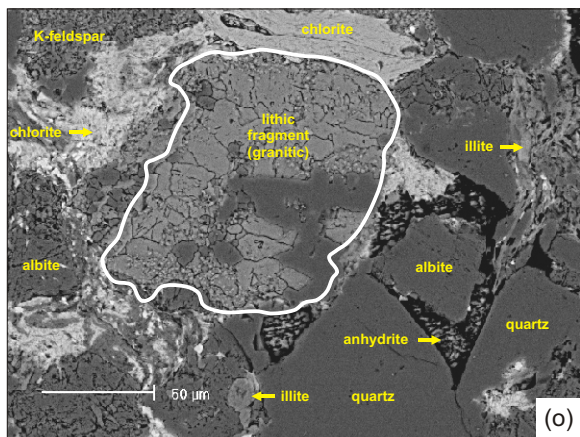
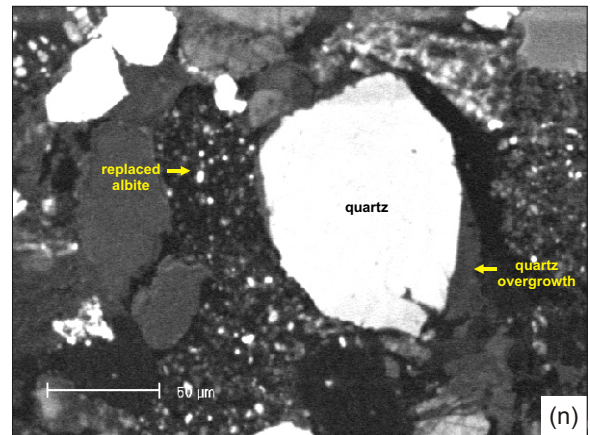
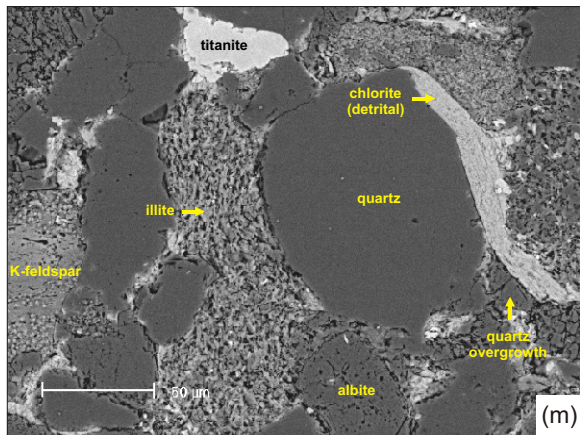


Figure 4.8 continued. Images of sandstone (3116) from the delta front facies in the Waterford Formation, Tanqua depocentre. (m) Quartz, chlorite, albite and illite, SEM. The detrital chlorite was deformed by mechanical compaction, after which the quartz overgrowth grew up to the edge of the chlorite grain. (n) Same field of view under CL showing the extent of quartz overgrowths and an albite grain completely replaced by illite. (o) SEM image of a lithic grain with inherited fractures and annealing. (p) Same field of view under CL showing the extent of quartz overgrowths. (q) Quartz grain with an altered rim and overgrowth, chlorite and albite, SEM. The detrital albite shows a rim of authigenic chlorite overgrowth. (r) Same field of view under CL showing the inherited annealed quartz grain, with quartz overgrowths on both the quartz grain and its quartz cement.

### **4.3.2 Kookfontein Formation**

The schematic stratigraphy of the Kookfontein Formation and sample locations relative to the overall stratigraphy are shown in Figure 4.9, whereas a summary of the texture and composition of the sandstones are given in Table 4.3. Photographs of sample locations are shown in Figure 4.10.

#### **4.3.2.1 Lower slope, low-density turbidite deposits**

The shales and siltstones are dark grey and fine-grained (max. grain size ~0.05 mm), with a colour index ~40. They consist primarily of clay minerals, mica, quartz and opaques. The shales and siltstones show faint parallel-lamination. The sandstones are lithofeldspathic, light brown to grey coloured and fine-grained (max. grain size ~0.25 mm), with a colour index of ~20. The outcrops vary from being massive to showing either ripple- or planar-lamination. Some fine-grained (max. grain size <0.50 mm) whitish layers (avg. thickness ~1 cm) are present within the siltstone outcrop (Figure 4.10a) at V6. The grains are randomly oriented, moderately sorted, and angular to sub-rounded and show no obvious grading. Grain boundaries are moderately to well defined and there are some quartz grain and secondary mineral overgrowths. The rocks are grain supported and show very little compaction, due to early cementation.

#### **4.3.2.2 Sandstones with soft-sediment deformational features**

The sandstones are lithofeldspathic, grey coloured and fine- to lower medium-grained (max. grain size <0.50 mm), with a colour index ~10. The grain boundaries are well defined and are angular to sub-rounded. Some quartz overgrowths and cementation can be seen, and there is no apparent grading. The grains are well sorted and there is no porosity due to early cementation.

#### **4.3.2.3 Mid-slope to shelf edge delta deposits**

The sandstones are feldspathic to lithofeldspathic, generally grey coloured and medium-grained (avg. grain size ~0.50 mm), with a colour index ranging from 15 to 20 and mostly showing ripple-lamination. The grains are moderately to well sorted and angular to rounded. They show very little compaction (due to early cementation), no grading and some preferred mica grain orientation parallel to the lamination.

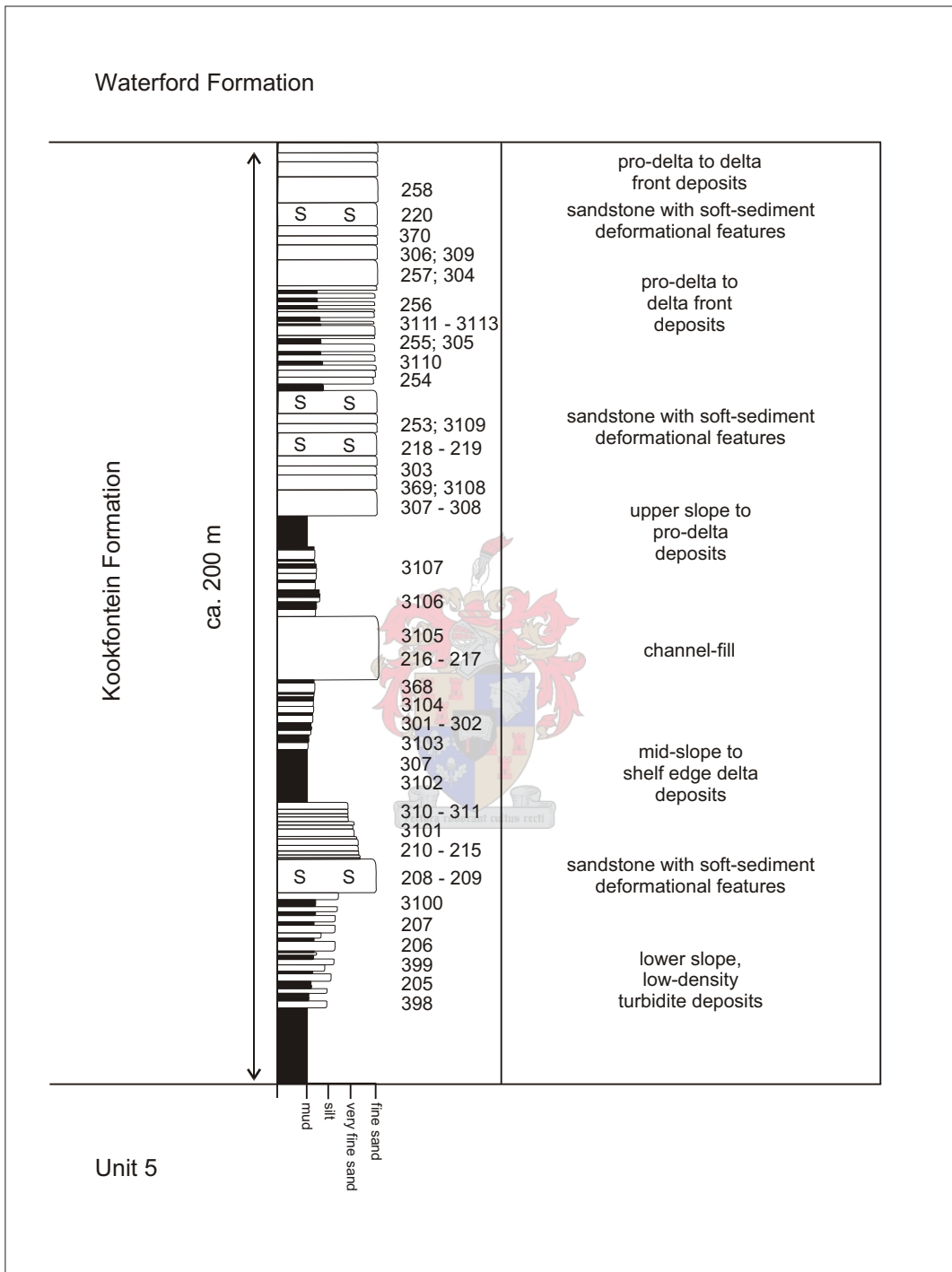


Figure 4.9 Schematic stratigraphy of the Kookfontein Formation, Tanqua depocentre. The sample locations relative to the overall stratigraphy are shown.

Table 4.3 Summary of texture and composition (%) of sandstones from the Kookfontein Formation, Tanqua deprocentre.

Stratigraphic unit	Detrital components						Authigenic minerals					Texture		Rock classification	
	Quartz	Feldspar	Mica	Litho-clasts	Accessory minerals	Matrix	Opagues	Quartz cement and overgrowths	Illite	Chlorite	Calcite	Mica	Grain size		Sorting
Lower slope, low-density turbidite deposits	34.29	15.38	13.93	5.30	0.41	10.00	3.30	5.56	6.10	1.00	2.00	3.48	fine-grained	moderately to well sorted	lithofeldspathic
Sandstone with soft-sediment deformational features	40.05	21.32	8.15	3.61	1.19	9.75	2.69	5.30	5.63	0.52	2.04		fine- to medium-grained	moderately to well sorted	lithofeldspathic
Mid-slope to shelf edge delta deposits	39.42	20.66	9.02	3.83	0.96	8.88	3.90	5.60	4.97	1.03	1.25	2.25	medium-grained	moderately to well sorted	feldspathic to lithofeldspathic
Channel-fill deposits	34.75	18.61	9.21	4.89		6.00	4.16	8.57	10.04	0.74	0.74	2.30	fine-grained	poorly to well sorted	feldspathic to lithofeldspathic
Upper slope to pro-delta deposits	35.47	18.14	11.18	7.42		3.67	2.29	7.37	8.90	1.23	1.54	2.79	fine- to medium-grained	moderately to well sorted	lithofeldspathic
Pro-delta to delta front deposits	37.33	20.01	8.34	4.64	0.91	5.00	3.91	6.34	10.00	0.85	1.36	2.09	fine- to medium-grained	moderately to well sorted	feldspathic to lithofeldspathic

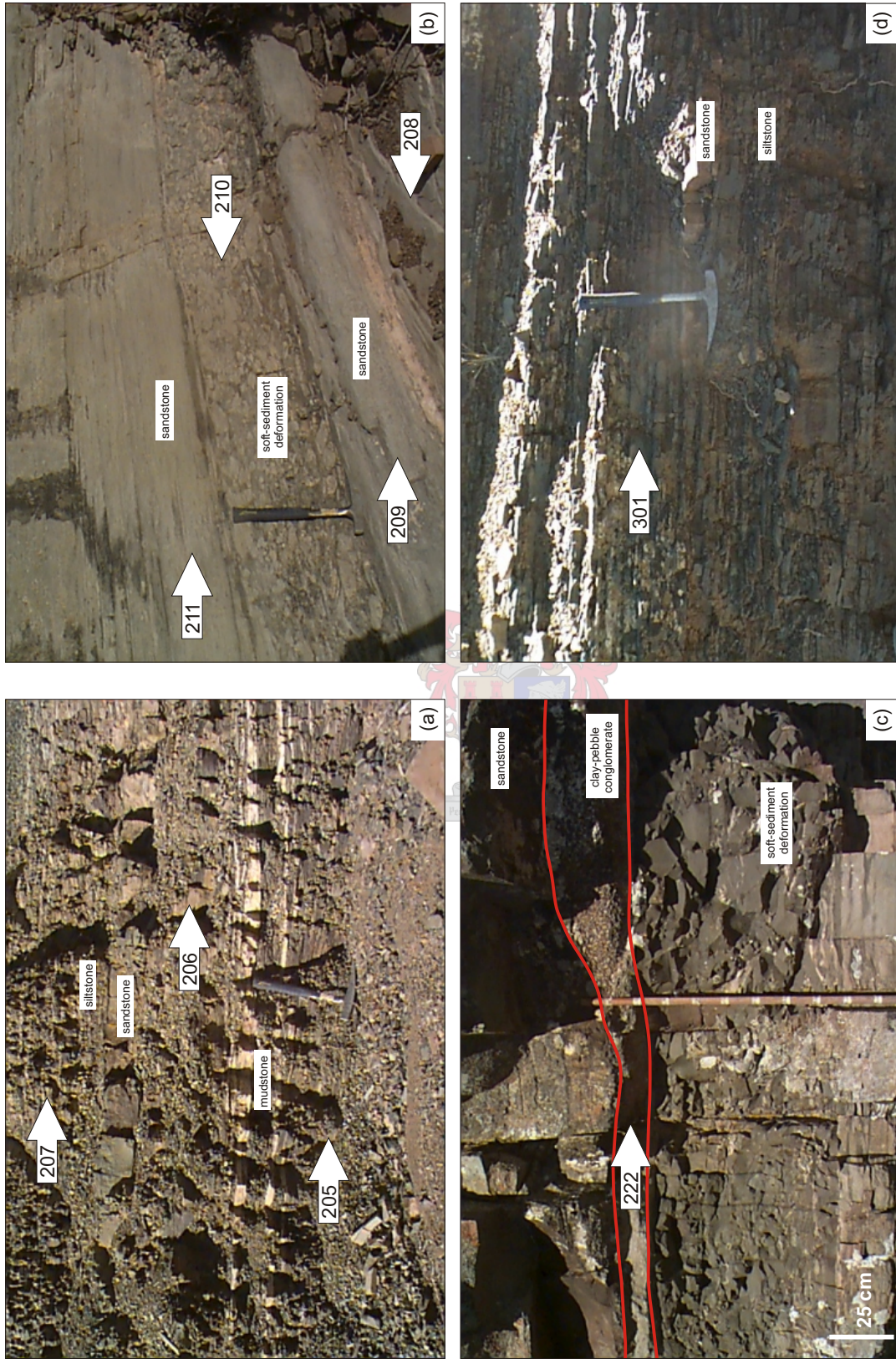


Figure 4.10 Kookfontein and Waterford Formations, Tanqua depocentre. Sample locations:

- (a) Samples 205 - 207 (Pienaarsfontein (V6) - Kookfontein Formation).
- (b) Samples 208 - 211 (Pienaarsfontein (V6) - Kookfontein Formation).
- (c) Sample 222 (Pienaarsfontein (V6) - Waterford Formation).
- (d) Sample 301 (Bitterberg (V11) - Kookfontein Formation).

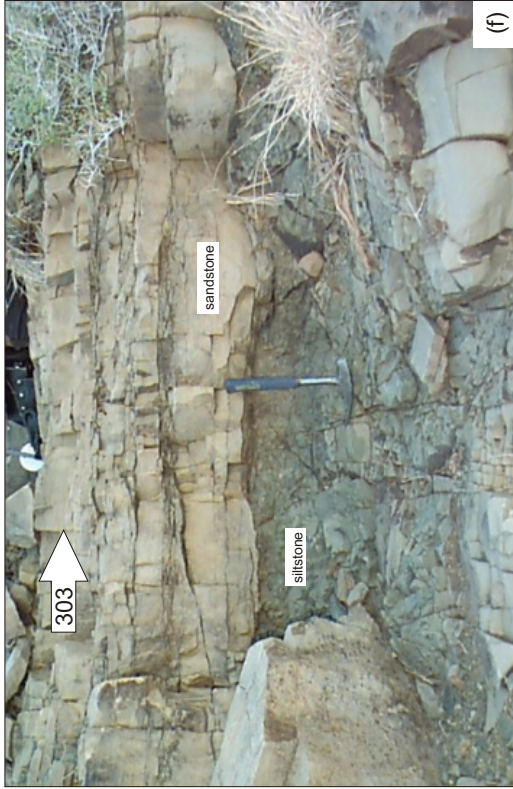


Figure 4. 10 continued. Kookfontein and Waterford Formations, Tanqua deocentre. Sample locations:  
 (e) Sample 302 (Bitterberg (V11) - Kookfontein Formation).  
 (f) Sample 303 (Bitterberg (V11) - Kookfontein Formation).  
 (g) Sample 256 (Skoorsteenberg (V135) - Kookfontein Formation).  
 (h) Samples 256 and 257 (Skoorsteenberg (V135) - Kookfontein Formation).

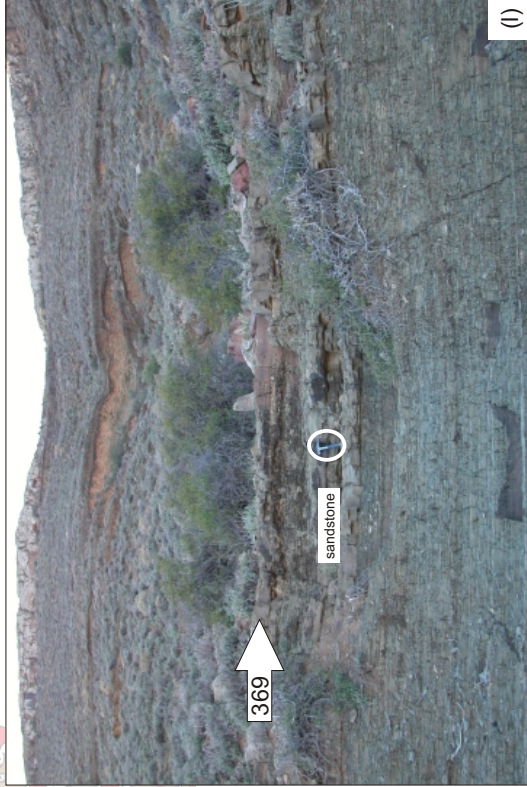
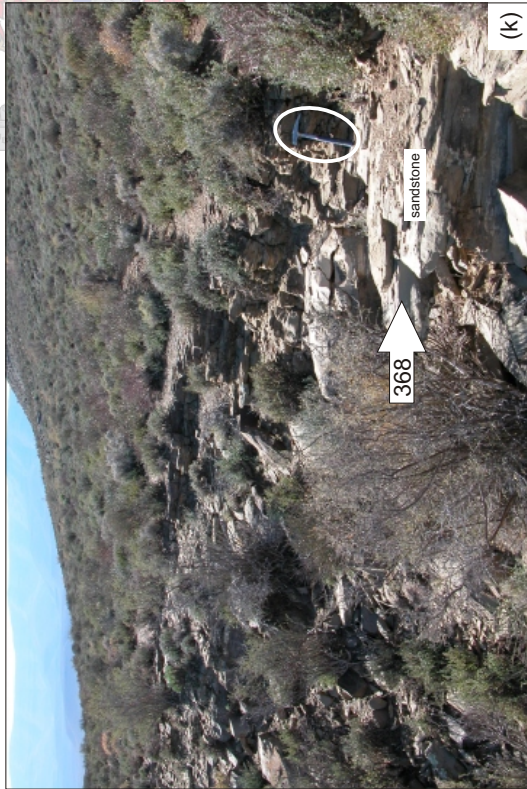
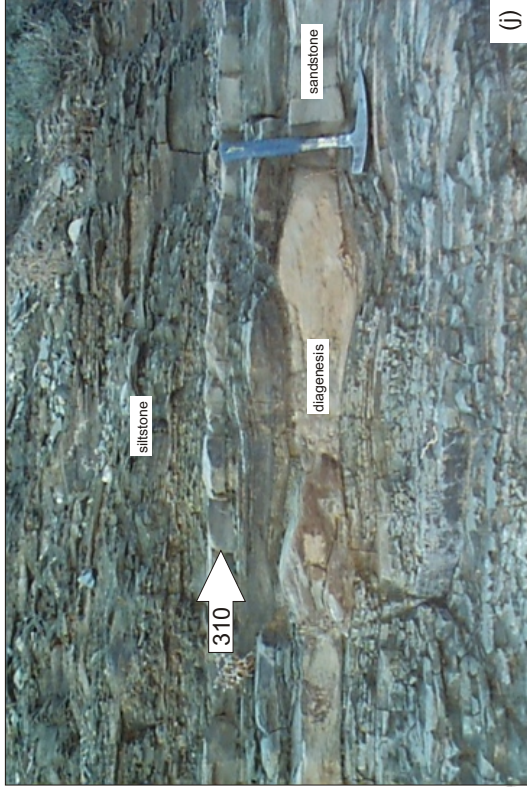
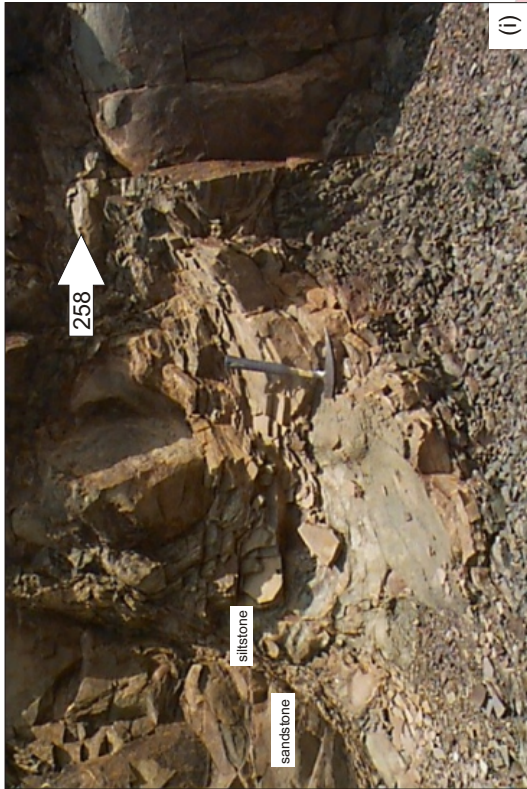


Figure 4. 10 continued. Kookfontein and Waterford Formations, Tanqua depocentre. Sample locations:

(i) Sample 258 (Skoorsteenberg (V135) - Kookfontein Formation).

(j) Sample 310 (Soutrivierspunt (V13) - Kookfontein Formation).

(k) Sample 368 (Ouberg (V18) - Kookfontein Formation). Hammer for scale (30 cm) is circled.

(l) Sample 369 (Ouberg (V18) - Kookfontein Formation). Hammer for scale (30 cm) is circled.

#### **4.3.2.4 Channel-fill deposits**

The channel-fill sandstones are feldspathic to lithofeldspathic, light grey coloured and fine-grained (max. grain size <0.25 mm), with a colour index ~5. The grains are poorly to well sorted, angular to sub-rounded and show no obvious grading. The sandstones show planar-lamination, defined by preferred parallel grain orientation, and very little compaction, due to early cementation.

#### **4.3.2.5 Upper slope to pro-delta deposits**

The sandstones are lithofeldspathic, grey coloured and fine- to lower medium-grained (avg. grain size ~0.50 mm), with a colour index ~10. There appears to be an overall increase in grain size and quartz in the sandstone beds upwards in the stratigraphic succession measured at Pienaarsfontein (V6). The grains are moderately to well sorted, angular to rounded and most of the grain boundaries are defined by primarily quartz, and in some cases calcite, cementation. Quartz overgrowths are common and there is no porosity. There is no apparent grading and very little compaction, due to early cementation. Sedimentary structures range from massive to planar-lamination to ripple-lamination. Preferred grain orientation of mica parallel to the lamination is present in some of the sandstones.

#### **4.3.2.6 Pro-delta to delta front deposits**

The sandstones are feldspathic to lithofeldspathic, grey to light brown coloured and fine- to lower medium-grained (avg. grain size <0.50 mm), with a colour index ~20. There is no obvious grading and very little compaction (due to early cementation); the sandstones are grain supported and show planar-lamination. The lamination is defined by the preferred grain orientation. The grains are moderately to well sorted. Most grain boundaries are obscured by quartz and secondary mineral overgrowths, but are angular to sub-rounded.

The sandstones from the above mentioned stratigraphic units are mineralogically very similar. The channel-fill sandstones are texturally less mature and not as well sorted as the rest of the facies. Higher energy depositional environments, such as the delta front facies, show coarser grain size.

Samples 208, 210 – 212, 214, 217 and 310 fall in the feldspathic sandstone field and samples 209, 213, 215, 216, 219, 220, 302 – 309, 311, 368 - 370, 3106 and 3109 – 3113 fall in the lithofeldspathic sandstone field on the QmFLt diagram (Figure 4.5; Table 4.2). The sandstones fall preferentially in the continental block and mixed provenance categories on the QmFLt and QFL diagrams (Figures 4.6 and 4.7; Table 4.2).

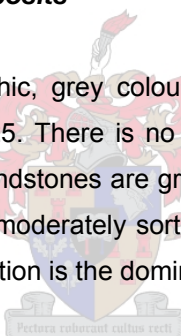
Images taken from the SEM show quartz overgrowths on quartz grains, quartz cement and replacement of albite and K-feldspar by illite (Figure 4.8). The relative timing for these processes are suggested to be albite and K-feldspar weathering and alteration to kaolinite and smectite, pore filling and alteration of kaolinite/smectite to illite, ductile deformation of detrital biotite and chlorite, followed by the formation of quartz overgrowths while the movement of formation waters were still relatively unrestricted and porosity and permeability much higher, followed by the formation of authigenic chlorite, which further decreased porosity and permeability.

### **4.3.3 Waterford Formation**

The schematic stratigraphy of the Waterford Formation and sample locations relative to the overall stratigraphy are shown in Figure 4.11, whereas a summary of the texture and composition of the sandstones are given in Table 4.4. Photographs of sample locations are shown in Figure 4.10.

#### **4.3.3.1 Pro-delta and delta front deposits**

The sandstones are lithofeldspathic, grey coloured, and fine-grained (max. grain size ~0.40 mm), with a colour index of ~25. There is no obvious grading, very little compaction (due to early cementation) and the sandstones are grain supported. The grains are randomly oriented, angular to sub-angular and moderately sorted. Grain boundaries are poorly to well defined by cementation. Ripple-lamination is the dominant primary sedimentary structure.



#### **4.3.3.2 Channel-fill deposits**

Sandstones are lithofeldspathic, light to dark grey coloured and fine- to lower medium-grained (max. grain size ~0.25 mm), with a colour index ~15. The grains are poorly to well sorted, sub-rounded and show no grading. Quartz grain overgrowths obscure some of the grain boundaries. The sandstones show planar- and cross-lamination, defined by lighter and darker coloured bands.

Mineralogically the sandstones are very similar. The main differences between sandstones from the different facies are grain size and sorting, with the sandstones from the wave influenced delta facies being finer grained and better sorted than the sandstones from the channel-fills, due to the reworking of the sands.

Samples 254 and 257 fall in the feldspathic sandstone field and samples 223, 224, 253, 255 and 3114 - 3116 fall in the lithofeldspathic sandstone field on the QmFLt diagram (Figure

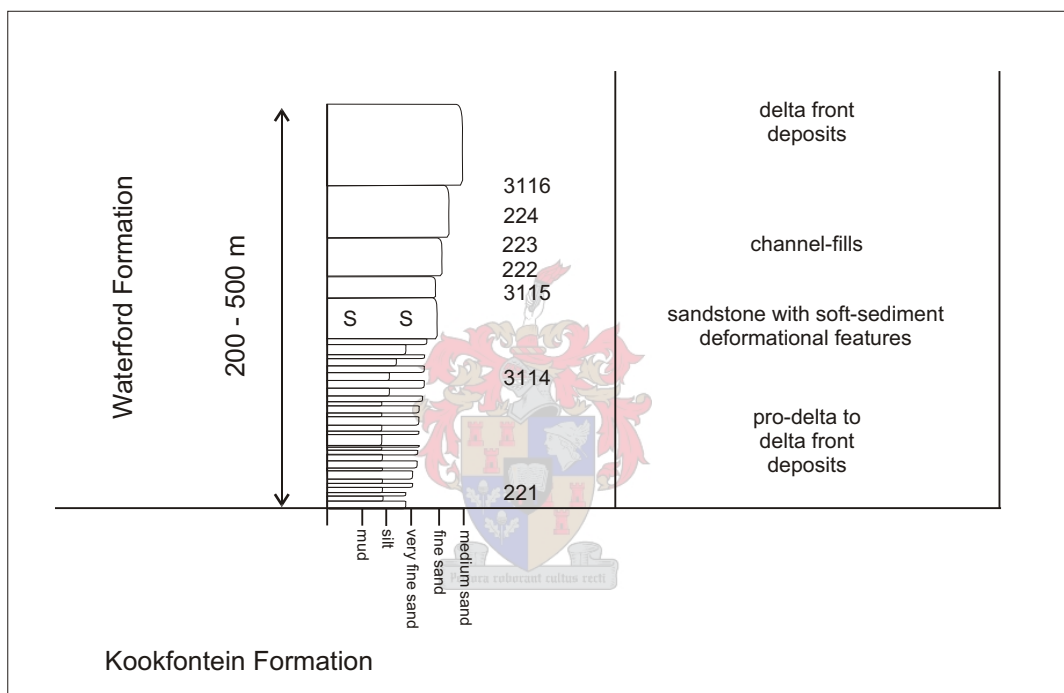


Figure 4.11 Schematic stratigraphy of the Waterford Formation, Tanqua depocentre. The sample locations relative to the overall stratigraphy are shown.

Table 4.4 Summary of texture and composition (%) of sandstones from the Waterford Formation, Tanqua depocentre.

Stratigraphic unit	Detrital components						Authigenic minerals					Texture		Rock classification	
	Quartz	Feldspar	Mica	Litho-clasts	Accessory minerals	Matrix	Opauques	Quartz cement and overgrowths	Illite	Chlorite	Calcite	Mica	Grain size		Sorting
Pro-delta to delta front deposits	40.50	15.97	10.50	5.13		15.00	2.85	2.28	2.28	0.57	2.28	2.62	fine-grained	moderately sorted	lithofeldspathic
Channel-fill deposits	39.18	19.65	9.77	3.55	0.51	7.00	2.39	7.14	5.62	1.55	1.37	2.44	fine- to medium-grained	poorly to well sorted	lithofeldspathic

4.5; Table 4.2). The sandstones fall preferentially in the continental block and mixed provenance categories on the QmFLt and QFL diagrams (Figures 4.6 and 4.7; Table 4.2).

SEM images show quartz overgrowths on quartz grains, quartz cement and replacement of albite and K-feldspar with illite (Figure 4.8). The relative timing for these processes are suggested to be albite and K-feldspar weathering and alteration to kaolinite and smectite, pore filling and alteration of kaolinite/smectite to illite, ductile deformation of detrital biotite and chlorite, followed by the formation of quartz overgrowths while the movement of formation waters were still relatively unrestricted and porosity and permeability much higher, followed by the formation of authigenic chlorite, which further decreased porosity and permeability.

#### **4.4 Laingsburg depocentre**

The Collingham, Vischkuil, Laingsburg and Fort Brown Formations, with the measured sedimentological profiles and sample locations, are shown in Figure 4.12. Photographs of sample locations are shown in Figure 4.13.

##### **4.4.1 Collingham Formation**

The schematic stratigraphy of the Collingham Formation and sample locations relative to the overall stratigraphy are shown in Figure 4.14, whereas a summary of the texture and composition of the sandstones are given in Table 4.5.

##### **4.4.1.1 Basin-floor, very fine-grained turbidites**

The Collingham Formation consists of alternating thin beds of mudstone, very thin beds of tuff, subordinate siltstone, very fine-grained sandstone and chert beds (Viljoen, 1992a).

The sandstones are light to dark grey coloured, fine-grained (avg. grain size ~0.10 mm), with a colour index ~45. The grains are randomly oriented, moderately to well sorted, angular to rounded and shows no grading, preferred orientation and very little compaction, due to early cementation. Quartz grain and secondary mineral overgrowths obscure some of the grain boundaries. The sandstones show planar-lamination and are grain supported.

The shales and siltstones are dark grey to brown on outer weathering surfaces, and very fine-grained (avg. grain size <0.05 mm), with a colour index ~35. They consist of larger grains of quartz, clay minerals, opaques, biotite, muscovite, albite and K-feldspar in a finer matrix of the same composition and are finely laminated. There is very little compaction, due to early cementation, and the grains show random orientation and grain overgrowths.

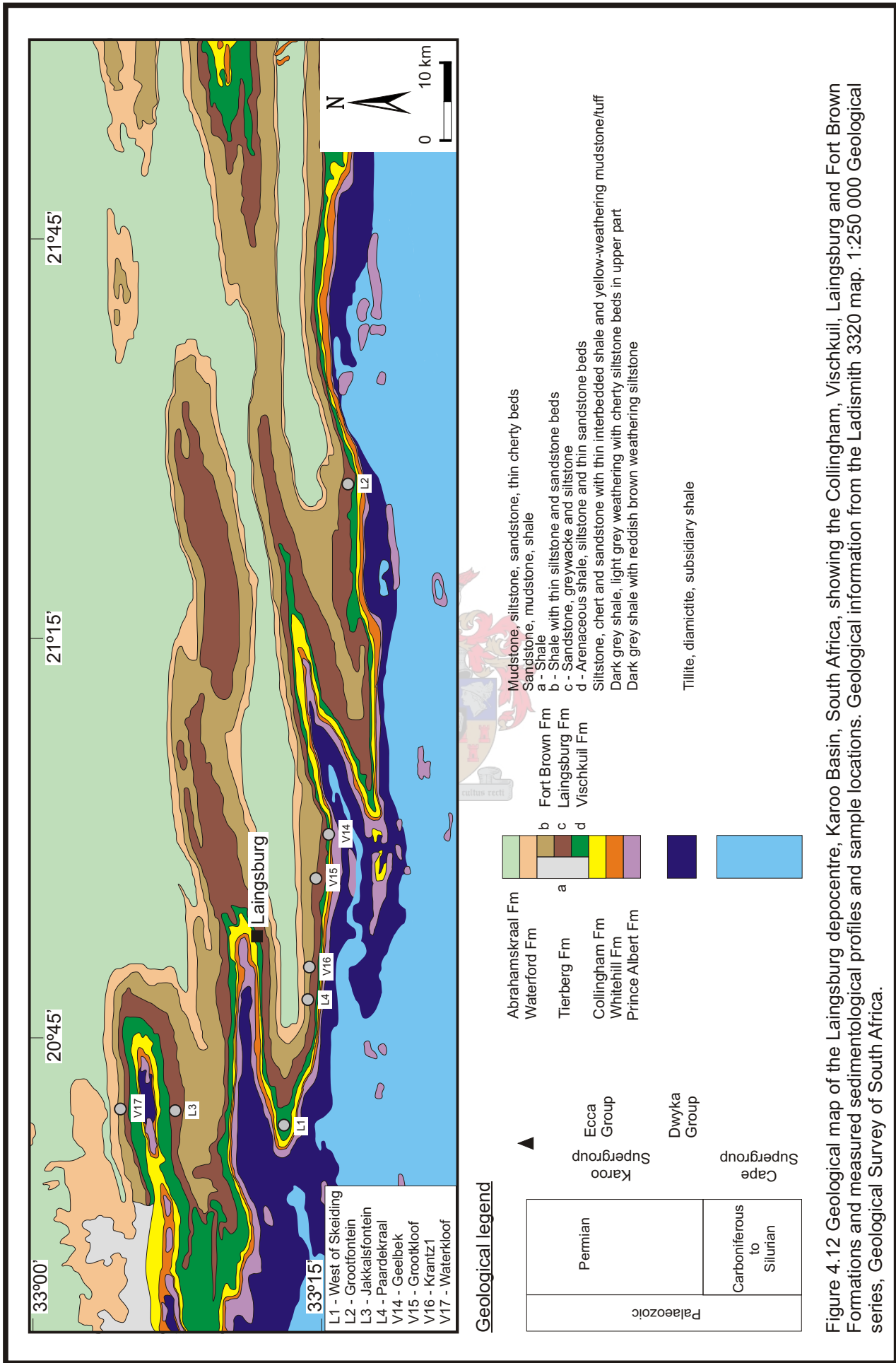


Figure 4.12 Geological map of the Laingsburg depocentre, Karoo Basin, South Africa, showing the Collingham, Vischkuil, Laingsburg and Fort Brown Formations and measured sedimentological profiles and sample locations. Geological information from the Ladismith 3320 map. 1:250 000 Geological series, Geological Survey of South Africa.

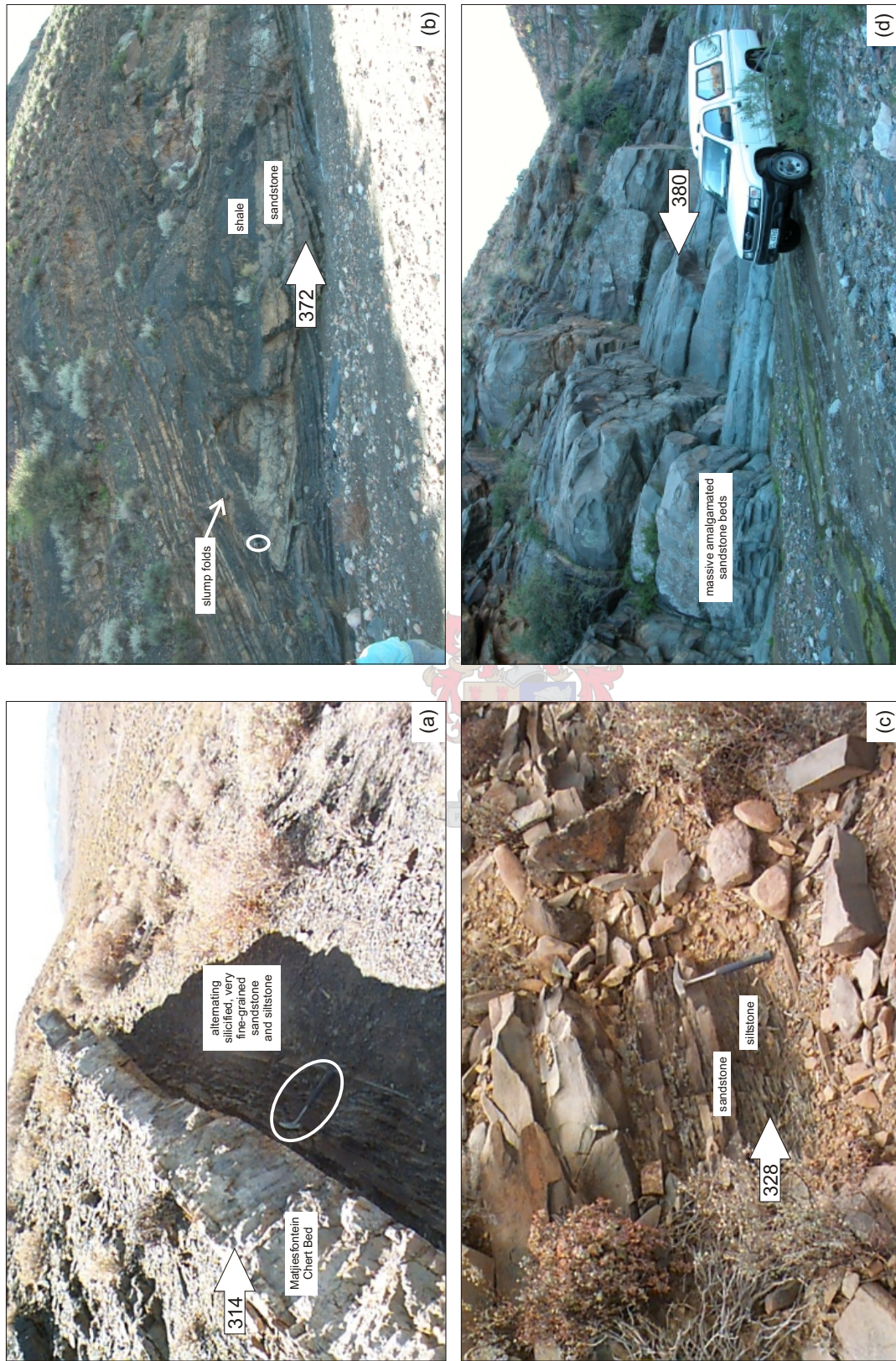


Figure 4.13 Laingsburg depocentre. Sample locations:  
 (a) Sample 314 (Geelbek (V14) - Collingham Formation). Hammer for scale (30 cm) is circled.  
 (b) Sample 372 (west of Skeiding (L1) - Vischkuil Formation). Hammer for scale (30 cm) is circled.  
 (c) Sample 328 (Grootkloof (V15) - Unit 1, Fan A from the Laingsburg Formation).  
 (d) Sample 380 (Grootfontein (L2) - Unit 2, Fan A from the Laingsburg Formation).

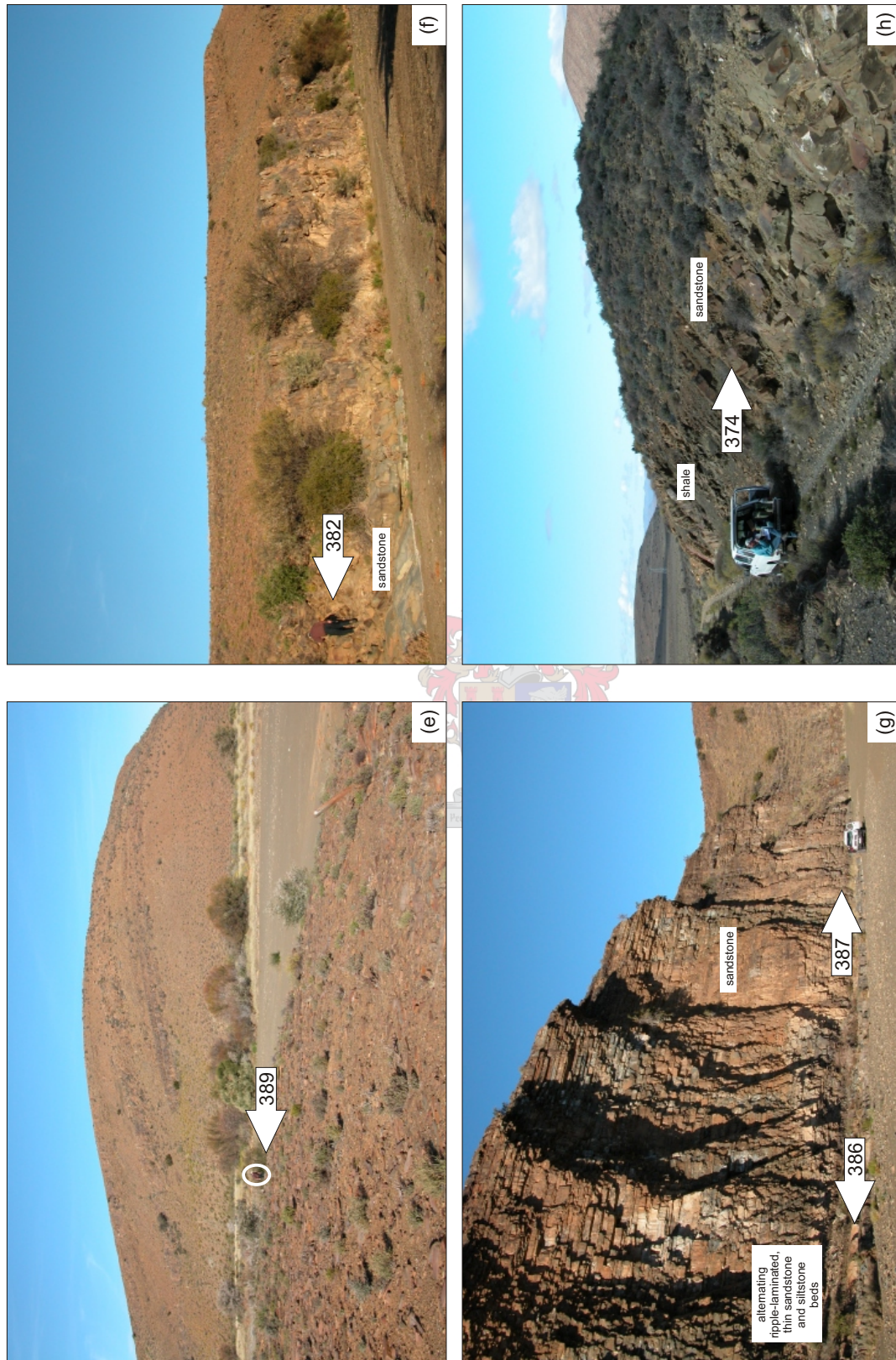


Figure 4.13 continued. Laingsburg depocentre. Sample locations:  
 (e) Sample 389 (Jakkalsfontein (L3) - Unit 3, Fan A, Laingsburg Formation). Person for scale is circled.  
 (f) Sample 382 (Jakkalsfontein (L3) - Unit 4, Fan A, Laingsburg Formation).  
 (g) Samples 386 and 387 (Jakkalsfontein (L3) - Fan B, Laingsburg Formation).  
 (h) Sample 374 (Paardekraal (L4) - Fan C, Laingsburg Formation).

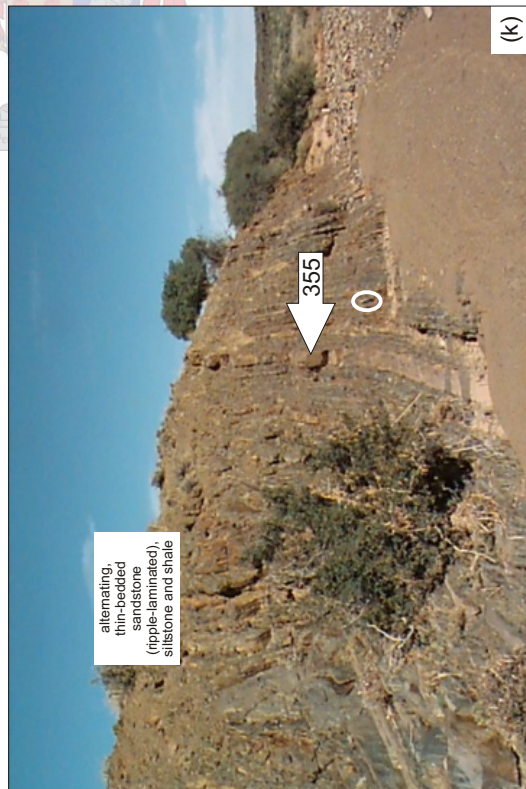
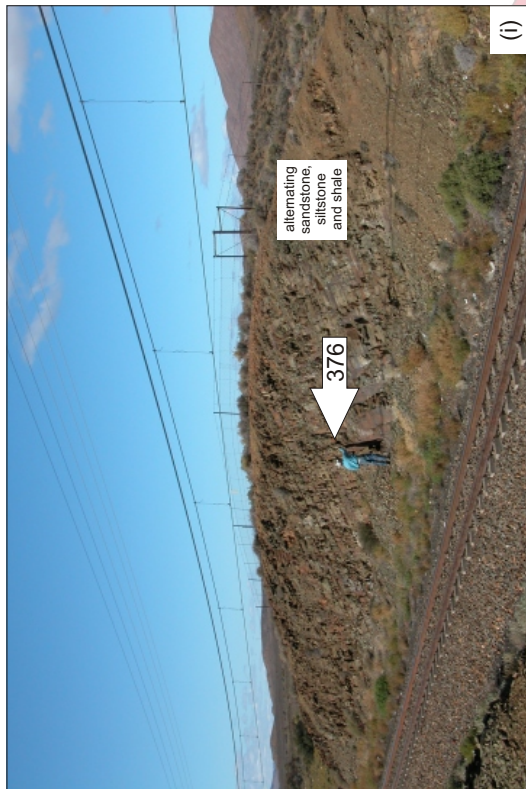
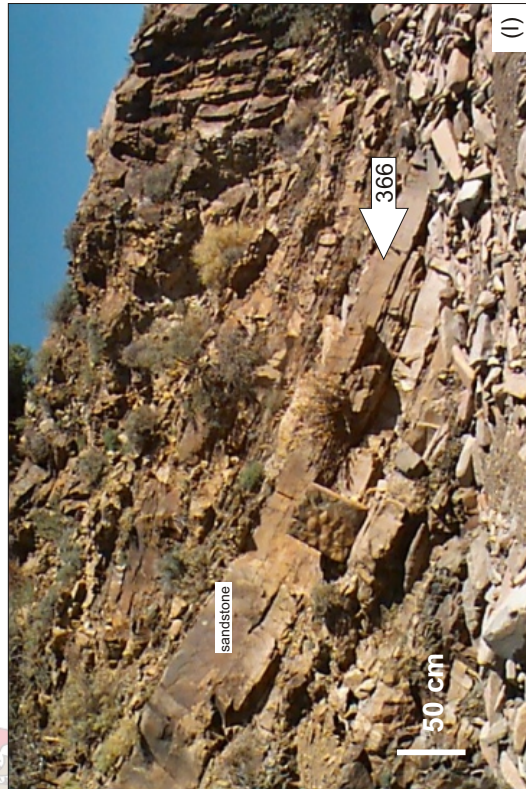


Figure 4.13 continued. Laingsburg deposcentre. Sample locations:  
 (i) Sample 376 (Paardekraal (L4) - Fan D, Laingsburg Formation).  
 (j) Sample 375 (Paardekraal (L4) - Fan E, Laingsburg Formation).  
 (k) Sample 355 (Waterkloof (V17) - Fan F, Laingsburg Formation).  
 (l) Sample 366 (Waterkloof (V17) - Fort Brown Formation).  
 Hammer for scale (30 cm) is circled.

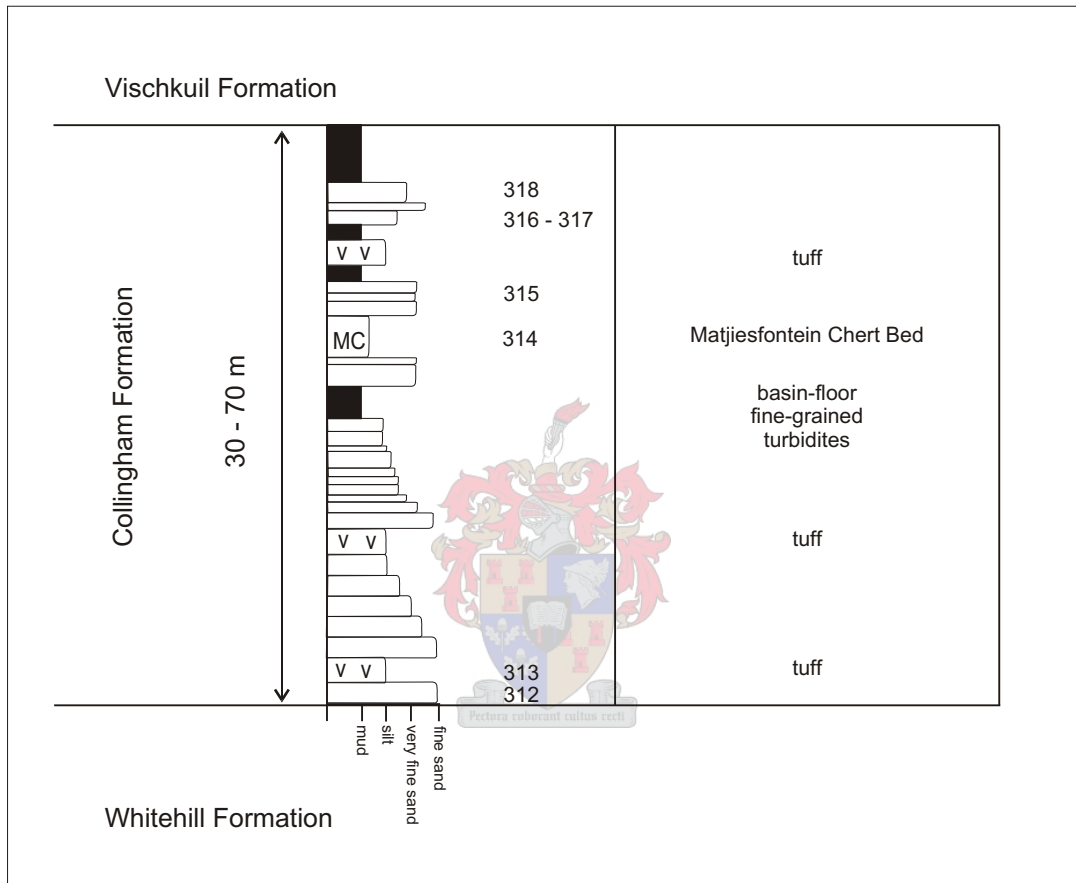


Figure 4.14 Schematic stratigraphy of the Collingham Formation, Laingsburg depocentre. The sample locations relative to the overall stratigraphy are shown.

Table 4.5 Summary of texture and composition (%) of sandstones from the Collingham Formation, Laingsburg deponentre.

Stratigraphic unit	Detrital components						Authigenic minerals				Texture		Rock classification		
	Quartz	Feldspar	Mica	Litho-clasts	Accessory minerals	Matrix	Opagues	Quartz cement and overgrowths	Illite	Chlorite	Calcite	Mica		Grain size	Sorting
Basin-floor, fine-grained turbidites	37.33	8.99	10.61	4.05		15.00	4.05	9.22	6.75	0.45	0.90	2.65	fine-grained	moderately to well sorted	lithofeldspathic

The K-bentonite layers are khaki coloured, fine-grained (avg. grain size <0.20 mm) and have a colour index ~15. The tuffs consist mainly of quartz, feldspar, opaques, biotite and accessory muscovite, chlorite, calcite and clay minerals. The grains are randomly oriented and the larger grains are angular. Grain intergrowths are present and there is no preferred grain orientation. The bentonite is massive.

#### **4.4.1.2 Matjiesfontein Chert Bed**

The Matjiesfontein Chert Bed is dark grey coloured, fine-grained (avg. grain size <0.05 mm), with a colour index ~60. The rock consists mainly of authigenic silica, with larger grains of quartz, biotite, albite, hematite and other opaques in a finer grained quartz matrix. The larger grains are generally angular to sub-rounded and the rock is massive.

The rock falls in the lithofeldspathic field on the QmFLt diagram (Figure 4.15; Table 4.2) and in the recycled orogen category on the QFL and QmFLt diagrams (Figures 4.16 and 4.17; Table 4.2).

#### **4.4.2 Vischkuil Formation**

The schematic stratigraphy of the Vischkuil Formation and sample locations relative to the overall stratigraphy are shown in Figure 4.18, whereas a summary of the texture and composition of the sandstones are given in Table 4.6.

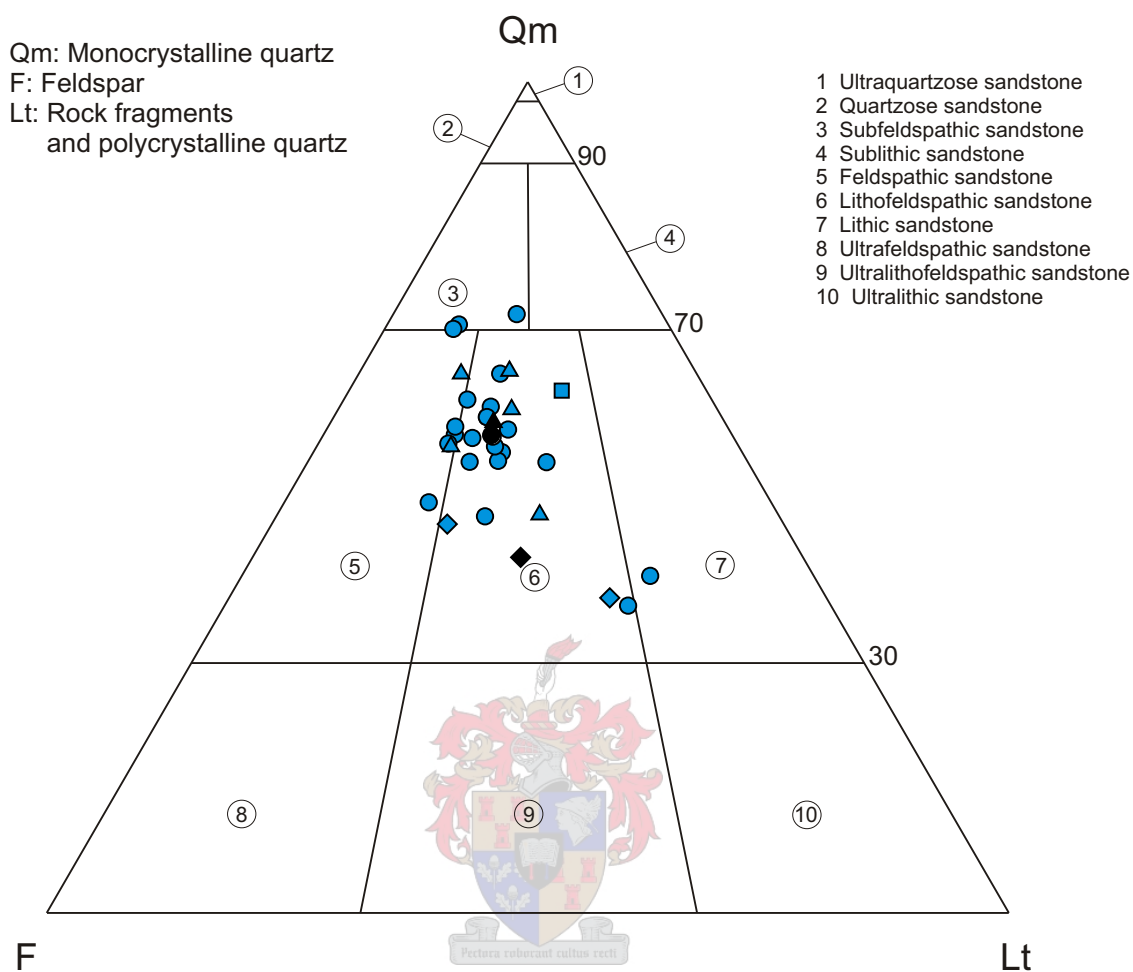
##### **4.4.2.1 Basin-floor, muddy turbidites**

The siltstones and shales are dark grey, fine-grained (max. grain size ~0.05 mm), with a colour index ~60. They consist of quartz, clay minerals, opaques, mica and feldspar. There is very little compaction, due to early cementation, and the grains show random orientation and grain overgrowth. The siltstones show pencil weathering.

The sandstones are lithofeldspathic, grey coloured, fine- to lower medium-grained (max. grain size <0.50 mm), with a colour index ~40. There is some compaction and no obvious grading. The long axes of the grains are perpendicular to the direction of compaction. The grains are angular to sub-angular, moderately sorted and the grain boundaries are well defined, even though there are some quartz grain and secondary mineral overgrowths. The sandstones are grain supported.

##### **4.4.2.2 Sandstone with soft-sediment deformational features**

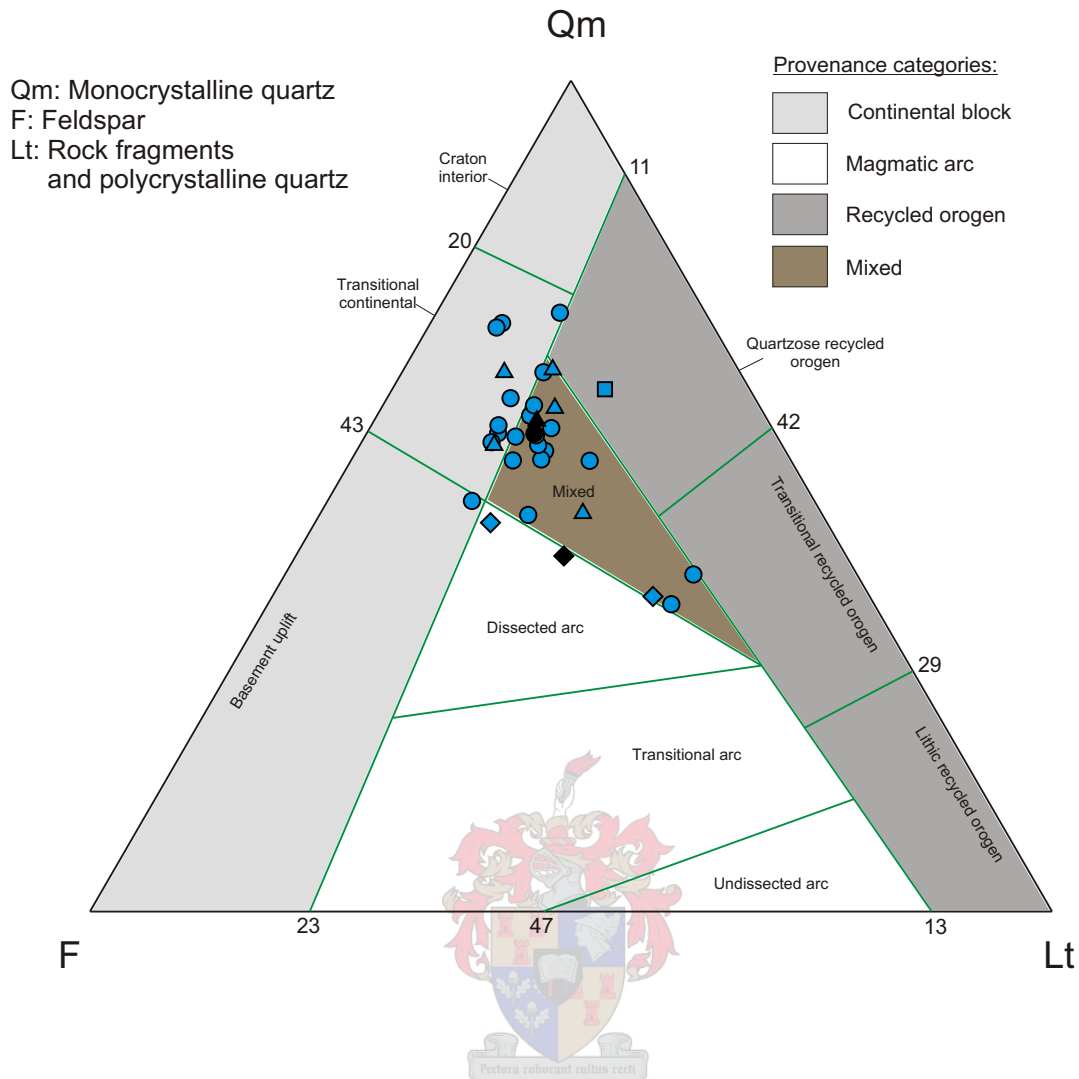
The sandstones are lithofeldspathic, grey coloured and fine-grained (avg. grain size ~0.15



Laingsburg depocentre:

- ▲ Fort Brown Formation
- ▲ Average Fort Brown Formation (n = 5)
- Laingsburg Formation
- Average Laingsburg Formation (n = 23)
- ◆ Vischkuil Formation
- ◆ Average Vischkuil Formation (n = 2)
- Collingham Formation (n = 1)

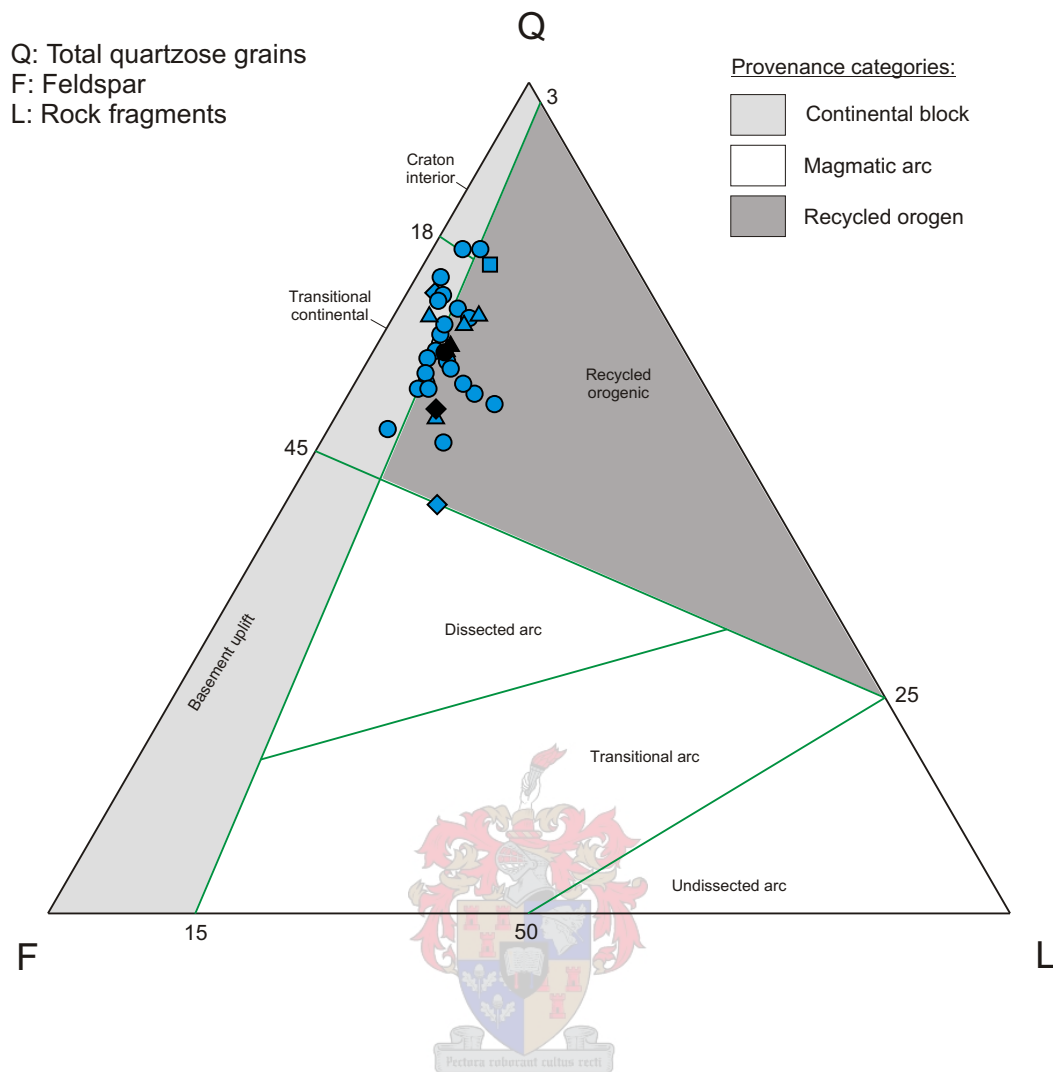
Figure 4.15 Sandstone classification (method after Johnson, 1976) and framework mineralogy (method after Johnson, 1991).



Laingsburg depocentre:

- ▲ Fort Brown Formation
- ▲ Average Fort Brown Formation (n = 5)
- Laingsburg Formation
- Average Laingsburg Formation (n = 23)
- ◆ Vischkuil Formation
- ◆ Average Vischkuil Formation (n = 2)
- Collingham Formation (n = 1)

Figure 4.16 QmFLt plot for framework modes of sandstones showing provisional subdivisions according to inferred provenance type (method after Dickinson *et al.*, 1983). Within continental blocks, sources are either on stable shields and platforms or in uplifts marking plate boundaries and trends of intraplate deformation that transects the continental blocks (Dickinson, 1985). Commonly granitic or gneissic exposures are supplemented by recycling of associated sediments (Dickinson, 1985; McCann, 1998). Within active magmatic arcs, sediment sources are mainly in the volcanic carapace capping the igneous belt and in granitic plutons of the arc roots (Dickinson *et al.*, 1983). Within recycled orogens, sediment sources are dominantly sedimentary strata and subordinate volcanic rocks, in part metamorphosed, exposed to erosion by the orogenic uplift of fold belts and thrust sheets (Dickinson and Suszek, 1979; Dickinson, 1985; McCann, 1998). Basement uplifts occur along incipient rift belts, transform ruptures, deep-seated thrusts, and zones of wrench tectonism (Dickinson *et al.*, 1983).



Laingsburg depocentre:

- ▲ Fort Brown Formation
- ▲ Average Fort Brown Formation (n = 5)
- Laingsburg Formation
- Average Laingsburg Formation (n = 23)
- ◆ Vischkuil Formation
- ◆ Average Vischkuil Formation (n = 2)
- Collingham Formation (n = 1)

Figure 4.17 QFL plot for framework modes of sandstones showing provisional subdivisions according to inferred provenance type (method after Dickinson *et al.*, 1983). Within continental blocks, sources are either on stable shields and platforms or in uplifts marking plate boundaries and trends of intraplate deformation that transects the continental blocks (Dickinson, 1985). Commonly granitic or gneissic exposures are supplemented by recycling of associated sediments (Dickinson, 1985; McCann, 1998). Within active magmatic arcs, sediment sources are mainly in the volcanic carapace capping the igneous belt and in granitic plutons of the arc roots (Dickinson *et al.*, 1983). Within recycled orogens, sediment sources are dominantly sedimentary strata and subordinate volcanic rocks, in part metamorphosed, exposed to erosion by the orogenic uplift of fold belts and thrust sheets (Dickinson and Suszek, 1979; Dickinson, 1985; McCann, 1998). Basement uplifts occur along incipient rift belts, transform ruptures, deep-seated thrusts, and zones of wrench tectonism (Dickinson *et al.*, 1983).

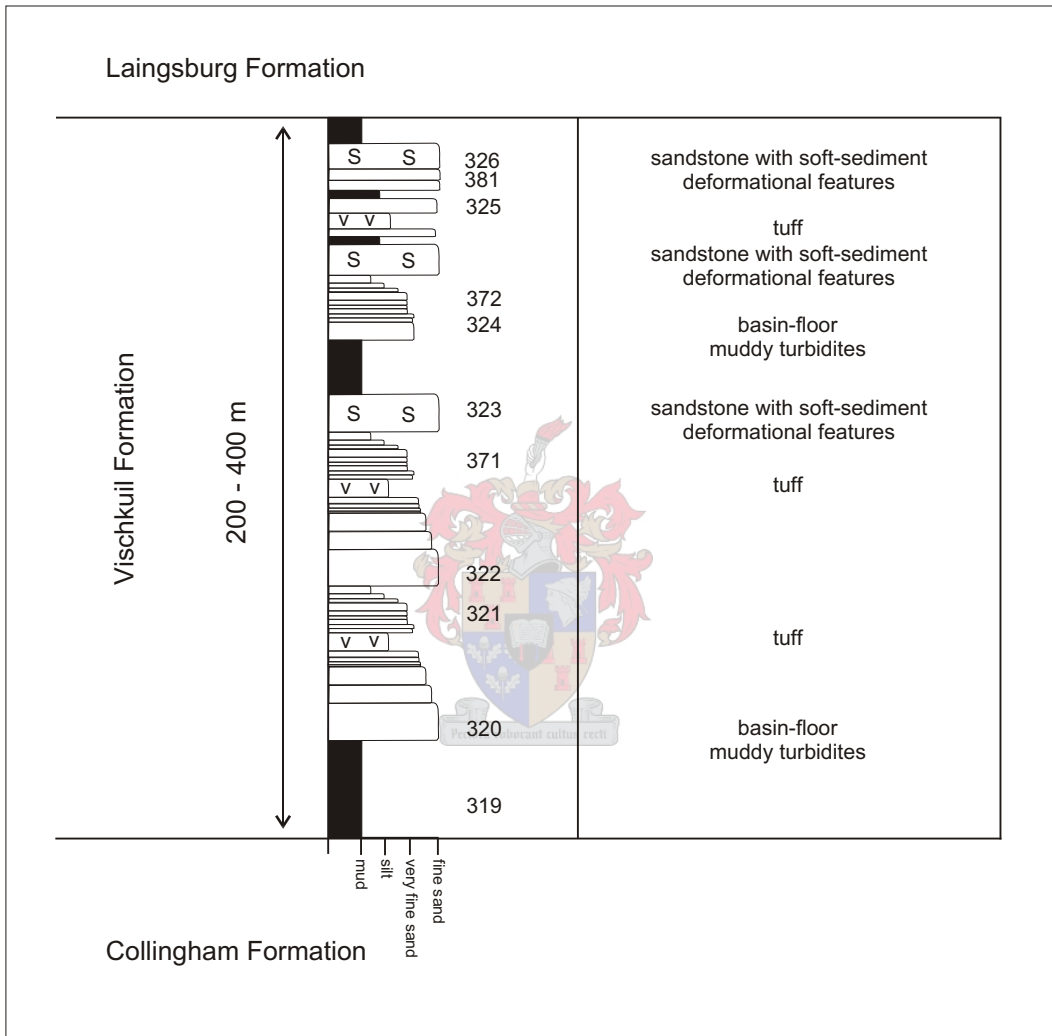


Figure 4.18 Schematic stratigraphy of the Vischkuil Formation, Laingsburg depocentre. The sample locations relative to the overall stratigraphy are shown.

Table 4.6 Summary of texture and composition (%) of sandstones from the Vischkuil Formation, Laingsburg depocentre.

Stratigraphic unit	Detrital components					Authigenic minerals					Texture		Rock classification		
	Quartz	Feldspar	Mica	Litho-clasts	Accessory minerals	Matrix	Opagues	Quartz cement and overgrowths	Illite	Chlorite	Calcite	Mica		Grain size	Sorting
Basin-floor muddy turbidites	26.24	34.38	5.79	11.76		5.00	7.24	1.81	4.52	1.81		1.45	fine- to medium-grained	moderately sorted	lithofeldspathic
Sandstone with soft-sediment deformational features	22.81	13.85	5.21	1.63	0.41	10.00	1.63	22.81	7.33	0.81	12.22	1.30	fine-grained	poorly to well sorted	lithofeldspathic

mm), with a colour index ~60. The grains are angular with secondary mineral overgrowths and show no preferred orientation and very little compaction.

The sandstones from both stratigraphic units are very similar, both mineralogically and texturally.

The sandstones fall in the lithofeldspathic field on the QmFLt diagram (Figure 4.15; Table 4.2) and fall mostly in the mixed provenance field in the QFL and QmFLt diagrams (Figures 4.16 and 4.17).

SEM images show inherited angular and fragmented quartz grains (some annealed), minimal quartz overgrowths, quartz cement and K-feldspar and albite replaced by illite (Figure 4.19). The relative timing for these processes are suggested to be albite and K-feldspar weathering and alteration to kaolinite and smectite, pore filling and alteration of kaolinite/smectite to illite, ductile deformation of detrital biotite and chlorite, followed by the formation of quartz overgrowths while the movement of formation waters were still relatively unrestricted and porosity and permeability much higher, followed by the formation of authigenic chlorite, which further decreased the porosity and permeability.

#### **4.4.3 Laingsburg Formation**

The schematic stratigraphy of the Laingsburg Formation and sample locations relative to the overall stratigraphy are shown in Figure 4.20, whereas a summary of the texture and composition of the sandstones are given in Table 4.7.

##### **4.4.3.1 Fan A**

The basin-floor turbidite deposits of Fan A, with sample locations and stratigraphic interpretation, are shown in Figure 4.21. Sixsmith (2000) has done extensive sequence stratigraphic work on Fan A of the Laingsburg Formation. He subdivided the Fan A system into seven time-stratigraphic depositional units (Units 1 to 7) bounded by regionally correlatable key surfaces, such as fan flooding surfaces and sequence boundaries. Sandstone samples were taken from each of these units and compared. It was found that they are texturally and compositionally very similar, and it was not possible to apply the same characteristic subdivisions based on petrographic data.

##### **4.4.3.1.1 Basin-floor turbidite deposits**

The shales are grey, fine-grained (max. grain size ~0.05 mm), finely laminated, with a colour index of 30 and showing pencil weathering. The main mineral constituents are quartz,

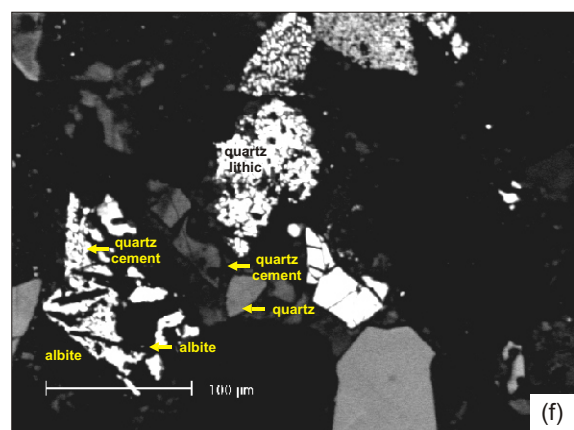
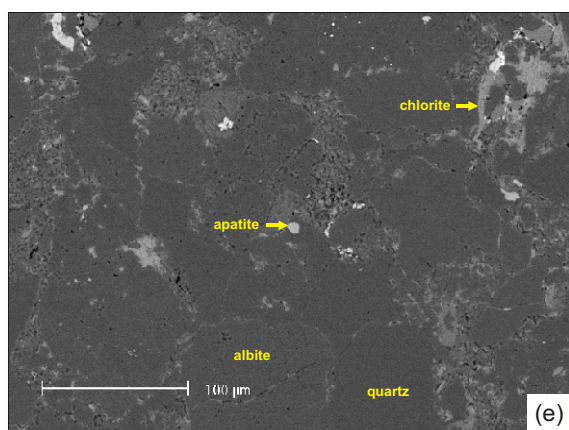
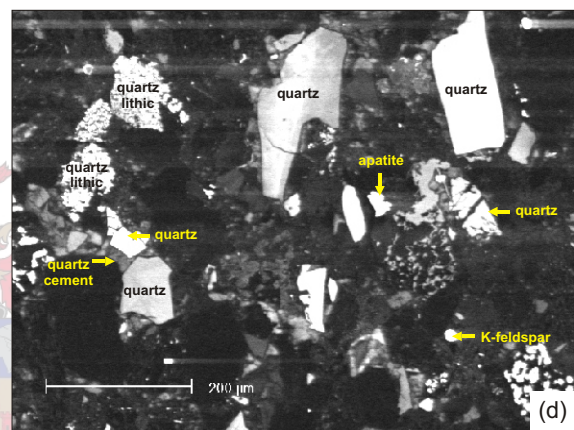
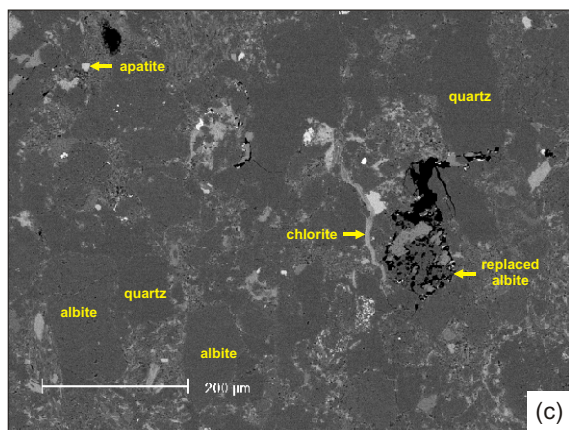
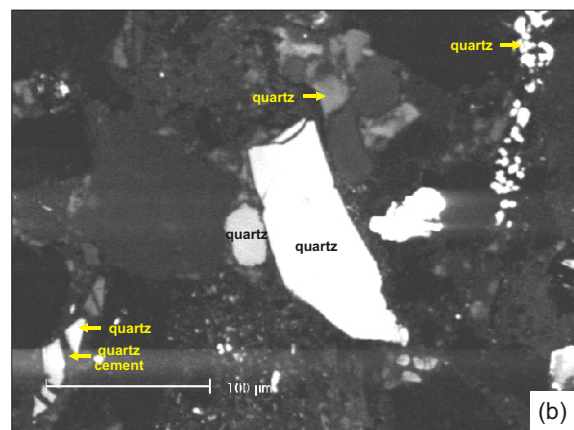
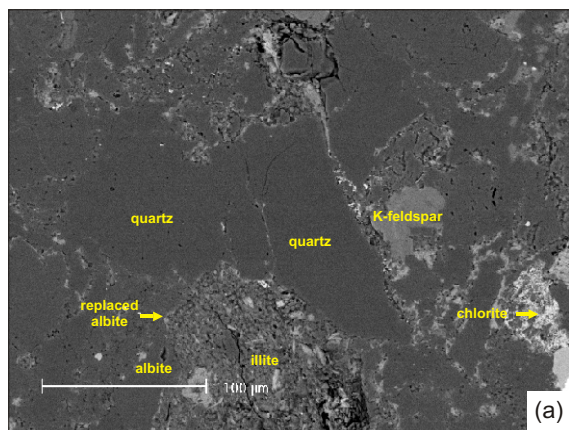


Figure 4.19 Images of sandstone (381) from the basin-floor turbidite deposits of the Vischkul Formation, Laingsburg depocentre. (a) Scanning electron microscopy (SEM) image of inherited fragmented and annealed quartz grains, K-feldspar and albite replaced by illite. (b) Same field of view under cathodoluminescence (CL) showing the extent of the quartz cement and no obvious quartz overgrowths. (c) SEM image of quartz, albite, K-feldspar, chlorite and apatite. (d) Same field of view under CL showing the angular and fragmented detrital quartz grains and quartz cement. (e) Quartz, albite, chlorite and apatite, SEM. (f) Same field of view under CL showing quartz lithics, fragmented and annealed quartz grains and detrital albite replaced by authigenic quartz cement.

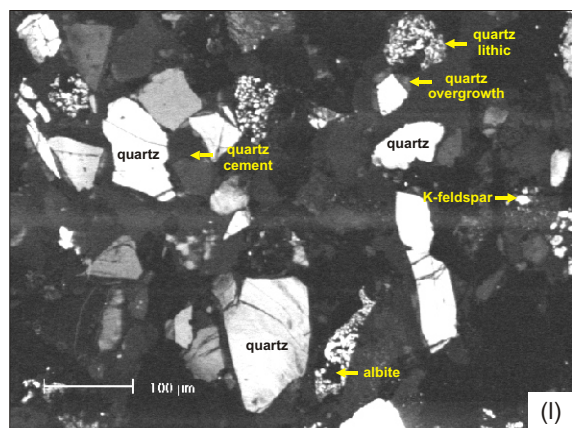
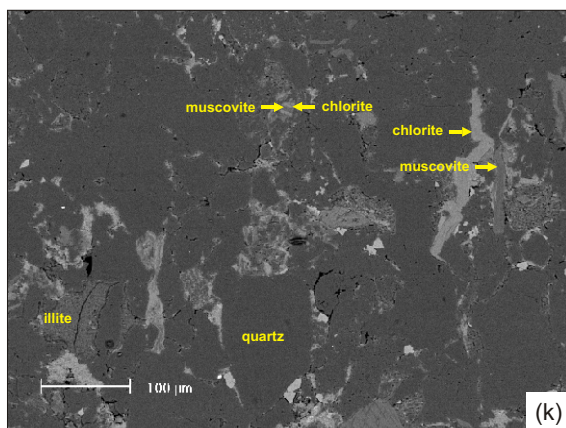
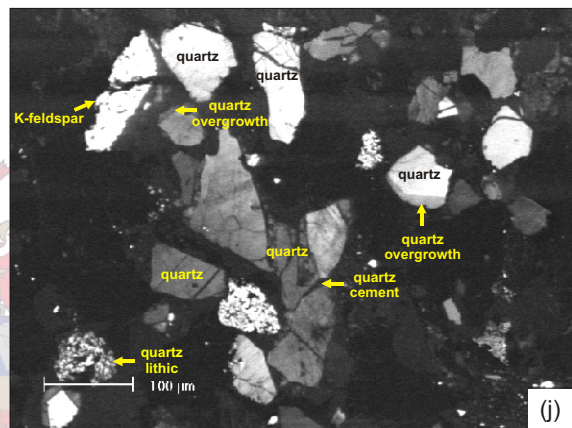
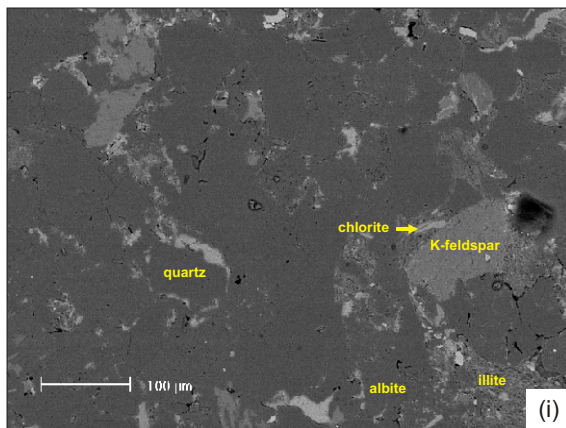
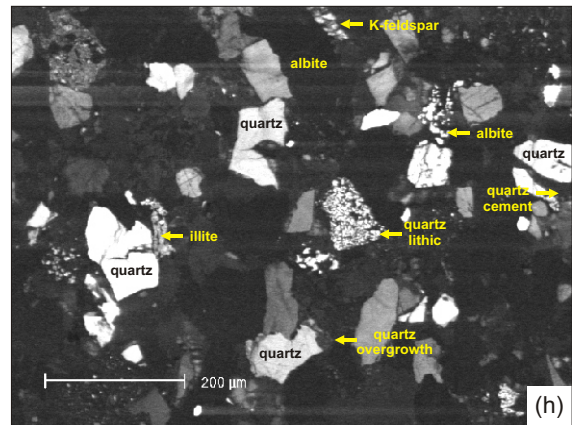
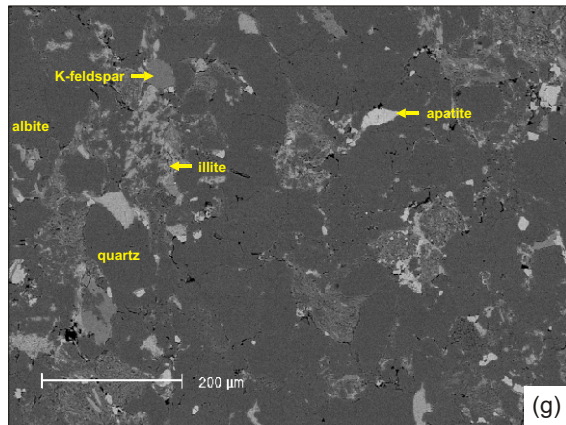


Figure 4.19 continued. Images of sandstone (385) from the basin-floor turbidite deposits of Fan A in the Laingsburg Formation, Laingsburg depocentre. (g) Quartz, albite, K-feldspar, apatite and illite, SEM. (h) Same field of view under CL showing inherited fragmented and annealed quartz grains, some quartz overgrowths on the quartz grains, lithic quartz fragments, and partially replaced K-feldspar and albite with illite. (i) SEM image of quartz, albite, K-feldspar, chlorite and illite. (j) Same field of view under CL, showing inherited fragmented and annealed quartz grains with authigenic quartz overgrowths, lithic quartz grains, albite and K-feldspar. (k) Detrital muscovite partially altered to chlorite, SEM. (l) Same field of view under CL showing quartz overgrowths, inherited fragmented and annealed quartz grains, quartz lithics and partially altered albite.

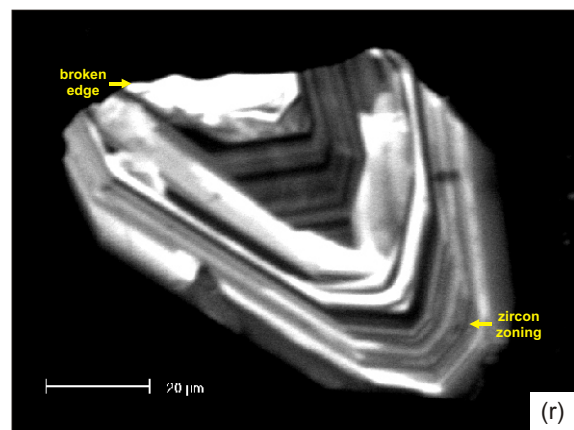
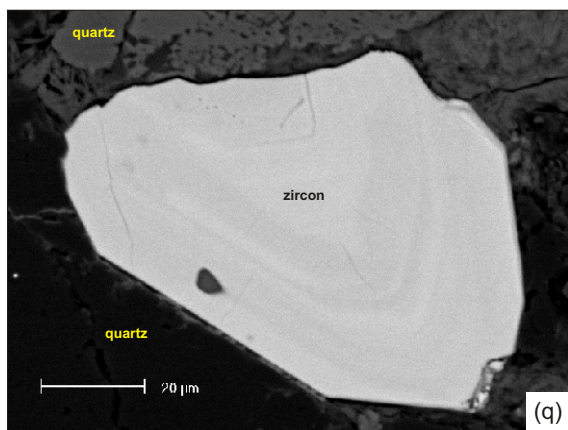
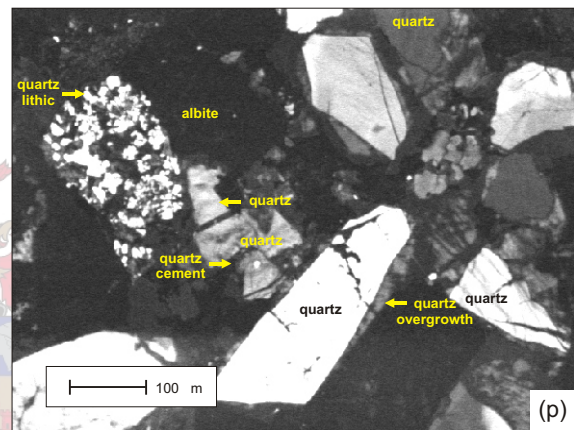
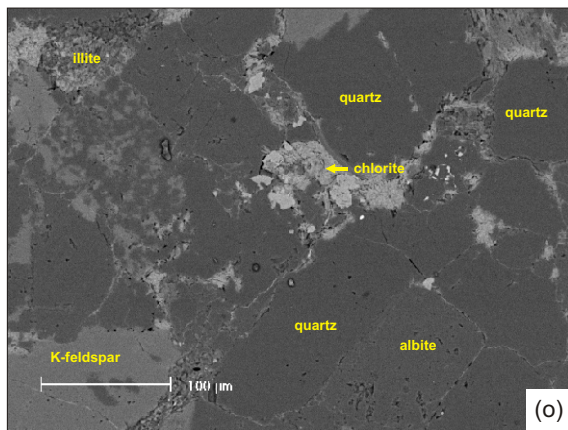
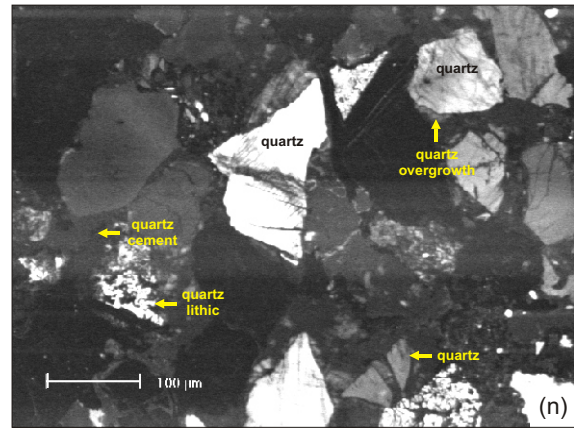
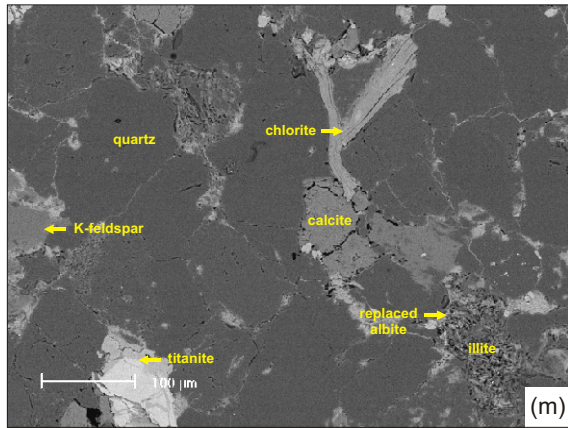


Figure 4.19 continued. Images of sandstone (366) from the deltaic deposits of the Fort Brown Formation, Laingsburg depocentre. (m) Quartz, chlorite, albite replaced with illite, calcite and titanite (the lighter coloured areas contains less Ti), SEM. The detrital chlorite has been deformed by compaction. (n) Same field of view under CL showing the extent of quartz overgrowths, quartz and calcite cement and quartz lithics. (o) SEM image of quartz, K-feldspar, albite, chlorite and illite. (p) Same field of view under CL showing the extent of quartz overgrowths, inherited fragmented and annealed quartz grains and quartz lithics. (q) Broken zircon grain, SEM. (r) Same field of view under CL showing the zoning in the zircon grain. These zones grew while in the source and the grain was broken during transport. No further growth zones formed after deposition.

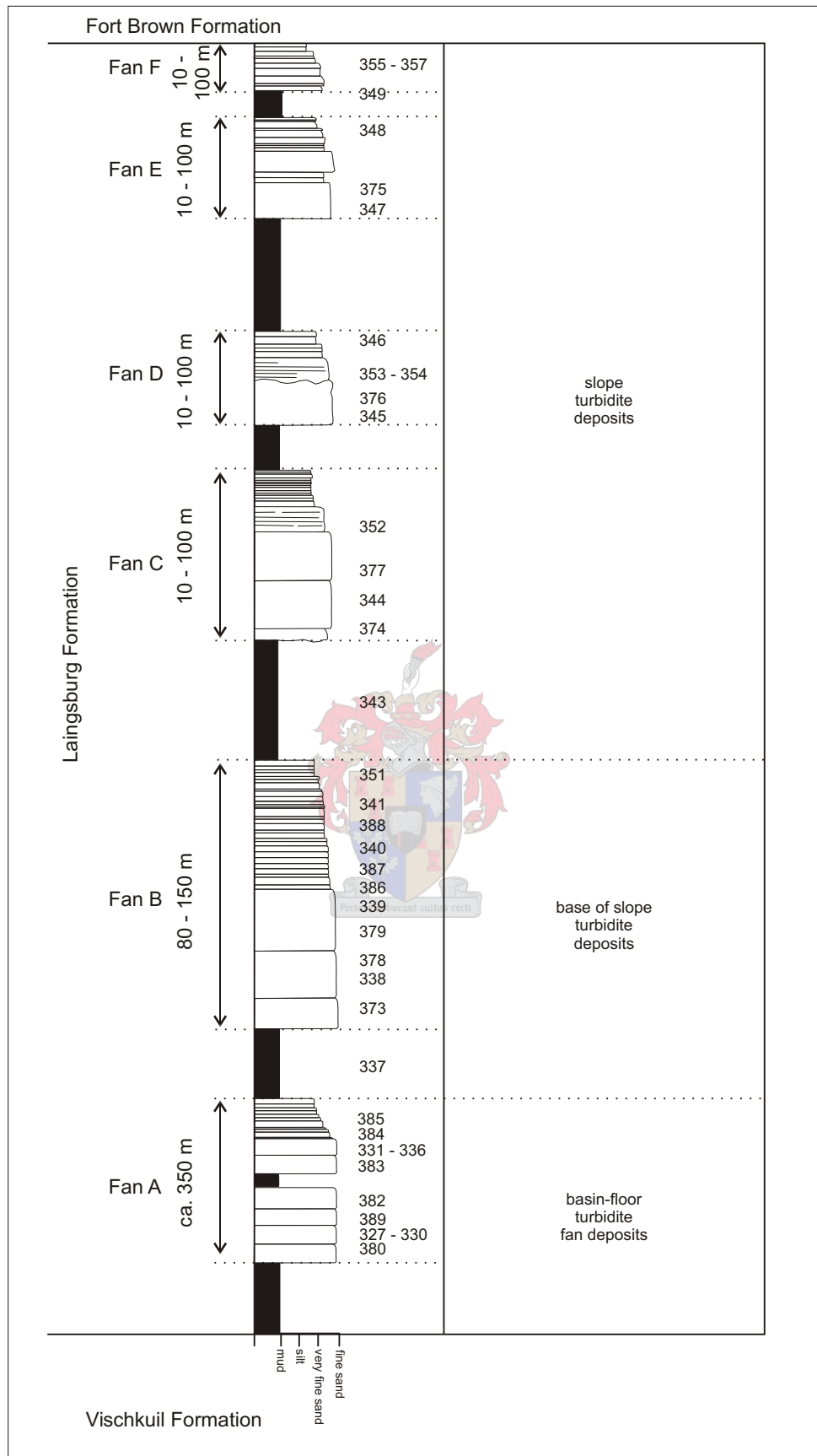


Figure 4.20 Schematic stratigraphy of the Laingsburg Formation, Laingsburg depocentre (after Grecula, 2000; Sixsmith, 2000). The sample locations relative to the overall stratigraphy are shown.

Table 4.7 Summary of texture and composition (%) of sandstones from the Laingsburg Formation, Laingsburg deponentre.

Stratigraphic unit	Detrital components						Authigenic minerals					Texture		Rock classification	
	Quartz	Feldspar	Mica	Litho-clasts	Accessory minerals	Matrix	Opagues	Quartz cement and overgrowths	Illite	Chlorite	Calcite	Mica	Grain size		Sorting
Basin-floor turbidites Fan A															
Unit 1	35.00	16.00	10.40	4.00		5.00	7.00	8.50	6.50	3.50	2.60		fine-grained	poorly to moderately sorted	lithofeldspathic
Unit 2	31.88	14.61	11.69	4.65		15.00	4.65	5.98	3.98	2.66	2.92		fine-grained	moderately sorted	lithofeldspathic
Unit 3	42.61	18.86	6.15	8.38		5.00	3.49	4.89	4.89	2.79	1.54		fine-grained	moderately sorted	lithofeldspathic
Unit 4	42.67	13.87	11.09	2.13	1.07	4.00	4.27	2.13	10.67	4.27	2.77		fine-grained	poorly sorted	subfeldspathic
Unit 5	31.98	16.14	11.42	6.13	0.91	6.00	3.88	3.54	7.92	6.70	2.86		fine-grained	moderately sorted	lithofeldspathic
Unit 6	41.57	16.63	10.28	11.34		4.00	4.57	2.27	2.27	2.27	2.57		fine-grained	moderately sorted	lithofeldspathic
Unit 7	36.28	26.66	8.29	4.44	1.48	3.00	2.22	6.66	4.44	2.96	2.07		fine-grained	moderately to well sorted	feldspathic
Base of slope turbidites Fan B															
Slope facies Fan C															
Fan D	35.76	16.19	8.15	4.92	0.76	13.33	3.26	6.50	5.50	3.00	2.04		fine-grained	poorly to well sorted	feldspathic to lithofeldspathic
Fan E	38.99	15.43	8.04	3.24	1.05	4.67	2.31	5.13	8.32	9.81	2.01		fine- to medium-grained	poorly to well sorted	subfeldspathic to lithofeldspathic
Fan F	37.99	11.16	9.99	2.13	1.52	5.00	3.55	9.61	6.42	9.43	2.50		fine-grained	poorly to well sorted	subfeldspathic to lithofeldspathic
	35.78	17.77	11.36	4.37	0.55	9.00	3.18	6.29	5.70	5.57	2.84		fine-grained	poorly to well sorted	feldspathic to lithofeldspathic
	38.84	16.11	10.23	3.79		10.00	0.47	6.63	6.63	2.84	2.56		fine-grained	poorly to moderately sorted	feldspathic

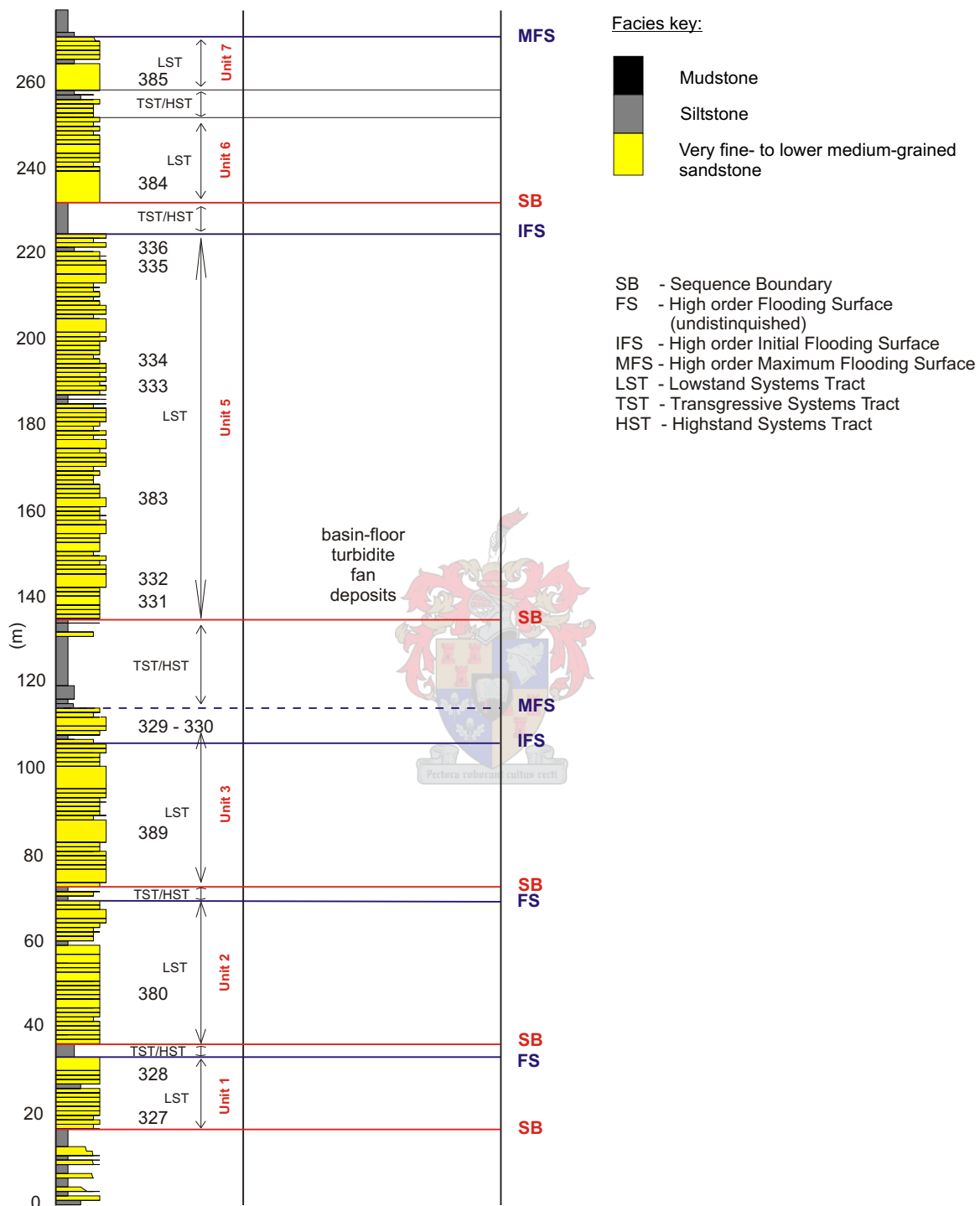


Figure 4.21 Basin-floor turbidite deposits of Fan A in the Laingsburg Formation, measured at Grootkloof (V15). The sample locations are indicated next to the lithology and stratigraphic interpretation is after Sixsmith (2000). Note that Unit 4 has shaded out at this position.

clay minerals, opaques and mica. Siltstones are brown to grey, fine-grained (max. grain size ~0.05 mm), with a colour index of 20 to 30. The siltstones consist of quartz, clay minerals, opaques and mica and occasionally show planar-lamination.

The sandstones are mainly lithofeldspathic, dark grey coloured and fine-grained (avg. grain size ~0.20 mm), with a colour index of 30 to 50. There is no obvious grading and some compaction. The long axes of the grains are perpendicular to the direction of compaction. The grains are angular to sub-rounded and poorly to well sorted. Grain boundaries are poorly to well defined, depending on the degree of quartz grain and secondary mineral overgrowths. The sandstones are grain supported and range from being massive to showing planar-lamination.

Sandstones from Units 1 – 3 and 5 – 6 are lithofeldspathic, sandstones from Unit 4 are subfeldspathic and sandstones from Unit 7 fall in the feldspathic field on the QmFLt diagram (Figure 4.15; Table 4.2). The sandstones from Units 1 – 3 and 6 fall in the mixed provenance category, sandstones from Units 4 and 7 fall in the continental block provenance category, and sandstones from Unit 5 fall in both the mixed and continental block provenance categories on the QFL and QmFLt diagrams (Figures 4.16 and 4.17; Table 4.2).

#### **4.4.3.2 Fan B**

##### **4.4.3.2.1 Base of slope turbidite deposits**

The shales and siltstones are generally dark grey and fine-grained (max. grain size ~0.05 mm), with a colour index ~45. The rocks consist primarily of clay minerals, mica, quartz and opaques and are finely laminated.

The sandstones are feldspathic to lithofeldspathic, grey coloured and fine-grained (avg. grain size ~0.25 mm), with a colour index ~45. There is no obvious grading and very little to some compaction. The long axes of the grains are perpendicular to the direction of compaction and the rocks are grain supported. The sandstones range from being massive to showing planar-lamination. The grains are angular to rounded and poorly to well sorted. Grain boundaries are poorly to well defined, depending on the degree of the quartz grain overgrowths and secondary mineral alterations.

Sample 337 falls in the lithic sandstone field, samples 373, 386 and 388 fall in the lithofeldspathic sandstone field and samples 378 and 379 fall in the feldspathic sandstone field on the QmFLt diagram (Figure 4.15; Table 4.2). Sandstone samples 337, 373, 386 and 388 fall in the mixed provenance field and samples 378 and 379 in the continental block provenance category on the QFL and QmFLt diagrams (Figures 4.16 and 4.17; Table 4.2).

#### **4.4.3.3 Fan C**

##### **4.4.3.3.1 Slope facies deposits**

The shales are dark grey and fine-grained (max. grain size ~0.05 mm), with a colour index ~55. The rocks consist of quartz, clay minerals, biotite and opaques. There is no grading or preferred grain orientation and the rocks show pencil weathering.

The sandstones are subfeldspathic to lithofeldspathic, grey coloured and fine- to lower medium-grained (max. grain size <0.50 mm), with a colour index ~35. The grains are randomly oriented, poorly to well sorted, angular to sub-rounded and show no obvious grading and very little compaction, due to early cementation. Grain boundaries are poorly to well defined and there are secondary quartz grain overgrowths and secondary mineral alterations. The sandstones are grain supported and massive.

Sample 374 falls in the subfeldspathic sandstone field and samples 352 and 377 fall in the lithofeldspathic sandstone field on the QmFLt diagram (Figure 4.15; Table 4.2). Sandstones 374 and 377 fall in the continental block provenance and sandstone 352 in the mixed provenance fields on the QFL and QmFLt diagrams (Figures 4.16 and 5.17; Table 4.2).

#### **4.4.3.4 Fan D**

##### **4.4.3.4.1 Slope facies deposits**



The siltstones are dark grey and fine-grained (max. grain size ~0.05 mm), with a colour index ~50. The rocks consist of quartz, clay minerals, opaques and mica and are finely laminated.

The sandstones are subfeldspathic to lithofeldspathic, grey coloured and fine-grained (avg. grain size ~0.10 mm), with a colour index ~30. There is no grading and very little compaction, due to early cementation, and the grain boundaries are poorly to well defined, with some quartz grain and secondary mineral overgrowths. The primary internal structures of the rocks range from massive to planar-lamination to ripple-lamination. The preferred grain orientation of biotite defines the lamination. The sandstones are grain supported and the grains are angular to sub-rounded and poorly to well sorted.

Sample 345 falls in the lithofeldspathic sandstone field and sample 353 falls in the subfeldspathic sandstone field on the QmFLt diagram (Figure 4.15; Table 4.2). These sandstones (345 and 353) fall in the mixed and continental block provenance categories on the QFL and QmFLt diagrams (Figures 4.16 and 4.17; Table 4.2).

#### **4.4.3.5 Fan E**

##### **4.4.3.5.1 Slope facies deposits**

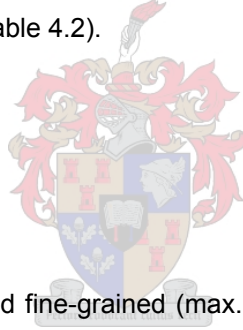
The siltstones are dark grey and fine-grained (max. grain size ~0.05 mm), with a colour index ~45. The rocks consist of quartz, clay minerals, opaques and mica and are finely laminated.

The sandstones are feldspathic to lithofeldspathic, light brown to light grey coloured and fine-grained (avg. grain size ~0.15 mm), with a colour index ~30. The grains are angular to sub-rounded, poorly to well sorted and show no obvious preferred grain orientation, grading and very little compaction, due to early cementation. Grain boundaries are moderately defined as a result of quartz grain overgrowths and secondary mineral alterations.

Sample 347 falls in the lithofeldspathic sandstone field and sample 375 in the feldspathic sandstone field on the QmFLt diagram (Figure 4.15; Table 4.2). These sandstones (347 and 375) fall in the mixed and continental block provenance categories on the QFL and QmFLt diagrams (Figures 4.16 and 4.17; Table 4.2).

#### **4.4.3.6 Fan F**

##### **4.4.3.6.1 Slope facies deposits**



The siltstones are dark grey and fine-grained (max. grain size <0.05 mm), with a colour index ~60. The rocks consist primarily of clay minerals, opaques, mica and quartz and are finely laminated.

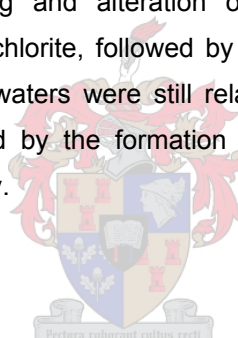
The sandstones are feldspathic, brown to grey coloured and fine-grained (max. grain size ~0.25 mm), with a colour index ~35. The grains are poorly to moderately sorted, angular to sub-rounded with poorly to well defined grain boundaries and quartz grain and secondary mineral overgrowths. There is no apparent grading and minimal compaction. The primary internal structures of the rocks range from planar-lamination to ripple-lamination, defined by lighter and darker layers and preferred grain orientation of biotite, muscovite and some opaques.

Sample 349 falls in the feldspathic sandstone field on the QmFLt diagram (Figure 4.15; Table 4.2). The sandstone (349) falls in the continental block provenance category on the QFL and QmFLt diagrams (Figures 4.16 and 4.17; Table 4.2).

Mineralogically the sandstones from all the fans in the Laingsburg Formation are very similar, with differences only in the modal percentages of feldspar and lithic fragments. Textural differences are present in grain size and sorting, with the sandstones from the basin-floor and base of slope turbidite deposits being finer grained on average than the slope facies deposits. The basin-floor turbidite deposits are also generally better sorted than the base of slope and slope facies deposits, probably due to the higher energy conditions in the slope environment during sediment deposition (more proximal and channelised).

SEM images show a large percentage of inherited annealed quartz grains that were broken and repaired with quartz cement in the source terrane(s). Quartz overgrowths are more prominent than in the Vischkuil Formation sandstones. This might be due to the fact that the Laingsburg Formation was open to formation waters for a longer period of time than the Vischkuil Formation, probably as a result of tectonic processes starting to play an increasingly larger role. Albite, K-feldspar and lithic quartz fragments have been partially replaced by illite, while detrital muscovite has been partially altered to chlorite (Figure 4.19). The relative timing for these processes are suggested to be albite and K-feldspar weathering and alteration to kaolinite and smectite, pore filling and alteration of kaolinite/smectite to illite, ductile deformation of detrital biotite and chlorite, followed by the formation of quartz overgrowths while the movement of formation waters were still relatively unrestricted and porosity and permeability much higher, followed by the formation of authigenic chlorite, which further decreased porosity and permeability.

#### **4.4.4 Fort Brown Formation**



The schematic stratigraphy of the Fort Brown Formation and sample locations relative to the overall stratigraphy are shown in Figure 4.22, whereas a summary of the texture and composition of the sandstones are given in Table 4.8.

##### **4.4.4.1 Pro-delta deposits**

The siltstones are dark greenish-grey and fine-grained (max. grain size <0.05 mm), with a colour index ~50. The rocks consist mainly of a finely grained matrix of quartz, clay minerals, opaques and biotite, with some larger grains of quartz, biotite and opaques. The siltstones are matrix to grain supported and finely laminated.

The sandstones are lithofeldspathic, grey coloured and fine- to lower medium-grained (max. grain size <0.50 mm), with a colour index ~30. The grains are poorly sorted, sub-angular to sub-rounded and show no grading or preferred orientation. The poorly to well defined grain boundaries are partially obscured by quartz grain and secondary mineral

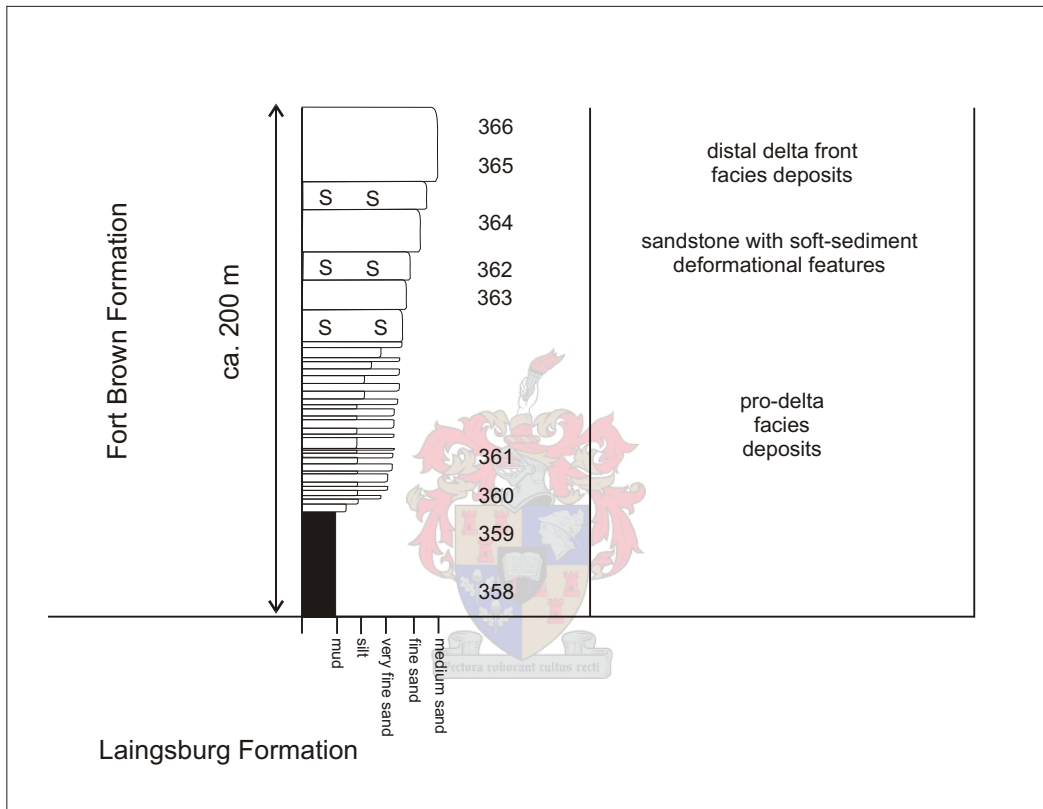


Figure 4.22 Schematic stratigraphy of the Fort Brown Formation, Laingsburg depocentre. The sample locations relative to the overall stratigraphy are shown.

Table 4.8 Summary of texture and composition (%) of sandstones from the Fort Brown Formation, Laingsburg depocentre.

Stratigraphic unit	Detrital components						Authigenic minerals					Texture		Rock classification	
	Quartz	Feldspar	Mica	Litho-clasts	Accessory minerals	Matrix	Opauques	Quartz cement and overgrowths	Illite	Chlorite	Calcite	Mica	Grain size		Sorting
Pro-delta facies	41.88	12.50	13.00	5.63		10.00	1.25	4.38	5.63		2.50	3.25	fine- to medium-grained	poorly sorted	lithofeldspathic
Sandstone with soft-sediment deformational features	37.95	13.55	12.14	4.88		10.00	1.63	6.51	7.05	1.08	2.17	3.04	fine-grained	poorly to moderately sorted	lithofeldspathic
Distal delta front facies	40.33	18.42	10.97	4.71		6.00	2.36	3.52	7.03	1.57	3.91	2.74	medium-grained	moderately to well sorted	feldspathic

overgrowths. The sandstones show very little compaction, due to early cementation, and are massive and grain supported.

#### **4.4.4.2 Sandstone with soft-sediment deformational features**

The sandstones are lithofeldspathic, dark grey coloured and fine-grained (max. grain size ~0.25 mm), with a colour index ~55. The grains are poorly to moderately sorted, angular to sub-rounded and show very little compaction (due to early cementation), grading or preferred grain orientation. The grain boundaries are poorly to well defined, due to partial quartz grain and secondary mineral overgrowths.

#### **4.4.4.3 Distal delta front deposits**

The sandstones grey coloured, sometimes showing light brown and darker grey coloured layers, and medium-grained (max. grain size <0.50 mm), with a colour index ~25. The grains are moderately to well sorted, angular to rounded and grain boundaries are generally well defined, although there are quartz and secondary mineral overgrowths. There is no apparent grading, very little compaction (due to early cementation) and no preferred grain orientation. The sandstones are grain supported and range from being massive to showing cross-lamination.

The sandstones from the above mentioned stratigraphic units are mineralogically very similar. Texturally there are some differences, with an increase in grain size from the pro-delta facies deposits to the distal delta front facies deposits, as well as sandstones from the distal delta front facies showing better sorting, due to the higher energy and wave-influenced shallower depositional environment.

Samples 350, 360 and 362 fall in the lithofeldspathic sandstone field and samples 363 and 366 fall in the feldspathic sandstone field on the QmFLt diagram (Figure 4.15; Table 4.2). Sandstone samples 350, 360 and 362 fall in the mixed provenance category and samples 363 and 366 in the continental block provenance category on the QFL and QmFLt diagrams (Figures 4.16 and 4.17; Table 4.2).

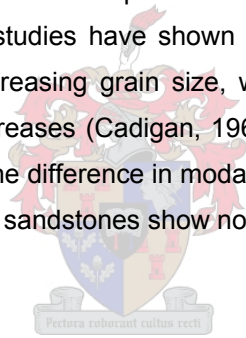
SEM images show that the detrital quartz grains are generally larger and have more quartz overgrowths on average than the Laingsburg Formation sandstones. This might be due to the fact that the Fort Brown Formation was open to formation waters for a longer period of time than the Laingsburg Formation. Quartz grains were broken and repaired with quartz cement in the source terrane(s) (Figure 4.19). Lithic quartz grains, albite and K-feldspar are partially replaced with illite. Zoned and broken zircon grains and a minor amount of titanite and calcite cement are present as well. The relative timing for these processes are

suggested to be albite and K-feldspar weathering and alteration to kaolinite and smectite, pore filling and alteration of kaolinite/smectite to illite, ductile deformation of detrital biotite and chlorite, followed by the formation of quartz overgrowths while the movement of formation waters were still relatively unrestricted and porosity and permeability much higher, followed by the formation of authigenic chlorite, which further decreased porosity and permeability. Detrital zircon grains show multiple zones of overgrowth. They were broken during transport and no further growth zones that might have formed after deposition, are present.

## 4.5 Discussion

### 4.5.1 Detrital and authigenic mineralogy

The petrographic study shows that all the sandstones range in size from very fine- to lower medium-grained, are tightly packed, poorly to well sorted, and have undergone both mechanical and chemical compaction (pressure solution). They have no visible porosity or permeability, primarily due to the fine grain size and the formation of authigenic quartz cement and secondary chlorite and illite. Mineral composition in sediments varies considerably as a function of particle size. Previous studies have shown that the percentage of feldspar and heavy minerals increases with decreasing grain size, whereas the amount of quartz, rock fragments, chert, and quartzite decreases (Cadigan, 1967, Odom *et al.*, 1976, Hunter *et al.*, 1979). Even though this is true for the difference in modal mineralogy between the sandstone, siltstone and shale of this study, the sandstones show no changes in modal mineralogy based on grain size.



Sorting is related to the kind of depositing current and the degree of sorting can be measured. The sandstones from the present study range from poorly to well sorted, giving an indication of the changing turbidity-current strength. Sand grains are abraded as currents knock them against each other and angular grains of various shapes usually imply a short transportation distance. The sandstone grains from this study are angular to rounded. However, a long transport distance is suggested for these sediments based on their provenance in the following chapter. Their grain shape might be explained by the fact that the degree of erosion on grains in suspension depends upon the velocity of the currents. Slow-moving currents might be too slow to accomplish much erosion, but still have enough mild turbulence to keep fine-grained sedimentary particles in suspension for a long time before they settle (Press and Siever, 1986).

An overall visual comparison between sandstones from the Tanqua and Laingsburg depocentres is demonstrated in Figure 4.23, whereas a summary of the detrital composition of sandstones from the Tanqua and Laingsburg depocentres are shown in Table 4.9.

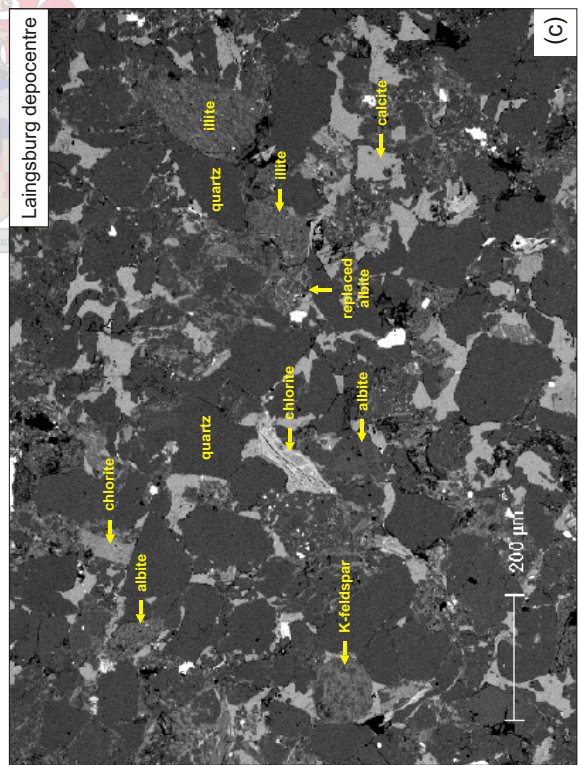
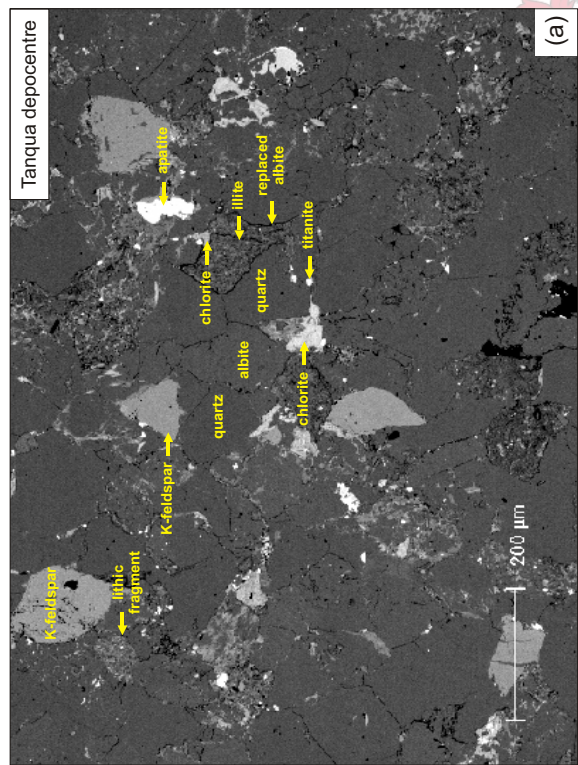
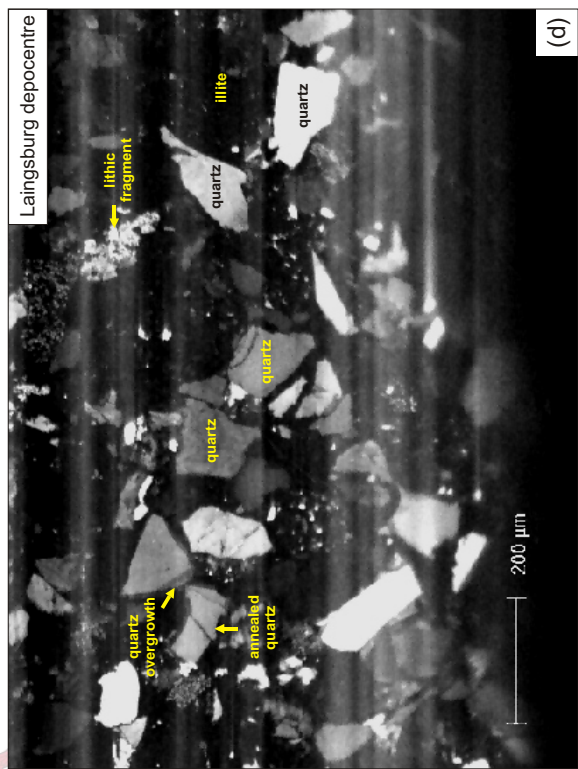
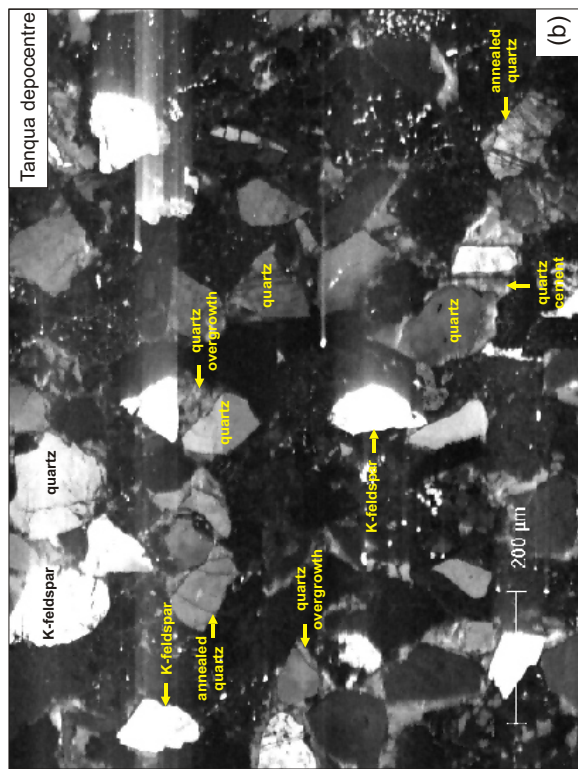


Figure 4.23 Images of sandstones (303 and 374) from the Kookfontein Formation, Tanqua depocentre and Laingsburg Formation, Laingsburg depocentre. The images demonstrate the similarity in overall mineralogy and texture between sandstones from the two depocentres. (a) Scanning electron microscopy (SEM) image of quartz, K-feldspar, apatite, chlorite and albite replaced by illite. (b) Same field of view under cathodoluminescence (CL) showing inherited annealed quartz grains, the extent of the authigenic quartz overgrowths and the overall angularity of the grains. (c) SEM image of quartz, albite, K-feldspar, chlorite and calcite. (d) Same field of view under CL showing the angular, inherited annealed quartz grains and authigenic quartz overgrowths.

Table 4.9 Summary of the detrital mineralogy (%) of sandstones from the different stratigraphic units of the Tanqua and Laingsburg depocentres.

Stratigraphy	Quartz	Feldspar	Mica	Litho-clasts	Accessory minerals	Matrix	Opaques
Tanqua depocentre							
Waterford Formation	39.84	17.81	10.14	4.34	0.51	11.00	2.62
Kookfontein Formation	36.89	19.02	9.97	4.95	0.87	7.22	3.38
Skoorsteenbergr Formation	37.62	18.94	10.35	4.34	0.70	10.12	4.20
Laingsburg depocentre							
Fort Brown Formation	40.05	14.82	12.04	5.07		8.67	1.75
Laingsburg Formation	37.45	16.62	9.76	4.96	1.05	7.00	3.57
Vischkuil Formation	24.53	24.12	5.50	6.70	0.41	7.50	4.44
Collingham Formation	37.33	8.99	10.61	4.05		15.00	4.05

The primary detrital mineralogy in both the Tanqua and Laingsburg depocentres was originally quartz, albite, K-feldspar, opaques, titanite, biotite, lithic fragments and accessory muscovite, apatite and zircon, identifying them as greywackes and arkoses.

After burial and subsequent mineral alteration, the secondary or authigenic mineral assemblages that formed are chlorite, illite, hematite, calcite, quartz (cement and microquartz) and minor amounts of mica. The primary cement is authigenic quartz, due to pressure solution (chemical compaction). The quartz overgrowth development was inhibited in the more lithic sandstones where the quartz grains were not in contact. Biotite, muscovite and some lithoclasts were altered to chlorite and illite.

The Tanqua and Laingsburg depocentres had a high-latitude palaeoposition (~42°S) during the late Permian (Smith *et al.*, 1973; Grunow, 1999), indicating a cold climate (Scotese *et al.*, 1999). In cold zones chemical weathering is at a minimum (Reading, 1996). Faster plagioclase reaction can thus be attributed to wetter and warmer climate. A possible explanation for the preservation of detrital feldspar during sediment transport from the provenance to the Tanqua and Laingsburg depocentres might thus be attributed to the cold palaeoclimate.

An extensive study on the diagenesis in Karoo sediments was done by Rowsell and De Swardt (1976). They found that the illite and chlorite which constitute most of the southern Karoo shales, and particularly those of the Ecca and Dwyka Groups, are of diagenetic and not detrital origin. It was therefore concluded that they correspond to the stage of deep diagenesis, where the transformation of montmorillonite has been completed.

It might be expected that the heavier grains, containing elements such as Zr and iron oxides, would sink to the bottom, leaving the lighter quartz and feldspar grains and finer particles to settle later (Weber and Middleton, 1961). A concentration of heavy minerals could thus be expected at the base of the turbidite beds as the result of rapid fall-out of suspension. However, this is not true in this case, since the sandstones show little variation from top to bottom.

## **4.5.2 Burial history**

### **4.5.2.1 Pressure/temperature processes**

Compaction and pressure solution are two diagenetic processes dependant largely on depth of burial. Chemical processes of diagenesis include the precipitation of minerals, leading to the cementation of the sediments, the dissolution of unstable grains, and the replacement of grains by other minerals (Tucker, 1991). Changes in clay mineralogy during diagenesis take place principally through the rise in temperature, accompanying increased depth of burial (Tucker, 1991). Studies show that the main change is an alteration of smectites to illite via mixed-layer clays of smectite-illite (Hower *et al.*, 1976; Iman and Shaw, 1985; Jennings and Thompson, 1986; Tucker, 1991). The process is largely temperature dependent and the temperature at which smectite begins to disappear is in the order of 70 – 95°C, that is at depths of 2 – 3 km, in areas of average geothermal gradient (30°C/km) (Tucker, 1991). Smectites, mixed-layer clays and kaolinite do not survive into metamorphism, and are replaced by illite and chlorite (Tucker, 1991). With very advanced diagenesis and early metamorphism, only illite, chlorite and occasional poryphyllite are usually present (Kubler, 1966; Rowsell and De Swardt, 1976). Clay minerals are thus modified and altered during early and late diagenesis, and into metamorphism (Figure 4.24).

Regional metamorphism is a more severe version of the mild changes caused in sediments by diagenesis during moderate and deep burial (Figure 4.25). The dividing line between diagenesis and metamorphism is thus more or less arbitrarily drawn at low temperatures and pressures (Press and Siever, 1986). The example given in Figure 4.26 was drawn up from shales.

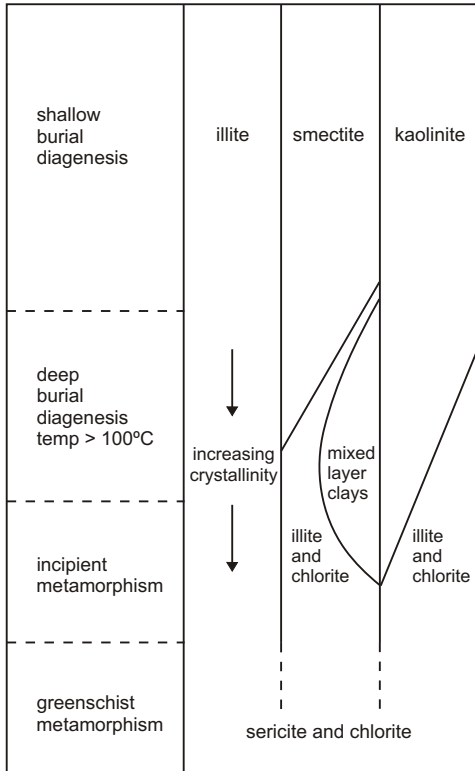


Figure 4.24 Diagram illustrating the changes of clay minerals with increasing depth of burial and into metamorphism (Tucker, 1991).

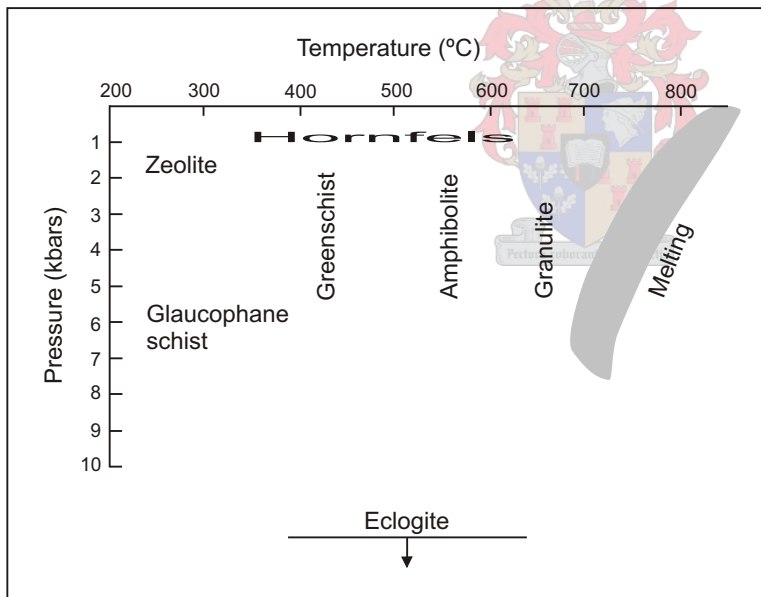


Figure 4.25 Generalised and simplified metamorphic facies diagram, showing the distribution of metamorphic rock types in relation to the temperature and pressure fields in which they are formed. There are no sharp boundaries between any of these facies (Press and Siever, 1986).

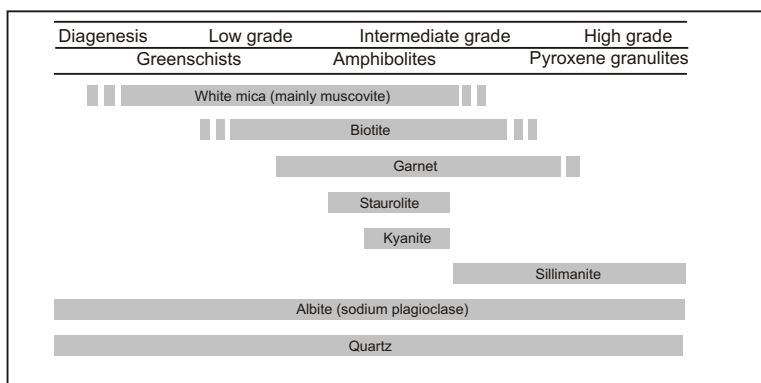


Figure 4.26 Changes in mineral composition of shales metamorphosed under conditions of intermediate pressure and temperature (Press and Siever, 1986).

The mineralogical composition and texture of the Tanqua and Laingsburg sandstones suggest that the rocks have undergone high-grade diagenesis to low-grade regional burial metamorphism to the lower greenschist facies (90 – 250°C; ~2 kbars using the schemes of Winkler (1965) and Press and Siever (1986)). Based in vitrinite reflectance profiles, geothermal gradients of 26 to >33 °C/km can be reached in foreland basins, depending on thermal regimes and structural provinces (Zhang and Davis, 1993). Under conditions of average basinal heat flow (32.5°C/km), hydrostatic conditions, average fluid density of 1.1 g/cm<sup>3</sup> (Ambers, 2001), and a surface temperature of 20°C, a temperature of 250°C would be obtained at 7 km burial depth. Such a burial depth may be likely, since the upper zone of the Karoo strata is represented by the bulk of the Beaufort Group, as well as the overlying Molteno, Elliot and Clarens Formations in the main basin, and has a total cumulative thickness of up to 7000 m (Johnson *et al.*, 1996). The Clarens Formation is in turn overlain by 1400 m of basaltic lavas of the Drakensberg Group and its equivalents (Johnson *et al.*, 1996; Turner, 1999). However, other processes, such as heat-flow (hydrothermal circulation), magmatic activity and tectonic pressure probably had an influence as well.

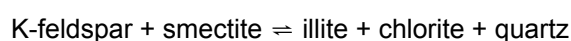
Rowell and De Swardt (1976) estimated that palaeotemperatures in the main Karoo Basin ranged between 270 to 300°C for the most deeply buried sediments, while the thickness of the overburden was between 6 and 7 km in the Tanqua and Laingsburg depocentre areas. Brown *et al.* (1994) found that sedimentary-hosted U ore deposits of the Eccra Group in the Laingsburg area (DR-3 Laingsburg) experienced maximum palaeotemperatures of at least 250 ± 50°C subsequent to deposition (for heating times of the order of 10<sup>6</sup> yr). They interpreted the high temperatures to be the result of magmatically driven hydrothermal circulation within the sedimentary sequence, accompanied by the intrusion of the Karoo sills/dykes. Excess heat was dissipated over a more extensive thickness of the stratigraphic sequence through the hydrothermal activity than it would have occurred under a system controlled by conductive heat transfer alone. The duration of heating resulting from any single intrusive body is very short (≤ 10<sup>5</sup> yr). However, hydrothermal activity (and associated moderately elevated regional temperatures) could be expected to occur throughout the duration of the Karoo magmatic episode between ~200 Ma and ~160 Ma (Brown *et al.*, 1994).

It is likely that temperature is more important than pressure in controlling quartz cementation in both cataclasites and undeformed sandstones (Rimstidt and Barnes, 1980; Oelkers *et al.*, 1996; Fisher *et al.*, 2000). The onset of quartz cementation invariably occurs at ~90°C (Giles *et al.*, 2000), illite formation occurs at >100°C, whereas diagenesis occurs at <300°C (Press and Siever, 1986). In the most advanced stages of diagenesis and in early metamorphism there is often a considerable new formation of chlorite, while the more aluminous illites gradually change into normal muscovite (Velde, 1965; Rowell and De

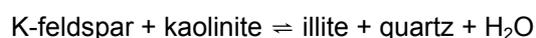
Swardt, 1976). Clay formation is usually an early or the first diagenetic event, often predating quartz overgrowths or calcite cementation (Tucker, 1991).

The origin of the silica for quartz overgrowths has frequently been attributed to pressure solution. Pore solutions become enriched in silica, which is then reprecipitated as overgrowths when supersaturation is achieved (Tucker, 1991). Waugh (1970) studied the formation of quartz overgrowths in the Penrith sandstone (Lower Permian) of northwest England. He found no apparent marked difference in the morphology of overgrowths formed on unstrained or strained grains. Due to burial, sandstone compaction and deformation of some mica and ductile clasts occurred, which formed a pseudomatrix in some samples. Deep burial mechanical compaction involving grain crushing may occur if the rate of grain-contact quartz dissolution and/or quartz overgrowth development cannot compete with the rate of stress increase at grain contacts (Fisher *et al.*, 1999).

The detrital quartz in the Tanqua and Laingsburg rocks has undergone compaction and some grains were broken and were then repaired by the formation of quartz cement in the source terrane(s). Detrital zircon grains show multiple zones of overgrowth. They were broken during transport and no further growth zones that might have formed after deposition in the depocentres, are present. There is no evidence for zonation in the quartz overgrowths, showing that there was only one episode of authigenic quartz formation. Feldspars have been altered, and in some cases completely replaced, by illite and chlorite. Minor cements include calcite and some iron oxides. The matrix is of a diagenetic origin, which might explain the fine grain size of the sandstones. Chlorite and illite replaced kaolinite and smectite, and K-feldspar and kaolinite are metastable, thus the following reactions occurred (Hoffman and Hower, 1979; Bjørkum and Gjelsvik, 1988; Worden and Burley, 2003):



and



The relative timing for these processes in the both the Tanqua and Laingsburg depocentres are suggested to be albite and K-feldspar weathering and alteration to kaolinite and smectite, pore filling and alteration of kaolinite/smectite to illite, ductile deformation of detrital biotite and chlorite, followed by the formation of quartz overgrowths while the movement of formation waters were still relatively unrestricted and porosity and permeability much higher, followed by the formation of authigenic chlorite. A paragenetic scheme for diagenesis of the Tanqua and Laingsburg sandstones is presented in Figure 4.27, whereas regional aspects of diagenetic mineralogies are summarised in Figure 4.28.

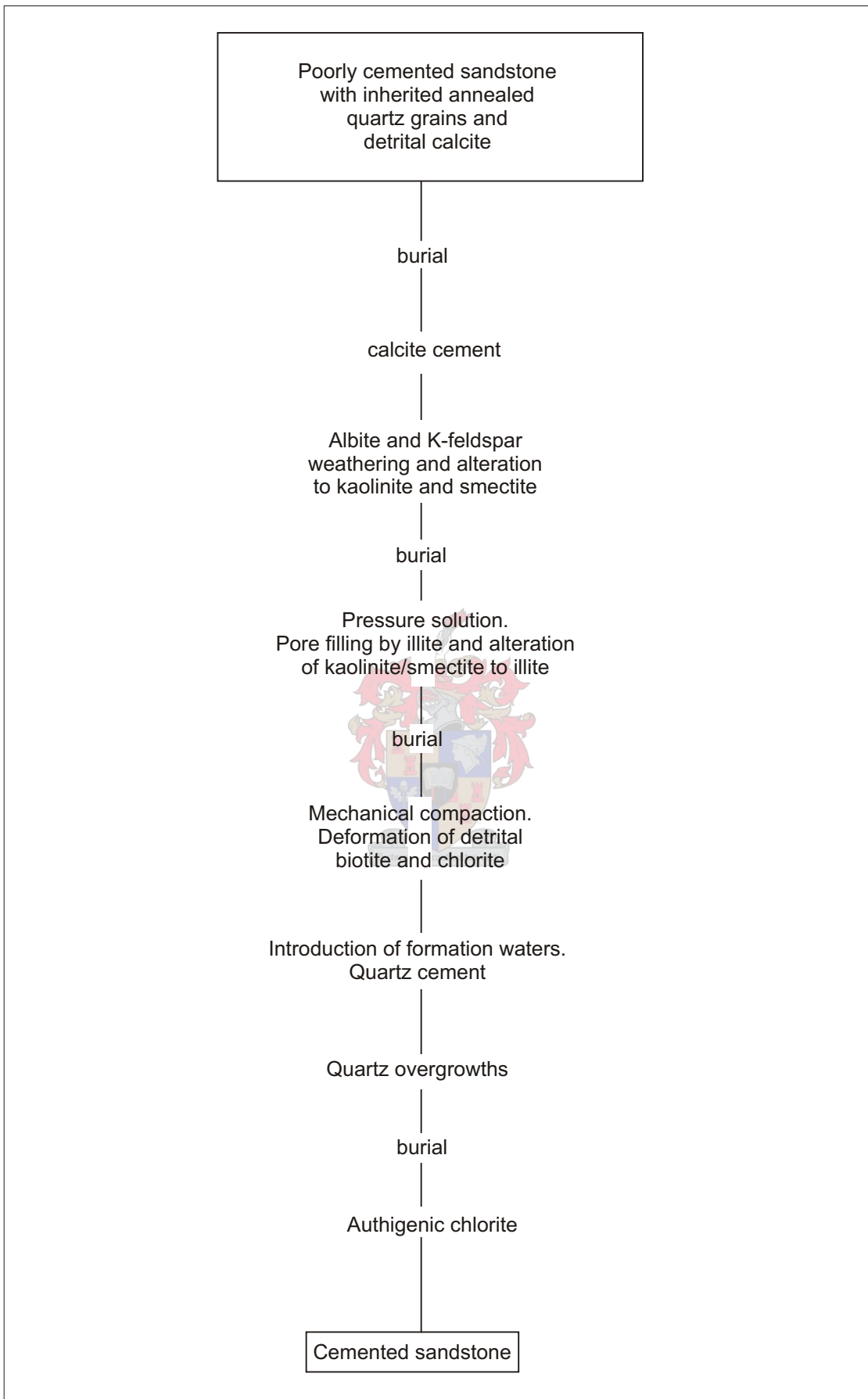
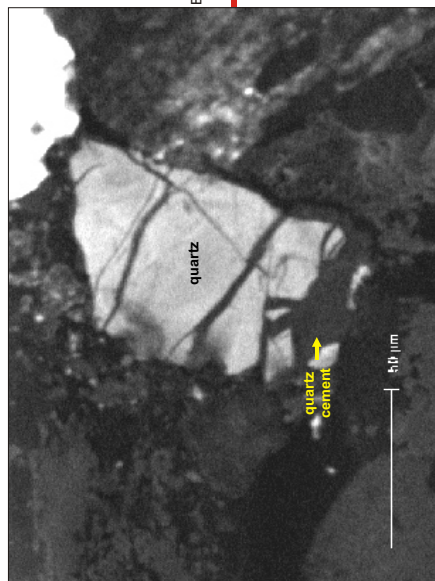
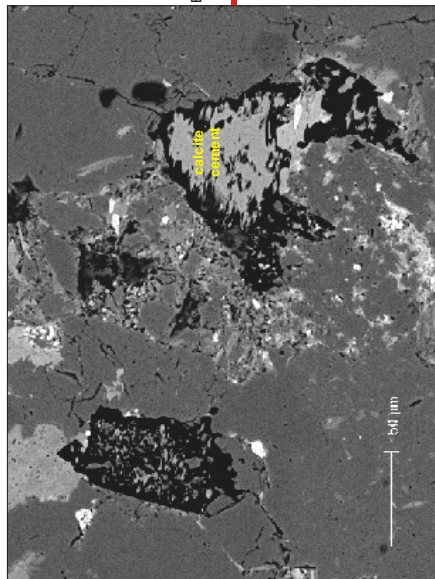


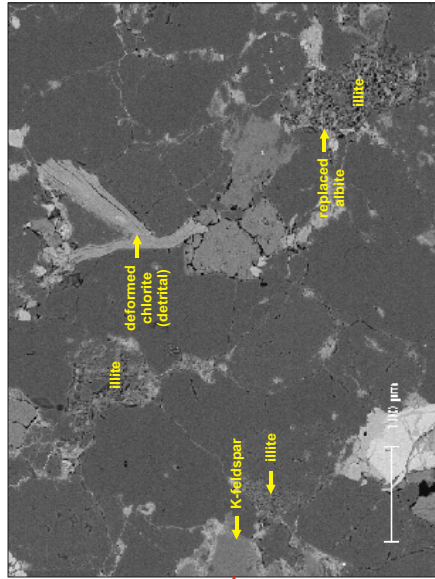
Figure 4.27 Flow chart illustrating simplified schematic diagenetic pathways in the Tanqua and Laingsburg depocentres.



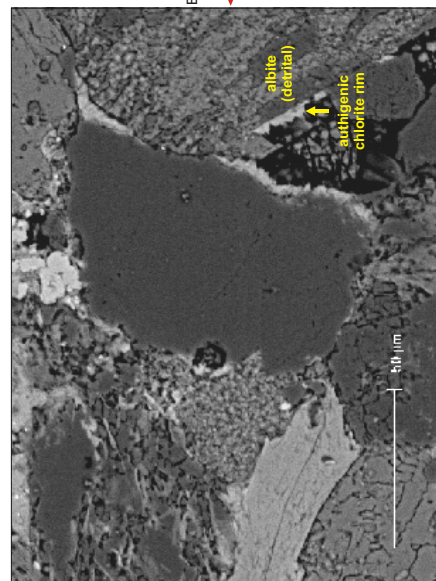
Inherited annealed quartz



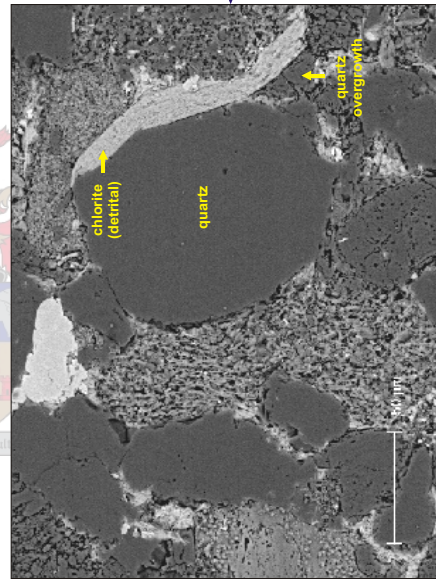
Early calcite cement



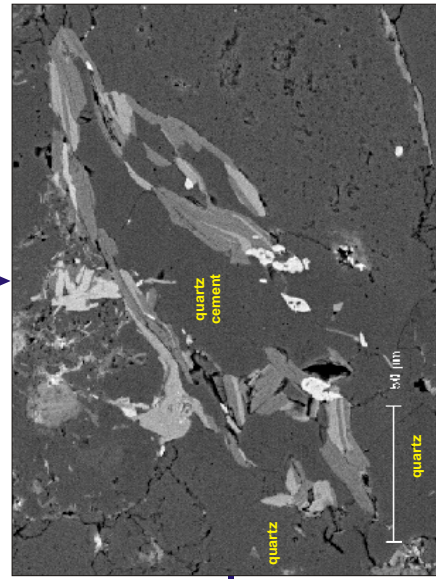
Illite pore filling and replacement of feldspar by kaolinite and smectite, now altered to illite, followed by further burial, mechanical compaction and the deformation of detrital chlorite



Authigenic chlorite rim growing on a detrital albite grain



Quartz overgrowths, growing up to the edge of the deformed detrital chlorite



Quartz cement

Figure 4.28 Summary of authigenic aspects of diagenetic mineralogies in the Tanqua and Laingsburg depocentres.

Undulatory extinction in some of the quartz grains was caused by deformation of the quartz after crystallisation (Deer *et al.*, 1992). In this study most interstitial material that represented distorted remains of lithic grains were assigned to the rock fragment category. The quartz grains range from angular to sub-rounded, and poorly to well sorted in the sandstone samples. Fisher *et al.* (1999) studied the effects of mechanical compaction on deeply buried sandstones in the North Sea. They found that crushed detrital grains are extensively quartz cemented and probably formed during deep burial. Cataclastic faults within the Rotliegendes of the southern North Sea are believed to have formed at depths of 2 – 3 km, suggesting that mechanical compaction must have occurred beyond this depth, due to the lack of quartz fragments containing quartz-cemented microcracks within the cataclastic faults (Fisher *et al.*, 1999). These authors concluded that sandstones susceptible to mechanical compaction during deep burial are those that maintain a high porosity and small grain contact area at depth, due to (i) the generation of secondary porosity, and/or (ii) the suppression of grain-to-grain quartz dissolution and quartz overgrowth precipitation. The sandstones from the Tanqua and Laingsburg depocentres have little quartz grain-to-grain contact and quartz overgrowths, and there is no evidence of authigenic grain fracturing due to mechanical compaction during deep burial.

#### **4.5.2.2 Sensitivity models**

The geodynamic and thermal consequences of the tectonic model for the southwestern Karoo Basin are tested through the use of sensitivity models via a computer program called WinheatXL. This is a 1D forward modelling program for predicting heat flow, maturation and horizon temperature histories from well or cross-section data. The program has been written by Professor Nick Kusznir (head of the Basin Modelling Group at the University of Liverpool, UK) and is distributed by Badley Geoscience Limited (Lincolnshire, UK).

The program allows the user to input a 1D stratigraphic section and model the thermal and maturation history and, in the case of this study, the burial history (defined by input stratigraphy and lithology - compaction is incorporated). The lithostratigraphy of the complete Karoo Supergroup (preserved in the Eastern Cape Province) is shown in Table 4.10. The horizon depth and interval lithologies of the sediments in the southwestern Karoo Basin used for the calculations in this program are shown in Table 4.11. The thicknesses of the formations, as well as the sedimentary units overlying the Tanqua and Laingsburg depocentre rocks, were calculated from borehole data (KL1/65 and SA1/66 from Rowsell and De Swardt, 1976) and extrapolated from the present day exposure of these successions in other parts of the Karoo Basin (Johnson, 1976; Tankard *et al.*, 1982; Turner, 1983; Cole, 1992; Johnson *et al.*, 1996; Catuneanu *et al.*, 1998; Turner, 1999). The possible thermal consequences of the igneous intrusions from the Drakensberg Group into the sediment pile were also tested. The results are presented in Figures 4.29 and 4.30.

Table 4.10 Lithostratigraphy of the Karoo Supergroup in the Eastern Cape Province. Tectonic pulse dates (P1 - P5) from Hälbich *et al.* (1983). Average stratigraphic thicknesses after Tankard *et al.* (1982), Johnson (1991), Visser (1991), Viljoen (1992a), Viljoen and Wickens (1992), Wickens (1994), Johnson *et al.* (1996), Turner (1999), Grecula (2000), Sixsmith (2000), and references therein.

KAROO SUPERGROUP	GROUP	SUBGROUP	FORMATION	Approximate thickness	
		DRAKENSBERG			1400 m
	STORMBERG		CLARENS	300 m	← 215 Ma <sup>(P5)</sup>
			ELLIOT	≤ 500 m	
			MOLTENO	≤ 600 m	← 230 Ma <sup>(P4)</sup>
	BEAUFORT	TARKASTAD	BURGERSDORP	7000 m	← 247 Ma <sup>(P3)</sup>
			KATBERG		
		ADELAIDE	BALFOUR		
			TEEKLOOF/MIDDLETON		
			ABRAHAMSKRAAL/ KOONAP		
	ECCA		WATERFORD	200 - 500 m	← 258 Ma <sup>(P2)</sup>
			FORT BROWN	200 m	
			LAINGSBURG	750 m	
			VISCHKUIL	200 - 400 m	
			COLLINGHAM	30 - 70 m	← 270 Ma <sup>b</sup>
			WHITEHILL	30 m	← 277 Ma <sup>a</sup>
			PRINCE ALBERT	165 m	← 278 Ma <sup>(P1)</sup>
	DWYKA			800 m	

Dating techniques:

- ← 270 Ma: Biostratigraphic or radiometric dates:-
  - <sup>a</sup>Biostratigraphic age from Oelofsen and Araujo (1987).
  - <sup>b</sup>Radiometric date from Turner (1999).
  - Biostratigraphic age from Rubridge (1991).
  - <sup>c</sup>Radiometric date from Duncan *et al.* (1997).

← 278 Ma<sup>(P1)</sup> Major tectonic episode (Hälbich *et al.*, 1983).

Table 4.11 Horizon depth and interval lithologies of the sediments in the southwestern Karoo Basin.

Tanqua depocentre

Unit	Thickness* (m)	Depth (km)	Age* (Ma)	Lithologies
Surface (fictitious)	50	0	0	Fictitious
Second (fictitious)	50	0.05	178	Basalt
Drakensberg Group lavas	1400	0.10	179	Basalt
Upper Beaufort Group**	8000	1.50	183	Sandstone
Abrahamskraal Formation	500	9.50	255	Sandstone
Waterford Formation (top)	500	10.00	257	60% sandstone/ 40% shale
Kookfontein Formation (top)	220	10.50	258.5	60% sandstone/ 40% shale
Skoorsteenberg Formation Fans 1 - 4 and Unit 5	340	10.72	259.7	90% sandstone
Tierberg Formation	500	11.06	263.7	95% shale
Collingham Formation Whitehill/Prince Albert	30	11.56	270	Siltstone/mudstone
Formations	130	11.59	288	Shale
Dwyka Group	305	11.72	297	Tillite and diamictite
Cape Supergroup	8000	12.03	330	Sandstone
Basement (top)		20.03	400	Top basement

\* The ages and thicknesses of the stratigraphic units are from Johnson (1976), Tankard *et al.* (1982), Turner (1983, 1999), Cole (1992), Johnson *et al.* (1996), Catuneanu *et al.* (1998), and references therein.

\*\* The thickness of the Upper Beaufort Group varies from 4000 to 10000 m, depending on the sensitivity model test.

Laingsburg depocentre

Unit	Thickness* (m)	Depth (km)	Age* (Ma)	Lithologies
Surface (fictitious)	50	0	0	Fictitious
Second (fictitious)	50	0.05	178	Basalt
Drakensberg Group lavas	1400	0.10	179	Basalt
Upper Beaufort Group**	8000	1.50	183	Sandstone
Abrahamskraal Formation	500	9.50	255	Sandstone
Waterford Formation (top)	500	10.00	257	60% sandstone/ 40% shale
Fort Brown Formation (top)	300	10.50	258.5	60% sandstone/ 40% shale
Laingsburg Formation Fans A - F	760	10.80	263	60% sandstone
Vischkuij Formation	250	11.56	269.5	30% shale
Collingham Formation Whitehill/PrinceAlbert	45	11.81	270	Siltstone/mudstone
Formations	190	11.86	288	Shale
Dwyka Group	430	12.05	297	Tillite and diamictite
Cape Supergroup	8000	12.48	330	Sandstone
Basement (top)		20.48	400	Top basement

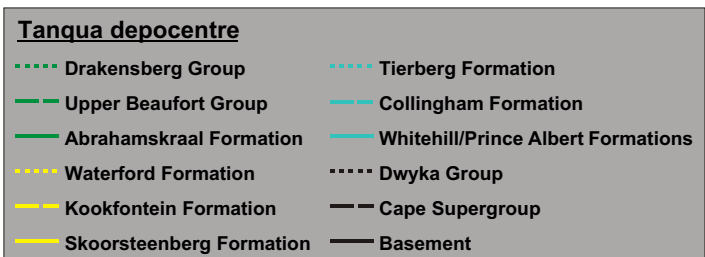
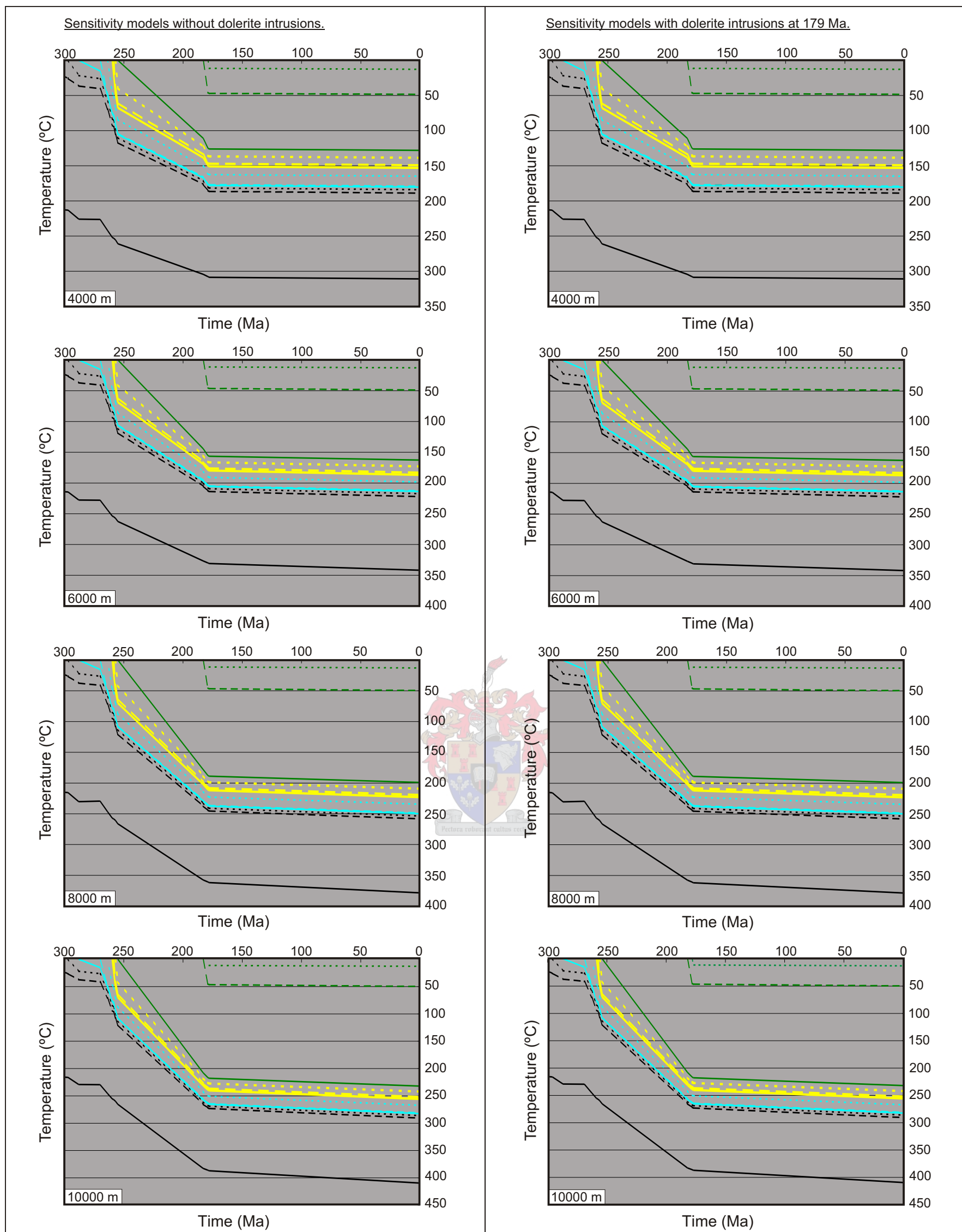


Figure 4.29 Tanqua depocentre burial sensitivity models. The parameters were for an Upper Beaufort Group thickness of 4000, 6000, 8000 and 10000 m. The other variable tested is the effect of dolerite intrusions at 179 Ma on the temperature history of the Skoorsteenberg, Kookfontein and Waterford Formations.

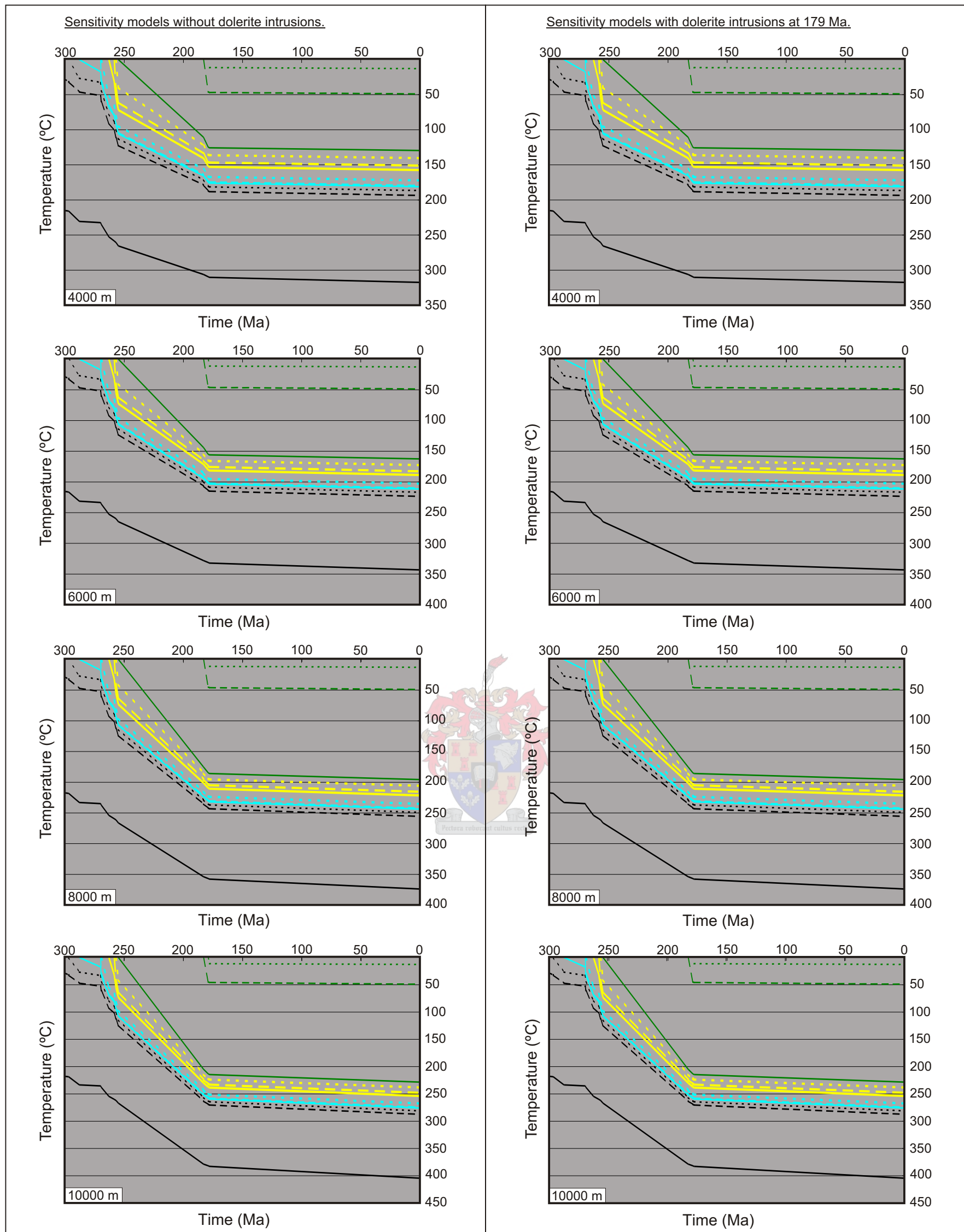


Figure 4.30 Laingsburg depocentre burial sensitivity models. The parameters were for an Upper Beaufort Group thickness of 4000, 6000, 8000 and 10000 m. The other variable tested is the effect of dolerite intrusions at 179 Ma on the temperature history of the Collingham, Vischkuil, Laingsburg and Fort Brown Formations.

From these sensitivity models it can be seen that the intrusion of basaltic dykes, during the Jurassic, do not affect or elevate the temperatures of the sediments from this study (Skoorsteenbergh, Kookfontein and Waterford Formations in the Tanqua depocentre and Collingham, Vischkuil, Laingsburg and Fort Brown Formations in the Laingsburg depocentre) to a significant extent. The thermal history of these sediments is the same, whether the intrusions are present or not. Temperature conditions of  $250 \pm 50^\circ\text{C}$  can be reached through burial under overlying strata with a thickness of at least 7000 m. These modelling results strongly suggest that at least 7 km of Upper Karoo overburden has been stripped off the study area.

#### **4.5.3 Petrographic differences between depositional facies**

There are differences in the sandstone compositions between the Tanqua and Laingsburg depocentres. Their detrital quartz and mica compositions are about the same, whereas the Tanqua depocentre sandstones have a slightly higher amount of feldspar, and slightly less lithic fragments, than the Laingsburg depocentre sandstones. The Vischkuil Formation sandstones differ from all the other analysed rocks, both from the Tanqua and Laingsburg depocentres, in that it has much less detrital quartz and mica, but a larger percentage of feldspar and lithic fragments. The most likely reason for this is probably a change in provenance, due to the short-term exposure of an unknown source rock.

Facies-related variability is a function of textural change within the sandstones, i.e. differences in grain size and sorting. Sandstones from channel-fills are generally slightly coarser grained than interchannel/overbank deposits, due to the higher energy depositional environments of channels. Sandstones from the delta facies are finer grained and better sorted than the sandstones from the channel-fills, due to the wave reworking of the sands. Sandstones from the basin-floor and base of slope turbidite deposits are finer grained on average than the slope facies deposits. The basin-floor turbidite deposits are also generally better sorted than the base of slope and slope facies deposits, probably due to the higher energy conditions in the slope environment during sediment deposition. The better sorting is also due to the fact that the sediments travelled further and were in suspension longer before settling. There is an increase in grain size from the pro-delta facies deposits to the delta front facies deposits, as well as sandstones from the delta front facies showing better sorting, due to the higher energy of the depositional environment.

#### **4.5.4 Petrographic differences between the Tanqua and Laingsburg depocentre sandstones**

Within the Tanqua depocentre, there are differences in the overall or primary sandstone compositions between formations, which infer different provenance terranes. These are: the

Skoorsteenberg Formation (feldspathic; continental provenance), the Kookfontein Formation (lithofeldspathic; mixed provenance), and the Waterford Formation (lithofeldspathic; continental provenance) (Table 4.2).

The sandstones within the Laingsburg depocentre show less compositional variation between the formations, and are as follows: the Collingham Formation (lithofeldspathic; recycled orogen), the Laingsburg Formation (lithofeldspathic; mixed provenance), and the Fort Brown Formation (lithofeldspathic; mixed provenance), with the exception of the Vischkuil Formation (lithofeldspathic; mixed and magmatic arc provenance), which has larger amounts of detrital feldspar and lithic fragments, and less detrital quartz compared to the rest (Tables 4.2 and 4.9).

From this data it can be seen that the sandstones from the Laingsburg depocentre are generally less feldspathic and contain more lithic fragments than the Tanqua depocentre sandstones. The amount of feldspar present in the rocks of both the Tanqua and Laingsburg depocentres has been underestimated in the past, due to the fine-grained nature of the sandstones and the difficulty involved in distinguishing optically between feldspar and quartz. Studies carried out by Den Boer (2002) confirm this. Sandstones from Fan 3 in the Skoorsteenberg Formation of the Tanqua depocentre were identified as very fine- to fine-grained arkoses, i.e. the sandstones contain quartz, lithic fragments and more than 25% feldspar. Overall, the Tanqua depocentre sandstones are finer grained and the grains are better sorted and less angular than the Laingsburg depocentre sandstones. Sandstones from the Laingsburg depocentre also show more evidence of compaction. Although the provenance terranes for the sediments from both depocentres are primarily from a continental and a mixed source, the continental provenance is dominant in the Tanqua depocentre, whereas the mixed provenance is dominant in the Laingsburg depocentre.

#### **4.5.5 Synthesis of the textural and detrital mineralogy data**

Sandstone provenance can be inferred from quantitative detrital framework modes (Dickinson *et al.*, 1983). These authors identified the following major provenance types: continental blocks (stable cratons), magmatic arcs, and recycled orogens, showing that mean compositions of sandstone suites derived from these different kinds of provenance terranes controlled by plate tectonics tend to lie within discrete and separate fields on QFL and QmFLt diagrams. However, anomalous lithic fragments in variable amounts locally can be introduced by recycling of cover rocks overlying basement. The QmFLt ratios plotted in Figures 4.5 – 4.6 and 4.15 – 4.16 show the compositional categories as well as the provenance fields of Dickinson *et al.* (1983).

The above data suggest the following provenance evolution for the Laingsburg depocentre: the source terrane for the Collingham Formation was a recycled orogen with lithofeldspathic material, which switched to a magmatic arc or mixed provenance with a lithofeldspathic composition for the Vischkuil Formation. The overlying Laingsburg Formation source terrane was a mixed provenance, with a lithofeldspathic composition. The Fort Brown Formation deltaic deposits are from the same mixed provenance, also with a lithofeldspathic composition. The provenance evolution for the Tanqua depocentre is as follows: starting from Unit 5 lower slope deposits in the Skoorsteenberg Formation, the sediment source terrane started as continental, with a mainly feldspathic composition. It then switched to a mixed provenance for the Kookfontein Formation, which consisted of predominantly lithofeldspathic material (similar to the Laingsburg Formation). For the Waterford Formation, it switched back to a continental provenance, now with a lithofeldspathic composition. It should be noted that the compositional differences of all the sandstones in both the Tanqua and Laingsburg depocentres are not major.

The high quartz content in sandstone reflects intense weathering on cratons with low relief and prolonged transport across continental surfaces having low gradients (Dickinson and Suczek, 1979). Kingsley (1977, 1981) suggested that the abundance of undulatory quartz, the predominance of low-temperature feldspar and the rarity of volcanic fragments indicated that the primary provenance areas for the Ecca Group and lower part of the Beaufort Group were low-grade metamorphic rocks and sedimentary rocks (mainly quartzite). Geochemistry shows that this is partially true for the rocks from this study; they were derived from mixed sources of granitoid and schist composition. Granites are coarse- to very coarse-grained and mineralogically consist of quartz, alkali feldspar, sodic plagioclase, accessory apatite, titanite, zircon and magnetite (Hamilton *et al.*, 1980). Schists refer to sedimentary rocks that have undergone low- to medium-grade regional metamorphism. They are coarse-grained with a marked layering, defined by platy or elongate minerals (such as biotite or muscovite), often finely interleaved with quartz and feldspar (Hamilton *et al.*, 1980). The primary detrital mineralogy of the studied rocks from the Tanqua and Laingsburg depocentres is consistent with this.

#### **4.6 Gondwana palaeogeography and possible source area(s)**

The geotectonic and palaeogeographic setting of Gondwana, showing the distribution of Archean to Mesozoic geology, and that of western Gondwana (South America and southern Africa) during the late Palaeozoic, are shown in Figure 4.31. The major amount of sediment was transported across the broad coastal plain and shelf (during lowstand periods) to the Tanqua and Laingsburg depocentres at approximately 270 – 255 Ma, after which time sediment input was cut off. Using the constraints that the source rocks had a granitic to upper crust composition and had to be exposed at the time of Tanqua and Laingsburg depocentre

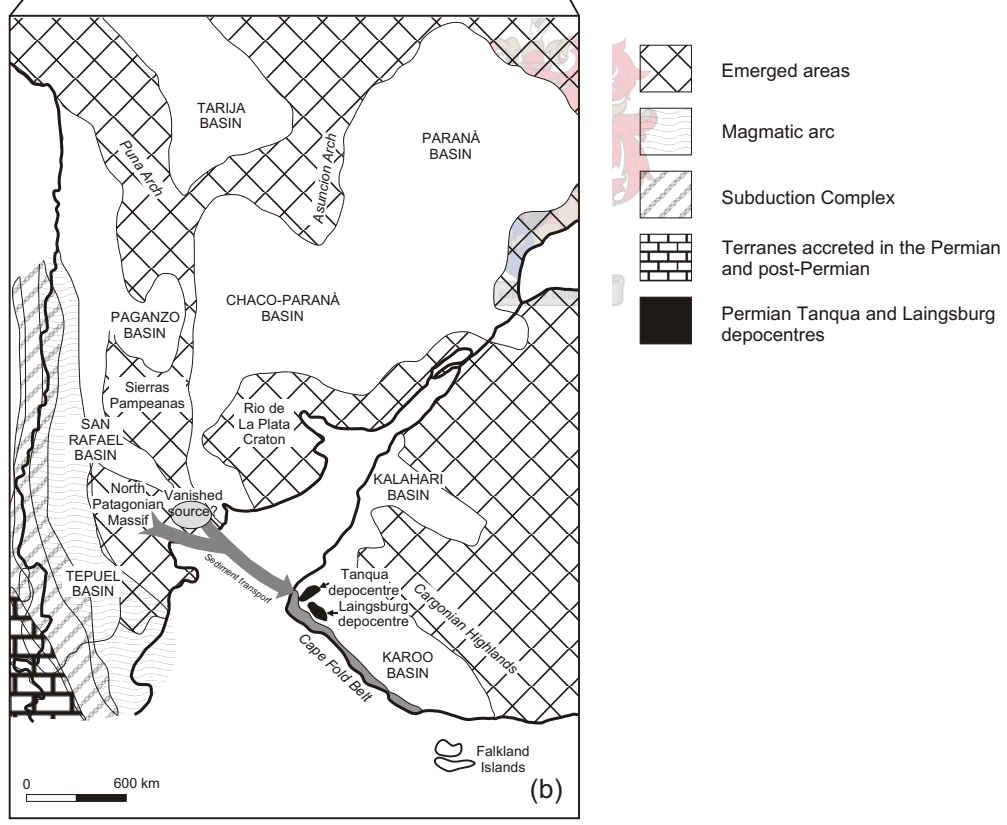
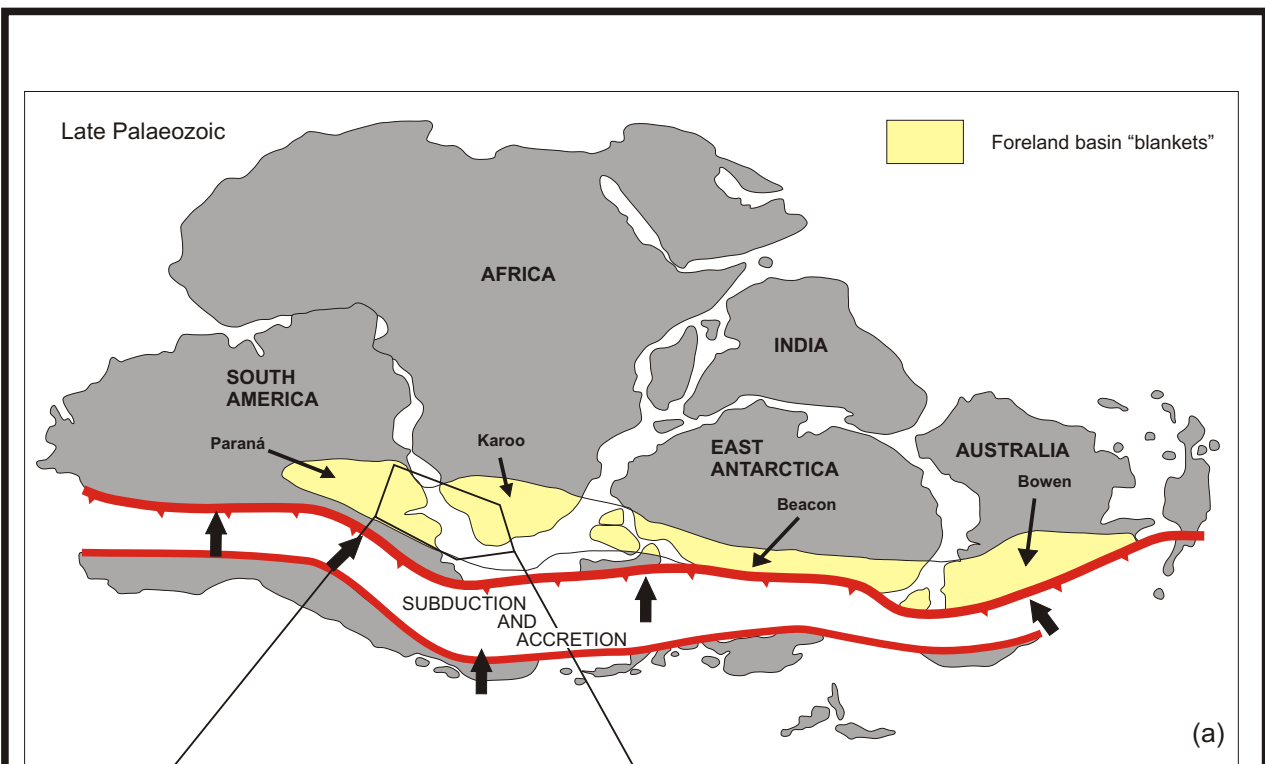


Figure 4.31 (a) Karoo, Paraná and Beacon Basins in response to accretion tectonics during the late Palaeozoic along the southern margin of Gondwana (after De Wit and Ransome, 1992). (b) Palaeogeography and geotectonic setting of western Gondwana (South America and southern Africa) during the late Palaeozoic (after Lòpez-Gamundi and Rosello, 1998). The arrow indicating sediment transport is to illustrate the linkage between the source terranes and the Tanqua and Laingsburg depocentres.

sediment deposition at 270 - 255 Ma (Turner, 1999), the source terranes are identified in Chapter Five as Sierras Pampeanas (SP) granites and schists, and the Patagonian batholith from the North Patagonian Massif (NPM).

The source area(s) infer a sediment transport distance of approximately 600 to 1350 km, dependent on the accuracy of the Gondwana reconstructions. Even though the geochemistry of rocks from the SP shows them as a possible source terrane, they are located too far from the Laingsburg and Tanqua depocentres to be a source, based on petrographic evidence. The NPM is still considered to be a possible source, with the mixed provenance signature coming in from either a vanished source that was possibly located very close to the NPM, or a source even closer to the Karoo Basin, such as the Cape Granite Suite (CGS). The distance of the NPM is consistent with the overall fine grain size of the sediments. A large transport distance would lead to well rounded grains. As shown by petrography, however, most of the grains are angular to sub-rounded. It is not clear why this is, although a possible explanation might be that the deposits resulted from glaciofluvial processes (rapid transport).

Gondwana reconstruction for the Permo-Carboniferous glacial event is shown in Figure 4.32. The possibility that the Dwyka Group sediments could have been a source for the Tanqua and Laingsburg depocentre rocks would infer recycling of glacial sediments (Figure 4.33). It would be one explanation for the mixed provenance signature, angular to sub-rounded grain shapes and fine-grained nature of the sediments. The receding Dwyka glaciation (early Permian) deposited sediments into the Karoo Basin, over the still submerged Cape Fold Belt (CFB). During the late Permian, as the uplift of the CFB started, the overlying Dwyka sediment would have been uplifted as well, resulting in their reworking and recycling and deposition into the Laingsburg and Tanqua depocentres.

A ternary diagram shows the compositions of the Tanqua and Laingsburg depocentre sediments compared to Dwyka Group rocks, and sediments originating from the SP and NPM (Figure 4.34). The diagram shows that the Dwyka rocks are very similar to the Tanqua and Laingsburg depocentre sediments. However, the Tanqua and Laingsburg depocentre sediments are more closely related to the rocks from the Sauce Grande Basin in the Sierras Australes Fold Belt of east central Argentina (in the region of the NPM) deposited during the Permian.

The units of the Pillahuincó Group (Sauce Grande Basin) show a depositional history that can be explained in terms of glaciomarine sedimentation (Sauce Grande Formation - equivalent to the Dwyka Group), postglacial transpression (Piedra Azul and Bonete Formations), followed by deltaic deposition (Tunas Formation) (Lopez-Gamundi *et al.*, 1995). The provenance areas are suggested to be located to the southwest for the Tunas Formation deposits and northeast (Tandil cratonic area) for the underlying succession (Sauce Grande,

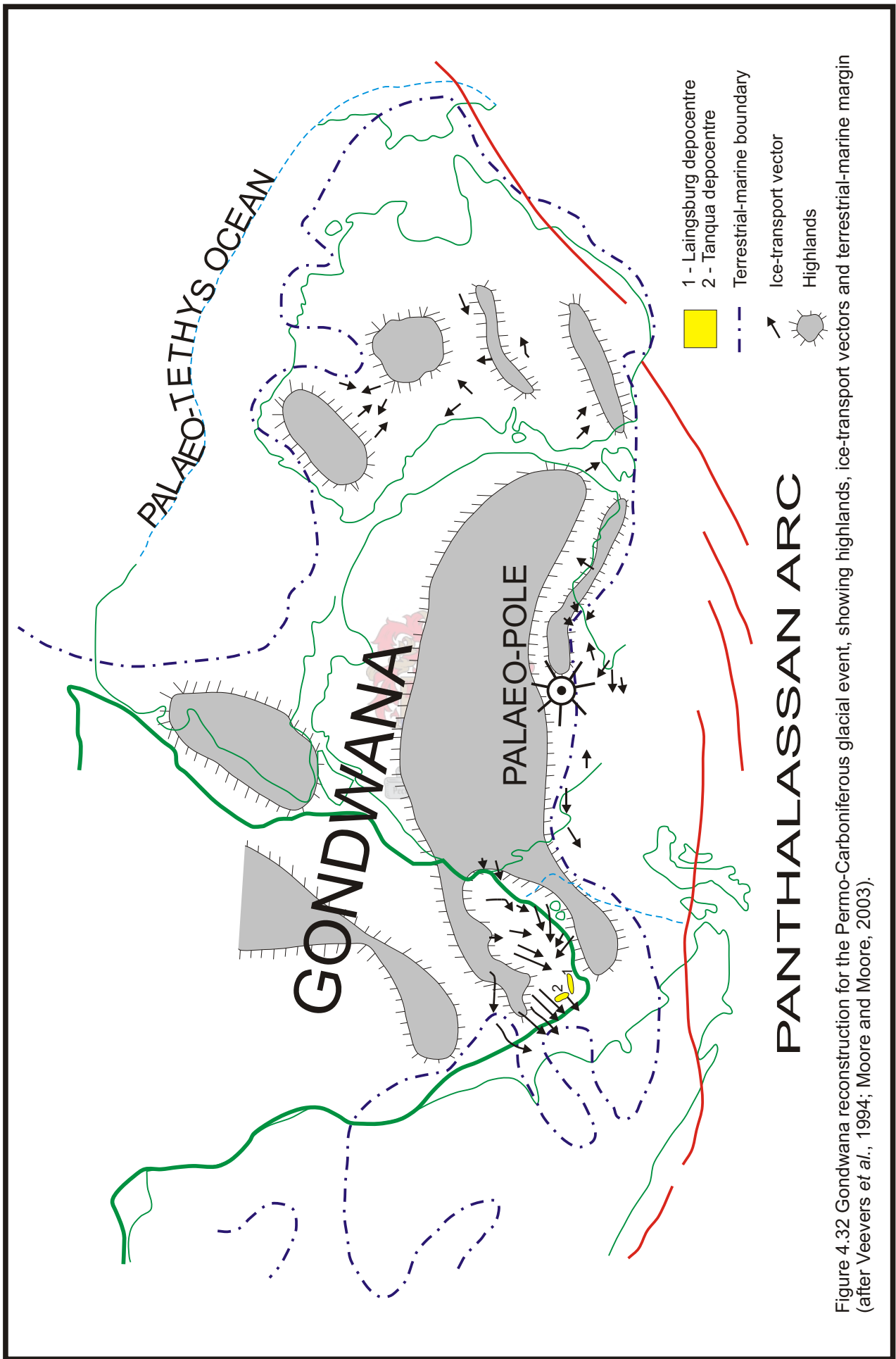
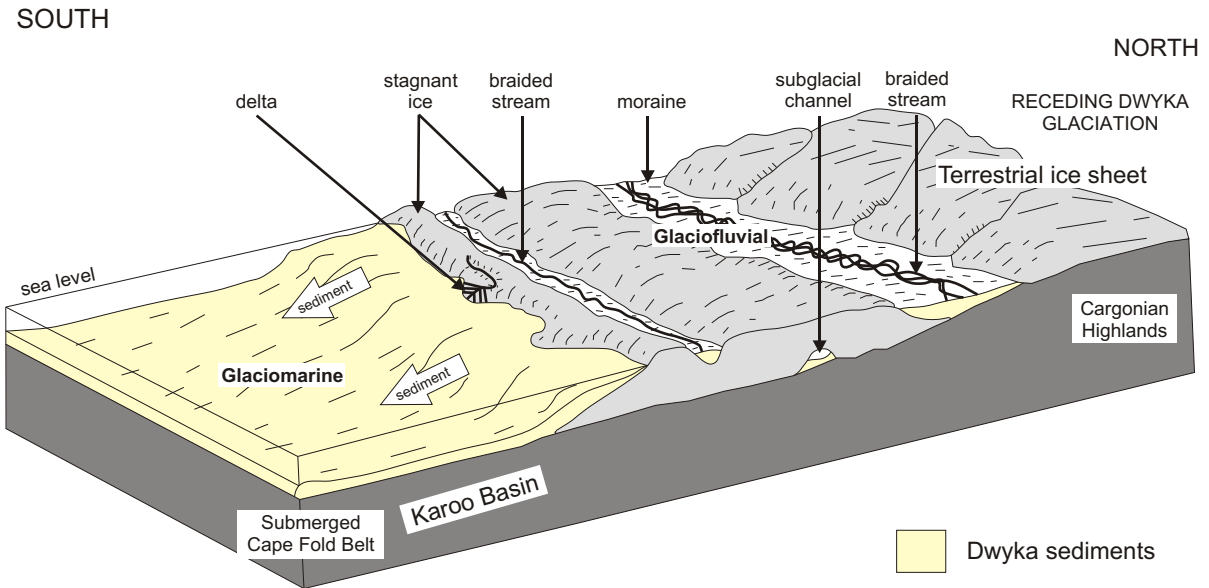


Figure 4.32 Gondwana reconstruction for the Permo-Carboniferous glacial event, showing highlands, ice-transport vectors and terrestrial-marine margin (after Veevers *et al.*, 1994; Moore and Moore, 2003).

(a) Early Permian



(b) Late Permian

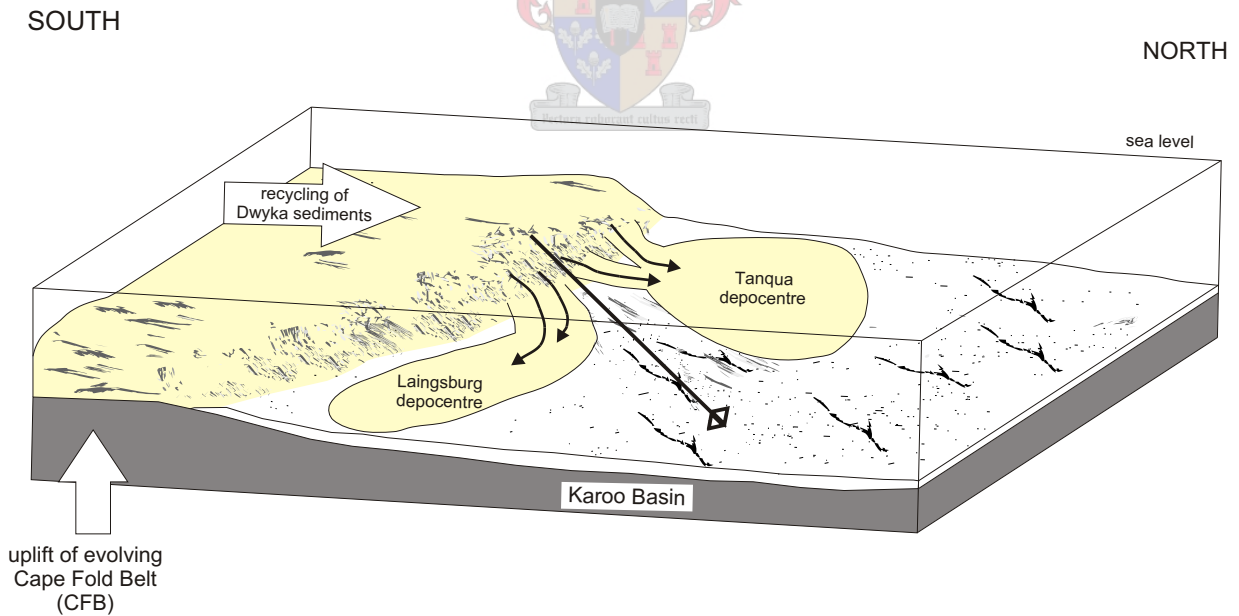
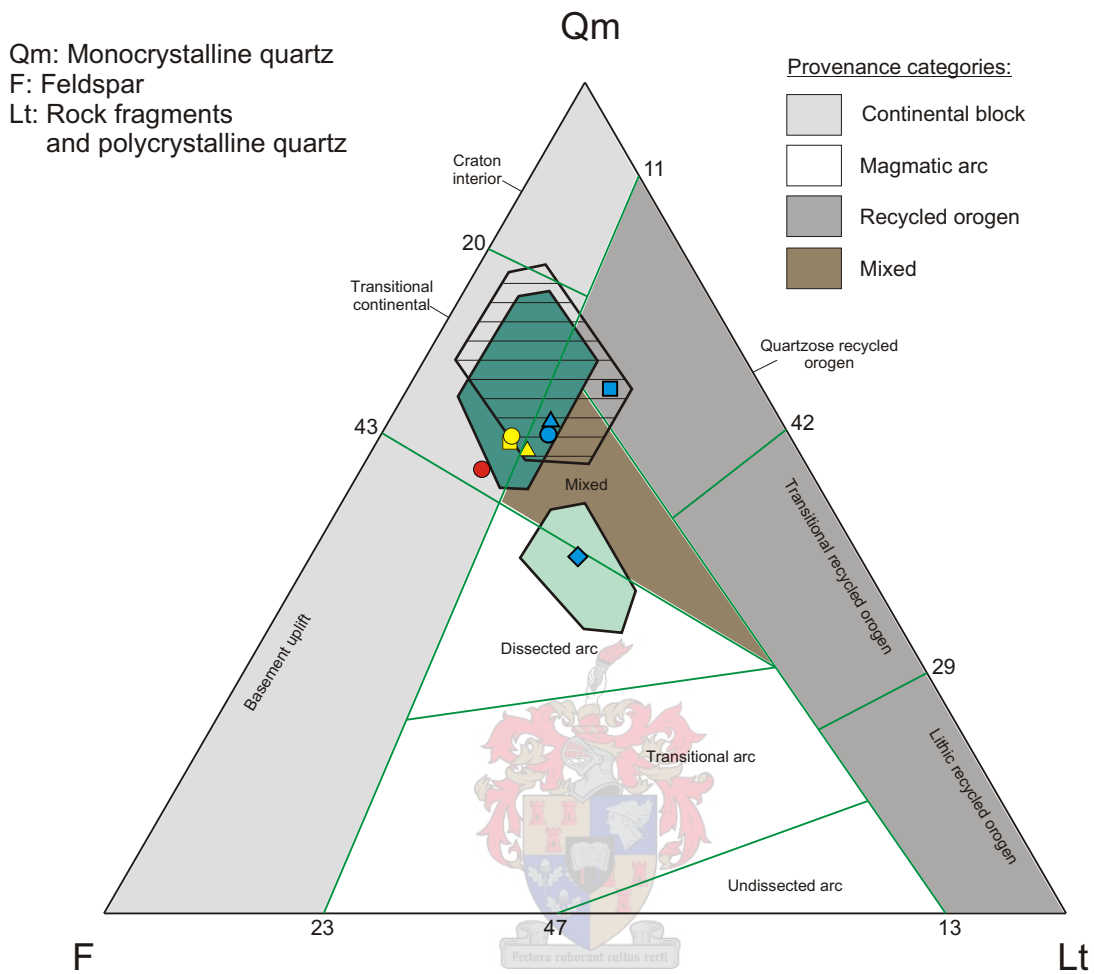


Figure 4.33 Schematic block diagrams showing (a) the receding Dwyka glaciation during the early Permian. Sediment is deposited through glaciofluvial and glaciomarine processes into the Karoo Basin (modified after Allen, 1997), and (b) the proposed deposition of reworked and recycled Dwyka sediment, firstly into the Laingsburg depocentre and later into the Tanqua depocentre, during the late Permian, as a result of the uplift of the evolving CFB.



Tanqua depocentre:

- Average Waterford Formation (n = 4)
- ▲ Average Kookfontein Formation (n = 34)
- Average Skoorsteenberg Formation (Unit 5) (n = 14)

Laingsburg depocentre:

- ▲ Average Fort Brown Formation (n = 5)
- Average Laingsburg Formation (n = 23)
- ◆ Average Vischkuil Formation (n = 2)
- Collingham Formation (n = 1)

Dwyka Group:

- Average Dwyka Group (n = 3) (after Johnson, 1991)

Sauce Grande Basin:

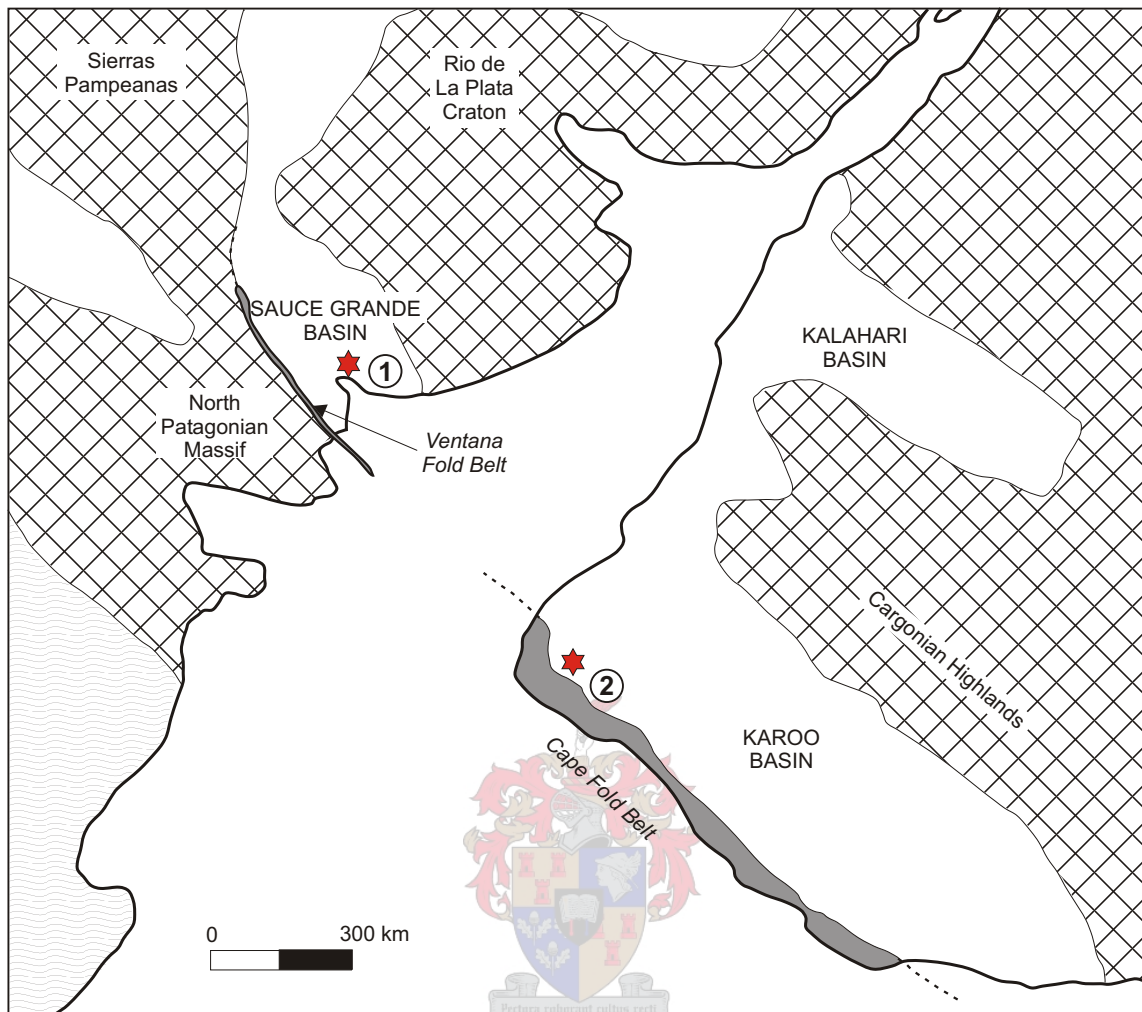
- Tunas Formation (after Lopez-Gamundi *et al.*, 1995)
- ▨ Piedra Azul and Bonete Formations (after Lopez-Gamundi *et al.*, 1995)
- Sauce Grande Formation (after Lopez-Gamundi *et al.*, 1995)

Figure 4.34 QmFLt plot for framework modes of sandstones showing provisional subdivisions according to inferred provenance type (method after Dickinson *et al.*, 1983).

Piedra Azul and Bonete Formations). The age constraints and similarities in composition between the tuff horizons present in the Sauce Grande and Karoo Basins suggest a genetic linkage between them (Lopez-Gamundi *et al.*, 1995). These tuffs are associated with the silicic volcanism along the Andes and Patagonia that peaked during the Permian and are present in the Tunas Formation (Sauce Grande Basin) and Whitehill Formation (Karoo Basin) (Rossello *et al.*, 1997). The similar palaeotectonic evolution identified in the Sauce Grande Basin – Ventana Fold Belt and Karoo Basin – CFB is shown in Figure 4.35.

The Brenton Loch Formation in the Falkland Islands has been correlated to the Ripon Formation (Adie, 1952; Curtis and Hyam, 1998; Aldiss and Edwards, 1999; Trewin *et al.*, 2002). The Ripon Formation, overlying the Collingham Formation in the Eastern Cape (South Africa) and overlain by the Fort Brown Formation, is considered to stratigraphically be the same as the Vischkuil and Laingsburg Formations in the Laingsburg depocentre. The Brenton Loch Formation consists of basin-floor, delta-derived turbidites, with the sand-mud couplets in the interbedded rhythmite units representing annual freeze-thaw cycles in the source area, deposited during highstand intervals (Trewin *et al.*, 2002). The rhythmic facies association, where turbidite units are generally subordinate, dominates the lower part of the Brenton Loch Formation and comprises of mudstone-sandstone couplets on a sub-millimetre to centimetre scale (Trewin *et al.*, 2002). The turbidite facies association consists of sandstone-dominated units tens of metres thick, separated either by rhythmites with thin sandstone beds, or massive or irregularly laminated mudstone (Trewin *et al.*, 2002). Petrographically, the sandstones from the Brenton Loch Formation are similar to those of the Tanqua and Laingsburg depocentres. They are generally fine- to lower medium-grained, with angular to sub-angular grains and sorting that ranges from poor in the turbidites to moderate in channel-fill sandstones of the delta tops (Trewin *et al.*, 2002). The total quartz ranges from 16 to 42% and feldspar comprises 13 – 34%, sedimentary and metamorphic clasts, as well as volcanic rock fragments (Trewin *et al.*, 2002). These sandstones differ from the sandstones in the present study in that they have volcanic fragments in their compositions, were derived from a provenance typical of a transitional arc regime, and have different secondary mineral assemblages, due to different processes of diagenesis and metamorphism. A late Palaeozoic-Mesozoic arc has been recognised in South America (Dalziel and Elliot, 1982), which probably continues into the Antarctic Peninsula area (Milne and Millar, 1989) and is a possible source of the volcanoclastic detritus (Trewin *et al.*, 2002).

Work done by Flint *et al.* (2004) suggests that the majority of the Laingsburg depocentre deep-water deposits are older than the Tanqua depocentre deposits (Figure 4.36). This would mean that sediment routing changed progressively from the Laingsburg to the Tanqua depocentre (Figure 4.37) as a result of the evolving structures of the CFB.



- ★ Tuffs in Permian units:
  - ① Tunas Formation (Pillahuincó Group - Sauce Grande Basin)
  - ② Whitehill and Collingham Formations (Ecca Group - Karoo Basin)
- ☒ Emerged areas
- ▨ Magmatic arc
- Ventana and Cape Fold Belts

Figure 4.35 Palaeogeography and geotectonic setting of the Karoo and Sauce Grande Basins in western Gondwana (South America and southern Africa) during the late Palaeozoic (modified after Lopez-Gamundi and Rosello, 1998). The CFB is inferred to be subaqueous at this time.

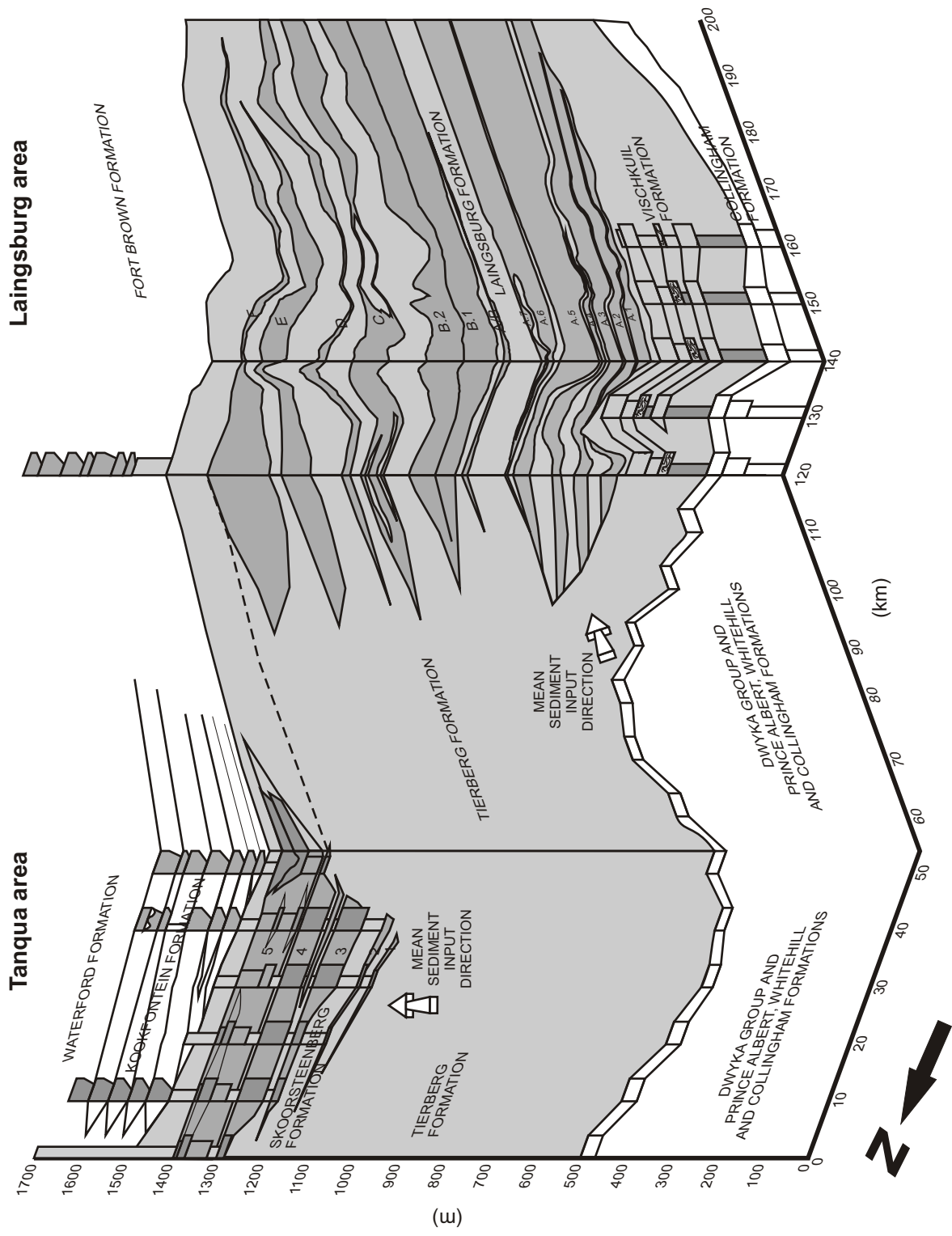


Figure 4.36 Stratigraphic relation between the Tanqua and Laingsburg depocentres, showing that the majority of the Laingsburg depocentre deposits are older than the Tanqua depocentre deposits (after Flint *et al.*, 2004).

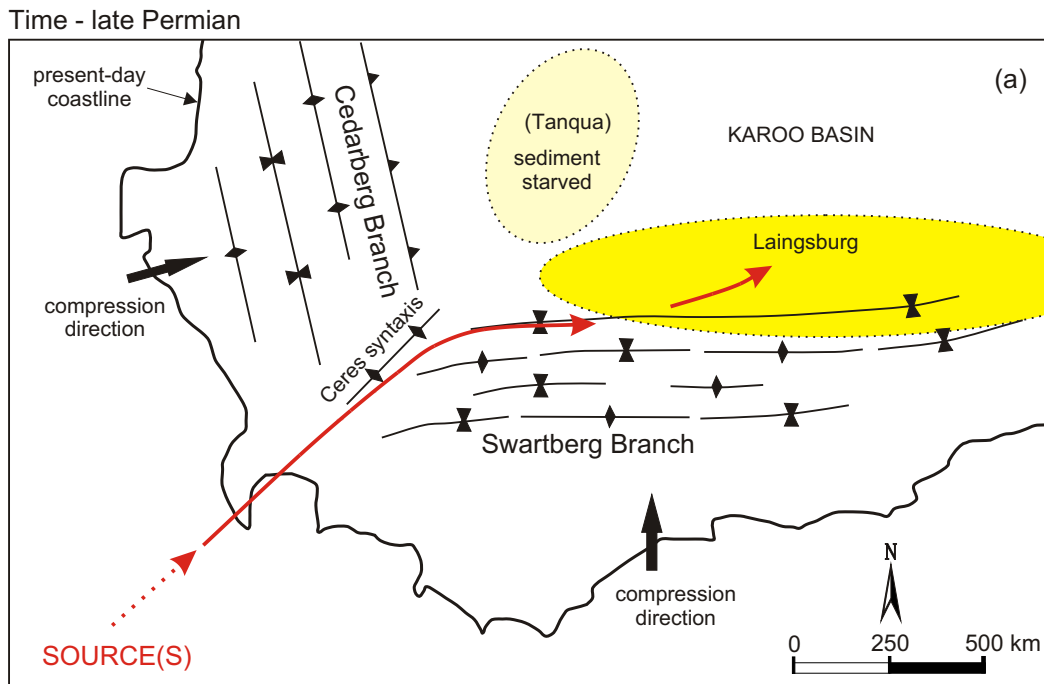


Figure 4.37 (a) Diagram showing the sediment supply and deposition in the Laingsburg depocentre (modified after King *et al.*, 2004). Sediment pathways follow the actively deforming synclines.

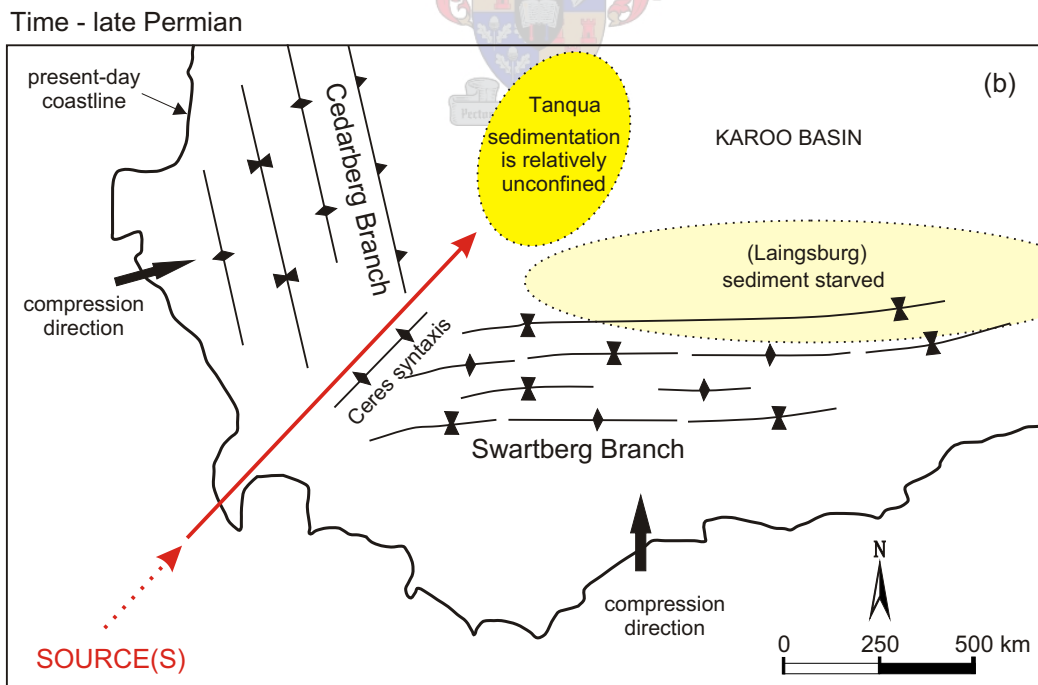


Figure 4.37 (b) Diagram showing the sediment supply and deposition in the Tanqua depocentre (modified after King *et al.*, 2004). The frontal monoclines of the Cedarberg Branch act as a confining barrier to the Tanqua depocentre.

#### 4.7 Conclusions (answers to initial objectives)

- i. The primary detrital mineralogy for the sandstones of both the Tanqua and Laingsburg depocentres before burial, metamorphism and alteration was originally quartz, albite, K-feldspar, opaques, titanite, biotite, lithic fragments and accessory muscovite, apatite and zircon, identifying them as arkoses.
- ii. The main secondary mineral assemblages in these sandstones are illite (alteration of kaolinite and feldspar), chlorite (alteration of feldspar), quartz overgrowths and cement, minor calcite cement, and some authigenic mica. The rocks of both the Tanqua and Laingsburg depocentres have undergone high-grade diagenesis to low-grade regional burial metamorphism to the lower greenschist facies (90 – 250°C; ~2 kbars).
- iii. Based upon the identified primary mineralogy, the sandstone classifications in the Tanqua depocentre range from subfeldspathic (2%) to feldspathic (33%) to lithofeldspathic (65%) with the provenance(s) being continental (50%), mixed (44%) and magmatic (6%). The Laingsburg depocentre sandstones range in composition from lithic (3%) to subfeldspathic (10%) to feldspathic (23%) to lithofeldspathic (64%), with provenance(s) being magmatic (3%), recycled orogen (3%), continental (39%) and mixed (55%).
- iv. Within the Tanqua depocentre, there are differences in the primary sandstone compositions between formations. The sandstones within the Laingsburg depocentre show less compositional variation between the formations, with the exception of the Vischkuil Formation, which has larger amounts of detrital feldspar and lithic fragments, and less detrital quartz compared to the rest. Sandstones from the Laingsburg depocentre are generally less feldspathic and contain more lithic fragments than the Tanqua depocentre sandstones. Overall, the Tanqua depocentre sandstones are finer grained and the grains are better sorted and less angular than the Laingsburg depocentre sandstones. Sandstones from the Laingsburg depocentre also show more evidence of compaction. There are no differences in sandstone composition and texture for samples taken within the same stratigraphic units, but at different locations.
- v. Cathodoluminescence (CL) shows that the original grain shape of the detrital quartz was angular to rounded and that fracture and annealed quartz grains were inherited from the source(s). Most of the feldspar and kaolinite have been altered to illite, which is a diagenetic effect of burial. The loss of porosity and permeability was thus a result of the alterations to authigenic clay minerals (illite and chlorite) and the formation of quartz overgrowths and cement.

## Chapter Five

### 5 Geochemistry

#### 5.1 Analytical techniques

Whole rock chemical analyses, including major (XRF), minor and trace element (ICP-MS) compositions, of the Tanqua and Laingsburg depocentre rocks are given in Appendix C and these data have been plotted on variation diagrams. The concentrations of many elements in fine-grained sedimentary rocks in continental platforms around the world are similar as a consequence of mixing through repeated cycles of erosion (Rollinson, 1993). The North American Shale Composite (NASC) was used for normalisation purposes and to identify subtle enrichments and deficiencies in certain elements. The tectonic setting of the depositional environment is assumed to influence sedimentation, diagenesis and composition of sandstones (Chamley, 1990). Chemical and physical modification of source material during weathering, erosion, transport and deposition make it difficult to determine provenance of sandstones in ancient sedimentary systems. Geochemistry can, however, help to reveal the nature of source regions and the tectonic setting of sedimentary basins, since sandstone composition has been shown, in some circumstances, to reflect the tectonic history of the source area. X-ray Fluorescence (XRF) spectrometry and Inductively Coupled Plasma Emission Mass Spectrometry (ICP-MS) were used for geochemical analyses. The details of analytical procedure are discussed in the following sections.

##### 5.1.1 X-ray Fluorescence (XRF) Spectrometry

Concentrations of thirteen major elements, Si, Ti, Al, Fe, Mn, Mg, Ca, Na, K, P, S, Ni and Cr were determined with a Phillips 1404 wavelength dispersive XRF spectrometer (University of Stellenbosch, South Africa) using the following techniques: Representative samples (>60 g) of each whole rock were cleaned and trimmed of weathering rinds. They were then crushed in a jaw crusher and powdered in a carbon steel Sieb technik mill for two minutes, taking the necessary precautions against contamination. Fusion disks for each sample were prepared with 6 g of LiT-LiM flux in the proportion 57:43 (Sigma Chemicals) and LiBr as releasing agent, mixed with 0.7 g of the sample, according to the methods described in Norrish *et al.* (1969), Duncan *et al.* (1984), Heinrich (1986) and Thompson *et al.* (1997).

The spectrometer is fitted with an Rh tube, six analysing crystals, namely: LIF200, LIF220, LIF420, PE, TLAP and PX1 and the detectors are a gas-flow proportional counter, scintillation detector or a combination of the two. The gas-flow proportional counter uses P10 gas, which is a mixture of 90% argon and 10% methane. All measurements were made on a fused glass bead at 60 kV and 40 mA tube operating conditions. Intensity data were collected

using the SuperQ Philips software and matrix effects in the samples were corrected for by applying theoretical alpha factors and measured line overlap factors to the raw intensities. Standards that were used in the calibration procedures for both major and trace element analyses are as follows: AGV-1 (andesite from USGS), BHVO-1 (basalt from USGS), JG-1 (granodiorite from GSJ), JB-1 (granodiorite from GSJ), GSP-1 (granodiorite from USGS), SY-2 (syenite from CCRMP), SY-3 (syenite from CCRMP), STM-1 (syenite from USGS), NIM-G (granite from MINTEK), NIM-S (syenite from MINTEK), NIM-N (norite from MINTEK), NIM-P (pyroxenite from MINTEK), NIM-D (dunite from MINTEK), BCR (basalt from USGS), GA (granite from CRPG), GH (granite from CRPG), DRN (diorite from ANRT), and BR (basalt from CRPG).

Abbreviations used:

ANRT: Association Nationale de la Recherche Technique, Paris

CCRMP: Canadian certified Reference Materials Project

CRPG: Centre de Recherches Petrographiques et Geochimiques, Nancy

MINTEK: Council for Mineral Technology, South Africa

GSJ: Geological Survey of Japan

NIM: National Institute of Metallurgy, South Africa

USGS: United States Geological Survey, Reston

### **5.1.2 Inductively Coupled Plasma Emission Mass Spectrometry (ICP-MS)**

Trace elements, including REE, were analysed by ICP-MS by means of the following techniques and the methods described in Le Roex *et al.* (2001). Sample powders, as prepared for XRF, were carefully weighed out to 50 mg in clean, small (~5 ml) Savillex beakers, a 4 ml of HF/HNO<sub>3</sub> stock solution was added and the lids tightly closed and placed on hotplates for approximately 48 hours at a temperature of 50 - 60°C. The samples were then dried down, 2 ml of concentrated 2-bottled HNO<sub>3</sub> was added to each sample and the lids were again tightly closed and placed on the hotplates until complete dissolution. The samples were then evaporated to complete dryness at a temperature of ~75°C, after which the process was repeated by the addition of 2 ml of concentrated 2-bottled HNO<sub>3</sub>.

Four ml of internal standard stock solution (University of Cape Town, South Africa) was added to each of the samples and allowed to dissolve. Each of the dissolved samples was then quantitatively transferred to clean and dry 50 ml centrifuge tubes, after which the sample beakers were washed with internal standard stock solution twice and quantitatively transferred to the centrifuge tube on the microbalance. The dissolved samples were made up to 50 mg with internal standard stock solution, 4 drops of concentrated 2-bottled HF were added to each and the weights were recorded. The solutions represented 1000-fold dilutions of the original solid sample and were analysed in the ICP-MS.

## 5.2 Objectives

- i. Are there changes in major, trace and rare earth element chemistry with the chemical index of alteration (CIA), palaeocurrent direction and stratigraphic location, within the individual Skoorsteenberg and Kookfontein Formations in the Tanqua depocentre, and between the Laingsburg and Fort Brown Formations within the Laingsburg depocentre?
- ii. Can any correlations in these geochemical parameters be drawn between the Tanqua and Laingsburg depocentres?
- iii. What, if any, are the differences in geochemical classification for the Tanqua and Laingsburg rocks and what do they indicate?
- iv. Are the provenance signatures and tectonic settings within the individual depocentres constant with stratigraphic location and position in the systems tract?
- v. With the available geochemical data, what was the transport distance of the sediments and the most probable source terrane in ancient Gondwana during the late Palaeozoic?

## 5.3 Major element chemistry

The  $\text{SiO}_2$  content and  $\text{SiO}_2/\text{Al}_2\text{O}_3$  ratio can determine geochemical sediment maturity, reflected by the abundance of quartz and the clay and feldspar content. The alkali content can also be a good measure of the feldspar content, however, potassium in clay should be taken into account. Classification for the sandstones based upon geochemistry was made through the use of a plot of  $\log (\text{Na}_2\text{O}/\text{K}_2\text{O})$  vs.  $\log (\text{SiO}_2/\text{Al}_2\text{O}_3)$  (Pettijohn *et al.*, 1972, Herron, 1988, Rollinson, 1993) (Figure 5.1). The chemical index of alteration ( $\text{CIA} = \text{Al}_2\text{O}_3/(\text{Al}_2\text{O}_3 + \text{CaO} + \text{Na}_2\text{O} + \text{K}_2\text{O}) \times 100$ ) is an indicator of major element changes due to weathering and the conversion of feldspars, volcanic glass and other labile components to clay minerals (Nesbitt and Young, 1982; Andersson and Worden, 2004). Analysed sandstones and siltstones have been grouped depending on the stratigraphy, with the mean chemical compositions and standard deviations of these groups reported in Appendix D.

### 5.3.1 Tanqua depocentre

#### 5.3.1.1 Skoorsteenberg Formation

The Skoorsteenberg Formation sandstones are classified as litharenites (Figure 5.1). The sandstones range in  $\text{SiO}_2$  between 68.89 and 77.28 wt.% (avg. = 74.79 wt.%,  $n = 17$ ) (Appendix C). In the Harker plots, some of the major elements ( $\text{Al}_2\text{O}_3$  and  $\text{MgO}$ ) show a decrease with  $\text{SiO}_2$ , whereas the trends on the  $\text{TiO}_2$  and  $\text{Fe}_2\text{O}_3^{\text{T}}$  diagrams are due to dissolution, as shown by the auto-correlations (Figure 5.2). The sandstones show weak

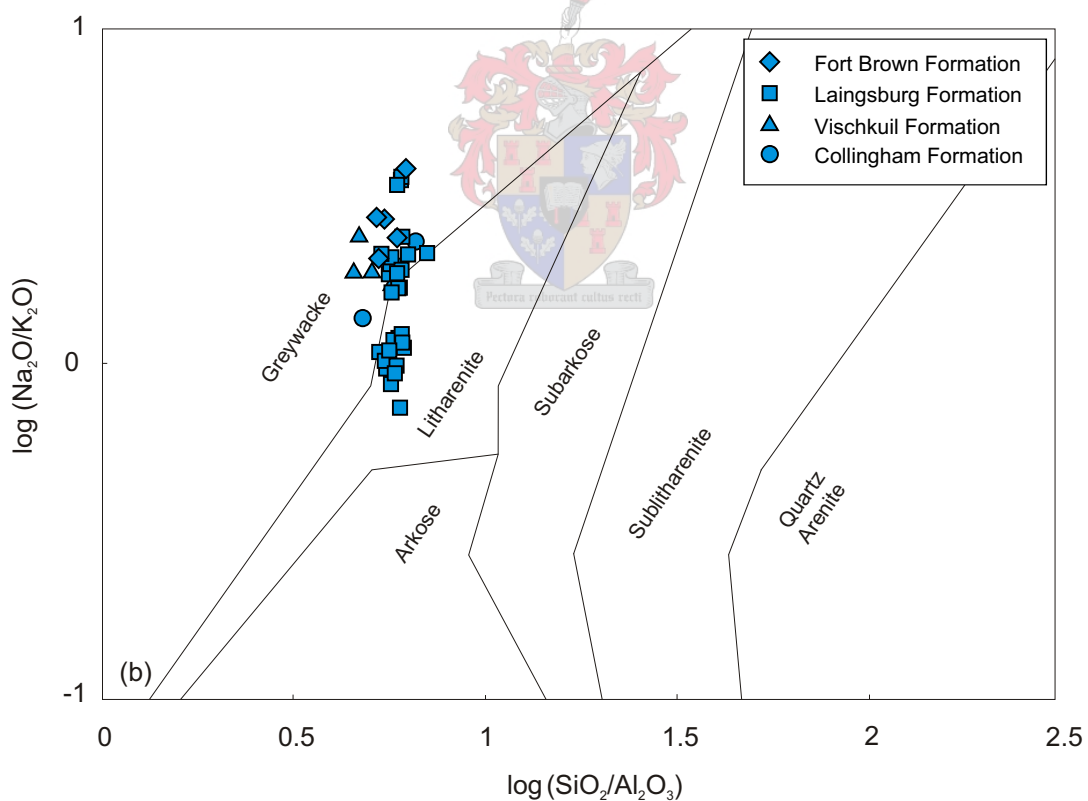
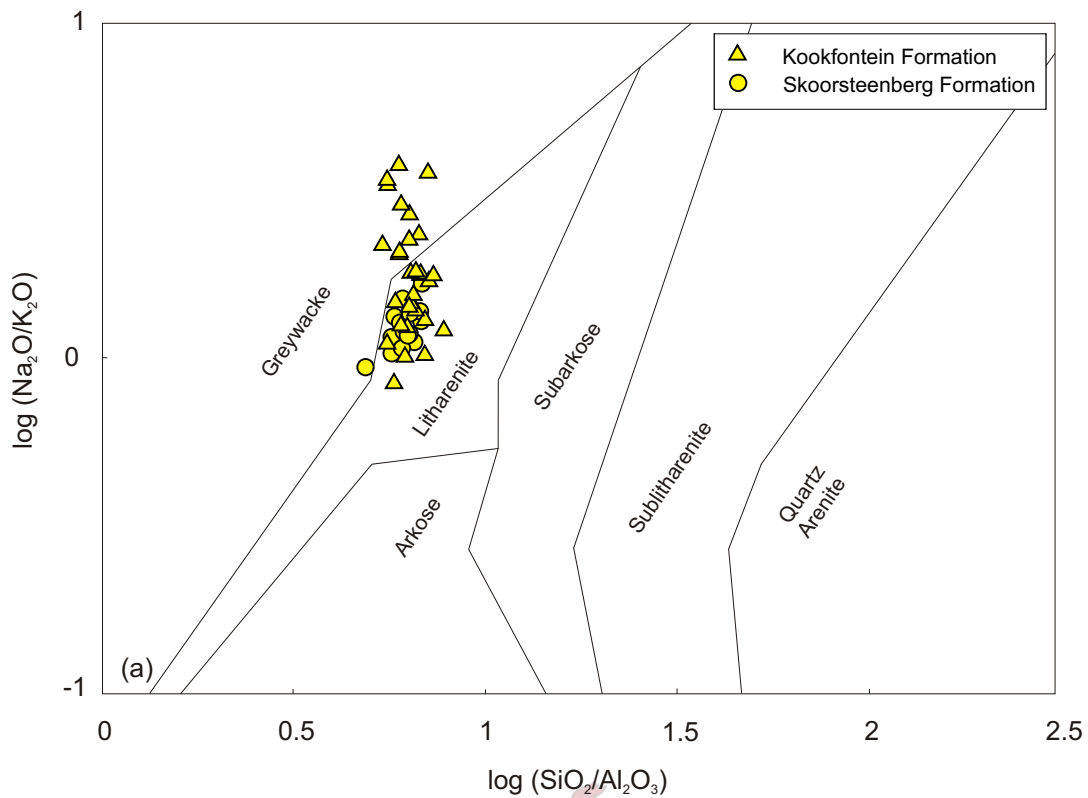


Figure 5.1 The classification of sandstones using  $\log (\text{Na}_2\text{O}/\text{K}_2\text{O})$  vs.  $\log (\text{SiO}_2/\text{Al}_2\text{O}_3)$  from Pettijohn *et al.* (1972) with the boundaries redrawn by Herron (1988) after Rollinson (1993). Sandstones from the Tanqua and Laingsburg depocentres, respectively, are plotted together based on the assumption that they had the same provenance. (a) Sandstones from the Skoorsteenberg Formation (basin-floor deposits) and Kookfontein Formation (slope and deltaic deposits) (Tanqua depocentre). (b) Sandstones from the Laingsburg Formation (basin-floor and slope deposits) and Fort Brown Formation (deltaic deposits) (Laingsburg depocentre).

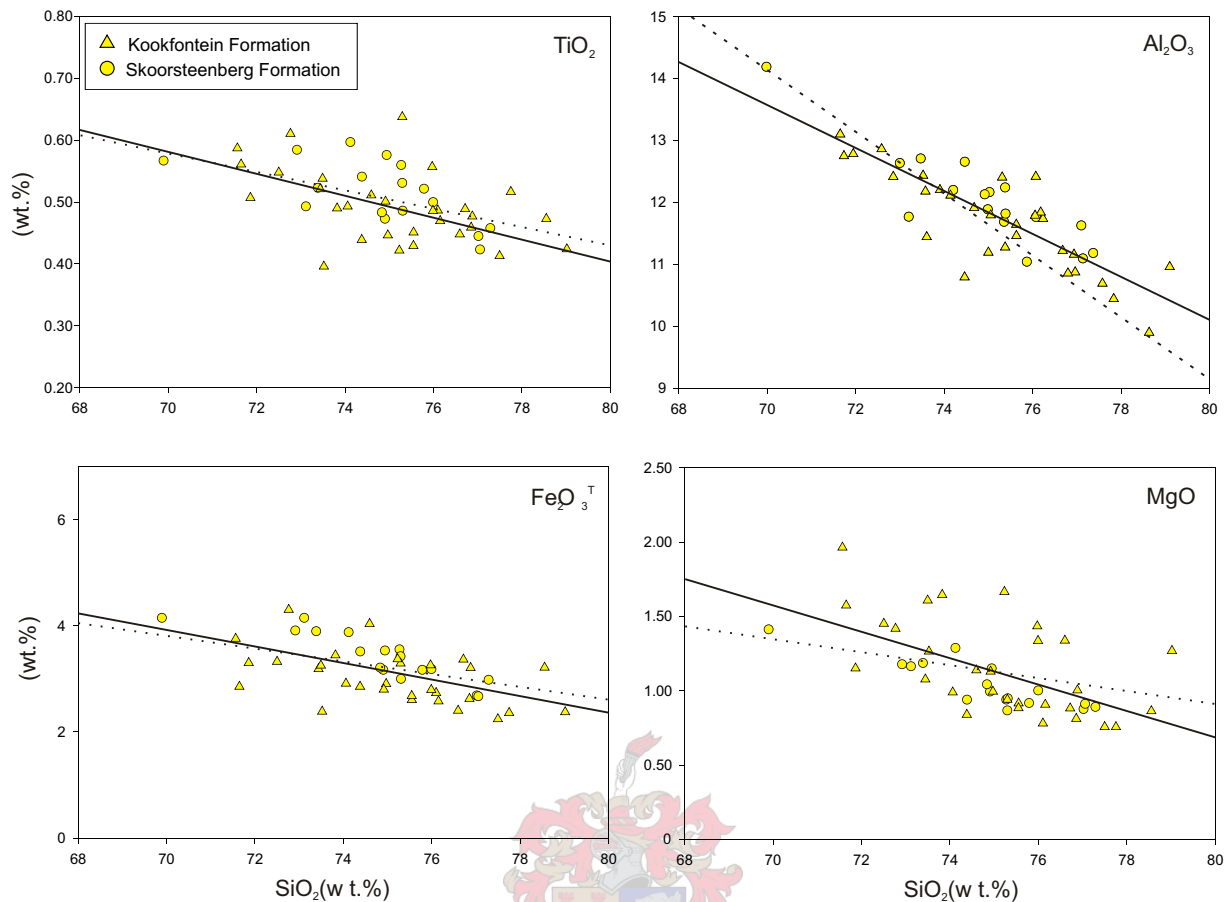


Figure 5.2 Harker variation diagrams for quartz-rich sandstones from the Tanqua depocentre. The increase in  $\text{SiO}_2$  reflects an increased mineralogical maturity, i.e. a greater quartz content and a smaller proportion of detrital grains (after Rollinson, 1993). The solid line shows the data regression line, whereas the dashed line shows the auto-correlation (dissolution trend).

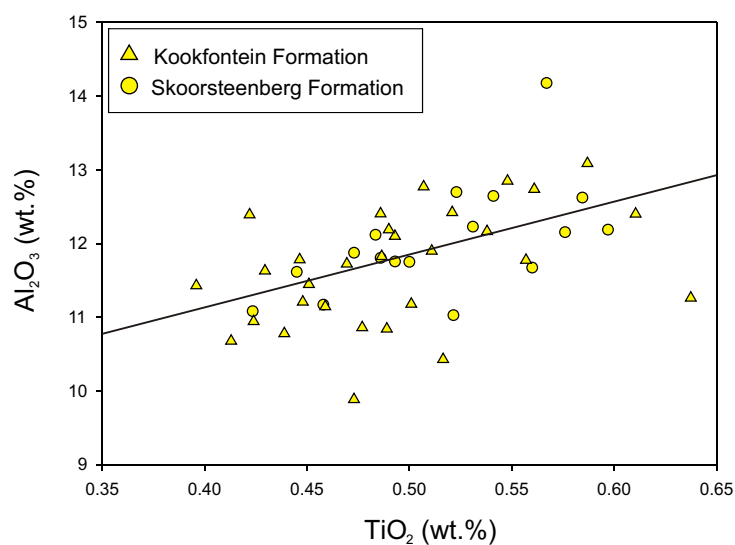


Figure 5.3 Diagram of  $\text{TiO}_2$  vs.  $\text{Al}_2\text{O}_3$  of sandstones from the Tanqua depocentre, to determine the accumulation of immobile elements and chemical weathering in the provenance (method after Young and Nesbitt, 1998).

positive correlation of  $\text{TiO}_2$  with  $\text{Al}_2\text{O}_3$  (Figure 5.3). There is no change in  $\text{TiO}_2/\text{Al}_2\text{O}_3$  against the individually measured stratigraphic intervals (V7, V8, V9 and V10).

Sandstones of the Skoorsteenberg Formation all have CIA values ranging from 65 to 69 (avg. = 67.41, n = 17) (Appendix C). There is no apparent correlation between  $\text{SiO}_2$  and CIA (Figure 5.4). CIA is represented in a ternary diagram (Figure 5.5), in which the sandstones plot in the NASC field.

Diagrams of major element ratios plotted against palaeocurrent direction of Unit 5, indicate no apparent correlations with  $\text{K}_2\text{O}/(\text{K}_2\text{O} + \text{CaO})$  or  $\text{TiO}_2/\text{Al}_2\text{O}_3$  (Figure 5.6). Variation diagrams of major elements against stratigraphic position in the Skoorsteenberg Formation indicate that  $\text{K}_2\text{O}$  decreases up the succession; whereas  $\text{Na}_2\text{O}$  and  $\text{CaO}$  show very weak increases and  $\text{MgO}$  show no change (Figure 5.7).

Multi-element and log multi-element spider diagrams show enrichment and depletion in various elements, depending on whether the Skoorsteenberg Formation sandstones were normalised to averages of granite, basalt, NASC, upper crust and Phanerozoic quartz arenite (Figure 5.8). The least amount of variation for the major elements is when normalised to average granite composition, except for the elements Ni, Co, Cr and Ce.

### 5.3.1.2 Kookfontein Formation

Sandstones from the Kookfontein Formation are classified as litharenites and greywackes (Figure 5.1). They range in  $\text{SiO}_2$  between 71.56 and 79.02 wt.% (avg. = 75.10%, n = 30) (Appendix C). In the Harker plots, some major elements ( $\text{Al}_2\text{O}_3$  and  $\text{MgO}$ ) show a decrease with  $\text{SiO}_2$ , barring  $\text{TiO}_2$  and  $\text{Fe}_2\text{O}_3^{\text{T}}$ , which show no relationship, except for dissolution trends (Figure 5.2). Two siltstones (205 and 207) collected show differences in their compositions (Appendix C). The siltstone (205) with whitish, what was interpreted to be thin calcareous layers, appears to have lower  $\text{SiO}_2$  and  $\text{Na}_2\text{O}$  values than the unaltered siltstone (207), but higher values of  $\text{Al}_2\text{O}_3$ ,  $\text{Fe}_2\text{O}_3^{\text{T}}$ ,  $\text{MgO}$ ,  $\text{K}_2\text{O}$  and loss on ignition (LOI). The sample (206) of alternating sandstone and siltstone exhibits values averaged between those for the sandstones and siltstones.  $\text{TiO}_2$  shows weak positive correlation with  $\text{Al}_2\text{O}_3$  for the sandstones (Figure 5.3). There is no change in  $\text{TiO}_2/\text{Al}_2\text{O}_3$  against the individually measured stratigraphic intervals (V6, V135, V11, V12, V13 and V18).

CIA values for the sandstones from the Kookfontein Formation ranges from 59 to 73 (avg. = 66.00, n = 30) (Appendix C). The sandstones plot in the NASC field on a ternary diagram representing CIA (Figure 5.5).

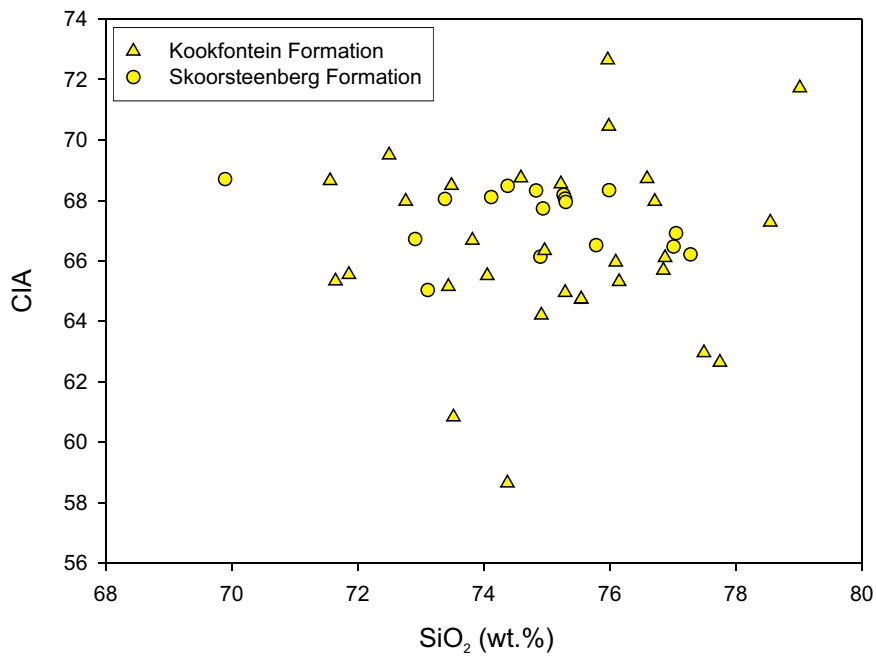


Figure 5.4 CIA vs. SiO<sub>2</sub> for the Tanqua depocentre sandstones (method after Nesbitt and Young, 1982). CIA is a potentially useful index to characterise sediments in terms of the degree of weathering of the sediment source and in terms of variable source terranes.

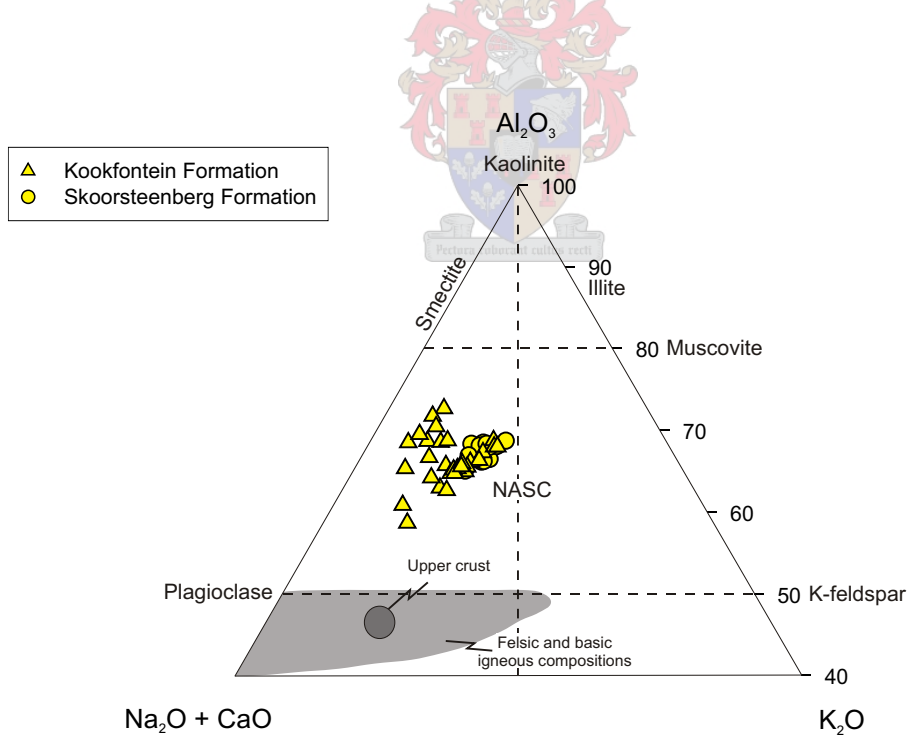


Figure 5.5 CIA as an indicator of the degree of alteration for the Tanqua depocentre sandstones (method after Cingolani *et al.*, 2003). The samples plot mostly in the middle part of the triangle, in the illite-muscovite-plagioclase and illite-plagioclase-K-feldspar compositional fields. NASC = North American Shale Composite.

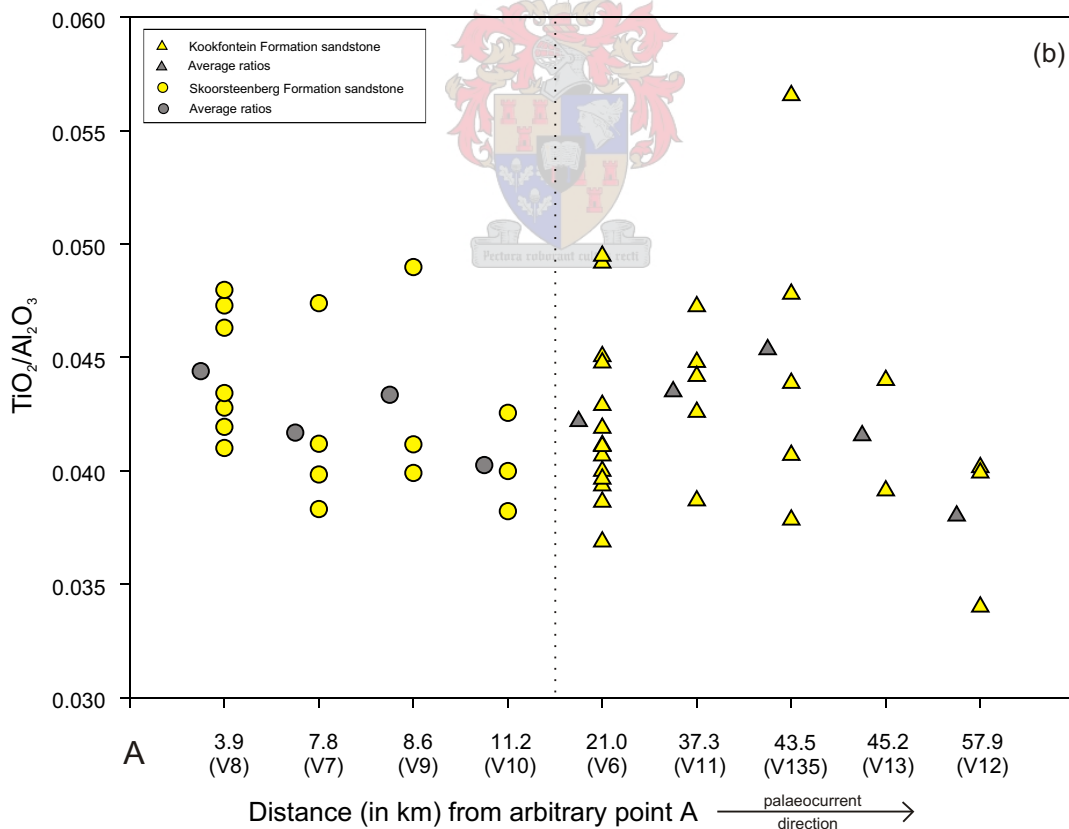
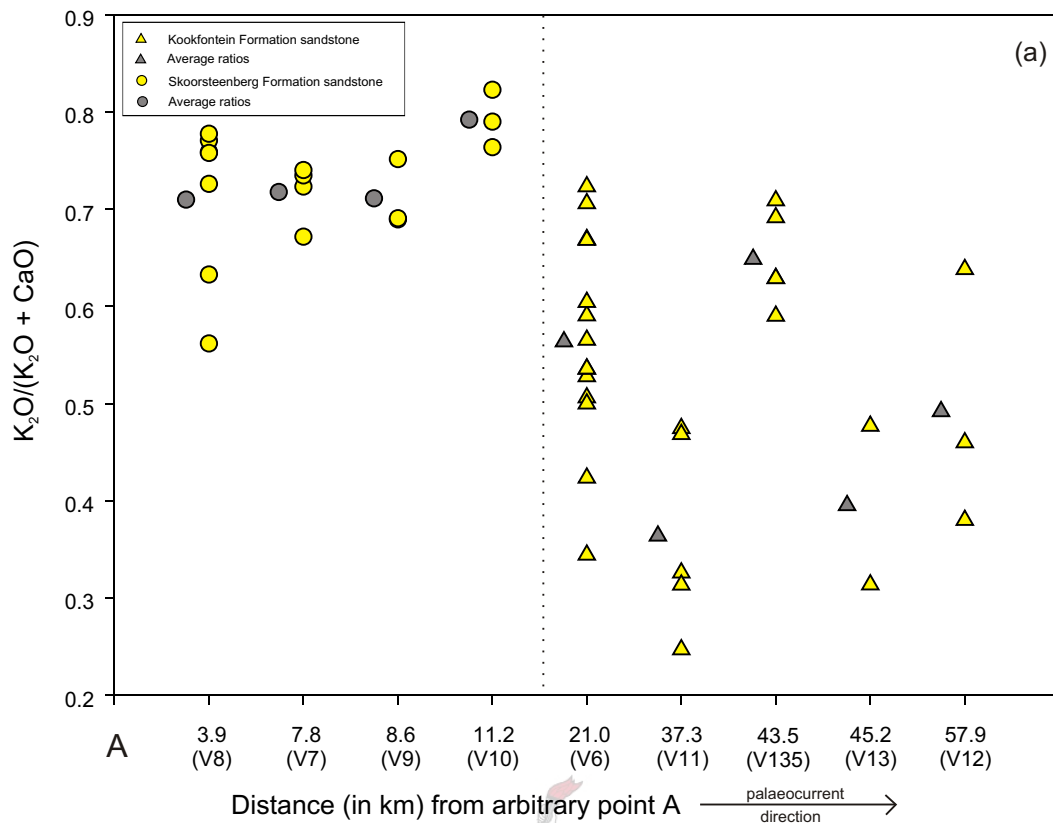
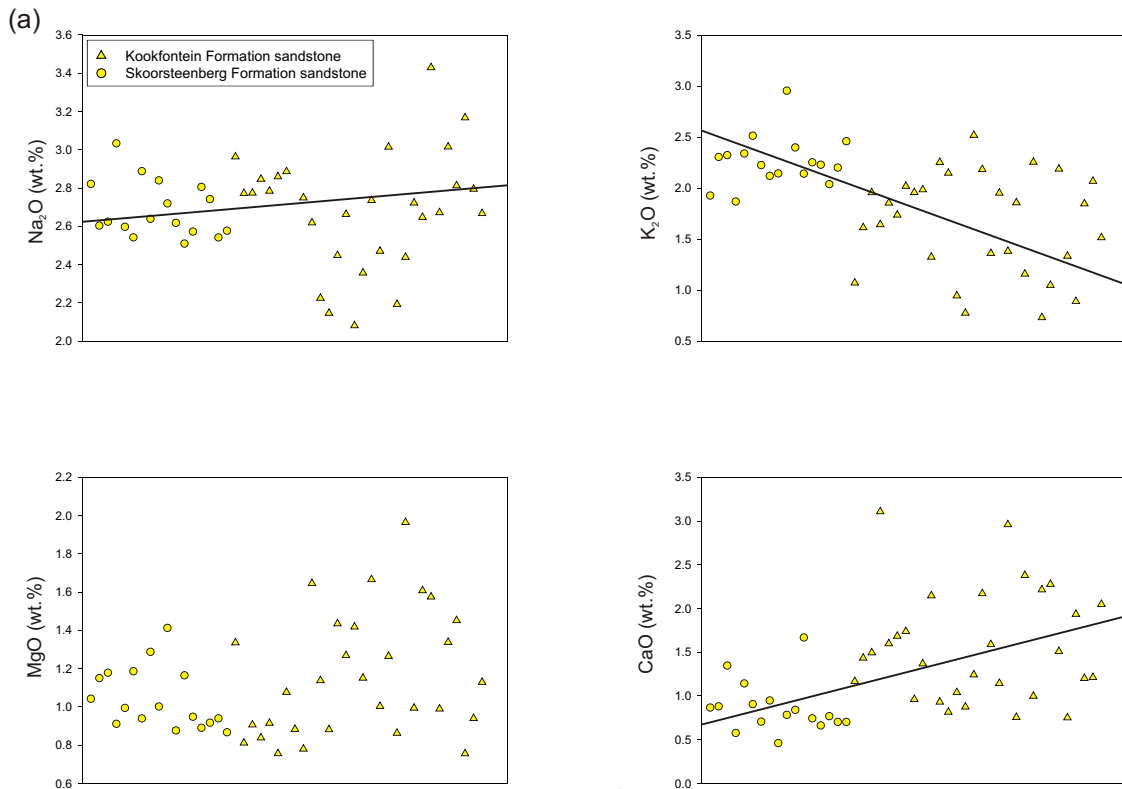
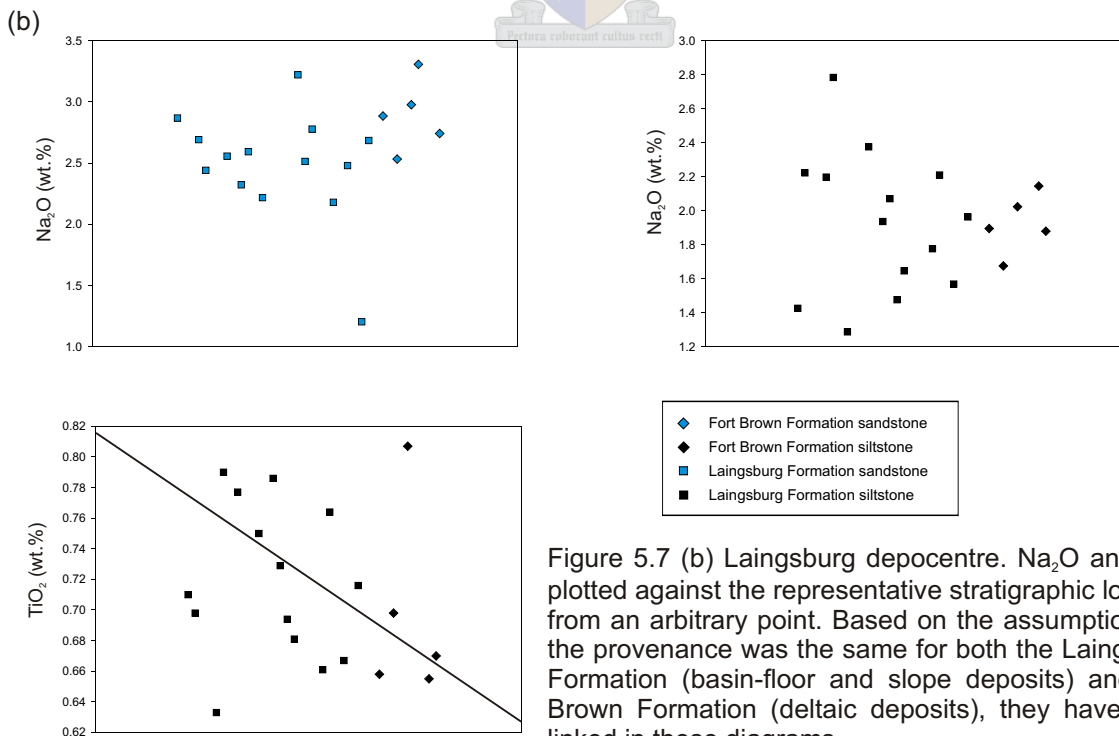


Figure 5.6 Tanqua depocentre sandstones. (a)  $K_2O/(K_2O + CaO)$  and (b)  $TiO_2/Al_2O_3$  ratios plotted against distance (in km) down-current from an arbitrary point A. The dashed line separates the Skoorsteenberg Formation (basin-floor deposits) and Kookfontein Formation (slope and deltaic deposits). Based on the assumption that the provenance was the same for both formations, they have been linked in these diagrams to determine any variations in  $K_2O/(K_2O + CaO)$  and  $TiO_2/Al_2O_3$  ratios with palaeocurrent.



Representative stratigraphic location from an arbitrary point →

Figure 5.7 (a) Tanqua depocentre. Na<sub>2</sub>O, K<sub>2</sub>O, MgO and CaO plotted against the representative stratigraphic location from an arbitrary point. Based on the assumption that the provenance was the same for both the Skoorsteenberg Formation (basin-floor deposits) and Kookfontein Formation (slope and deltaic deposits), they have been linked in these diagrams.



Representative stratigraphic location from an arbitrary point →

Figure 5.7 (b) Laingsburg depocentre. Na<sub>2</sub>O and TiO<sub>2</sub> plotted against the representative stratigraphic location from an arbitrary point. Based on the assumption that the provenance was the same for both the Laingsburg Formation (basin-floor and slope deposits) and Fort Brown Formation (deltaic deposits), they have been linked in these diagrams.

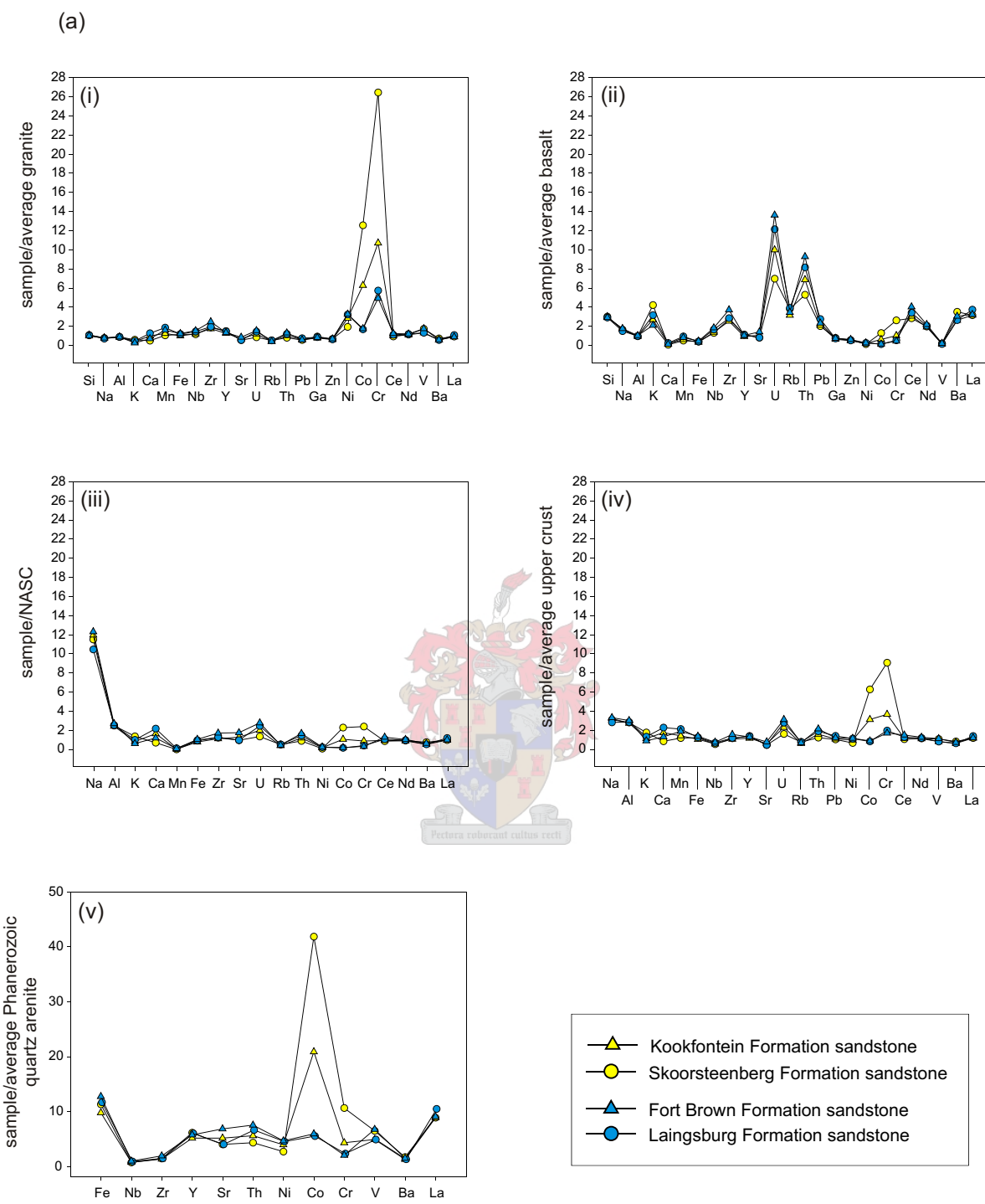


Figure 5.8 (a) Tanqua and Laingsburg depocentres. Multi-element concentrations for the Skoorsteenberg, Kookfontein, Laingsburg and Fort Brown Formations average sandstones normalised to the compositions of average (i) granite, (ii) basalt, (iii) North American Shale Composite (NASC), (iv) upper continental crust, and (v) Phanerozoic quartz arenite (method after Rollinson, 1993). The normalising data are in Table 5.1.

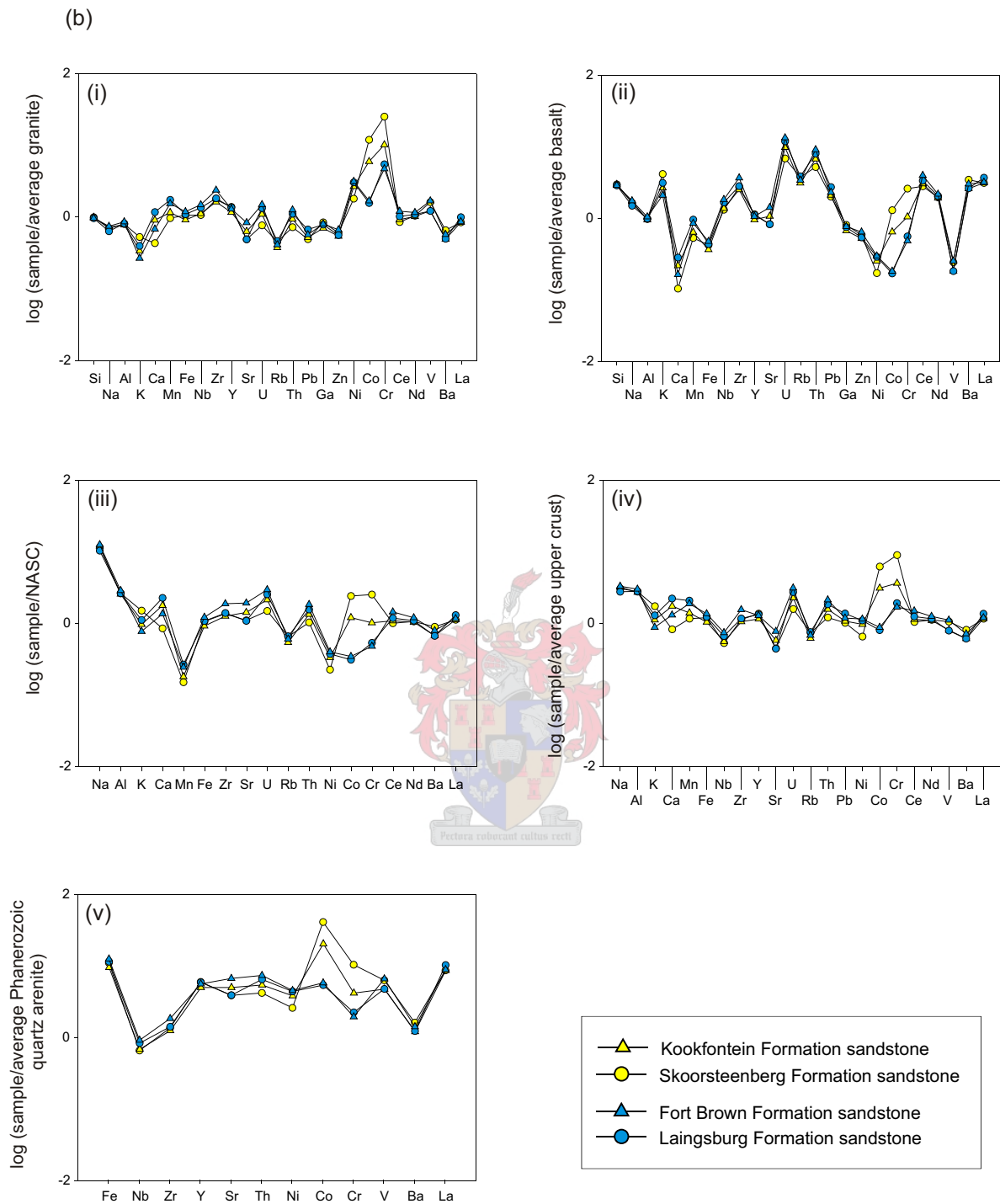


Figure 5.8 (b) Tanqua and Laingsburg depocentres. Log multi-element concentrations for the Skoorsteenberg, Kookfontein, Laingsburg and Fort Brown Formations average sandstones normalised to the compositions of average (i) granite, (ii) basalt, (iii) North American Shale Composite (NASC), (iv) upper continental crust, and (v) Phanerozoic quartz arenite (method after Rollinson, 1993).

Multi-element and log multi-element spider diagrams comparing the Kookfontein Formation sandstones to the normalised compositions of averages for basalt, granite, NASC, upper crust and Phanerozoic quartz arenite, show variations in the major element trends, depending on which composition they were normalised to (Figure 5.8). The diagram comparing the normalised average granite composition to the sandstones show the least variation, except for the elements Ni, Co, Cr and Ce.

### **5.3.1.3 Discussion on trends in the Tanqua depocentre rocks**

Major element oxides of the Tanqua depocentre sandstones are shown with mineral oxides (Figure 5.9). These diagrams show which minerals the oxides in the sandstones are concentrated in. The following is indicated:  $\text{Al}_2\text{O}_3$  in illite, biotite, K-feldspar and albite;  $\text{TiO}_2$  in biotite, muscovite and illite;  $\text{Fe}_2\text{O}_3^{\text{T}}$  in biotite, chlorite and illite;  $\text{Na}_2\text{O}$  in albite; and  $\text{K}_2\text{O}$  in illite and K-feldspar. This corresponds to the main mineral composition of the samples as determined with petrography.

The Kookfontein Formation sandstones have higher  $\text{Na}_2\text{O}/\text{K}_2\text{O}$  and lower  $\text{K}_2\text{O}/(\text{K}_2\text{O} + \text{CaO})$  ratios than the Skoorsteenberg Formation sandstones. This might be due to their slightly higher compositional albite to K-feldspar ratio, as seen with petrographic studies.

The extreme insolubility of  $\text{TiO}_2$  and  $\text{Al}_2\text{O}_3$  in common rock-forming fluids causes them to be the most immobile of oxides during diagenesis. They are highly resistant to weathering in all but the most extreme environments, such as in long-lived weathering profiles in hot and humid conditions (Hill *et al.*, 2000). A correlation between these elements might thus be expected and ratios of these elements may reveal details of the change in provenance of the sediments, or even changes in the weathering environment in the hinterland. Only a weak correlation between  $\text{TiO}_2$  and  $\text{Al}_2\text{O}_3$  can be seen for both the Skoorsteenberg and Kookfontein Formation sandstones. Processes, such as chemical weathering in the source area(s), might have affected these oxides to a different extent. This might be due to the fact that, individually, the  $\text{TiO}_2$  and  $\text{Al}_2\text{O}_3$  contents vary due to dilution by quartz, calcite and other non-clay minerals (Hill *et al.*, 2000).

The CIA vs.  $\text{SiO}_2$  plot show that the Kookfontein Formation sandstones have a much more varied data spread than the Skoorsteenberg Formation sandstones. The alteration of rocks during weathering results in depletion of alkalis and alkaline earths and the preferential enrichment of  $\text{Al}_2\text{O}_3$ . A higher degree of open system diagenesis might have caused more loss of these alkali and alkali earth elements in the sandstones from the Kookfontein Formation. The ternary CIA diagram indicate that samples from both formations plot in the triangles between illite-muscovite-plagioclase and illite-plagioclase-K-feldspar, due to their similar compositions and degrees of alteration. However, it can also be seen that the

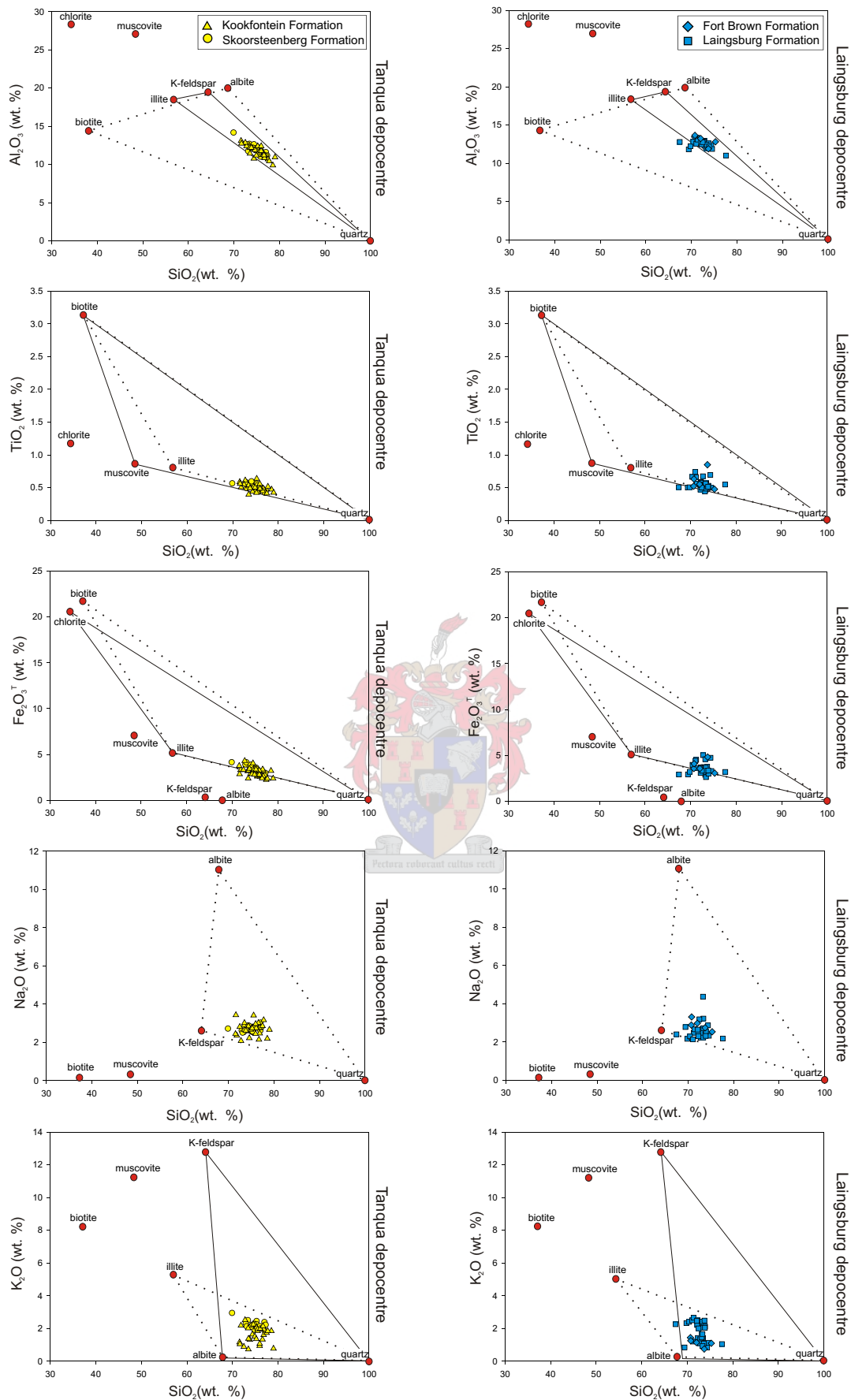


Figure 5.9 Major oxide compositions of Tanqua and Laingsburg depocentre sandstones, plotted with mineral oxides (weight percentage). Triangles show the major compositional fields that the sandstones fall in. Mineral compositions after Deer *et al.* (1992).

Kookfontein Formation sandstones are compositionally generally more enriched in plagioclase than the Skoorsteenberg Formation sandstones, confirming the above statement. Andersson and Worden (2004) found that mudstones of the Skoorsteenberg Formation have, with few exceptions, CIA ratios between 58 and 75, indicating a slightly to moderately weathered source terrane.

The significance of the variations of the Tanqua depocentre sandstones from the average compositions of possible source rocks in the multi-element spider diagrams, show how likely it was that the sediments were derived from these specific rock types. The smaller the variations, or the less the number of variations, the closer the rocks are compositionally, and the more likely that the source(s) had a similar composition.

### **5.3.2 Laingsburg depocentre**

#### **5.3.2.1 Laingsburg Formation**

Laingsburg Formation sandstone classification, based upon a bivariate plot of the log of major element ratios, identifies the rocks primarily as litharenites, and secondary as greywackes (Figure 5.1). The sandstones range in  $\text{SiO}_2$  between 67.45 and 77.62 wt.% (avg. = 72.62 wt.%,  $n = 30$ ) (Appendix C). The siltstones show  $\text{SiO}_2$  values of 58.25 to 69.63 wt.% (avg. = 65.09 wt.%,  $n = 14$ ). In the Harker plots for the sandstones,  $\text{Al}_2\text{O}_3$  shows weak negative correlation with  $\text{SiO}_2$ , whereas  $\text{Fe}_2\text{O}_3^{\text{T}}$  shows no correlation (Figure 5.10). The Harker variation diagrams for the major elements of the siltstones show a positive correlation of  $\text{SiO}_2$  with  $\text{TiO}_2/\text{Al}_2\text{O}_3$ , and negative correlations with  $\text{Fe}_2\text{O}_3^{\text{T}}$  and  $\text{MgO}$ , whereas  $\text{Al}_2\text{O}_3$  shows auto-correlation or a dissolution trend with  $\text{SiO}_2$  (Figure 5.10). The sandstones and siltstones show positive correlation of  $\text{TiO}_2$  with  $\text{Al}_2\text{O}_3$  (Figure 5.11).

Sandstones of the Laingsburg Formation have CIA values ranging from 53 to 75 (avg. = 67.46,  $n = 30$ ), whereas the siltstones show values of 73 to 81 (avg. = 77.53,  $n = 14$ ) (Appendix C). There is also a negative correlation between  $\text{SiO}_2$  and CIA for the siltstones, whereas the sandstones show no obvious correlation (Figure 5.12). On a ternary diagram representing CIA (Figure 5.13), the sandstones plot in the NASC field, whereas the siltstones plot mostly in this field as well, although some in and around the muscovite composition.

Variation diagrams of major elements against the stratigraphic column for the Laingsburg Formation indicate that  $\text{TiO}_2$  decreases upward in the succession for the siltstones, whereas  $\text{Na}_2\text{O}$  show no correlation in either the sandstones or siltstones (Figure 5.7).

Multi-element spider diagrams show enrichment and depletion in various elements, depending on whether the Laingsburg Formation sandstones were normalised to averages of

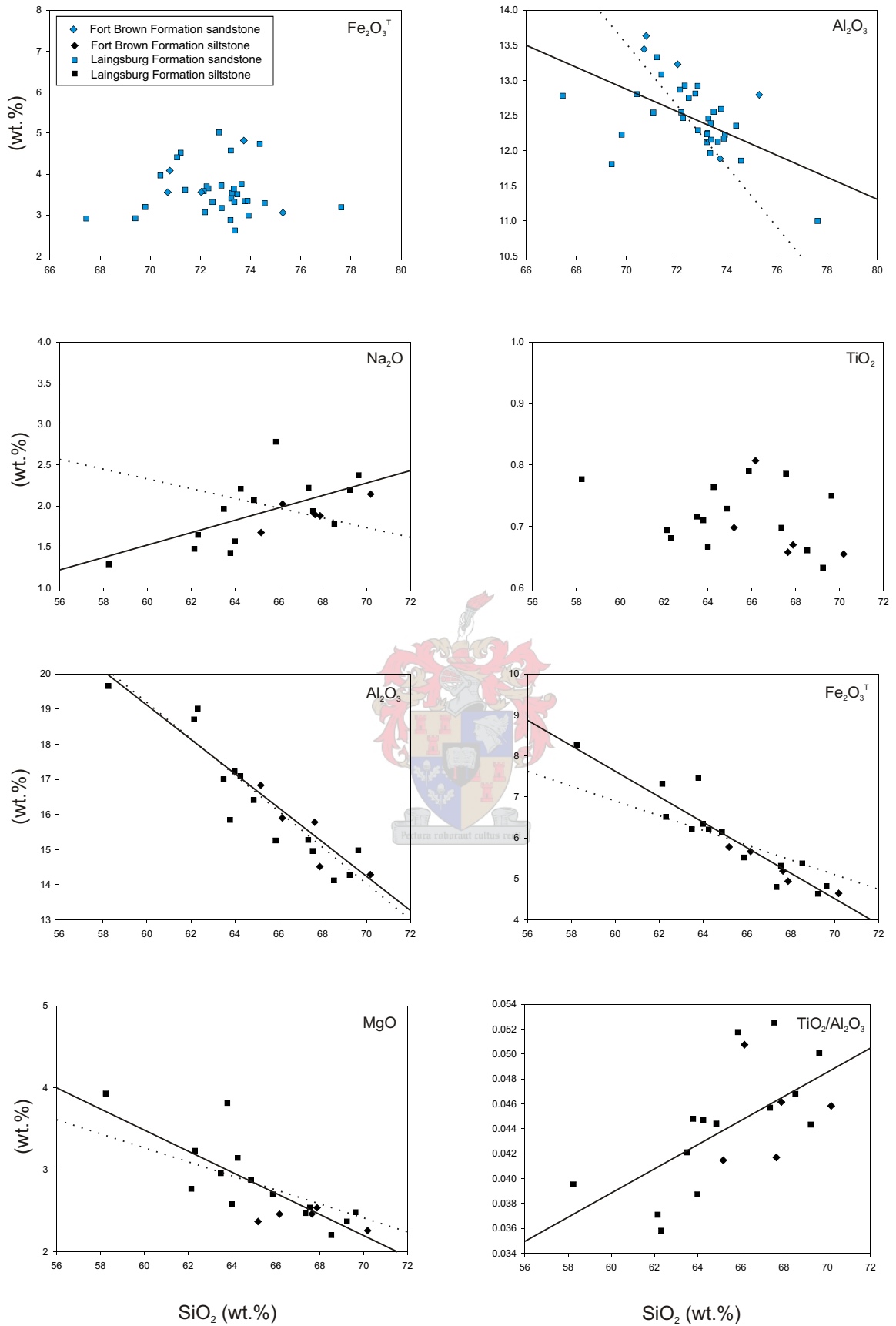


Figure 5.10 Harker variation diagrams for sandstones and siltstones from the Laingsburg depocentre. The increase in  $\text{SiO}_2$  reflects an increased mineralogical maturity, i.e. greater quartz content and a smaller proportion of detrital grains (after Rollinson, 1993). The solid line shows the data regression, whereas the dashed line shows the auto-correlation (dissolution trend).

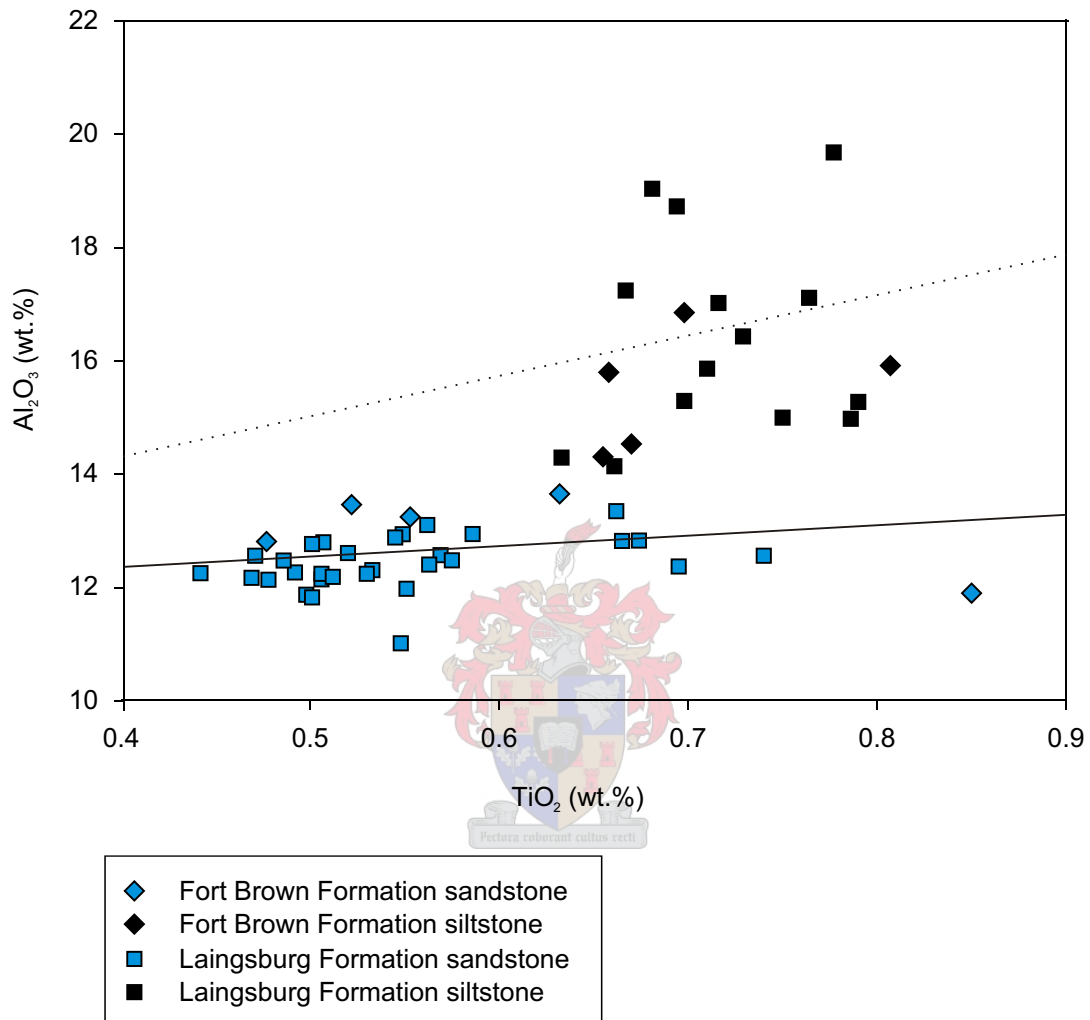


Figure 5.11 Diagram of  $\text{TiO}_2$  vs.  $\text{Al}_2\text{O}_3$  of sandstones and siltstones from the Laingsburg depocentre, to determine the accumulation of immobile elements and chemical weathering in the source area(s) (method after Young and Nesbitt, 1998). The sandstones and siltstones from the Laingsburg Formation (basin-floor and slope deposits) and Fort Brown Formation (deltaic deposits) are shown on the same diagram to discriminate between any differences in the oxides concentrated in different sediment size fractions, as well as differences in the sediments between the formations. The dashed line shows the data regression for the siltstones, whereas the solid line shows the data regression for the sandstones.

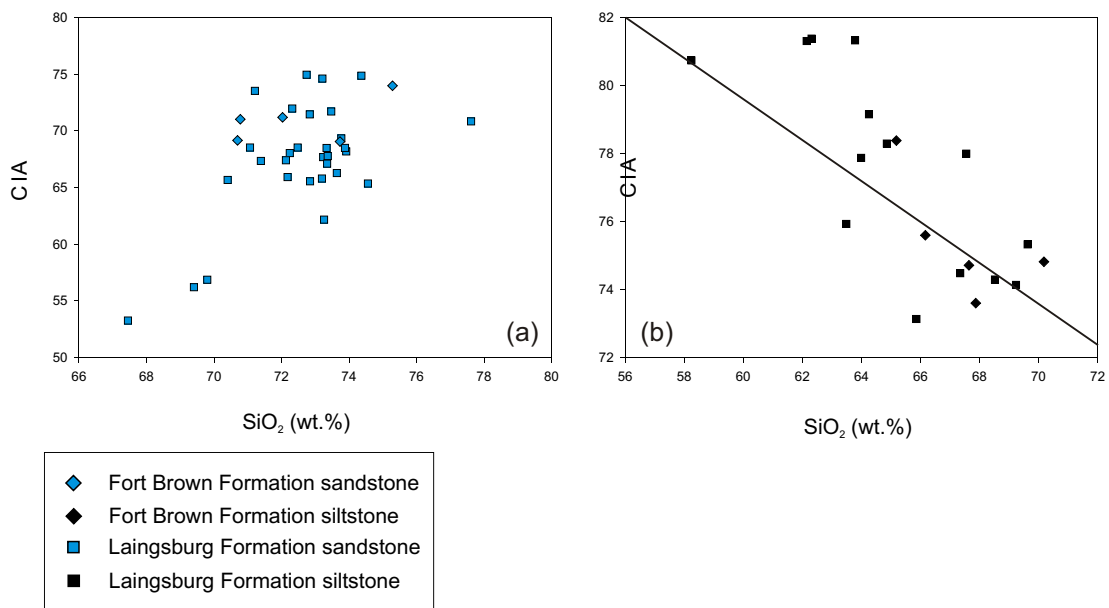


Figure 5.12 CIA vs. SiO<sub>2</sub> for the Laingsburg depocentre (a) sandstones and (b) siltstones (method after Nesbitt and Young, 1982). CIA is a potentially useful index to characterise sediments in terms of the degree of weathering of the sediment source and in terms of variable source terranes.

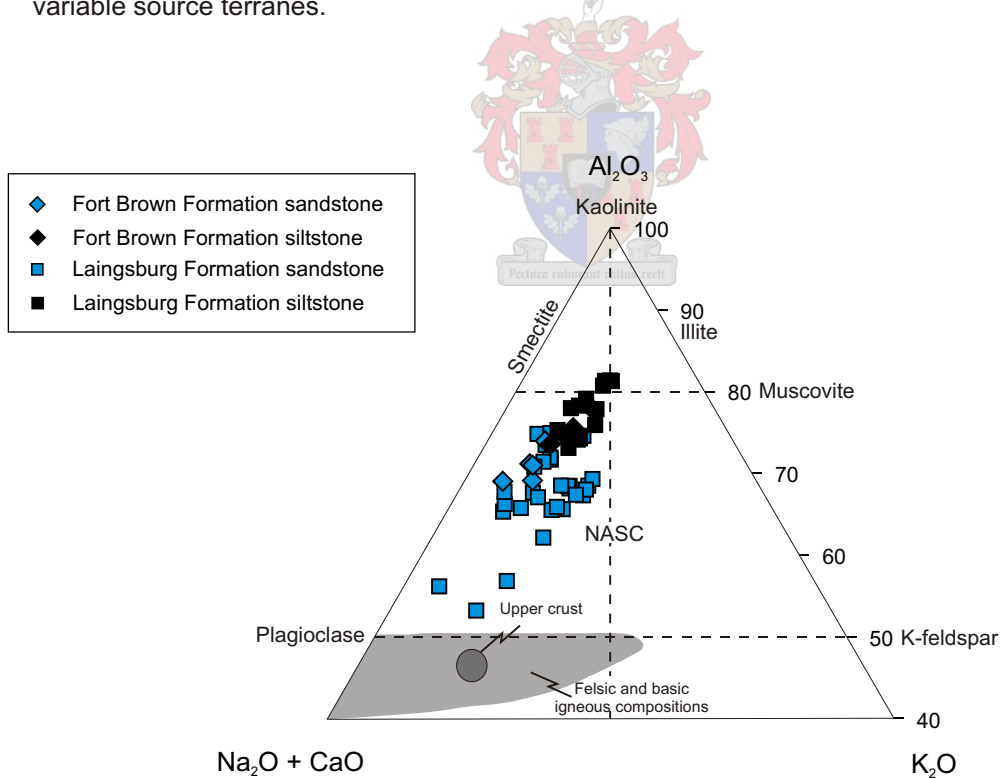


Figure 5.13 CIA as an indicator of the degree of alteration for the Laingsburg depocentre sandstones and siltstones (method after Cingolani *et al.*, 2003). The sandstones plot mostly in the middle part of the triangle, in the illite-plagioclase-K-feldspar field, whereas the siltstones plot closer to the muscovite and illite compositions. NASC = North American Shale Composite.

granite, basalt, NASC, upper crust and Phanerozoic quartz arenite (Figure 5.8). The least amount of variation for the major elements is when normalised to average granite composition. Based on the sandstone mineralogy identified with petrographic studies, the most probable source(s) to normalise to is granite and upper crust, with a metamorphic element.

### **5.3.2.2 Fort Brown Formation**

The Fort Brown Formation sandstones are classified as greywackes (Figure 5.1). They range in  $\text{SiO}_2$  between 70.70 and 75.29 wt.% (avg. = 72.51%, n = 5) (Appendix C). The siltstones have  $\text{SiO}_2$  values ranging from 65.19 to 70.18 wt.% (avg. = 67.41 wt.%, n = 5). In the Harker plots for the sandstones,  $\text{Al}_2\text{O}_3$  shows a decrease with  $\text{SiO}_2$  (Figure 5.10). The Harker diagrams for siltstones are more defined, showing positive correlations between  $\text{SiO}_2$  and  $\text{TiO}_2/\text{Al}_2\text{O}_3$  and  $\text{Na}_2\text{O}$ , negative correlations between  $\text{SiO}_2$  and  $\text{Fe}_2\text{O}_3^{\text{T}}$  and  $\text{MgO}$ , and auto-regression (dissolution trend) between  $\text{SiO}_2$  and  $\text{Al}_2\text{O}_3$  (Figure 5.10).  $\text{TiO}_2$  shows weak positive correlation with  $\text{Al}_2\text{O}_3$  for the sand- and siltstones (Figure 5.11).

CIA values for the sandstones from the Fort Brown Formation ranges from 69 to 74 (avg. = 70.88, n = 5), whereas those for the siltstones range from 74 to 78 (avg. = 75.42, n = 5) (Appendix C). The siltstone CIA shows a negative correlation with  $\text{SiO}_2$  (Figure 5.12). The sandstones plot mostly in the illite-plagioclase-K-feldspar field of the ternary diagram of CIA (Figure 5.13), whereas the siltstones plot closer to the muscovite and illite compositions.

$\text{Na}_2\text{O}$  shows no change in either sandstones or siltstones upwards in the Fort Brown Formation succession, whereas  $\text{TiO}_2$  shows a decrease up section in siltstones (Figure 5.7).

Multi-element spider diagrams show enrichment and depletion in various elements, depending on whether the Fort Brown Formation sandstones were normalised to averages of granite, basalt, NASC, upper crust and Phanerozoic quartz arenite (Figure 5.8). The least amount of variation for the major elements is when normalised to average granite composition, which together with varying degrees of influence from possible upper crust and metamorphic sources, are the most likely source rocks based on petrography.

### **5.3.2.3 Discussion on trends in the Laingsburg depocentre rocks**

Major element oxides of the Laingsburg depocentre sandstones are shown with mineral oxides (Figure 5.9). These diagrams show which minerals the oxides in the sandstones are concentrated in. The following is indicated:  $\text{Al}_2\text{O}_3$  in illite, biotite, K-feldspar and albite;  $\text{TiO}_2$  in biotite, muscovite and illite;  $\text{Fe}_2\text{O}_3^{\text{T}}$  in biotite, chlorite and illite;  $\text{Na}_2\text{O}$  in albite; and  $\text{K}_2\text{O}$  in illite and K-feldspar. This corresponds to the main mineral composition of the samples as

determined by petrography. Based on these diagrams, there is very little variation between sandstones from the Laingsburg and Fort Brown Formations.

The increase in the  $\text{TiO}_2/\text{Al}_2\text{O}_3$  ratio with the increase in  $\text{SiO}_2$  in siltstones might indicate that  $\text{TiO}_2$  is a heavy mineral fraction. Further data shows that Ti is in fact concentrated in mica and clay minerals. The co-variance is more likely to be due to a decrease in  $\text{Al}_2\text{O}_3$  with an increase in  $\text{SiO}_2$  in the siltstones, a result of dissolution between these two oxides.

The positive correlation between  $\text{Al}_2\text{O}_3$  and  $\text{TiO}_2$  for sandstones is much weaker than that for the siltstones (Figure 5.11). The concentrations of these oxides are more evenly distributed in the siltstone, since it contains more Al and Ti bearing minerals, such as chlorite, biotite and illite than the sandstones. This diagram shows that  $\text{TiO}_2$  is coming in from the fine fraction, also indicating that it is not a heavy mineral fraction.

The siltstones of the Laingsburg depocentre show a negative correlation between  $\text{SiO}_2$  and CIA. The mudstones of the Skoorsteenberg Formation (Tanqua depocentre) show a negative correlation between CIA and  $\text{SiO}_2$  as well (Andersson and Worden, 2004). A possible grain size control on the individual CIA values is suggested, since higher  $\text{SiO}_2$  contents will be induced by a higher quartz silt or sand content. However, the sandstones from neither the Tanqua, nor the Laingsburg depocentre, show any correlation between CIA and  $\text{SiO}_2$ . The CIA ternary diagram shows that the siltstones plot closer to the illite composition than the sandstones, which indicates a higher degree of alteration.

#### ***5.3.2.4 Discussion on the major element chemistry of the Tanqua and Laingsburg depocentres***

The mineralogy of the studied samples is reflected by their geochemistry, with sandstones having higher  $\text{SiO}_2$  and correspondingly lower  $\text{Al}_2\text{O}_3$  as a consequence of their higher quartz content, and depletion in  $\text{K}_2\text{O}$ ,  $\text{Fe}_2\text{O}_3^{\text{T}}$  and  $\text{TiO}_2$ , relative to the siltstones of the same age, reflecting their higher content in clay and clay-sized phases. Andersson and Worden (2004) found mineralogical and geochemical differences between the interfan and intrafan mudstones of the Skoorsteenberg Formation mudstones and attributed these differences as being the result of changes in relative sea-level.

The geochemical composition of the Tanqua depocentre sandstones analysed is consistent with that of litharenites (lithic arenites). The sandstones from the Kookfontein Formation that were identified as greywackes are all from sections measured in the northeastern part of the study area (V11 – V13). A possible explanation for this difference in classification from the rest of the sandstones from both the Skoorsteenberg and Kookfontein Formations is that during burial, reactions with clay minerals, dissolution of unstable grains,

precipitation of authigenic minerals and mixing with waters from other sources may have modified the pore waters to different degrees. Petrography shows that the differences must be due to secondary processes, since the detrital mineralogy of these sandstones are similar to the rest of the sandstones from the Tanqua depocentre. Greywacke can be used as a term to include both feldspathic and lithic arenites. Feldspathic arenites include all sandstones that contain less than 90% quartz and more feldspars than rock fragments, whereas lithic arenites include all sandstones that contain less than 90% quartz and more rock fragments than feldspars.

The Laingsburg depocentre sandstones analysed have the geochemical composition of litharenites and greywackes in the Laingsburg Formation and greywackes in the Fort Brown Formation. Sandstone classification based on geochemistry [ $\log (\text{SiO}_2/\text{Al}_2\text{O}_3)$  vs.  $\log (\text{Na}_2\text{O}/\text{K}_2\text{O})$ ] thus shows differences in the overall composition of the sandstones, with the Tanqua depocentre sandstones being slightly more mature than the Laingsburg depocentre sandstones. Petrography shows the Laingsburg depocentre sandstones to have more detrital lithic fragments than the Tanqua depocentre sandstones.

An increase in mineralogical maturity is reflected by an increase in  $\text{SiO}_2$ , i.e. greater quartz content and a smaller proportion of detrital grains. The  $\text{SiO}_2$  content for the Tanqua depocentre sandstones from the Skoorsteenberg Formation have an average of 74.79 wt.% (standard deviation = 1.81;  $n = 17$ ), whereas the Kookfontein Formation sandstones have an average  $\text{SiO}_2$  content of 75.10 wt.% (standard deviation = 1.98;  $n = 30$ ). The sandstones are thus very similar, although all relatively immature. Sandstones from the Laingsburg Formation have an average  $\text{SiO}_2$  content of 72.62 wt.% (standard deviation = 1.84;  $n = 30$ ) and the Fort Brown Formation sandstones an average  $\text{SiO}_2$  content of 72.51 wt.% (standard deviation = 1.98;  $n = 5$ ). The Laingsburg depocentre sandstones are thus geochemically less mature than the Tanqua depocentre sandstones.

The  $\text{K}_2\text{O}$  and  $\text{Na}_2\text{O}$  concentrations for the Skoorsteenberg Formation sandstones are generally the same, indicating a possible equal amount of K-feldspar and plagioclase. This is also true for some of the Kookfontein Formation sandstones, although most of them show values for  $\text{Na}_2\text{O}$  higher than for  $\text{K}_2\text{O}$ . The  $\text{Na}_2\text{O}$  values of the Laingsburg and Fort Brown Formation sandstones are all basically double that of their  $\text{K}_2\text{O}$  values. However, the petrography shows that the sandstones do not contain equal amounts of K-feldspar and albite, but do contain illite and mica, which accounts for a large part of the  $\text{K}_2\text{O}$  concentrations.

The litharenites and greywackes of this study contain markedly less silica and considerably more aluminium, sodium, and potassium than do quartz arenites. A poor correlation between quartz content and total  $\text{SiO}_2$  concentration indicates that feldspars, rock

fragments, and other silicate minerals also influence total silica content (Boggs Jr., 1992). The aluminium content is influenced particularly by feldspars, micas, and clay minerals, which are all commonly more abundant in greywackes than in quartz arenites (Boggs Jr., 1992). The greater content of sodium and potassium in greywackes is mainly a function of the higher content of sodium and potassium feldspars in these rocks (Boggs Jr., 1992).

Displacement in the plot of the ratio of  $K_2O/Na_2O$  is affected by the degree of maturity of the sediments, maturity being directly reflected in the relative feldspar ratios (McCann, 1991). These vertical distributions are true for the Skoorsteenberg and Kookfontein Formation sandstones in the Tanqua depocentre and the Laingsburg and Fort Brown Formation sandstones in the Laingsburg depocentre from this study.

The CIA values for the Skoorsteenberg Formation sandstones and Kookfontein Formation sandstones measured range from 65 to 69 and 59 to 73, respectively. CIA values for the Laingsburg Formation sandstones (53 to 75) have a larger range than those for the Fort Brown Formation sandstones (69 to 74), with the lower values of the Laingsburg Formation sandstones indicating a source with less intense chemical weathering in most cases. However, the CIA values for the siltstones from the Laingsburg Formation are slightly higher than those for the Fort Brown Formation siltstones. Finer grained rocks should show stronger evidence of weathering than associated sandstones (McLennan *et al.*, 1990), since a subsidiary control on the CIA value in sedimentary rocks is grain size. In general, coarse-grained siliciclastic materials tend to have a higher feldspar/clay ratio than those that are fine-grained and thereby have lower CIA values (Visser and Young, 1990).

Depletion of alkalis and alkaline earths and preferential enrichment of  $Al_2O_3$  is the result of alteration of rocks during weathering (Cingolani *et al.*, 2003). The ternary diagrams representing CIA (Figures 5.5 and 5.13) show that the sandstones of the Skoorsteenberg, Kookfontein, Laingsburg and Fort Brown Formations are all from an intermediately weathered source. Higher  $SiO_2$  contents will be induced by a higher quartz silt or sand content. The source(s) of the Skoorsteenberg Formation sandstones have undergone moderate weathering, since unweathered rocks give CIA values of around 50, whereas higher values (up to 100) are obtained from rocks that have undergone strong weathering (Visser and Young, 1990). Andersson and Worden (2004) found that the CIA for the mudstones of the Skoorsteenberg Formation indicates that the hinterland did not experience extreme weathering conditions. The range of CIA values for the Kookfontein Formation is much wider, indicating little weathering to a much higher degree of weathering. This is probably due to the change in source area(s). The sediment source terrane for the Skoorsteenberg Formation started out as continental, with a mainly feldspathic composition. It then switched to a mixed provenance for the Kookfontein Formation, which consisted of predominantly lithofeldspathic

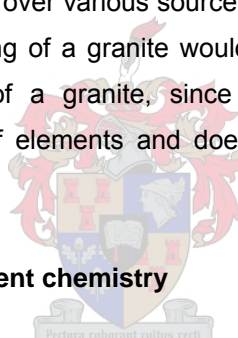
material. The even wider range of CIA values for the Laingsburg Formation sandstones is probably as a result of changes in the source terrane(s) as well.

Comparison between the geochemical data from this study and the average chemical composition of greywackes from other studies show broadly similar chemical composition. It should be noted that the greywackes from these other studies were derived from predominantly acidic precursors of acidic composition (Floyd *et al.*, 1990; Floyd *et al.*, 1991; Floyd and Leveridge, 1987). The similarities in composition might thus point to the fact that the source rocks for the sediments from this study was acidic in composition as well.

Comparing multi-element spider diagrams for the Skoorsteenberg, Kookfontein, Laingsburg and Fort Brown Formations sandstones to the normalised averages of basalt, granite, NASC, upper crust and Phanerozoic quartz arenite, show that their compositions all deviate least from the normalised average granite composition, which indicates that the source terrane(s) were predominantly composed of granitic material.

The normalisation of sediments over various source materials may represent a problem if not carefully considered. Weathering of a granite would not necessarily produce sediments with the geochemical signature of a granite, since the technique presumes complete weathering, complete deposition of elements and does not take into account elements in solution, adsorption and absorption.

## 5.4 Trace and rare earth element chemistry



### 5.4.1 *Tanqua depocentre*

#### 5.4.1.1 *Skoorsteenberg Formation*

The trace elemental variations in the Skoorsteenberg Formation sandstones are as follows: Rb = 61 – 113 ppm, Nb = 11 – 16 ppm, Th = 9 – 15 ppm, Ba = 392 - 765 ppm, Pb = 11 – 19 ppm, U = 0 – 7 ppm and Zr = 220 – 396 ppm (Appendix C). The alternating sandstone and siltstone has higher values of Rb, Ba and Pb and similar values of Nb, Th, U and Zr. The Harker diagrams (Figure 5.14) illustrate a weak negative correlation between SiO<sub>2</sub> and Rb, and weak positive correlations between Rb and Al<sub>2</sub>O<sub>3</sub>, Fe<sub>2</sub>O<sub>3</sub><sup>T</sup> and K<sub>2</sub>O; TiO<sub>2</sub> and Zr and V; and MgO and Pb. The correlation between K<sub>2</sub>O and Rb are only for K<sub>2</sub>O values above 1.50 wt.%. Compared to NASC the sandstones are similar in Th and U, depleted in Rb and Ba and enriched in Zr. Anomalous values for Cr have been found in sandstone samples (203, 204, 227, 228 and 230) above and below deposits with soft-sediment deformation (V7 and V8).

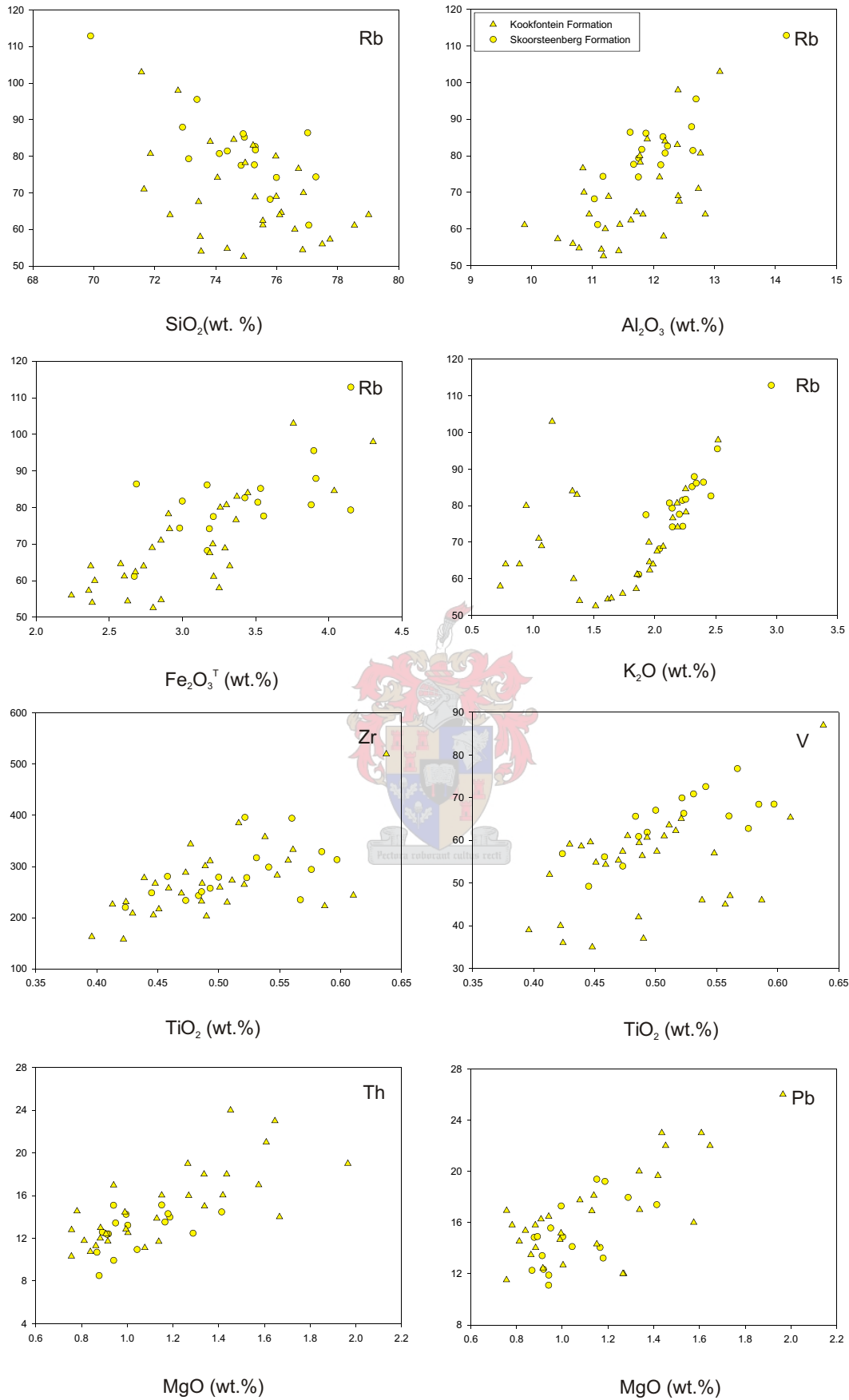


Figure 5.14 Harker diagrams for quartz-rich sandstones from the Tanqua depocentre, showing variations of trace elements (in ppm) with major elements.

Diagrams of trace elements and trace element ratios against the palaeocurrent direction of the slope fan indicate no change in Zr, whereas Th/(Th + Y) show a weak increase with the flow direction (Figure 5.15). Sr is fairly low and constant and there are no changes in Zr, Rb and La up the Skoorsteenberg Formation stratigraphic section (Figure 5.16).

The Skoorsteenberg Formation sandstones show average values of La = 35 ppm (n = 17), Ce = 67 ppm (n = 17) and Nd = 29 ppm (n = 17) (Appendix D). Compared to NASC, the sandstones are slightly enriched in La and Ce, and slightly depleted in Nd.

Multi-element spider diagrams of the Skoorsteenberg Formation sandstones, normalised to averages of basalt, granite, upper crust, NASC and Phanerozoic quartz arenite, show a pattern similar to that of the normalised average upper crust and average granite (Figure 5.8). The sandstones are, however, enriched in Ni, Co and Cr compared to average granite (Figure 5.8).

#### **5.4.1.2 Kookfontein Formation**

The Kookfontein Formation sandstones are characterised as follows: Rb = 53 – 103 ppm, Nb = 10 – 18 ppm, Th = 10 – 24 ppm, Ba = 273 - 633 ppm, Pb = 9 – 26 ppm, U = 0 – 9 ppm and Zr = 158 – 519 ppm; whereas the siltstones show higher values of Rb, Nb and Pb, similar values of Th, Ba and U and lower values of Zr (Appendix C). The Harker diagrams (Figure 5.14) show weak positive correlations between Rb and  $\text{Al}_2\text{O}_3$ ,  $\text{Fe}_2\text{O}_3^T$  and  $\text{K}_2\text{O}$ ;  $\text{TiO}_2$  and Zr and V; and MgO and Th and Pb. The correlation between  $\text{K}_2\text{O}$  and Rb are only for  $\text{K}_2\text{O}$  values above 1.50 wt.%. Compared to NASC, the sandstones are similar in Th, Ba, and U, enriched in Zr and depleted in Rb. Anomalous values for Cr have been found in sandstone samples (210, 253 and 257) above and below deposits with soft-sediment deformation (V6 and V135).

There are no changes in Sr, Zr, Rb or La upwards in the Kookfontein Formation stratigraphic succession (Figure 5.16).

Kookfontein Formation sandstone average REE values are as follows: La = 37 ppm (n = 30), Ce = 72 ppm (n = 30) and Nd = 30 ppm (n = 30) (Appendix D). The siltstone values are generally higher at La = 36 ppm (n = 3), Ce = 88 ppm (n = 3) and Nd = 34 ppm (n = 3). Compared to NASC the sandstones are depleted in La, Ce and Nd, whereas the siltstones are very consistent with NASC values.

Kookfontein Formation sandstone multi-element spider diagrams, normalised to averages of basalt, granite, upper crust, NASC and Phanerozoic quartz arenite, show a similar pattern to that of the normalised average upper crust and average granite (Figure 5.8). The sandstones are, however, enriched in Ni, Co and Cr relative to average granite (Figure 5.8).

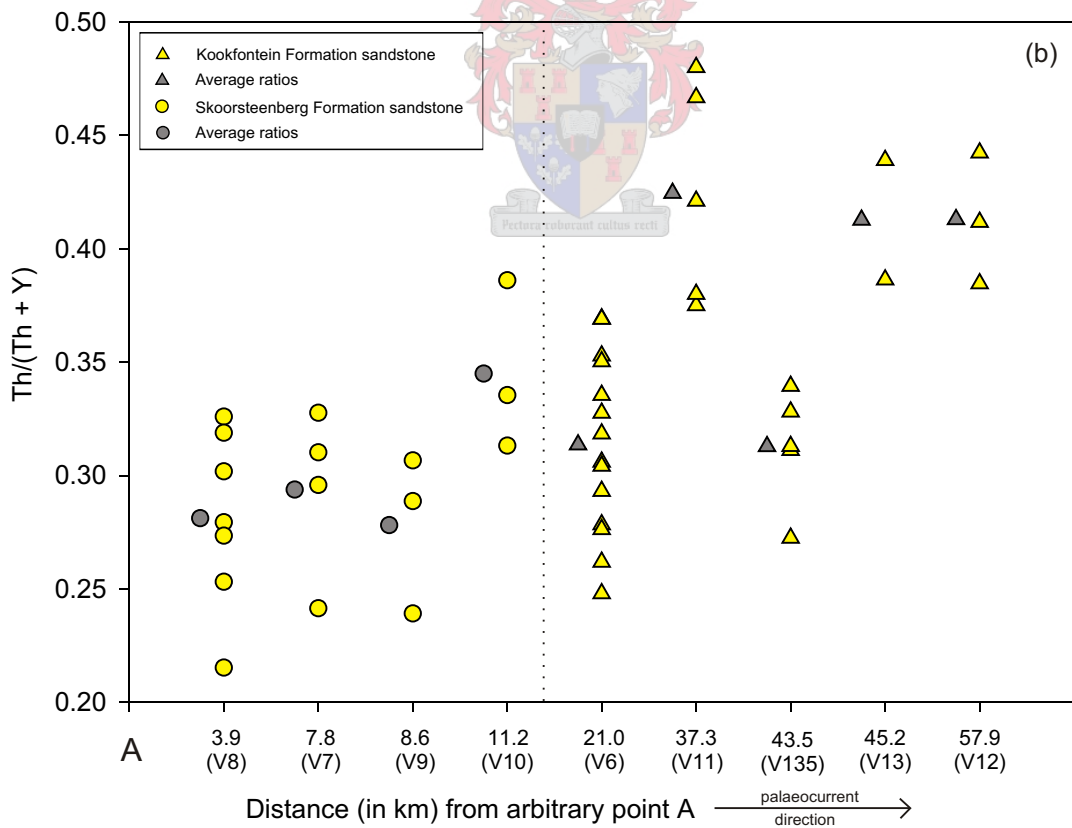
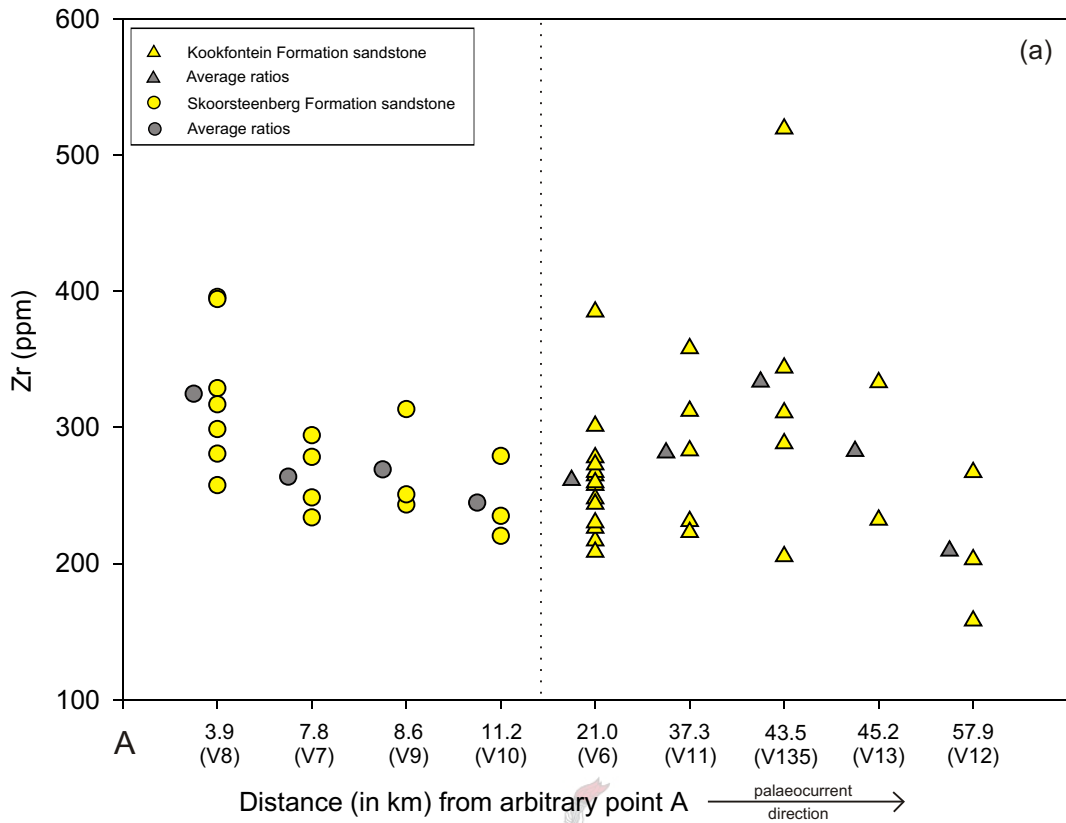


Figure 5.15 Tanqua depocentre sandstones. (a) Zr (ppm) and (b) Th/(Th + Y) ratios plotted against distance (in km) down-current from an arbitrary point A. The dashed line separates the Skoorsteenberg Formation (basin-floor deposits) and Kookfontein Formation (slope and deltaic deposits). Based on the assumption that the provenance was the same for both formations, they have been linked in these diagrams to determine any variations in Zr and Th/(Th + Y) ratios with palaeocurrent.

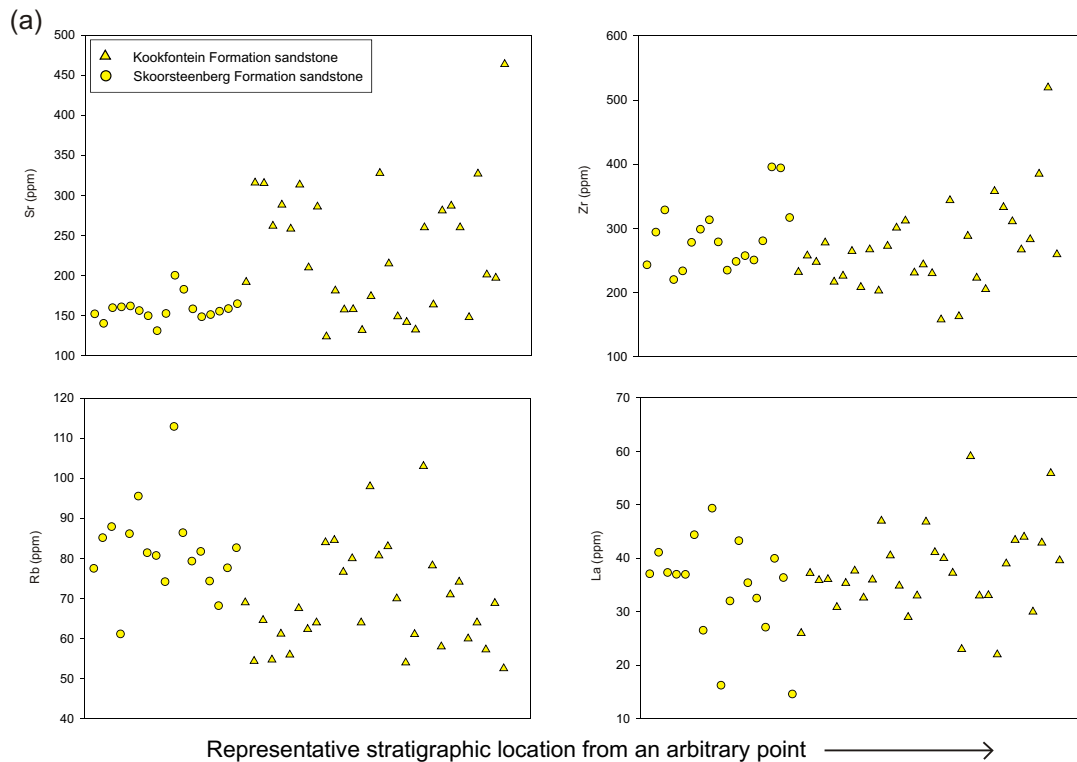


Figure 5.16 (a) Tanqua depocentre. Sr, Zr, Rb and La plotted against the representative stratigraphic location from an arbitrary point. Based on the assumption that the provenance was the same for both the Skoorsteenberg Formation (basin-floor deposits) and Kookfontein Formation (slope and deltaic deposits), they have been linked in these diagrams.

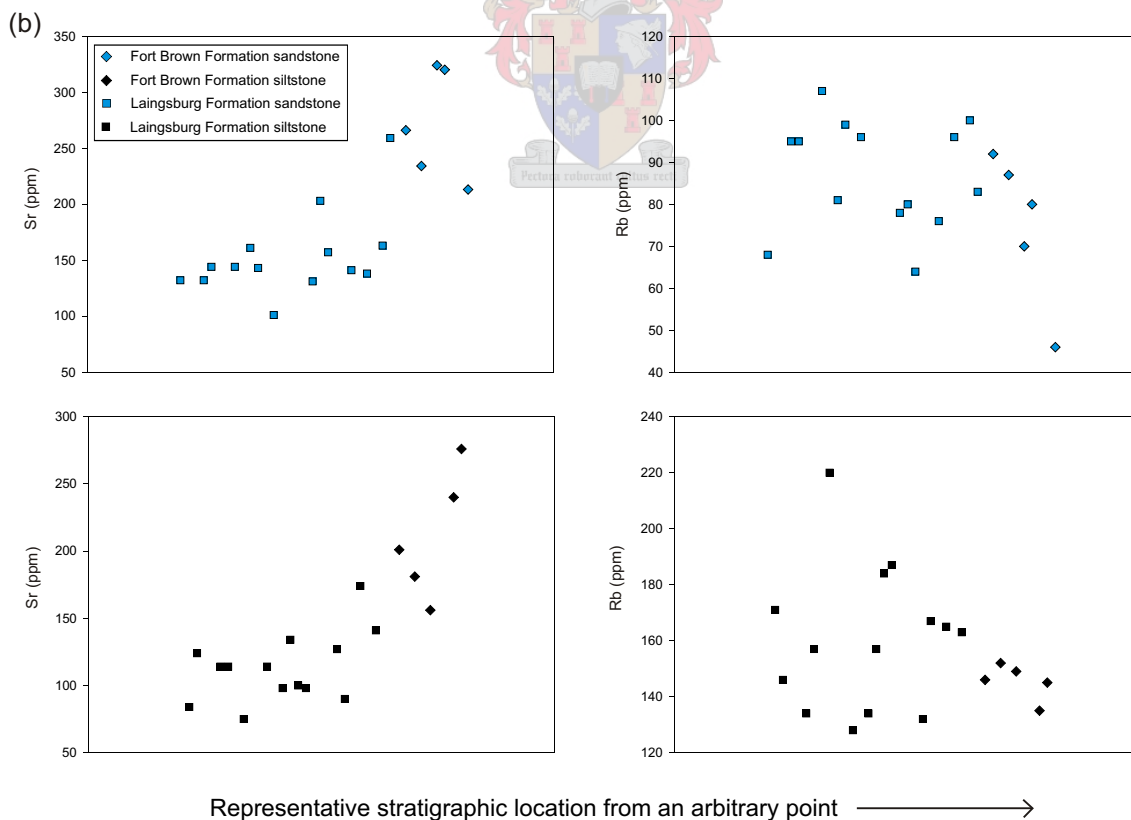


Figure 5.16 (b) Laingsburg depocentre. Sr and Rb plotted against the representative stratigraphic location from an arbitrary point. Based on the assumption that the provenance was the same for both the Laingsburg Formation (basin-floor and slope deposits) and Fort Brown Formation (deltaic deposits), they have been linked in these diagrams.

### 5.4.1.3 Discussion on trends in the Tanqua depocentre rocks

Rb is a mobile element and shows weak positive correlations with  $\text{Al}_2\text{O}_3$ ,  $\text{Fe}_2\text{O}_3^{\text{T}}$  and  $\text{K}_2\text{O}$ . Fe and K are mobile as well, but Al is not. This might show that even though Rb was moved within the system, it was not moved out of the system. Ti - Zr and Ti - V correlate, since they are immobile during hydrothermal alteration and weathering.

Andersson and Worden (2004) found that the chondrite normalised REE pattern for the interfan and intrafan mudstones from the Skoorsteenberg Formation is similar, which suggests that both types of mudstones form part of the same evolutionary pattern and that the sediments have one common origin. The similar evolving REE trend in the intrafan mudstones can also be explained by the mixing of sediment from two weathering terranes with a steadily growing importance of one of them in stratigraphically younger rocks.

The weak increase in  $\text{Th}/(\text{Th} + \text{Y})$  with palaeocurrent direction is a function of an increase in Th concentration. Both Th and Y are immobile. The slight increase is probably due to a change in the source composition(s) for the rocks from the Skoorsteenberg and Kookfontein Formations, as discussed in previous chapters.

The diagram of Sr plotted against the representative stratigraphic location, shows that the values for the Skoorsteenberg Formation sandstones are low and fairly constant, whereas those of the Kookfontein Formation sandstones are more varied. Sr was more mobile in the Kookfontein Formation than in the Skoorsteenberg Formation.



## 5.4.2 Laingsburg depocentre

### 5.4.2.1 Laingsburg Formation

The trace elemental variations in the Laingsburg Formation sandstones are as follows: Rb = 61 – 107 ppm, Nb = 14 – 26 ppm, Th = 15 – 28 ppm, Ba = 270 - 675 ppm, Pb = 11 – 29 ppm, U = 1 – 12 ppm and Zr = 190 - 669 ppm (Appendix C). The siltstones, on average, have higher values, except for Nb and Zr: Rb = 128 – 220 ppm, Nb = 15 – 21 ppm, Th = 19 – 28 ppm, Ba = 460 - 978 ppm, Pb = 20 – 32 ppm, U = 3 – 12 ppm and Zr = 123 - 285 ppm (Appendix C). The sandstone Harker diagrams (Figure 5.17) illustrate weak positive correlations between  $\text{TiO}_2$  and Zr and V. The siltstone Harker diagrams show positive correlations between  $\text{Al}_2\text{O}_3$  and Rb and V; and  $\text{Fe}_2\text{O}_3^{\text{T}}$  and Rb and V, with negative correlations between  $\text{SiO}_2$  and Rb and V (Figure 5.17). Compared to NASC the sandstones are similar in Th and U, depleted in Rb and Ba and enriched in Zr.

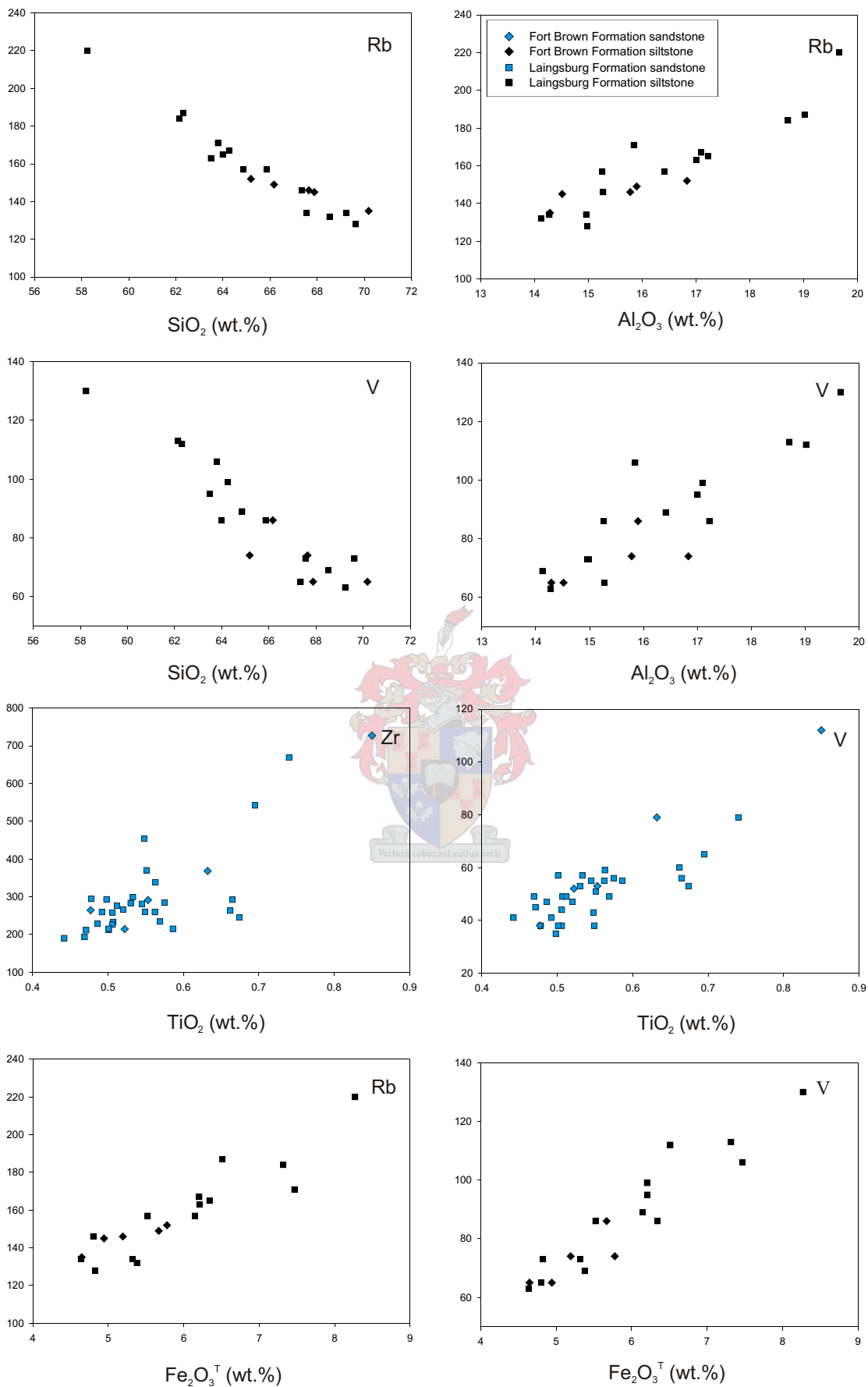


Figure 5.17 Harker diagrams for sandstones and siltstones from the Laingsburg depocentre, showing variations of trace elements (in ppm) with major elements.

Diagrams of trace elements against the Laingsburg Formation stratigraphic location from an arbitrary point show a weak increase in Sr in sandstones and siltstones, and no change in Rb in the rocks, up the succession (Figure 5.16).

The Laingsburg Formation sandstones show average values of La = 35 ppm (n = 30), Ce = 83 ppm (n = 30) and Nd = 30 ppm (n = 30) (Appendix D). Compared to NASC, the sandstones are slightly enriched in La and Ce, and slightly depleted in Nd. The siltstones have the following average values: La = 37 ppm (n = 14), Ce = 109 ppm (n = 14) and Nd = 36 ppm (n = 14) (Appendix D).

The multi-element spider diagrams for the Laingsburg Formation sandstones, normalised to averages of granite, basalt, NASC, upper crust and Phanerozoic quartz arenite, show patterns most closely related to that of the average upper crust and average granite (Figure 5.8). Compared to average granite, the sandstones are enriched in Ni, Co and Cr (Figure 5.8).

#### **5.4.2.2 Fort Brown Formation**

The Fort Brown Formation trace elemental variations in the sandstones are as follows: Rb = 46 – 92 ppm, Nb = 13 – 29 ppm, Th = 19 – 30 ppm, Ba = 363 - 729 ppm, Pb = 12 – 25 ppm, U = 6 – 12 ppm and Zr = 214 - 727 ppm (Appendix C). The siltstones have the following values: Rb = 135 – 152 ppm, Nb = 15 – 21 ppm, Th = 21 – 26 ppm, Ba = 514 - 667 ppm, Pb = 22 – 29 ppm, U = 2 – 12 ppm and Zr = 154 - 226 ppm (Appendix C). The sandstone Harker diagrams (Figure 5.17) illustrate weak positive correlations between  $\text{TiO}_2$  and Zr and V. The siltstone Harker diagrams show positive correlations between  $\text{Al}_2\text{O}_3$  and Rb and V; and  $\text{Fe}_2\text{O}_3^{\text{T}}$  and Rb and V, with negative correlations between  $\text{SiO}_2$  and Rb and V (Figure 5.17). Compared to NASC the sandstones are similar in Th and U, depleted in Rb and Ba and enriched in Zr.

From an arbitrary point diagrams of trace elements against the Fort Brown Formation stratigraphic location show a weak increase in Sr in sandstones and siltstones up the succession, and no change in Rb (Figure 5.16).

The sandstones from the Fort Brown Formation show average values of La = 36 ppm (n = 5), Ce = 96 ppm (n = 5) and Nd = 33 ppm (n = 5) (Appendix D). Compared to NASC, the sandstones are slightly enriched in La and Ce, and slightly depleted in Nd. The siltstones have the following average values: La = 43 ppm (n = 5), Ce = 99 ppm (n = 5) and Nd = 34 ppm (n = 5) (Appendix D).

Comparison of the average composition of Fort Brown Formation sandstones normalised to averages of granite, basalt, NASC, upper crust and Phanerozoic quartz arenite in multi-element spider diagrams, show patterns most similar to that of average upper crust and average granite (Figure 5.8). The sandstones are enriched in Ni, Co and Cr relative to average granite (Figure 5.8).

#### **5.4.2.3 Discussion on trends in the Laingsburg depocentre rocks**

The negative correlations between  $\text{SiO}_2$  and Rb and V, and positive correlations between  $\text{Al}_2\text{O}_3$  and  $\text{Fe}_2\text{O}_3^{\text{T}}$  and these elements, indicate a dissolution effect between  $\text{SiO}_2$  and  $\text{Al}_2\text{O}_3$  and  $\text{SiO}_2$  and  $\text{Fe}_2\text{O}_3^{\text{T}}$ . The behaviour of Rb and V (both mobile elements) are very similar. Rb moves with K in K-feldspar and muscovite and has probably been affected by the alteration of these elements to illite and chlorite. The weak positive correlations between  $\text{TiO}_2$  and Zr and V are only present in the sandstones, and not in the siltstones. This effect is controlled by the concentration of these elements in the heavy fraction.

The diagram of Sr plotted against the representative stratigraphic location show that the values for the Laingsburg and Kookfontein Formation rocks are equally varied. Sr was mobile to the same extent in the sandstones and siltstones of both the formations.

#### **5.4.2.4 Discussion on the trace and rare earth element chemistry of the Tanqua and Laingsburg depocentres**

Zircon is usually concentrated in the coarser, more quartz-rich fraction of sediments, leading to a positive correlation between Zr,  $\text{SiO}_2$  and grain size (Viljoen, 1995). Compared to the siltstones, the sandstones are more enriched in heavy minerals and thus also in elements associated with these heavy minerals, such as: Zr and Nb (zircon, rutile), REE and Th (zircon, apatite, monazite). Th shows affinity for the fine-grained sediments, however, is less grain size dependent than U (Svendsen and Hartley, 2001). Th also shows a much stronger affinity to Zr than U, indicating that Th is a much more dominant heavy mineral component, primarily in zircon and monazite (Hartley, 2001). U is removed under oxidising conditions with V.

The significant difference in the trace and REE composition of the Tanqua and Laingsburg depocentres is that the Laingsburg depocentre sandstones contain higher amounts of Nb, Zr, Sr, U, Rb, Th, Pb, Ni, Ce, Nd and La, but markedly lower amounts of Co and Cr than the Tanqua depocentre sandstones. The amounts for Y, Ga, Zn, V and Ba are similar for the sandstones from both depocentres.

Comparing multi-element spider diagrams for the Skoorsteenberg, Kookfontein, Laingsburg and Fort Brown Formations sandstones to the normalised averages of basalt,

granite, NASC, upper crust and Phanerozoic quartz arenite, show that their compositions all deviate least from the normalised average granite and average upper crust compositions. However, they are all enriched in Ni, Co and Cr, although not to the same extent. The enrichment in these elements in the sandstones from highest to lowest are: Skoorsteenberg, Kookfontein, Laingsburg and Fort Brown Formations. The possibility of contamination during sample preparation, resulting in the high values of Co and Cr, was considered. Fifteen siltstone and sandstone samples were re-analysed at a different facility, using an agate mortar during the sample preparation. The results were found to be consistent.

The highest concentrations of trace elements are found in clay-rich sediments, as can be seen by the higher values found in the siltstones compared to those in the sandstones. It is not possible to draw a correlation between the anomalous Cr values for some of the sandstone samples. Andersson and Worden (2004) studied the mudstones of the Skoorsteenberg Formation (Tanqua depocentre) and found depleted values of Cr, V and Ni. Trace elements such as Zn are considered a better indicator of total clay than  $Al_2O_3$ , since  $Al_2O_3$  is also a dominant component of K-feldspar (Svendsen and Hartley, 2001). The Zn is higher in the siltstones than the sandstones for the samples in this study.

Rare earth elements are insoluble and present in very low concentrations in sea and river water and thus reflect the chemistry of their source. The effects of weathering and diagenesis are minor (Rollinson, 1993). The REE data collected for the Skoorsteenberg and Kookfontein Formation rocks in this study can thus be inferred to reflect the REE compositions of the source rocks. It should, however, be noted that the clay-bearing rocks have higher concentrations of total REE than other sediments and therefore more faithfully represent the provenance (Cullers *et al.*, 1987). The reasons for this are that quartz has a diluting effect on REE concentrations and that the presence of heavy minerals, such as zircon, monazite and allanite, may have a significant but erratic effect on the REE pattern of an individual sample (Rollinson, 1993)

The Nd values for the Skoorsteenberg and Kookfontein Formation sandstones are almost the same, although the La and Ce values differ.

The Laingsburg Formation trace element values for the sandstones and siltstones are generally higher than those of the Fort Brown Formation, except for Pb and Zr.

## **5.5 Tectonic discrimination**

Previous studies of clastic sediments have aimed at using element ratios in various major element provenance diagrams to fingerprint the tectonic or lithological sources of sediment.

### **5.5.1 *Tanqua depocentre***

A discriminant plot of provenance and, by implication, of tectonic setting of sedimentary suites, was used to determine the provenance signatures for both the Skoorsteenberg and Kookfontein Formations (Figure 5.18), indicating a primarily felsic igneous provenance for both. The felsic source reflects acid plutonic and volcanic detritus. The fields are based on analyses of sandstone-mudstone suites from ancient sedimentary successions that were crosschecked against modern sediments from known tectonic setting. Multi-element spider diagrams show the source to be closest in composition to average granite (Figure 5.8).

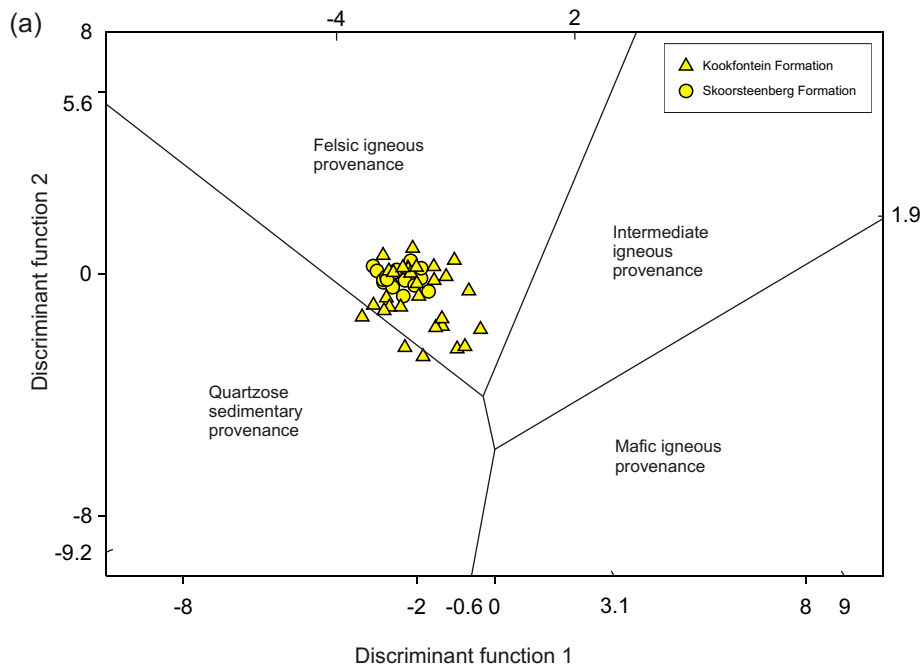
Diagrams based upon bivariate plots of major element oxides and major element oxide ratios are thought to be capable of discriminating provenance tectonic settings (Bhatia, 1983; Roser and Korsch, 1986; Rollinson, 1993). These all indicate an active continental margin as the major tectonic setting for the provenance of the Tanqua depocentre sandstones (Figure 5.19). This could mean either a collisional margin, transform margin or subduction zone. The Tanqua depocentre forms part of the Karoo foreland basin, indicating a subduction zone associated with an arc and orogenic belt as the major tectonic setting.

Diagrams of Th and U show no obvious correlation between these two elements (Figure 5.20). In a plot of Cr/V vs. Y/Ni (Figure 5.21), the sandstone samples of both the Skoorsteenberg and Kookfontein Formations have higher concentration in these elements than the post-Archean Australian Shale (PAAS) and the upper crust (UC). The Cr/Th and Co/Th ratios for the sandstones from the Skoorsteenberg Formation are 27.9 and 5.13, whereas those for the Kookfontein Formation sandstones are 14.1 and 4.03. Differences in these ratios may reflect compositional variation in provenance.

A discrimination diagram of the Ti/Nb ratios (Figure 5.22) shows slightly higher ratios of Ti/Nb for the Tanqua depocentre sandstones when compared to the Laingsburg depocentre sandstones.

### **5.5.2 *Laingsburg depocentre***

A discriminant function diagram of provenance and, by implication tectonic setting of sedimentary suites, was used to determine the provenance signatures for the Laingsburg and Fort Brown Formations (Figure 5.18). The fields are based on analyses of sandstone-mudstone suites from ancient sedimentary successions that were crosschecked against modern sediments from known tectonic setting. The primary signature for the Laingsburg Formation is that of a felsic igneous provenance ( $n = 22$ ), although some samples plot in the quartzose sedimentary provenance field ( $n = 8$ ). This could indicate source mixing or two different source areas. The Fort Brown Formation indicates a felsic igneous provenance

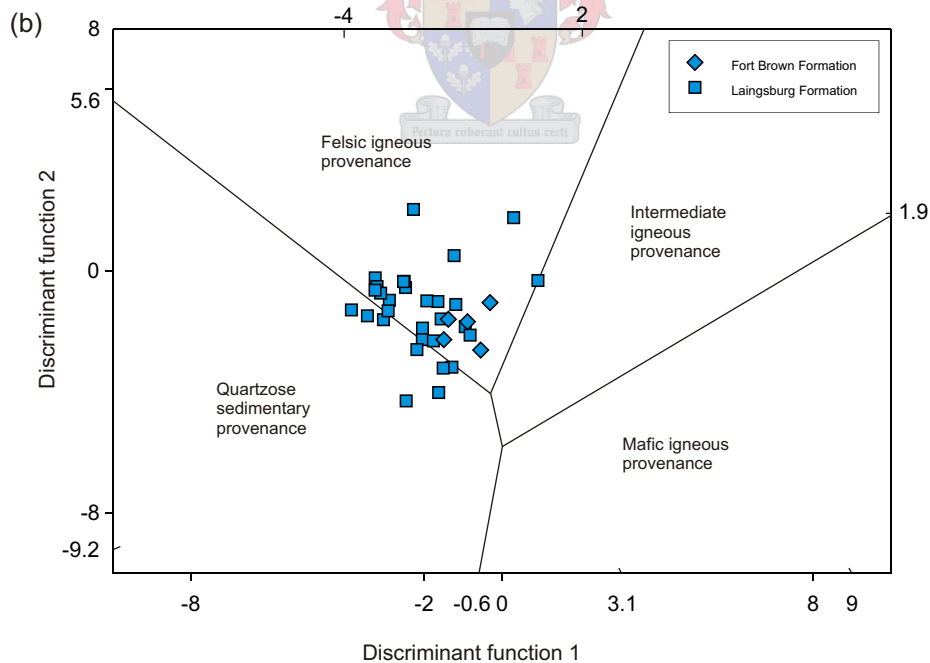


The discriminant functions are:

$$\text{Discriminant function 1} = -1.773\text{TiO}_2 + 0.607\text{Al}_2\text{O}_3 + 0.76\text{Fe}_2\text{O}_3^{\text{T}} - 1.5\text{MgO} + 0.616\text{CaO} + 0.509\text{Na}_2\text{O} - 1.224\text{K}_2\text{O} - 9.09$$

$$\text{Discriminant function 2} = 0.445\text{TiO}_2 + 0.07\text{Al}_2\text{O}_3 - 0.25\text{Fe}_2\text{O}_3^{\text{T}} - 1.142\text{MgO} + 0.438\text{CaO} + 1.475\text{Na}_2\text{O} + 1.426\text{K}_2\text{O} - 6.861$$

Figure 5.18 (a) Tanqua depocentre. Discriminant function diagram for the provenance signatures of sandstone-mudstone suites using major elements. Fields for dominantly mafic, intermediate and felsic igneous provenances are shown with the field for a quartzose sedimentary provenance (method after Roser and Korsch, 1988; Rollinson, 1993).



The discriminant functions are:

$$\text{Discriminant function 1} = -1.773\text{TiO}_2 + 0.607\text{Al}_2\text{O}_3 + 0.76\text{Fe}_2\text{O}_3^{\text{T}} - 1.5\text{MgO} + 0.616\text{CaO} + 0.509\text{Na}_2\text{O} - 1.224\text{K}_2\text{O} - 9.09$$

$$\text{Discriminant function 2} = 0.445\text{TiO}_2 + 0.07\text{Al}_2\text{O}_3 - 0.25\text{Fe}_2\text{O}_3^{\text{T}} - 1.142\text{MgO} + 0.438\text{CaO} + 1.475\text{Na}_2\text{O} + 1.426\text{K}_2\text{O} - 6.861$$

Figure 5.18 (b) Laingsburg depocentre. Discriminant function diagram for the provenance signatures of sandstone-mudstone suites using major elements. Fields for dominantly mafic, intermediate and felsic igneous provenances are shown with the field for a quartzose sedimentary provenance (method after Roser and Korsch, 1988; Rollinson, 1993).

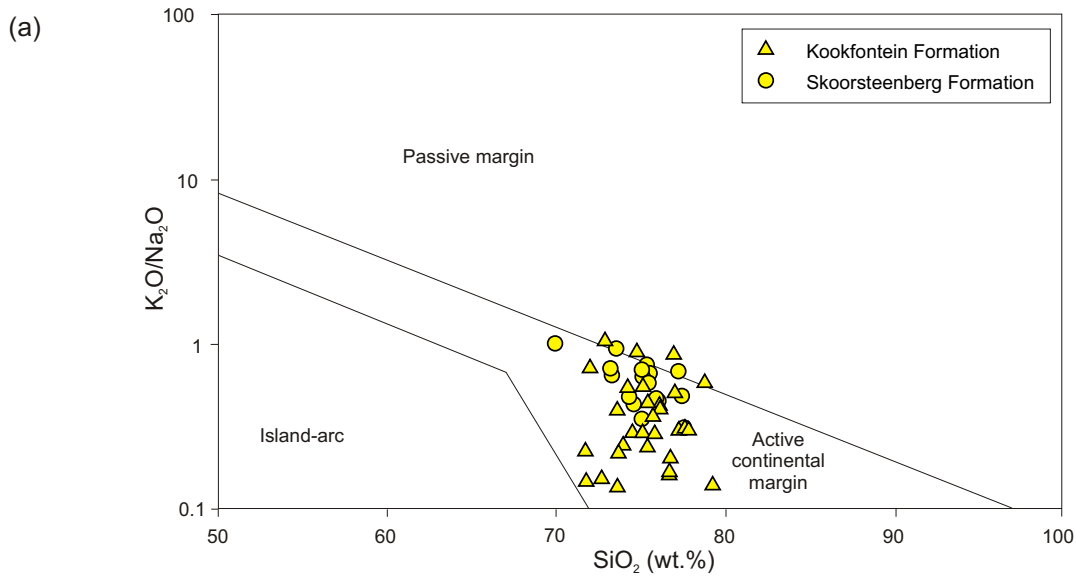


Figure 5.19 (a) Tanqua depocentre.  $\text{SiO}_2$  vs.  $\text{K}_2\text{O}/\text{Na}_2\text{O}$  discriminant plot of tectonic setting (method after Roser and Korsch, 1986).

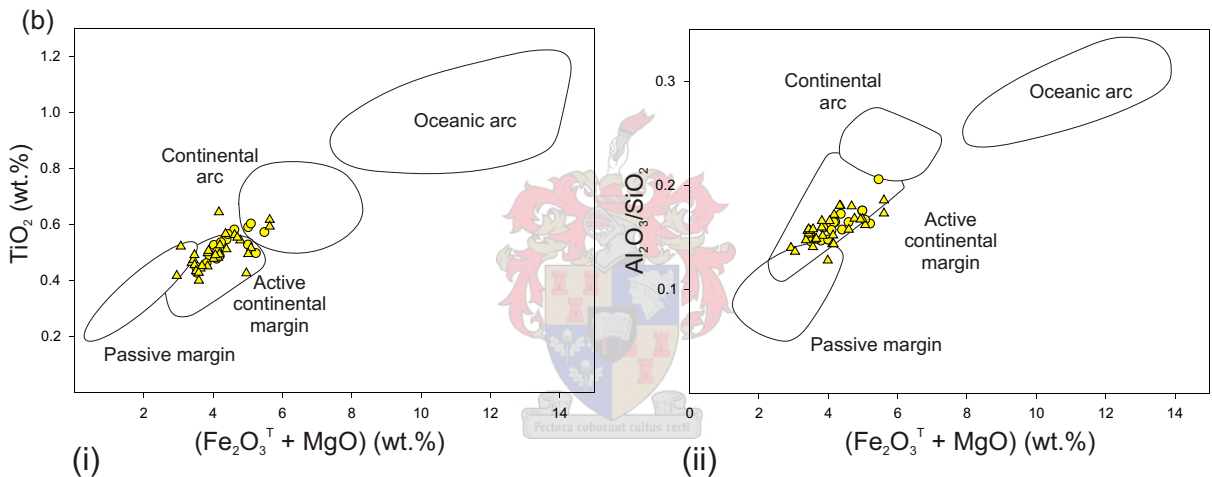


Figure 5.19 (b) Tanqua depocentre. Discrimination diagrams for sandstones, based upon (i) a bivariate plot of  $\text{TiO}_2$  vs.  $(\text{Fe}_2\text{O}_3^T + \text{MgO})$  and (ii) a bivariate plot of  $\text{Al}_2\text{O}_3/\text{SiO}_2$  vs.  $(\text{Fe}_2\text{O}_3^T + \text{MgO})$ . The fields are oceanic island-arc, continental island-arc, active continental margin and passive margin (method after Bhatia, 1983; Rollinson, 1993).

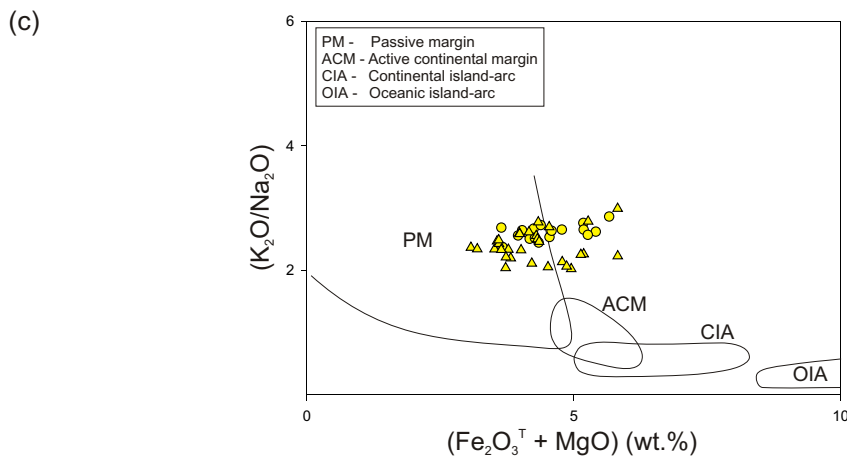


Figure 5.19 (c) Tanqua depocentre. Discrimination diagram for sandstones, based upon a bivariate plot of  $(\text{K}_2\text{O}/\text{Na}_2\text{O})$  vs.  $(\text{Fe}_2\text{O}_3^T + \text{MgO})$ . The fields are oceanic island-arc, continental island-arc, active continental margin and passive margin (method after Bhatia, 1983; Rollinson, 1993).

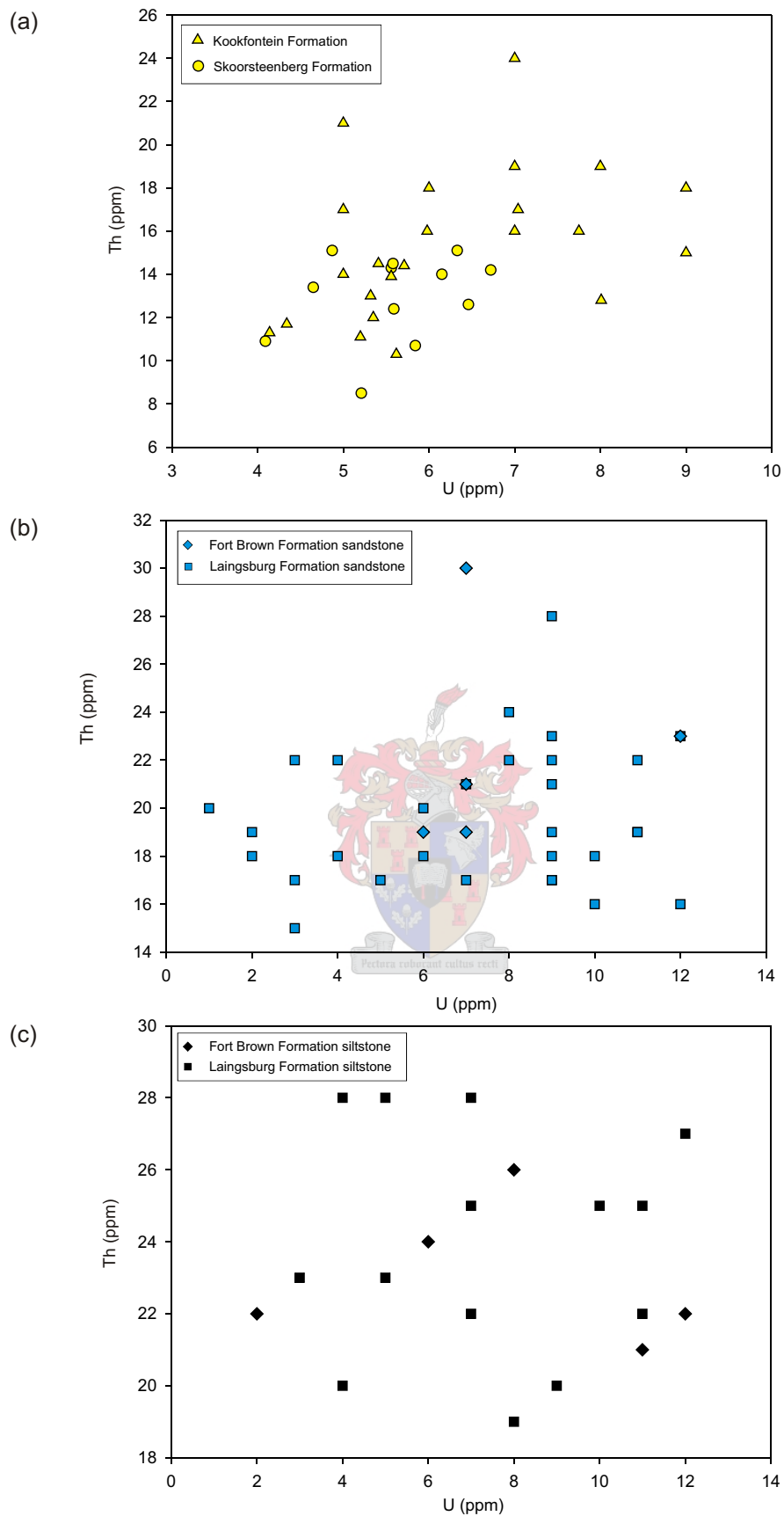


Figure 5.20 (a) Tanqua depocentre. Trace element variation diagram of Th vs. U for sandstones from the Skoorsteenberg Formation (basin-floor deposits) and Kookfontein Formation (slope and deltaic deposits). (b) and (c) Laingsburg depocentre. Trace element variation diagrams of Th vs. U for sandstones and siltstones from the Laingsburg Formation (basin-floor and slope deposits) and Fort Brown Formation (deltaic deposits).

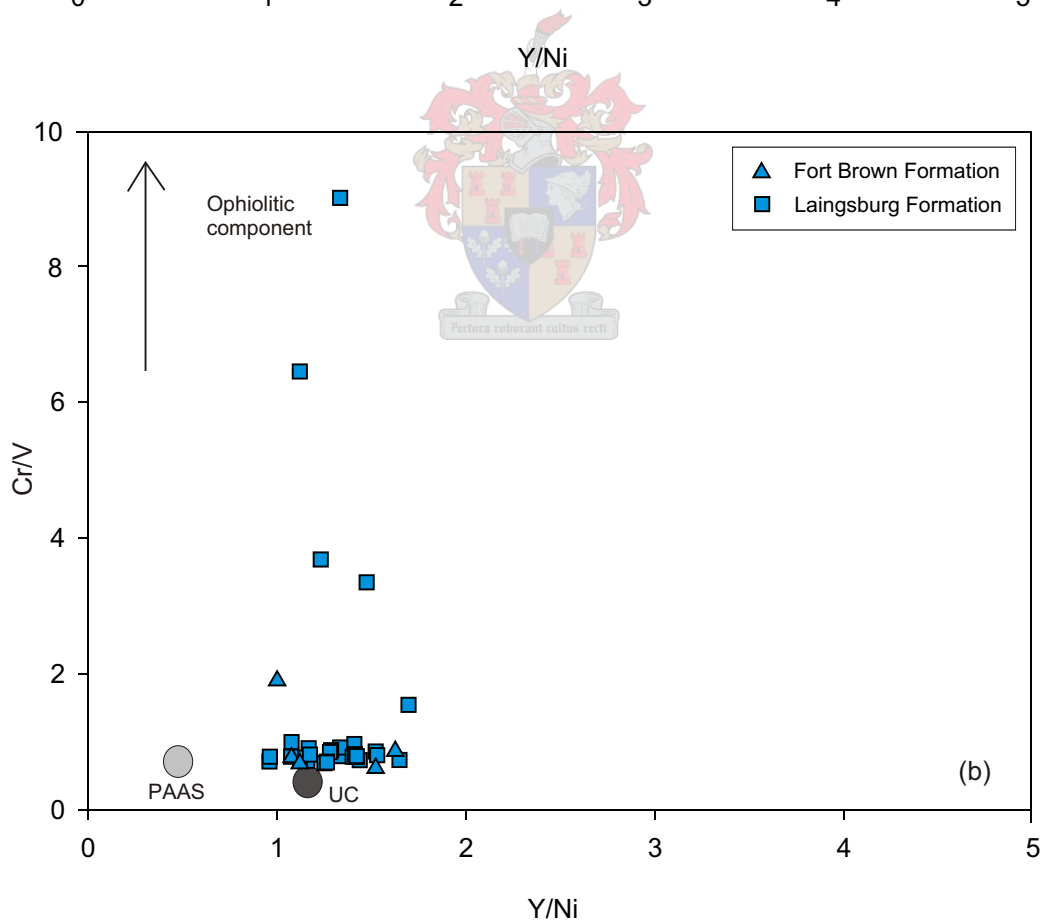
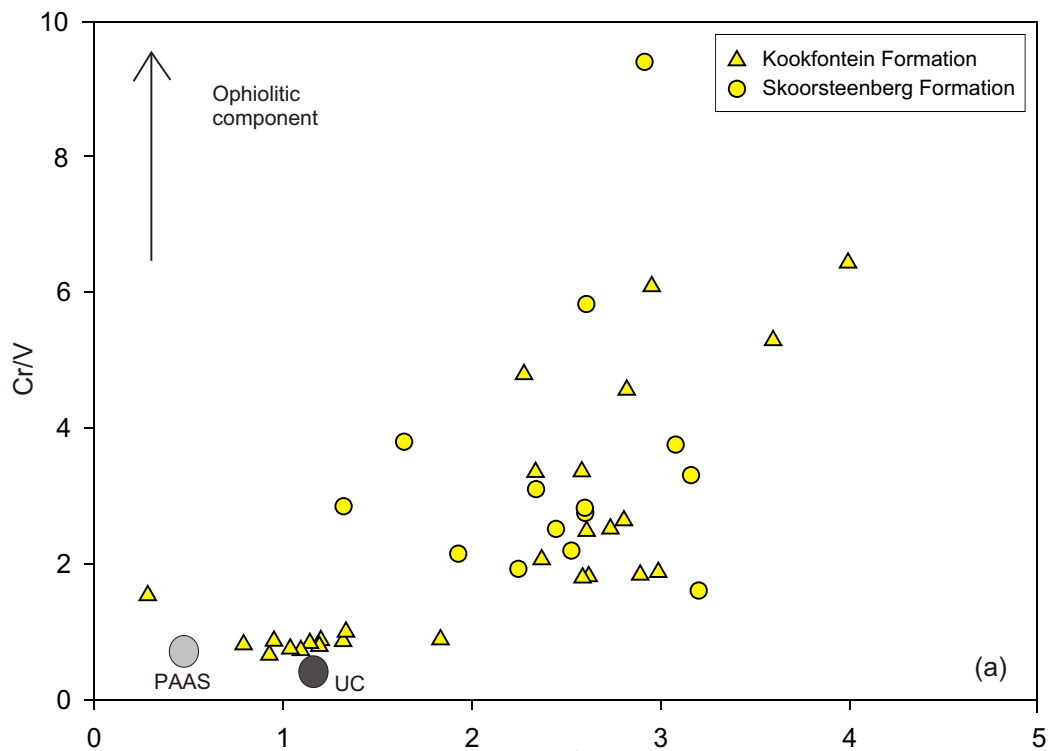
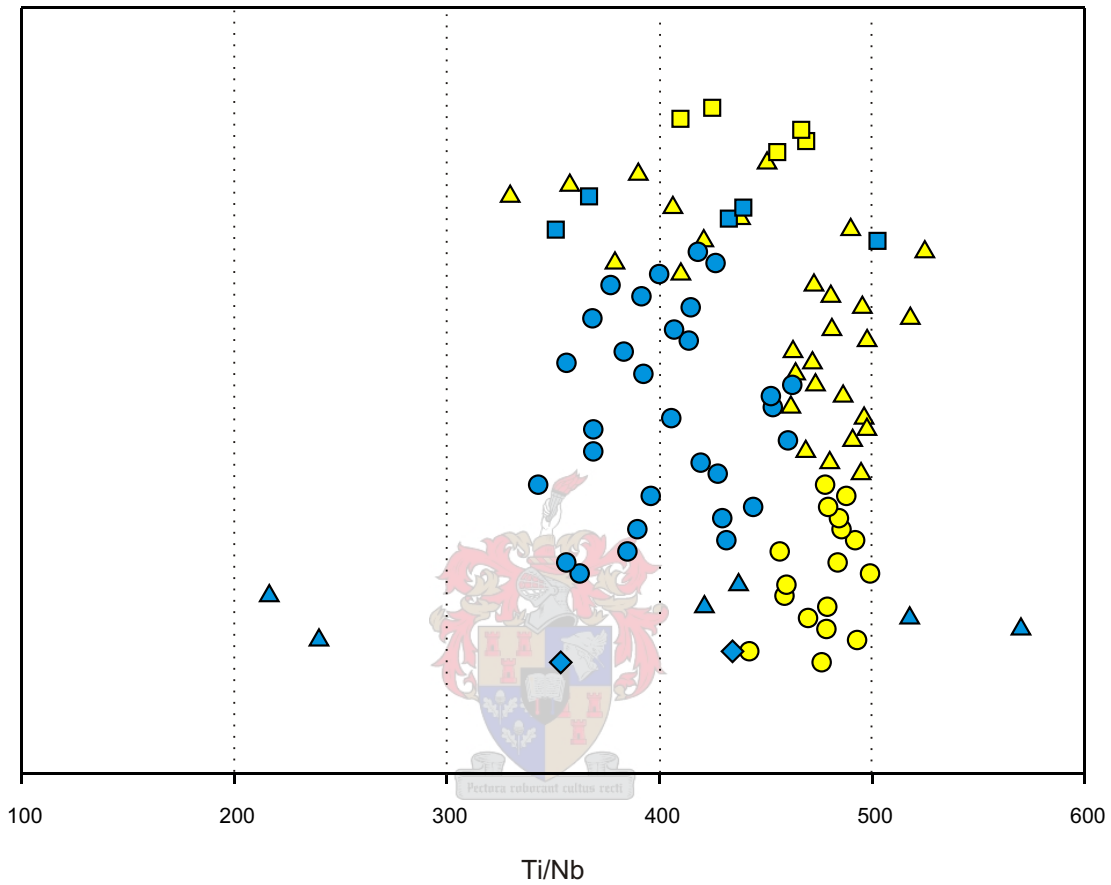


Figure 5.21 Diagrams of Cr/V vs. Y/Ni (method after Cingolani *et al.*, 2003). (a) Tanqua depocentre. (b) Laingsburg depocentre. PAAS = Post-Archaean Australian Shales; UC = Upper Crust. The arrow points towards an ophiolite end member composition with extremely high Cr/V ratios.



Tanqua depocentre sandstones:

- Waterford Formation
- ▲ Kookfontein Formation
- Skoorsteenberg Formation

Laingsburg depocentre sandstones:

- Fort Brown Formation
- Laingsburg Formation
- ▲ Vischkuil Formation
- ◆ Collingham Formation

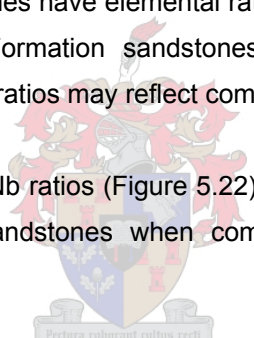
Figure 5.22 Summary diagram for sandstones from the Tanqua and Laingsburg depocentres, showing the alternation of higher Ti/Nb ratios in the Tanqua rocks compared to the lower Ti/Nb ratios of the Laingsburg rocks (method after Boulter *et al.*, 2004).

signature. Samples that plot in the felsic source field are generally thought to reflect acid plutonic and volcanic detritus, whereas samples that plot in the quartzose sedimentary provenance have been derived from a passive margin setting (Roser and Korsch, 1988). Average granite composition as source rock is shown to be closest in composition to both the average Laingsburg and Fort Brown Formations sandstone compositions (Figure 5.8).

Bivariate plots of major element oxides and major element oxide ratios are thought to be capable of discriminating provenance tectonic settings (Bhatia, 1983; Roser and Korsch, 1986; Rollinson, 1993). These mainly indicate an active continental margin tectonic setting as provenance for the Laingsburg depocentre sandstones (Figure 5.23). The Laingsburg depocentre forms part of the Karoo foreland basin, indicating a subduction zone associated with an arc and orogenic belt as the major tectonic setting.

Plots of Th and U show no obvious correlation between them (Figure 5.20). The sandstones of the Laingsburg and Fort Brown Formations have higher concentrations of Cr, V, Ni and Y than PAAS and UC, as can be seen in a diagram of Cr/V vs. Y/Ni (Figure 5.21). The Laingsburg Formation sandstones have elemental ratios for Cr/Th and Co/Th of 3.34 and 0.42, whereas the Fort Brown Formation sandstones have values of 2.68 and 0.40. Differences in the Cr/Th and Co/Th ratios may reflect compositional variation in provenance.

A discrimination diagram of Ti/Nb ratios (Figure 5.22) shows slightly lower ratios of Ti/Nb for the Laingsburg depocentre sandstones when compared to the Tanqua depocentre sandstones.



### **5.5.3 Discussion on the tectonic setting of Tanqua and Laingsburg depocentre source rocks**

Plate tectonic setting may be indicated by the geochemical analysis of sedimentary rocks. Roser and Korsch (1988) define three main tectonic provenances: (i) Active continental margin (ACM) – quartz-intermediate sediments derived from tectonically active continental margins on or adjacent to active plate boundaries (e.g. trench, fore-arc and retro-arc settings); (ii) Passive continental margin (PM) – quartz-rich sediments deposited in plate interiors at stable continental margins of intracratonic basins; (iii) Oceanic island-arc (OIA) – quartz-poor volcanoclastic sediments derived from oceanic island-arcs (i.e. sediments derived from an island-arc source and deposited in a variety of settings including fore-arc, intra-arc and retro-arc basins and trenches).

Oxides such as CaO, Na<sub>2</sub>O (the most mobile phases) and enrichment of SiO<sub>2</sub>, TiO<sub>2</sub>, etc. (the most immobile elements), are assumed to show enrichment or depletion in quartz, K-feldspar, micas and plagioclase (Getaneh, 2002). TiO<sub>2</sub> shows positive correlation with Al<sub>2</sub>O<sub>3</sub>

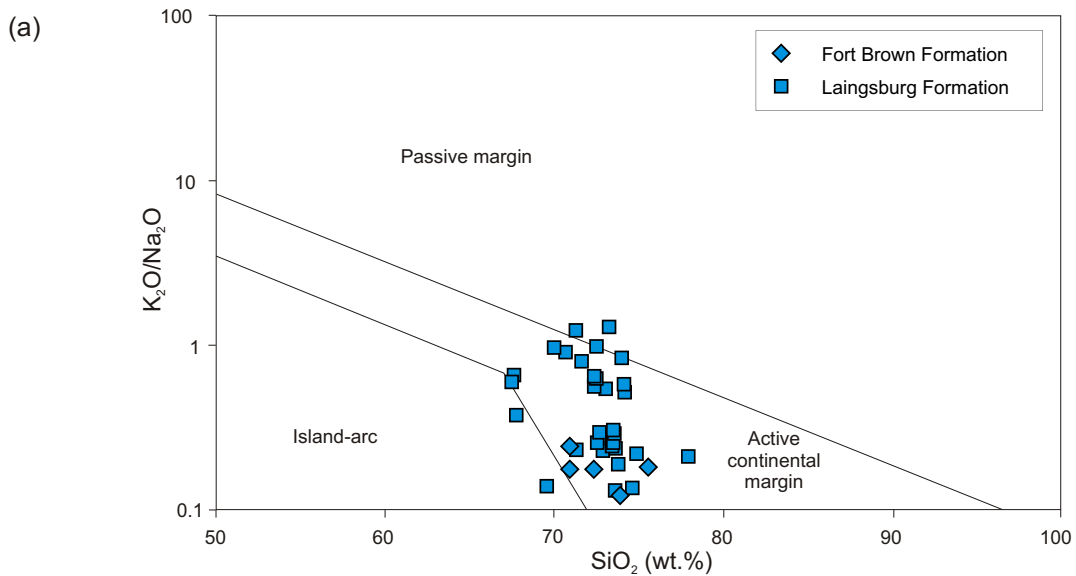


Figure 5.23 (a) Laingsburg depocentre.  $\text{SiO}_2$  vs.  $\text{K}_2\text{O}/\text{Na}_2\text{O}$  discriminant plot of tectonic setting (method after Roser and Korsch, 1986).

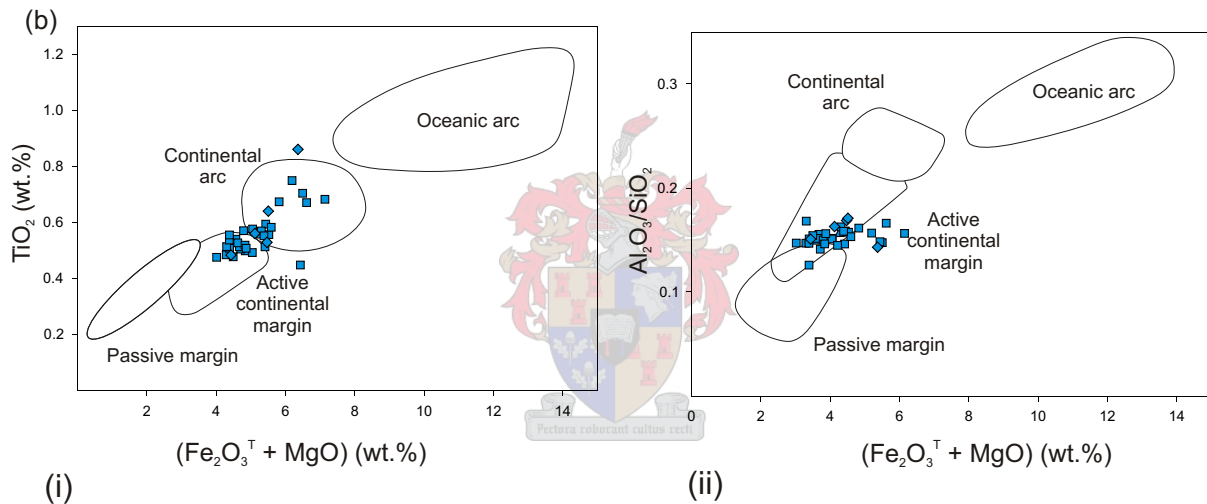


Figure 5.23 (b) Laingsburg depocentre. Discrimination diagrams for sandstones, based upon (i) a bivariate plot of  $\text{TiO}_2$  vs.  $(\text{Fe}_2\text{O}_3^{\text{T}} + \text{MgO})$  and (ii) a bivariate plot of  $\text{Al}_2\text{O}_3/\text{SiO}_2$  vs.  $(\text{Fe}_2\text{O}_3^{\text{T}} + \text{MgO})$ . The fields are oceanic island-arc, continental island-arc, active continental margin and passive margin (method after Bhatia, 1983; Rollinson, 1993).

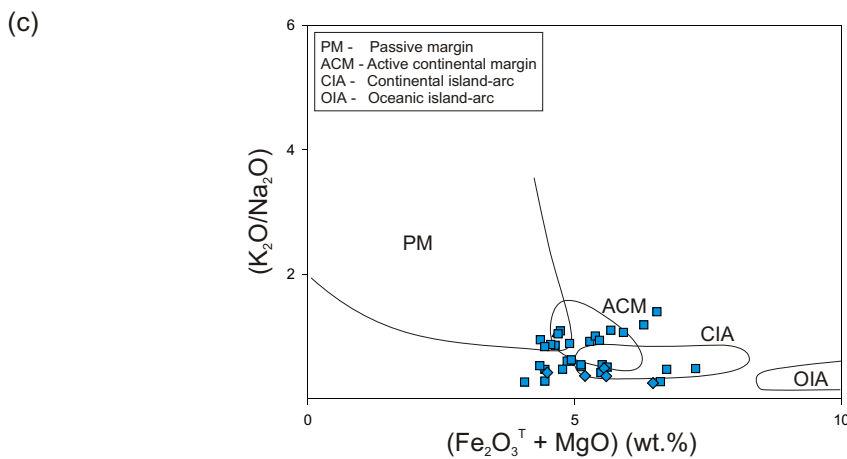


Figure 5.23 (c) Laingsburg depocentre. Discrimination diagram for sandstones, based upon a bivariate plot of  $(\text{K}_2\text{O}/\text{Na}_2\text{O})$  vs.  $(\text{Fe}_2\text{O}_3^{\text{T}} + \text{MgO})$ . The fields are oceanic island-arc, continental island-arc, active continental margin and passive margin (method after Bhatia, 1983; Rollinson, 1993).

for the Tanqua and Laingsburg depocentre rocks, suggesting accumulation of immobile elements and intense chemical weathering in the provenance. The ratios of the most immobile elements to the most mobile ones increases towards the passive margin tectonic setting due to relative tectonic stability and thus protracted weathering and a high degree of recycling of sediments (Bhatia, 1983; Roser and Korsch, 1988). Tectonic discrimination diagrams for the sandstones, from both the Tanqua and Laingsburg depocentres, using major elements, show relatively consistent results. In the  $\text{TiO}_2$  wt.% and  $\text{Al}_2\text{O}_3/\text{SiO}_2$  plots (Figures 5.19 and 5.23) most of the points fall within the active continental margin setting, although some plot within the continental and passive margin settings. Figure 5.18 shows that the sandstones originated from a felsic igneous provenance. The source materials were thus acidic rocks. Plotting the ratio of  $\text{K}_2\text{O}/\text{Na}_2\text{O}$  (Figures 5.19 and 5.23) produce distributions where most of the sandstones of the Skoorsteenberg and Kookfontein Formations, and the sandstones and siltstones of the Laingsburg and Fort Brown Formations, fall within the active continental margin field. Care should be taken when interpreting Figures 5.19(c) and 5.23(c), since the fields are not very well defined. Comparison of the geochemical data from this study with the average composition of late Proterozoic and Phanerozoic greywackes associated with different tectonic environments (Appendix D) indicates that the data are consistent with an active margin setting.

U and Th reflect the characteristic signatures of felsic components in the source area (Naqvi *et al.*, 2002) through the process of extra-basinal leaching of felsic source rocks and the expulsion of U- and Th-rich pore waters. The geochemical behaviour of U and Th under various conditions, specifically oxidation and reduction conditions, are significantly different. These elements thus show no obvious correlation, which also shows that they might have been disturbed during sedimentary processes, such as slope instability, in both the Tanqua or Laingsburg depocentre sandstones.

The sandstones of the Tanqua and Laingsburg depocentres are enriched in Cr compared to the average upper continental crust and have higher values of Ni and V. The data might reflect mixed sources, since it is not compatible with typical upper continental crust. The relative abundances of Cr, Ni and Co in the sandstones may indicate some mafic input, and the Cr/V and Y/Ni values are higher than the PAAS and upper crust average compositions. The Cr/Th and Co/Th ratios for the Tanqua and Laingsburg depocentre rocks differ, which may reflect compositional variation in source area(s). Compositional variation in source area(s) is further discussed in this chapter under source terrane identification. The Tanqua sandstone values compare best to the elemental ratios for andesites (Cr/Th = 9.77 and Co/Th = 4.65), with the possible influence of some basic rocks, which give values of Cr/Th = 22 – 100 and Co/Th = 7.1 – 8.3 for sands (Condie, 1993; Cullers, 1994; Cullers *et al.*, 1988). The Laingsburg sandstone values are more compatible with values from the upper continental crust of Cr/Th = 3.3 and Co/Th = 0.9 (Taylor and McLennan, 1985). However, the variations in

Co/Th and Cr/Th must be used with caution, since the values may also be due to changes in the oxidation state, therefore not reflecting source area composition (Bauluz *et al.*, 2000).

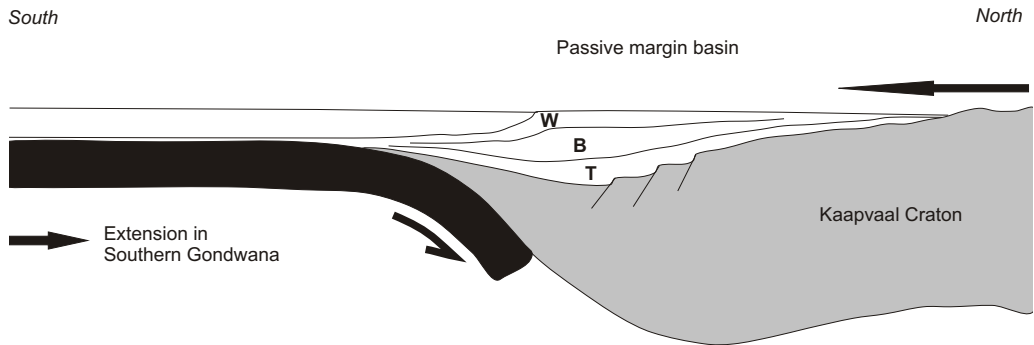
Ti/Nb are good provenance indicators in clastic sedimentary rocks, because these elements undergo little fractionation during weathering or diagenesis, and the residence time of Nb in the ocean is rather short (Taylor and McLennan, 1985; Bonjour and Dabard, 1991; Slack and Stevens, 1994; Boulter *et al.*, 2004). Generally, the Ti/Nb ratios for the Tanqua and Laingsburg depocentre sandstones are constant, with the Tanqua rocks having slightly higher ratios (Figure 5.22). This may be interpreted in terms of either detrital inheritance, or some homogenisation during low temperature geochemical processes. Nb is generally considered to be almost immobile during weathering, low temperature geochemical processes and diagenesis (Colley *et al.*, 1984; Middleburg *et al.*, 1988). The relatively constant Ti/Nb ratios must thus be due to inheritance from source rocks, either as a result from a mixture of different clastic supplies or a single homogenous source area. The diagram of the Ti/Nb ratios for the Tanqua and Laingsburg sandstones (Figure 5.22) show that the distribution of these elements segregate samples in accordance with their petrography (Laingsburg depocentre rocks have more lithic fragments, and less quartz, than the Tanqua depocentre rocks), with the Tanqua depocentre sandstones having higher Ti/Nb ratios than the Laingsburg depocentre sandstones. However, there is overlap of the Tanqua and Laingsburg sandstone data in these diagrams, which further supports the mixed source(s) theory.

The most probable provenance for the Skoorsteenberg, Kookfontein, Laingsburg and Fort Brown Formation sandstones is granitic in composition, as shown in multi-element spider diagrams. There are, however, deviations in the average sandstone compositions, in that they are enriched in Ni, Co and Cr relative to average granite composition. This could either indicate that the source itself was enriched in these elements, or that there were influxes at times from another source, containing higher values of these elements in its composition, such as average basalt.

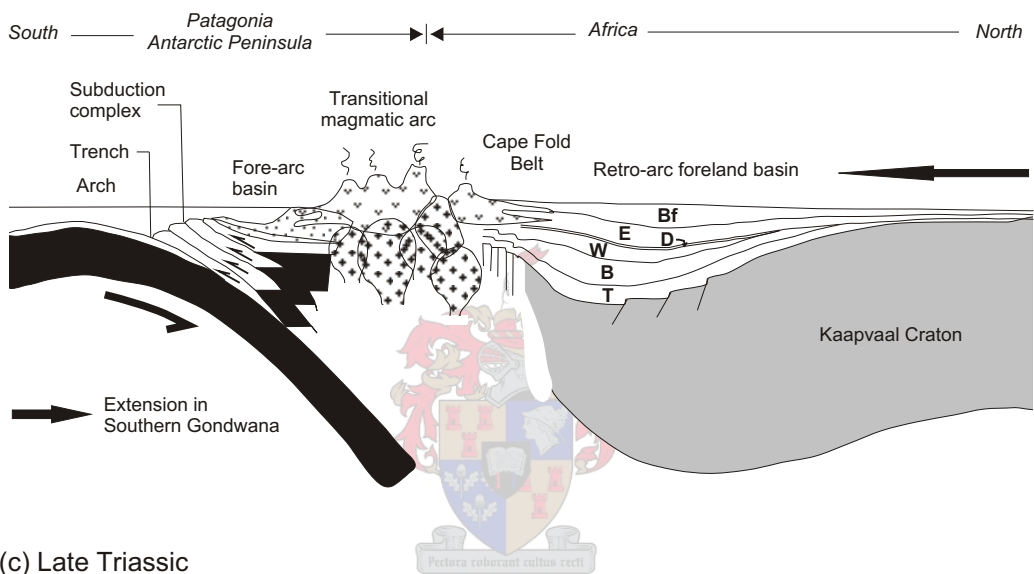
## 5.6 Source terrane identification

The Tanqua and Laingsburg depocentre submarine fan systems were deposited in a foreland basin in relation to an active continental margin setting, the subduction of the palaeo-Pacific plate under the southern edge of Gondwana (Figure 5.24) (Johnson, 1991; De Wit and Ransome, 1992). Scott *et al.* (2000) proposed that these submarine fan systems were deposited during a tectonic quiescence, and represent the subsequent weathering and erosion of the uplifted orogenic belt a substantial distance away. A large change in the sediment transport paths to their depositional basins could be caused by small changes in topography of the sea floor, particularly closer to the deltaic sediment supply system (Scott *et*

(a) Early Carboniferous



(b) Late Permian



(c) Late Triassic

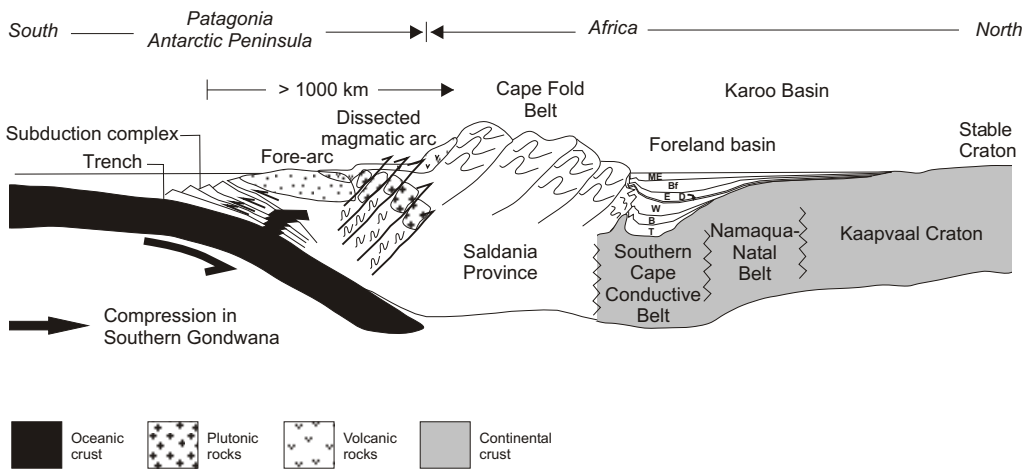


Figure 5.24 (a) to (c) Schematic representation of three stages in the evolution of the southern part of the Cape-Karoo Basin, showing the inferred position of the magmatic arc and subduction zone (modified after Johnson, 1991; Siegfried, 1993; Turner, 1999). The sediments in the Tanqua and Laingsburg depocentres were deposited before the emergence of the transitional magmatic arc (b). B = Bokkeveld Group; Bf = Beaufort Group; D = Dwyka Group; E = Ecca Group; ME = Molteno and Elliot Formations; T = Table Mountain Group; W = Witteberg Group.

*al.*, 2000). The alteration of sand-rich deposition between the depocentres and the switching of palaeocurrent directions, is likely related to this and deltaic switching (Scott *et al.*, 2000).

Andersson and Worden (2004) conducted a study on the Tanqua depocentre mudstones and suggested two different sediment supply regions within the same drainage basin, feeding the fan systems and the interfan mudstones. One source relatively close to the basin centre and exposed during low relative sea-level and intrafan deposition, the other source relatively distant from the basin centre and dominant during high sea-level stand and deposition of the interfan mudstones. Further Sm-Nd isotope studies done by Andersson *et al.* (2003) propose that the source rocks of the Skoorsteenberg Formation is a mixture of older (Archean (?) and Palaeoproterozoic) and successively younger source materials recycled repeatedly and a later Carboniferous to Permian juvenile component. Based on this and palaeocurrent data, these authors concluded that the source area was probably a late Palaeozoic thrust belt and a contemporaneous magmatic arc to the south.

Johnson (1991) proposed an active magmatic arc as exclusive provenance area for the southeastern Karoo Basin during the Permian. He noted that neither the uplifted Cape Fold Belt (CFB), nor a gneiss/granite basement constituted the main source for Ecca and Lower Beaufort Group sediments and that the influence of the CFB increased only during the lower Triassic (Upper Beaufort Group).

A contradicting model was proposed by Kingsley (1981), stating that the emergence of the southern source area was caused by folding of the southern Cape strata during the Permian, as a result of the drifting of a crustal plate (Antarctica (?)) towards Africa. Eventually the southern plate would have collided with southern Africa, forming the CFB. During and after uplift, the metamorphosed fine-grained strata of the Cape Supergroup could have acted as the provenance for the Ecca and Beaufort sediments.

The geotectonic and palaeogeographic setting of Gondwana, showing the distribution of Archean to Mesozoic geology, and that of western Gondwana (South America and southern Africa) during the late Palaeozoic, are shown in Figure 5.25. The majority of sediment was transported across the broad coastal plain and shelf (during lowstand periods) to the Tanqua and Laingsburg depocentres between approximately 270 – 255 Ma, after which time sediment input was cut off (Figure 5.26). Although the term shelf is commonly used to denote the fringe of a continent – the continental shelf – it is suggested that the same term is fully appropriate for a shallow-marine platform located around the margin of a deeper basin irrespective of the basin's tectonic setting (Porębski and Steel, 2003). This is a morphological shelf. Such shelves, commonplace on the edges of marine basins, can vary in their width from a few kilometres to several hundred kilometres, and generally slope basinwards at less than 0.1° (Posamentier and Allen, 1999). During a sea-level highstand, the shelf can support a water

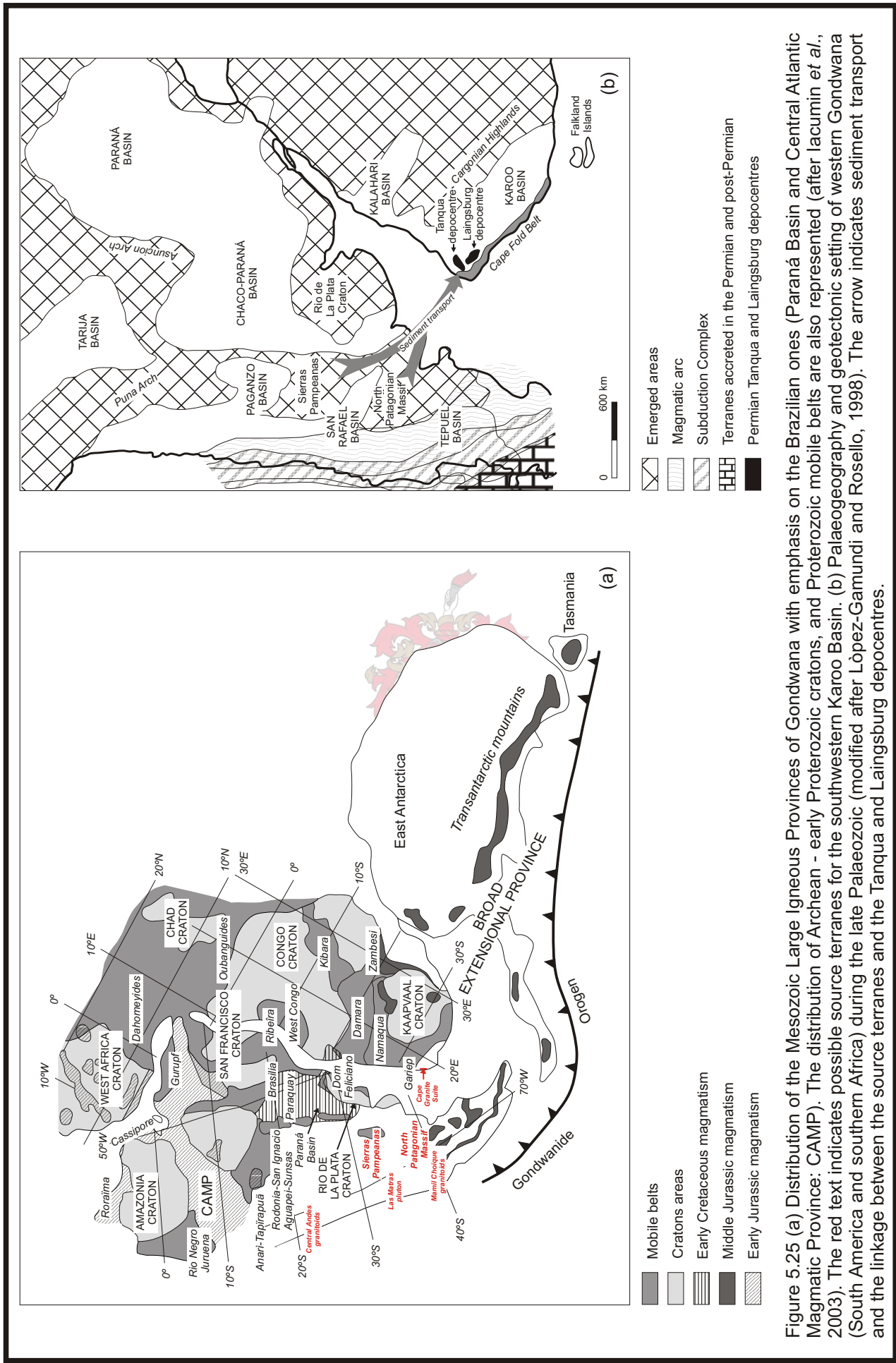


Figure 5.25 (a) Distribution of the Mesozoic Large Igneous Provinces of Gondwana with emphasis on the Brazilian ones (Paraná Basin and Central Atlantic Magmatic Province: CAMP). The distribution of Archean - early Proterozoic cratons, and Proterozoic mobile belts are also represented (after Jacumin *et al.*, 2003). The red text indicates possible source terranes for the southwestern Karoo Basin. (b) Palaeogeography and geotectonic setting of western Gondwana (South America and southern Africa) during the late Palaeozoic (modified after López-Gamundi and Rosello, 1998). The arrow indicates sediment transport and the linkage between the source terranes and the Tanqua and Laingsburg depository basins.

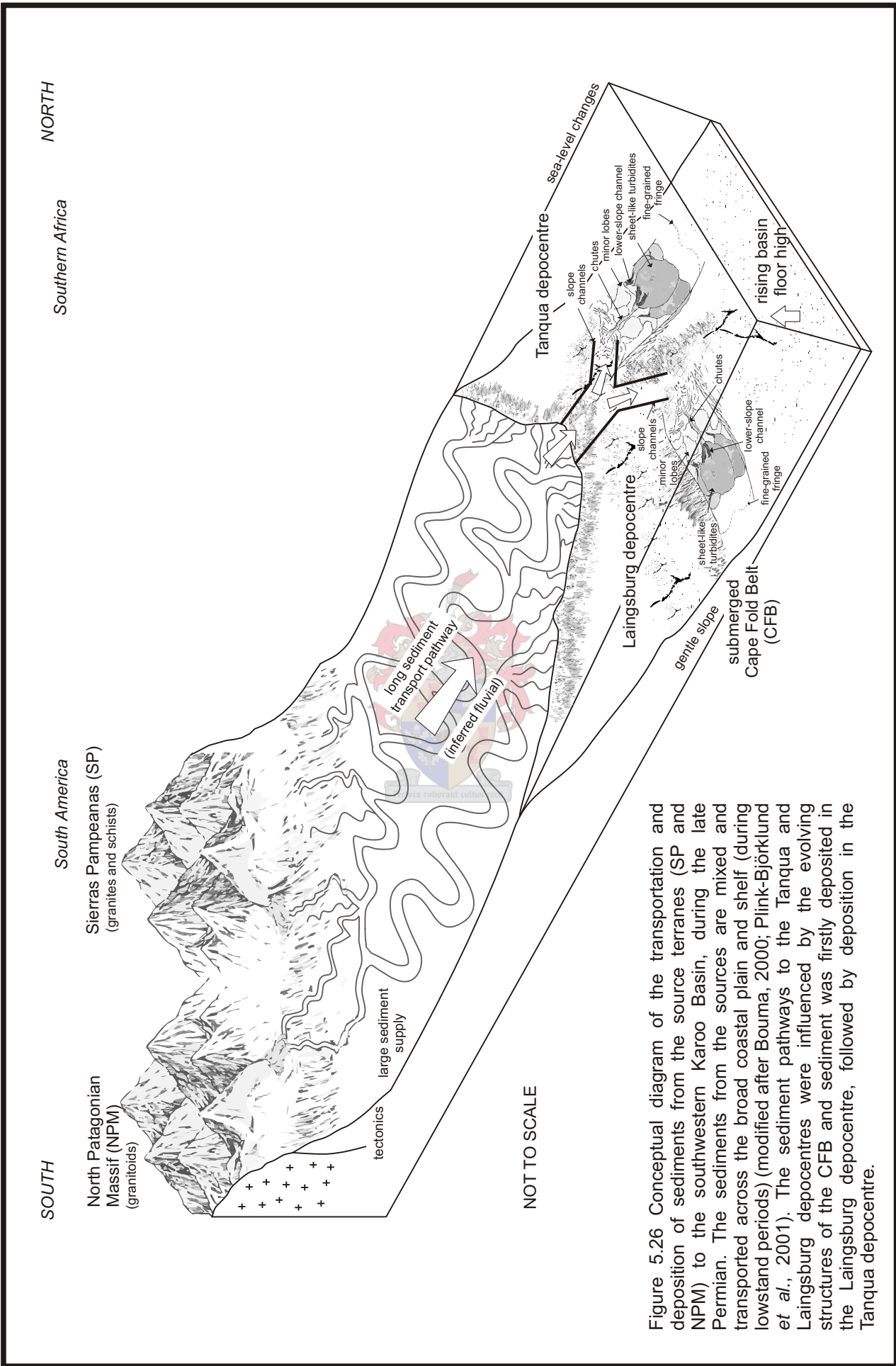


Figure 5.26 Conceptual diagram of the transportation and deposition of sediments from the source terranes (SP and NPM) to the southwestern Karoo Basin, during the late Permian. The sediments from the sources are mixed and transported across the broad coastal plain and shelf (during lowstand periods) (modified after Bourma, 2000; Plink-Björklund *et al.*, 2001). The sediment pathways to the Tanqua and Laingsburg depocentres were influenced by the evolving structures of the CFB and sediment was firstly deposited in the Laingsburg depocentre, followed by deposition in the Tanqua depocentre.

column of up to several hundred metres at its outer edge (Porębski and Steel, 2003). Such basin-margin platforms are constructed by the long-term balance between sediment accommodation and sediment bypass, and the gradual extension or progradation of the front margin of this platform into the basin (Posamentier and Allen, 1999).

Using the constraints that the source rocks had a granitic to upper crust composition and had to be exposed at the time of Tanqua and Laingsburg depocentre sediment deposition between 270 - 255 Ma (Turner, 1999), the possible source terranes were narrowed down to the following (Table 5.1):

- Las Matras pluton – 1200 Ma (Sato *et al.*, 2000);
- Cape Granite Suite (CGS) – 552 to 515 Ma (Scheepers and Armstrong, 2002);
- Mamil Choique granitoids from the southwestern North Patagonian Massif (NPM) – 505 to 286 Ma (Dalla Salda *et al.*, 1994; Cerredo and López de Luchi, 1998);
- Central Andes granitoids – 505 to 245 Ma (Lucassen *et al.*, 2001);
- Sierras Pampeanas (SP) granites and schists – 384 Ma (Otamendi *et al.*, 1998); and
- Patagonian batholith from the NPM – 580 to 235 Ma (Bruhn *et al.*, 1978; Pankhurst *et al.*, 1992, 2003).

The geochemical compositions of the above were compared to the sandstone geochemical compositions of the Tanqua and Laingsburg depocentres, with the use of multi-element spider diagrams (Figure 5.27). Variations in these diagrams ruled out the A-type granites from the CGS, which intruded into the Malmesbury Group metasediments, although the I- and S-type granites are very similar in composition. Based on their geochemistry, the Ordovician and late Palaeozoic average granitoids from the Central Andes, Las Matras pluton average trondhjemites and tonalities and the NPM average tonalities, granodiorites and monzogranites, are unlikely source rocks. The most likely provenance(s) appear to be the SP and Patagonian batholith rocks. The source composition was that of granites, and to a minor extent schists, from the SP, and granitoids from the Patagonian batholith. The geochemical signature from the I- and S-type granites of the CGS may have been incorporated when sediment was transported across these rocks, if they were exposed during the time of deposition. A combination of these rock types, with granitoids being the primary constituent and schists contributing in elements such as Ni, Co, Cr and V, will give a result closest to the sandstone compositions of the Tanqua and Laingsburg depocentres. This infers a sediment transport distance of approximately 600 to 1350 km (Figure 5.25), dependent on the accuracy of the Gondwana reconstructions, or a source area that no longer exists.

The Tanqua and Laingsburg depocentre sediments are compared to rocks from the proposed source terrane(s). Willan (2003) did a study on the Hope Bay Formation, which forms part of the Trinity Peninsula Group in the Antarctic Peninsula. Provenance ages are sparse and undiagnostic. The rocks are weakly deformed, mostly unfossiliferous, and consist

Table 5.1 Normalising values for multi-element diagrams for sedimentary and igneous rocks and Tanqua and Laingsburg depocentre sandstones (values in ppm).

No. of samples Reference	Tanqua depocentre		Laingsburg depocentre		NASC	Average upper crust	Average Phanerozoic quartz arenite	Average granite [4, 5] <i>n</i> = 2485	Average basalt	Cape Granite Suite		
	Skoorsteenberg Formation sandstone <i>n</i> = 17	Kookfontein Formation sandstone <i>n</i> = 30	Laingsburg Formation sandstone <i>n</i> = 30	Fort Brown Formation sandstone <i>n</i> = 5						Average A-type granite	Average I-type granite	Average S-type granite
	[1]	[2]	[3]	[4]	[5]	[6]	[7]	[8]	[9]	[10]	[11]	[12]
Si	1243801	1243468	1205192	1206690	7479	28200	1198203	407722	1245632	1229822	1180230	
Na	87125	90674	79380	93256	89471	84700	120039	51630	142304	110358	97128	
Al	236956	231463	241467	255002	31546	27400	284425	236956	252452	253040	268733	
K	47983	30786	36093	24204	24303	25000	87261	11253	102760	95329	102123	
Ca	20844	43672	56576	32754	4646	600	46154	195037	9429	27543	33995	
Mn	705	846	1269	1128	39565	35000	700	1290	282	705	1551	
Fe	42457	36696	43835	47843	200	240	38413	97815	21166	26426	52727	
Nb	13	14	17	19	142	25	12	10	144	16	12	
Zr	275	255	286	373	3	22	150	99	219	154	188	
Y	30	26	30	28	125	22	21	26	137	57	33	
Sr	158	204	158	271	142	350	310	186	17	85	102	
U	4	6	7	8	3	3	5	1	12	15	7	
Rb	83	68	85	75	12	110	175	21	640	279	255	
Th	13	17	20	22	12	11	17	2	107	33	18	
Pb	15	16	21	18	3	15	30	8				
Ga	14	12	13	13			16	17				
Zn	50	45	47	56			80	84				
Ni	13	20	22	23	58	20	7	75				
Co	63	31	8	9	26	10	5	47				
Cr	317	128	68	59	125	35	12	119				
Ce	68	73	81	96	67	64	76	24	120	56	88	
Nd	29	29	31	33	27	26	27	15	40	27	36	
V	64	49	48	67		60	38	257				
Ba	575	432	436	502	636	700	840	162				
La	35	35	42	36	31	30	40	11	76	30	46	

- [1] Gromet *et al.* (1984).  
 [2] Taylor and McLennan (1981).  
 [3] Boryta and Condie (1990).  
 [4] Taylor and McLennan (1985).  
 [5] Govindaraju (1989).  
 [6] Scheepers and Rozendaal (1995).

Table 5.1 continued

No. of samples Reference	Central Andes		Las Matras pluton		Sierras Pampeanas		North Patagonian Massif			
	Average Late Palaeozoic granitoid n = 89 [7]	Average Ordovician granitoid n = 42 [7]	Average trondhjemites n = 6 [8]	Average tonalites n = 4 [8]	Average anatectic granites n = 3 [9]	Average schist n = 4 [9]	Average Patagonian batholith n = 13 [10]	Tonalites n = 3 [11, 12]	Average Mamil Choique granitoids n = 2 [11, 12]	Monzogranites n = 5 [11, 12]
Si	1144949	1168248	1200200	1061408	1159760	1167249	1241305	1083375	1104843	1201198
Na	116167	102291	131655	133591	115521	79058	125524	116812	114553	104873
Al	286387	266771	264614	307375	305610	251275	251667	322087	320322	295214
K	60085	76433	57749	39915	117197	59023	78132	49894	60934	89172
Ca	74938	62283	50868	120099	42184	42928	35980	95533	89082	44665
Mn	1128	1128	846	1833	423	1128	705	1128	846	423
Fe	53228	47592	37573	82034	28180	72140	27418	54731	47342	18411
Nb	14	17	8	7	10	14	25		4.67	7.20
Zr	171	186	189	136	291	264	171	166	159	150
Y	34	50	32	30	33	32			12.3	8.60
Sr	189	155	207	328	315	154	117	478	470	410
U			2	1						
Rb	113	142	64	64	174	162	143	101	83.7	135
Th			5	3	17	13				
Pb										
Ga	24	21								
Zn	11	8								
Ni										
Co										
Cr	51	62								
Ce	47	56	54	43	142	93				
Nd	20	25	26	25	60	43				
V	47	55			21	107				
Ba	525	410	859	531	855	367	573			
La	23	27	25	19	72	46				

[7] Lucassen *et al.* (2001).

[8] Sato *et al.* (2000).

[9] Otamendi *et al.* (1998).

[10] Bruhn *et al.* (1978).

[11] Cerredo and López de Luchi (1998).

[12] Dalla Salda *et al.* (1994).

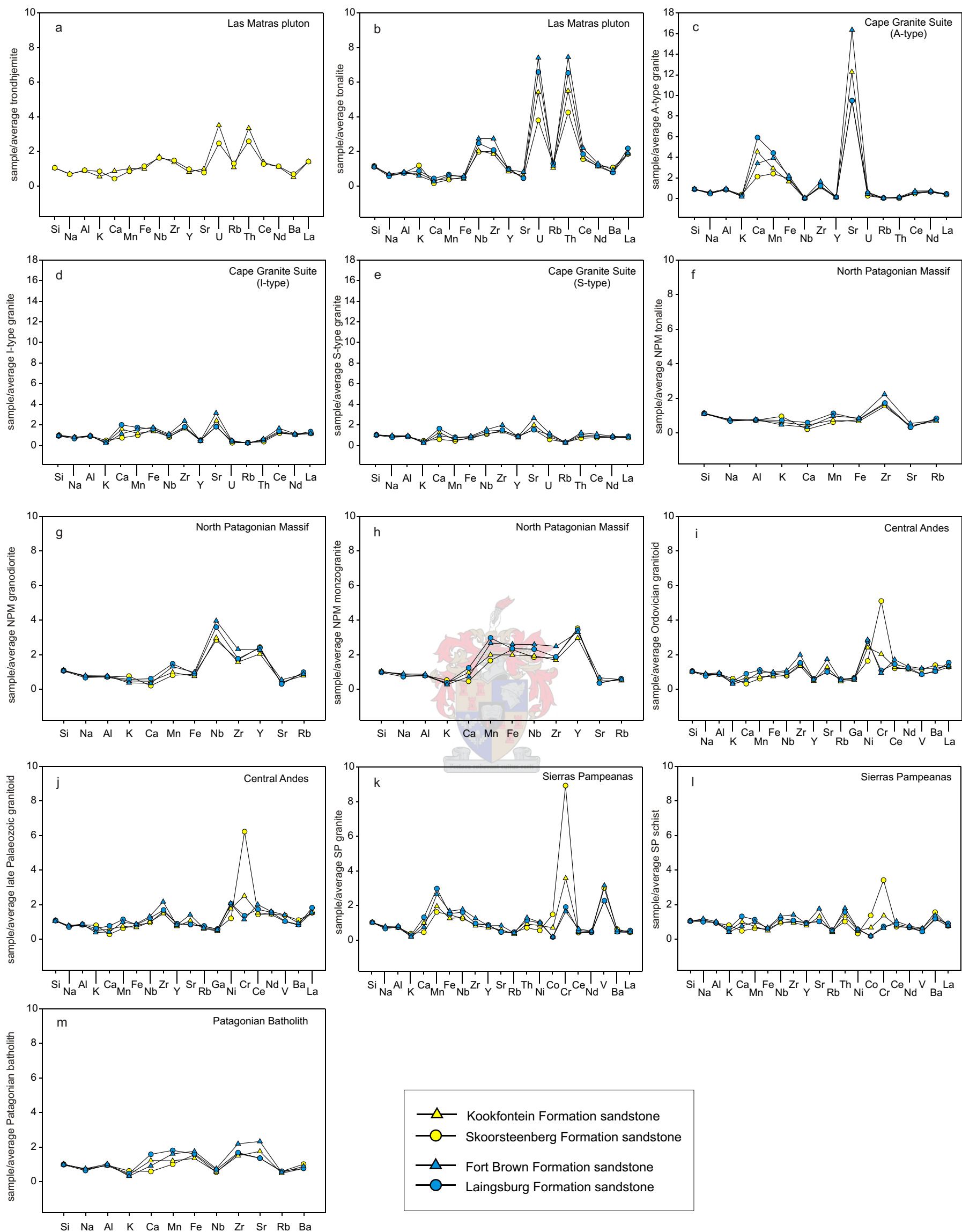


Figure 5.27 Multi-element concentrations for the Skoorsteenberg, Kookfontein, Laingsburg and Fort Brown Formations average sandstones normalised to the compositions of average (a) Las Matras pluton trondhjemite, (b) Las Matras pluton tonalite, (c) Cape Granite Suite A-type granite, (d) Cape Granite Suite I-type granite, (e) Cape Granite Suite S-type granite, (f) NPM tonalite, (g) NPM granodiorite, (h) NPM monzogranite, (i) Central Andes Ordovician granitoid, (j) Central Andes late Palaeozoic granitoid, (k) SP granite, (l) SP schist, and (m) Patagonian batholith (method after Rollinson, 1993). The normalising data are in Table 5.1.

of a marine turbidite sequence of amalgamated, thick lithic sandstones, mudstones, and thin interbedded siltstones and mudstones. Hope Bay Formation sandstones are lithic arkoses dominated by quartz, plagioclase and K-feldspar and minor quantities of biotite, muscovite, chlorite and lithic fragments. These rocks were derived from a deeply eroded continental-margin arc, possibly the early Permian arc of the Patagonian Massif. The sedimentary succession and sandstone compositions compare well to the sediments from the present study.

## **5.7 Geological overview of central South America**

### **5.7.1 Introduction**

The geologic history of western Gondwana (Africa and South America in pre-drift reconstruction) is dominated by the events related to the Brasiliano/Pan-African tectonomagmatic cycle (Brito Neves and Cordani, 1991). These events encompassed the entire late Proterozoic and ceased effectively by Cambro-Ordovician times (Cowie and Bassett, 1989). Post-orogenic tectonism, magmatism and sedimentation took place in several regions of South America and Africa, which were by then united as part of the Gondwana supercontinent (Brito Neves and Cordani, 1991).

The Brasiliano/Pan-African events were orogenic within the different late Proterozoic mobile belts and tectonic reactivation was common in all cratonic borders of the existing continental plates, including widespread folding of platform cover within the interiors of the plates (Brito Neves and Cordani, 1991). In the context of the amalgamation of western Gondwana, the Brasiliano/Pan-African domains can be seen as the result of the approach, complex collision and adjustments of at least five large continental masses: the Amazonian Craton, the West African Craton (including the São Luiz cratonic fragment in Brazil), the Congo-Kasai/São Francisco Craton, the Rio de La Plata Craton and the Kalahari Craton (Brito Neves and Cordani, 1991).

Exposures of pre-Mesozoic basement rocks are sparse, and in southern Patagonia they consist of restricted sedimentary and metasedimentary rocks of late Palaeozoic age, and smaller, scattered outcrops of older granite and metamorphic rocks (Pankhurst *et al.*, 2003). The basement of Patagonia east of the Andes was buried during successive episodes. These processes began with basin formation during Triassic extension and intrusion of late Triassic calc-alkaline batholiths (Pankhurst *et al.*, 2003). Extensive rhyolite volcanism during Jurassic rifting of Gondwana and shallow marine basin sedimentation during the Cretaceous followed this (Pankhurst *et al.*, 2003).

A series of foreland basins that developed behind a foldbelt/magmatic zone from southern South America to Australia, lay along a continental margin characterised by synchronous stages of extension and punctuated by diachronous Panthalassan subduction during the Permian and Triassic (Veevers *et al.*, 1994). This palaeotectonic evolution is particularly clear in the Sauce Grande Basin – Ventana Fold Belt (Argentina) and Karoo Basin – CFB (South Africa) of western Gondwana (López-Gamundi and Rossello, 1998).

### **5.7.2 Sierras Pampeanas (SP)**

The SP, situated east of the Andes as a group of north-south trending mountain chains in central and northwestern Argentina, form a tectono-stratigraphic terrane comprised of mainly early and mid-Palaeozoic metamorphic and igneous rocks (Figure 5.28). The mountain blocks are separated by valleys that formed as a result of uplift and tilt along reverse faults during the Upper Tertiary Andean orogeny (Lira *et al.*, 1997). Sedimentary rocks of Carboniferous, Permian, Triassic and Tertiary-Quaternary ages partially cover the metamorphic-igneous basement rocks of the SP. The latter comprises three lithostratigraphic domains, characterised by metasedimentary rocks deposited in the late Neoproterozoic to Cambrian, Cambro-Ordovician, and the Ordovician, respectively (Sims *et al.*, 1998; Skirrow *et al.*, 2000). All three domains share a common tectonic history since the early Devonian.

The SP orogeny is characterised by two major deformation events, namely the Pampean (Neoproterozoic-Cambrian) and Famatinian (Ordovician) cycles, and include pre-, syn- and post-tectonic granitoids (Tourn *et al.*, 2004). Convergence on the western margin of Gondwana in the mid-Palaeozoic resulted in compressive deformation and the development of an early Devonian magmatic arc extending over much of the southern SP. This tectonism has been termed the Achalian Orogeny (Sims *et al.*, 1998; Skirrow *et al.*, 2000). The deformation was dominated by orthogonal westerly directed thrusting, with a component of sinistral shearing, both at greenschist facies, and the development of regionally extensive ductile and brittle-ductile, conjugate faults and shear zones (Skirrow *et al.*, 2000). Peraluminous to slightly peraluminous granites were widely emplaced in the metamorphic basement during and after Achalian shear zone development. Major uplift of the central SP took place before the late Devonian. At that time batholith-scale post-orogenic weakly peraluminous monzonitic magmas intruded the plutono-metamorphic basement, which was already established by that time (Rapela *et al.*, 1992; Otamendi *et al.*, 1998). Felsic magmatism may have continued into the Carboniferous, with granites ranging from monzogranite and syenogranite to granite and leucogranite (Rapela *et al.*, 1990; Skirrow *et al.*, 2000). Most are two-mica granites, although hornblende has been reported in a few intrusions. Accessory ilmenite is present in some Devonian granites, whereas others contain accessory magnetite (Skirrow *et al.*, 2000).



Figure 5.28 Location map of the Sierras Pampeanas, the North Patagonian Massif and the Sierras Australes Fold Belt in Argentina (modified after Jordan, 1995; López de Luchi and Rapalini, 2002; Tomezzoli *et al.*, 2003). The conjectural extensions of the Pampean (P) and Famatinian (F) orogenic belts of Neoproterozoic to mid-Ordovician age are also shown (after Pankhurst *et al.*, 2003). The inset shows South America, with the generalised location of the Rio de La Plata Craton (RPC).

A division between the eastern and western SP has been recognised (Caminos, 1979). The western zone is characterised by an abundance of mafic, ultramafic, and carbonate-bearing rocks, high-pressure metamorphic grade rocks, and a lack of major batholiths (Lira *et al.*, 1997). The eastern SP (Central Argentina), consist of several mountain chains, such as the Sierra Grande, Sierra de San Luis and Sierra de Altutina (Tourn *et al.*, 2004). The metamorphic rocks of the eastern SP are primarily characterised by phyllites, schists and gneisses, subordinate marbles and amphibolites (greenschist to amphibolite metamorphic grade), and a granulite facies (Lira *et al.*, 1997). There are abundant intrusives into the metamorphic complex, dominated by granitoid rocks over mafic and ultramafic bodies. The metamorphic grade generally increases southward.

The stratigraphic sequence of the eastern SP is not well known. This is largely due to a lack of geochronological data and the intensity of deformation and metamorphism.

The youngest igneous activity in the area are: thick middle-Cretaceous alkaline basalts erupted in an intra-continental basin, the Sierra de Córdoba, and late-Tertiary alkali-calcic intermediate to felsic and/or calc-alkaline volcanic rocks, constituting small volcanic necks in both Sierra de Córdoba and Sierra de San Luis (Otamendi *et al.*, 1998).

### **5.7.3 North Patagonian Massif (NPM)**

The Famatinian Orogenic Belt (early Palaeozoic) of deformation, metamorphism, and plutonism in the SP, continues southward into northern Patagonia and thereby traverses the inferred terrane boundary of the NPM (Ramos, 1988; Dalla Salda *et al.*, 1994). Rosello *et al.* (1997) postulated a dextral transpression under N-S contraction that affected northeast Patagonia, the Sierras Australes, and Tandilia during the late Palaeozoic – early Mesozoic.

In southern Argentina, the NPM covers an area south of the Colorado and Neuquén Basins between the Atlantic coast on the east and the foothills of the Patagonian Cordillera to the west (Figure 5.28). The northern margin against the Colorado Basin is assumed to be a W-E to NW-SE-striking fault system (Turner and Baldis, 1978), whereas the southern margin of the massif is indicated by the Tecka-Tepuel Basin (Von Gosen, 2002).

The granites of the NPM constitute two batholithic series. These are (i) the Somuncura Batholith, which lies largely in the north of the massif, and (ii) the Batholith of Central Patagonia, which lies along its southwestern border (Pankhurst *et al.*, 1992). In terms of both age and composition, the most voluminous granites of the Somuncura Batholith and the Batholith of Central Patagonia are correlative with the Permo-Triassic Choiyoi Province of the Central Andes and present post-collisional magmatism (Pankhurst *et al.*, 1992).

The early to late Palaeozoic intrusive activity in the NPM, as well as acid volcanics, is related to an inner cordilleran arc, formed during east-directed subduction beneath the western margin of Gondwana during the Devonian-Permian (Cingolani *et al.*, 1991). Caminos *et al.* (1988) proposed a post-middle Carboniferous uplift and cratonisation of the massif.

The NPM is widely covered by Triassic, Jurassic, and Tertiary volcanics, while Proterozoic to early Palaeozoic rocks, and late Palaeozoic-Mesozoic intrusions are only exposed in a few areas (Von Gosen, 2002). Isolated outcrops of siliciclastic sediments in the NPM have been recognised that can be correlated to the Sierra Grande Formation (Rossello *et al.*, 1997).

Jurassic volcanism represents a major magmatic event in the evolution of Patagonia. The volcanic rocks are predominantly rhyolitic and form one of the world's most voluminous silicic provinces, which extent from the Atlantic margin to Chile (Pankhurst *et al.*, 1992).

In general, compression in the northeastern segment of the NPM can be regarded as part of the Gondwanide deformation in the Samfrau Orogenic Zone of Du Toit (1937), which is also recorded in the CFB (Söhnge and Hälbich, 1983), the Falkland Islands (Marshall, 1994; Curtis, 1998), and probably continues in the Ellsworth Mountains (Dalziel *et al.*, 1987; Curtis, 1998) and the Pensacola Mountains (Ford, 1972) of Antarctica (Von Gosen, 2002).

## 5.8 Conclusions (answers to initial objectives)

- i + ii The sandstones in the Tanqua and Laingsburg depocentres show no changes in major, trace and rare earth element data with the chemical index of alteration (CIA), whereas only the siltstones and mudstones show a negative correlation between CIA and SiO<sub>2</sub>. A possible grain size control on the individual CIA values is suggested, since higher SiO<sub>2</sub> contents will be induced by a higher quartz silt or sand content. An increase in mineralogical maturity is reflected by an increase in SiO<sub>2</sub>, i.e. greater quartz content and a smaller proportion of detrital grains. Based on this, the Laingsburg depocentre sandstones are geochemically less mature than the Tanqua depocentre sandstones. In the Tanqua sandstones, Al<sub>2</sub>O<sub>3</sub> and MgO show a decrease with SiO<sub>2</sub>, whereas the negative correlation trends of TiO<sub>2</sub> and Fe<sub>2</sub>O<sub>3</sub><sup>T</sup> with SiO<sub>2</sub> are due to dissolution of these elements. The Laingsburg depocentre sandstones show weak negative correlation between Al<sub>2</sub>O<sub>3</sub> and SiO<sub>2</sub>, whereas Fe<sub>2</sub>O<sub>3</sub><sup>T</sup> shows no correlation with SiO<sub>2</sub>. The major elements of the Laingsburg depocentre siltstones show a positive correlation of SiO<sub>2</sub> with TiO<sub>2</sub>/Al<sub>2</sub>O<sub>3</sub>, and negative correlations of SiO<sub>2</sub> with Fe<sub>2</sub>O<sub>3</sub><sup>T</sup> and MgO, whereas Al<sub>2</sub>O<sub>3</sub> shows a dissolution trend. There are no changes in K<sub>2</sub>O/(K<sub>2</sub>O + CaO) or TiO<sub>2</sub>/Al<sub>2</sub>O<sub>3</sub> with the palaeocurrent direction of the slope fan in the Tanqua

depocentre.  $K_2O$  decreases upwards in the Skoorsteenberg Formation succession; whereas  $Na_2O$  and  $CaO$  show very weak increases and  $MgO$  show no change. In the Laingsburg depocentre  $TiO_2$  decreases up the stratigraphic succession for the siltstones, whereas  $Na_2O$  show no correlation in either the sandstones or siltstones. The positive correlation between  $Al_2O_3$  and  $TiO_2$  for sandstones is much weaker than that for the siltstones. The concentrations of these oxides are more evenly distributed in the siltstone, since it contains more Al and Ti bearing minerals, such as chlorite, biotite and illite, than the sandstones. This shows that  $TiO_2$  is coming in from the fine fraction, indicating that it is not a heavy mineral fraction.

- iii. The geochemical composition of both the Tanqua and Laingsburg depocentre sandstones is consistent with that of litharenites and greywackes, with the Laingsburg depocentre sandstones containing more lithic fragments than the Tanqua depocentre sandstones. Sandstone classification based on geochemistry [ $\log(SiO_2/Al_2O_3)$  vs.  $\log(Na_2O/K_2O)$ ] shows differences in the overall composition of the sandstones, with the Tanqua depocentre sandstones being slightly more mature than the Laingsburg depocentre sandstones. The reason for this might be that the Tanqua depocentre sediments are slightly younger than the Laingsburg depocentre rocks in that source rocks were unroofed and sediment was first deposited in the Laingsburg depocentre, after which, sediments derived from previously covered rocks, were deposited in the Tanqua depocentre.
- iv. The provenance signatures for the Tanqua and Laingsburg depocentres are constant with their stratigraphic location and position in the systems tract. The provenance signatures for both depocentres indicate a felsic igneous provenance, which agrees with the proposed source composition(s) of granitoids and schists. The depocentres form part of the Karoo foreland basin, indicating a subduction zone in an active continental margin as the major tectonic setting for both depocentre sediments.
- v. The most likely source terranes for the Tanqua and Laingsburg depocentre sediments are the SP granites, and to a minor extent, schist, and the Patagonian batholith granitoids, putting the sediment transport distance at approximately 600 to 1350 km, dependent on the accuracy of the Gondwana reconstructions, or a source area that no longer exists. The long distance between the subduction zone and its foreland basin, created a longer transportation distance for the sediments, causing their fine-grained nature. Based on proximity and normalisation data of the CGS, the I- and S-type granites also have the potential of being a minor source.

## Chapter Six

### 6 Sm-Nd Isotope Chemistry

#### 6.1 Analytical techniques

The initial Nd values of rocks should approximate that of their source rocks at their time of formation, unless secondary processes such as crustal contamination have modified them. Metamorphic and sedimentary processes do not significantly fractionate Sm and Nd isotopes within the continental crust and the parent/daughter ratio of their source region is thus preserved. A model age is a measure of the length of time a sample has been separated from the mantle from which it was originally derived and in the case of Nd isotopes there are two frequently quoted models for the mantle reservoir – CHUR (Chondritic Uniform Reservoir) and DM (Depleted Mantle) (Rollinson, 1993). Sediment eroded from a segment of continental crust will possess a crustal residence age (generally well in excess of the stratigraphic age of the sediment), which may reflect the crust formation age, and is the average crustal residence time of all the components of the rock, since minimal fractionation of Sm/Nd accompanies their generation (Rollinson, 1993). Model Nd ages are the average model age of the sediment and provide a minimum estimate of the crustal residence age or an average crustal residence age, since many continental sediments are a mixture of materials from different sources.

The CHUR model is based on the assumption that the Earth's primitive mantle had the same isotopic composition as the average chondritic meteorite at the formation of the Earth and, therefore, for Nd isotopes CHUR is synonymous with the composition of the bulk Earth (Rollinson, 1993).  $T_{\text{CHUR}}$  (a model age calculated relative to CHUR) is the time in the past at which the sample rock separated from the mantle reservoir and acquired a different Sm/Nd ratio, as well as the time at which the sample had the same  $^{143}\text{Nd}/^{144}\text{Nd}$  ratio as CHUR (Rollinson, 1993).

The mantle, which supplied the continental crust, has evolved since earliest times with an Sm/Nd ratio greater than that of CHUR, and for this reason  $T_{\text{DM}}$  (a model age calculated relative to depleted mantle) for the continental crust are usually calculated with reference to the depleted mantle reservoir rather than CHUR (Rollinson, 1993).

The epsilon parameter in the study of Nd isotopes is a measure of the difference between the  $^{143}\text{Nd}/^{144}\text{Nd}$  ratio of a sample or suite of samples and a reference value, which is either CHUR or DM. These values can be used in three different ways, which are (i)  $\epsilon_{\text{Nd}}$ -values for an isochron; (ii)  $\epsilon_{\text{Nd}}$ -values for individual rocks at their time of formation; and (iii)  $\epsilon_{\text{Nd}}$ -values for individual rocks at the present day (Rollinson, 1993). Information about the magma source is provided by the 'initial' value of  $\epsilon_{\text{Nd}}$  in the rock at its time of crystallisation, and is denoted as

$\epsilon_{Nd}^t$ . An isochron calculation of  $\epsilon_{Nd}^t = 0$  indicates that the magma was derived from a mantle reservoir which has had a chondritic Sm/Nd from the origin of the Earth until time  $t$ , a positive  $\epsilon_{Nd}^t$ -value implies a depleted mantle source region (derived from a source with a greater Sm/Nd than CHUR); whereas a negative  $\epsilon_{Nd}^t$ -value implies an enriched mantle source or a crustal source (derived from a source with a lower Sm/Nd than CHUR) (Rollinson, 1993).

### 6.1.1 Isotope dilution analyses

Concentrations of Sm and Nd in the samples were determined by isotope dilution, using a multi-collector Finnigan Mat 262 mass spectrometer in static mode housed at the Memorial University of Newfoundland, Canada. The isotopic values of  $^{147}\text{Sm}$ ,  $^{143}\text{Nd}$  and  $^{144}\text{Nd}$ , were determined respectively. The chemical separation that preceded this procedure involved the crushing and powdering of the clean samples (>30 g) in a jaw crusher and a porcelain disc mill, respectively. The powdered samples were weighed and added to previously weighed aliquots of Sm-Nd spike.

Approximately 0.10 g of rock powder was dissolved in savilex using a mixture of concentrate HF–HNO<sub>3</sub> acids. A mixed  $^{150}\text{Nd}/^{149}\text{Sm}$  spike was added to each sample prior to acid digestion. After five days of digestion, the solution was evaporated to dryness and then dissolved in 6N HCl acid for two days. The solution was then dried, dissolved in 2.5N HCl and loaded on a cationic exchange chromatography column using AG50W–X8 resin. The REE fraction was then purified and Sm and Nd were isolated using a secondary column loaded with Eichrom Ln resin. All reagents were distilled in order to ensure a low contamination level. The measured total chemical blanks range between 40 and 90 pg and are thus negligible.

The Nd isotopic ratio is normalized to  $^{146}\text{Nd}/^{144}\text{Nd} = 0.7219$ . The reported values were adjusted to the La Jolla Nd standard ( $^{143}\text{Nd}/^{144}\text{Nd} = 0.511860$ ). During the course of data acquisition replicates of the standard gave a mean value of  $^{143}\text{Nd}/^{144}\text{Nd} = 0.511886 \pm 26$  (2 $\sigma$ , n = 18). The in-run precisions on the Nd isotopic ratio are given at 95% confidence level. Error on Nd isotopic compositions are <0.002% and errors on the  $^{147}\text{Sm}/^{144}\text{Nd}$  ratio are estimated to be less than 0.1%.

The  $\epsilon_{Nd}$ -values are calculated using  $^{147}\text{Sm}/^{144}\text{Nd} = 0.1967$  and  $^{143}\text{Nd}/^{144}\text{Nd} = 0.512638$  values for the present day CHUR. The  $^{147}\text{Sm}$  decay constant is  $6.54 \times 10^{-12} \text{ y}^{-1}$  (Steiger and Jäger, 1977), and  $T_{DM}$  was calculated both with respect to a depleted mantle with a  $\epsilon_{Nd(0)}$  value of +10 isolated from the CHUR since 4.55 Ga and following a linear evolution, and the De Paolo mantle model (DePaolo, 1991).

## 6.2 Objectives

- i. How do the Sm-Nd isotope data for the Tanqua and Laingsburg depocentre sandstones compare?
- ii. Are there differences in the Sm-Nd isotope data between Fans A to F of the Laingsburg Formation?
- iii. How do the Sm-Nd isotope data relate to the geochemistry?
- iv. What do the Sm-Nd isotope data tell us about the nature of the source rocks?

## 6.3 Examples of Sm-Nd isotope studies of sedimentary rocks from the literature

Sm-Nd isotope data are usually used in conjunction with geochemical data, and where possible, zircon U-Pb age data, to constrain the provenance. Even though Sm-Nd concentrations are more reliable than, e.g. Rb-Sr systems, due to the fact that they are less easily altered and less mobile than most other elements, they do have the disadvantage that small amounts of recycled crust, mixed with a large proportion of a mantle component, become isotopically invisible (Rollinson, 1993). Three examples from the literature are discussed in the following section. These were chosen to illustrate how Sm-Nd data was used to (i) distinguish between different provenance signatures for succeeding formations within the same basin; (ii) draw up new constraints on tectonic evolution; and (iii) estimate the relative proportions of different source rock material in sediments.

### (i) *Karoo Supergroup mudstones of the Ellisras Basin, South Africa (Faure et al., 1996)*

The Swartrant and Grootegeluk Formations of the Ecca Group, and the Eendragtpan Formation of the Beaufort Group (Karoo Supergroup) in the Ellisras Basin, consist of sediments deposited predominantly during the Permian. The Ellisras Basin sediments are preserved in faulted blocks and a half-graben that parallels the ancient Limpopo mobile belt. The Swartrant Formation is composed of sandstone, grit, siltstone, carbonaceous mudrock and coal seams, whereas the overlying Grootegeluk Formation is composed of a repetitive sequence of carbonaceous mudstones with interbedded bright coal seams. These are overlain by the massive mudstones of the Eendragtpan Formation.

Whole rock chemical and rare earth element compositions were used in combination with Sm-Nd isotope analyses to determine the provenance of the rocks. Based on the concentrations and inter-element ratios of relatively immobile elements, the mudstones of the Grootegeluk and Eendragtpan Formations analysed have the same predominant provenance, with an average granodioritic composition, whereas the source composition of the underlying Swartrant Formation is more mafic. These findings are confirmed by the variation of the Sm-Nd model ages and  $\epsilon_{Nd}$ -values of the mudstones. The Swartrant Formation mudstones have

model ages between 1898 and 2362 Ma and  $\epsilon_{Nd}$ -values between  $-15$  and  $-16$ . The Grootegeluk and Eendragtpan Formations have much younger Sm-Nd model ages (850 to 1570 Ma) and significantly different  $\epsilon_{Nd}$ -values ( $-6.4$  to  $-2.9$ ). This is consistent with the fact that the source of the Swartrant Formation mudrocks was more mafic, as indicated by the whole rock and rare earth element geochemistry. The very low  $\epsilon_{Nd}$ -values must thus be as a result of older crustal residence ages than the source rocks of the Grootegeluk and Eendragtpan Formation mudrocks.

The authors found that evidence for a unique provenance of the sediments was inconclusive, but that the Sm-Nd isotope data and sedimentological interpretations of the Grootegeluk and Eendragtpan Formations are more consistent with a source from northward retreating glaciers and for the Swartrant Formation a provenance from Antarctica.

(ii) *Permian to Mesoproterozoic sediments from the southern margin of the Yangtze Block, southeast China (Li and McCulloch, 1996)*

The southern margin of the Yangtze Block is composed of a Proterozoic basement rock series (1850 – 800 Ma), Sinian (800 – 570 Ma) and post-Sinian cover sequences. The Proterozoic basement is separated into Meso- and Neoproterozoic by an unconformity, where the Mesoproterozoic rocks, collectively termed as the Sibao Group in northern Guangxi, consist of meta-sandstones, siltstones and slates with metamorphosed mafic-ultramafic volcanic intercalations. The time-interval represented by the Sibao Group is considered to be  $\sim 1740$  Ma to 1050 Ma. The Sibao Group and its equivalents are unconformably overlain by a series of Pre-Sinian, Neoproterozoic rocks, named the Danzhou Group in northern Guangxi, and consisting of basal conglomerates with granitic clasts, slates and phyllites. The age interval of the Danzhou Group and its equivalents is inferred to be  $\sim 1050$  to 800 Ma. The Sinian sequence ( $\sim 800$  to 570 Ma) forms the cover strata on the folded basement, and is in turn overlain by Lower Cambrian black shale.

The Sibao Group sediments have relatively high  $\epsilon_{Nd}$ -values ( $-0.5$  to  $+1.4$ ) and a uniform  $T_{DM}$  age of  $\sim 1.8$  Ga. These sediments were derived dominantly from immature continental crustal materials, and are probably the product of the first stage of sediment recycling of these materials. The Neoproterozoic Upper Danzhou Group sediments show significantly younger  $T_{DM}$  ages (1.36 to 1.66 Ga) than those of the Lower Danzhou Group sediment  $T_{DM}$  ages (1.60 to 1.89 Ga). This indicates that a large amount of fresh mantle-derived materials has been incorporated in the sediments. Deposition of the Danzhou Group was coeval with the Jingning Orogeny during the Neoproterozoic in the Yangtze Craton, causing Nd isotopic shifts. The Lower Sinian sediments with  $T_{DM}$  ages of  $\sim 1.3$  Ga also contain large amounts of juvenile materials, which decreases gradually following deposition of the Upper Sinian sediments. The

younger Upper Sinian to Permian sediments are again characterised by provenances having 'normal' inter-orogenic Nd composition and  $T_{DM}$  ages of  $\sim 1.8$  Ga.

These authors concluded that the provenance of sediments from a convergent continental margin has been strongly controlled by regional tectonic events. The 'Nd isotopic shift' is closely related to the Jingning Orogeny and during this orogenic event the Nd isotopic evidence indicates that a large amount of newly mantle-derived materials has been incorporated in the sedimentary provenance, after the collision between the Yangtze and Huanan Blocks.

*(iii) Metagreywackes from the Palaeoproterozoic Karrat Group, Rinkian Belt, West Greenland (Kalsbeek et al., 1998)*

The Karrat Group, overlying the Rinkian mobile belt, consists of a sequence of metasediments with subordinate metavolcanic rocks, which, in the centre of the belt, is intruded by a large igneous complex, the Prøven charnokite, dated at  $1860 \pm 25$  Ma. The Karrat Group has been subdivided into three formations, of which the Nûkavsak Formation is the most important rock unit in the Rinkian Belt. It is a monotonous flysch unit, consisting almost entirely of metagreywacke-pelite couplets interpreted as turbidites.

Archean gneisses are the only known rocks to underlie the Karrat Group, and were considered to be the major source of detritus to form the sedimentary sequences. SHRIMP U-Pb data, however, showed that this was not the case and that a significant proportion of the greywackes must have been derived from Palaeoproterozoic sources. Association of the Karrat greywackes with volcanic activity in a Palaeoproterozoic arc, relatively close to or just within an Archean continent, agrees with the chemical data, as well as the presence in the metasediments of both Archean and Proterozoic detrital zircons.

Sm-Nd data in this study are used to estimate the relative proportions of Archean and Proterozoic material in the Karrat greywackes. At 2000 Ma, the Karrat sediments had  $\epsilon_{Nd} = -3$ . Arc rocks derived from depleted mantle 2000 Ma ago would have  $\epsilon_{Nd} = +3.5$ , and Archean crustal material, derived 2900 Ma ago from depleted mantle and with Sm/Nd similar to Greenland Archean crust, would have  $\epsilon_{Nd} = -9$  at 2000 Ma. The Archean and Proterozoic components in the greywackes thus contributed more or less equal amounts of Nd to the rock. However, the Archean component probably had much higher Nd than the Proterozoic arc component. It is therefore very likely that the Proterozoic arc provided much more than half of the material that formed the Karrat greywackes.

## 6.4 Tanqua and Laingsburg depocentres

Sandstones from the Laingsburg depocentre were analysed to constrain their Sm-Nd isotopic signatures and evolution. These data are not used here for magmatic geochronology, but to determine how they compare to sandstones from the Tanqua depocentre. Analytical data are given in Table 6.1. All Sm-Nd isotopic data and geochemical data for the Skoorsteenberg Formation sandstones from the Tanqua depocentre used in this chapter are from Andersson *et al.* (2003).

The estimated time of deposition for the Skoorsteenberg and Laingsburg Formations is 270 - 260 Ma, based on an age of 270 Ma determined for the underlying Collingham Formation (Turner, 1999) and subsequent shale depositional rates within the Skoorsteenberg and Laingsburg Formations, and an average age of 265 Ma was thus chosen for the calculation of  $\epsilon_{Nd}$ . Overall, the sandstones from the Tanqua and Laingsburg depocentres show little variation in  $^{147}\text{Sm}/^{144}\text{Nd}$ , as can be seen on a Sm-Nd isotope ratios diagram (Figure 6.1). However, the sandstone from Fan F (357) of the Laingsburg Formation seems to be slightly different when compared to the rest of the samples. Sm-Nd isotopic evolution of the sandstones from the Tanqua and Laingsburg depocentres are illustrated on an age versus  $\epsilon_{Nd}$  diagram in Figure 6.2. This diagram indicates a range in  $\epsilon_{Nd}$  from  $-8.2$  to  $-7.6$  for the Tanqua sandstones and the depleted mantle model ages range from 730 to 810 Ma, with the sandstone from Unit 5 (Skoorsteenberg Formation) giving the youngest model age. The sandstones analysed from the Laingsburg depocentre have slightly more radiogenic initial  $^{143}\text{Nd}/^{144}\text{Nd}$ , corresponding to  $\epsilon_{Nd}$ -values from  $-8.2$  to  $-6.7$  (Figure 6.2). The depleted mantle model ages range from 696 to 945 Ma, with the sandstone from Fan F (357) (Laingsburg Formation) giving the youngest model age.  $\epsilon_{Nd,265 \text{ Ma}}$  ranges for the Tanqua and Laingsburg rocks, along with evolution fields for the possible source rocks, are shown in Figure 6.3. A combination of these two diagrams is given in Figure 6.4, showing that the evolution fields for the Tanqua and Laingsburg depocentre sandstones are most compatible with the evolution field of the North Patagonian Massif (NPM).

Discrimination diagrams for  $\epsilon_{Nd,265 \text{ Ma}}$  versus major oxides, trace and REE of the Tanqua and Laingsburg sandstones are illustrated in Figures 6.5 and 6.6. In most of these diagrams, the Tanqua and Laingsburg samples are distinguishable in that they plot in two separate 'fields'. However, there is some overlap of data. The  $\text{TiO}_2$ ,  $\text{K}_2\text{O}$ ,  $\text{MgO}$  and  $\text{Fe}_2\text{O}_3^{\text{T}}$  increase with decreasing  $\epsilon_{Nd,265 \text{ Ma}}$ , whereas the  $\text{Na}_2\text{O}$  increases. There is no obvious relation between the  $\epsilon_{Nd,265 \text{ Ma}}$  and the rest of the major oxides (Figure 6.5).  $\epsilon_{Nd,265 \text{ Ma}}$ -values show slight covariance with Sr and Cr, whereas V and Y show a decrease with increasing  $\epsilon_{Nd,265 \text{ Ma}}$ .

Table 6.1 Sm and Nd isotopic compositions for Tanqua and Laingsburg depocentre sandstones.

Locality and sample no.	Stratigraphic position	Rock type	Sm (ppm)	Nd (ppm)	Sm/Nd	$^{147}\text{Sm}/^{144}\text{Nd}$ 2 m	$^{143}\text{Nd}/^{144}\text{Nd}$	Nd (now) <sup>b</sup>	Nd (265 Ma) <sup>b</sup>	$T_{\text{CHUR}}^{\text{c}}$ Ma	$T_{\text{DM}}^{\text{d}}$ Ma
<b>Skoorsteenberg Formation<sup>a</sup></b>											
1:36	Fan 1	Sandstone	4.86	25.3	0.192	0.1163	0.512247 ± 13	-7.6	-4.9	740	1246
1:71	Fan 2	Sandstone	5.44	27.7	0.196	0.1189	0.512249 ± 13	-7.6	-5.0	760	1277
1:156	Fan 3	Sandstone	6.29	32.3	0.195	0.1179	0.512238 ± 6	-7.8	-5.1	770	1281
1:97	Fan 3	Sandstone	5.27	27.0	0.195	0.1179	0.512244 ± 9	-7.7	-5.0	760	1271
2:48	Fan 4	Sandstone	5.28	26.0	0.203	0.1228	0.512244 ± 12	-7.7	-5.2	810	1339
2:47	Unit 5	Sandstone	5.46	30.6	0.178	0.1080	0.512215 ± 9	-8.2	-5.3	730	1195
<b>Laingsburg Formation</b>											
380	Fan A	Sandstone	6.128	32.11	0.191	0.1153	0.512227 ± 4	-8.0	-5.3	826	1264
378	Fan B	Sandstone	8.420	42.71	0.197	0.1192	0.512216 ± 4	-8.2	-5.6	770	1333
377	Fan C	Sandstone	5.734	29.80	0.192	0.1163	0.512232 ± 3	-7.9	-5.2	770	1269
376	Fan D	Sandstone	6.612	30.59	0.216	0.1307	0.512229 ± 3	-8.0	-5.7	830	1493
375	Fan E	Sandstone	5.929	29.94	0.198	0.1197	0.512221 ± 4	-8.1	-5.5	945	1332
357	Fan F	Sandstone	6.916	34.36	0.201	0.1217	0.512296 ± 4	-6.7	-4.1	696	1238

a) Andersson *et al.* (2003).

b) Present-day and initial  $\epsilon_{\text{Nd}}$  values at 265 Ma, according to Jacobsen and Wasserburg (1984): present-day chondritic  $^{143}\text{Nd}/^{144}\text{Nd}$  ratio 0.1967, present-day chondritic  $^{143}\text{Nd}/^{144}\text{Nd}$  ratio 0.512638.

c) Model age calculated relative to the chondritic uniform reservoir (CHUR) of Jacobsen and Wasserburg (1984), using a decay constant for  $^{147}\text{Sm}$  of  $6.54 \times 10^{-12}$ .

d) Model age calculated relative to the depleted mantle curve (DM) of DePaolo (1991).

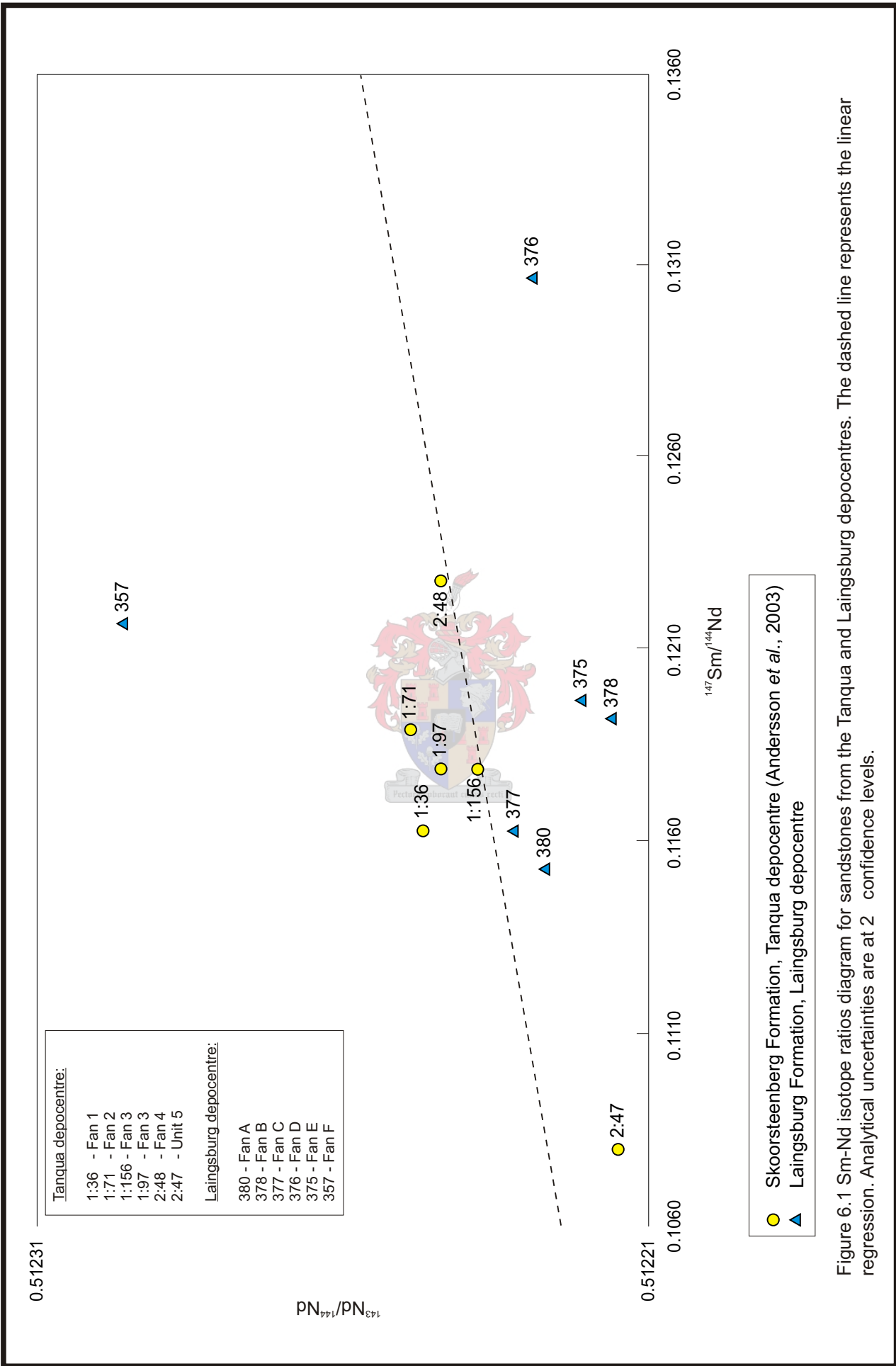


Figure 6.1 Sm-Nd isotope ratios diagram for sandstones from the Tanqua and Laingsburg depocentres. The dashed line represents the linear regression. Analytical uncertainties are at 2 confidence levels.

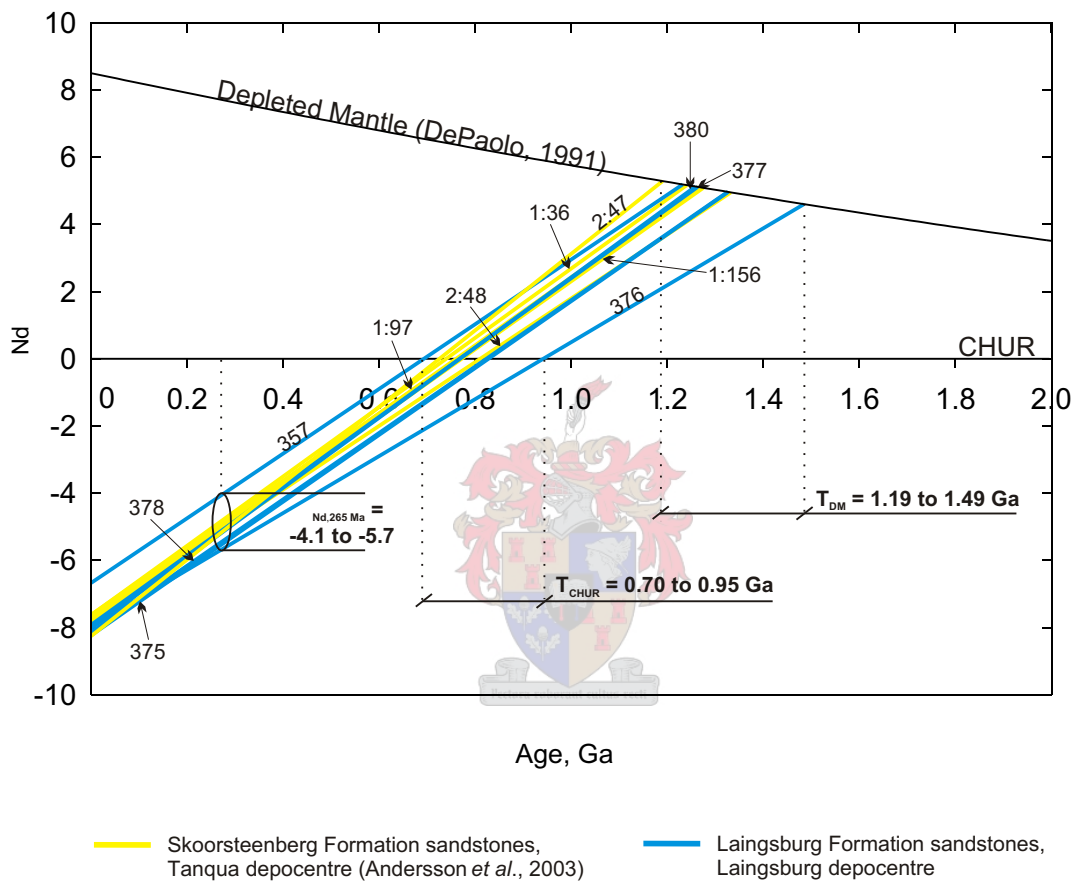


Figure 6.2  $\epsilon_{Nd}$  vs. age for the Tanqua and Laingsburg depocentre sandstones, showing how the geographic groupings also have coherence in their isotopic characteristics. Initial  $\epsilon_{Nd}$ -values at 265 Ma (inferred depositional age) are highlighted as well as model ages calculated relative to the Chondritic Uniform Reservoir (CHUR) and the depleted mantle (DM) curve of DePaolo (1991).

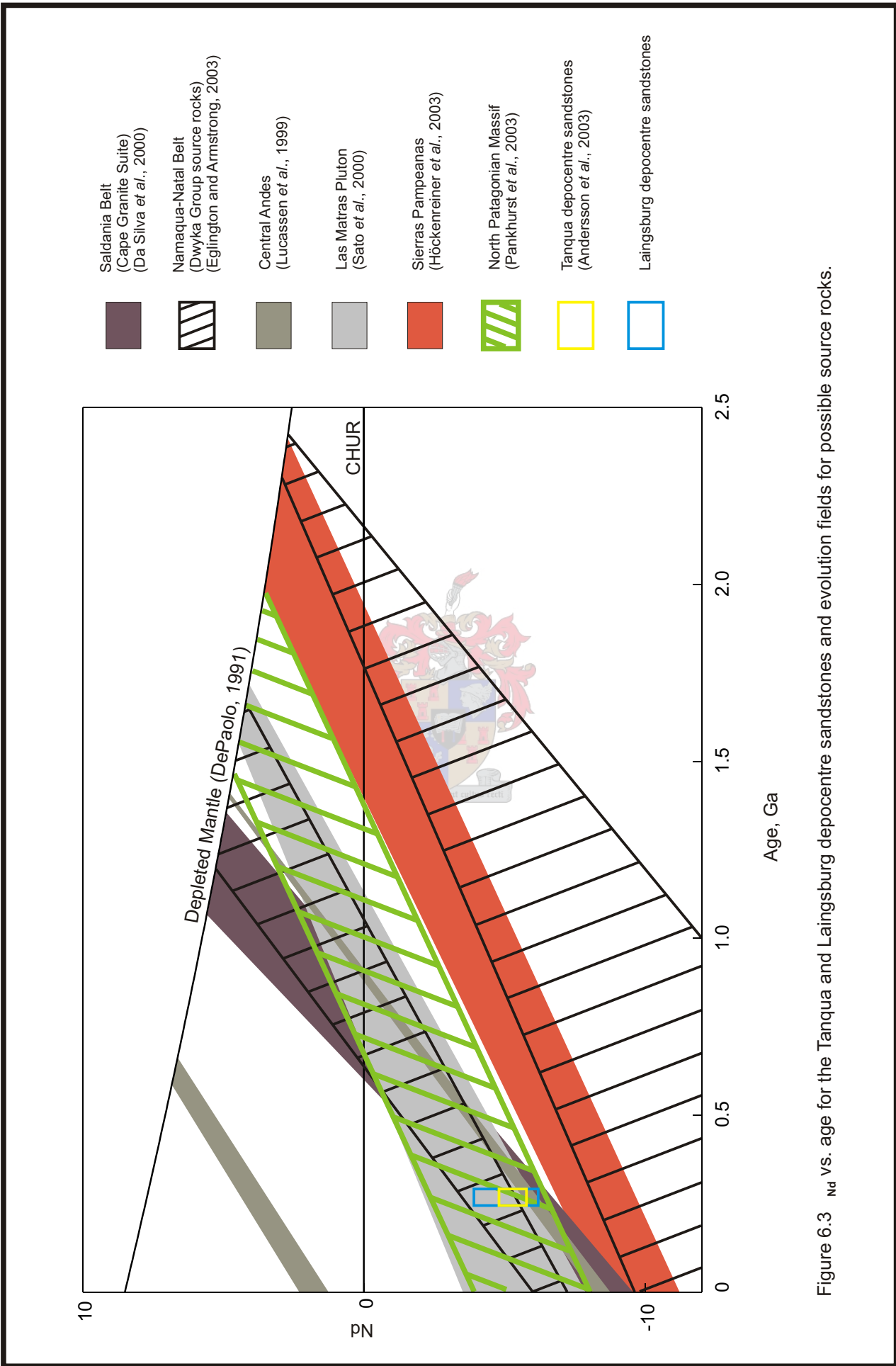
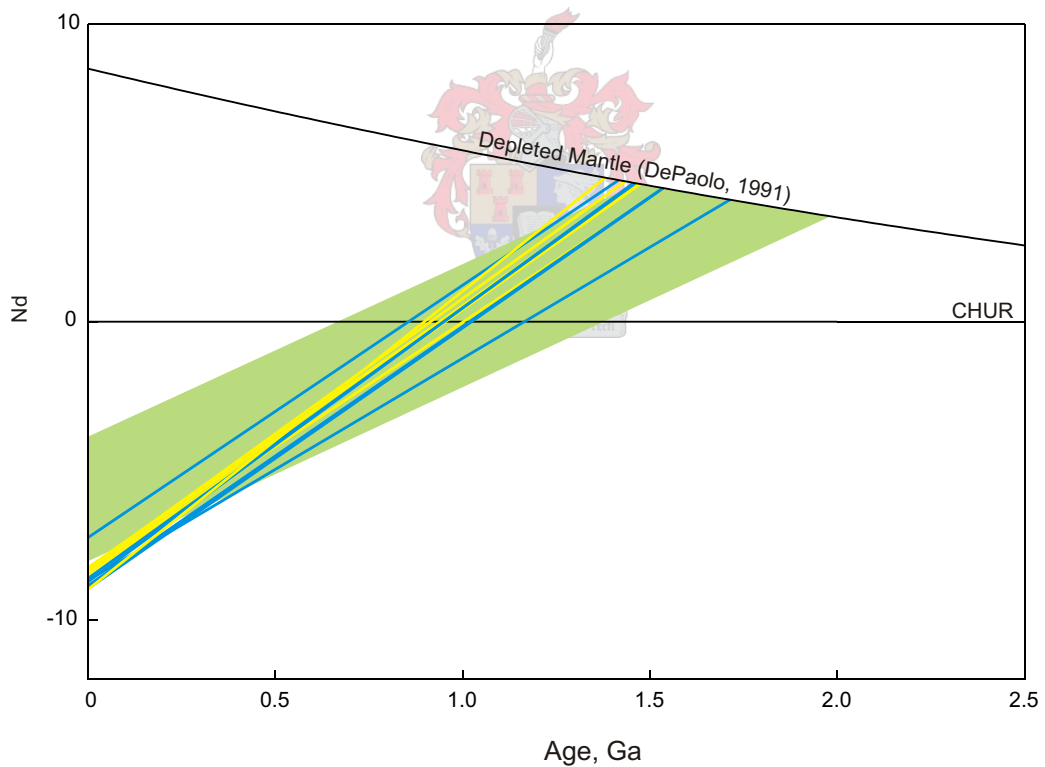
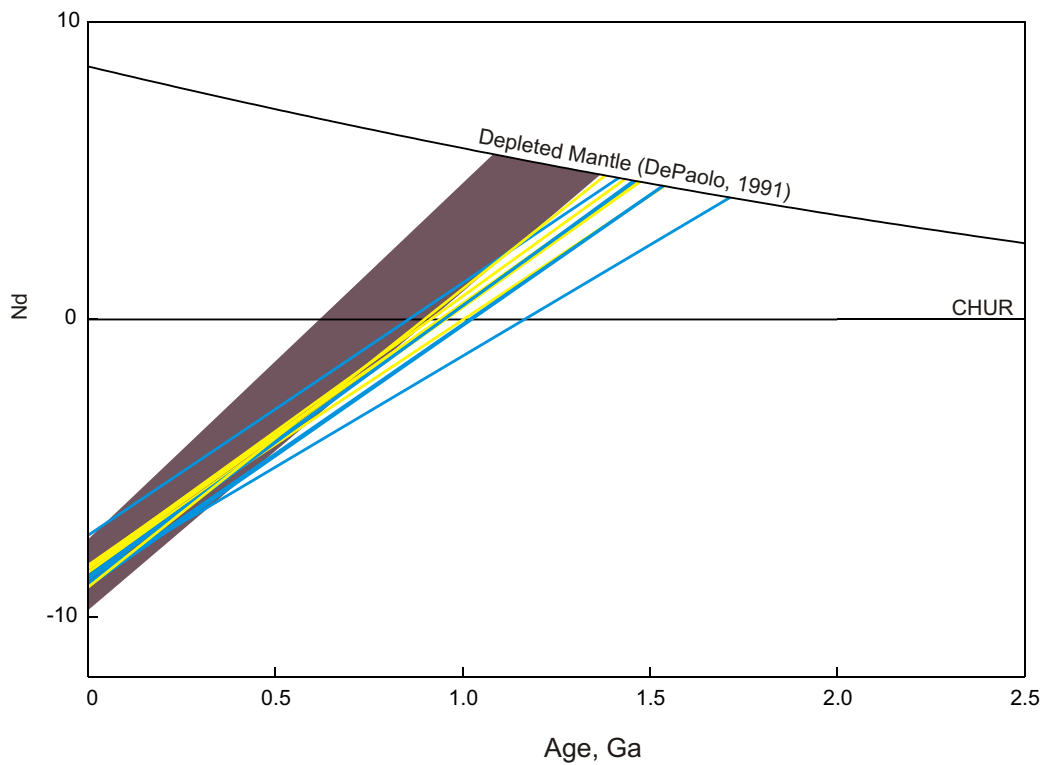


Figure 6.3  $Nd$  vs. age for the Tanqua and Laingsburg depocentre sandstones and evolution fields for possible source rocks.



- |  |  |
|--|--|
| <ul style="list-style-type: none"> <li><span style="display: inline-block; width: 15px; height: 15px; background-color: #654321; margin-right: 5px;"></span> Saldania Belt<br/>(Cape Granite Suite)<br/>(Da Silva <i>et al.</i>, 2000)</li> <li><span style="display: inline-block; width: 15px; height: 15px; background-color: #90EE90; margin-right: 5px;"></span> North Patagonian Massif<br/>(Pankhurst <i>et al.</i>, 2003)</li> </ul> | <ul style="list-style-type: none"> <li><span style="display: inline-block; width: 15px; height: 15px; background-color: yellow; margin-right: 5px;"></span> Skoorsteenberg Formation sandstones,<br/>Tanqua depocentre (Andersson <i>et al.</i>, 2003)</li> <li><span style="display: inline-block; width: 15px; height: 15px; background-color: cyan; margin-right: 5px;"></span> Laingsburg Formation sandstones,<br/>Laingsburg depocentre</li> </ul> |
|--|--|

Figure 6.4  $\epsilon_{Nd}$  vs. age evolution fields for the Tanqua and Laingsburg depocentre sandstones and possible source rocks. The isotopic characteristics of the sandstones are most consistent with the evolution field of the North Patagonian Massif, indicating it to be the most likely source for these rocks.

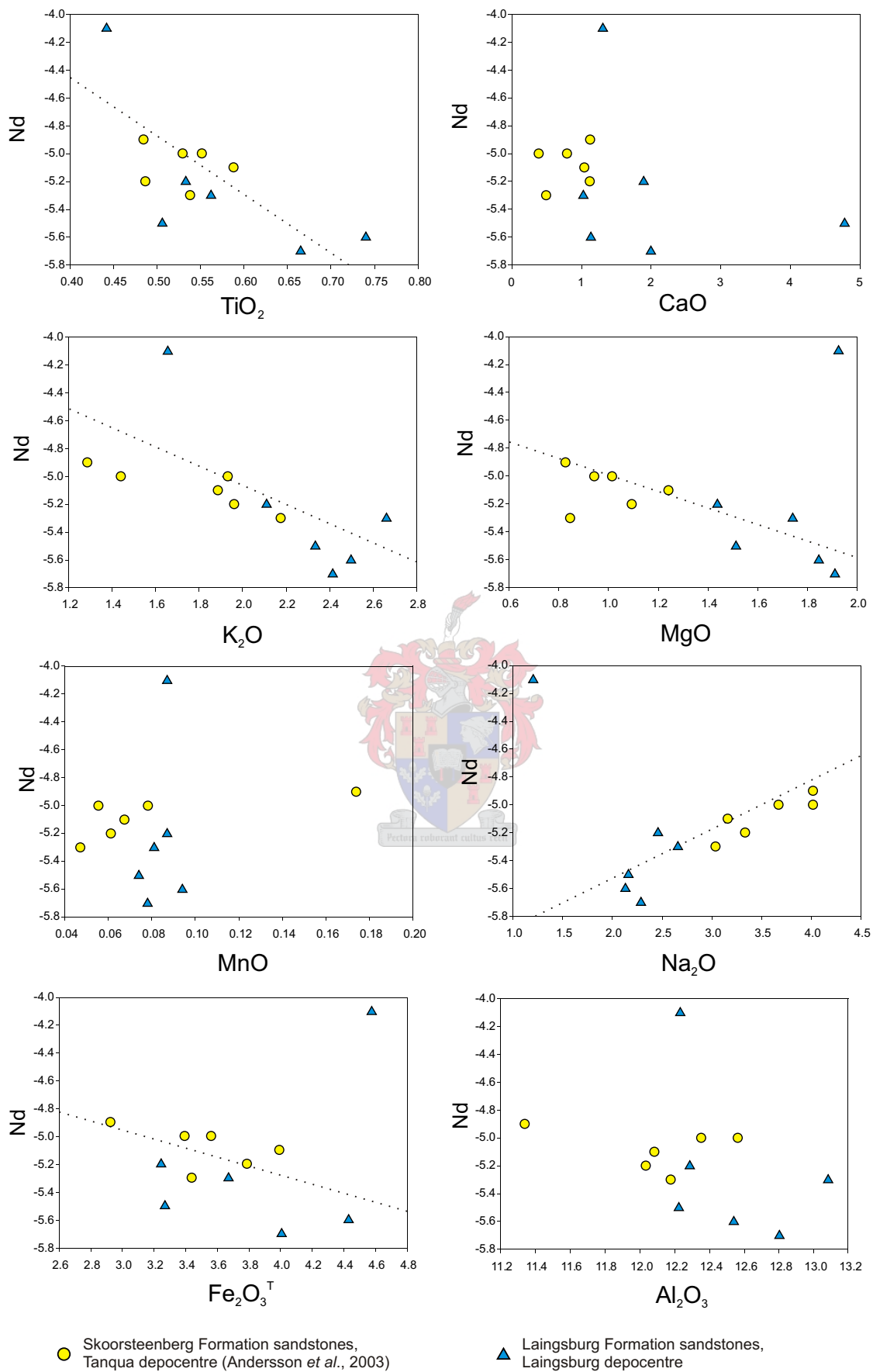


Figure 6.5  $^{265}\text{Ma}$  Nd vs. major oxides (wt.%) for sandstones from the Tanqua and Laingsburg depocentres. Linear regressions are at a confidence level of 95%.

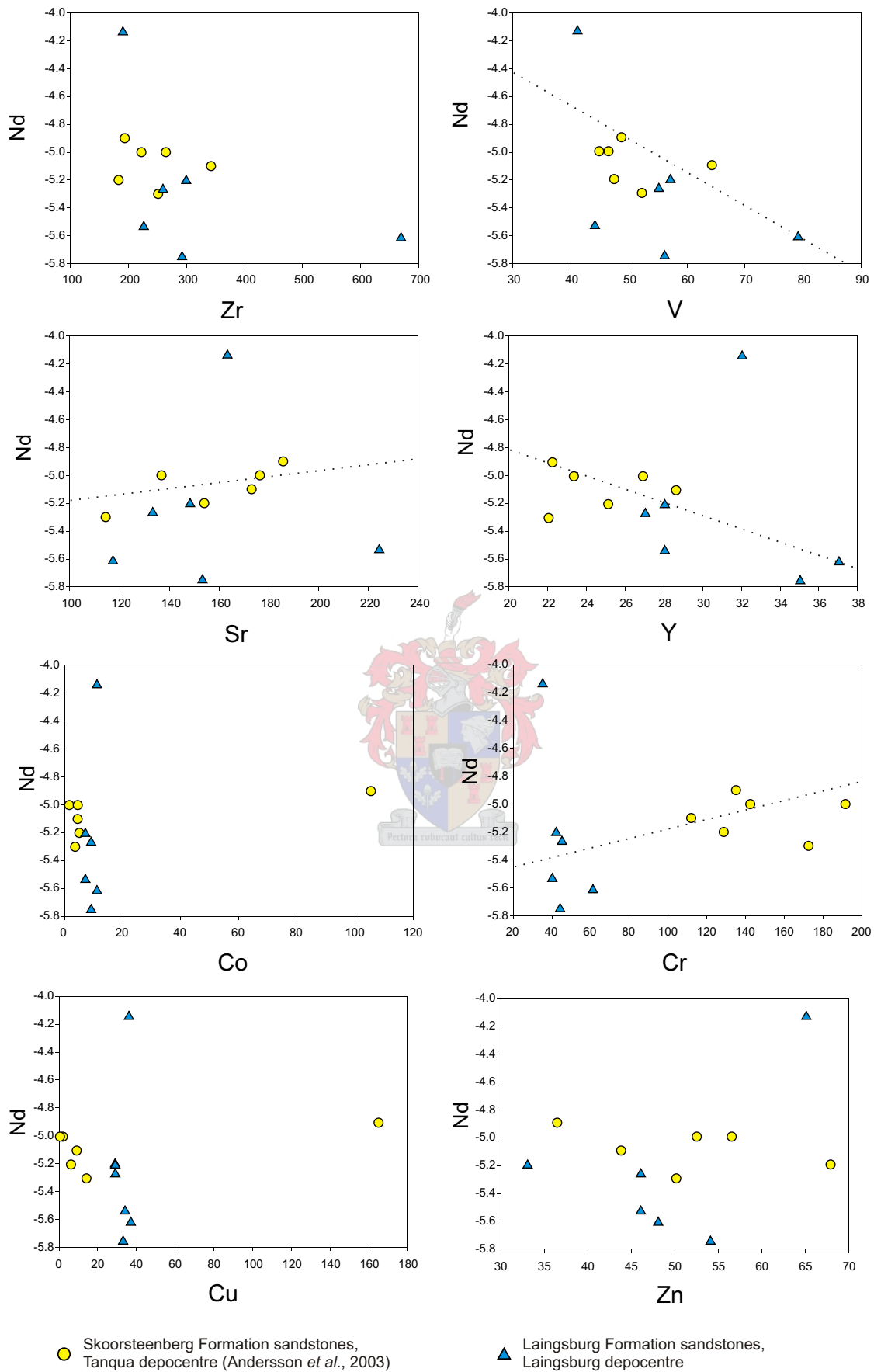


Figure 6.6  $Nd_{265\text{ Ma}}$  vs. trace and rare earth elements (ppm) for sandstones from the Tanqua and Laingsburg depocentres. Linear regressions are at a confidence level of 95%.

## 6.5 Provenance

The Tanqua and Laingsburg depocentre submarine fan systems were deposited in the Karoo foreland basin, which formed as a result of the northward subduction of the oceanic crust under the palaeo-Pacific margin of Gondwana (De Wit *et al.*, 1988; Visser, 1991; Catuneanu *et al.*, 1998).

The Cape Fold Belt (CFB) has been suggested by various authors to be the source area for the Ecca and Beaufort Groups of the Karoo Supergroup in the Karoo Basin (Kingsley, 1981; Hälbich, 1983; Cole, 1992; Veevers *et al.*, 1994; Adelman and Fiedler, 1998). Kingsley (1981) stated that the emergence of the southern source area was caused by folding of the southern pile of Cape sediments during the Permian, as a result of the drifting of a crustal plate (Antarctica (?)) towards Africa. The CFB would have been formed by the eventual collision of the southern plate with southern Africa. Metamorphosed fine-grained sediments of the Cape strata could thus have acted as the provenance for the Ecca and Beaufort sediments during and after uplift. Adelman and Fiedler (1998) also suggested the CFB as source area for the upper Ecca and lowermost Beaufort deposits (in the Laingsburg depocentre), together with an active magmatic arc presumably south of the CFB.

Contrary to this, Lock (1980) and Smellie (1981) considered the provenance to be a magmatic arc, located much closer than 1500 to 2000 km south of the basin during the Permian. Visser (1985, 1989, 1992) agreed with this and placed the early Karoo Basin in a retro-arc position north of a northward migrating orogenic belt at the palaeo-Pacific margin of Gondwana. During the early Permian, the uplifted region was initially situated more than 1200 km south of South Africa, but only a few hundred kilometres to the south during Ecca Group deposition. The concept of northward subduction of oceanic crust under the palaeo-Pacific margin of Gondwana also points to the existence of a subduction-related, volcanically active source area situated somewhere between the CFB and the palaeo-Pacific subduction site (De Wit *et al.*, 1988). Johnson (1991) considered an active magmatic arc as exclusive provenance area for the southeastern Karoo Basin during the Permian, based on sandstone petrography and the large volcanoclastic component in the lower Karoo succession. He noted that neither the uplifted CFB, nor a gneiss/granite basement constituted the main source for Ecca and Lower Beaufort Group sediments and that the influence of the CFB came into play only during the lower Triassic (Upper Beaufort Group).

Scott *et al.* (2000) proposed that the submarine fan systems of the Tanqua depocentre were deposited during a tectonic quiescence, and represent the subsequent weathering and erosion of the uplifted orogenic belt a substantial distance away. Based on microprobe studies of detrital heavy minerals (biotite, garnet and tourmaline) from the sandstones of the Vischkuil, Skoorsteenberg and Laingsburg Formations, Scott (1997) suggested mixed

source(s) for these successions, namely a granitic source and a high-grade metamorphic source, situated between the magmatic arc on top of the subduction zone and the still submerged evolving fold/thrust belt. Andersson *et al.* (2003) proposed that the source rocks for the Skoorsteenberg Formation (Tanqua depocentre) was a mixture of older (Archean (?) and Palaeoproterozoic) and successively younger source materials recycled repeatedly and a later Carboniferous to Permian juvenile component, the source area being a late Palaeozoic thrust belt and a contemporaneous magmatic arc to the south.

## 6.6 Discussion

The initial Nd values of the Tanqua and Laingsburg depocentre rocks should approximate that of their source rocks at their time of formation. The Sm/Nd ratio is not especially sensitive to changes in bulk composition (McLennan and Hemming, 1992). The Skoorsteenberg and Laingsburg Formation sandstones show Sm/Nd ratios ranging from 0.178 to 0.216 (Table 6.1), which correspond well to Archean and Post Archean Upper Continental Crust geochemical reservoir Sm/Nd ratios of 0.200 and 0.173, respectively (Taylor and McLennan, 1985). Nd isotopic data from rock units that might have been possible sources have been recalculated to  $\epsilon_{\text{Nd}}$ -values at 265 Ma, which is the estimated time of deposition for the Skoorsteenberg and Laingsburg Formations, and are summarised in Table 6.2 and Figure 6.7. The Nd-model ages (both  $T_{\text{CHUR}}$  and  $T_{\text{DM}}$ ) are well in excess of the stratigraphic age, which can be taken as indication that a substantial fraction of the sediment provenance must be composed of old or recycled crust (McLennan and Hemming, 1992). The  $\epsilon_{\text{Nd},265 \text{ Ma}}$ -values at the inferred time of deposition are around -5 for all samples, implying a substantial input of older continental material to these sediments. The Nd signatures are very homogeneous, probably due to repeated recycling.

The Tanqua sandstones all have negative  $\epsilon_{\text{Nd},265 \text{ Ma}}$ -values (-4.9 to -5.3), whereas the Laingsburg sandstones have  $\epsilon_{\text{Nd},265 \text{ Ma}}$ -values ranging from -4.1 to -5.7. This isotopic similarity indicates that the Tanqua and Laingsburg sequences represent two continuous rock suites and have not been differentially affected by alteration. This is consistent with the geochemical and petrographic record of these formations, which show a mixing of a major granitic component and a minor metamorphic component. The low  $\epsilon_{\text{Nd},265 \text{ Ma}}$ -values for the Tanqua and Laingsburg sandstones can be interpreted in terms of crustal contamination or enriched mantle to the igneous source rocks.  $T_{\text{DM}}$  model ages of 1.19 to 1.49 Ga, and  $T_{\text{CHUR}}$  model ages of 0.70 to 0.95 Ga, resulted from a mixture of Archean and Proterozoic material in unknown proportions.

A mid- to late Proterozoic origin for the sediments of the Skoorsteenberg and Laingsburg Formations is suggested by the narrow interval of initial  $\epsilon_{\text{Nd},265 \text{ Ma}}$ -values and model ( $T_{\text{DM}}$ ) ages (Andersson *et al.*, 2003; this study). Many individual source rocks of different ages could have

Table 6.2  $\epsilon_{Nd}$ -values at 265 Ma for possible source rock units in southern Africa and South America, including rock units from the Karoo Basin (modified after Andersson *et al.*, 2003). For location of the various rock units, the reader should refer to the original papers, respectively.

Crustal domain	Rock unit	Age (Ga) <sup>a</sup>	$\epsilon_{Nd}$ (265 Ma) <sup>b</sup>	References
Karoo Supergroup	Ecca Group shales	0.25	-1 to -12	Dia <i>et al.</i> (1990)
	Skoorsteenberg Formation	0.27	-5	Andersson <i>et al.</i> (2003)
Cape Supergroup	Laingsburg Formation	0.27	-5	(this study)
	Witteberg Group shales	0.40	-8 to -16	Dia <i>et al.</i> (1990)
	Bokkeveld Group shales	0.45	-6 to -8	Dia <i>et al.</i> (1990)
	Cape Granite Suite	0.55	-5 to -6	Da Silva <i>et al.</i> (2000)
Saldania Belt	Dwyka Group <sup>c</sup>	1.00 to 2.00	-4 to -20	Eglington and Armstrong (2003)
Namaqua-Natal Belt	Sierra de Limón Verde rocks	0.27	3 to -6	Lucassen <i>et al.</i> (1999)
Central Andes	Sierras Pampeanas rocks	0.40 to 0.42	-3 to -10	Höcknerreiner <i>et al.</i> (2003)
Sierras Pampeanas	Dos Hermanos rocks	0.46 to 0.58	-2 to -7	Pankhurst <i>et al.</i> (2003)
North Patagonian Massif	Las Matras rocks	1.20	0 to -6	Sato <i>et al.</i> (2000)

a) Suggested age of formation of rock units. Average depositional age for the shales and greywackes of Saldania Belt and Cape and Karoo Supergroups.

b)  $\epsilon_{Nd}$  values at 265 Ma, according to Jacobsen and Wasserburg (1984): present-day chondritic  $^{147}\text{Sm}/^{144}\text{Nd}$  ratio 0.1967, present-day chondritic  $^{143}\text{Nd}/^{144}\text{Nd}$  ratio 0.512638.

c) The Namaqua-Natal Belt is a major source for the glacial Dwyka Group sediments.

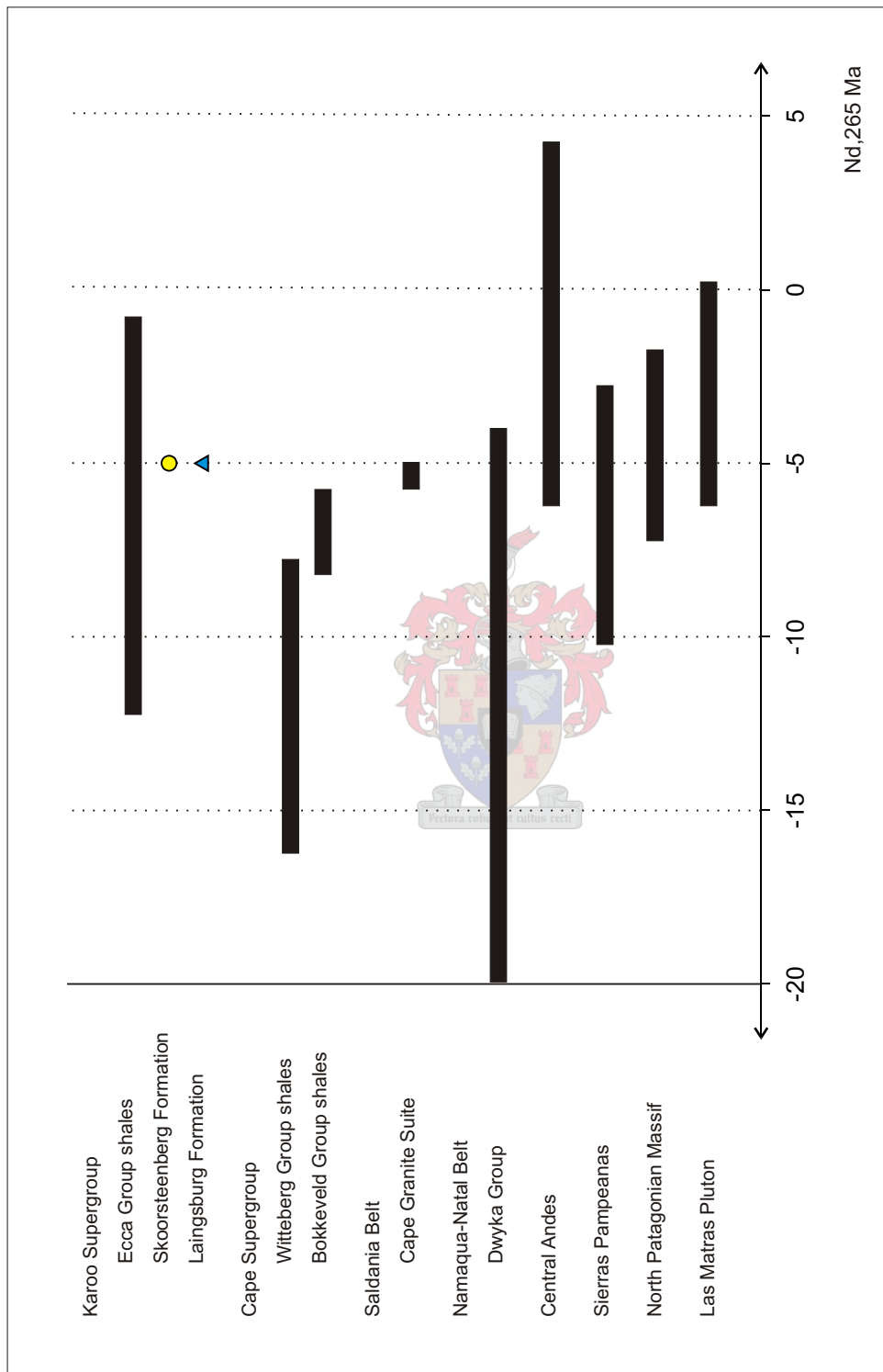


Figure 6.7  $Nd_{265}$  values for the sandstones of the Skoorsteenberg (Tanqua depocentre) and Laingsburg (Laingsburg depocentre) Formations and possible source areas (modified after Andersson *et al.*, 2003). The Namaqua-Natal Belt is a major source for the glacial Dwyka Group sediments.

been available either directly or indirectly (through recycling) at the time of deposition of these sandstones (Figure 6.8). Based on the 'best fit' evolution fields ( $\epsilon_{Nd}$  vs. age) of the Tanqua and Laingsburg sandstones to the NPM (Figures 6.3 and 6.4), it is thought to be the most likely source terrane. There is a fair bit of overlap with the evolution field of the Cape Granite Suite (CGS) as well. This could be due to minor sediment contribution by these granites, incorporated when sediment was transported across these rocks, if they were exposed during the time of deposition. Sm-Nd data from the NPM yield model ages of 1.3 to 1.6 Ga for the initial mantle extraction to form the continental source material of the granites, with the age of low-grade metamorphism experienced by some of these rocks at  $540 \pm 20$  Ma (Pankhurst *et al.*, 2003 and references therein). These units show Nd isotopic compositions corresponding to  $\epsilon_{Nd}$ -values between  $-7$  and  $-2$  at 265 Ma, with an average of  $-5$  ( $n = 6$ ). The Palaeozoic magmatic record of Patagonia is based on small outcrops of granitoid rocks whose tectonic environment is not easily interpreted. The oldest recognised episode is deposition of latest Neoproterozoic to early Cambrian sediment, followed in Cambrian times by mafic magmatism and calc-alkaline granitoid plutonism (Pankhurst *et al.*, 2003).

The Tanqua and Laingsburg sandstones plot closely on a diagram of  $\epsilon_{Nd,265 \text{ Ma}}$  vs.  $SiO_2$ , showing that these rocks have undergone the same degree of crustal contamination (Figure 6.9). Crustal rocks of granitic composition, similar to rocks from the CGS and Sierras Pampeanas (SP), probably caused this contamination. Figures 6.5 and 6.6 show trends in  $\epsilon_{Nd,265 \text{ Ma}}$  vs.  $TiO_2$ ,  $MgO$ ,  $Fe_2O_3^T$ ,  $Sr$ ,  $Y$ ,  $Cr$  and  $V$ , which could be inferred as the result of crustal contamination, and  $\epsilon_{Nd,265 \text{ Ma}}$  vs.  $K_2O$  and  $Na_2O$ , which could be inferred as the result of alteration and diagenesis (Rollinson, 1993).



## 6.7 Conclusions (answers to initial objectives)

- i. The Sm-Nd isotope data for the Tanqua and Laingsburg depocentre sandstones are very similar and it can be inferred that they originated from the same, or very similar, source(s). The data overlap in many instances, and the  $T_{DM}$  ages are generally consistent for both depocentre sandstones, showing that the rocks were separated from the mantle at the same time, confirming the same source rock units.
- ii. Fans A to E of the Laingsburg Formation show very similar results, with the exception of Fan F.  $\epsilon_{Nd}$ ,  $T_{CHUR}$  and  $T_{DM}$  values for Fan F are lower when compared to the Sm-Nd isotope data of the other fans, even when compared to the data for the Tanqua sandstones. This result is not consistent with stratigraphic, structural and geochemical data constraints, and should be considered as anomalous.
- iii. The geochemistry shows some variation with the Sm-Nd isotope data. It is possible to discriminate between the sandstones from the two depocentres in that they generally plot in two different fields on diagrams, however, there is data overlap and the fields

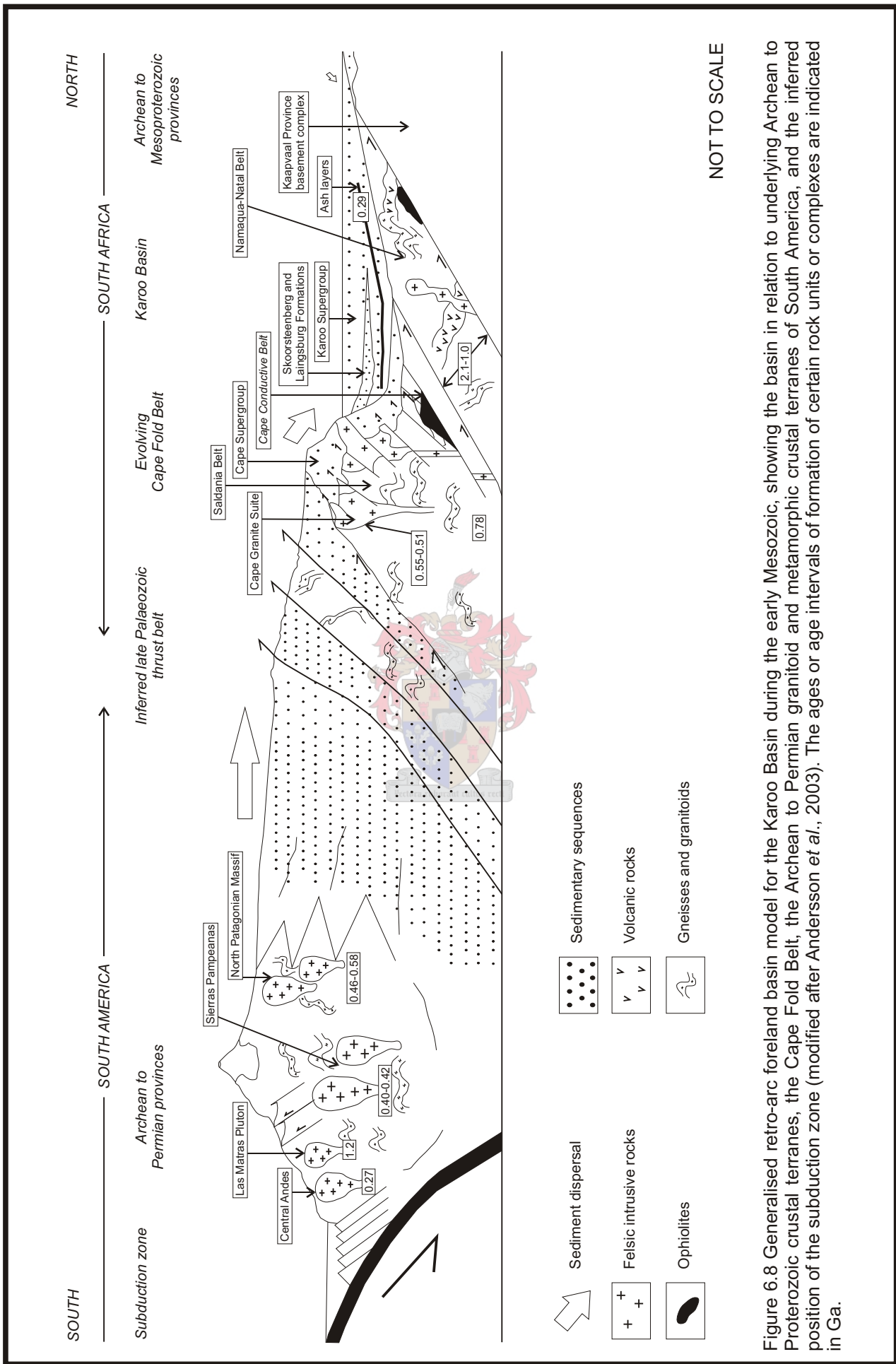
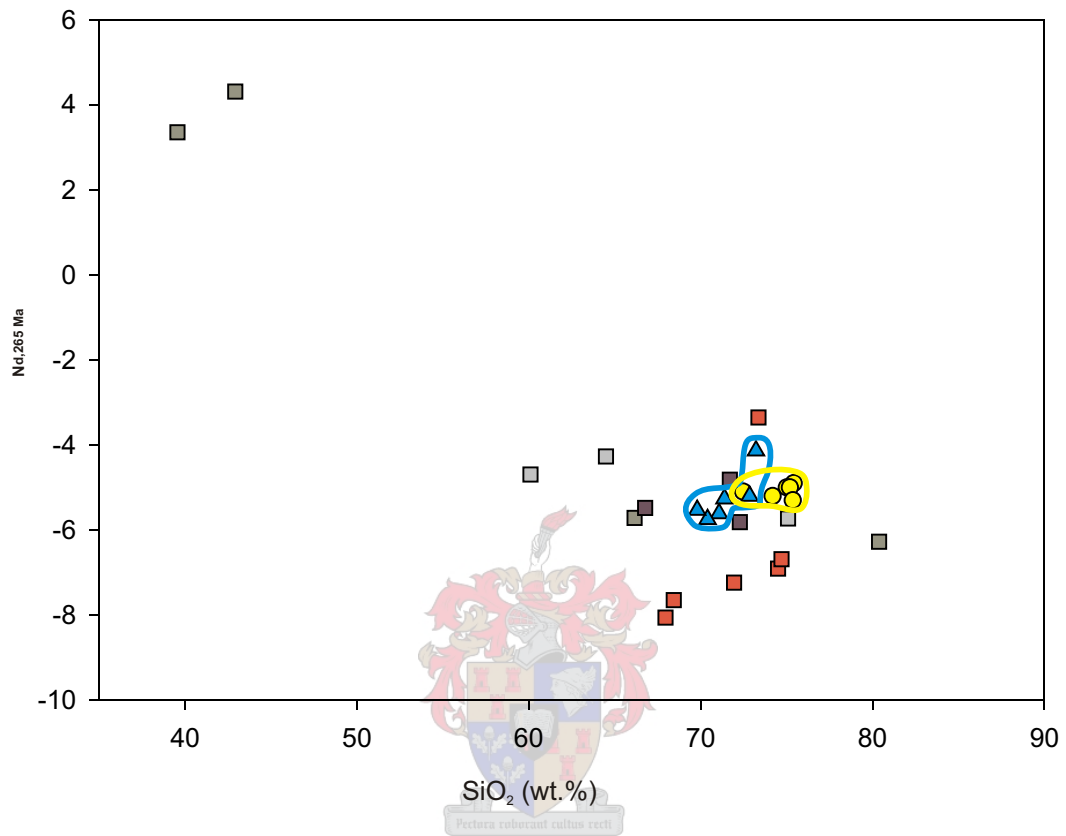


Figure 6.8 Generalised retro-arc foreland basin model for the Karoo Basin during the early Mesozoic, showing the basin in relation to underlying Archean to Proterozoic crustal terranes, the Cape Fold Belt, the Archean to Permian granitoid and metamorphic crustal terranes of South America, and the inferred position of the subduction zone (modified after Anderson *et al.*, 2003). The ages or age intervals of formation of certain rock units or complexes are indicated in Ga.

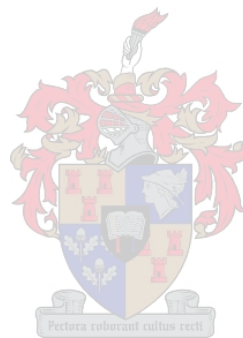


- Skoorsteenberg Formation, Tanqua depocentre (Andersson *et al.*, 2003)
- ▲ Laingsburg Formation, Laingsburg depocentre
- Sierras Pampeanas (Höckenreiner *et al.*, 2003)
- Central Andes (Lucassen *et al.*, 1999)
- Cape Granite Suite (Da Silva *et al.*, 2000)
- Las Matras Pluton (Sato *et al.*, 2000)

Figure 6.9  $Nd_{265\text{ Ma}}$  vs.  $SiO_2$  (wt.%) for the Tanqua and Laingsburg depocentre sandstones and possible source terrane rocks.

are very closely spaced to each other. Trends also show that processes such as crustal contamination of the source rocks, and alteration, occurred.

- iv. Very homogenous  $\epsilon_{Nd}$ -values of around -5 at the time of deposition (265 Ma) are yielded by the sandstones from the Skoorsteenberg and Laingsburg Formations, indicating that there is little or no variation in provenance between the two formations. The NPM, consisting of granitoids and gneisses of different ages and showing Nd isotopic compositions corresponding to  $\epsilon_{Nd}$ -values between -7 and -2 at 265 Ma, with an average of -5, is thought to be the most likely source terrane, with the possibility of minor contributions from the CGS.



## Chapter Seven

### 7 Conclusions

A summary of the most important findings regarding the spectral gamma ray (SGR), mineralogical and geochemical studies from the Permian southwestern Karoo Basin is given in this section. These studies have helped to reveal information about the sedimentary processes and the characteristics and evolution of the unknown provenance. Areas of possible future research, based on results of this project, are also outlined.

#### 7.1 Spectral gamma ray (SGR)

- K-bearing minerals (illite and chlorite) were responsible for the majority of the total gamma radiation in the mudstones and identified clay mineral peaks. The narrow trends in the Th/K ratios, ranging around 6 to 8, can also be explained by relatively constant clay mineralogy. The distinct compositional fields of Th vs. K reflect similarities in original mineralogy, suggesting the same provenance for both the Tanqua and Laingsburg depocentres. The Th/K data of the logs can also be correlated with the quartz/feldspar ratio, where decreases in the Th/K data points to decreases in the quartz/feldspar ratio.
- The SGR pattern for total counts, K, U, Th and ratios of these elements are erratic in the mudstone successions, and K-bearing minerals are responsible for the majority of the total gamma radiation in the mudstones and identified clay mineral peaks. There are no major changes between the interfan and intrafan mudstones in the SGR data set that could imply different origin, and no distinct signals in the SGR pattern of the mudstone intervals, which potentially correspond to maximum flooding surfaces.
- The total GR motif for the sand-rich turbidite sequences of the Tanqua depocentre, generally show a blocky character with a sharp base and top, typical for basin floor fans. The same can be seen for the sand-rich Fan A of the Laingsburg Formation. It was not possible to identify the subdivisions (Unit 1 to 7) indicated by maximum flooding surfaces in Fan A by applying the SGR data.
- The Th/U and U/K ratios recorded from the GR measurements, show a basinward and vertical stratigraphic evolution, primarily from the sandstones in the Tanqua depocentre, and from both siltstones and sandstones in the Laingsburg depocentre. The Th/U ratio increases, indicating an overall decrease in U. This could be due to either a decrease in the amount of U from the provenance, or a decrease in U as a result of the early settling of U-bearing heavy minerals, such as zircon.
- The distribution of the SGR data, in combination with lithology, show that it is possible to correlate successions in the Skoorsteenbergh, Kookfontein and Waterford Formations in the Tanqua depocentre. The same is true for the Laingsburg and Fort

Brown Formations in the Laingsburg depocentre. The Collingham Formation can be distinguished from the rest of the formations and measured sections based on just the SGR data. The data show higher and more erratic values with comparisons. The reason for this is the large amount of pyroclastic deposits in the form of K-bentonites within the Collingham Formation.

- Within the Tanqua depocentre, good correlation is possible between the SL1 (V20) borehole GR pattern, and the measured GR patterns from the outcrop sections, indicating the diminished effect of weathering on the accuracy of the spectrometer readings in this study.

## 7.2 Mineralogy

- The sandstones range in grain size from very fine- to lower medium-grained, are tightly packed, poorly to well sorted, and have undergone mechanical compaction and pressure solution. They have no visible porosity or permeability, primarily due to the fine grain size and the formation of authigenic quartz cement and secondary chlorite and illite.
- The primary detrital mineralogy in both the Tanqua and Laingsburg depocentre sandstones was originally quartz, albite, K-feldspar, opaques, titanite, biotite, lithic fragments and accessory muscovite, apatite and zircon, identifying them as greywackes and arkoses. The authigenic mineral assemblages that formed were chlorite, illite, hematite, calcite, quartz (cement and microquartz) and minor amounts of mica.
- The mineralogical composition and texture of the Tanqua and Laingsburg sandstones suggest that the rocks have undergone high-grade diagenesis to low-grade regional burial metamorphism to the lower greenschist facies ( $250 \pm 50^\circ\text{C}$ ;  $\sim 2$  kbars). Under conditions of average basal heat flow ( $32.5^\circ\text{C}/\text{km}$ ), hydrostatic conditions, average fluid density of  $1.1 \text{ g}/\text{cm}^3$ , and a surface temperature of  $20^\circ\text{C}$ , a temperature of  $250^\circ\text{C}$  would be obtained at 7 km burial depth.
- The sensitivity models predicting the thermal history of the southwestern Karoo Basin indicate that temperature conditions of  $250 \pm 50^\circ\text{C}$  can be reached through burial under overlying strata with a thickness of at least 7000 m. These modelling results strongly suggest that at least 7 km of Upper Karoo overburden has been stripped off the study area.
- The relative timing of the diagenetic processes in both depocentres are suggested to be albite and K-feldspar weathering and alteration to kaolinite and smectite, pore filling and alteration of kaolinite/smectite to illite. This was followed by the ductile deformation of detrital biotite and chlorite and the formation of quartz overgrowths, while the movement of formation waters were still relatively unrestricted and porosity and permeability much higher. Finally, authigenic chlorite was formed.

- The Tanqua depocentre sandstones are generally more feldspathic and contain less lithic fragments than the Laingsburg depocentre sandstones. Overall, the Tanqua depocentre sandstones are finer grained and the grains are better sorted and less angular than the Laingsburg depocentre sandstones. A possible reason for this might be the slightly longer transport distance of the sediments to the younger Tanqua depocentre. Although the provenance terrane(s) for the sediments from both depocentres are primarily from a continental and a mixed source, the continental provenance is dominant in the Tanqua depocentre, whereas the mixed provenance is dominant in the Laingsburg depocentre.
- The provenance terrane was comprised of mixed sources of granitoid and schist composition. Granites were coarse- to very coarse-grained and mineralogically consisted of quartz, alkali feldspar, sodic plagioclase, accessory apatite, titanite, zircon and magnetite. Schists, sedimentary rocks that have undergone low- to medium-grade regional metamorphism, are coarse-grained with layering defined by mica, often finely interleaved with quartz and feldspar. The primary detrital mineralogical composition of the rocks from the Tanqua and Laingsburg depocentres is consistent with this.

### 7.3 General geochemical characteristics of the southwestern Karoo Basin

- The oxides in the sandstones are concentrated in the following minerals:  $\text{Al}_2\text{O}_3$  in illite, biotite, K-feldspar and albite;  $\text{TiO}_2$  in biotite, muscovite and illite;  $\text{Fe}_2\text{O}_3^{\text{T}}$  in biotite, chlorite and illite;  $\text{Na}_2\text{O}$  in albite; and  $\text{K}_2\text{O}$  in illite and K-feldspar. Based on these, there is very little variation between sandstones from the Tanqua and Laingsburg depocentres.
- The CIA for the Tanqua depocentre rocks average between 59 and 73, and for the Laingsburg depocentre between 53 and 75, indicating a slightly to moderately weathered provenance. The ternary diagrams representing CIA, indicate that samples from the sediments of both the Tanqua and Laingsburg depocentres plot in the fields between illite-muscovite-plagioclase and illite-plagioclase-K-feldspar, due to their similar compositions and the intermediate weathering conditions in the hinterland.
- The Tanqua and Laingsburg depocentre sandstones are geochemically classified as lithic arenites and greywackes. Lithic arenites include all sandstones that contain less than 90% quartz and more rock fragments than feldspars, whereas the term greywacke can be used to include both feldspathic and lithic arenites. Geochemistry also shows that the Tanqua depocentre sandstones are slightly more mature than the Laingsburg depocentre sandstones.
- Chondrite normalised REE patterns for the sandstones from the Tanqua and Laingsburg depocentres are similar, suggesting that both form part of the same

evolutionary pattern and that the sediments have one common origin. The similar evolving REE trend in the sandstones can also be explained by the mixing of sediment from two weathering terranes with a steadily growing importance of one of them in stratigraphically younger rocks. Comparing multi-element spider diagrams for the Tanqua and Laingsburg depocentre sandstones to the normalised averages of basalt, granite, NASC, upper crust and Phanerozoic quartz arenite, show that their compositions all deviate least from the normalised average granite composition, which indicates that the provenance was predominantly composed of granitic material.

#### 7.4 Sm-Nd isotope chemistry constraints

- The Skoorsteenberg and Laingsburg Formation sandstones show Sm/Nd ratios ranging from 0.178 to 0.216, which correspond well to Archean and Post Archean Upper Continental Crust geochemical reservoir Sm/Nd ratios of 0.200 and 0.173, respectively. Homogenous  $\epsilon_{\text{Nd},265 \text{ Ma}}$ -values for all sandstone samples are around  $-5$  at the inferred time of deposition, implying a substantial input of older continental material to these sediments.
- The isotopic similarity indicates that the Tanqua and Laingsburg successions represent two continuous rock suites that have not been differentially affected by alteration. The geochemical and petrographic record of these successions, which show a mixing of a major granitic component and a minor metamorphic component, are consistent with this. The low  $\epsilon_{\text{Nd},265 \text{ Ma}}$ -values for the Tanqua and Laingsburg sandstones can be interpreted in terms of crustal contamination or enriched mantle to the igneous source rocks.  $T_{\text{CHUR}}$  model ages of 0.70 to 0.95 Ga, and  $T_{\text{DM}}$  model ages of 1.19 to 1.49 Ga, resulted from a mixture of Archean and Proterozoic material in unknown proportions.
- The most likely source terrane is thought to be the North Patagonian Massif (NPM), based on the 'best fit' evolution fields ( $\epsilon_{\text{Nd}}$  vs. age) for the Tanqua and Laingsburg sandstones compared to it. The NPM rock suites show Nd isotopic compositions corresponding to  $\epsilon_{\text{Nd}}$ -values between  $-7$  and  $-2$  at 265 Ma, with an average of  $-5$  ( $n = 6$ ). Some overlap with Cape Granite Suite (CGS) data show that these granites could also have contributed to Permian Karoo sedimentation.

#### 7.5 Provenance and tectonic setting

- The provenance for the Tanqua and Laingsburg depocentre sediments is very similar throughout, despite their thickness and great spatial extent.

- Major element data suggest that the sediments in the Tanqua and Laingsburg depocentres were derived from a felsic igneous source and deposited in an active continental margin setting.
- The sandstones of the Tanqua and Laingsburg depocentres are enriched in Cr compared to the average upper continental crust and have higher values of Ni and V. The data might reflect mixed sources, with the relative abundances of Cr, Ni and Co in the sandstones indicating some mafic/metamorphic input.
- The geochemical compositions of the sandstones from the Tanqua and Laingsburg depocentres were compared to possible sources with the use of multi-element spider diagrams. These diagrams ruled out the A-type granites of the CGS, which intruded into the Malmesbury Group metasediments. However, the I- and S-type granites are very similar in composition. The most likely provenance appears to be the NPM. The geochemical signature from the I- and S-type granites of the CGS, however, may have been incorporated when sediment was transported across these rocks, if they were exposed during the time of deposition. A combination of these rock types, with granitoids being the primary constituent and schists contributing in elements such as Ni, Co, Cr and V, will give a result closest to the sandstone compositions of the Tanqua and Laingsburg depocentres. This infers a sediment transport distance of at least 600 km, depending on the accuracy of the Gondwana reconstructions.

## **7.6 Suggestions for future work**

- U-Pb dating of single zircons will allow a more accurate dating of the sources of the Eccca Group succession. This will also help to constrain the duration of the accumulation of the Tanqua and Laingsburg depocentre successions.
- Constraining the vertical (stratigraphic) metamorphic trends, particularly in the Laingsburg depocentre, will increase the understanding of the burial history.
- Chemostratigraphic correlation between the Tanqua and Laingsburg depocentres, in particular following the Tanqua depocentre mudstone geochemistry work of Andersson and Worden (2004), into the Laingsburg depocentre, will further constrain the temporal and spatial relationship between the depocentres.
- Correlation of the Tanqua and Laingsburg depocentres to Grahamstown and the Falkland Islands to increase the understanding of Permian source area evolution.

## References

- Adams, A. E., MacKenzie, W. S. and Guilford, C. (1997). *Atlas of sedimentary rocks under the microscope*. Longman Group Limited, 104 p.
- Adelmann, D. and Fiedler, K. (1998). Origin and characteristics of Late Permian submarine fan and deltaic sediments in the Laingsburg sub-basin (SW Karoo Basin, Cape Province, South Africa). *Z. dt. Geol. Ges.* **149**, pp. 27 – 38.
- Adie, R. J. (1952). The position of the Falkland Islands in a reconstruction of Gondwanaland. *Geological Magazine* **89**, pp. 401 – 410.
- Ahmad, R., Tipper, J. C. and Eggleton, R. A. (1994). Compositional trends in the Permian sandstones from the Denison Through, Bowen Basin, Queensland reflect changing provenance and tectonics. *Sedimentary Geology* **89**, pp. 197 – 217.
- Aigner, T., Schauer, M., Junghans, W. D. and Reinhardt, L. (1995). Outcrop gamma-ray logging and its applications: examples from the German Triassic. *Sedimentary Geology* **100**, pp. 47-61.
- Aldiss, D. T. and Edwards, E. J. (1999). The Geology of the Falkland Islands. *British Geological Survey Technical Reports WC/99/10*.
- Allen, P. A. (1997). *Earth surface processes*. Blackwell Scientific Publications, UK, 404 p.
- Ambers, C. P. (2001). Evidence of elevated pressure and temperature during burial of the Salem Limestone in south-central Indiana, USA, and its implications for surprisingly deep burial. *Sedimentary Geology* **143**, pp. 245 – 257.
- Andersson, P. O. D., Johansson, Å. and Kumpulainen, R. A. (2003). Sm–Nd isotope evidence for the provenance of the Skoorsteenberg Formation, Karoo Supergroup, South Africa. *Journal of African Earth Sciences* **36 (3)**, pp. 173 – 183.
- Andersson, P. O. D. and Worden, R. H. (2004). Mudstones of the Tanqua Basin, South Africa: an analyses of lateral and stratigraphic variations within mudstones and a comparison of mudstones within and between turbidite fans. *Sedimentology*, in press.
- Bain, A. G. (1856). On the geology of southern Africa. *Transactions of the Geological Society, London (second series)* **7**, pp. 175 – 192.
- Basu, D. and Bouma, A. H. (2000). Thin-bedded turbidites of the Tanqua Karoo: physical and depositional characteristics. In: A. H. Bouma and G. Stone (eds.), *Fine-grained turbidite systems. AAPG Memoir 72/SEPM Special Publication* **68**, pp. 263 – 278.
- Bauluz, B., Mayayo, M. J., Fernandez-Nieto, C. and Gonzalez Lopez, J. M. (2000). Geochemistry of Precambrian and Paleozoic siliciclastic rocks from the Iberian Range (NE Spain): implications for source-area weathering, sorting, provenance, and tectonic setting. *Chemical Geology* **168**, pp. 135 – 150.
- Bhatia, M. R. (1983). Plate tectonics and geochemical composition of sandstones. *Journal of Geology* **91**, pp. 611 – 627.

- Bhatia, M. R. and Crook, K. A. W. (1986). Trace element characteristics of greywackes and tectonic setting discrimination of sedimentary basins. *Contributions to Mineralogy and Petrology* **92**, pp. 181 – 193.
- Bjørkum, P. A. and Gjelsvik, N. (1988). An isochemical model for the formation of authigenic kaolinite, K-feldspar and illite in sandstones. *Journal of Sedimentary Petrology* **58**, pp. 506 – 511.
- Blignaut, J. J. G., Rossouw, P. J., De Villiers, J. and Russell, H. D. (1948). The geology of the Skoorsteenberg area, Cape Province. Explan. Sheet 166 (Schoorsteenberg). *Geological Survey of South Africa*, 48 p.
- Boggs Jr., S. (1992). *Petrology of sedimentary rocks*. Macmillan Publishing Company, New York, 707 p.
- Bonjour, J. –L. and Dabard, M. –P. (1991). Ti/Nb ratios of clastic terrigenous sediments used as an indicator of provenance. *Chemical Geology* **91**, pp. 257 – 267.
- Booth, P. W. K. and Shone, R. W. (2002). A review of thrust faulting in the Eastern Cape Fold Belt, South Africa, and the implications for current lithostratigraphic interpretation of the Cape Supergroup. *Journal of African Earth Sciences* **34**, pp. 179 – 190.
- Boryta, M. and Condie, K. C. (1990). Geochemistry and origin of the Archean Beit Bridge Complex, Limpopo Belt, South Africa. *Journal of the Geological Society, London* **147**, pp. 229 – 239.
- Boulter, C. A., Hopkinson, L. J., Ineson, M. G. and Brockwell, J. S. (2004). Provenance and geochemistry of sedimentary components in the Volcano-Sedimentary Complex, Iberian Pyrite Belt: discrimination between the sill-sediment-complex and volcanic-pile models. *Journal of the Geological Society, London* **161**, pp. 103 – 115.
- Bouma, A. H. (1962). *Sedimentology of some flysch deposits*. Elsevier, Amsterdam. 168 p.
- Bouma, A. H. (2000). Fine-grained, mud-rich turbidite systems: model and comparison with coarse-grained, sand-rich systems. In: A. H. Bouma and C. G. Stone (eds.), *Fine-grained turbidite systems, AAPG Memoir 72/SEPM Special Publication* **68**, pp. 9 – 20.
- Bouma, A. H., Stelling, C. E. and Coleman, J. M. (1985). Mississippi Fan, Gulf of Mexico. In: A. H. Bouma, W. R. Normark and N. E. Barnes (eds.), *Submarine fans and related turbidite systems*. Springer-Verlag, New York, pp. 143 – 150.
- Bouma, A. H., Coleman, J. M., Stelling, C. E. and Kohl, B. (1989). Influence of relative sea-level changes on the construction of the Mississippi fan. *Geo-Marine Letters* **9**, pp. 161 – 170.
- Bouma, A. H. and Wickens, H. DeV. (1991). Permian passive margin fan complex, Karoo Basin, South Africa: possible model to Gulf of Mexico. *Trans. Gulf Coast Assoc. Geol. Soc.* **41**, pp. 30 – 42.
- Brito Neves, B. B. de and Cordani, U. G. (1991). Tectonic evolution of South America during the Late Proterozoic. *Precambrian Research* **53**, pp. 23 – 40.

- Brown, R., Gallagher, K. and Duane, M. (1994). A quantitative assessment of the effects of magmatism on the thermal history of the Karoo sedimentary sequence. *Journal of African Earth Sciences* **18 (3)**, pp. 227 – 243.
- Bruhn, R. L., Stern, C. R. and De Wit, M. J. (1978). Field and geochemical data bearing on the development of a Mesozoic volcano-tectonic rift zone and back-arc basin in southernmost South America. *Earth and Planetary Science Letters* **41**, pp. 32 – 46.
- Burchell, W. J. (1811). *Travels in the interior of southern Africa*. Facsimile Reprint (1976), C. Struik (Bpk), Cape Town, South Africa, 582 p.
- Burgess, P. M. and Moresi, L. N. (1999). Modelling rates and distribution of subsidence due to dynamic topography over subducting slabs: is it possible to identify dynamic topography from ancient strata? *Basin Research* **11**, pp. 305 – 314.
- Cadigan, R. A. (1967). Petrology of the Morrison Formation in the Colorado Plateau Region. *US Geological Survey Prof. Paper* **556**, 113 p.
- Caminos, R. (1979). Sierras Pampeanas noroccidentales. Salta, Tucumán, Catamarca, La Rioja y San Juan. In: *Segundo Simposio de Geología Regional Argentina* **1**, Academia Nacional de Ciencias, Córdoba, pp. 225 – 291.
- Caminos, R., Llambías, E. J., Rapela, C. W. and Parica, C. A. (1988). Late Paleozoic – Early Triassic magmatic activity of Argentina and the significance of new Rb-Sr ages from northern Patagonia. *Journal of South American Earth Sciences* **1 (2)**, pp. 137 – 145.
- Catuneanu, O., Sweet, A. R. and Miall, A. D. (1998). Reciprocal architecture of Bearpaw T-R Sequences, Uppermost Cretaceous, Western Canada Sedimentary Basin. *Bulletin of Canadian Petroleum Geology* **45**, pp. 75 – 94.
- Catuneanu, O., Hancox, P. J. and Rubidge, B. S. (1998). Reciprocal flexural behaviour and contrasting stratigraphies: a new basin development model for the Karoo retroarc foreland system, South Africa. *Basin Research* **10**, pp. 417 – 439.
- Catuneanu, O., Hancox, P. J., Cairncross, B. and Rubidge, B. S. (2002). Foredeep submarine fans and forebulge deltas: orogenic off-loading in the underfilled Karoo Basin. *Journal of African Earth Sciences* **35**, pp. 489 – 502.
- Cerrodo, M. E. and López de Luchi, M. G. (1998). Mamil Choique Granitoids, southwestern North Patagonian Massif, Argentina: magmatism and metamorphism associated with a polyphasic evolution. *Journal of South American Earth Sciences* **11 (5)**, pp. 499 – 515.
- Chamberlain, A. K. (1984). Surface gamma-ray logs: a correlation tool for frontier areas. *The American Association of Petroleum Geologists Bulletin* **68 (8)**, pp. 1040 – 1043.
- Chamley, H. (1990). *Sedimentology*. Springer-Verlag, Berlin.
- Cingolani, C. A., Dalla Salda, F., Hervé, F., Munizaga, F., Pankhurst, R. J., Parada, M. A. and Rapela, C. W. (1991). The magmatic evolution of northern Patagonia: new impressions of pre-Andean and Andean tectonics. *Geological Society of America Special Paper* **265**, pp. 29 – 44.

- Cingolani, C. A., Manassero, M. and Abre, P. (2003). Composition, provenance, and tectonic setting of Ordovician siliciclastic rocks in the San Rafael block: Southern extension of the Precordillera crustal fragment, Argentina. *Journal of South American Earth Sciences* **16**, pp. 91 – 106.
- Coe, A. L., Bosence, D. W. J., Church, K. D., Flint, S. S., Howell, J. A. and Wilson, R. C. L. (2003). *The sedimentary record of sea-level change*. Edited by A. L. Coe, Cambridge University Press, 288 p.
- Cole, D. I. (1992). Evolution and development of the Karoo Basin. In: M. J. De Wit and I. G. D. Ransome (eds.), *Inversion Tectonics of the Cape Fold Belt, Karoo and Cretaceous Basins of Southern Africa*, pp. 87 – 99.
- Cole, D., Wickens, H. DeV. and Viljoen, J. (1998). Lower Karoo Supergroup: glacial, basinal and terrestrial environments in the southwestern part of the main Karoo Basin. *Guidebook 10<sup>th</sup> Gondwana Conference*, University of Cape Town, South Africa, 77 p.
- Coleman, J. M. and Prior, D. B. (1982). Deltaic environments of deposition. In: P. A. Scholle and D. Spearing (eds.), *Sandstone depositional environments*. American Association of Petroleum Geologists, Tulsa, Oklahoma, pp. 139 – 178.
- Coleman, J. M., Prior, D. B. and Lindsay, J. F. (1983). Deltaic influences on shelf edge instability processes. In: D. J. Stanley and G. T. Moore (eds.), *The shelf break, critical interface on continental margins*. SEMP Special Publications **33**, pp. 121 – 137.
- Colley, S., Thomson, J., Wilson, T. R. S. and Higgs, N. C. (1984). Post-depositional migration of elements during diagenesis in brown clay and turbidite sequences in the North East Atlantic. *Geochimica et Cosmochimica Acta* **48**, pp. 1223 – 1235.
- Condie, K. C. (1993). Chemical composition and evolution of the upper continental crust: contrasting results from surface samples and shales. *Chemical Geology* **104**, pp. 1 – 37.
- Cowie, J. D. and Bassett, M. G. (1989). International Union of Geological Sciences: 1989 global stratigraphic chart with geochronometric and magnetostratigraphic calibration. *Episodes* **12 (2)**, (supplement).
- Crampton, S. L. and Allen, P. A. (1995). Recognition of forebulge unconformities associated with early stage foreland basin development: Example from the North Alpine foreland basin. *Bulletin of the American Association of Petroleum Geologists* **79**, pp. 1495 – 1514.
- Crook, K. A. W. (1974). Lithogenesis and geotectonics: the significance of compositional variations in flysch arenites (graywackes). In: Dott, R. H., Jr. and Shaver, R. H. (eds.), *Modern and ancient geosynclinal sedimentation: Society of Economic Palaeontologists and Mineralogists Special Publication* **19**, pp. 304 – 310.
- Cullers, R. L. (1994). The controls of the major and trace element variation of shales, siltstones, and sandstones of Pennsylvanian-Permian age from uplifted continental blocks in Colorado to platform sediments in Kansas, USA. *Geochimica et Cosmochimica Acta* **58**, pp. 4955 – 4972.

- Cullers, R. L., Barrett, T., Carlson, R. and Robinson, B. (1987). Rare-earth element and mineralogic changes in Holocene soil and stream sediment: a case study in the Wet Mountains, Colorado, U.S.A. *Chemical Geology* **63**, pp. 275 – 297.
- Cullers, R. L., Basu, A. and Suttner, L. (1988). Geochemical signature of provenance in sand-size material in soils and stream sediments near the Tobacco Root batholite, Montana, USA. *Chemical Geology* **70**, pp. 335 – 348.
- Curtis, M. L. (1998). Development of kinematic partitioning within a pure-shear dominated dextral transpression zone: the southern Ellsworth Mountains, Antarctica. *Geological Society of London Special Publication* **135**, pp. 289 – 306.
- Curtis, M. L. and Hyam, D. M. (1998). Late Paleozoic to Mesozoic structural evolution of the Falkland Islands: a displaced segment of the Cape Fold Belt. *Journal of the Geological Society* **155**, pp. 115 – 129.
- Dalla Salda, L., Varela, R., Cingolani, C. and Aragón, E. (1994). The Rio Chico Paleozoic Crystalline Complex and the evolution of Northern Patagonia. *Journal of South American Earth Sciences* **7 (34)**, pp. 377 – 386.
- Dalziel, I. W. D. and Elliot, D. H. (1982). West Antarctica: problem child of Gondwanaland. *Tectonics* **1**, pp. 3 – 19.
- Dalziel, I. W. D., Garrett, S. W., Grunow, A. M., Pankhurst, R. J., Storey, B. C. and Vennum, W. R. (1987). The Ellsworth-Whitmore Mountains crustal block: its role in the tectonic evolution of West Antarctica. *Geophysical Monograph* **40**, pp. 173 – 182.
- Da Silva, L. C., Gresse, P. G., Scheepers, R., McNaughton, N. J., Hartmann, L. A. and Fletcher, I. (2000). U-Pb SHRIMP and Sm-Nd age constraints on the timing and sources of the Pan-African Cape Granite Suite, South Africa. *Journal of African Earth Sciences* **30 (4)**, pp. 795 – 815.
- De'Ath, N. G. and Schuyleman, S. F. (1981). The geology of the Magnus oil field. In: L. V. Illing, G. D. Hobson and Heyden (eds.), *Petroleum geology of the continental shelf of N. W. Europe*, pp. 342 – 351.
- De Beer, C. H. (1989). Structure of the Cape Fold Belt in the Ceres Syntaxis. *M.Sc. thesis (unpublished)*, University of Stellenbosch, South Africa, 134 p.
- De Beer, C. H. (1990). Simultaneous folding in the western and southern branches of the Cape Fold Belt. *South African Journal of Geology* **93**, pp. 583 – 591.
- De Beer, C. H. (1992). Structural evolution of the Cape Fold Belt syntaxis and its influence on syntectonic sedimentation in the SW Karoo Basin. In: M. J. De Wit and I. G. D. Ransome (eds.), *Inversion Tectonics of the Cape Fold Belt, Karoo and Cretaceous Basins of Southern Africa*, pp. 197 – 206.
- De Beer, C. H. (1995). Fold interference from simultaneous shortening in different directions: the Cape Fold Belt syntaxis. *Journal of African Earth Sciences* **21 (1)**, pp. 157 – 169.
- De Beer, J. H., Van Zijl, J. S. V. and Gough, D. I. (1982). The Southern Cape Conductive Belt (South Africa): its composition, origin and tectonic significance. *Tectonophysics* **83**, pp. 205 – 225.

- DeCelles, P. G. and Giles, K. A. (1996). Foreland basin systems. *Basin Research* **8**, pp. 105 – 123.
- Deer, W. A., Howie, R. A. and Zussman, J. (1992). *An introduction to the rock-forming minerals*. (2<sup>nd</sup> Edition). Longman Scientific & Technical, 528 p.
- Den Boer, L. C. (2002). Development of a petrophysical flow model of turbidites in the Permian Tanqua subbasin, southwestern Karoo, South Africa. *M.Sc. dissertation*, Delft University of Technology, Delft, 92 p.
- DePaolo, D. J., Linn, A. M. and Schubert, G. (1991). The continental crustal age distribution: methods of determining mantle separation ages from Sm-Nd isotopic data and applications to the southwestern United States. *Journal of Geophysical Research* **96**, pp. 2071 – 2088.
- De Wit, M. J., Jeffery, M., Nicolaysen, L. O. N. and Bergh, H. (1988). *Explanatory notes on the Geologic Map of Gondwana*. American Association Petroleum Geology, Tulsa.
- De Wit, M. J. and Ransome, I. G. D. (1992). Regional inversion tectonics along the southern margin of Gondwana. In: M. J. De Wit and I. G. D. Ransome (eds.), *Inversion Tectonics of the Cape Fold Belt, Karoo and Cretaceous Basins of Southern Africa*, pp. 15 – 21.
- Dia, A., Allegre, C. J. and Erlank, A. J. (1990). The development of continental crust through geological time: the South African case. *Earth and Planetary Science Letters* **98**, pp. 74 – 89.
- Dickinson, W. R. (1974). Plate tectonics and sedimentation. *SEMP Special Publication* **22**, pp. 1 – 27.
- Dickinson, W. R. (1985). Interpreting detrital modes of greywacke and arkose. *Journal of Sedimentary Petrology* **40**, pp. 695 – 707.
- Dickinson, W. R. and Suczek, C. A. (1979). Plate tectonics and sandstone compositions. *Bulletin of the American Society of Petroleum Geologists* **63**, pp. 2164 – 2182.
- Dickinson, W. R., Beard, L. S., Brackenridge, G. R., Erjavec, J. L., Ferguson, R. C., Inman, K. F., Knepp, R. A., Lindberg, F. A. and Ryberg, P. T. (1983). Provenance of North American Phanerozoic sandstones in relation to tectonic setting. *Bulletin of the Geological Society of America* **94**, pp. 222 – 235.
- Dingle, R. V., Siesser, W. G. and Newton, A. R. (1983). *Mesozoic and Tertiary geology of southern Africa*. Balkema, Rotterdam, 375 p.
- Du Toit, A. L. (1937). *Our wandering continents*. Oliver and Boyd, Edinburgh, 366 p.
- Du Toit, A. L. (1954). *The geology of South Africa*. (Third edition). Oliver and Boyd, 611 p.
- Duncan, A. R., Erlank, A. J. and Betton, P. J. (1984). Analytical techniques and database descriptions. *Special Publications of the Geological Society of South Africa* **13**, Appendix 1, pp. 389 – 395.
- Duncan, R. A., Hooper, P. R., Rehacek, J., Marsh, J. S. and Duncan, A. R. (1997). The timing and duration of the Karoo igneous event, southern Gondwana. *Journal of Geophysical Research* **102**, pp. 127 – 138.

- Dunn, E. J. (1879). Reports on the coal outcrops of the Camdeboo and Nieuweveld Mountains. *Parliamentary Report. C. G. H.* **G37**, 31 p.
- Dunn, E. J. (1886). Reports on a supposed extensive deposit of coal underlying the central districts of the Colony. *Parliamentary Report. C. G. H.* **G8**, 12 p.
- Eglington, B. M. and Armstrong, R. A. (2003). Geochronological and isotopic constraints on the Mesoproterozoic Namaqua-Natal Belt: evidence from deep borehole intersections in South Africa. *Precambrian Research* **125**, pp. 179 – 189.
- Embry, A. F. (1995). Sequence boundaries and sequence hierarchies: problems and proposals. In: R. J. Steel, V. L. Velt, E. P. Johannessen, and C. Mathieu (eds.), *Sequence Stratigraphy on the Northwest European Margin. NPF Special Publication* **5**, pp. 1 – 11.
- Englund, J-O. and Jorgensen, P. (1973). A chemical classification scheme for argillaceous sediments and factors affecting their composition. *Geol. Foren. Stockholm Forh.* **95**, pp. 87 – 97.
- Faure, K., Armstrong, R. A., Harris, C. and Willis, J. P. (1996). Provenance of mudstones in the Karoo Supergroup of the Ellisras basin, South Africa: geochemical evidence. *Journal of African Earth Sciences* **23 (2)**, pp. 189 – 204.
- Fisher, Q. J., Casey, M., Clennell, M. B. and Knipe, R. J. (1999). Mechanical compaction of deeply buried sandstones of the North Sea. *Marine and Petroleum Geology* **16**, pp. 605 – 618.
- Fisher, Q. J., Knipe, R. J. and Worden, R. H. (2000). Microstructures of deformed and non-deformed sandstones from the North Sea: implications for the origins of quartz cement in sandstones. In: R. H. Worden and S. Morad (eds.), *Special Publication of the International Association of Sedimentologists* **29**, pp. 129 – 146.
- Flint, S. S., Hodgson, D. M., King, R. C., Potts, G. J., Van Lente, B. and Wild, R. J. (2004). The Karoo Basin Slope Project – Final Report: Phase 1. *Industry consortium report (unpublished). The Universities of Liverpool and Stellenbosch. (CD-ROM)*.
- Floyd, P. A. and Leveridge, B. E. (1987). Tectonic environment of the Devonian Gramscatho basin, south Cornwall: framework mode and geochemical evidence from turbiditic sandstones. *Journal of the Geological Society, London* **144**, pp. 531 – 542.
- Floyd, P. A., Franke, W., Shail, R. and Dorr, W. (1990). Provenance and depositional environment of Rhenohercynian synorogenic greywacke from the Giessen nappe, Germany. *Geologische Rundschau*, in press.
- Floyd, P. A., Shail, R., Leveridge, B. E. and Franke, W. (1991). Geochemistry and Provenance of Rhenohercynian synorogenic sandstones: implications for tectonic environment discrimination. In: Morton, A. C., Todd, S. P. and Haughton, P. D. W. (eds). *Developments in Sedimentary Provenance Studies. Geological Society Special Publication* **57**, pp. 173 – 188.

- Ford, A. B. (1972). Weddell Orogeny – Latest Permian to Early Mesozoic deformation at the Weddell Sea margin of the Transantarctic Mountains. *International Union of Geological Science, Series B* **1**, pp. 419 – 425.
- Getaneh, W. (2002). Geochemistry provenance and depositional tectonic setting of the Adigrat sandstone northern Ethiopia. *Journal of African Earth Sciences* **35**, pp. 185 – 198.
- Giles, M. R., Indrelid, S. L., Beynon, G. V. and Amthor, J. (2000). The origin of large-scale quartz cementation: evidence from large data sets and coupled heat-fluid mass transport modelling. In: R. H. Worden and S. Morad (eds.), *Special Publication of the International Association of Sedimentologists* **29**, pp. 21 – 38.
- Goldhammer, R. K., Wickens, H. DeV., Bouma, A. H. and Wach, G. (2000). Sequence stratigraphic architecture of the Late Permian Tanqua submarine fan complex, Karoo Basin, South Africa. In A. H. Bouma and C. G. Stone (eds.), *Fine-grained turbidite systems, AAPG Memoir 72/SEPM Special Publication* **68**, pp. 165 - 172.
- Götze, J. and Zimmerle, W. (2000). Quartz and silica as guide to provenance and sedimentary rocks. In: T. Aigner, T. Cross and V. P. Wright (eds.), *Contributions to Sedimentary Geology* **21**, 91 p.
- Govindaraju, K. (1989). 1988 compilation report on trace element in 6 anrt rock reference samples – diorite DR-N, serpentine UB-N, bauxite BX-N, disthene DT-N, granite GS-N and potash feldspar FK-N. *Geostandards Newsletter* **13 (1)**, pp. 5 – 67.
- Graham, S. A., Ingersoll, R. V. and Dickinson, W. R. (1976). Common provenance for lithic grains in Carboniferous sandstones from Quachita Mountains and Black Warrior basin. *Journal of Sedimentary Petrology* **46**, pp. 620 – 632.
- Grecula, M. (2000). Stratigraphy and architecture of tectonically controlled turbidite systems: Laingsburg Formation, Karoo Basin, South Africa. *Ph.D. thesis*, University of Liverpool, United Kingdom, 291 p.
- Grecula, M., Flint, S. S., Wickens, H. DeV. and Johnson, S. D. (2003). Upward-thickening patterns and lateral continuity of Permian sand-rich turbidite channel fills, Laingsburg Karoo, South Africa. *Sedimentology* **50**, pp. 831 – 853.
- Gresse, P. G., Theron, J. N., Fitch, F. J. and Miller, J. A. (1992). Tectonic inversion and radiometric resetting of the basement in the Cape Fold Belt. In: M. J. De Wit and I. G. D. Ransome (eds.), *Inversion Tectonics of the Cape Fold Belt, Karoo and Cretaceous Basins of Southern Africa*, pp. 217 – 228.
- Groenewald, G. H. (1989). Stratigraphy of the Tarkastad Subgroup, Karoo Supergroup, South Africa. *Ph.D. thesis (unpublished)*, University of Port Elizabeth, South Africa.
- Gromet, L. P., Dymek, R. F., Haskin, L. A. and Korotev, R. L. (1984). The “North American Shale Composite”: its compilation, major and trace element characteristics. *Geochimica et Cosmochimica Acta* **48**, pp. 2469 – 2482.
- Grunow, A. M. (1999). Gondwana events and palaeogeography: a palaeomagnetic review. *Journal of African Earth Sciences* **28 (1)**, pp. 53 – 69.

- Hälbich, I. W. (1978). Fold profiles and tectonic shortening in the Cape Fold Belt. *Geological Society of South Africa Transactions* **80**, pp. 253 – 265.
- Hälbich, I. W. (1983). A tectogenesis of the Cape Fold Belt (CFB). In: A. P. G. Söhngge and I. W. Hälbich (eds.), *Geodynamics of the Cape Fold Belt. Special Publications of the Geological Society of South Africa* **12**, pp. 165 – 175.
- Hälbich, I. W. (1992). The Cape Fold Belt Orogeny: State of the art 1970s – 1980s. In: M. J. De Wit and I. G. D. Ransome (eds.), *Inversion Tectonics of the Cape Fold Belt, Karoo and Cretaceous Basins of Southern Africa*, pp. 141 – 158.
- Hälbich, I. W. and Swart, J. (1983). Structural zoning and dynamic history of the cover rocks of the Cape Fold Belt. In: A. P. G. Söhngge and I. W. Hälbich (eds.), *Geodynamics of the Cape Fold Belt. Special Publications of the Geological Society of South Africa* **12**, pp. 165 – 175.
- Hälbich, I. W., Fitch, F. J. and Miller, J. A. (1983). Dating the Cape Orogeny. In: A. P. G. Söhngge and I. W. Hälbich (eds.), *Geodynamics of the Cape Fold Belt. Special Publications of the Geological Society of South Africa* **12**, pp. 149 – 164.
- Hamilton, W. R., Woolley, A. R. and Bishop, A. C. (1980). *The Hamlyn guide to minerals, rocks and fossils*. Hamlyn Publishing Group Limited, 320 p.
- Hartley, N. R. (2001). The geochemistry of barren Triassic sequences: Implications for chemostratigraphic correlation and reservoir characterisation. *Ph.D. thesis (unpublished)*, University of London, United Kingdom.
- Haq, B. U. (1991). Sequence stratigraphy, sea-level change, and significance for the deep sea. In: D. I. M. Macdonald (ed.), *Sedimentation, tectonics and eustasy. International Society of Sedimentologists Special Publication* **12**, pp. 3 – 39.
- Hawkesworth, C., Kelley, S., Turner, S., Le Roex, A. and Storey, B. (1999). Mantle processes during Gondwana break-up and dispersal. *Journal of African Earth Sciences* **28**, pp. 239 – 261.
- Heinrich, K. F. J. (1986). Mass absorption coefficients for electron probe microanalysis. In: J. B. Brown and R. H. Packwood (eds.), *Proceedings of the 11<sup>th</sup> International Congress on X-ray Optics and Microanalysis, London, Canada*.
- Herron, M. M. (1988). Geochemical classification of terrigenous sands and shales from core or log data. *Journal of Sedimentary Petrology* **58**, pp. 820 – 829.
- Herron, M. M. and Herron, S. L. (1990). Geological applications of geochemical well logging. In: Hurst, A., Lovell, M. A. and Morton, A. C. (eds.), *Geological applications of wireline logs, Special Publications of the Geological Society* **48**, pp. 165 – 175.
- Hesselbo, S. P. (1996). Spectral gamma-ray logs in relation to clay mineralogy and sequence stratigraphy, Cenozoic of the Atlantic margin, offshore New Jersey. In: G. S. Mountain, K. G. Miller, P. Blum, C. W. Poag and D. C. Twichell (eds.), *Proceedings of the Ocean Drilling Program, Scientific Results* **150**, pp. 411 – 422.

- Hill, I. G., Worden, R. H. and Meighan, I. G. (2000). Geochemical evolution of a palaeolaterite: the interbasaltic formation, Northern Ireland. *Chemical Geology* **166**, pp. 65 – 84.
- Hiller, N. and Stavrakis, N. (1984). Permo-Triassic fluvial systems in the southwestern Karoo Basin. *Palaeogeography, Palaeoclimatology, Palaeoecology* **45**, pp. 1 – 21.
- Höckenreiner, M., Söllner, F. and Miller, H. (2003). Dating the TIPA shear zone: an Early Devonian terrane boundary between the Famatinian and Pampean systems (NW Argentina). *Journal of South American Earth Sciences* **16**, pp. 45 – 66.
- Hoffman, J. and Hower, J. (1979). Clay mineral assemblages as low grade metamorphic geothermometers: application to the thrust faulted disturbed belt of Montana, U.S.A. In: P. A. Scholle and P. R. Schluger (eds.), *Aspects of diagenesis, SEMP Special Publication* **26**, pp. 55 – 79.
- Holzer, L., Frei, R., Barton, J.M., Kramers, J. (1998). Unraveling the record of successive high-grade events in the Central Zone of the Limpopo Belt using Pb single phase dating of metamorphic minerals. *Precambrian Research* **87**, pp. 87-115.
- Hower, J., Eslinger, E. V., Hower, M. E. and Perry, E. A. (1976). Mechanism of burial metamorphism of argillaceous sediment: 1. Mineralogical and chemical evidence. *Bulletin of the Geological Society of America* **87**, pp. 725 – 737.
- Hunter, R. E., Clifton, H. E. and Phillips, R. L. (1979). Depositional processes, sedimentary structures, and predicted vertical sequences in barred near-shore systems, southern Oregon Coast. *Journal of Sedimentary Petrology* **49**, pp. 711 – 726.
- Hurst, A. (1990). Natural gamma-ray spectrometry in hydrocarbon-bearing sandstones from the Norwegian continental shelf. In: A. Hurst, M A. Lovell and A. C. Morton (eds.), *Geological applications of wireline logs, Geological Society Special Publication* **48**, pp. 211 - 222.
- Iacumin, M., De Min, A., Piccirillo, E. M. and Bellieni, G. (2003). Source mantle heterogeneity and its role in the genesis of Late Archean-Proterozoic (2.7–1.0 Ga) and Mesozoic (200 and 130 Ma) tholeiitic magmatism in the South American Platform. *Earth-Science Reviews* **62**, pp. 365 – 397.
- Iman, M. B. and Shaw, H. F. (1985). The diagenesis of Neogene clastic sediments from the Bengal Basins Bangladesh. *Journal of Sedimentary Petrology* **55**, pp. 665 – 671.
- Ingersoll, R. V. and Busby, C. J. (1995). Tectonics of sedimentary basins. In: C. J. Busby and R. V. Ingersoll (eds.), *Tectonics of sedimentary basins*. Blackwell Scientific Publications, USA, pp. 1 – 51.
- Jacobsen, S. B. and Wasserburg, G. J. (1984). Sm-Nd isotopic evolution of chondrites and achondrites, II. *Earth and Planetary Science Letters* **67**, pp. 137 – 150.
- Jennings, S. and Thompson, G. R. (1986). Diagenesis of Plio-Pleistocene sediments of the Colorado River Delta, southern California. *Journal of Sedimentary Petrology* **56**, pp. 89 – 98.

- Jervey, M.T. (1988). Quantitative geological modelling of siliciclastic rock sequences and their seismic expression. *SEMP Special Publications* **42**, pp. 47 – 69.
- Johnson, M. R. (1976). Stratigraphy and sedimentology of the Cape and Karoo sequences in the Eastern Cape Province. *Ph.D. thesis*, Rhodes University, South Africa, 336 p.
- Johnson, M. R. (1991). Sandstone petrography, provenance and plate tectonic setting in Gondwana context of the southeastern Cape-Karoo Basin. *South African Journal of Geology* **94 (2/3)**, pp. 137 – 154.
- Johnson, M. R., Van Vuuren, C. J., Hegenberger, W. F., Key, R. and Shoko, U. (1996). Stratigraphy of the Karoo Supergroup in southern Africa: an overview. *Journal of African Earth Sciences* **23 (1)**, pp. 3 – 15.
- Johnson, M. R., Van Vuuren, C. J., Visser, J. N. J., Cole, D. I., Wickens, H. DeV., Christie, A. D. M. and Roberts, D. L. (1997). The Foreland Karoo Basin, South Africa. In: K. J. Hsü (Series editor). R. C. Selley (ed.) *Sedimentary basins of the world. African Basins*. Elsevier, pp. 269 – 317.
- Johnson, S. D., Flint, S., Hinds, D. and Wickens, H. DeV. (2001). Anatomy, geometry and sequence stratigraphy of basin floor to slope turbidite systems, Tanqua Karoo, South Africa. *Sedimentology* **48**, pp. 987 - 1023.
- Jopling, A. V. and Walker, R. G. (1968). Morphology and origin of ripple-drift cross-lamination and examples from the Pleistocene of Massachusetts. *Journal of Sedimentary Petrology* **38**, pp. 971 – 984.
- Jordan, T. E. (1995). Retroarc foreland and related basins. In: C. J. Busby and R. V. Ingersoll (eds.), *Tectonics of sedimentary basins*. Blackwell Scientific Publications, USA, pp. 331 – 362.
- Jordan, T. E. and Flemings, P. B. (1991). Large-scale stratigraphic architecture, eustatic variation, and unsteady tectonism: a theoretical evaluation. *Journal of Geophysical Research* **96 (B4)**, pp. 6681 – 6699.
- Kalsbeek, F., Pulvertaft, T. C. R. and Nutman, A. P. (1998). Geochemistry, age and origin of metagreywackes from the Palaeoproterozoic Karrat Group, Rinkian Belt, West Greenland. *Precambrian Research* **91**, pp. 383 – 399.
- Killeen, P. G. and Carmichael, C. M. (1970). Gamma-ray spectrometer calibration for field analysis of thorium, uranium and potassium. *Canadian Journal of Earth Sciences* **7**, pp. 1093 – 1098.
- King, R., Van Lente, B., Potts, G., Hodgson, D. M., Andersson, P. O. D., Worden, R. H., Flint, S. S. and Wickens, H. DeV. (2004). Extra-foreland source to turbidite sink in the early Karoo Basin, South Africa. *AAPG Annual Meeting 2004: Embrace the Future, Celebrate the Past Technical Program*.
- Kingsley, C. S. (1977). Stratigraphy and sedimentology of the Eccca Group in the Eastern Cape Province, South Africa. *Ph.D. thesis*, University of Port Elizabeth, South Africa, 290 p.

- Kingsley, C. S. (1981). A composite submarine fan-delta-fluvial model for the Ecca and lower Beaufort Groups of Permian age in the Eastern Cape Province, South Africa. *Transcripts of the Geological Society of South Africa* **84**, pp. 27 – 40.
- Kubler, B. (1966). La cristallinité de l'illite et les zones tout à fait supérieures du métamorphisme. *Inst. Geol. Univ. Neuchâtel. Colloque sur les étages tectoniques Neuchâtel*.
- Kübler, M. (1977). The sedimentology and uranium mineralisation of the Beaufort Group in the Beaufort West – Fraserburg – Merweville area, Cape Province. *M.Sc. thesis (unpublished)*, University of the Witwatersrand, South Africa, 106 p.
- Kuenen, Ph. H. (1963). Turbidites in South Africa. *Transactions of the Geological Society of South Africa* **66**, 191 p.
- Leeder, M., Raiswell, R., Al-Biatty, H., McMahon, A. and Hardman, M. (1990). Carboniferous stratigraphy, sedimentation and correlation of well 48/3-3 in the southern North Sea Basin: integrated use of palynology, natural gamma/sonic logs and carbon/sulphur geochemistry. *Journal of the Geological Society, London* **147**, pp. 287 – 300.
- Le Roex, A. P., Späth, A. and Zartman, R. E. (2001). Lithospheric thickness beneath the southern Kenya Rift: implications from basalt geochemistry. *Contributions to Mineral Petrology* **142**, pp. 89 – 106.
- Le Roux, J. P. (1993). Genesis of stratiform U-Mo deposits in the Karoo Basin of South Africa. *Ore Geology Reviews* **7 (6)**, pp. 485 – 509.
- Li, X. and McCulloch, M. T. (1996). Secular variation in the Nd isotopic composition of Neoproterozoic sediments from the southern margin of the Yangtze Block: evidence for a Proterozoic continental collision in southeast China. *Precambrian Research* **76**, pp. 67 – 76.
- Lira, R., Millone, H. O., Kirschbaum, A. M. and Moreno, R. S. (1997). Calc-alkaline arc granitoid activity in the Sierra Norte-Ambargasta Ranges, Central Argentina. *Journal of South American Earth Sciences* **10 (2)**, pp. 157 – 177.
- Lock, B. E. (1980). Flat-plate subduction and the Cape Fold Belt of South Africa. *Geology* **8**, pp. 35 – 39.
- López de Luchi, M. G. and Rapalini, A. E. (2002). Middle Jurassic dyke swarms in the North Patagonian Massif: the Lonco Trapial Formation in the Sierra de Mamil Choique, Río Negro province, Argentina. *Journal of South American Earth Sciences* **15**, pp. 625 – 641.
- López-Gamundi, O. R., Conaghan, P. J., Rossello, E. A. and Cobbold, P. R. (1995). The Tunas Formation (Permian) in the Sierras Australes Foldbelt, east central Argentina: evidence for syntectonic sedimentation in a foreland basin. *Journal of South American Earth Sciences* **8 (2)**, pp. 129 – 142.

- López-Gamundi and Rossello, E. A. (1998). Basin fill evolution and paleotectonic patterns along the Samfrau geosyncline: the Sauce Grande basin–Ventana foldbelt (Argentina) and Karoo basin-Cape foldbelt (South Africa) revisited. *Geologische Rundschau* **86**, pp. 819 – 934.
- Løvborg, L., Wollenberg, H., Sørensen, P. and Hansen, J. (1971). Field determination of uranium and thorium by gamma-ray spectrometry, exemplified by measurements in the Ilímaussaq Alkaline Intrusion, South Greenland. *Economic Geology* **66**, pp. 368 – 384.
- Løvborg, L. and Mose, E. (1987). Counting statistics in radioelement assaying with a portable spectrometer. *Geophysics* **52**, pp. 555 – 563.
- Lucassen, F., Franz, G. and Laber, A. (1999). Permian high pressure rocks – the basement of the Sierra de Limón Verde in Northern Chile. *Journal of South American Earth Sciences* **12**, pp. 183 – 199.
- Lucassen, F., Becchio, R., Harmon, R., Kasemann, S., Franz, G., Trumbull, R., Wilke, H-G., Romer, R. L. and Dulski, P. (2001). Composition and density model of the continental crust at an active continental margin – the Central Andes between 21° and 27°S. *Tectonophysics* **341**, pp. 195 – 223.
- Mack, G. H. (1984). Exceptions to the relationship between plate tectonics and sandstone composition. *Journal of Sedimentary Petrology* **54**, pp. 212 –220.
- MacKenzie, W. S., Donaldson, C. H. and Guilford, C. (1982). *Atlas of igneous rocks and their textures*. Longman Group Limited, 148 p.
- Marshall, J. E. A. (1994). The Falkland Islands: a key element in Gondwana paleogeography. *Tectonics* **13 (2)**, pp. 499 – 514.
- Martini, J. E. J. (1974). On the presence of ash beds and volcanic fragments in the greywackes of the Karroo System in the southern Cape Province (South Africa). *Transactions of the Geological Society of South Africa* **77**, pp. 113 – 116.
- Mayall, M. and Stewart, I., (2000). The architecture of turbidite slope channels. In: Weimar, P., Slatt, R.M., Coleman, J., Rosen, N.C., Nelson, H., Bouma, A.H., Styzen M.J. and Lawrence, D.T., (eds.), *Deep water reservoirs of the world, Gulf Coast Section SEPM. (CD-ROM)*.
- McCann, T. (1991). Petrological and geochemical determination of provenance in the southern Welsh Basin. In: A. C. Morton, S. P. Todd and P. D. W. Haughton (eds.), *Developments in Sedimentary Provenance Studies. Geological Society Special Publication* **57**, pp. 215 – 230.
- McCann, T. (1998). Sandstone composition and provenance of the Rotliegend of the NE German Basin. *Sedimentary Geology* **116**, pp. 177 – 198.
- McKee, E. D. (1965). Experiments on ripple lamination. In: G. V. Middleton (ed.), *Primary sedimentary structures and their hydrodynamic interpretation. Society of Economic Palaeontologists and Mineralogists Special Publication* **12**, pp. 66 – 83.

- McLachlan, I. R. (1990). Tuff beds in the northwestern part of the Karoo Basin. *South African Journal of Geology* **93** (2), pp. 329 – 338.
- McLennan, S. M. and Hemming, S. (1992). Samarium/neodymium elemental and isotopic systematics in sedimentary rocks. *Geochimica et Cosmochimica Acta* **56**, pp. 887 – 898.
- McLennan, S. M., Taylor, S. R., McCulloch, M. T. and Maynard, J. B. (1990). Geochemical and Nd-Sr isotopic composition of deep-sea turbidites: crustal evolution and plate tectonic associations. *Geochimica et Cosmochimica Acta* **54**, pp. 2051 – 2050.
- McRoberts, C. A., Furrer, H. and Jones, D. S. (1997). Palaeoenvironmental interpretation of a Triassic-Jurassic boundary section from Western Austria based on palaeoecological and geochemical data. *Palaeogeography, Palaeoclimatology, Palaeoecology* **136**, pp. 79 - 95.
- Mellere, D., Plink-Björklund, P. and Steel, R. (2002). Anatomy of shelf deltas at the edge of a prograding Eocene shelf margin, Spitsbergen. *Sedimentology* **49**, pp. 1181 – 1206.
- Middleburg, J. J., Van der Weiden, C. H. and Woittiez, J. R. W. (1988). Chemical processes affecting the mobility of major, minor and trace element during weathering of granitic rocks. *Chemical Geology* **68**, pp. 253 – 273.
- Middleton, G. V. and Hampton, M. A. (1973). Sediment gravity flows: mechanics of flow and deposition. In: G. V. Middleton and A. H. Bouma (eds.), *Turbidites and deep water sedimentation. Special Publication of the Society of Economic Palaeontologists and Mineralogists, Pacific Section*, pp. 1 – 38.
- Migeon, S., Savoye, B., Zanella, E., Mulder, T., Faugères, J.-C. and Weber, O. (2001). Detailed seismic-reflection and sedimentary study of turbidite sediment waves on the Var Sedimentary Ridge (SE France): significance for sediment transport and deposition and for the mechanisms of sediment-wave construction. *Marine and Petroleum Geology* **18**(2), pp. 179 – 208.
- Milodowski, A. E. and Zalasiewicz, J. A. (1991). Redistribution of rare earth elements during diagenesis of turbidite/hemipelagite mudrock sequences of Llandovery age from central Wales. In: A. C. Morton, S. P. Todd and P. D. W. Haughton (eds.), *Developments in Sedimentary Provenance Studies. Geological Society Special Publication* **57**, pp. 101 – 124.
- Milne, A. J. and Millar, I. L. (1989). The significance of mid-Paleozoic basement in Graham Land, Antarctic Peninsula. *Journal of the Geological Society, Special Publications* **153**, pp. 445 – 464.
- Milton, N. J. and Emery, D. (1996). Outcrop and well data. In: D. Emery and K. J. Myers (eds.), *Sequence Stratigraphy*. Blackwell Science, Oxford. pp. 61 – 79.
- Moore, J. M. and Moore, A. E. (2003). The roles of primary kimberlitic and secondary Dwyka glacial sources in the development of alluvial and marine diamond deposits in Southern Africa. *Journal of African Earth Sciences*, in press.

- Murti, K. S., Rao, R. U. M. and Aswathanarayana, U. (1984). Radioactive elements in the sediments of the Upper Proterozoic Chhattisgarh Basin, India, as indicators of palaeoenvironments. *Precambrian Research* **25**, pp. 325 – 328.
- Mutti, E. (1984). The Hecho Eocene Submarine Fan System, South-Central Pyrenees, Spain. *Geo-Marine Letters* **3**, pp. 199 – 202.
- Myers, K. J. and Bristow, C. S. (1989). Detailed sedimentology and gamma-ray log characteristics of a Namurian deltaic succession II: Gamma-ray logging. In: M. K. G. Whateley and K. T. Pickering (eds.), *Deltas: Sites and traps for fossil fuels*, Geological Society Special Publication **41**, pp. 81 – 88.
- Naqvi, S. M., Uday Raj, B., Subba Rao, D. V., Manikyamba, C., Nirmal Charan, S., Lalaram, V. and Srinivasa Sarma, D. (2002). Geology and geochemistry of arenite-quartzwacke from the Late Archean Sandur schist belt – implications for provenance and accretion processes. *Precambrian Research* **114**, pp. 177 – 197.
- Nesbitt, H. W. and Young, G. M. (1982). Early Proterozoic climates and plate motions inferred from major element chemistry of lutites. *Nature* **299**, pp. 715 – 717.
- Norrish, K. and Hutton, J. T. (1969). An accurate X-ray spectrographic method for the analysis of a wide range of geological samples. *Geochimica et Cosmochimica Acta* **33**, pp. 431 – 453.
- Odom, I. E., Doe, T. W. and Dott Jr., R. H. (1976). Nature of feldspar-grain size relations in some quartz-rich sandstones. *Journal of Sedimentary Petrology* **46**, pp. 862 – 870.
- Oelkers, E. H., Bjørkum, P. A. and Murphy, W. M. (1996). A petrographic and computational investigation of quartz cementation and porosity reduction in North Sea sandstones. *American Journal of Science* **296**, pp. 420 – 452.
- Oelofsen, B. W. and Araujo, D. C. (1987). Mesosaurus tenuidens and Stereosternum tumidum from the Permian Gondwana of both southern Africa and South America. *South African Journal of Science* **83**, pp. 370 – 372.
- Otamendi, J. E., Nullo, F. E., Patiño Douce, A. E. and Fagiano, M. (1998). Geology, mineralogy and geochemistry of syn-orogenic anatectic granites from the Achiras Complex, Córdoba, Argentina: some petrogenic and geodynamic implications. *Journal of South American Earth Sciences* **44 (4)**, pp. 407 – 423.
- Pankhurst, R. J. (1983). Rb-Sr constraints on the ages of basement rocks of the Antarctic Peninsula. In: R. L. Oliver, P. R. James and J. B. Jago (eds.), *Antarctic Earth Science: Cambridge, U.K.*, pp. 367 – 371.
- Pankhurst, R. J., Rapela, C. W., Caminos, R., Llambias, E. and Parica, C. (1992). A revised age for the granites of the central Somuncura Batholith, North Patagonian Massif. *Journal of South American Earth Sciences* **5 (3/4)**, pp. 321 – 325.
- Pankhurst, R. J., Rapela, C. W., Loske, W. P., Márquez, M. and Fanning, C. M. (2003). Chronological study of the pre-Permian basement rocks of southern Patagonia. *Journal of South American Earth Sciences* **16**, pp. 27 – 44.

- Pawellek, T. and Aigner, T. (2003). Stratigraphic architecture and gamma ray logs of deeper ramp carbonates (Upper Jurassic, SW Germany). *Sedimentary Geology* **159**, pp. 203 – 240.
- Pettijohn, F. J., Potter, P. E. and Siever, R. (1972). *Sand and sandstones*. Springer-Verlag, New York.
- Pitts, B. E., Maher, M. J., De Beer, J. H. and Gough, D. I. (1992). Interpretation of magnetic, gravity and magnetotelluric data across the Cape Fold Belt and Karoo Basin. In: M. J. De Wit and I. G. D. Ransome (eds.), *Inversion tectonics of the Cape Fold Belt, Karoo and Cretaceous Basins of Southern Africa*. A. A. Balkema, Rotterdam, pp. 27 – 32.
- Plink-Björklund, P., Steel, R.J. and Mellere, D. (2001). Turbidite variability and architecture of sand-prone, deep water slopes: Eocene clinofolds in the Central Basin, Spitsbergen. *Journal of Sedimentary Research* **71**, pp. 895 – 912.
- Plink-Björklund, P. and Steel, R.J. (2002). Perched-delta architecture and the detection of sea-level fall and rise in a slope-turbidite accumulation, Eocene Spitsbergen. *Geology* **30**, pp. 115 – 118.
- Plint, A. G. and Nummendal, D. (2000). The falling stage systems tract: recognition and importance in sequence stratigraphic analysis. In: D. Hunt and R. L. Gawthorpe (eds.), *Sedimentary responses to forced regressions*. Geological Society of London Special Publication **172**, pp. 1 – 17.
- Porębski, S. J. and Steel, R. J. (2003). Shelf-margin deltas: their stratigraphic significance and relation to deepwater sands. *Earth-Science Reviews* **62**, pp. 283 – 326.
- Posamentier, H. W. and Vail, P. R. (1988). Eustatic controls on clastic deposition II – sequence and systems tract models. In: C. K. Wilgus, B. S. Hastings, C. G. St. C. Kendall, H. W. Posamentier, C. A. Ross and J. C. Van Wagoner (eds.), *Sea Level Change – An integrated approach*. Special Publications of the Society of Economic Palaeontology and Mineralogy **42**, pp. 125 – 154.
- Posamentier, H. W., Jervey, M. T. and Vail, P. R. (1988). Eustatic controls on clastic deposition I. Conceptual framework. In: C. K. Wilgus, B. S. Hastings, C. G. St. C. Kendall, H. W. Posamentier, C. A. Ross and J. C. Van Wagoner (eds.), *Sea Level Change – An integrated approach*. Special Publications of the Society of Economic Palaeontology and Mineralogy **42**, pp. 109 – 124.
- Posamentier, H. W. and Allen, G. P. (1999). Siliciclastic sequence stratigraphy: concepts and applications. *SEMP Concepts in Sedimentology and Palaeontology* **9**, 210 p.
- Prather, B.E., (2000). Calibration and visualisation of depositional process models for above-grade slopes; a case study from the Gulf of Mexico. *Marine and Petroleum Geology* **17**, pp. 419-438.
- Prather, B. E. (2003). Controls on reservoir distribution, architecture and stratigraphic trapping in slope settings. *Marine and Petroleum Geology* **20**, pp. 529 – 545.
- Press, F. and Siever, R. (1986). *Earth*. W. H. Freeman and Company, New York, 656 p.

- Pysklywec, R. N. and Mitrovica, J. X. (1999). The role of subduction-induced subsidence in the evolution of the Karoo Basin. *Journal of Geology* **107**, pp. 155 – 164.
- Ramos, V. A. (1986). Discussion on “Tectonostratigraphy as applied to analysis of South African Phanerozoic basins”, by H. de la R. Winter. *Transactions of the Geological Society of South Africa* **89**, pp. 427 – 429.
- Ramos, V. A. (1988). Late Proterozoic – Early Paleozoic of south America – a collisional history. *Episodes* **11 (3)**, pp. 168 – 174.
- Rapela, C. W., Toselli, A., Heaman, L. and Saavedra, J. (1990). Granite plutonism of the Sierras Pampeanas: an inner cordilleran Paleozoic arc in the southern Andes. *Geological Society of America Special Paper* **241**, pp. 77 – 90.
- Rapela, C. W., Coira, B., Toselli, A. and L., Saavedra, J. (1992). El magmatismo del Paleozoico inferior en el Sudoeste de Gondwana. In: J. G. Gutierrez, J. Saavedra and I. Rabano (eds.), *Paleozoico inferior de Ibero-América*. Universidad de Extremadura, Merida. pp. 21 – 68.
- Reading, H. G. (editor). (1996). *Sedimentary environments: processes, facies and stratigraphy*. Blackwell Scientific Publications, UK, 688 p.
- Reading, H. G. and Richards, M. (1994). Turbidite systems in deep water basin margins classified by grain size and feeder system. *Bulletin of the American Association of Petroleum Geologists* **78**, pp. 792 – 822.
- Rex, D. C. (1976). Geochronology in relation to the stratigraphy of the Antarctic Peninsula: British Antarctic Survey, *Bulletin* **43**, pp. 49 – 58.
- Rider, M. H. (1986). *The geological interpretation of well logs*. Blackie Halsted Press, London – New York, 171 p.
- Rider, M. H. (1990). Gamma-ray log shape used as a facies indicator: critical analysis of an oversimplified methodology. In: A. Hurst, M. A. Lovell and A. C. Morton (eds.), *Geological applications of wireline logs. Geological Society Special Publication* **48**, pp. 27 – 37.
- Rimstidt, J. D. and Barnes, H. L. (1980). The kinetics of silica-water reactions. *Geochimica et Cosmochimica Acta* **44**, pp. 1683 – 1699.
- Rogers, A. W. (1910). Geological survey of parts of the Divisions of Beaufort West, Fraserburg, Victoria West, Sutherland and Laingsburg. *Ann. Rep. Geol. Comm. C. G. H.* **15**, pp. 9 – 66.
- Rogers, A. W. (1925). The geology of the country near Laingsburg. Explan. Cape Sheet No. 5 (Laingsburg). *Geological Survey of South Africa* **5**, 29 p.
- Rogers, A. W. and Du Toit, A. L. (1903). Geological surveys of parts of the Divisions of Ceres, Sutherland and Calvinia. *Ann. Rep. Geol. Comm. C. G. H.*, pp. 25 – 32.
- Rogers, A. W. and Schwarz, E. H. L. (1902). Report on a survey of parts of the Beaufort West, Prince Albert, and Sutherland Divisions. *Ann. Rep. Geol. Comm. C. G. H.*, pp. 100 – 106.

- Rollinson, H. (1993). *Using Geochemical Data: Evaluation, Presentation, Interpretation*. Longman Group UK Limited, 352 p.
- Rosales-Hoz, L. and Carranza-Edwards, A. (1995). Geochemistry of two Mexican tropical basins in an active margin and their influence on littoral sediments. *Journal of South American Earth Sciences* **8 (2)**, pp. 221 – 228.
- Roser, B. P. and Korsch, R. J. (1986). Provenance signatures of sandstone-mudstone suites determined using SiO<sub>2</sub> content and K<sub>2</sub>O/Na<sub>2</sub>O ratio. *Journal of Geology* **94**, pp. 635 – 650.
- Roser, B. P. and Korsch, R. J. (1988). Provenance signatures of sandstone-mudstone suites determined using discriminant function analysis of major-element data. *Chemical Geology* **67 (1 - 2)**, pp. 119 – 139.
- Rossello, E. A., Massabie, A. C., López-Gamundi, O. R., Cobbold, P. R. and Gapais, D. (1997). Late Paleozoic transpression in Buenos Aires and northeast Patagonia ranges, Argentina. *Journal of South American Earth Sciences* **10 (5 – 6)**, pp. 389 – 402.
- Rossouw, P. J., Meyer, E. I., Mulder, M. P. and Stocken, C. G. (1964). Die geologie van die Swartberge, die Kangovallei en die omgewing van Prins Albert. K. P. Explan. Sheets 3321B (Gamkapoort) and 3322A (Prince Albert). *Geological Survey of South Africa*, 93 p.
- Rowell, D. M. and De Swardt, A. M. J. (1976). Diagenesis in Cape and Karoo sediments, South Africa, and its bearing on their hydrocarbon potential. *Transactions of the Geological Society of South Africa* **79 (1)**, pp. 81-145.
- Rubridge, B. S. (1991). A new primitive dinocephalian mammal-like reptile from the Permian of southern Africa. *Palaeontology* **34**, pp. 547 – 559.
- Ruffell, A. and Worden, R. (2000). Palaeoclimate analysis using spectral gamma-ray data from the Aptian (Cretaceous) of southern England and southern France. *Palaeogeography, Palaeoclimatology, Palaeoecology* **155**, pp. 265 - 283.
- Rust, I. C. (1975). Tectonic and sedimentary framework of Gondwana Basins in southern Africa. *Third Gondwana Symposium* **5**, pp. 554 – 564.
- Ryan, P. J. (1967). Stratigraphic and Palaeocurrent analysis of the Ecca Series and lowermost Beaufort Beds in the Karroo Basin of South Africa. *Ph.D. thesis (unpublished)*. University of the Witwatersrand, South Africa, 210 p.
- Sato, A. M., Tickyj, H., Llambías, E. J. and Sato, K. (2000). The Las Matras tonalitic-trondhjemitic pluton, central Argentina: Grenvillian-age constraints, geochemical characteristics, and regional implications. *Journal of South American Earth Sciences* **13**, pp. 587 – 610.
- Scheepers, R. and Rozendaal, A. (1995). Phosphorus as a typological and mineralization potential indicator: the Cape Granite Suite of the Saldania belt as a case study. *Journal of African Earth Sciences* **21(1)**, pp. 127 – 140.

- Scheepers, R. and Armstrong, R. (2002). New U-Pb SHRIMP zircon ages of the Cape Granite Suite: implications for the magmatic evolution of the Saldania Belt. *South African Journal of Geology* **105**, pp. 241 – 256.
- Schlumberger (1987). *Log interpretation principles/applications*. Schlumberger Educational Services, 198 p.
- Schwarz, E. H. L. (1897). Geological survey of the Beaufort West District. *Ann. Rep. Geol. Comm. C. G. H. for 1896* **G81**, 12 p.
- Scotese, C. R., Boucot, A. J. and McKerrow, W. S. (1999). Gondwanan palaeogeography and palaeoclimatology. *Journal of African Earth Sciences* **28 (1)**, pp. 99 – 114.
- Scott, E. D. (1997). Tectonics and sedimentation: the evolution, tectonic influences and correlation of the Tanqua and Laingsburg subbasins, southwest Karoo Basin, South Africa. *Ph.D. thesis (unpublished)*. Louisiana State University, USA.
- Scott, E. D., Bouma, A. H. and Wickens, H. DeV. (2000). Influence of tectonics on submarine fan deposition, Tanqua and Laingsburg subbasins, South Africa. In A. H. Bouma and C. G. Stone (eds.), *Fine-grained turbidite systems, AAPG Memoir 72/SEPM Special Publication* **68**, pp. 47-56.
- Serra, O. (1984). Fundamentals of well-log interpretation. 1. The acquisition of logging data. In: *Developments of petroleum science* **15A**, Elsevier. Amsterdam – Oxford – New York – Tokyo, 423 p.
- Serra, O. (1985). *Sedimentary environments from wireline logs*. Schlumberger, 211 p.
- Siegfried, H. P. (1993). The Malmesbury Batholith and its relationship to granitic plutons in the Swartland tectonic domain. *Ph.D. thesis*, University of Stellenbosch, South Africa, 137 p.
- Simon-Brygoo, C. (1980). Analyse qualitative des diagraphies. Essai de methods d'interprétation. Thèse, University of Bordeaux, No. 1557 (*unpublished*).
- Sims, J. P., Ireland, T. R., Camacho, A., Lyons, P., Pieters, P. E., Skirrow, R. G., Stuart-Smith, P. G. and Miró, R. (1998). U-Pb, Th-Pb and Ar-Ar geochronology from the southern Sierras Pampeanas, Argentina: implications for the Paleozoic tectonic evolution of the western Gondwana margin. In: R. J. Pankhurst and C. W. Rapela (eds.), *The Proto-Andean Margin of Gondwana. Geological Society of London Special Publication* **142**, pp. 259 – 281.
- Sinclair, H. D., Coakley, B. J., Allen, P. A. and Watts, A. B. (1991). Simulation of foreland basin stratigraphy using a diffusion model of mountain belt uplift and erosion: an example from the Central Alps, Switzerland. *Tectonics* **10**, pp. 599 – 620.
- Sixsmith, P. J. (2000). Stratigraphic development of a Permian turbidite system on a deforming basin floor: turbidite systems: Laingsburg Formation, Karoo Basin, South Africa. *Ph.D. thesis*, University of Liverpool, United Kingdom, 229 p.

- Skirrow, R. G., Camacho, A., Lyons, P., Pieters, P. E., Sims, J. P., Stuart-Smith, P. G. and Miró, R. (2000). Metallogeny of the southern Sierras Pampeanas, Argentina: geological,  $^{40}\text{Ar}$ - $^{39}\text{Ar}$  dating and stable isotope evidence for Devonian Au, Ag-Pb-Zn and W ore formation. *Ore Geology Reviews* **17**, pp. 39 – 81.
- Slack, J. F. and Stevens, B. P. J. (1994). The metasediments of the Early Proterozoic Broken Hill Group, New South Wales, Australia: geochemistry, provenance, and metallogenic significance. *Geochimica et Cosmochimica Acta* **58**, pp. 3633 – 3652.
- Smellie, J. L. (1981). A complete arc-trench system recognised in Gondwana sequences of the Antarctic Peninsula region. *Geological Magazine* **118**, pp. 139 – 159.
- Smith, A. G. (1999). Gondwana: its shape, size and position from Cambrian to Triassic times. *Journal of African Earth Sciences* **28** (1), pp. 71 – 97.
- Smith, A. G., Briden, J. C. and Drewry, G. E. (1973). Phanerozoic world maps. *Special Papers in Palaeontology* **12**, pp. 1 – 42.
- Smith, R. M. H., Erickson, P. A. and Botha, W. J. (1993). A review of the stratigraphy and sedimentary environments of the Karoo-aged basins of southern Africa. *Journal of African Earth Sciences* **16**, pp. 143 – 169.
- Söhnge, A. P. G. and Hälbich, I. W. E. (1983). Geodynamics of the Cape Fold Belt. *Geological Society of South Africa Special Publication* **12**, pp. 1 – 184.
- Sprague, A.R.G., Garfield, T.R., Goulding, F.J., Beaubouef, R.T., Sullivan, M.D., Rossen, C., Campion, K.M., Sickafoose, D.K., Abreu, V., Schellpeper, M.E., Jensen, G.N., Jennette, D.C., Pirmez, C. and Dixon, B.T., (2003). Integrated slope channel depositional models: The key to successful prediction of reservoir presence and quality in offshore West Africa. *Conference Proceedings of Submarine Slope Systems: Processes, Products and Prediction*, University of Liverpool, United Kingdom, 87 p.
- Steiger, R. H. and Jäger, E. (1977). Subcommittee on geochronology: Convention on the use of decay constants in geo- and cosmochronology. *Earth and Planetary Science Letters* **36**, pp. 359-362.
- Strachan, L. J. (2002). Slump-initiated and controlled syndepositional sandstone remobilisation: an example from the Namurian of County Clare, Ireland. *Sedimentology* **49**, pp. 25 – 41.
- Svendsen, J. B. and Hartley, N. R. (2001). Comparison between outcrop-spectral gamma-ray logging and whole rock geochemistry: implications for quantitative reservoir characterisation in continental sequences. *Marine and Petroleum Geology* **18**, pp. 657 - 670.
- Tankard, A. J., Jackson, M. P. A., Eriksson, K. A., Hobday, D. K. and Minter, W. E. L. (1982). *Crustal evolution of Southern Africa – 3.8 billion years of Earth history*. Springer-Verlag, New York, 523 p.

- Taylor, S. R. and McLennan, S. M. (1981). The composition and evolution of the continental crust: rare earth element evidence from sedimentary rocks. *Phil. Trans. R. Soc.* **A301**, pp. 381 – 399.
- Taylor, S. R. and McLennan, S. M. (1985). *The continental crust: its composition and evolution*. Blackwell Scientific Publications, UK. 312 p.
- Theron, A. C. (1967). The sedimentology of the Koup Subgroup near Laingsburg. *M.Sc. thesis (unpublished)*. University of Stellenbosch, South Africa, 22 p.
- Thomas, R. J., Von Veh, M. W. and McCourt, S. (1993). The tectonic evolution of southern Africa – an overview. *Journal of African Earth Sciences* **16 (1 – 2)**, pp. 5 – 24.
- Thompson, M., Potts, P. J., Kane, J. S. and Webb, P. C. (1997). GEOPT2. International proficiency test for analytical geochemistry laboratories – Report on Round 2 (Preliminary report, May 1997). To be published in *Journal of Geostandards and Geoanalysis*.
- Tomezzoli, R. N., MacDonald, W. D. and Tickyj, H. (2003). Composite magnetic fabrics and S-C structure in granitic gneiss of Cerro de los Viejos, La Pampa province, Argentina. *Journal of Structural Geology* **25**, pp. 159 – 169.
- Tourn, S. M., Herrmann, C. J., Ametrano, S. and De Brodtkorb, M. K. (2004). Tourmalinites from the Eastern Sierras Pampeanas, Argentina. *Ore Geology Reviews* **24**, pp. 229 – 240.
- Trewin, N. H., Macdonald, D. I. M. and Thomas, C. G. C. (2002). Stratigraphy and sedimentology of the Permian of the Falkland Islands: lithostratigraphic and palaeoenvironmental links with South Africa. *Journal of the Geological Society* **159**, pp. 5 – 19.
- Tucker, M. E. (editor). (1988). *Techniques in sedimentology*. Blackwell Scientific Publications, UK, 394 p.
- Tucker, M. E. (1991). *Sedimentary Petrology: An introduction to the origin of sedimentary rocks*. Second edition. Blackwell Scientific Publications, UK, 260 p.
- Turner, B. R. (1975). The stratigraphy and sedimentary history of the Molteno Formation in the main Karoo Basin of South Africa and Lesotho. *Ph.D. thesis (unpublished)*, University of the Witwatersrand, South Africa.
- Turner, B. R. (1983). Braidplain deposition of the Upper Triassic Molteno Formation in the main Karoo (Gondwana) Basin, South Africa. *Sedimentology* **30**, pp. 77 – 89.
- Turner, B. R. (1999). Tectonostratigraphical development of the Upper Karoo foreland basin: orogenic unloading versus thermally-induced Gondwana rifting. *Journal of African Earth Sciences* **29 (1)**, pp. 215 – 238.
- Turner, J. C. M. and Baldis, B. A. J. (1978). La estructura transcontinental del límite septentrional de la Patagonia. *7 Congreso Geológico Argentino, Actas* **2**, pp. 225 – 238.

- Vail, P. R., Mitchum, R. M. and Thompson, S. (1977). Seismic stratigraphy and global changes of sea level. *In: C. E. Payton (ed.), Seismic stratigraphy – Applications to hydrocarbon exploration. American Association of Petroleum Geologists Memoir 26*, pp. 83 – 97.
- Vail, P. R., Audemard, F., Bowman, S. A., Eisner, P. N. and Perez-Cruz, C. (1991). The stratigraphic signature of tectonics, eustacy and sedimentology – an overview. *In: G. Einsele, W. Ricken and A. Seilacher (eds.), Cycles and events in stratigraphy. Springer-Verlag, New York, N. Y.*, pp. 611 – 659.
- Valloni, R., Lazzari, D. and Calzolari, M. A. (1991). Selective alteration of arkose framework in Oligo-Miocene turbidites of the Northern Apennines foreland: impact on sedimentary provenance analysis. *In: A. C. Morton, S. P. Todd and P. D. W. Haughton (eds.), Developments in sedimentary provenance studies. Geological Society Special Publication 57*, pp. 125 – 136.
- Van Der Werff, W., Flint, S. S., Johnson, S. D. and Wickens, H. DeV. (2000). High-resolution 3-D architecture and pinchout geometries of basin floor fans, Tanqua Karoo, South Africa. *In: AAPG Annual Meeting Abstract Volume, April 16 – 19 2000, New Orleans*, A151.
- Van Buchem, F. S. P., Melnyk, D. H. and McCave, I. N. (1992). Chemical cyclicity and correlation of Lower Lias mudstones using gamma-ray logs, Yorkshire, UK. *Journal of the Geological Society, London 149*, pp. 991 – 1002.
- Van Wagoner, J. C., Mitchum, R. M. Jr., Campion, K. M. and Rahmanian, V. D. (1990). Siliciclastic sequence stratigraphy in well logs, cores and outcrop. *American Association of Petroleum Geologists. Methods in Exploration 7*, 55 p.
- Veevers, J. J. and Powell, C. M. (1987). Late Palaeozoic glacial episodes in Gondwanaland reflected in transgressive-regressive depositional sequences in Euramerica. *Geological Society of America Bulletin 98*, pp. 475 – 487.
- Veevers, J. J., Powell, C., Collinson, J. W. and López-Gamundi, O. R. (1994). Synthesis. *In J. J. Veevers and C. Powell (eds.), Permian-Triassic Pangean Basins and Foldbelts along the Panthalassan Margin of Gondwanaland. Geological Society of America Memoir 184*, pp. 223 – 279.
- Velde, B. (1965). Phengite micas: synthesis, stability, and natural occurrences. *American Journal of Science 263*, pp. 886 – 913.
- Viljoen, J. H. A. (1992a). Lithostratigraphy of the Collingham Formation (Ecca Group), including the Zoute Kloof, Buffels River and Wilgehout River members and the Matjiesfontein Chert Bed. *South African Committee for Stratigraphy, Lithostratigraphic Series 22*, 10 p.
- Viljoen, J. H. A. (1992b). Lithostratigraphy of the Laingsburg Formation (Ecca Group). *South African Committee for Stratigraphy, Lithostratigraphic Series 20*, 7 p.

- Viljoen, J. H. A. (1995). Piroklastiese afsettings van Perm-ouderdom in die hoof-Karookom met spesiale verwysing na die Collingham Formasie, Ecca Groep. *Ph.D. thesis*. University of Stellenbosch, South Africa, 274 p.
- Viljoen, J. H. A. and Wickens, H. DeV. (1992). Lithostratigraphy of the Vischkuil Formation (Ecca Group). *South African Committee for Stratigraphy, Lithostratigraphic Series* **19**, 7 p.
- Visser, J. N. J. (1984). A review of the Stormberg Group and Drakensberg volcanics in southern Africa. *Palaeontol. Afr.* **25**, pp. 5 – 27.
- Visser, J. N. J. (1985). Discussion on “Tectonostratigraphy as applied to analysis of South African Phanerozoic basins”, by H. de la R. Winter. *Transactions of the Geological Society of South Africa* **88**, pp. 183 – 185.
- Visser, J. N. J. (1986). Lateral lithofacies relationships in the glaciogene Dwyka Formation in the western and central parts of the Karoo Basin. *Transactions of the Geological Society of South Africa* **89**, pp. 373 – 383.
- Visser, J. N. J. (1989). The Permo-Carboniferous Dwyka Formation of Southern Africa: deposition by a predominantly subpolar marine ice-sheet. *Palaeogeography, Palaeoclimatology, Palaeoecology* **70**, pp. 377 – 391.
- Visser, J. N. J. (1991). Self-destructive collapse of the Permo-Carboniferous marine ice sheet in the Karoo Basin: evidence from the southern Karoo. *South African Journal of Geology* **94**, pp. 255 – 262.
- Visser, J. N. J. (1992). Basin tectonics in southwestern Gondwana during the Carboniferous and Permian. In: M. J. De Wit and I. G. D. Ransome (eds.), *Inversion Tectonics of the Cape Fold Belt, Karoo and Cretaceous Basins of Southern Africa*, pp. 109 – 115.
- Visser, J. N. J. (1997). Deglaciation sequences in the Permo-Carboniferous Karoo and Kalahari basins of southern Africa: a tool in the analysis of cyclic glaciomarine basin fills. *Sedimentology* **44 (3)**, pp. 507 – 521.
- Visser, J. N. J. and Loock, J. C. (1978). Water depth in the main Karoo Basin in South Africa during Permian sedimentation. *Transactions of the Geological Society of South Africa* **81**, pp. 185 – 191.
- Visser, J. N. J. and Young, G. M (1990). Major element geochemistry and palaeoclimatology of the Permo-Carboniferous glaciogene Dwyka Formation and post-glacial mudrocks in southern Africa. *Palaeogeography, Palaeoclimatology, Palaeoecology* **81**, pp. 49 – 57.
- Visser, J. N. J. and Praekelt, H. E. (1998). Late Palaeozoic crustal block rotations within the Gondwana sector of Pangea. *Tectonophysics* **287**, pp. 201 – 212.
- Visser, J. N. J., Loock, J. C. and Jordaan, M. J. (1980). Permian deltaic sedimentation in the western half of the Karoo Basin, South Africa. *Transactions of the Geological Society of South Africa* **83**, pp. 415 – 424.

- Von Gosen, W. (2002). Polyphase structural evolution in the northeastern segment of the North Patagonian Massif (southern Argentina). *Journal of South American Earth Sciences* **15** (6), pp. 591 – 623.
- Wach, G. D., Lukas, T. C., Goldhammer, R. K., Wickens, H. DeV., Bouma, A. H. and Wach, G. (2000). Submarine fan through slope to deltaic transition basin-fill succession, Tanqua Karoo, South Africa. In A. H. Bouma and C. G. Stone (eds.), *Fine-grained turbidite systems, AAPG Memoir 72/SEPM Special Publication* **68**, pp. 173-180.
- Watts, A. B. (1992). The effective elastic thickness of the lithosphere and the evolution of foreland basins. *Basin Research* **4**, pp. 169 – 178.
- Waugh, B. (1970). Formation of quartz overgrowths in the Penrith sandstone (Lower Permian) of northwest England as revealed by scanning electron microscopy. *Sedimentology* **14**, pp. 309 – 320.
- Weber, J. N. and Middleton, G. V. (1961). Geochemistry of the turbidites of the Normanskill and Charny formations – I. Effects of turbidity currents on the chemical differentiation of turbidites. *Geochimica et Cosmochimica Acta* **22**, pp. 200 – 243.
- Weber, J. N. and Middleton, G. V. (1961). Geochemistry of the turbidites of the Normanskill and Charny formations – II. Distribution of trace elements. *Geochimica et Cosmochimica Acta* **22**, pp. 244 – 288.
- Wickens, H. DeV. (1992). Submarine fans of the Permian Ecca Group in the SW Karoo Basin: their origin and reflection on the tectonic evolution of the basin and its source areas. In: M. J. De Wit and I. G. D. Ransome (eds.), *Inversion Tectonics of the Cape Fold Belt, Karoo and Cretaceous Basins of Southern Africa*, pp. 117 – 125.
- Wickens, H. DeV. (1994). Basin floor fan building turbidites of the southwestern Karoo Basin, Permian Ecca Group, South Africa. *Ph.D. thesis*, University of Port Elizabeth, South Africa, 233 p.
- Wickens, H. DeV., Brink, G. J., Basson, V. A. and Van Rooyen, W. (1990). The sedimentology of the Skoorsteenberg Formation and its applicability as a model for submarine fan turbidite deposits in the Bredasdorp Basin. *Unpublished report*, SOEKOR, Parow, 47 p.
- Wickens, H. DeV., Brink, G. J., Van Rooyen, W., Bouma, A. H. and Brown, L. F., Jr. (1992). The Tanqua turbidite and deltaic complexes: Depositional models, reservoir realities and the application of sequence stratigraphy. *AAPG Field Seminar Guidebook. April 1992*. SOEKOR, Parow, South Africa, 180 p.
- Wickens, H. DeV. and Bouma, A. H. (2000). The Tanqua Fan Complex, Karoo Basin, South Africa – Outcrop analog for fine-grained, deepwater deposits. In: A. H. Bouma and C. G. Stone (eds.), *Fine-grained turbidite systems, AAPG Memoir 72/SEPM Special Publication* **68**, pp. 153 – 164.
- Wild, R. J. (*in preparation*). Sedimentology and sequence stratigraphy of a siliciclastic lower slope to shelf-edge depositional system, Tanqua depocentre, S.W. Karoo Basin, South Africa. *Ph.D. thesis*, University of Liverpool, United Kingdom.

- Willan, R. C. R. (2003). Provenance of Triassic-Cretaceous sandstones in the Antarctic Peninsula: implications for terrane models during Gondwana breakup. *Journal of Sedimentary Research* **73 (6)**, pp. 1062 – 1077.
- Winchester, J. A. and Floyd, P. A. (1977). Geochemical discrimination of different magma series and their differentiation products using immobile elements. *Chemical Geology* **20**, pp. 325 – 343.
- Winkler, H. F. (1965). Petrogenesis of metamorphic rocks. *Springer-Verlag*.
- Winter, H. de la R. (1984). Tectonostratigraphy as applied to analysis of South African Phanerozoic basins. *Transactions of the Geological Society of South Africa* **87**, pp. 169 – 179.
- Worden, R. H. and Burley, S. D. (2003). Sandstone diagenesis: the evolution of sand to stone. In: S. D. Burley and R. H. Worden (eds.), *Sandstone diagenesis: recent and ancient, International Association of Sedimentologists Reprint Series 4*, pp. 3 – 44.
- Worden, R. H. and Morad, S. (2003). Clay minerals in sandstones: controls on formation, distribution and evolution. *International Association of Sedimentologists Special Publication 34*, pp. 3 – 41.
- Young, G. M. and Nesbitt, H. W. (1998). Process controlling the distribution of Ti and Al in weathering profiles, siliciclastic sediments and sedimentary rocks. *Journal of Sedimentary Research* **68**, pp. 448 – 455.
- Zhang, E. and Davis, A. (1993). Coalification patterns of the Pennsylvanian coal measures in the Appalachian foreland basin, western and south-central Pennsylvania. *Geological Society of America Bulletin* **105 (2)**, pp. 162 – 174.
- Zimmermann, U. and Bahlburg, H. (2003). Provenance analysis and tectonic setting of the Ordovician clastic deposits in the southern Puna Basin, NW Argentina. *Sedimentology* **50**, pp. 1079 – 1104.
- Zuffa, G. G. (1991). On the use of turbidite arenites in provenance studies: critical remarks. In: A. C. Morton, S. P. Todd and P. D. W. Haughton (eds.), *Developments in sedimentary provenance studies. Geological Society Special Publication 57*, pp. 23 – 29.

## Appendix A

### Table for modal compositions of Tanqua and Laingsburg depocentre rocks



Appendix A Modal compositions of Tanqua and Laingsburg depocentre rocks.

Sample Description	202 Sandstone	203 Sandstone	204 Sandstone	208 Sandstone	209 Sandstone	210 Sandstone	211 Sandstone
Location	Waterfall	Waterfall	Waterfall	Pienaarsfontein	Pienaarsfontein	Pienaarsfontein	Pienaarsfontein
Quartz							
Monocrystalline	48.50	26.76	47.53	44.43	45.41	45.58	32.48
Polycrystalline	5.28	1.49	5.06	4.87	8.36	5.19	5.82
Feldspar							
Albite	3.84	2.23	4.55	5.48	6.57	6.35	4.36
K-feldspar	7.68	7.06	14.66	23.13	11.95	15.00	14.06
Biotite	4.80	5.57	3.54	8.52	6.57	8.08	11.15
Muscovite		0.37	1.01		0.60		0.97
Chlorite	0.96	1.86	0.51	1.22	1.19	0.58	
Calcite	1.44						0.97
Opaques	9.12	4.46	5.06	3.04	3.58	2.31	2.91
Zircon	0.48	0.74			1.19		0.48
Lithic fragments	0.96	1.86	3.54	3.04	1.79		2.91
Clay minerals	1.92	2.60	4.55	4.26	7.77	6.92	3.88
Matrix	15.00	45.00	10.00	2.00	5.00	10.00	20.00

Sample Description	212 Sandstone	213 Sandstone	214 Sandstone	215 Sandstone	216 Sandstone	217 Sandstone	219 Sandstone
Location	Pienaarsfontein						
Quartz							
Monocrystalline	42.65	39.65	45.37	35.20	37.54	31.97	28.37
Polycrystalline	2.06	7.12	7.80	8.55	9.26	7.87	3.32
Feldspar							
Albite	8.94	4.57	6.38	5.03	4.88	6.39	4.79
K-feldspar	16.51	15.76	17.01	13.07	13.65	12.30	10.68
Biotite	4.82	10.17	9.22	13.07	10.73	11.31	11.42
Muscovite	0.69		0.71	1.01	0.49	0.49	0.74
Chlorite	2.06	1.02		0.50	0.49	0.98	0.74
Calcite	1.38	1.02	0.71	2.51	0.49	0.98	0.37
Opaques	8.94	3.05	2.13	2.01	3.90	4.43	1.47
Zircon	1.38	1.02					
Lithic fragments	3.44	5.59	2.84	2.51	6.83	2.95	2.95
Clay minerals	4.13	3.05	2.84	6.54	9.75	10.33	5.16
Matrix	3.00	8.00	5.00	10.00	2.00	10.00	30.00

Sample Description	220 Sandstone	223 Sandstone	224 Sandstone	226 Sandstone	227 Sandstone	228 Sandstone	229 Sandstone
Location	Pienaarsfontein	Pienaarsfontein	Pienaarsfontein	Groot Hangklip	Groot Hangklip	Groot Hangklip	Groot Hangklip
Quartz							
Monocrystalline	42.00	38.48	37.92	40.97	38.40	35.63	30.52
Polycrystalline	4.67	9.62	9.58	2.21	9.50	1.62	1.36
Feldspar							
Albite	6.00	5.41	4.58	4.98	2.28	2.70	3.39
K-feldspar	16.67	15.63	8.33	15.50	15.59	21.59	18.99
Biotite	10.67	10.22	9.17	12.73	11.79	12.41	20.35
Muscovite	1.33	0.60	4.17	0.55	2.28	1.62	0.68
Chlorite	1.33	1.20	1.25	1.66	0.76	0.54	1.36
Calcite	0.67	1.80	0.83	1.11	1.14	0.54	
Opaques	2.67	1.20	3.75	4.98	2.28	3.78	4.75
Zircon		0.60	0.42		0.38		
Lithic fragments	6.67	3.01	2.50	6.09	1.14	4.32	10.85
Clay minerals	5.33	4.21	7.50	7.20	6.46	10.26	4.75
Matrix	2.00	8.00	10.00	2.00	8.00	5.00	3.00

Sample Description	230 Sandstone	231 Sandstone	232 Sandstone	234 Sandstone	235 Sandstone	236 Sandstone	239 Sandstone
Location	Groot Hangklip	Groot Hangklip	Droëkloof	Droëkloof	Klein Hangklip	Klein Hangklip	KL 1/65
Quartz							
Monocrystalline	36.01	35.25	35.39	35.84	43.98	30.67	30.17
Polycrystalline	1.74	3.92	1.86	6.21	7.72	7.67	1.53
Feldspar							
Albite	1.74	3.13	1.86	4.78	10.03	2.56	4.09
K-feldspar	15.10	18.02	18.63	20.55	11.57	18.53	12.78
Biotite	20.91	14.88	18.01	14.33	3.86	17.25	7.67
Muscovite	1.16	1.57	1.24	1.43	1.54		1.53
Chlorite	0.58	0.78	1.86	0.96			1.53
Calcite	1.74	1.57	0.62	1.43	1.54	1.28	0.51
Opaques	2.32	1.57	4.97	4.78	0.77	1.28	20.45
Zircon	0.58	0.78		0.48	1.54		0.51
Lithic fragments	8.13	4.70	6.83	2.39	1.54	7.67	6.65
Clay minerals	6.97	7.83	3.73	3.82	13.89	5.11	2.56
Matrix	3.00	6.00	5.00	3.00	2.00	8.00	10.00

Appendix A continued

Sample Description	240 Sandstone	245 Bentonite	248 Bentonite	253 Sandstone	254 Sandstone	255 Sandstone	257 Sandstone
Location	KL 1/65	NS1	NS1	Skoorsteenberg	Skoorsteenberg	Skoorsteenberg	Skoorsteenberg
Quartz							
Monocrystalline	33.30		50.85	39.08	30.68	35.05	33.20
Polycrystalline	3.82		2.68	9.77	5.80	8.38	5.77
Feldspar							
Albite	4.37	26.22	28.10	4.19	8.29	3.81	10.11
K-feldspar	21.29	7.86	8.03	13.26	15.75	15.24	11.55
Biotite	10.37	26.22	1.34	7.68	5.80	16.76	8.66
Muscovite	0.55	7.86	1.34	0.70	1.66	1.52	1.44
Chlorite	1.09	1.31		2.09	0.83	0.76	0.72
Calcite	0.55	3.93	1.34	2.09	0.83	0.76	2.89
Opaques	7.64	15.73	1.34	1.40	8.29	2.29	6.50
Zircon	0.55	1.31			0.83		1.44
Lithic fragments	4.37	1.31		5.58	4.15	4.57	3.61
Clay minerals	7.10	5.24		11.17	14.09	6.86	10.11
Matrix	5.00	3.00	5.00	3.00	3.00	4.00	4.00
Sample Description	258 Sand-/siltstone	302 Sandstone	303 Sandstone	305 Sandstone	306 Sandstone	307 Sandstone	308 Sandstone
Location	Skoorsteenberg	Bitterberg	Bitterberg	Bitterberg	Bitterberg	Katjiesberg	Katjiesberg
Quartz							
Monocrystalline	39.32	33.70	31.11	42.02	41.72	35.68	36.22
Polycrystalline	2.27	8.22	8.24	7.31	10.31	6.42	4.10
Feldspar							
Albite	4.54	4.52	4.58	2.44	3.28	2.00	2.05
K-feldspar	15.12	9.45	14.64	14.62	14.06	14.43	15.72
Biotite	1.51	15.62	12.81	9.74	9.38	7.22	19.14
Muscovite	1.51	1.64	0.92	2.44	2.34	2.00	0.68
Chlorite	1.51	1.23	0.92	0.61		0.40	0.68
Calcite	2.27	2.05	1.83	1.22	0.94	1.20	0.68
Opaques	3.02	2.47	2.75	1.83	0.94	4.01	2.73
Zircon	0.76	0.41		0.61		0.40	
Lithic fragments	5.29	3.29	9.15	4.87	0.94	4.41	7.52
Clay minerals	15.88	7.40	10.07	7.31	6.09	6.82	5.47
Matrix	7.00	10.00	3.00	5.00	10.00	15.00	5.00
Sample Description	309 Sandstone	310 Sandstone	311 Sandstone	318 Sandstone	326 Sandstone	327 Sandstone	331 Sandstone
Location	Katjiesberg	Soutrivierspunt	Soutrivierspunt	Geelbek	Geelbek	Grootkloof	Grootkloof
Quartz							
Monocrystalline	39.33	34.10	40.36	37.33	22.81	35.00	17.27
Polycrystalline	4.51	3.65	4.64	9.22	22.81	8.50	17.27
Feldspar							
Albite	3.22	8.53	2.78	1.35	3.67	4.50	
K-feldspar	18.05	17.66	9.28	7.65	10.18	11.50	10.08
Biotite	8.38	12.18	12.53	6.52	4.89	11.00	17.27
Muscovite		2.44	0.93	6.75	1.63	2.00	
Chlorite	0.64	0.61	1.39	0.45	0.81	1.50	1.44
Calcite	0.64	1.22	0.93	0.90	12.22	3.50	17.99
Opaques	4.51	2.44	7.42	4.05	1.63	7.00	3.60
Zircon					0.41		
Lithic fragments	9.03	4.87	4.64	4.05	1.63	4.00	2.88
Clay minerals	9.67	7.31	5.10	6.75	7.33	6.50	7.20
Matrix	2.00	5.00	10.00	15.00	10.00	5.00	5.00
Sample Description	336 Sandstone	337 Sandstone	345 Sandstone	347 Sandstone	349 Sandstone	350 Sandstone	352 Sandstone
Location	Grootkloof	Krantz 1	Waterkloof				
Quartz							
Monocrystalline	23.75	17.51	34.87	33.25	38.84	29.31	39.38
Polycrystalline	4.57	17.51	14.65	8.31	6.63	12.34	6.56
Feldspar							
Albite	3.65	1.29	1.52	1.66	4.26	2.57	7.29
K-feldspar	11.88	6.18	12.13	14.41	11.84	12.86	8.02
Biotite	20.10	5.92	7.58	12.75	11.37	11.83	8.75
Muscovite	0.91	1.55	0.51	1.66	1.42	1.03	0.73
Chlorite	0.91	0.77	2.02	1.11	1.89	1.54	0.73
Calcite	10.05	2.06	6.06	3.33	2.84	2.57	7.29
Opaques	2.74	0.77	2.53	3.33	0.47	3.09	2.19
Zircon	0.91	0.77	1.52	0.55		1.03	0.73
Lithic fragments	6.39	1.29	1.52	3.88	3.79	4.63	3.65
Clay minerals	9.13	4.38	10.11	7.76	6.63	7.20	11.67
Matrix	5.00	40.00	5.00	8.00	10.00	10.00	3.00

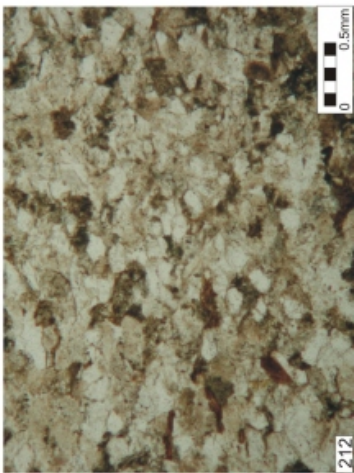
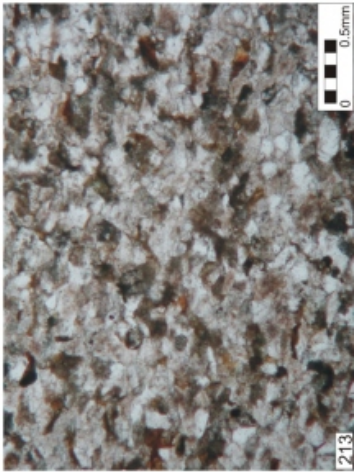
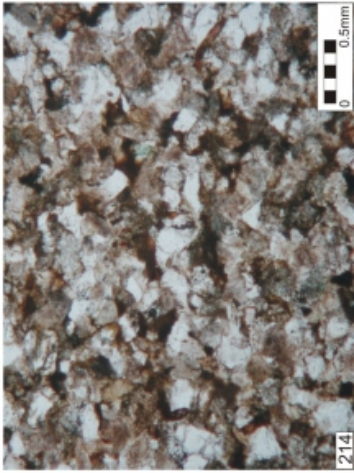
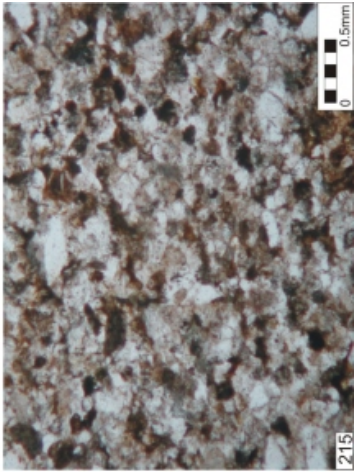
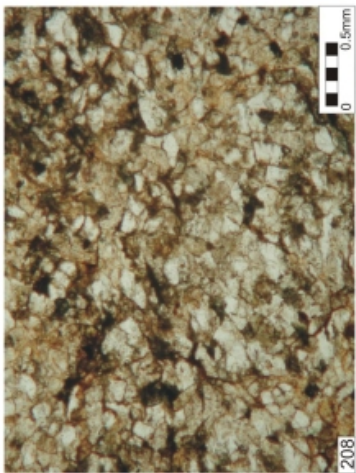
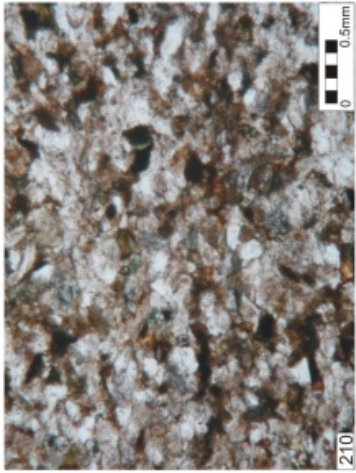
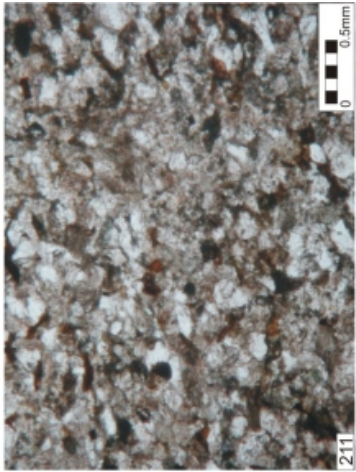
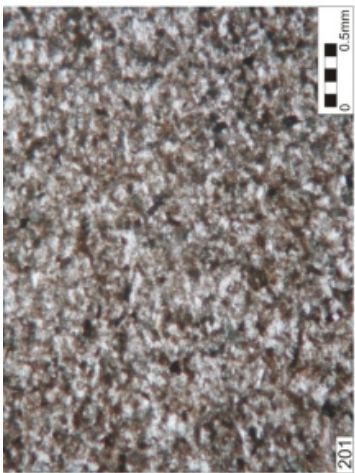
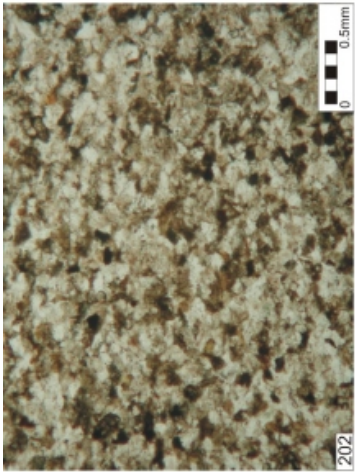
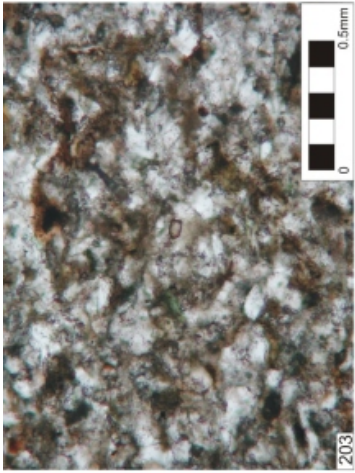
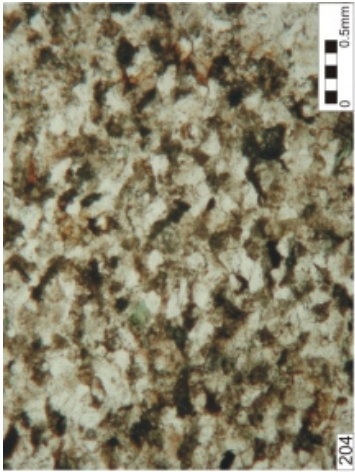
Appendix A continued

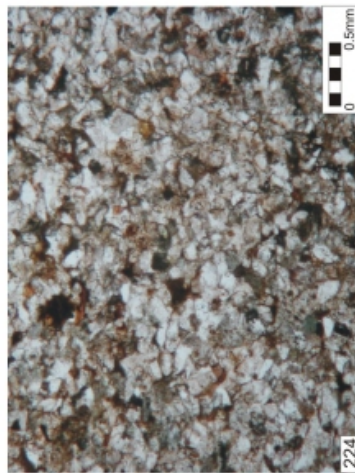
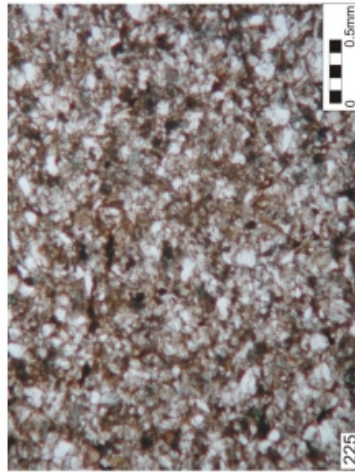
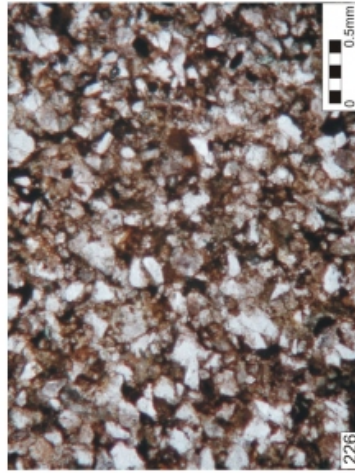
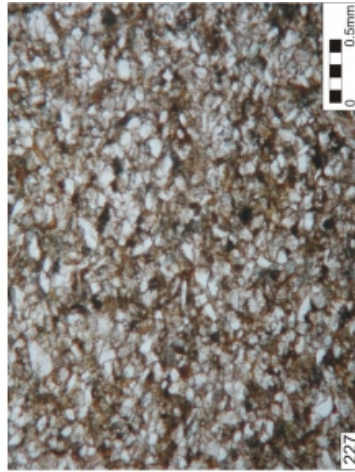
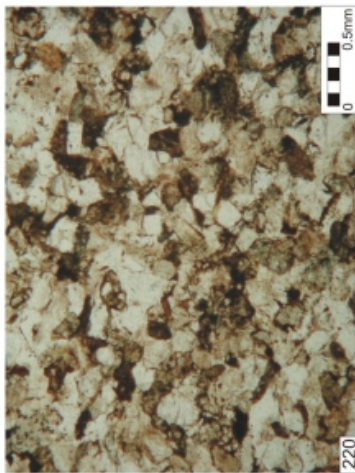
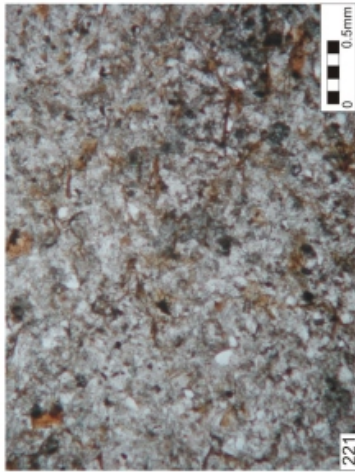
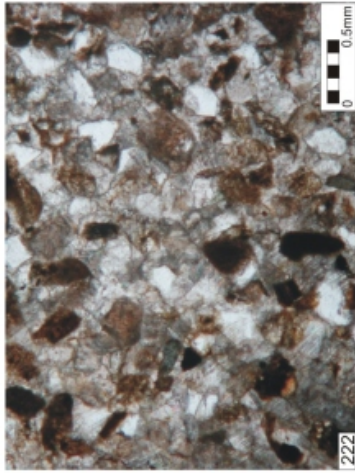
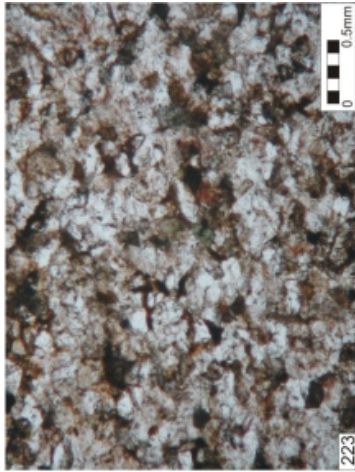
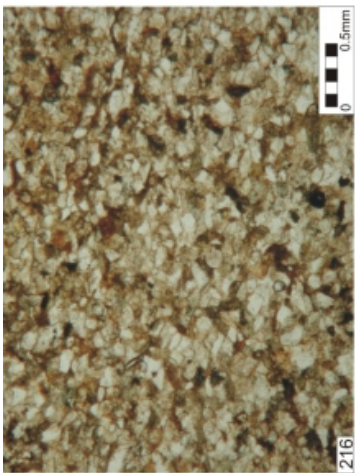
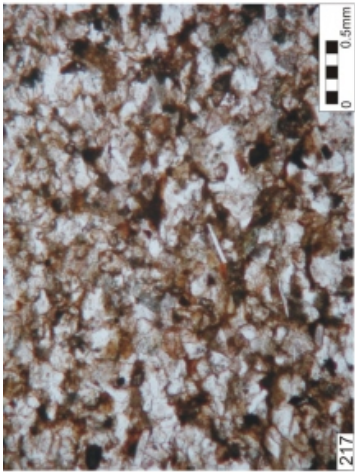
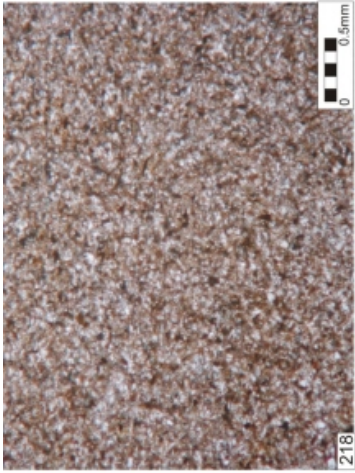
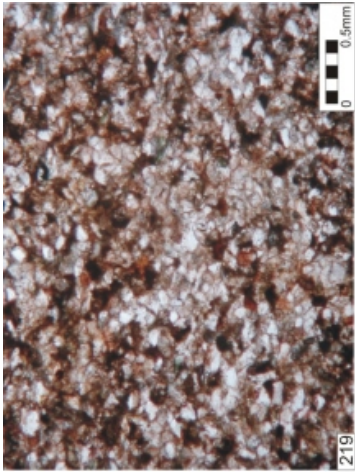
Sample Description	353	360	362	363	366	368	369	370
Location	Sandstone Waterkloof	Sandstone Ouberg	Sandstone Ouberg	Sandstone Ouberg				
Quartz								
Monocrystalline	41.11	41.88	37.95	42.83	37.83	33.49	41.15	40.50
Polycrystalline	4.57	4.38	6.51	4.67	2.36	2.05	2.20	2.28
Feldspar								
Albite	1.37	3.75	2.71	6.23	6.31	2.05	5.88	2.28
K-feldspar	7.31	8.75	10.84	10.12	14.19	13.67	19.11	13.69
Biotite	14.62	15.63	13.55	13.24	12.61	23.92	11.76	13.12
Muscovite	2.28	0.63	1.63		0.79		0.73	
Chlorite	0.91		1.08	0.78	2.36	1.37	2.20	0.57
Calcite	12.79	2.50	2.17	4.67	3.15	2.73	1.47	2.28
Opagues	4.57	1.25	1.63		2.36	3.42	2.20	2.85
Zircon								
Lithic fragments	2.74	5.63	4.88	2.34	7.09	8.20	5.14	5.13
Clay minerals	2.74	5.63	7.05	10.12	3.94	4.10	5.14	2.28
Matrix	5.00	10.00	10.00	5.00	7.00	5.00	3.00	15.00
Sample Description	373	374	375	377	378	379	380	381
Location	Sandstone Skeiding	Sandstone Paardekraal	Sandstone Paardekraal	Sandstone Grootfontein	Sandstone Grootfontein	Sandstone Grootfontein	Sandstone Grootfontein	Sandstone Grootfontein
Quartz								
Monocrystalline	39.71	37.62	38.31	39.96	37.11	42.67	31.88	34.38
Polycrystalline	1.94	1.95	4.26	6.89	4.45	4.83	5.98	1.81
Feldspar								
Albite	1.94	5.19	1.82	2.07	4.45	4.83	2.66	12.67
K-feldspar	14.53	6.49	17.64	17.22	15.59	16.10	11.95	13.57
Biotite	9.68	9.08	13.38	7.58	4.45	12.08	12.62	7.24
Muscovite	0.97	1.95	0.61	2.07	2.23		1.99	
Chlorite	0.97	1.95	0.61	1.38	2.23	0.81	1.99	1.81
Calcite	2.91	20.76	1.82	1.38	7.42	1.61	2.66	
Opagues	5.81	1.30	3.04	3.44	2.97	3.22	4.65	7.24
Zircon				1.38	0.74	0.81		
Lithic fragments	8.72	1.95	4.86	4.13	4.45	4.83	4.65	11.76
Clay minerals	4.84	7.78	3.65	5.51	8.91	3.22	3.98	4.52
Matrix	8.00	4.00	10.00	7.00	5.00	5.00	15.00	5.00
Sample Description	382	383	384	385	386	388	389	398
Location	Sandstone Jakkalsfontein	Sandstone SL1						
Quartz								
Monocrystalline	42.67	40.22	41.57	36.28	43.84	33.72	42.61	40.49
Polycrystalline	2.13	2.51	2.27	6.66	4.65	5.62	4.89	2.34
Feldspar								
Albite	4.27	5.03	3.02	9.63	1.99	5.62	4.19	3.11
K-feldspar	9.60	11.73	13.61	17.03	11.96	12.64	14.67	14.02
Biotite	10.67	6.70	11.34	9.63	9.30	9.13	6.99	15.57
Muscovite	3.20	0.84	1.51	0.74	2.66	1.40	0.70	1.56
Chlorite	1.07	5.03	2.27	1.48	1.33	0.70	1.40	1.56
Calcite	4.27	3.35	2.27	2.96	3.32	0.70	2.79	2.34
Opagues	4.27	5.03	4.54	2.22	3.99	2.81	3.49	0.78
Zircon	1.07			1.48		0.70		0.78
Lithic fragments	2.13	5.86	11.34	4.44	5.31	4.92	8.38	7.79
Clay minerals	10.67	6.70	2.27	4.44	4.65	7.02	4.89	4.67
Matrix	4.00	7.00	4.00	3.00	7.00	15.00	5.00	5.00
Sample Description	3106	3109	3110	3112	3113	3114	3115	3116
Location	Sandstone SL1	Sandstone SL1						
Quartz								
Monocrystalline	42.04	37.81	32.66	41.72	38.32	37.37	32.88	29.12
Polycrystalline	4.60	6.39	1.48	7.06	9.80	9.47	1.86	3.31
Feldspar								
Albite	3.94	5.33	5.94	3.85	3.56	4.74	3.10	7.28
K-feldspar	15.11	13.31	19.30	16.69	11.58	12.63	11.17	13.24
Biotite	5.26	14.38	4.45	11.55	11.58	8.42	8.07	11.91
Muscovite	0.66	0.53		0.64	1.78		1.86	0.66
Chlorite	1.31	2.66	1.48	0.64	1.78	1.05	1.86	2.65
Calcite	3.28	1.60	2.97	0.64	1.78	2.63	2.48	2.65
Opagues	2.63	1.60	7.42	1.93	2.23	1.58	3.72	3.97
Zircon					0.45	1.05	1.24	0.66
Lithic fragments	5.26	2.66	11.88	5.14	4.01	3.68	7.45	7.94
Clay minerals	5.91	3.73	7.42	5.14	3.12	7.37	9.31	6.62
Matrix	10.00	10.00	5.00	5.00	10.00	10.00	15.00	10.00

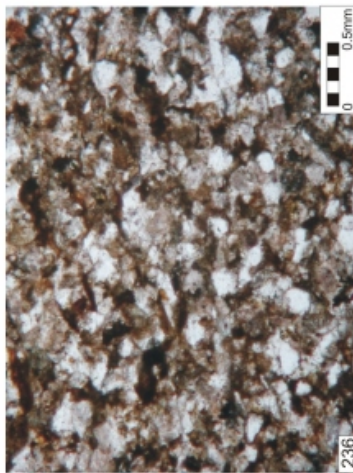
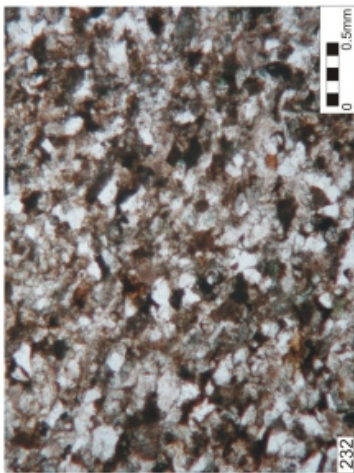
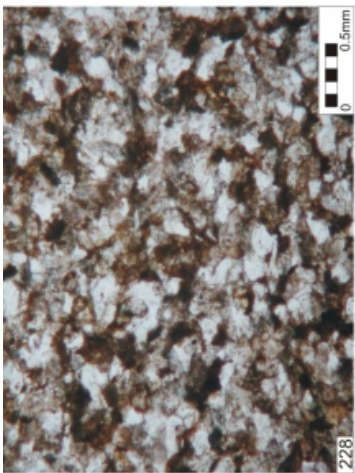
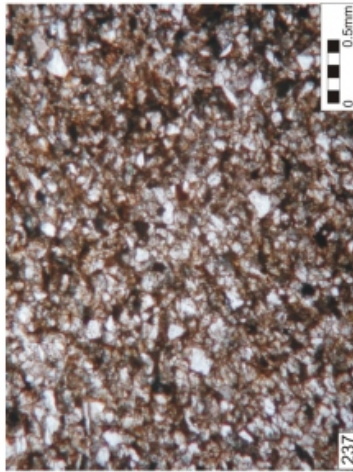
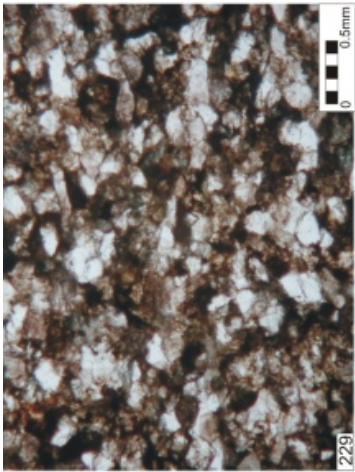
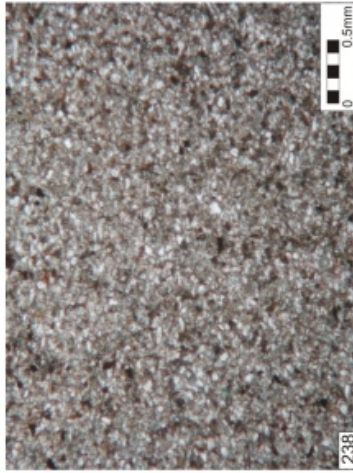
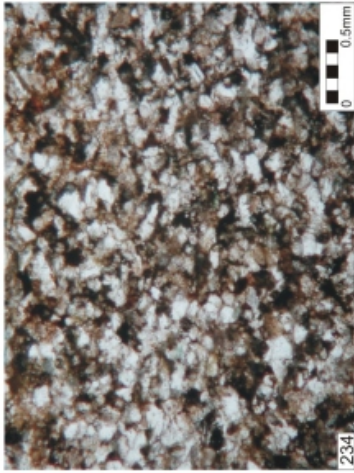
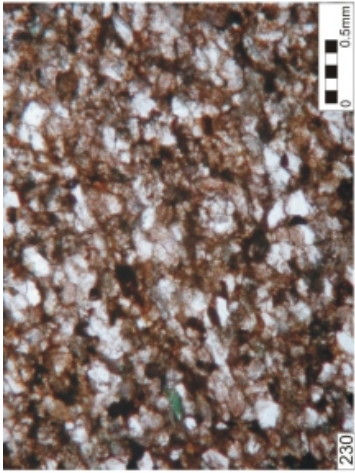
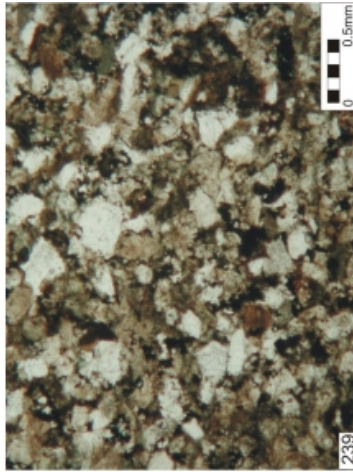
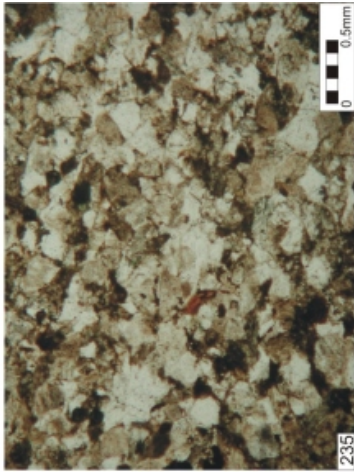
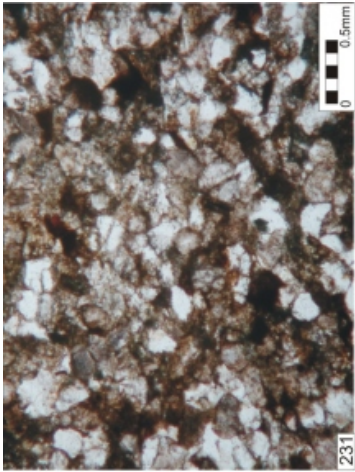
## Appendix B

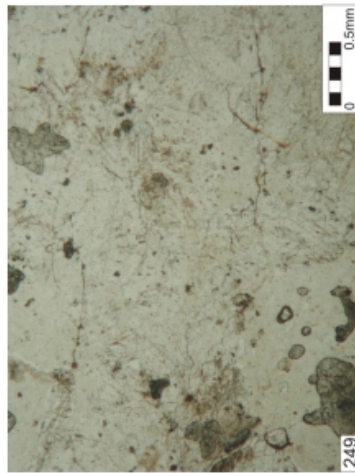
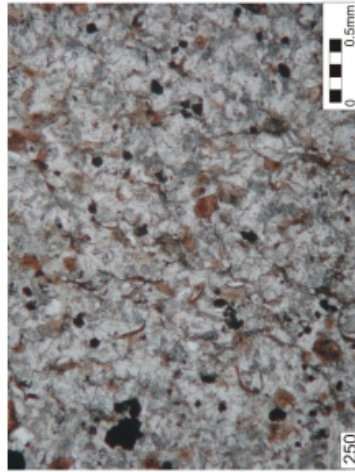
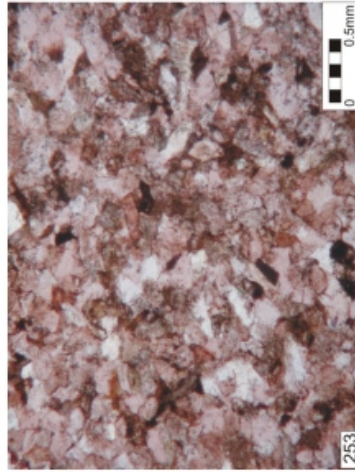
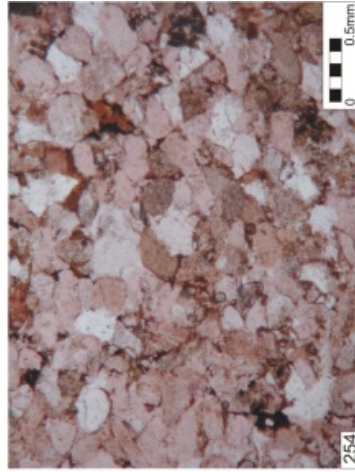
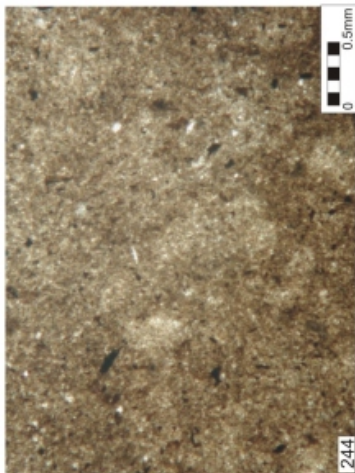
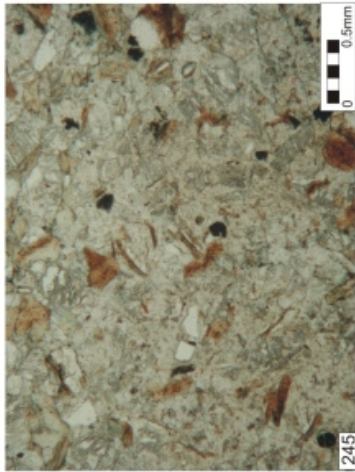
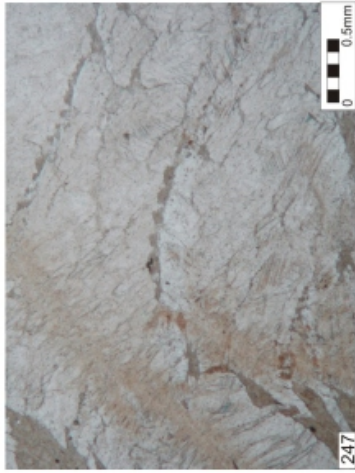
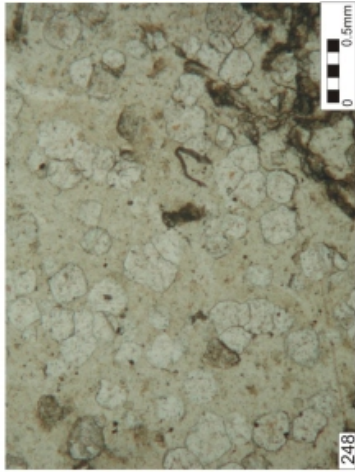
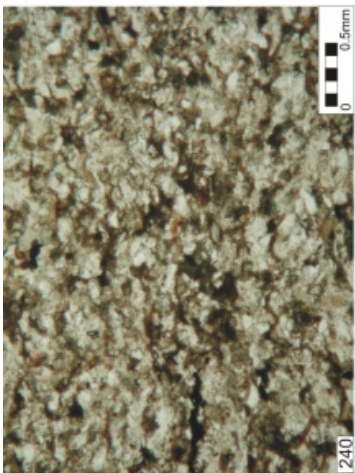
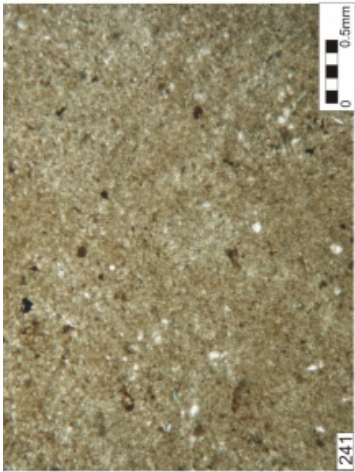
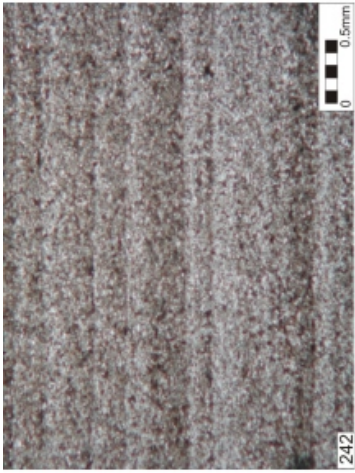
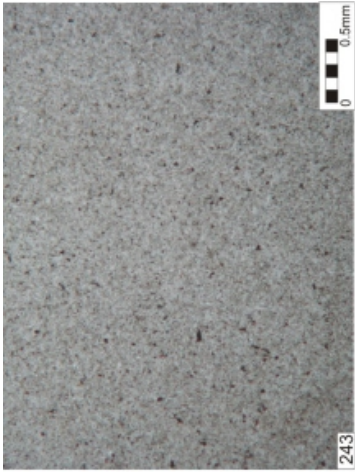
### Sample microphotographs

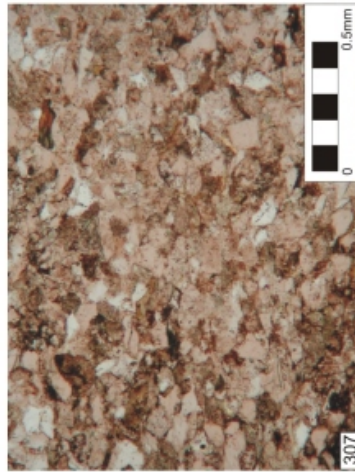
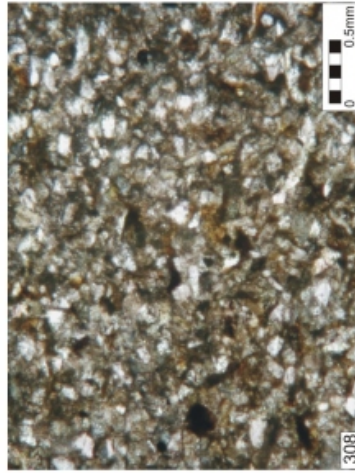
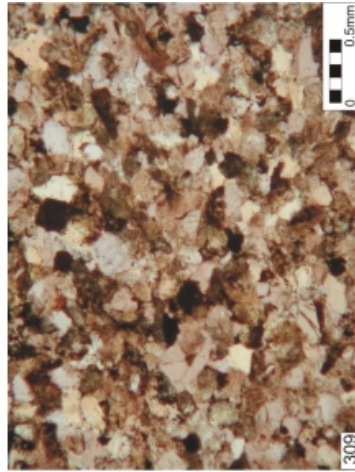
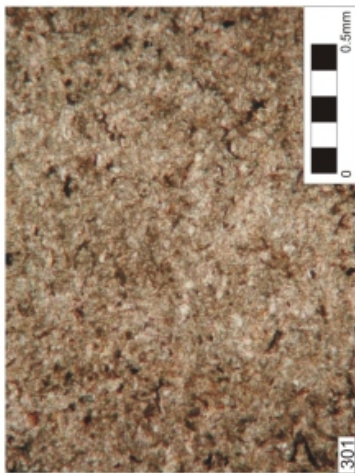
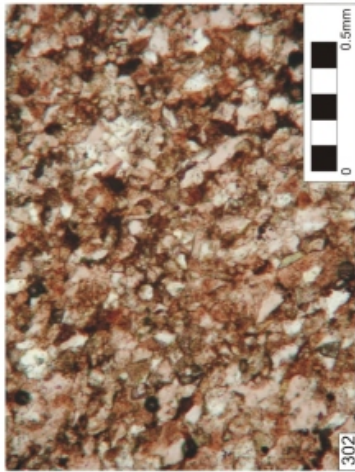
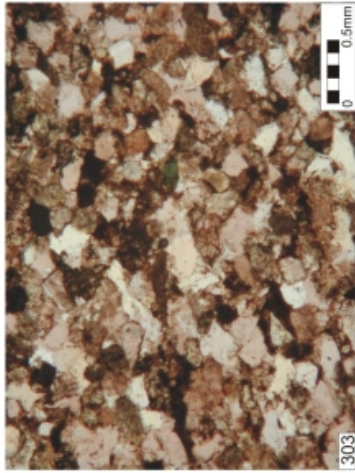
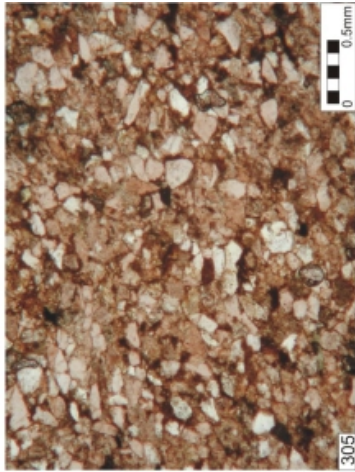
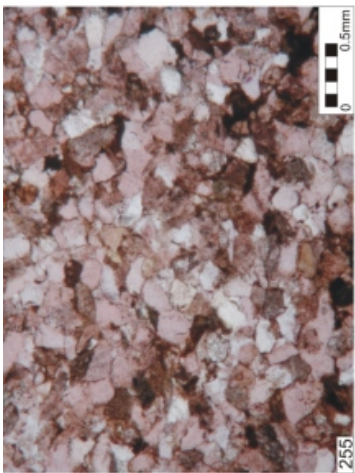
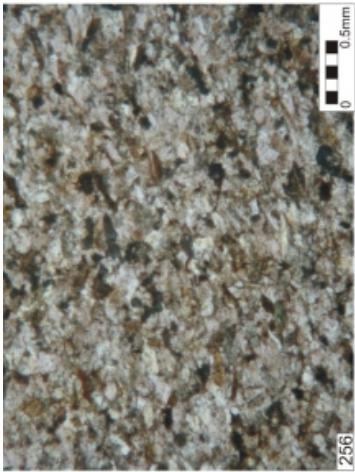
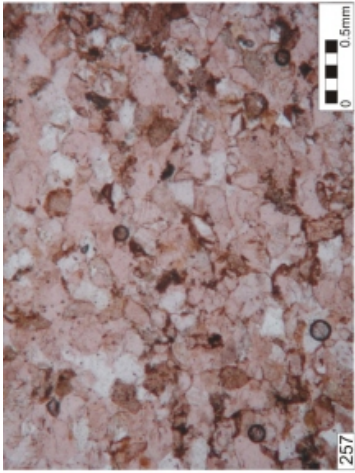
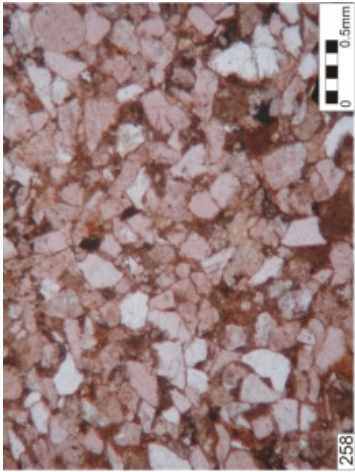


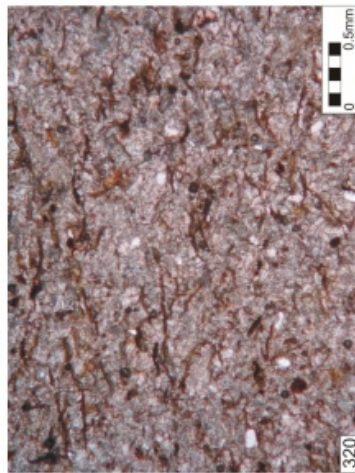
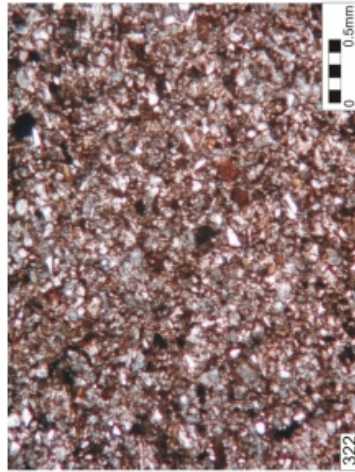
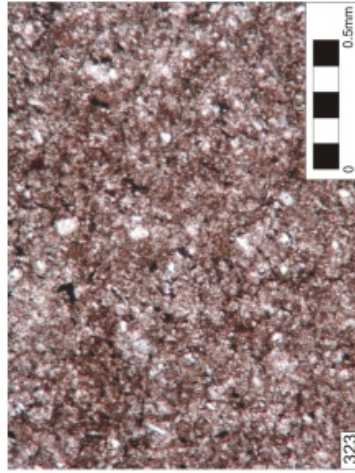
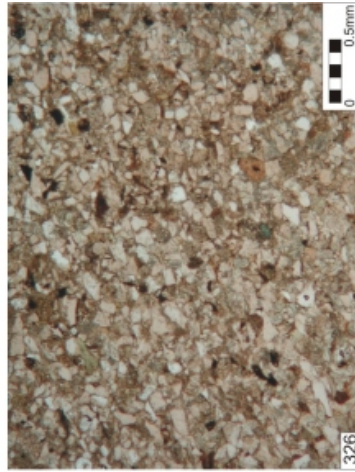
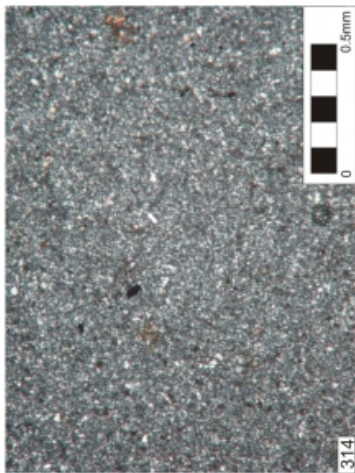
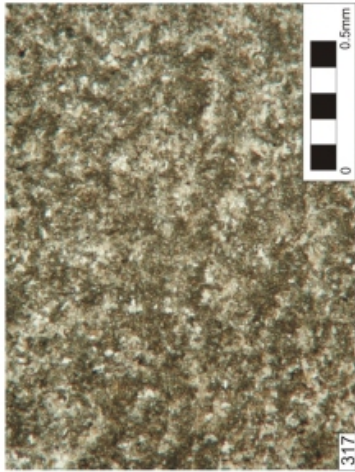
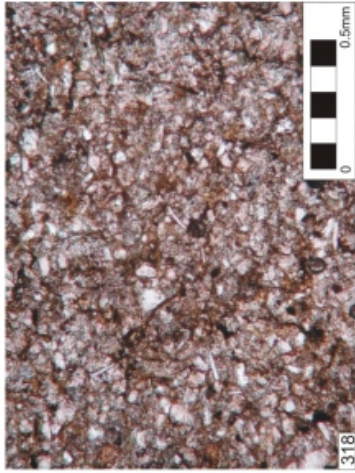
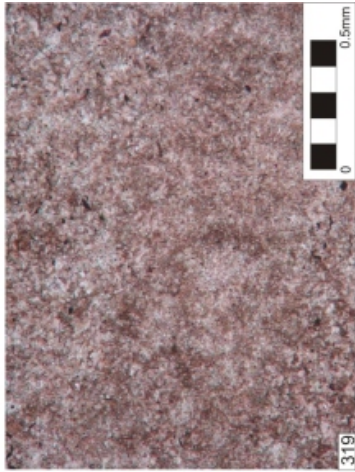
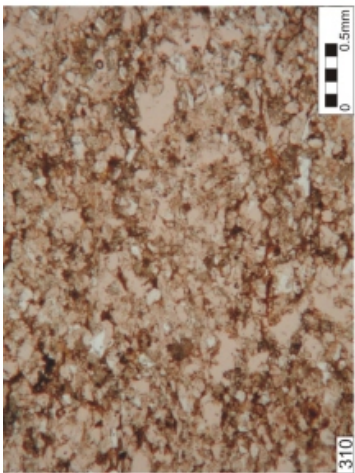
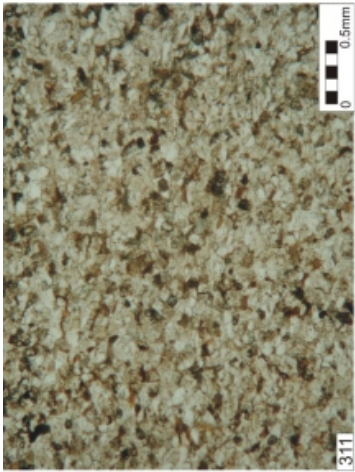
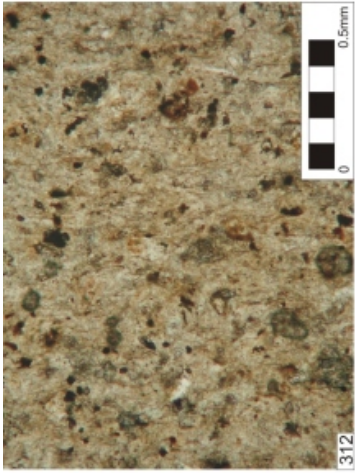
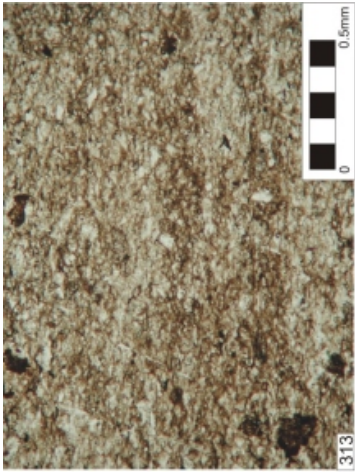


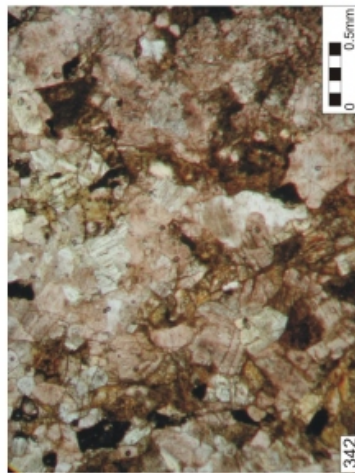
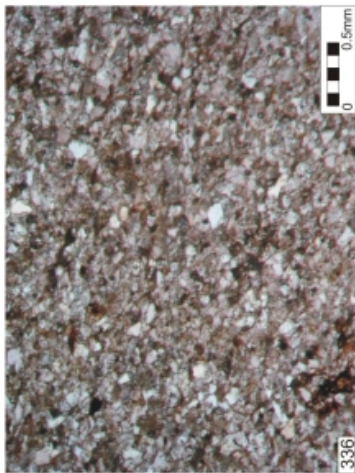
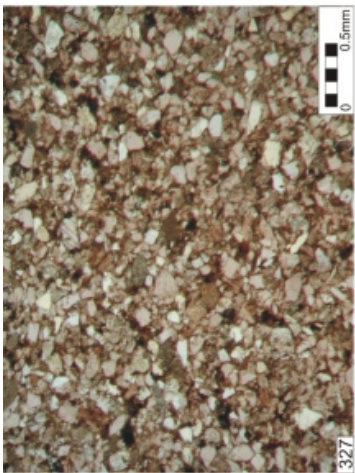
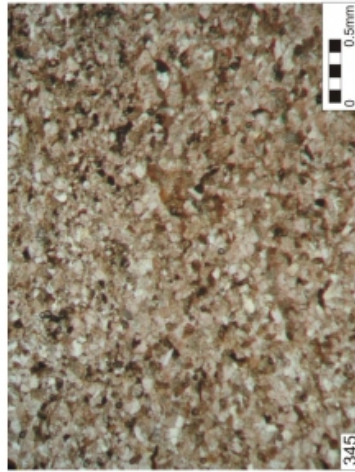
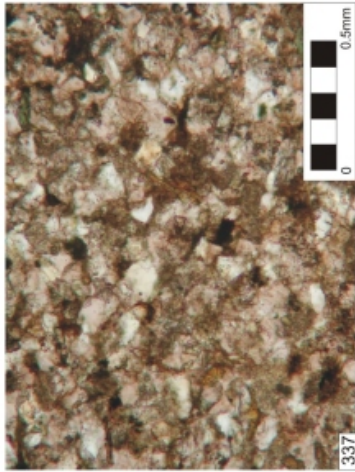
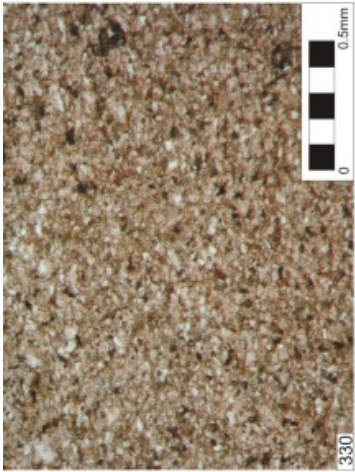
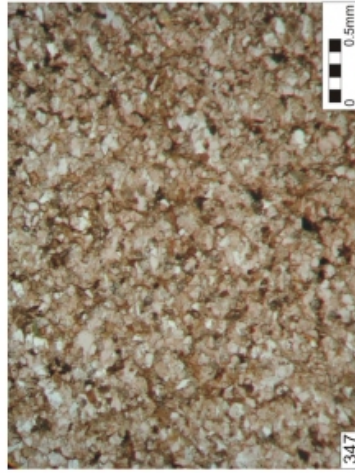
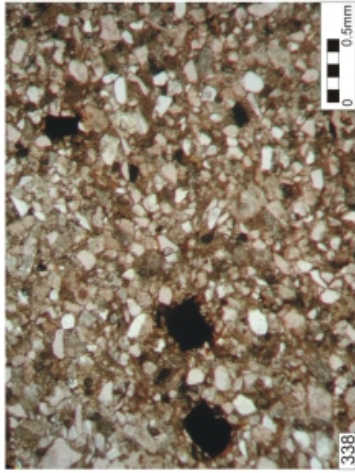
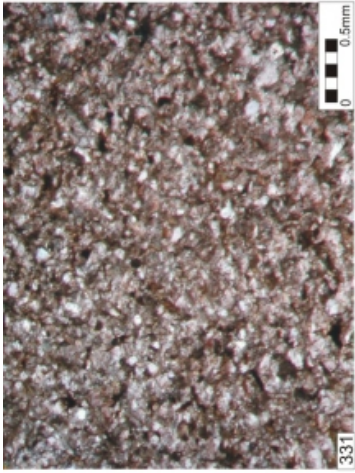
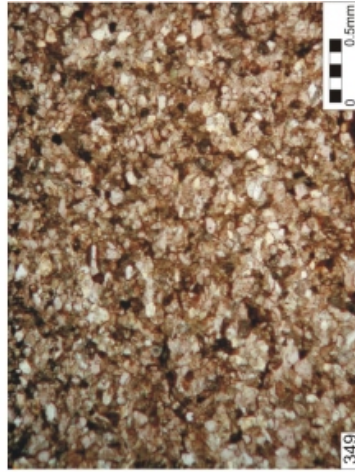
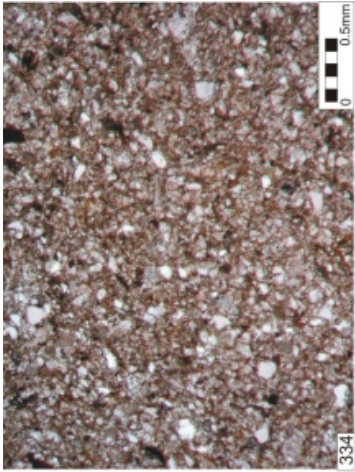


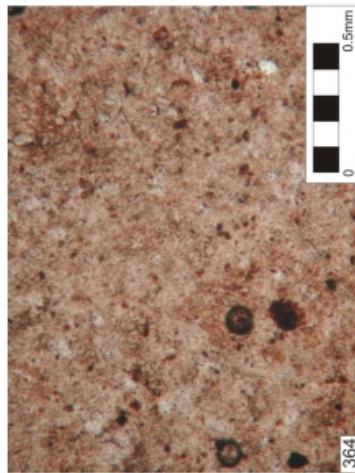
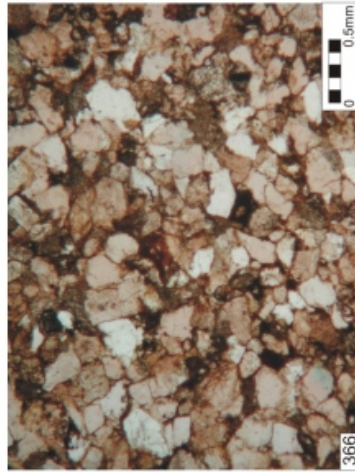
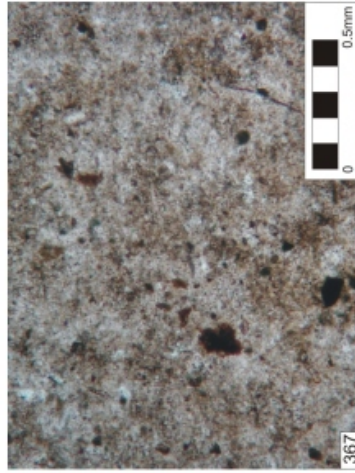
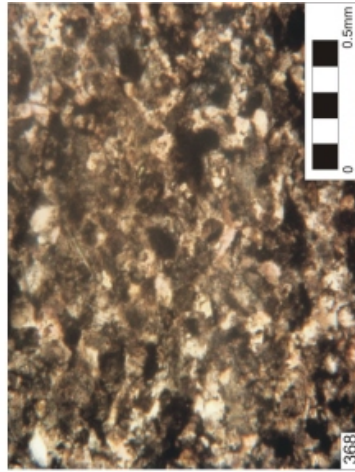
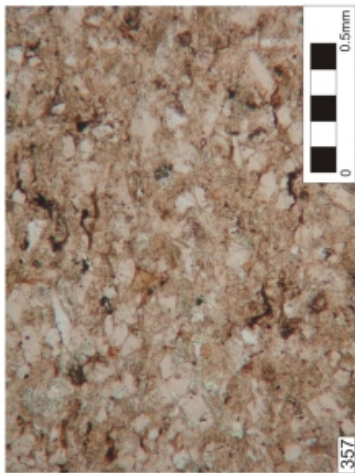
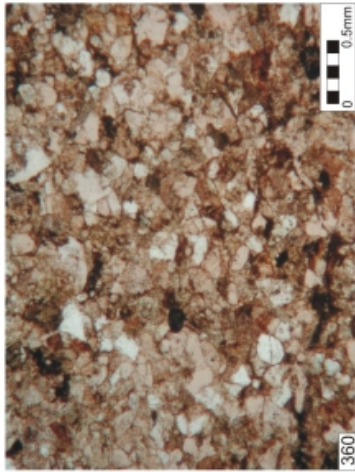
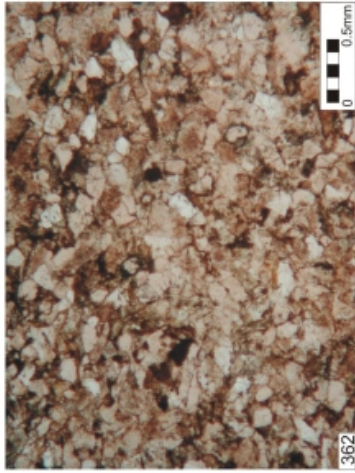
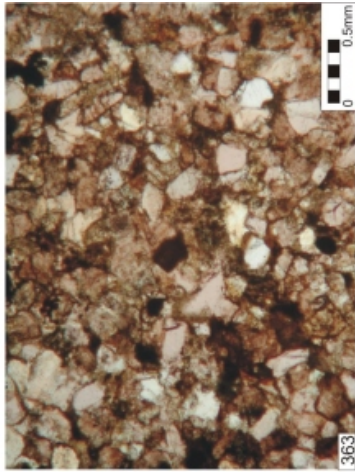
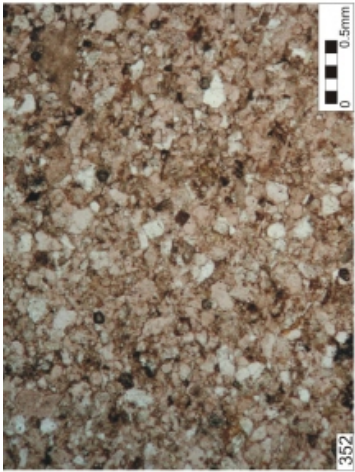
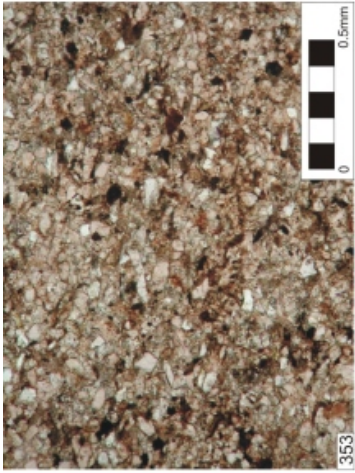
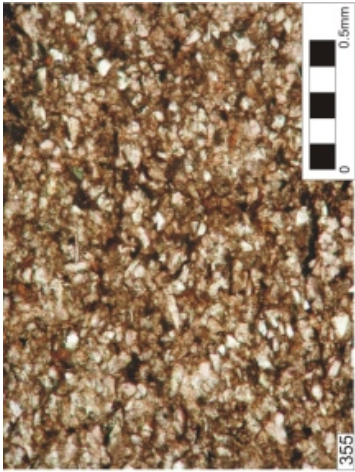


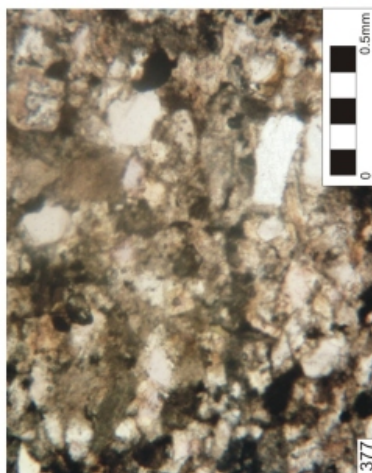
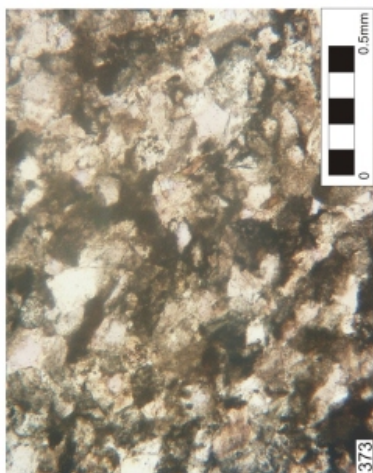
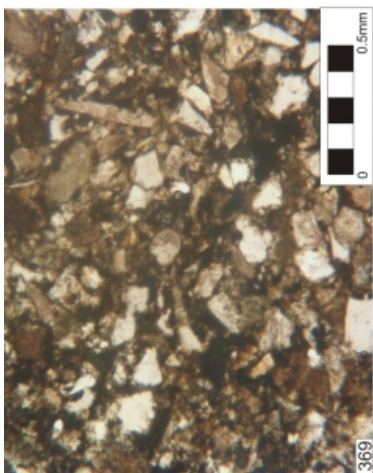
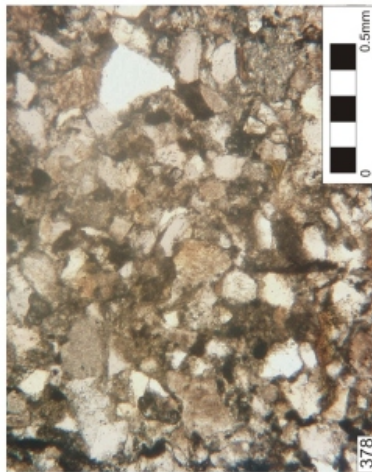
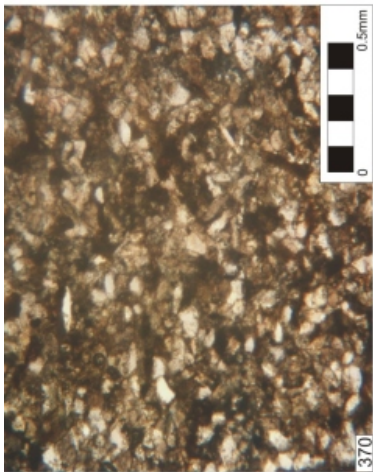
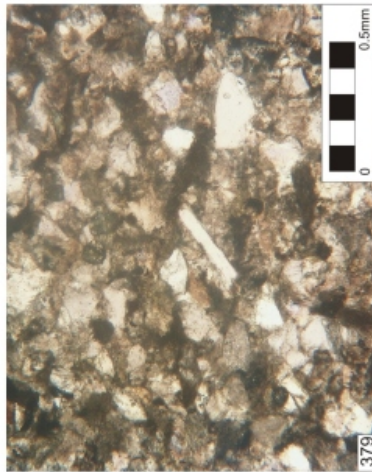
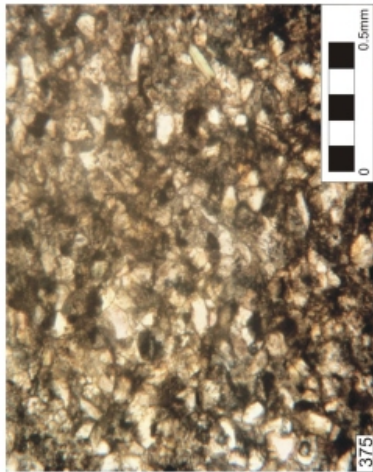
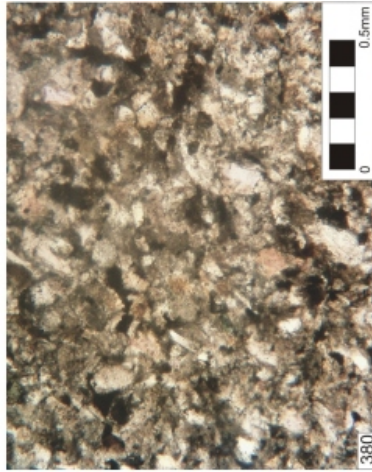
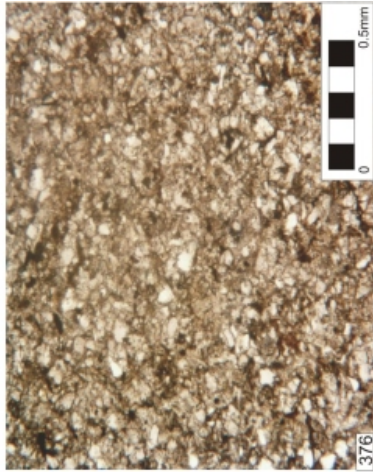
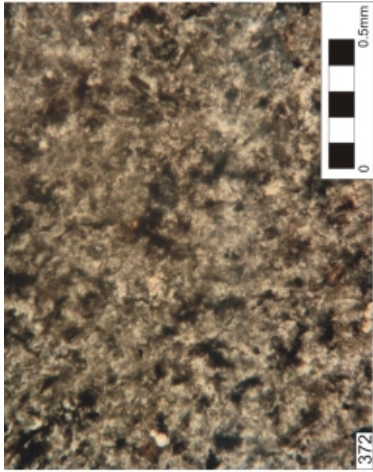


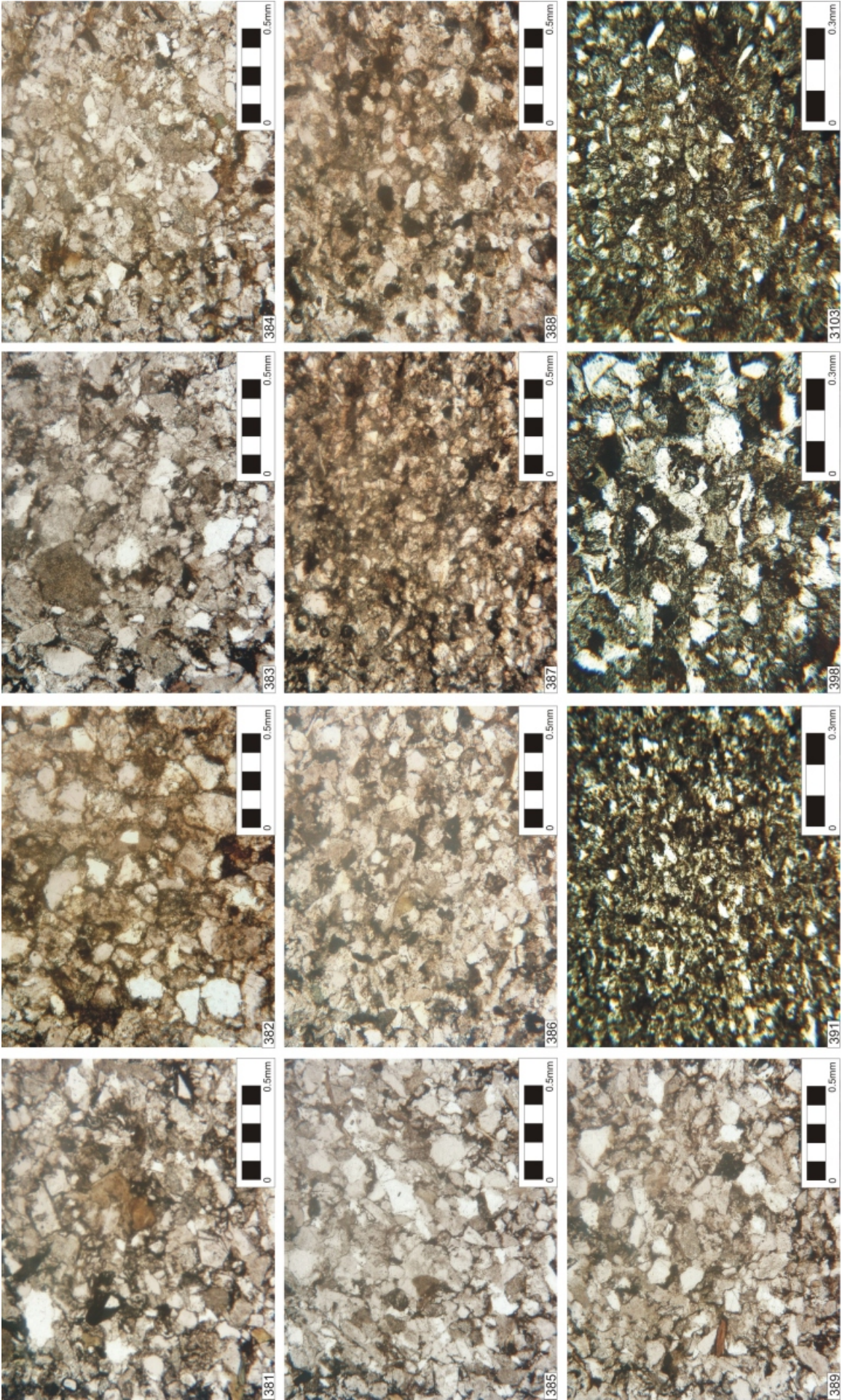


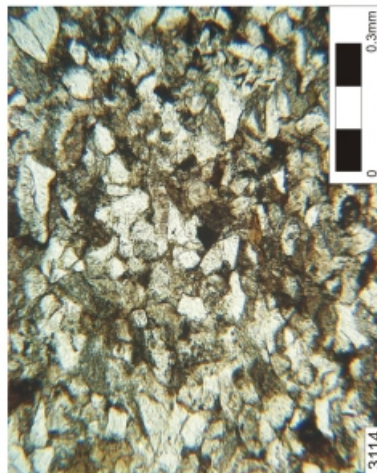
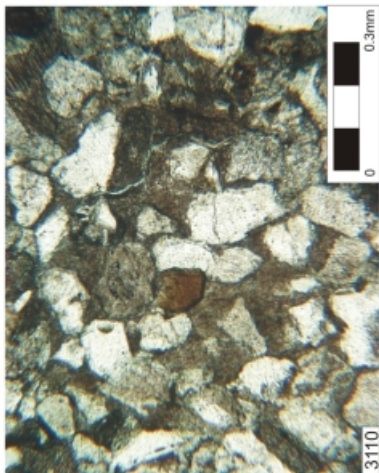
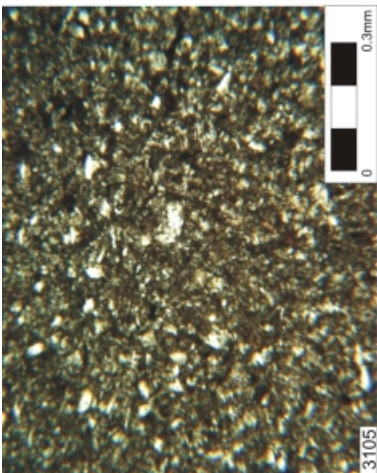
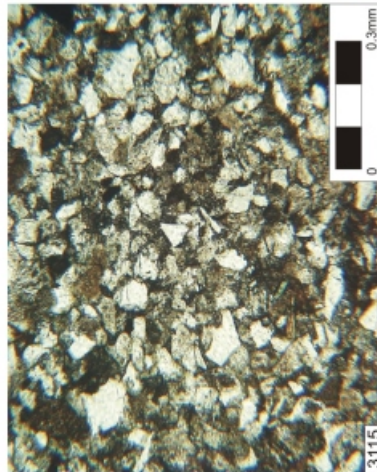
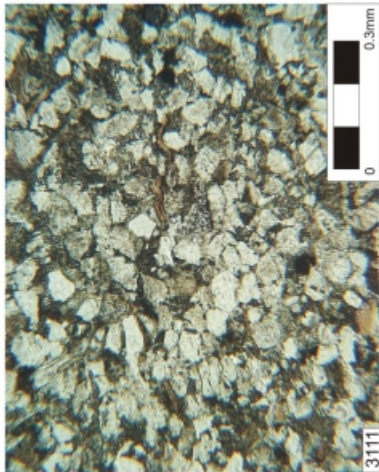
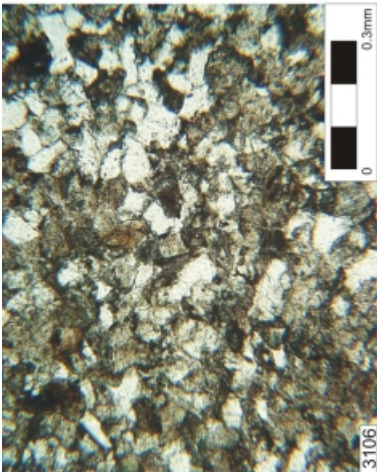
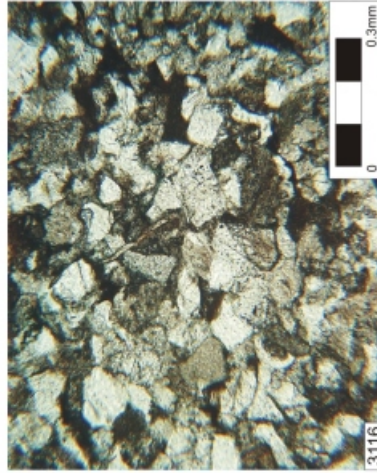
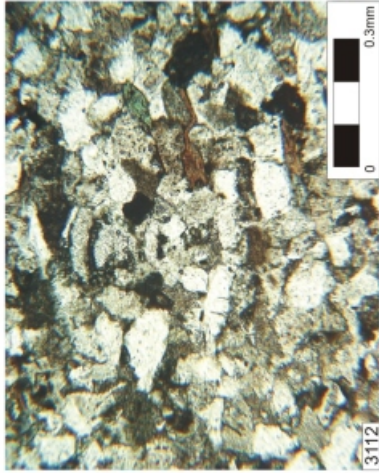
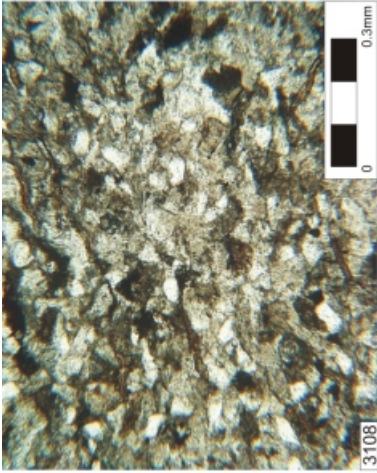
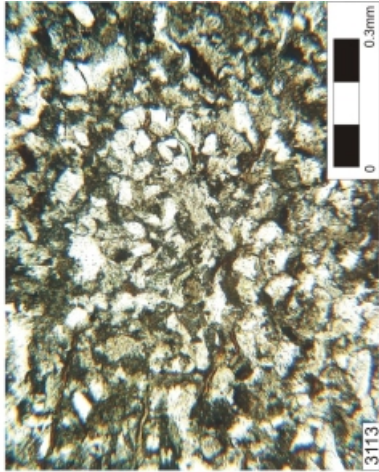
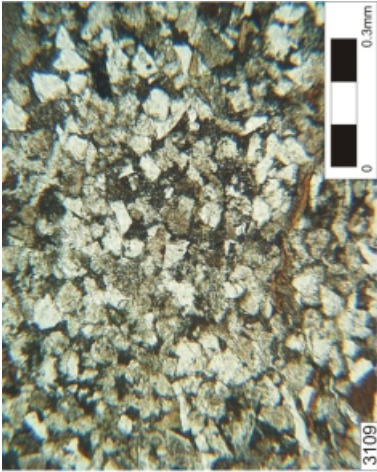






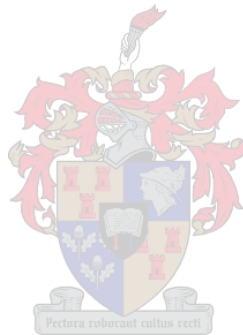






## Appendix C

**Table for major, trace and rare earth elements for the Tanqua and  
Laingsburg depocentre rocks**



Appendix C Table for major, trace and REE, given in percentage and ppm respectively, for the Tanqua and Laingsburg depocentre rocks.

Sample description and location	201		202		203		204		205		206		207		208		209		210		211		212		213			
	Sandstone	Waterfall	Sandstone	Waterfall	Sandstone	Waterfall	Sandstone	Waterfall	Shale	Plenaarsfontein	Sand-/siltstone	Plenaarsfontein	Shale	Plenaarsfontein	Sandstone	Plenaarsfontein												
SiO <sub>2</sub>	74.94	73.38	74.90	77.01	60.24	70.40	68.05	76.85	76.15	74.37	75.55	77.49	73.44	73.44	76.85	76.15	74.37	75.55	77.49	73.44	73.44	75.55	77.49	73.44	73.44	73.44	73.44	
TiO <sub>2</sub>	0.58	0.52	0.47	0.45	0.70	0.43	0.68	0.46	0.41	0.44	0.45	0.41	0.41	0.41	0.46	0.47	0.44	0.45	0.41	0.41	0.41	0.45	0.41	0.41	0.41	0.41	0.41	
Al <sub>2</sub> O <sub>3</sub>	12.15	12.70	11.88	11.62	18.09	12.01	14.81	11.15	11.72	10.78	11.45	10.68	12.42	12.42	11.15	11.72	10.78	11.45	10.68	10.68	10.68	11.45	10.68	10.68	10.68	10.68	10.68	
Fe <sub>2</sub> O <sub>3</sub>	3.53	3.90	3.17	2.69	7.36	2.33	5.12	2.63	2.58	2.85	2.60	2.24	3.19	3.19	2.63	2.58	2.85	2.60	2.24	2.24	2.60	2.60	2.24	2.24	2.24	2.24	2.24	
MnO	0.06	0.06	0.05	0.04	0.08	0.18	0.07	0.04	0.05	0.06	0.04	0.05	0.05	0.05	0.04	0.05	0.06	0.04	0.04	0.04	0.04	0.04	0.04	0.04	0.04	0.04	0.04	
NiO	0.01	0.01	0.01	0.01	0.01	0.00	0.01	0	0	0	0	0	0	0	0	0	0	0	0	0	0	0	0	0	0	0	0	
MgO	1.15	1.19	1.00	0.88	2.25	1.22	1.73	0.81	0.91	0.84	0.81	0.81	0.81	0.81	0.81	0.81	0.84	0.92	0.76	0.76	0.84	0.92	0.76	0.76	0.76	0.76	0.76	
CaO	0.88	0.91	1.14	0.84	0.99	2.23	1.07	1.43	1.50	1.68	1.60	1.68	1.74	1.74	1.43	1.50	1.68	1.60	1.68	1.68	1.60	1.60	1.68	1.68	1.68	1.68	1.68	
Na <sub>2</sub> O	2.60	2.54	2.60	2.62	0.80	0.41	1.88	2.77	2.88	2.77	2.77	2.77	2.88	2.88	0.80	0.41	1.88	2.77	2.88	2.88	2.77	2.77	2.88	2.88	2.88	2.88	2.88	
K <sub>2</sub> O	2.30	2.51	2.34	2.40	4.07	1.95	3.15	1.61	1.96	1.64	1.85	1.74	2.02	2.02	4.07	1.95	1.64	1.85	1.74	1.74	1.85	1.85	1.74	1.74	1.74	1.74	1.74	
P <sub>2</sub> O <sub>5</sub>	0.16	0.14	0.12	0.12	0.17	0.10	0.17	0.13	0.13	0.13	0.13	0.13	0.14	0.14	0.17	0.10	0.13	0.13	0.13	0.13	0.13	0.13	0.13	0.13	0.13	0.13	0.13	0.13
H <sub>2</sub> O <sup>-</sup>	0.55	0.50	0.45	0.39	1.13	4.40	0.64	1.48	0.52	0.45	0.45	0.45	0.63	0.63	1.13	4.40	0.64	1.48	0.52	0.45	0.45	0.45	0.45	0.45	0.45	0.45	0.45	
LOI	1.77	1.93	1.98	1.59	3.90	3.69	2.95	0.03	2.08	3.21	2.20	2.04	2.44	2.44	3.90	3.69	2.95	0.03	2.08	3.21	2.20	2.20	2.04	2.04	2.04	2.04	2.04	
Total	100.70	100.32	100.10	100.67	99.80	99.35	100.35	99.42	100.83	100.77	100.14	100.77	100.46	100.46	99.80	99.35	100.35	99.42	100.83	100.77	100.14	100.14	100.77	100.77	100.77	100.77	100.77	
Nb	15.1	13.3	13.4	11.6	17.6	15.2	18.0	11.6	12.2	11.7	11.5	10.4	13.1	13.1	15.2	15.2	12.2	11.6	12.2	11.7	11.5	11.5	10.4	10.4	10.4	10.4	10.4	
Zr	294	278	234	249	143	115	160	258	248	278	217	226	285	285	294	294	248	217	226	278	217	217	226	226	226	226	226	
Y	36.0	31.1	29.2	26.7	37.0	18.6	36.6	26.7	26.6	36.6	26.7	26.6	28.8	28.8	36.0	36.0	26.6	26.7	26.6	26.6	26.7	26.7	26.6	26.6	26.6	26.6	26.6	26.6
Sr	140	156	162	183	108	427	179	316	315	262	288	258	313	313	140	140	315	288	258	262	288	288	258	258	258	258	258	258
U	6.33	6.15	6.72	5.21	7.23	9.66	6.87	0	0	0	0	0	5.20	5.20	6.33	6.33	0	0	0	0	0	0	0	0	0	0	0	0
Rb	85.2	95.5	86.2	86.4	181	77.3	131	54.4	64.6	61.2	61.2	56.0	67.6	67.6	85.2	85.2	64.6	61.2	64.6	61.2	61.2	61.2	56.0	56.0	56.0	56.0	56.0	
Th	15.1	14.0	14.2	8.50	20.5	18.2	14.7	11.8	12.4	10.7	11.7	12.8	11.1	11.1	15.1	15.1	12.4	11.7	12.4	10.7	11.7	11.7	12.8	12.8	12.8	12.8	12.8	
Pb	19.4	19.2	17.3	14.8	35.3	56.8	22.6	14.5	16.3	15.4	12.4	16.9	17.8	17.8	19.4	19.4	16.3	12.4	16.3	15.4	12.4	12.4	16.9	16.9	16.9	16.9	16.9	
Ga	14.3	13.2	14.2	12.0	28.6	21.7	12.6	12.6	13.7	11.1	11.1	11.1	14.8	14.8	14.3	14.3	13.7	11.1	13.7	11.1	11.1	11.1	11.8	11.8	11.8	11.8	11.8	
Zn	52.7	58.1	56.8	39.3	136	91.8	86.8	39.8	41.4	41.7	41.9	36.2	47.6	47.6	52.7	52.7	41.4	41.9	41.4	41.7	41.9	41.9	36.2	36.2	36.2	36.2	36.2	
Cu	0	0	0	0	0	0	0	0	0	0	0	0	0	0	0	0	0	0	0	0	0	0	0	0	0	0	0	0
Ni	11.4	14.6	17.8	9.83	27.7	11.7	20.8	7.43	8.91	9.02	8.82	7.42	11.0	11.0	11.4	11.4	8.91	8.82	8.91	9.02	8.82	8.82	7.42	7.42	7.42	7.42	7.42	
Co	85.4	59.9	88.1	83.9	-	-	-	76.2	84.2	69.5	89.7	88.0	84.8	84.8	85.4	85.4	84.2	89.7	84.2	69.5	89.7	89.7	88.0	88.0	88.0	88.0	88.0	
Cr	211	951	208	895	182	44.1	143	290	107	724	141	319	122	122	211	211	107	141	107	724	141	141	319	319	319	319	319	
Ce	91.7	68.9	64.0	69.5	76.3	111	76.1	63.5	71.3	62.9	61.2	48.2	65.5	65.5	91.7	91.7	71.3	61.2	71.3	62.9	61.2	61.2	48.2	48.2	48.2	48.2	48.2	
Nd	40.6	32.9	30.8	29.0	37.4	23.4	38.7	27.9	28.1	22.8	27.3	24.4	24.6	24.6	40.6	40.6	28.1	27.3	28.1	22.8	27.3	27.3	24.4	24.4	24.4	24.4	24.4	
V	62.8	66.3	54.0	49.2	126	39.8	90.4	54.3	55.3	58.6	54.8	52.0	65.1	65.1	62.8	62.8	55.3	54.8	55.3	58.6	54.8	54.8	52.0	52.0	52.0	52.0	52.0	
Ba	526	598	561	600	686	555	632	483	588	476	543	541	589	589	526	526	588	543	588	476	543	543	541	541	541	541	541	
La	41.1	44.4	37.0	43.3	46.7	23.4	38.0	37.2	35.9	36.1	30.9	35.4	37.7	37.7	41.1	41.1	35.9	30.9	35.9	36.1	30.9	30.9	35.4	35.4	35.4	35.4	35.4	
(SiO <sub>2</sub> /Al <sub>2</sub> O <sub>3</sub> )	6.17	5.78	6.31	6.63	3.33	5.86	4.59	6.90	6.50	6.90	6.60	7.26	5.91	5.91	6.17	6.17	6.50	6.60	6.50	6.90	6.60	6.60	7.26	7.26	7.26	7.26	7.26	
log (Na <sub>2</sub> O+K <sub>2</sub> O)	0.69	0.70	0.69	0.70	0.66	0.37	0.70	0.64	0.67	0.65	0.67	0.66	0.69	0.69	0.69	0.69	0.67	0.67	0.67	0.65	0.67	0.67	0.66	0.66	0.66	0.66	0.66	
log (SiO <sub>2</sub> /Al <sub>2</sub> O <sub>3</sub> )	0.79	0.76	0.80	0.82	0.52	0.77	0.66	0.84	0.81	0.84	0.82	0.86	0.77	0.77	0.79	0.79	0.81	0.82	0.81	0.84	0.82	0.82	0.86	0.86	0.86	0.86	0.86	
K <sub>2</sub> O/(K <sub>2</sub> O + CaO)	0.72	0.73	0.67	0.74	0.80	0.47	0.75	0.53	0.57	0.35	0.54	0.54	0.51	0.51	0.72	0.72	0.57	0.54	0.57	0.35	0.54	0.54	0.54	0.54	0.54	0.54	0.54	
(K <sub>2</sub> O/Na <sub>2</sub> O)	0.88	0.99	0.90	0.92	5.06	4.77	1.68	0.58	0.70	0.58	0.67	0.61	0.70	0.70	0.88	0.88	0.70	0.67	0.70	0.58	0.67	0.67	0.61	0.61	0.61	0.61	0.61	
(Fe <sub>2</sub> O <sub>3</sub> + MgO)	4.68	5.08	4.16	3.56	9.62	3.55	6.85	3.44	3.48	3.69	3.52	3.00	4.26	4.26	4.68	4.68	3.48	3.52	3.48	3.69	3.52	3.52	3.00	3.00	3.00	3.00	3.00	
(TiO <sub>2</sub> /Al <sub>2</sub> O <sub>3</sub> )	0.05	0.04	0.04	0.04	0.05	0.04	0.05	0.04	0.04	0.04	0.04	0.04	0.04	0.04	0.05	0.05	0.04	0.04	0.04	0.04	0.04	0.04	0.04	0.04	0.04	0.04	0.04	
ClA	68	68	66	66	76	72	71	66	65	59	65	63	65	65	68	68	65	65	65	59	65	65	63	63	63	63	63	
Th/(Th + Y)	0.30	0.31	0.33	0.24	0.36	0.49	0.29	0.31	0.32	0.29	0.33	0.28	0.28	0.28	0.30	0.30	0.32	0.33	0.32	0								

Appendix C continued

Sample description and location	214		215		216		217		218		219		220		221		222		223		224		225		226		
	Sandstone	Pienaarsfontein																									
SiO <sub>2</sub>	75.55	76.10	74.59	76.71	72.76	71.86	77.75	74.91	28.36	75.43	74.86	72.91	74.38	74.86	75.43	72.91	74.38	74.86	75.43	72.91	74.38	74.86	75.43	72.91	74.38	74.86	75.43
TiO <sub>2</sub>	0.43	0.49	0.51	0.49	0.61	0.51	0.52	0.50	0.26	0.50	0.53	0.50	0.54	0.53	0.50	0.58	0.54	0.53	0.50	0.58	0.54	0.53	0.50	0.58	0.54	0.53	0.50
Al <sub>2</sub> O <sub>3</sub>	11.63	11.83	11.90	10.84	12.40	12.77	10.43	11.18	6.39	11.18	11.18	10.43	11.18	12.41	12.62	12.62	12.62	12.41	12.62	12.62	12.62	12.41	12.62	12.62	12.62	12.41	12.62
Cr <sub>2</sub> O <sub>3</sub>	0.01	0.01	0.02	0.01	0.01	0.01	0.01	0.01	0.01	0.01	0.01	0.01	0.01	0.01	0.01	0.01	0.01	0.01	0.01	0.01	0.01	0.01	0.01	0.01	0.01	0.01	0.01
Fe <sub>2</sub> O <sub>3</sub> <sup>T</sup>	2.68	2.73	4.04	3.37	4.30	3.30	2.36	2.80	2.27	2.80	2.80	2.36	2.80	2.92	2.69	2.69	2.92	2.92	2.69	2.69	2.92	2.92	3.91	3.51	3.51	3.51	3.51
MnO	0.05	0.05	0.06	0.04	0.06	0.05	0.04	0.05	0.04	0.05	0.05	0.04	0.05	0.04	0.05	0.05	0.04	0.04	0.05	0.05	0.04	0.04	0.06	0.04	0.04	0.04	0.04
NiO	0	0	0	0	0	0	0	0	0	0	0	0	0	0	0	0	0	0	0	0	0	0	0	0	0	0	0
MgO	0.88	0.78	1.14	0.88	1.42	1.15	0.76	1.13	0	1.13	1.15	0.76	1.13	0.90	0.82	0.82	0.90	0.90	0.82	0.82	0.90	0.90	1.18	0.94	0.94	0.94	0.94
CaO	0.96	1.37	0.93	0.82	1.24	2.17	1.20	2.05	31.82	2.05	2.05	1.20	2.05	0.96	0.96	0.96	0.96	0.98	0.96	0.96	0.98	1.35	0.71	0.71	0.71	0.71	
Na <sub>2</sub> O	3.41	2.75	2.23	2.15	2.08	2.36	2.36	2.67	3.24	2.67	2.67	2.36	2.67	3.22	3.24	3.22	3.22	3.22	3.24	3.22	3.22	2.62	2.89	2.89	2.89	2.89	
K <sub>2</sub> O	1.96	1.99	2.25	2.15	2.52	2.18	1.85	1.51	1.58	1.51	1.51	1.85	1.51	2.63	2.35	2.35	2.63	2.63	2.35	2.35	2.63	2.32	2.23	2.23	2.23	2.23	
P <sub>2</sub> O <sub>5</sub>	0.12	0.13	0.14	0.15	0.20	0.15	0.13	0.27	0.04	0.15	0.15	0.13	0.27	0.18	0.15	0.15	0.18	0.18	0.15	0.15	0.18	0.16	0.12	0.12	0.12	0.12	
H <sub>2</sub> O	0.45	0.46	0.47	0.53	0.52	0.50	0.27	0.53	0.52	0.50	0.50	0.27	0.53	0.36	0.36	0.36	0.36	0.34	0.36	0.36	0.34	0.51	0.68	0.68	0.68	0.68	
LOI	1.59	1.93	1.96	1.72	2.43	3.25	1.64	2.29	26.15	2.29	2.29	1.64	2.29	1.62	1.59	1.62	1.62	1.62	1.59	1.62	1.62	2.40	2.03	2.03	2.03	2.03	
Total	99.72	100.60	100.23	99.85	100.56	100.26	100.12	99.91	98.86	99.91	99.91	100.12	99.91	100.63	100.22	100.63	100.22	100.63	100.22	100.63	100.63	100.63	100.64	100.72	100.72	100.72	100.72
Nb	11.6	12.5	13.5	13.2	16.2	13.7	13.0	13.8	7.30	13.8	13.8	13.0	13.8	14.1	13.33	14.1	13.33	14.1	13.33	13.33	14.1	15.6	14.1	14.1	14.1	14.1	
Zr	208	267	273	301	244	230	385	259	85.8	259	259	385	259	293	334	293	334	293	334	334	293	329	299	299	299	299	
Y	23.8	27.0	33.0	31.4	36.7	27.4	31.3	27.5	42.3	27.5	27.5	31.3	27.5	30.6	29.0	30.6	29.0	30.6	29.0	29.0	30.6	36.9	31.2	31.2	31.2	31.2	
Sr	210	286	181	158	174	328	201	464	395	464	464	201	464	211	227	211	227	211	227	227	211	160	150	150	150	150	
U	5.32	5.41	4.34	5.35	5.98	7.75	5.62	5.56	11.8	5.56	5.56	5.62	5.56	6.85	4.95	6.85	4.95	6.85	4.95	4.95	6.85	5.56	4.87	4.87	4.87	4.87	
Rb	62.4	64.0	84.6	76.6	80.7	76.6	57.3	52.6	70.9	76.6	76.6	57.3	52.6	82.4	72.3	82.4	72.3	82.4	72.3	72.3	82.4	87.9	81.4	81.4	81.4	81.4	
Th	13.0	14.5	11.7	12.0	16.0	16.0	10.3	13.9	0	13.9	13.9	10.3	13.9	16.8	12.1	16.8	12.1	16.8	12.1	12.1	16.8	14.3	15.1	15.1	15.1	15.1	
Pb	14.0	15.8	18.1	15.8	19.7	14.3	11.5	16.9	11.7	16.9	16.9	11.5	16.9	17.6	16.1	17.6	16.1	17.6	16.1	16.1	17.6	13.2	11.1	11.1	11.1	11.1	
Ga	11.3	13.6	12.8	11.2	15.0	15.1	10.8	14.3	9.12	14.3	14.3	10.8	14.3	13.3	13.3	13.3	13.3	13.3	13.3	13.3	13.3	14.7	15.8	15.8	15.8	15.8	
Zn	42.5	42.5	61.0	44.4	59.5	41.9	39.3	48.0	33.1	48.0	48.0	39.3	48.0	53.3	46.4	53.3	46.4	53.3	46.4	46.4	53.3	57.0	36.1	36.1	36.1	36.1	
Cu	0	0	0	0	0	0	44.7	68.7	0	68.7	68.7	44.7	68.7	0	0	0	0	0	0	0	0	0	0	0	0	0	
Ni	9.13	11.4	14.5	11.2	12.7	10.6	6.01	9.65	19.2	10.6	10.6	6.01	9.65	13.3	15.1	13.3	15.1	13.3	15.1	15.1	13.3	42.2	13.9	13.9	13.9	13.9	
Co	99.5	82.3	49.8	63.7	25.7	41.6	91.4	51.8	11.5	41.6	41.6	91.4	51.8	56.1	68.0	56.1	68.0	56.1	68.0	68.0	56.1	42.2	59.6	59.6	59.6	59.6	
Cr	150	126	308	152	124	113	204	91.5	42.7	91.5	91.5	204	91.5	250	581	250	581	250	581	581	250	176	144	144	144	144	
Ce	57.2	69.8	67.8	67.4	97.3	67.4	80.9	72.8	59.0	67.4	67.4	80.9	72.8	66.9	72.9	66.9	72.9	66.9	72.9	72.9	66.9	69.8	65.8	65.8	65.8	65.8	
Nd	18.9	26.7	32.3	27.4	43.5	26.4	37.2	37.2	27.4	26.4	26.4	37.2	37.2	29.5	26.5	29.5	26.5	29.5	26.5	26.5	29.5	32.9	32.4	32.4	32.4	32.4	
V	59.1	59.4	63.6	56.4	65.4	61.0	62.3	57.4	44.7	61.0	61.0	62.3	57.4	67.8	63.2	67.8	63.2	67.8	63.2	63.2	67.8	68.5	72.6	72.6	72.6	72.6	
Ba	633	600	508	494	459	446	449	392	306	446	446	449	392	530	508	530	508	530	508	508	530	559	543	543	543	543	
La	32.6	36.0	40.5	34.9	46.8	41.1	42.9	39.6	34.8	41.1	41.1	42.9	39.6	35.7	26.3	35.7	26.3	35.7	26.3	26.3	35.7	37.3	26.5	26.5	26.5	26.5	
(SiO <sub>2</sub> /Al <sub>2</sub> O <sub>3</sub> )	6.50	6.43	6.27	7.08	5.87	5.63	7.46	6.70	4.44	6.70	6.70	7.46	6.70	6.03	6.26	6.03	6.26	6.03	6.26	6.26	6.03	5.78	5.88	5.88	5.88	5.88	
log (Na <sub>2</sub> O+K <sub>2</sub> O)	0.73	0.68	0.65	0.63	0.66	0.66	0.70	0.62	0.40	0.62	0.62	0.70	0.62	0.77	0.75	0.77	0.75	0.77	0.75	0.75	0.77	0.69	0.71	0.71	0.71	0.71	
log (SiO <sub>2</sub> /Al <sub>2</sub> O <sub>3</sub> )	0.81	0.81	0.80	0.85	0.77	0.75	0.87	0.83	0.65	0.83	0.83	0.87	0.83	0.78	0.80	0.78	0.80	0.78	0.80	0.80	0.78	0.76	0.77	0.77	0.77	0.77	
K <sub>2</sub> O/(K <sub>2</sub> O + CaO)	0.67	0.59	0.71	0.72	0.67	0.50	0.61	0.57	0.05	0.57	0.57	0.61	0.57	0.73	0.73	0.73	0.73	0.73	0.73	0.73	0.73	0.89	0.77	0.77	0.77	0.77	
(K <sub>2</sub> O/Na <sub>2</sub> O)	0.57	0.72	1.01	1.00	1.21	0.93	0.58	0.57	1.71	0.93	0.93	0.58	0.57	0.82	0.73	0.82	0.73	0.82	0.73	0.73	0.82	0.89	0.77	0.77	0.77	0.77	
(Fe <sub>2</sub> O <sub>3</sub> + MgO)	3.56	3.52	5.18	4.25	5.72	4.45	3.12	3.93	2.27	3.93	3.93	3.12	3.93	3.82	3.51	3.82	3.51	3.82	3.51	3.51	3.82	5.09	4.45	4.45	4.45	4.45	
(TiO <sub>2</sub> /Al <sub>2</sub> O <sub>3</sub> )	0.04	0.04	0.04	0.05	0.05	0.04	0.05	0.04	0.04	0.04	0.04	0.05	0.04	0.04	0.04	0.04	0.04	0.04	0.04	0.04	0.04	0.05	0.05	0.05	0.05	0.05	
Cl/Al	65	66	69	68	68	66	63	64	16	66	66	63	64	65	65	65	65	65	65	65	65	67	68	68	68	68	
Th/(Th + Y)	0.35	0.35	0.26	0.28	0.30	0.37	0.25	0.34	0.00	0.34	0.34	0.25	0.34	0.35	0.29	0.35	0.29	0.35	0.29	0.29	0.35	0.28	0				

Appendix C continued

Sample description and location	227 Sandstone		228 Sandstone		229 Sandstone		230 Sandstone		231 Sandstone		232 Sandstone		233 Sandstone		234 Sandstone		235 Sandstone		236 Sandstone		237 Sandstone		246 Bentonite		249 Limestone		251 Bentonite		252 Limestone	
	Groot Hangklip	Droëkloof	Droëkloof	Droëkloof	Droëkloof	Droëkloof	Droëkloof	Klein Hangklip	NS1	NS1	NS1	NS1	NS1	NS1	NS1															
SiO <sub>2</sub>	73.11	77.28	75.78	75.27	75.29	74.83	74.12	75.30	75.30	77.05	77.05	75.39	69.89	75.39	69.89	75.39	77.05	77.05	75.39	69.89	75.39	69.89	46.35	20.37	46.35	20.37	46.35	20.37	22.24	
TiO <sub>2</sub>	0.49	0.46	0.52	0.56	0.48	0.48	0.60	0.49	0.53	0.48	0.48	0.60	0.49	0.53	0.48	0.42	0.42	0.50	0.57	0.57	0.57	0.31	0.16	0.31	0.16	0.31	0.16	0.71		
Al <sub>2</sub> O <sub>3</sub>	11.76	11.17	11.03	11.67	12.23	12.12	12.19	11.81	12.23	12.12	12.19	11.81	11.81	12.23	12.12	11.08	11.08	11.75	14.18	14.18	14.18	25.23	11.20	25.23	11.20	25.23	11.20	12.34		
Cr <sub>2</sub> O <sub>3</sub>	0.03	0.03	0.01	0.02	0.01	0.01	0.02	0.01	0.01	0.01	0.01	0.02	0.01	0.01	0.01	0.01	0.01	0.01	0.01	0.01	0.01	0.01	0.01	0.01	0.01	0.01	0.01	0.01	0.01	
Fe <sub>2</sub> O <sub>3</sub> T	4.15	2.98	3.17	3.55	3.43	3.21	3.88	3.00	3.43	3.21	3.88	3.00	3.00	3.43	3.21	2.67	2.67	3.18	4.15	4.15	4.15	2.66	1.17	2.66	1.17	2.66	1.17	1.67		
MnO	0.07	0.04	0.05	0.05	0.03	0.05	0.06	0.04	0.03	0.05	0.06	0.04	0.04	0.03	0.05	0.04	0.04	0.03	0.04	0.04	0.04	0.15	1.23	0.15	1.23	0.15	0.85	0.85		
NiO	0	0	0	0	0	0	0	0	0	0	0	0	0	0	0	0	0	0	0	0	0	0	0	0	0	0	0	0	0	
MgO	1.17	0.89	0.92	0.94	0.87	1.04	1.29	0.95	0.87	1.04	1.29	0.95	0.95	0.87	1.04	0.91	0.91	1.00	1.41	1.41	1.41	1.71	0	0	1.71	0	1.71	0	0	
CaO	1.67	0.86	0.77	0.70	0.70	0.87	0.95	0.74	0.70	0.87	0.95	0.74	0.74	0.87	0.58	0.58	0.46	0.46	0.79	0.79	0.79	5.16	32.07	5.16	32.07	5.16	32.07	29.58	29.58	
Na <sub>2</sub> O	2.51	2.81	2.74	2.54	2.58	2.82	2.57	2.57	2.58	2.82	2.57	2.57	2.57	2.58	2.82	3.03	3.03	2.84	2.72	2.72	2.72	0.42	0.17	0.42	0.17	0.42	0.17	0	0	
K <sub>2</sub> O	2.14	2.23	2.04	2.20	2.46	1.93	2.12	2.25	2.46	1.93	2.12	2.25	2.25	1.93	2.12	1.87	1.87	2.14	2.95	2.95	2.95	6.92	3.04	6.92	3.04	6.92	3.04	3.45	3.45	
P <sub>2</sub> O <sub>5</sub>	0.12	0.12	0.12	0.15	0.11	0.12	0.19	0.12	0.11	0.12	0.19	0.12	0.12	0.11	0.12	0.10	0.10	0.11	0.13	0.13	0.13	0.04	0	0.04	0	0.04	0	0	0	
H <sub>2</sub> O	0.60	0.54	0.50	0.65	0.75	0.64	0.53	0.56	0.75	0.64	0.53	0.56	0.56	0.64	0.37	0.37	0.61	0.61	0.64	0.64	0.64	2.87	1.84	2.87	1.84	2.87	1.84	1.51	1.51	
H <sub>2</sub> O	2.70	1.56	1.84	1.94	2.10	2.48	2.15	2.09	2.10	2.48	2.15	2.09	2.09	2.15	1.64	1.64	1.97	1.97	2.56	2.56	2.56	8.23	27.01	8.23	27.01	8.23	27.01	25.13	25.13	
LOI	100.53	100.77	99.49	100.25	101.09	100.61	100.72	99.92	101.09	100.61	100.72	99.92	99.92	100.61	99.78	99.78	100.60	100.60	100.05	100.05	100.05	100.05	98.30	100.05	100.05	98.30	100.05	97.50	97.50	
Nb	13.5	12.5	13.1	14.5	14.6	12.3	15.4	12.6	14.6	12.3	15.4	12.6	12.6	14.6	11.1	11.1	12.8	12.8	14.9	14.9	14.9	26.8	14.2	26.8	14.2	26.8	14.2	30.0	30.0	
Zr	298	281	396	394	317	243	313	251	317	243	313	251	251	317	220	220	279	279	235	235	235	519	213	519	213	519	213	586	586	
Y	39.9	26.9	33.0	36.2	24.7	27.0	39.7	30.4	24.7	27.0	39.7	30.4	30.4	24.7	24.5	24.5	21.0	21.0	31.7	31.7	31.7	90.4	74.3	90.4	74.3	90.4	74.3	169	169	
Sr	159	151	156	159	165	152	131	149	165	152	131	149	149	165	161	161	153	153	200	200	200	506	462	506	462	506	462	702	702	
U	0	6.46	0	0	5.84	4.09	0	4.65	5.84	4.09	0	4.65	4.65	5.84	5.59	5.59	0	0	5.58	5.58	5.58	15.4	12.3	15.4	12.3	15.4	12.3	25.7	25.7	
Rb	79.3	74.4	68.2	77.7	82.7	77.5	80.7	81.7	82.7	77.5	80.7	81.7	81.7	80.7	74.2	74.2	74.2	74.2	113	113	113	243	249	243	249	243	249	131	131	
Th	13.5	12.6	12.4	9.93	10.7	10.9	12.5	13.4	10.7	10.9	12.5	13.4	13.4	12.5	12.4	12.4	13.2	13.2	14.5	14.5	14.5	41.5	18.3	41.5	18.3	41.5	18.3	27.9	27.9	
Pb	14.1	14.9	12.3	11.9	12.3	14.1	18.0	15.6	12.3	14.1	18.0	15.6	15.6	14.1	13.4	13.4	14.9	14.9	17.4	17.4	17.4	114	22.0	114	22.0	114	22.0	36.6	36.6	
Ga	15.0	13.4	12.9	13.5	15.8	14.8	13.2	12.7	15.8	14.8	13.2	12.7	12.7	13.2	13.9	13.9	12.2	12.2	18.9	18.9	18.9	29.2	14.7	29.2	14.7	29.2	14.7	14.6	14.6	
Zn	51.5	44.3	53.1	53.3	36.0	51.4	58.5	48.1	36.0	51.4	58.5	48.1	48.1	51.4	43.6	43.6	33.7	33.7	70.9	70.9	70.9	249	59.2	249	59.2	249	59.2	227	227	
Cu	0	0	0	0	0	0	0	0	0	0	0	0	0	0	0	0	0	0	0	0	0	51.9	0	0	51.9	0	51.9	74.9	74.9	
Ni	13.7	11.4	12.7	13.9	7.72	10.4	12.9	13.0	7.72	10.4	12.9	13.0	13.0	12.9	9.70	9.70	10.9	10.9	24.0	24.0	24.0	12.9	0	12.9	0	12.9	0	0	0	
Co	45.3	71.1	66.3	70.2	69.2	76.3	31.0	57.3	69.2	76.3	31.0	57.3	57.3	62.3	62.3	70.9	70.9	148	223	223	33.5	-	-	-	-	-	-	-	-	
Cr	584	648	196	386	118	189	261	192	118	189	261	192	192	128	128	148	148	288	288	288	33.5	0	0	0	0	0	0	0	0	
Ce	51.3	56.0	82.9	41.3	41.3	67.4	79.7	60.2	41.3	67.4	79.7	60.2	60.2	63.3	63.3	60.6	60.6	63.3	69.5	69.5	69.5	20.7	115	20.7	115	20.7	115	150	150	
Nd	26.3	24.6	38.5	30.6	12.4	32.0	33.8	26.6	12.4	32.0	33.8	26.6	26.6	27.5	27.5	15.0	15.0	32.8	32.8	32.8	32.8	0	57.8	0	57.8	0	57.8	76.8	76.8	
V	61.9	56.1	69.9	65.7	70.9	65.6	68.5	60.9	70.9	65.6	68.5	60.9	60.9	56.9	56.9	67.1	67.1	67.1	76.8	76.8	76.8	33.6	0	33.6	0	33.6	0	46.7	46.7	
Ba	523	541	525	541	617	392	595	553	617	392	595	553	553	624	624	607	607	607	1862	1862	1862	1690	863	1690	863	1690	863	869	869	
La	35.4	27.1	40.0	36.4	14.6	37.1	49.4	32.6	14.6	37.1	49.4	32.6	32.6	37.0	37.0	16.3	16.3	32.0	32.0	32.0	32.0	0	56.6	0	56.6	0	60.5	60.5		
(SiO <sub>2</sub> /Al <sub>2</sub> O <sub>3</sub> )	6.22	6.92	6.87	6.45	6.16	6.18	6.08	6.38	6.16	6.18	6.08	6.38	6.38	6.08	6.95	6.95	6.47	6.47	4.93	4.93	4.93	1.84	1.82	1.84	1.82	1.84	1.82	1.80	1.80	
log (Na <sub>2</sub> O/H <sub>2</sub> O)	0.67	0.70	0.68	0.68	0.70	0.68	0.68	0.68	0.68	0.68	0.68	0.68	0.68	0.68	0.69	0.69	0.70	0.70	0.75	0.75	0.75	0.67	0.51	0.67	0.51	0.67	0.51	0.54	0.54	
log (SiO <sub>2</sub> /Al <sub>2</sub> O <sub>3</sub> )	0.79	0.84	0.84	0.81	0.79	0.79	0.78	0.80	0.79	0.79	0.78	0.80	0.80	0.79	0.84	0.84	0.81	0.81	0.69	0.69	0.69	0.26	0.26	0.26	0.26	0.26	0.26	0.26	0.26	
K <sub>2</sub> O/(K <sub>2</sub> O + CaO)	0.56	0.77	0.78	0.76	0.78	0.79	0.69	0.75	0.78	0.79	0.69	0.75	0.75	0.78	0.79	0.75	0.75	0.82	0.79	0.79	0.79	0.57	0.09	0.57	0.09	0.57	0.09	0.10	0.10	
(K <sub>2</sub> O/Na <sub>2</sub> O)	0.85	0.79	0.74	0.87	0.95	0.68	0.80	0.88	0.95	0.68	0.80	0.88	0.88	0.87	0.62	0.62	0.75	0.75	1.09	1.09	1.09	16.3	17.9	16.3	17.9	16.3	17.9	0	0	
(Fe <sub>2</sub> O <sub>3</sub> + MgO)	5.31	3.87	4.09	4.50	4.29	4.25	5.17	3.95	4.																					



Appendix C continued

Sample description and location	310	311	312	313	314	315	316	317	318	319	320	321	322	323	324	325	326	327
	Sandstone Soutrivierspunt	Sandstone Soutrivierspunt	Bentonite Geelbek	Sandstone Geelbek	Chert Geelbek	Shale Geelbek	Siltstone Geelbek	Siltstone Geelbek	Sandstone Geelbek	Sandstone Geelbek	Limestone Geelbek	Sandstone Geelbek	Shale Geelbek	Limestone Geelbek	Sandstone Geelbek	Shale Geelbek	Shale Geelbek	Sandstone Geelbek
SiO <sub>2</sub>	75.99	71.65	76.54	78.88	78.66	71.69	71.97	70.64	64.18	18.86	67.34	60.69	31.91	61.18	65.86	62.43	66.93	74.37
TiO <sub>2</sub>	0.49	0.56	0.11	0.34	0.12	0.54	0.56	0.47	0.59	0.25	0.23	0.63	0.35	0.59	0.66	0.77	0.58	0.70
Al <sub>2</sub> O <sub>3</sub>	12.40	13.65	13.65	11.98	10.69	14.59	14.54	15.91	13.47	5.90	12.08	20.04	9.13	13.55	16.27	18.03	14.34	12.36
Cr <sub>2</sub> O <sub>3</sub>	0.02	0.02	0.02	0.03	0.02	0.01	0.03	0.02	0.02	0.02	0.02	0.03	0.02	0.02	0.01	0.03	0.02	0.03
Fe <sub>2</sub> O <sub>3</sub> <sup>T</sup>	2.79	2.85	1.50	1.80	0.97	3.59	3.38	3.08	4.11	8.16	3.08	6.38	8.55	10.03	5.92	7.05	5.15	4.74
MnO	0.07	0.06	0.03	0.07	0.06	0.04	0.03	0.03	0.20	1.55	0.33	0.06	1.37	0.27	0.08	0.08	0.09	0.06
NiO	0.01	0	0	0	0	0.01	0	0	0	0	0	0	0	0	0	0	0	0
MgO	1.34	1.58	1.23	0.84	0.33	1.35	1.14	2.11	1.45	1.33	1.56	2.87	1.61	2.98	2.57	3.18	2.06	1.83
CaO	1.17	2.28	0.14	0.96	1.84	0.35	0.20	0.28	7.03	33.28	7.79	0.97	24.24	4.54	0.89	0.48	2.50	0.44
Na <sub>2</sub> O	2.96	3.43	0.73	2.57	4.24	2.13	1.81	1.54	2.56	1.28	1.36	1.48	1.70	1.81	1.79	1.57	2.79	2.87
K <sub>2</sub> O	1.07	1.05	2.05	1.15	0.43	2.25	2.31	2.58	1.92	0.23	1.40	2.38	0.39	1.00	1.47	1.77	1.21	0.85
P <sub>2</sub> O <sub>5</sub>	0.17	0.24	0.05	0.08	0.15	0.16	0.13	0.12	0.16	0.64	0.14	0.44	0.42	0.43	0.21	0.17	0.22	0.19
H <sub>2</sub> O	-	-	-	-	-	-	-	-	-	-	-	-	-	-	-	-	-	-
LOI	1.98	2.11	2.24	2.06	1.83	2.20	2.31	2.23	2.45	4.50	2.95	2.71	3.86	2.50	2.82	2.94	2.52	2.28
Total	100.45	98.55	98.28	100.34	99.33	98.90	98.41	98.97	98.13	76.00	98.28	98.68	83.54	98.88	98.55	98.50	98.40	100.69
Nb	17.0	18.0	16.0	12.0	10.0	17.0	17.0	13.0	17.0	5.00	12.0	12.0	4.00	13.0	18.0	20.0	14.0	24.0
Zr	232	333	203	111	90.0	175	160	105	176	59.0	94.0	155	124	134	184	175	222	542
Y	23.0	27.0	42.0	18.0	12.0	39.0	38.0	18.0	39.0	28.0	35.0	57.0	44.0	39.0	39.0	37.0	34.0	35.0
Sr	192	287	44.0	107	258	127	124	79.0	249	67.0	215	116	504	157	120	130	263	132
U	9.00	5.00	14.0	13.0	11.0	13.0	14.0	6.00	7.00	0	11.0	6.00	8.00	4.00	16.0	10.0	10.0	9.00
Rb	69.0	71.0	132	86.0	19.0	149	163	192	105	16.0	110	242	28.0	83.0	153	181	92.0	68.0
Th	18.0	17.0	25.0	15.0	27.0	20.0	19.0	32.0	17.0	6.00	25.0	25.0	24.0	22.0	31.0	22.0	21.0	23.0
Pb	16.0	16.0	14.0	29.0	23.0	15.0	38.0	19.0	24.0	0	28.0	29.0	23.0	19.0	42.0	31.0	30.0	24.0
Ga	14.0	15.0	21.0	14.0	7.00	18.0	19.0	20.0	16.0	9.00	15.0	27.0	11.0	20.0	22.0	24.0	12.0	15.0
Zn	36.0	48.0	10.0	37.0	22.0	66.0	37.0	41.0	97.0	26.0	33.0	78.0	48.0	92.0	94.0	109	73.0	76.0
Cu	24.0	27.0	14.0	15.0	10.0	31.0	28.0	24.0	44.0	134	42.0	50.0	115	70.0	43.0	51.0	40.0	35.0
Ni	21.0	26.0	13.0	15.0	6.00	19.0	20.0	17.0	26.0	19.0	14.0	45.0	22.0	30.0	34.0	31.0	26.0	23.0
Co	6.00	6.00	3.00	4.00	2.00	8.00	7.00	7.00	9.00	24.0	7.00	15.0	25.0	28.0	14.0	18.0	12.0	11.0
Cr	33.0	38.0	12.0	55.0	14.0	34.0	45.0	28.0	38.0	26.0	37.0	65.0	36.0	59.0	48.0	61.0	44.0	56.0
Ce	75.0	96.0	74.0	76.0	46.0	163	115	81.0	108	45.0	55.0	147	72.0	99.0	117	133	120	113
Nd	28.0	32.0	32.0	22.0	15.0	47.0	32.0	23.0	30.0	25.0	20.0	54.0	42.0	37.0	38.0	42.0	37.0	42.0
V	42.0	47.0	5.00	30.0	4.00	54.0	80.0	38.0	47.0	34.0	12.0	113	42.0	88.0	85.0	121	64.0	65.0
Ba	457	595	559	407	257	933	887	558	783	158	508	961	272	426	667	828	694	449
La	26.0	39.0	30.0	34.0	31.0	58.0	42.0	36.0	45.0	13.0	23.0	63.0	55.0	48.0	48.0	47.0	52.0	58.0
(SiO <sub>2</sub> /Al <sub>2</sub> O <sub>3</sub> )	6.13	5.63	5.61	6.58	7.36	4.91	4.95	4.44	4.77	3.20	5.68	3.03	3.49	4.52	4.05	3.46	4.67	6.02
log (Na <sub>2</sub> O+K <sub>2</sub> O)	0.61	0.65	0.44	0.57	0.67	0.64	0.62	0.61	0.65	0.18	0.44	0.59	0.32	0.45	0.51	0.52	0.60	0.57
log (SiO <sub>2</sub> /Al <sub>2</sub> O <sub>3</sub> )	0.79	0.75	0.75	0.82	0.87	0.89	0.89	0.85	0.68	0.50	0.75	0.48	0.54	0.65	0.61	0.54	0.67	0.78
K <sub>2</sub> O/(K <sub>2</sub> O + CaO)	0.48	0.31	0.87	0.67	0.19	0.87	0.92	0.92	0.21	0.01	0.15	0.71	0.02	0.18	0.62	0.79	0.33	0.66
(K <sub>2</sub> O/Na <sub>2</sub> O)	0.36	0.31	2.82	0.45	0.10	1.06	1.28	1.68	0.75	0.18	1.03	1.61	0.23	0.55	0.82	1.13	0.43	0.29
(Fe <sub>2</sub> O <sub>3</sub> + MgO)	4.13	4.43	2.73	2.64	1.30	4.94	4.52	5.19	5.56	9.49	4.64	9.24	10.2	13.0	8.49	10.2	7.21	6.57
(TiO <sub>2</sub> /Al <sub>2</sub> O <sub>3</sub> )	0.04	0.04	0.01	0.04	0.01	0.04	0.04	0.03	0.04	0.04	0.02	0.03	0.04	0.04	0.04	0.04	0.04	0.06
Cl/Al	70	65	82	74	62	76	77	78	54	15	53	81	26	65	80	83	69	75
Th/(Th + Y)	0.44	0.39	0.37	0.45	0.69	0.34	0.33	0.64	0.30	0.18	0.42	0.30	0.35	0.36	0.44	0.37	0.38	0.40
Cr/V	0.79	0.81	2.40	1.83	3.50	0.63	0.56	0.74	0.81	0.76	3.08	0.58	0.86	0.67	0.56	0.50	0.69	0.86
Y/Ni	1.10	1.04	3.23	1.20	2.00	2.05	1.90	1.06	1.50	1.47	2.50	1.27	2.00	1.30	1.15	1.19	1.31	1.52
Zr/ThO <sub>2</sub>	0.05	0.06	0.18	0.03	0.07	0.03	0.03	0.02	0.03	0.02	0.04	0.02	0.04	0.02	0.03	0.02	0.04	0.08
Nb/Y	0.74	0.67	0.38	0.67	0.83	0.44	0.45	0.72	0.44	0.18	0.34	0.21	0.09	0.33	0.46	0.54	0.41	0.69

Appendix C continued

Sample description and location	328	329	330	331	332	333	334	335	336	337	338	339	340	341	342	343	344	345
	Shale Grootkloof	Siltstone Grootkloof	Sandstone Grootkloof	Sandstone Grootkloof	Siltstone Grootkloof	Siltstone Grootkloof	Sandstone Grootkloof	Siltstone Grootkloof	Sandstone Grootkloof	Sandstone Krantz 1	Limestone Krantz 1	Siltstone Krantz 1	Sandstone Krantz 1	Shale Krantz 1	Gneiss Laingsburg	Shale Krantz 1	Shale Krantz 1	Sandstone Krantz 1
SiO <sub>2</sub>	63.79	67.35	73.47	73.24	69.24	65.86	72.32	58.25	74.56	72.84	49.88	69.63	72.74	67.55	61.67	62.15	62.31	73.64
TiO <sub>2</sub>	0.71	0.70	0.57	0.49	0.63	0.79	0.59	0.78	0.50	0.55	0.41	0.75	0.67	0.79	1.66	0.69	0.68	0.51
Al <sub>2</sub> O <sub>3</sub>	15.85	15.28	12.56	12.25	14.28	15.26	12.93	19.66	11.86	12.92	9.30	14.98	12.81	14.96	13.81	18.71	19.02	12.13
Cr <sub>2</sub> O <sub>3</sub>	0.02	0.02	0.02	0.09	0.03	0.02	0.02	0.02	0.02	0.05	0.02	0.03	0.02	0.02	0.04	0.02	0.02	0.06
Fe <sub>2</sub> O <sub>3</sub> <sup>T</sup>	7.47	4.80	3.51	3.41	4.64	5.52	3.65	8.27	3.29	3.72	2.68	4.82	5.02	5.32	6.06	7.32	6.51	3.76
MnO	0.09	0.07	0.07	0.07	0.07	0.07	0.07	0.09	0.06	0.08	0.41	0.08	0.09	0.09	0.19	0.08	0.08	0.08
NiO	0.01	0	0	0	0	0.01	0	0.01	0	0	0	0	0	0	0	0	0	0
MgO	3.81	2.47	1.59	1.48	2.37	2.70	1.83	3.93	1.46	1.86	1.08	2.48	2.20	2.54	2.39	2.77	3.23	1.71
CaO	0.45	1.01	0.84	1.92	0.91	0.89	1.05	1.19	2.83	1.22	16.98	1.14	0.96	0.92	5.10	0.58	0.47	2.57
Na <sub>2</sub> O	1.43	2.22	2.69	2.44	2.20	2.78	2.56	1.29	2.32	2.59	1.92	2.38	2.22	1.94	3.20	1.48	1.65	2.51
K <sub>2</sub> O	1.76	2.00	1.42	1.49	1.87	1.93	1.42	2.22	1.13	1.35	0.62	1.39	1.10	1.36	1.34	2.25	2.23	1.09
P <sub>2</sub> O <sub>5</sub>	0.26	0.18	0.16	0.13	0.18	0.23	0.17	0.22	0.16	0.15	0.12	0.21	0.19	0.19	0.53	0.21	0.22	0.14
H <sub>2</sub> O <sup>+</sup>	-	-	-	-	-	-	-	-	-	-	-	-	-	-	-	-	-	-
LOI	2.55	2.11	1.98	1.99	2.00	2.35	2.20	2.56	2.12	2.07	3.46	2.47	2.31	2.46	2.52	2.47	2.57	2.04
Total	98.19	98.20	98.89	98.99	98.40	98.41	98.81	98.47	100.31	99.40	86.87	100.36	100.34	98.14	98.50	98.72	99.00	100.24
Nb	15.0	18.0	20.0	16.0	18.0	21.0	17.0	19.0	16.0	16.0	12.0	20.0	19.0	20.0	34.0	17.0	18.0	16.0
Zr	123	229	234	259	185	187	215	125	293	260	245	285	245	226	519	161	149	258
Y	39.0	44.0	32.0	28.0	33.0	36.0	29.0	32.0	28.0	32.0	30.0	43.0	39.0	41.0	86.0	35.0	29.0	28.0
Sr	84.0	124	132	144	114	114	144	75.0	161	143	339	114	101	98.0	445	100	98.0	203
U	7.00	12.0	11.0	8.00	11.0	4.00	12.0	10.0	9.00	10.0	6.00	7.00	2.00	8.00	2.00	7.00	5.00	9.00
Rb	171	146	95.0	95.0	134	157	107	220	81.0	99.0	64.0	128	96.0	134	37.0	184	187	80.0
Th	25.0	27.0	22.0	24.0	22.0	20.0	16.0	25.0	18.0	16.0	16.0	22.0	18.0	19.0	5.00	28.0	28.0	21.0
Pb	25.0	20.0	17.0	23.0	24.0	24.0	22.0	29.0	22.0	29.0	15.0	27.0	26.0	22.0	12.0	30.0	31.0	26.0
Ga	25.0	18.0	15.0	12.0	16.0	18.0	13.0	26.0	9.00	12.0	12.0	17.0	16.0	18.0	26.0	24.0	26.0	10.0
Zn	107	73.0	50.0	37.0	74.0	92.0	58.0	138	47.0	48.0	38.0	64.0	60.0	82.0	166	109	114	44.0
Cu	56.0	39.0	30.0	30.0	39.0	43.0	30.0	59.0	31.0	31.0	59.0	38.0	38.0	42.0	61.0	52.0	47.0	32.0
Ni	42.0	32.0	24.0	21.0	29.0	32.0	25.0	36.0	26.0	26.0	16.0	21.0	23.0	24.0	24.0	37.0	27.0	25.0
Co	19.0	11.0	8.00	7.00	11.0	13.0	8.00	22.0	7.00	8.00	6.00	11.0	12.0	13.0	15.0	18.0	16.0	8.00
Cr	67.0	50.0	39.0	36.9	43.0	55.0	40.0	68.0	35.0	140	32.0	56.0	82.0	53.0	93.0	62.0	61.0	245
Ce	119	99.0	92.0	78.0	95.0	98.0	88.0	103	91.0	88.0	71.0	108	93.0	109	174	120	129	75.0
Nd	44.0	41.0	33.0	32.0	33.0	29.0	34.0	32.0	31.0	32.0	23.0	36.0	38.0	36.0	65.0	34.0	35.0	30.0
V	106	65.0	49.0	41.0	63.0	86.0	55.0	130	35.0	38.0	42.0	73.0	53.0	73.0	78.0	113	112	38.0
Ba	646	666	561	534	576	689	620	789	429	565	334	658	442	599	1163	978	905	321
La	32.0	50.0	31.0	36.0	34.0	13.0	39.0	9.00	34.0	35.0	44.0	36.0	48.0	34.0	57.0	39.0	57.0	26.0
(SiO <sub>2</sub> /Al <sub>2</sub> O <sub>3</sub> )	4.03	4.41	5.85	5.98	4.85	4.32	5.59	2.96	6.29	5.64	5.36	4.65	5.68	4.52	4.47	3.32	3.28	6.07
log (Na <sub>2</sub> O+K <sub>2</sub> O)	0.50	0.63	0.61	0.59	0.61	0.67	0.60	0.54	0.54	0.60	0.40	0.58	0.52	0.52	0.66	0.57	0.59	0.56
log (SiO <sub>2</sub> /Al <sub>2</sub> O <sub>3</sub> )	0.60	0.64	0.77	0.78	0.69	0.64	0.75	0.47	0.80	0.75	0.73	0.67	0.75	0.65	0.65	0.52	0.52	0.78
K <sub>2</sub> O/(K <sub>2</sub> O + CaO)	0.80	0.66	0.63	0.44	0.67	0.68	0.57	0.65	0.29	0.52	0.04	0.55	0.53	0.60	0.21	0.80	0.82	0.30
(K <sub>2</sub> O/Na <sub>2</sub> O)	1.23	0.90	0.53	0.61	0.85	0.69	0.56	1.72	0.49	0.52	0.33	0.59	0.50	0.70	0.42	1.52	1.35	0.43
(Fe <sub>2</sub> O <sub>3</sub> <sup>T</sup> + MgO)	11.3	7.27	5.10	4.89	7.00	8.22	5.48	12.2	4.75	5.58	3.76	7.31	7.22	7.86	8.45	10.1	9.74	5.46
(TiO <sub>2</sub> /Al <sub>2</sub> O <sub>3</sub> )	0.04	0.05	0.05	0.04	0.04	0.05	0.05	0.04	0.04	0.04	0.04	0.05	0.05	0.05	0.12	0.04	0.04	0.04
ClA	81	74	72	68	74	73	72	81	65	71	32	75	75	78	59	81	81	66
Th/(Th + Y)	0.39	0.38	0.41	0.46	0.40	0.36	0.36	0.44	0.39	0.33	0.35	0.34	0.32	0.32	0.05	0.44	0.49	0.43
CrV	0.63	0.77	0.80	9.00	0.68	0.64	0.73	0.52	1.00	3.68	0.76	0.77	1.00	3.68	1.19	0.55	0.54	6.45
Y/Ni	0.93	1.38	1.33	1.33	1.14	1.13	1.16	0.89	1.08	1.23	1.88	2.05	1.70	1.28	3.58	0.95	1.07	1.12
Zr/TiO <sub>2</sub>	0.02	0.03	0.04	0.05	0.03	0.02	0.04	0.02	0.06	0.05	0.06	0.04	0.04	0.03	0.03	0.02	0.02	0.05
Nb/Y	0.38	0.41	0.63	0.57	0.55	0.58	0.59	0.59	0.57	0.50	0.40	0.47	0.49	0.49	0.40	0.49	0.62	0.57



Appendix C continued

Sample description and location	364 Siltstone Waterkloof	365 Siltstone Waterkloof	366 Sandstone Waterkloof	367 Chert Perdekraal	368 Sandstone Uuberg	369 Sandstone Uuberg	370 Sandstone Uuberg	371 Sandstone W of Skelding	372 Sandstone W of Skelding	373 Sandstone Skelding	374 Sandstone Paardekraal	375 Sandstone Paardekraal	376 Sandstone Paardekraal	377 Sandstone Grootfontein	378 Sandstone Grootfontein	379 Sandstone Grootfontein
SiO <sub>2</sub>	70.18	67.87	73.73	80.10	73.52	67.75	70.85	69.65	76.11	73.26	67.45	69.80	70.41	72.85	71.07	73.34
TiO <sub>2</sub>	0.66	0.67	0.85	0.12	0.40	0.52	0.54	0.57	0.17	0.49	0.51	0.51	0.67	0.53	0.74	0.55
Al <sub>2</sub> O <sub>3</sub>	14.29	14.52	11.89	11.91	11.43	12.79	12.70	13.80	8.99	12.46	12.78	12.23	12.81	12.29	12.54	11.96
Cr <sub>2</sub> O <sub>3</sub>	0.01	0.02	0.02	0.02	0.02	0.02	0.02	0.02	0.01	0.03	0.03	0.02	0.02	0.02	0.03	0.02
Fe <sub>2</sub> O <sub>3</sub> T	4.65	4.94	4.82	0.98	2.38	3.75	3.63	4.61	2.24	3.54	2.92	3.20	3.97	3.17	4.41	3.64
MnO	0.08	0.08	0.10	0.02	0.07	0.07	0.07	0.08	0.23	0.08	0.19	0.07	0.08	0.09	0.09	0.07
NiO	0	0	0	0	0	0.01	0	0	0	0	0.01	0.01	0	0	0	0
MgO	2.26	2.54	1.61	0.40	1.27	1.98	1.68	1.81	1.35	1.55	1.42	1.51	1.91	1.44	1.85	1.61
CaO	1.16	1.92	1.84	0.13	2.96	3.96	2.13	0.44	4.73	0.79	6.55	4.78	1.99	1.89	1.13	1.23
Na <sub>2</sub> O	2.15	1.88	2.74	4.94	3.02	2.51	2.01	3.14	0.85	4.37	2.40	2.16	2.29	2.46	2.13	2.23
K <sub>2</sub> O	1.50	1.41	0.75	0.37	1.38	2.78	2.81	1.73	2.05	2.42	2.26	2.33	2.41	2.11	2.50	2.04
P <sub>2</sub> O <sub>5</sub>	0.19	0.20	0.21	0.10	0.13	0.14	0.16	0.23	0.10	0.14	0.13	0.15	0.19	0.16	0.16	0.14
H <sub>2</sub> O	-	-	-	-	-	-	-	-	-	-	-	-	-	-	-	-
LOI	2.33	2.42	2.04	1.72	1.70	1.75	1.60	1.58	1.79	1.53	1.86	1.75	1.65	1.51	1.45	1.42
Total	99.45	98.47	100.59	100.82	98.27	98.01	98.17	97.66	98.60	100.65	98.51	98.52	98.39	98.48	98.10	98.26
Nb	17.0	15.0	29.0	10.0	11.0	16.0	16.0	17.0	10.0	15.0	14.0	14.0	18.0	17.0	26.0	18.0
Zr	186	154	727	103	163	195	259	170	82.0	228	233	226	292	299	669	370
Y	33.0	36.0	35.0	14.0	19.0	28.0	32.0	26.0	17.0	26.0	24.0	28.0	35.0	28.0	37.0	27.0
Sr	240	276	213	105	142	203	151	172	167	125	186	224	153	148	117	135
U	11.0	6.00	7.00	13.0	8.00	13.0	9.00	10.0	7.00	11.0	7.00	1.00	4.00	5.00	9.00	3.00
Rb	135	145	46.0	13.0	54.0	101	96.0	66.0	78.0	86.0	87.0	93.0	98.0	80.0	92.0	77.0
Th	21.0	24.0	30.0	30.0	19.0	24.0	21.0	14.0	17.0	19.0	21.0	20.0	22.0	17.0	28.0	22.0
Pb	29.0	24.0	12.0	29.0	12.0	16.0	18.0	17.0	21.0	22.0	22.0	23.0	17.0	21.0	17.0	25.0
Ga	20.0	21.0	13.0	7.00	7.00	14.0	10.0	14.0	7.00	13.0	14.0	10.0	14.0	14.0	16.0	13.0
Zn	78.0	82.0	66.0	2.00	43.0	55.0	48.0	74.0	17.0	52.0	47.0	46.0	54.0	33.0	48.0	48.0
Cu	35.0	40.0	40.0	5.00	22.0	35.0	36.0	34.0	28.0	28.0	35.0	34.0	33.0	29.0	37.0	30.0
Ni	30.0	29.0	23.0	5.00	24.0	23.0	23.0	20.0	16.0	17.0	25.0	24.0	25.0	17.0	33.0	19.0
Co	11.0	12.0	11.0	2.00	5.00	8.00	8.00	11.0	5.00	8.00	6.00	7.00	9.00	7.00	11.0	9.00
Cr	45.0	55.0	69.0	15.0	34.0	35.0	41.0	39.0	17.0	38.0	35.0	40.0	44.0	42.0	61.0	40.0
Ce	99.0	92.0	132	58.0	55.0	101	96.0	94.0	56.0	75.0	73.0	81.0	70.0	80.0	114	87.0
Nd	31.0	30.0	48.0	20.0	22.0	32.0	36.0	32.0	23.0	28.0	23.0	28.0	32.0	28.0	39.0	34.0
V	65.0	65.0	112	2.00	39.0	51.0	47.0	58.0	8.00	47.0	49.0	44.0	56.0	57.0	79.0	51.0
Ba	667	514	371	346	273	599	535	508	265	444	309	524	395	430	527	399
La	38.0	47.0	68.0	34.0	23.0	36.0	49.0	43.0	29.0	28.0	36.0	32.0	18.0	43.0	44.0	35.0
(SiO <sub>2</sub> /Al <sub>2</sub> O <sub>3</sub> )	4.91	4.68	6.20	6.73	6.43	5.30	5.58	5.05	8.47	5.88	5.28	5.71	5.50	5.93	5.67	6.13
log (Na <sub>2</sub> O+K <sub>2</sub> O)	0.56	0.52	0.54	0.73	0.64	0.72	0.68	0.69	0.46	0.83	0.67	0.65	0.67	0.66	0.67	0.63
log (SiO <sub>2</sub> /Al <sub>2</sub> O <sub>3</sub> )	0.69	0.67	0.79	0.83	0.81	0.72	0.75	0.70	0.93	0.77	0.72	0.76	0.74	0.77	0.75	0.79
K <sub>2</sub> O/(K <sub>2</sub> O + CaO)	0.56	0.42	0.29	0.75	0.32	0.41	0.57	0.80	0.30	0.75	0.26	0.33	0.55	0.53	0.69	0.62
(K <sub>2</sub> O/Na <sub>2</sub> O)	0.70	0.75	0.27	0.07	0.46	1.11	1.40	0.55	2.41	0.55	0.94	1.08	1.06	0.86	1.17	0.92
(Fe <sub>2</sub> O <sub>3</sub> + MgO)	6.90	7.48	6.43	1.39	3.65	5.73	5.31	6.43	3.59	5.09	4.34	4.71	5.88	4.61	6.26	5.26
(TiO <sub>2</sub> /Al <sub>2</sub> O <sub>3</sub> )	0.05	0.05	0.07	0.01	0.03	0.04	0.04	0.04	0.02	0.04	0.04	0.04	0.05	0.04	0.06	0.05
Cr/Al	75	74	69	69	61	58	65	72	54	62	53	57	66	66	69	68
Th/(Th + Y)	0.39	0.40	0.46	0.68	0.50	0.46	0.40	0.35	0.50	0.42	0.47	0.42	0.39	0.38	0.43	0.45
Cr/V	0.69	0.85	0.62	7.50	0.87	0.69	0.87	0.91	0.71	0.81	0.71	0.91	0.79	0.78	0.77	0.74
Y/Ni	1.10	1.24	1.52	2.80	0.79	1.22	1.39	1.30	1.06	1.53	0.96	1.17	1.40	1.65	1.12	1.42
Zr/MO <sub>2</sub>	0.03	0.02	0.09	0.08	0.04	0.04	0.05	0.03	0.05	0.05	0.05	0.04	0.04	0.06	0.09	0.07
Nb/Y	0.52	0.42	0.83	0.71	0.58	0.57	0.50	0.65	0.59	0.58	0.58	0.50	0.51	0.61	0.70	0.67

Appendix C continued

Sample description and location	380 Sandstone Grooffontein	381 Sandstone Grooffontein	382 Sandstone Jakkalsfontein	383 Sandstone Jakkalsfontein	384 Sandstone Jakkalsfontein	385 Sandstone Jakkalsfontein	386 Sandstone Jakkalsfontein	387 Sandstone Jakkalsfontein	388 Sandstone Jakkalsfontein	389 Sandstone Jakkalsfontein	390 Siltstone SL1	392 Siltstone SL1	393 Siltstone SL1	394 Shale SL1
SiO <sub>2</sub>	71.39	72.35	73.77	72.18	73.92	73.35	73.88	72.25	72.13	72.48	57.96	61.31	59.67	61.10
TiO <sub>2</sub>	0.56	0.49	0.52	0.47	0.53	0.56	0.51	0.58	0.55	0.50	0.67	0.71	0.67	0.87
Al <sub>2</sub> O <sub>3</sub>	13.09	12.71	12.59	12.55	12.23	12.39	12.17	12.47	12.87	12.75	17.98	17.35	18.33	18.00
Cr <sub>2</sub> O <sub>3</sub>	0.02	0.02	0.01	0.02	0.02	0.01	0.02	0.02	0.02	0.02	0.02	0.02	0.02	0.03
Fe <sub>2</sub> O <sub>3</sub>	3.62	3.84	3.34	3.07	2.99	3.32	3.35	3.70	3.59	3.32	6.95	6.36	6.86	6.62
MnO	0.08	0.09	0.06	0.08	0.06	0.07	0.08	0.08	0.07	0.06	0.10	0.10	0.10	0.10
NiO	0	0	0	0	0	0	0	0.01	0	0	0	0	0	0
MgO	1.74	1.47	1.33	1.46	1.43	1.51	1.54	1.95	1.85	1.59	3.62	3.13	3.24	2.96
CaO	1.02	1.49	1.05	1.72	1.05	1.69	1.24	1.06	1.11	1.24	0.66	1.18	1.12	1.06
Na <sub>2</sub> O	2.66	2.81	2.41	2.55	2.54	2.72	2.31	2.30	2.64	3.18	1.30	1.48	1.24	1.22
K <sub>2</sub> O	2.86	1.89	2.49	2.22	2.12	1.67	2.05	2.50	2.47	2.01	4.64	4.09	4.49	4.40
P <sub>2</sub> O <sub>5</sub>	0.15	0.20	0.13	0.11	0.20	0.13	0.14	0.17	0.13	0.15	0.14	0.19	0.20	0.15
H <sub>2</sub> O <sup>-</sup>	-	-	-	-	-	-	-	-	-	-	-	-	-	-
LOI	1.34	1.41	1.34	1.42	1.38	1.21	1.18	1.15	1.13	1.16	2.31	2.22	2.29	2.31
Total	98.34	98.56	98.67	97.84	98.40	98.64	98.46	98.21	98.55	97.89	96.58	98.13	98.24	98.62
Nb	17.0	14.0	16.0	16.0	16.0	18.0	17.0	18.0	16.0	15.0	16.0	19.0	17.0	16.0
Zr	259	179	266	211	283	338	276	284	281	215	131	149	136	152
Y	19.0	19.0	25.0	24.0	24.0	24.0	27.0	29.0	30.0	24.0	36.0	38.0	41.0	39.0
Sr	133	195	128	147	140	136	127	125	140	150	161	188	169	171
U	3.00	7.00	6.00	6.00	9.00	2.00	3.00	9.00	11.0	7.00	12.0	11.0	10.0	9.0
Rb	92.0	60.0	80.0	80.0	77.0	61.0	79.0	91.0	85.0	68.0	218	181	202	192
Th	15.0	17.0	18.0	20.0	17.0	19.0	17.0	19.0	19.0	17.0	30.0	29.0	26.0	34.0
Pb	21.0	21.0	23.0	16.0	17.0	17.0	22.0	17.0	18.0	18.0	32.0	31.0	28.0	28.0
Ga	16.0	10.0	13.0	13.0	15.0	16.0	14.0	11.0	13.0	11.0	25.0	20.0	27.0	23.0
Zn	46.0	51.0	42.0	40.0	37.0	37.0	41.0	50.0	49.0	45.0	59.0	59.0	60.0	62.0
Cu	29.0	29.0	27.0	26.0	24.0	26.0	28.0	31.0	28.0	24.0	56.0	51.0	56.0	52.0
Ni	23.0	16.0	26.0	17.0	5.00	19.0	19.0	27.0	24.0	19.0	38.0	32.0	41.0	34.0
Co	9.00	9.00	8.00	7.00	7.00	8.00	8.00	9.00	8.00	8.00	19.0	16.0	18.0	17.0
Cr	45.0	38.0	37.0	37.0	39.0	42.0	39.0	44.0	38.0	40.0	80.0	60.0	70.0	59.0
Ce	91.0	80.0	85.0	77.0	78.0	72.0	69.0	74.0	88.0	71.0	119	118	117	121
Nd	27.0	28.0	24.0	30.0	25.0	27.0	25.0	27.0	34.0	23.0	107	105	106	107
V	55.0	52.0	47.0	45.0	53.0	59.0	49.0	56.0	55.0	57.0	84.0	82.0	83.0	81.0
Ba	597	617	675	530	472	270	338	522	534	458	529	516	554	523
La	35.0	23.0	19.0	28.0	27.0	31.0	25.0	35.0	44.0	39.0	46.0	52.0	58.0	43.0
(SiO <sub>2</sub> /Al <sub>2</sub> O <sub>3</sub> )	5.46	5.69	5.86	5.75	6.05	5.92	6.07	5.80	5.61	5.68	3.22	3.53	3.25	3.39
log (Na <sub>2</sub> O+K <sub>2</sub> O)	0.73	0.65	0.69	0.68	0.67	0.64	0.64	0.66	0.71	0.72	0.75	0.75	0.76	0.75
log (SiO <sub>2</sub> /Al <sub>2</sub> O <sub>3</sub> )	0.74	0.76	0.77	0.78	0.78	0.78	0.78	0.78	0.75	0.75	0.51	0.55	0.51	0.53
K <sub>2</sub> O/(K <sub>2</sub> O + CaO)	0.72	0.53	0.79	0.56	0.67	0.50	0.62	0.70	0.69	0.75	0.84	0.78	0.80	0.81
(K <sub>2</sub> O/Na <sub>2</sub> O)	1.00	0.60	1.03	0.87	0.84	0.61	0.89	1.09	0.93	0.63	3.56	2.77	3.61	3.61
(Fe <sub>2</sub> O <sub>3</sub> <sup>T</sup> + MgO)	5.36	5.31	4.67	4.53	4.42	4.84	4.88	5.65	5.43	4.91	10.1	9.49	10.1	9.58
(TiO <sub>2</sub> /Al <sub>2</sub> O <sub>3</sub> )	0.04	0.04	0.04	0.04	0.04	0.05	0.04	0.05	0.04	0.04	0.04	0.04	0.04	0.04
Cl/Al	67	68	69	66	68	67	68	68	67	69	72	72	73	73
Th/(Th + Y)	0.36	0.47	0.42	0.45	0.41	0.44	0.39	0.40	0.39	0.41	0.45	0.43	0.39	0.47
Cr/V	0.82	0.73	0.79	0.82	0.74	0.71	0.80	0.79	0.69	0.70	0.95	0.73	0.84	0.73
Y/Ni	1.17	1.19	1.04	1.41	4.80	1.26	1.42	1.07	1.25	1.26	0.95	1.19	1.00	1.15
Zr/TiO <sub>2</sub>	0.05	0.04	0.05	0.04	0.05	0.06	0.05	0.05	0.05	0.04	0.02	0.04	0.02	0.02
Nb/Y	0.63	0.74	0.64	0.67	0.67	0.75	0.63	0.62	0.53	0.63	0.44	0.50	0.41	0.41

Appendix C continued

Sample description and location	395 Shale		396 Shale		397 Shale		399 Siltstone		3100 Siltstone		3101 Shale		3102 Shale		3104 Siltstone		3107 Shale	
	SL1	SL1	SL1	SL1	SL1	SL1	SL1	SL1	SL1	SL1	SL1	SL1	SL1	SL1	SL1	SL1	SL1	SL1
SiO <sub>2</sub>	57.86	59.73	60.03	60.34	60.15	60.98	63.04	60.15	60.15	60.98	63.04	61.15	60.78	61.15	60.78	60.78	60.78	60.78
TiO <sub>2</sub>	0.67	0.70	0.69	0.68	0.74	0.74	0.68	0.74	0.74	0.68	0.68	0.73	0.71	0.73	0.71	0.71	0.71	0.71
Al <sub>2</sub> O <sub>3</sub>	18.47	18.57	18.52	16.75	17.71	17.96	16.04	16.75	17.71	17.96	16.04	17.68	16.95	17.68	16.95	16.95	16.95	16.95
Cr <sub>2</sub> O <sub>3</sub>	0.03	0.02	0.03	0.02	0.03	0.03	0.03	0.02	0.03	0.03	0.03	0.02	0.03	0.02	0.03	0.02	0.03	0.03
Fe <sub>2</sub> O <sub>3</sub> T	7.22	7.21	7.79	6.50	7.14	6.92	6.41	6.50	7.14	6.92	6.41	6.98	6.08	6.98	6.08	6.08	6.08	6.08
MnO	0.11	0.10	0.11	0.11	0.10	0.10	0.11	0.11	0.10	0.10	0.11	0.11	0.11	0.11	0.11	0.11	0.11	0.11
NiO	0	0	0	0	0	0	0	0	0	0	0	0	0	0	0	0	0	0
MgO	3.12	3.31	3.58	3.44	3.14	2.99	2.94	3.44	3.14	2.99	2.94	3.40	3.30	3.40	3.30	3.30	3.30	3.30
CaO	1.03	1.17	0.95	1.04	1.22	1.14	1.34	1.04	1.22	1.14	1.34	1.00	1.20	1.00	1.20	1.20	1.20	1.20
Na <sub>2</sub> O	1.17	1.08	1.07	1.47	1.23	1.26	1.89	1.47	1.23	1.26	1.89	1.22	1.53	1.22	1.53	1.53	1.53	1.53
K <sub>2</sub> O	4.65	4.63	4.82	3.90	4.13	4.33	3.74	3.90	4.13	4.33	3.74	4.42	4.44	4.42	4.44	4.44	4.44	4.44
P <sub>2</sub> O <sub>5</sub>	0.17	0.24	0.15	0.17	0.20	0.17	0.20	0.17	0.20	0.17	0.20	0.14	0.15	0.14	0.15	0.15	0.15	0.15
H <sub>2</sub> O <sup>-</sup>	-	-	-	-	-	-	-	-	-	-	-	-	-	-	-	-	-	-
LOI	2.30	2.31	2.33	2.23	2.33	2.32	2.34	2.23	2.33	2.32	2.34	2.29	2.32	2.29	2.32	2.32	2.32	2.32
Total	96.78	99.09	100.06	96.70	98.11	98.88	98.76	96.70	98.11	98.88	98.76	99.14	97.59	99.14	97.59	97.59	97.59	97.59
Nb	16.0	15.0	16.0	18.0	18.0	17.0	15.0	18.0	18.0	17.0	15.0	16.0	18.0	16.0	18.0	18.0	18.0	18.0
Zr	138	125	130	127	147	147	153	127	147	147	153	148	169	148	169	169	169	169
Y	38.0	40.0	40.0	42.0	45.0	40.0	37.0	42.0	45.0	40.0	37.0	41.0	41.0	41.0	41.0	41.0	41.0	41.0
Sr	148	140	132	178	171	180	225	178	171	180	225	170	230	170	230	230	230	230
U	13.0	14.0	13.0	15.0	9.0	12.0	16.0	15.0	9.0	12.0	16.0	13.0	12.0	13.0	12.0	12.0	12.0	12.0
Rb	205	208	218	186	187	186	165	186	187	186	165	205	207	205	207	207	207	207
Th	34.0	32.0	38.0	24.0	29.0	30.0	33.0	24.0	29.0	30.0	33.0	35.0	29.0	35.0	29.0	29.0	29.0	29.0
Pb	38.0	34.0	41.0	23.0	36.0	30.0	33.0	23.0	36.0	30.0	33.0	40.0	37.0	40.0	37.0	37.0	37.0	37.0
Ga	28.0	24.0	24.0	24.0	26.0	21.0	25.0	24.0	26.0	21.0	25.0	24.0	27.0	24.0	27.0	27.0	27.0	27.0
Zn	75.0	63.0	68.0	66.0	71.0	63.0	51.0	66.0	71.0	63.0	51.0	59.0	59.0	59.0	59.0	59.0	59.0	59.0
Cu	57.0	57.0	61.0	65.0	57.0	52.0	50.0	65.0	57.0	52.0	50.0	54.0	52.0	54.0	52.0	52.0	52.0	52.0
Ni	42.0	33.0	31.0	40.0	37.0	37.0	31.0	40.0	37.0	37.0	31.0	30.0	41.0	30.0	41.0	41.0	41.0	41.0
Co	19.0	19.0	21.0	18.0	19.0	18.0	16.0	18.0	19.0	18.0	16.0	18.0	15.0	18.0	15.0	15.0	15.0	15.0
Cr	68.0	73.0	73.0	76.0	64.0	66.0	55.0	76.0	64.0	66.0	55.0	64.0	61.0	64.0	61.0	61.0	61.0	61.0
Ce	114	108	118	135	123	116	116	135	123	116	116	117	128	117	128	128	128	128
Nd	106	104	107	109	107	105	105	109	107	105	105	106	107	106	107	107	107	107
V	84.0	85.0	87.0	96.0	90.0	82.0	80.0	96.0	90.0	82.0	80.0	88.0	84.0	88.0	84.0	84.0	84.0	84.0
Ba	574	543	514	489	496	518	468	489	496	518	468	522	512	522	512	512	512	512
La	62.0	54.0	64.0	63.0	64.0	58.0	42.0	63.0	64.0	58.0	42.0	46.0	61.0	46.0	61.0	61.0	61.0	61.0
(SiO <sub>2</sub> /Al <sub>2</sub> O <sub>3</sub> )	3.13	3.22	3.24	3.60	3.40	3.39	3.93	3.60	3.40	3.39	3.93	3.46	3.59	3.46	3.59	3.59	3.59	3.59
log (Na <sub>2</sub> O/K <sub>2</sub> O)	0.76	0.76	0.77	0.73	0.73	0.75	0.75	0.73	0.73	0.75	0.75	0.75	0.78	0.75	0.78	0.78	0.78	0.78
log (SiO <sub>2</sub> /Al <sub>2</sub> O <sub>3</sub> )	0.50	0.51	0.51	0.56	0.53	0.53	0.59	0.56	0.53	0.53	0.59	0.54	0.55	0.54	0.55	0.55	0.55	0.55
K <sub>2</sub> O/(K <sub>2</sub> O + CaO)	0.82	0.80	0.83	0.79	0.77	0.79	0.74	0.79	0.77	0.79	0.74	0.79	0.82	0.79	0.82	0.82	0.82	0.82
(K <sub>2</sub> O/Na <sub>2</sub> O)	3.97	4.29	4.52	2.66	3.36	3.44	1.98	2.66	3.36	3.44	1.98	3.61	2.90	3.61	2.90	2.90	2.90	2.90
(Fe <sub>2</sub> O <sub>3</sub> + MgO)	10.3	10.5	11.4	9.94	10.3	9.92	9.35	9.94	10.3	9.92	9.35	10.4	9.38	10.4	9.38	9.38	9.38	9.38
(TiO <sub>2</sub> /Al <sub>2</sub> O <sub>3</sub> )	0.04	0.04	0.04	0.04	0.04	0.04	0.04	0.04	0.04	0.04	0.04	0.04	0.04	0.04	0.04	0.04	0.04	0.04
Cl/Al	73	73	73	72	73	73	70	72	73	73	70	73	70	73	70	70	70	70
Th/(Th + Y)	0.47	0.44	0.49	0.36	0.39	0.43	0.47	0.36	0.39	0.43	0.47	0.46	0.41	0.46	0.41	0.41	0.41	0.41
Cr/V	0.81	0.86	0.84	0.79	0.71	0.80	0.69	0.79	0.71	0.80	0.69	0.73	0.73	0.73	0.73	0.73	0.73	0.73
Y/Ni	0.90	1.21	1.29	1.05	1.22	1.82	1.19	1.05	1.22	1.82	1.19	1.37	1.00	1.37	1.00	1.00	1.00	1.00
Zr/TiO <sub>2</sub>	0.02	0.02	0.02	0.02	0.02	0.02	0.02	0.02	0.02	0.02	0.02	0.02	0.02	0.02	0.02	0.02	0.02	0.02
Nb/Y	0.42	0.38	0.40	0.43	0.40	0.43	0.41	0.43	0.40	0.43	0.41	0.39	0.44	0.39	0.44	0.44	0.44	0.44

## Appendix D

**Table for average major, trace and rare earth element compositions of sandstones and siltstones from the Tanqua and Laingsburg depocentres**



Appendix D Average major, trace and rare earth element compositions of sandstones and siltstones from the Tanqua and Laingsburg depocentres.

Tanqua depocentre

	Skoorsteenberg Formation											
	Waterfall (V7)		Groot Hangklip (V8)		Droëkloof (V9)		Klein Hangklip (V10)					
	Average	Std dev	Average	Std dev	Average	Std dev	Average	Std dev	Average	Std dev	Average	Std dev
	<i>n</i> = 4		<i>n</i> = 7		<i>n</i> = 3		<i>n</i> = 3					
SiO <sub>2</sub>	75.06	1.49	74.86	1.54	74.75	0.60	74.31	0.60	74.31	3.86		
TiO <sub>2</sub>	0.50	0.06	0.53	0.04	0.52	0.06	0.50	0.06	0.50	0.07		
Al <sub>2</sub> O <sub>3</sub>	12.09	0.46	11.87	0.65	12.04	0.20	12.34	0.20	12.34	1.63		
Cr <sub>2</sub> O <sub>3</sub>	0.03	0.02	0.02	0.01	0.01	0	0.01	0	0.01	0		
Fe <sub>2</sub> O <sub>3</sub>	3.32	0.52	3.53	0.40	3.36	0.46	3.33	0.46	3.33	0.75		
MnO	0.05	0.01	0.05	0.01	0.05	0.01	0.04	0.01	0.04	0.01		
MgO	1.05	0.14	0.99	0.13	1.09	0.18	1.11	0.18	1.11	0.27		
CaO	0.94	0.14	0.94	0.40	0.85	0.10	0.61	0.10	0.61	0.16		
Na <sub>2</sub> O	2.59	0.03	2.67	0.14	2.68	0.13	2.86	0.13	2.86	0.16		
K <sub>2</sub> O	2.39	0.09	2.23	0.13	2.10	0.16	2.32	0.16	2.32	0.56		
P <sub>2</sub> O <sub>5</sub>	0.13	0.02	0.13	0.02	0.14	0.04	0.11	0.04	0.11	0.02		
Nb	13.4	1.43	14.0	1.04	13.4	1.71	12.9	1.71	12.9	1.90		
Zr	264	27.5	325	53.4	269	38.5	245	38.5	245	30.6		
Y	30.8	3.93	32.7	5.49	32.3	6.58	25.8	6.58	25.8	5.47		
Sr	160	17.6	157	5.19	144	11.2	171	11.2	171	25.5		
U	6.10	0.64	3.25	3.07	2.91	2.54	3.72	2.54	3.72	3.22		
Rb	88.3	4.84	78.8	6.31	80.0	2.21	82.8	2.21	82.8	26.9		
Th	13.0	3.01	12.6	1.86	12.3	1.26	13.4	1.26	13.4	1.06		
Pb	17.7	2.12	12.8	1.31	15.9	1.94	15.2	1.94	15.2	2.01		
Ga	13.4	1.09	14.4	1.18	13.6	1.11	15.0	1.11	15.0	3.49		
Zn	51.7	8.59	47.3	8.59	52.6	5.31	49.4	5.31	49.4	19.24		
Ni	13.4	3.53	12.6	2.44	12.1	1.50	14.9	1.50	14.9	7.95		
Co	79.3	13.0	60.5	12.1	54.9	22.7	55.6	22.7	55.6	19.6		
Cr	566	413	322	220	214	40.9	166	40.9	166	50.3		
Ce	73.5	12.3	63.5	14.8	69.1	9.85	64.5	9.85	64.5	4.54		
Nd	33.3	5.11	28.2	8.34	30.8	3.78	25.1	3.78	25.1	9.15		
V	58.1	7.86	66.5	5.79	65.0	3.83	66.9	3.83	66.9	9.97		
Ba	571	35.1	550	31.8	514	107.0	665	107.0	665	86.6		
La	41.4	3.28	31.1	8.88	39.7	8.70	28.4	8.70	28.4	10.83		

## Appendix D continued

	Kookfontein Formation													
	Pienaarsfontein (V6)		Shale		Skoorsteenberg (V135)		Bitterberg (V11)		Katjiesberg (V12)		Soutrivierspunt (V13)		Ouberg (V18)	
	Average	Std dev	Average	Std dev	Average	Std dev	Average	Std dev	Average	Std dev	Average	Std dev	Average	Std dev
	<i>n</i> = 14		<i>n</i> = 3	<i>n</i> = 5	<i>n</i> = 5	<i>n</i> = 5	<i>n</i> = 3	<i>n</i> = 3	<i>n</i> = 3	<i>n</i> = 2	<i>n</i> = 2	<i>n</i> = 1	<i>n</i> = 1	
SiO <sub>2</sub>	75.29	1.75	66.23	5.32	75.95	1.77	74.51	3.01	75.21	1.39	73.82	3.07	73.52	
TiO <sub>2</sub>	0.49	0.05	0.60	0.15	0.51	0.08	0.53	0.06	0.45	0.03	0.52	0.05	0.40	
Al <sub>2</sub> O <sub>3</sub>	11.51	0.71	14.97	3.04	11.18	0.87	12.16	0.86	11.93	0.63	12.57	0.23	11.43	
Cr <sub>2</sub> O <sub>3</sub>	0.01	0.01	0.01	0.00	0.02	0.01	0.02	0.00	0.02	0.00	0.02	0.00	0	
Fe <sub>2</sub> O <sub>3</sub>	2.98	0.60	4.94	2.52	3.11	0.18	3.19	0.50	3.07	0.58	2.82	0.04	2.38	
MnO	0.05	0.01	0.11	0.06	0.05	0.01	0.06	0.01	0.08	0.02	0.06	0.01	0.07	
MgO	0.96	0.19	1.74	0.51	0.96	0.06	1.55	0.26	1.55	0.18	1.46	0.17	1.27	
CaO	1.56	0.60	1.43	0.70	1.13	0.28	1.69	0.69	1.50	0.70	1.72	0.79	2.96	
Na <sub>2</sub> O	2.70	0.38	1.03	0.76	2.57	0.24	2.60	0.16	2.79	0.20	3.20	0.33	3.02	
K <sub>2</sub> O	1.94	0.27	3.06	1.06	2.06	0.16	0.90	0.17	1.34	0.02	1.06	0.02	1.38	
P <sub>2</sub> O <sub>5</sub>	0.15	0.04	0.15	0.04	0.14	0.04	0.17	0.03	0.15	0.02	0.20	0.05	0.13	
Nb	12.7	1.41	16.9	1.54	13.0	2.28	15.0	1.41	14.7	2.08	17.5	0.71	11.0	
Zr	261	43.7	139	22.8	333	116	281	56.5	209	54.8	283	71.4	163	
Y	28.0	3.96	30.7	10.5	29.9	4.57	26.6	3.85	24.3	4.51	25.0	2.83	19.0	
Sr	268	81.1	238	168	181	50.4	232	83.2	162	47.2	240	67.2	142	
U	4.18	2.91	7.92	1.52	3.38	3.25	6.40	0.89	5.33	3.51	7.00	2.83	8.00	
Rb	66.7	13.4	130	52.0	70.5	6.40	73.8	18.3	75.7	13.6	70.0	1.41	54.0	
Th	12.7	1.81	17.8	2.95	13.6	2.19	19.6	3.05	17.3	4.93	17.5	0.71	19.0	
Pb	15.7	2.21	38.3	17.3	14.5	1.48	21.2	5.36	16.0	6.56	18.0	2.83	12.0	
Ga	12.9	1.55	21.6	6.99	11.9	2.47	12.0	2.12	11.7	1.53	14.5	0.71	7.00	
Zn	44.8	7.20	105	26.9	50.3	4.36	46.8	10.6	43.7	7.02	42.0	8.49	43.0	
Ni	16.0	23.3	20.1	8.05	10.8	1.05	22.4	6.35	20.3	2.08	23.5	3.54	24.0	
Co	71.3	21.8	-	-	91.3	31.6	6.80	1.10	6.67	1.53	6.00	0	5.00	
Cr	212	166	123	71.0	413	274	39.4	3.21	36.0	1.73	35.5	3.54	34.0	
Ce	66.8	12.4	87.8	20.1	82.3	23.2	76.8	7.76	72.3	2.08	85.5	14.8	55.0	
Nd	28.9	6.55	33.5	8.80	33.0	11.5	30.6	3.91	28.3	1.53	30.0	2.83	22.0	
V	58.9	4.16	85.4	43.4	65.1	12.3	46.0	7.45	37.3	2.52	44.5	3.54	39.0	
Ba	514	70.1	624	66.1	508	36.0	426	135	343	38.0	526	97.6	273	
La	37.7	4.20	36.0	11.8	45.7	11.4	29.4	4.51	43.7	3.51	32.5	9.19	23.0	

Appendix D continued

Laingsburg\_deppcentre

	Collingham Formation				Vischkuil Formation			
	Sandstone		Siltstone		Sandstone		Shale	
	Average	Std dev	Average	Std dev	Average	Std dev	Average	Std dev
	<i>n</i> = 3		<i>n</i> = 3		<i>n</i> = 6		<i>n</i> = 3	
SiO <sub>2</sub>	71.53	10.39	71.43	0.70	68.93	5.11	62.99	2.63
TiO <sub>2</sub>	0.46	0.18	0.52	0.05	0.44	0.19	0.69	0.07
Al <sub>2</sub> O <sub>3</sub>	12.72	1.05	15.01	0.78	12.58	1.94	18.12	1.89
Cr <sub>2</sub> O <sub>3</sub>	0.02	0	0.02	0.01	0.02	0	0.02	0.01
Fe <sub>2</sub> O <sub>3</sub>	2.95	1.63	3.35	0.26	4.82	2.75	6.45	0.57
MnO	0.14	0.09	0.03	0.01	0.18	0.11	0.07	0.01
MgO	1.14	0.43	1.53	0.51	1.87	0.60	2.87	0.31
CaO	3.79	4.58	0.28	0.07	3.58	2.66	0.78	0.26
Na <sub>2</sub> O	2.57	0.00	1.83	0.30	2.12	0.92	1.61	0.16
K <sub>2</sub> O	1.53	0.55	2.38	0.17	1.51	0.38	1.88	0.47
P <sub>2</sub> O <sub>5</sub>	0.12	0.05	0.13	0.02	0.22	0.12	0.27	0.14
Nb	14.5	3.54	15.7	2.31	13.3	2.34	16.7	4.16
Zr	144	46.0	147	36.9	147	53.6	171	14.8
Y	28.5	14.8	31.7	11.8	28.3	9.07	44.3	11.0
Sr	178	100	110	26.9	195	39.4	122	7.21
U	10.0	4.24	11.0	4.36	8.17	2.64	10.7	5.03
Rb	95.5	13.4	168	21.9	81.5	18.1	192	45.5
Th	16.0	1.41	23.7	7.23	19.3	4.03	26.0	4.58
Pb	26.5	3.54	24.0	12.3	22.7	5.16	34.0	7.00
Ga	15.0	1.41	19.0	1.00	13.0	4.47	24.3	2.52
Zn	67.0	42.4	48.0	15.7	56.7	28.2	93.7	15.5
Ni	20.5	7.78	18.7	1.53	20.3	6.38	36.7	7.37
Co	6.50	3.54	7.33	0.58	12.0	8.25	15.7	2.08
Cr	46.5	12.0	35.7	8.62	39.0	13.5	58.0	8.89
Ce	92.0	22.6	120	41.2	84.0	25.5	132	15.0
Nd	26.0	5.66	34.0	12.1	29.5	7.12	44.7	8.33
V	38.5	12.0	57.3	21.2	47.0	31.2	106	18.9
Ba	595	266	793	205	503	150	819	147
La	39.5	7.78	45.3	11.4	36.3	12.9	52.7	8.96

Appendix D continued

	Laingsburg Formation															
	Fan A				Fan B				Fan C				Shale			
	Average	Std dev	Siltstone Average	Siltstone Std dev	Sandstone Average	Sandstone Std dev	Siltstone Average	Siltstone Std dev	Sandstone Average	Sandstone Std dev	Siltstone Average	Siltstone Std dev	Sandstone Average	Sandstone Std dev	Shale Average	Shale Std dev
	n = 11		n = 5		n = 8		n = 3		n = 3		n = 3		n = 3		n = 2	
SiO <sub>2</sub>	73.19	0.99	64.90	4.22	72.69	0.87	67.35	2.39	71.22	3.28	62.23	0.12	62.23	3.28	62.23	0.12
TiO <sub>2</sub>	0.54	0.06	0.72	0.06	0.58	0.09	0.76	0.03	0.50	0.03	0.69	0.01	0.69	0.03	0.69	0.01
Al <sub>2</sub> O <sub>3</sub>	12.50	0.34	16.06	2.09	12.53	0.34	15.45	0.83	12.41	0.83	18.86	0.22	18.86	0.33	18.86	0.22
Cr <sub>2</sub> O <sub>3</sub>	0.03	0.02	0.02	0.01	0.03	0.01	0.02	0.01	0.02	0.01	0.02	0	0.02	0	0.02	0
Fe <sub>2</sub> O <sub>3</sub>	3.48	0.46	6.14	1.64	3.87	0.56	5.43	0.67	2.91	0.67	6.92	0.57	6.92	0.27	6.92	0.57
MnO	0.07	0.01	0.08	0.01	0.08	0.01	0.08	0	0.11	0	0.08	0	0.08	0.07	0.08	0
MgO	1.57	0.17	3.06	0.76	1.80	0.23	2.63	0.21	1.43	0.21	3.00	0.33	3.00	0.01	3.00	0.33
CaO	1.26	0.71	0.89	0.27	1.09	0.15	0.97	0.15	3.36	0.15	0.53	0.07	0.53	2.77	0.53	0.07
Na <sub>2</sub> O	2.63	0.24	1.98	0.62	2.60	0.74	2.13	0.22	2.69	0.22	1.56	0.12	1.56	0.46	1.56	0.12
K <sub>2</sub> O	1.77	0.57	1.96	0.17	2.05	0.55	1.46	0.15	1.77	0.15	2.24	0.01	2.24	0.73	2.24	0.01
P <sub>2</sub> O <sub>5</sub>	0.15	0.02	0.21	0.04	0.15	0.02	0.19	0.02	0.13	0.02	0.22	0.01	0.22	0.01	0.22	0.01
Nb	17.4	2.58	18.2	2.17	18.1	3.44	18.7	2.31	16.0	2.31	17.5	0.71	17.5	1.73	17.5	0.71
Zr	283	94.1	170	45.4	327	145	229	54.6	264	54.6	155	8.49	155	61.2	155	8.49
Y	27.3	3.66	36.8	4.87	30.9	4.82	39.7	4.16	26.3	4.16	32.0	4.24	32.0	2.89	32.0	4.24
Sr	141	9.77	102	21.4	127	13.5	115	18.0	142	18.0	99.0	1.41	99.0	9.8	99.0	1.41
U	7.45	3.08	8.80	3.27	7.25	3.88	6.00	2.65	6.67	2.65	6.00	1.41	6.00	2.89	6.00	1.41
Rb	82.2	13.9	166	33.3	88.1	7.8	140	15.3	79.3	15.3	186	2.12	186	1.15	186	2.12
Th	19.0	2.93	23.8	2.77	19.8	3.77	21.3	2.08	17.3	2.08	28.0	0	28.0	0.58	28.0	0
Pb	20.0	3.00	24.4	3.21	22.0	4.47	27.0	5.00	21.0	5.00	30.5	0.71	30.5	0	30.5	0.71
Ga	13.1	2.07	20.6	4.56	13.5	1.77	18.7	2.08	13.7	2.08	25.0	1.41	25.0	0.58	25.0	1.41
Zn	46.8	11.6	96.8	27.0	49.5	5.29	80.7	16.0	32.7	16.0	112	3.54	112	0.58	112	3.54
Ni	21.2	6.06	34.2	5.02	23.5	5.24	31.3	10.0	16.7	10.0	32.0	7.07	32.0	0.58	32.0	7.07
Co	9.00	3.52	15.2	5.02	9.13	1.55	13.0	2.00	6.67	2.00	17.0	1.41	17.0	0.58	17.0	1.41
Cr	67.9	101	56.6	10.8	60.3	35.8	58.7	7.37	40.0	7.37	61.5	0.71	61.5	3.46	61.5	0.71
Ce	82.3	17.9	103	9.50	86.0	14.1	109	1.00	73.3	1.00	125	6.36	125	11.5	125	6.36
Nd	34.2	13.2	35.8	6.38	32.3	4.92	36.7	1.15	26.3	1.15	34.5	0.71	34.5	2.89	34.5	0.71
V	47.9	11.8	90.0	28.4	53.5	11.8	78.3	9.24	54.3	9.24	113	0.71	113	4.62	113	0.71
Ba	472	176	673	77.3	471	78.4	643	39.1	399	39.1	942	51.6	942	53.7	942	51.6
La	72.4	128	27.6	16.7	36.8	8.07	40.3	9.29	38.0	9.29	48.0	12.7	48.0	8.7	48.0	12.7

## Appendix D continued

	Laingsburg Formation												
	Fan D			Fan E			Fan F			Siltstone			
	Sandstone Average	Std dev	Siltstone Average	Sandstone Average	Siltstone Average	Siltstone Average	Sandstone Average	Std dev	Siltstone Average	Std dev	Sandstone Average	Std dev	Siltstone Average
	n = 3		n = 1	n = 2		n = 2	n = 3		n = 2		n = 3		n = 1
SiO <sub>2</sub>	71.15	2.21	68.52	73.71	5.52	64.12	72.54	0.19	64.12	0.19	72.54	1.15	63.49
TiO <sub>2</sub>	0.56	0	0.66	0.53	0.03	0.72	0.53	0.07	0.72	0.07	0.53	0.12	0.72
Al <sub>2</sub> O <sub>3</sub>	12.25	0.51	14.12	11.61	0.87	17.16	12.56	0.09	17.16	0.09	12.56	0.67	17.00
Cr <sub>2</sub> O <sub>3</sub>	0.04	0.02	0.03	0.03	0.02	0.02	0.02	0	0.02	0	0.02	0.01	0.03
Fe <sub>2</sub> O <sub>3</sub>	3.55	0.55	5.38	3.20	0	6.27	3.99	0.10	6.27	0.10	3.99	0.96	6.21
MnO	0.12	0.07	0.08	0.07	0	0.09	0.08	0.01	0.09	0.01	0.08	0.01	0.10
MgO	1.71	0.21	2.20	1.37	0.20	2.86	1.84	0.40	2.86	0.40	1.84	0.36	2.96
CaO	3.38	1.92	1.23	3.04	2.46	0.84	1.53	0.43	0.84	0.43	1.53	0.56	1.03
Na <sub>2</sub> O	2.53	0.25	1.78	2.17	0.01	1.89	2.12	0.45	1.89	0.45	2.12	0.80	1.96
K <sub>2</sub> O	1.45	0.84	1.88	1.69	0.91	1.97	1.44	0.30	1.97	0.30	1.44	0.23	2.39
P <sub>2</sub> O <sub>5</sub>	0.17	0.03	0.17	0.15	0	0.19	0.15	0.01	0.19	0.01	0.15	0.04	0.19
Nb	17.0	1.00	18.0	17.0	4.24	18.5	15.7	2.12	18.5	2.12	15.7	2.08	17.0
Zr	254	40.1	178	340	161	156	249	7.07	156	7.07	249	53.4	200
Y	33.0	4.36	35.0	28.0	0	36.5	33.0	0.71	36.5	0.71	33.0	2.65	36.0
Sr	171	27.8	127	183	58.7	132	187	59.4	132	59.4	187	63.9	141
U	7.33	2.89	5.00	5.00	5.66	10.0	8.00	1.41	10.0	1.41	8.00	4.00	4.00
Rb	80.7	17.0	132	84.5	12.0	166	93.0	1.41	166	1.41	93.0	8.89	163
Th	20.0	2.65	23.0	21.0	1.41	22.5	21.0	3.54	22.5	3.54	21.0	2.65	28.0
Pb	20.3	4.93	21.0	17.0	8.49	25.5	25.7	4.95	25.5	4.95	25.7	2.89	32.0
Ga	12.3	2.52	18.0	10.5	0.71	23.0	15.7	0	23.0	0	15.7	3.21	26.0
Zn	49.0	5.00	86.0	42.5	4.95	96.0	59.7	2.83	96.0	2.83	59.7	10.1	103
Ni	25.7	1.15	30.0	21.5	3.54	33.0	25.0	7.07	33.0	7.07	25.0	3.00	27.0
Co	7.67	1.53	13.0	7.00	0	15.5	9.67	0.71	15.5	0.71	9.67	2.31	15.0
Cr	108	119	51.0	92.0	73.5	61.0	41.7	4.24	61.0	4.24	41.7	9.87	56.0
Ce	71.7	2.89	98.0	82.0	1.41	108	91.3	8.49	108	8.49	91.3	11.0	120
Nd	30.7	1.15	35.0	30.0	2.83	34.5	30.7	6.36	34.5	6.36	30.7	0.58	39.0
V	44.0	10.4	69.0	43.5	0.71	92.5	46.3	9.19	92.5	9.19	46.3	11.9	95.0
Ba	339	49.5	460	416	153	674	520	52.3	674	52.3	520	140	797
La	25.7	7.51	36.0	36.5	6.36	40.5	40.3	19.1	40.5	19.1	40.3	6.51	46.0

Appendix D continued

	Fort Brown Formation			
	Sandstone	Siltstone		
	Average	Std dev	Average	Std dev
	<i>n</i> = 5		<i>n</i> = 5	
SiO <sub>2</sub>	72.51	1.98	67.41	1.90
TiO <sub>2</sub>	0.61	0.15	0.70	0.06
Al <sub>2</sub> O <sub>3</sub>	13.00	0.70	15.46	1.05
Cr <sub>2</sub> O <sub>3</sub>	0.02	0	0.02	0.01
Fe <sub>2</sub> O <sub>3</sub>	3.82	0.67	5.25	0.48
MnO	0.08	0.02	0.09	0.01
MgO	1.61	0.21	2.42	0.11
CaO	1.32	0.42	1.42	0.34
Na <sub>2</sub> O	2.89	0.29	1.92	0.18
K <sub>2</sub> O	1.14	0.26	1.68	0.21
P <sub>2</sub> O <sub>5</sub>	0.17	0.02	0.20	0.01
Nb	18.6	6.11	17.2	2.28
Zr	373	206	190	28.4
Y	28.4	3.91	36.4	2.30
Sr	271	49.9	211	47.7
U	7.80	2.39	7.8	4.02
Rb	75.0	18.2	145	6.43
Th	22.4	4.56	23.0	2.00
Pb	17.8	4.76	26.4	3.21
Ga	13.4	1.14	22.0	2.00
Zn	55.6	13.7	85.4	5.98
Ni	23.0	4.06	28.6	4.72
Co	8.80	1.64	12.4	1.14
Cr	59.2	26.1	50.6	5.68
Ce	95.8	28.0	99.2	5.72
Nd	32.6	8.88	33.6	3.21
V	66.8	29.3	72.8	8.64
Ba	502	165	596	57.9
La	36.0	19.7	42.8	7.76

